

Andreas Steimel

Electric Traction – Motive Power and Energy Supply –

**Basics and Practical
Experience**

**Oldenbourg
Industrieverlag**





Prof. Dr.-Ing. Andreas Steimel

Electric Traction – Motive Power and Energie Supply

Basics and Practical Experience

Oldenbourg Industrieverlag München

Bibliographic information of the German National Library

The German National Library records this publication in the German National Bibliography; detailed biographical data can be obtained on the Internet at <<http://dnb.ddb.de>>.

© 2008 Oldenbourg Industrierlag GmbH
Rosenheimer Straße 145,
D-81671 Munich
Phone: +49 89 45051-0
www.oldenbourg-industrieverlag.de

This work, including all figures, is copyrighted.

Any use outside the limits of the copyright law is not permitted without permission of the publisher and is punishable. This applies, in particular, to copying, translating, microfilming, and importing and editing in electronic systems.

Editor: Elmar Krammer
Production: Karl Heinz Pantke
Typesetting: Grafik + Druck GmbH
Printed on acid-free, chlorine-free paper

ISBN 978-3-8356-3132-8

Preface

Intention of this book and synopsis

This book has evolved from the lecture series “Elektrische Bahnen” (“Electric railways”) which has been held at Ruhr-Universität Bochum since 1996. Its primary audience are students of electrical energy technologies, control engineering and mechanical engineering as well as young engineers of electrical engineering, especially in the fields of power electronics, in railway industry and in railway-operating companies.

The book intends to convey mechanical fundamentals of electric railway propulsion, which includes rail-bound guidance, transmission of traction effort from wheel to rail under the influence of non-constant levels of adhesion and the transmission of motor torque to a spring-mounted and thus sliding drive set.

The focal point of the book will be the disposition of electric traction units powered by three-phase induction motors. We shall discuss the stationary and dynamical behaviour of the squirrel-cage induction motor and the principle and construction features of pulse-controlled inverters, as well as scalar and field-oriented control systems and four-quadrant power converters, feeding the DC link of the inverters.

As is appropriate to the lesser importance these drive systems have nowadays, we will consider DC and AC commutator motors only in a cursory fashion, as well as their voltage control. By example, we will take a look at high-performance locomotives, high-speed trains, diesel-electrically powered locomotives and commuter passenger systems.

Since the specific railway energy supply network being separate from the national power utility is a key factor in operating electrical railway systems, chapter 13 will offer a detailed look at the various systems of railway power supply, under special consideration of converter technology in this field as, for example, the line interference of inverter-fed traction units (see chapter 14). Chapter 15 features an abridged overview on the most important systems of field-oriented control of induction motors and about an innovative speed-sensorless control approach for induction motor drives, coming now into the commercial phase. Chapter 16 suggests further reading, while chapter 17 will provide lecture-oriented exercise (including sample solutions).

The Anglo-american reader may notice that the lion’s share of examples has been derived from central European (German, Swiss, Austrian) samples of Electric Traction. This is mainly due to the author’s personal experience as well as the fact that most fundamental research, design and construction of locomotives utilizing power electronics took place in these countries, notably with BBC and Siemens. We wish to apologize that British and American locomotives only feature rarely; however, an approach based on personal experience appeared to be the most sensible way to tackle the subject.

The translation follows the International Electrotechnical vocabulary (IEV, [31]) of IEC and the UIC Railway Dictionary [32]. Corresponding to the dominant use in international technical and scientific literature, the British English term ‘bogie’ will be used for the German word ‘Drehgestell’ and not the term ‘truck’, usual in American English. Finally, please excuse the use of German symbol standards in formulae and diagrams, since the vast number of variables involved would make a complete exchange a daunting task.

Basic knowledge

This book requires the following:

Basic knowledge of construction and operative behaviour of electrical machines and transformers according e.g. to lecture “Grundlagen der Energietechnik” ([V1], Basics of Electrical Power Engineering), basic knowledge of power electronics [V2], basic knowledge of mechanics.

Words of thanks

Every industrial engineer stands on the shoulders of the colleagues before him. So I want to express my gratitude first to my father Karl Steimel, 1956–1967 head of R&D of AEG in Frankfurt/ Germany, one of the indefatigable initiators of development in inverter-fed induction motors drives, and my academic teacher, R. Jötten at TU Darmstadt. Then – only to mention very few – my elder colleagues at Brown, Boveri & Cie. in power electronics as L. Abraham, E. Futterlieb, the late W. Lienau, H. Stemmler and W. Runge, as well as in locomotive engineering W. Teich, J. Körber, M. Schulz and the late R. Gammert, R. Pfeiffer from Technical University Darmstadt and W.-D. Weigel from Siemens Transportation Systems. Next my senior colleague at Ruhr-University Bochum, M. Depenbrock, the inventor of the Four-Quadrant Converter and of Direct Self Control (DSC), and our Ph. D. students working on perfection of DSC and the line behaviour of traction converters and on the development of robust sensorless operation of induction motors. Last but not least thank is to be said to my son Christian for the translation, the secretary and the draughtswoman of our chair in Bochum and the critical readers of the first two editions (in German), ferreting out hidden errors of the first edition.

Table of Contents

Preface	V
1	Basic principles	1
1.1	Definitions	1
1.1.1	So, what is a “railway“?	1
1.1.2	Classification of Railways	1
1.2	Historical development of electrical railwaying	2
1.3	A short overview of railway electrical supply networks	6
1.3.1	Direct-current railway systems	6
1.3.2	Single-phase alternating current railway systems	7
1.3.3	Three-phase three-conductor railway systems	8
1.3.4	Standardized voltages of the train line	8
1.3.5	State of electrification in selected countries	9
1.4	Comparison of traction systems	9
1.5	The European railway industry	10
2	The mechanics of railway transportation	13
2.1	Principles of rail-guidance	13
2.1.1	Gauges	13
2.1.2	Guidance of wheelset in track	14
2.1.3	Frame and bogie	16
2.1.4	Bogies with self-steering wheelsets	20
2.1.5	Curvature-dependant body-tilting equipment	21
2.2	Train resistance	23
2.2.1	Train rolling resistance	23
2.2.2	Train resistance due to curves	24
2.2.3	Train gradient resistance	24
2.2.4	Train acceleration resistance	25
2.2.5	Permanent and starting tractive efforts (F - v diagram)	25
2.2.6	Load transfer	26
2.3	Adhesion, slip-and-slide control	29
2.4	Traveling time loss by acceleration and braking	33
3	Running gear and drive of traction vehicles	35
3.1	Classification of traction vehicles and wheel arrangement	35
3.1.1	Classification of traction vehicle types	35
3.1.2	Wheel arrangement	36
3.2	Mechanical components of power transmission	37
4	Commutator traction motors and their control	47
4.1	DC traction motor	47
4.1.1	DC commutator motor	47
4.1.2	Variation of the terminal voltage by series resistors	52
4.1.3	Control of motor voltage in DC-supplied systems by means of a DC chopper	53
4.1.4	Control of the motor voltage with AC systems by phase-control rectifiers	58

4.2	AC traction motor	62
4.2.1	AC commutator motor	62
4.2.2	Control of motor voltage with the AC commutator motor	63
5	Synchronous traction motors and their control	67
5.1	Synchronous motor	67
5.2	Feeding the synchronous traction motor with a load-commutated inverter	69
6	Induction traction motors and their control	73
6.1	Construction and stationary behaviour of the induction machine	73
6.2	Voltage-source inverter (VSI)	81
6.3	Controlled operation of inverter-fed induction motor	85
6.4	Group supply of induction traction motors	89
6.5	Four-quadrant converter	91
6.6	Inverter circuit and construction technology	96
6.6.1	Forced-commutated thyristor voltage-source inverter	96
6.6.2	Inverter with Gate-Turn-Off (GTO) thyristors	98
6.6.3	IGBT Inverter	100
6.6.4	Three-level inverter	101
6.6.5	Current-source inverter	102
6.6.6	Cooling and constructional aspects	103
7	Electric traction vehicles for main-line service	111
7.1	Electric locomotives with DC traction motors	111
7.1.1	DC chopper control	111
7.1.2	Thyristor phase-angle control	111
7.2	Electric traction vehicles with AC commutator traction motors	115
7.3	Electric traction vehicles with synchronous traction motors	117
7.4	Electric traction vehicles with induction traction motors	118
7.4.1	Locomotives	118
7.4.2	High-speed trains	124
8	Multi-system traction vehicles	129
8.1	Examples with DC commutator motors and synchronous motors	129
8.2	Examples with inverter-fed induction motors	132
9	Diesel-electric traction vehicles	137
9.1	Conventional technologies – hydraulic and electric drive chain	137
9.2	Diesel-electric traction vehicles with three-phase drives	142
9.3	Dual-mode traction vehicles	150
10	Suburban and Light Rail traction vehicles	153
10.1	Metro and Underground trains	154
10.2	Light Rail and Light Rapid Transit vehicles, low-floor technology	157
10.2.1	Conventional tramway carriages and articulated trains	158
10.2.2	Dual-system Light Rapid Transit vehicles	160
10.2.3	Low-floor light rail vehicles	162
10.3	Traction vehicles with energy storage	170

11	Braking technology	173
11.1	Automatic air brake	173
11.2	Magnet rail brake	177
11.3	Linear eddy-current brake	178
12	Uncommon types of railways	179
12.1	Track-guided railways on pressurized rubber-tire wheels	179
12.2	Suspension Railways	181
12.3	Trackless "railway" transportation systems	184
12.4	Magnetic Levitation Railways (MagLev)	188
12.4.1	Support and Guidance	188
12.4.2	Contactless transmission of traction force	190
12.4.3	Converter	193
12.4.4	On-board power supply of vehicles	193
12.4.5	Application Pudong International Airport–Shanghai	194
13	Power supply of electric railways	195
13.1	AC railways operating at $16\frac{2}{3}$ (16.7) Hz	195
13.1.1	Centralized and decentralized supply in Germany	195
13.1.2	Rotary converters	199
13.1.3	Static converters	202
13.2	AC railways operating at 50 Hz	204
13.2.1	Properties, and a comparison to the $16\frac{2}{3}$ -Hz system	204
13.2.2	Autotransformer system	207
13.2.3	Increased operating voltage	208
13.3	DC railways	209
13.4	Contact lines and current collectors	212
14	Line interference	219
14.1	Survey	219
14.2	Emission sources in DC railway systems	220
14.2.1	Voltage harmonics of the substation rectifiers	220
14.2.2	Input-current harmonics of a step-down DC chopper	221
14.2.3	Input-current harmonics of an ASCI	222
14.2.4	Input-current harmonics of a VSI	223
14.3	Emission sources in AC railway systems	224
14.3.1	Voltage harmonics of the power supply	224
14.3.2	Input-current harmonics by phase-angle control	224
14.3.3	Input-current harmonics by inverter input current	228
14.3.4	Input voltage harmonics of the four-quadrant converter	228
14.3.5	Modulation of VSI input-current harmonics by the four-quadrant converter	233
14.4	Impedances of the railway power-supply system	234
14.5	Mechanisms of coupling, psophometric interference current	237
14.6	Track circuits	239
14.7	Suppression of low-frequent interference currents of power-electronic converters	240
14.8	High-frequent disturbance	241

15	Appendix	243
15.1	Control strategies for traction induction motor drives	243
15.1.1	Demands by railway traction	243
15.1.2	Space-phasor representation of three-phase systems	243
15.1.3	Dynamical equivalent circuit diagram of an Induction Machine	244
15.1.4	Field-oriented control	245
15.1.5	Direct Self Control	250
15.1.6	Indirect Stator-quantities Control	255
15.1.7	Conclusion	257
15.2	Speed-sensorless stator-flux-oriented control of induction motor drives in traction	258
15.2.1	Introduction	258
15.2.2	Model of the induction machine	259
15.2.3	Stator-flux oriented control	260
15.2.4	Field-weakening operation	262
15.2.5	Correction of inverter-voltage errors	263
15.2.6	Sensorless identification of speed	264
15.2.7	Stator-resistance estimation	267
15.2.8	Suppression of parasitic DC voltages	269
15.2.9	Operation with infinitely slow change between driving and breaking	269
15.2.10	Difference of Indirect Stator-Quantities Control and Direct Vector Control ..	272
15.2.11	Conclusion	273
15.3	Unified Notation of Carriages of UIC and OSShD	274
15.4	Symbols and Abbreviations	276
16	References	279
16.1	Books	279
16.2	Journals	281
16.3	Selected papers from journals and conferences	281
17	Exercises with exemplary solutions	295
17.1	F-v-Diagram of a Universal Locomotive	295
17.2	Mechanical design of a Universal Locomotive	297
17.3	Mean traveling speed of a Metro train	298
17.4	DC traction motor fed by a DC chopper	301
17.5	Two-pulse bridge in half-controllable connection of pairs of arms with sequential phase control	304
17.6	Three-phase induction traction motor for a Universal Locomotive with 6,400 kW	309
17.7	Wheel-tire diameter differences at group supply of traction IM	312
17.8	Four-quadrant converter for a Universal Locomotive 6,400 kW	315
17.9	Stopping distance of a Light Rapid Transit Train with and without magnetic rail brake	319
17.10	Supply of electric railway lines from the 50-Hz utility	321
Index	325

1 Basic principles

1.1 Definitions

1.1.1 So, what is a “railway“?

The most comprehensive definition of a “railway” is, according to DIN 57115 (VDE 0115)¹ part 1: “track-bound and non-track-bound transport systems for passenger and cargo transportation”. A more concise interpretation may be found in the 1962 edition of the Encyclopedia Britannica: “Railway, a mode of land transportation the roadway of which consists of one or more tracks, each having two parallel steel rails. Over these rails move freight and passenger carrying vehicles, or cars, with flanged wheels. The cars are usually pulled or pushed by a locomotive, although they may be self-propelled”.

We shall define a “railway“ in the narrower sense of “a self-propelled track-bound system of transport”. The defining features are track-bound rail guidance and the possibility of creating trains by linking single vehicular units, the iron rails not being necessarily a part of the system. In chapter 12, we will encounter various track-bound systems operating without such rails, which usually are considered key to the concept of “railwaying”.

The principle of track-bound rail guidance (rail-wheel system) allows for transport speeds peaking at 575 kilometres per hour (~360 mph); higher speeds are, in effect, inachievable for land-bound vehicles due to the power requirement rising by the speed to the third power. Regular high-speed train service in France, Germany and Japan operate at speeds of up to 330 kph (over 200 mph). Modern rail systems, on the other hand, allow for composition of trains of up to 20,000 metric tons of weight (4.4 *million* lbs.), which can be safely operated at speeds of up to 60 kph (37 mph) at minimal personnel requirements. Commuter transport may nowadays operate on a fully automatic basis (e.g. without drivers).

1.1.2 Classification of Railways

Railways may be classified by a host of different categories:

- By ownership

National railways and private enterprise railways

Whereas the 19th century had seen a co-existence of national and private railways, Europe and most of the worlds’ countries (excluding the United States of America) nationalized the majority of private rail networks in the years from 1880 onwards to about 1947. This was mainly due to structural and fiscal reasoning, especially in newly emerging national states such as Hungary, Italy and Germany and, later on, former colonies having achieved their independence; furthermore, to provide ample infrastructure for industrialization; finally, to meet the vast transport requirements of the two World Wars and their consequences.

¹ DIN: Deutsche Industrienorm, German Industrial Standard

During the second half of the 20th century, the railways' importance declined due to the rise of individual transport, in the form of the private motor car and lorry, as well as the airplane, whose speed and versatility the railway could not apparently match. Only by the close of the century, a change of mind set in: due to congestion of public traffic by individual transport, track-bound public mass transit becomes more and more appealing. In addition, governmental control proved inadequate to meet the demands to the railway systems; thus, programs of decentralization and deregulation were applied to railway transit. EU Directive 91/440 intended to enable and organize the barrier-free coexistence and competition of governmental and private railway operators. However, due to the massive governmental subsidies given to individual and airborne transport in the latter half of the century, public mass transit is unable to operate economically in most areas and is thus dependent on governmental additional funding.

- By specific task of traffic
Public-service railways (being subject to schedule operation and conveyance obligation);
Non-public service railways (including, for example, factory, harbor and mining railways).
- By importance of traffic
Major networks of national and international long-distance traffic;
Regional networks for a limited area of service;
Minor networks for local service;
Commuter networks for public mass transit in cities and conurbations. These are further specified as tramways or Light Rail Systems, Light Rapid Transit ('Stadtbahnen' in German), underground railways and suburban (mass transit) railways.
- Special transportation systems:
This includes purely touristic systems like funicular and other cable systems, automated cab railways ("people mover") on airport duty and isolated junction lines, for example the Haneda International Airport – Downtown Tokyo or the Pudong International Airport – Downtown Shanghai lines. Finally, there were barge tow railways, the sole surviving example being the system of the Panama Canal Authority.

1.2 Historical development of electrical railwaying

Having had a precursor in the tracks ground into Roman roads (with a width similar to modern standard gauge, 1435 mm or 4ft 8.5in), Europe only saw the return of track systems in the early modern age, in the shape of mining railways: wooden lorries, operating on wide wooden rails and guided by a track nail between the two rails. By the middle of the 18th century, coal-mining companies in England replaced the wooden tracks by iron ones; guidance was achieved by angle irons affixed to the outside of the track. The advantages were most obvious: The rolling friction was greatly reduced, the durability of the rails increased, and this actually laid the groundwork for the use of machine traction. Shortly after, the flanged wheel running on rails of "a mushroom-like" cross-section appeared.

In 1804, F. Trevithick used Watt's high-pressure steam engine on a rail-bound vehicle for the first time: the steam locomotive was born. From 1810 onwards, such locomotives were in widespread service in coal mines. In 1825, the very first public transport railway was established between Stockton and Darlington in North-East England, George and Robert Stevenson introducing today's 4ft 8.5in standard gauge on this occasion. In 1835, the first such railway opened service in Germany, connecting Nuremberg and Fuerth.

From isolated beginnings, European railwaying downright exploded in the following years; however, a bewildering variety of technical standards was used. By 1850, a necessary trend toward standardization of gauge, coupling system and general size of units emerged, leading to technical standards which allowed for a Europe-wide network of compatible standards. Some countries retained different gauges for strategic reasons, most notably Russia, but also including Spain and Portugal. Minor networks and colonial railways often chose narrow-gauge systems for financial reasons.

In the 1820s, A.M Ampere and M. Faraday had discovered electro-magnetic force and electrical induction, respectively. Subsequently, this led to research how to use this new source of power for railways. As early as in 1836, an electric railcar was tested in Scotland, being powered by electric motors which resemble recent Switched Reluctance Motors. These trials, however, did not yield considerable success, since there still was no effective, reliable and economically sound source of electrical power. Such machines could only operate using early batteries like Volta's elements. Only the discovery of the Electrodynamic Principle by W. von Siemens and Ch. Wheatstone in the 1860s allowed for effectively unlimited amounts of power using generators and thus to increase the output of electrical machines at discretion.

In 1879, Siemens displayed the first electrically powered locomotive at the Berlin Commerce Fair (Fig. 1.1). It was used for transporting visitors on the Fairgrounds, and operated on a direct current (DC) motor of 2.2 kilowatts continuous output, which was fed from a current-carrying rail placed between the two main rails, which in turn re-routed the current from the engine to the generator. Maximum speed attained was 13 kph (8 mph), and the engine's weight came to about two metric tons (4,400 pounds), which means a weight-to-power ratio of 1100 kilograms per kilowatt (modern high-power locomotives attain values of about 14 kilograms per kilowatt!). From 1882 onwards, this direct-current propulsion system was applied to tramways and mining railways, with power being usually supplied via an overhead contact line

The first fully electrified railway was opened in 1895 by the Baltimore & Ohio RR in the United States of America: a five-kilometre city tunnel was electrified using a 675 Volt overhead system; electrical motors of 4-270 kilowatt output were used, thus countering the smoke problem.



Fig. 1.1: First electric locomotive by W. v. Siemens 1879, Berlin

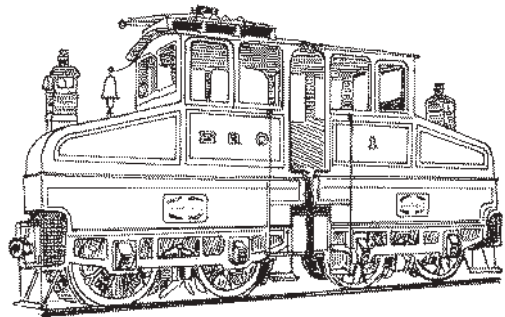


Fig. 1.2: DC locomotive of Baltimore & Ohio Railroad, 1895

The commutator bar voltage, however, limited maximum working voltage to about 750 Volt by the turn of the century. It was only about the time of the Great War that a maximum voltage limit of 1500 Volt was attained; this level is considered a practical economic limit even today. With such voltage, tramways and commuter railways could operate economically. Long-distance railways, however, experienced unacceptable voltage drop, even if using intermittent feeding rectifier units in very short intervals.

As was the case in national power supply, railways were keen on introducing alternating current systems, thus being able to transfer electrical energy at the required high voltage level (since direct current electricity's voltage level cannot easily be transformed). However, there were no traction motors running on AC yet that provided sufficient output levels. But there was already the squirrel-cage induction motor. From about 1890, secondary railways in Northern Italy and later on the Simplon Tunnel were electrified using three-phase alternating current (3AC). In 1903, the "Studiengesellschaft für elektrischen Schnellverkehr" (Research society for electrical rapid transport) held trials using two electric railcars fed from a three-pole overhead system (Fig. 1.3). These vehicles attained speeds of up to 210 kph (130 mph). The 3AC system, however, still suffered from being complicated to construct, especially at intersections and switches, and allowing only a limited number of economic speeds due to the fixed line frequency. As more advanced systems became available, most of the cumbersome three-phase systems had been eliminated by 1970.

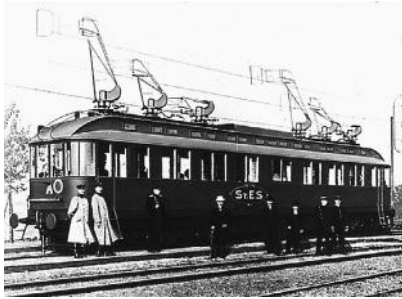


Fig. 1.3: Three-phase high speed experimental railcar by AEG 1903; 210 kph



Fig. 1.4: SBB Ce 6/8 II for single-phase AC 15 kV/16²/₃ Hz; 1920; 1650 kW

In 1903, H. Behn-Eschenburg, engineer at Maschinenfabrik Oerlikon/Switzerland succeeded in applying ohmic commutation-pole shunts to the series-wound commutator motor, thus achieving compatibility with alternating current feed. In 1905, trials at Seebach-Wettingen near Zurich met with success. In 1912, the German Länderbahnen of Prussia, Hesse, Bavaria and Baden signed an "Agreement on the execution of electrical railway transport", setting standards for single-phase alternating voltage (1AC) for traction at 15 kV and 16²/₃ Hz. This low special frequency was necessary to achieve sparkless commutation of the series-wound commutator motor. Shortly afterwards, Austria, Sweden, Switzerland and Norway introduced this system as well. Fig. 1.4 depicts the famous "Krokodil" electrical locomotive of the Swiss Federal Railway (SBB) used on the Gotthard Pass route in 1920.

A railway supply network separate from the national utility grid operating at proprietary frequency, however, was a burden many railway companies were unable to shoulder. Early experiments of using the 50-Hz "national" frequency for traction did not yield satisfying results until 1936, when the German electrical industry tested various prototype locomotives at the Höllental trial line in the Black Forest, of which those with mercury-vapor rectifiers proved most successful.

After the Second World War, that region was part of the French occupation zone; French engineers got to study the new system and learned of its advantages and peculiarities, using it then for electrification of the Lorraine–Nord France coal railways (Fig. 1.5), introducing a nominal voltage of 25 kV. From thereon, the 50-Hz system was adopted all over the world, using this frequency unless the national network operated at 60 Hz.

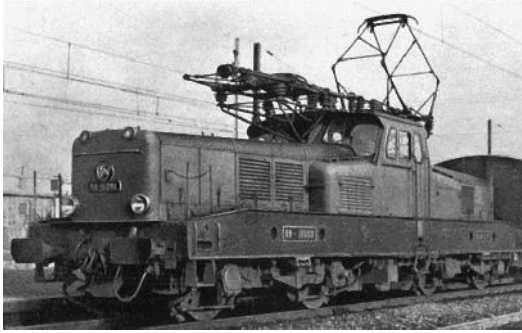


Fig. 1.5: 50-Hz goods locomotive of SNCF, Japan series 12 000, 1950, 2650 kW, 85 metric tons



Fig. 1.6: Shin-Kansen High Speed Train of national railroad, Series 0; 220 kph

Nowadays, high-speed trains like the “Shin Kansen” of Japan (Fig. 1.6) and the French “Train Grande Vitesse” (TGV) attain maximum speeds in excess of 200 mph.

1908 saw the advent of the diesel locomotive, designed by R. Diesel and the Sulzer company of Switzerland (Fig. 1.7). It yielded 1500 hp using a direct drive without gearing or clutch. Due to difficulties of starting up a heavy train using compressed air carried on board, this new technology first proved unsuccessful. Only in the 1930s, the success of Electro-Motive Division of General Motors in introducing diesel-electric drive technology in the U.S. and the introduction of the hydraulic flow converter in Germany allowed for economical use of the diesel motor in railway traction.

In 1971, the first successful diesel-electric locomotive with three-phase drive technology, produced by BBC and Henschel (Fig. 1.8) took up operations. Frequency converters now allowed (by variable frequency/variable amplitude feed) to employ the robust squirrel-cage induction motors in place of the cost- and maintenance-heavy commutator motors.

In 1979, three-phase drive technology was applied to overhead-system locomotives in the shape of the first high-performance universal locomotive, the class 120 of the DB (Deutsche Bundesbahn). Ever since 1990, this technology is general standard for high-speed trains (Fig. 1.10) and heavy and/or fast goods trains as well as most commuter service railways.

[B2], [B4], [B7], [B8], [B11], [B12]; [1]...[5].

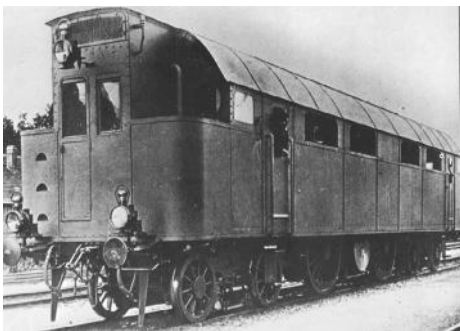


Fig. 1.7: Sulzer-Klose-Henschel diesel locomotive 1912 with direct drive; 1000 kW



Fig. 1.8: First diesel-electric locomotive with three-phase drive technology DE 2500 by BBC and Henschel 1971; 1840 kW

(Bombardier Transportation)



Fig. 1.9: Full-electric high-performance locomotive class 120 of DB; 1979, 5600 kW
(Bombardier Transportation)



Fig. 1.10: Electric High-Speed Train ICE3 class 403 of DB AG; 1999, 8000 kW, 330kph

1.3 A short overview of railway electrical supply networks

As indicated in the historical overview, the type of electrical supply network chosen – direct current, single-phase alternating current or three-phase alternating current – is of vital importance for the system “Electric Railway” and is thus inextricably linked to the evolution of traction technology. Therefore, this subchapter will provide a short overview on the various railway power systems of Europe, their development and current state. chapter 13 will focus on the various railway power systems *en détail*.

1.3.1 Direct-current railway systems

Tramways and underground railway systems run preferably on direct current (DC) voltage of 600–750 V; suburban commuter and city railways usually operate at voltages of 750–1500 V, this being due to the simple vehicle technology. 750 V is used in South-East England (Kent). In South and Southwest France as well as in the Netherlands, stemming from the suburban lines of the great capital terminal stations extended networks of 1500-V main-line systems have developed. Though their limitation of power (less than 5 MW per train) is a distinctive drawback, it is unlikely however, that they will be replaced by more efficient power supply systems. Fig. 1.11 depicts these direct current railways of $U_N = 1.5$ kV by hatching from top left to bottom right, the 750-V lines from bottom left to top right.

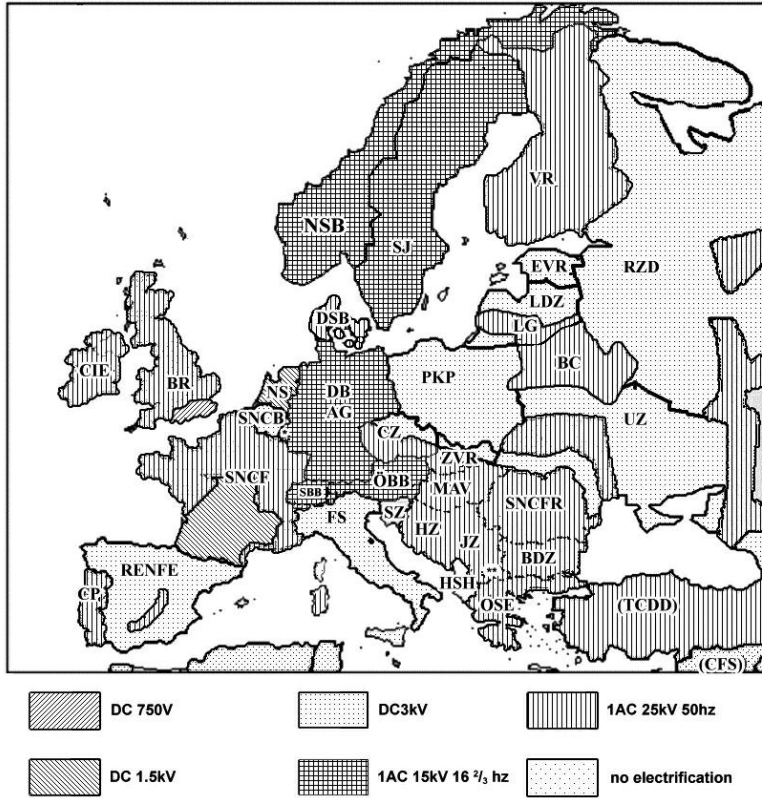


Fig. 1.11: Railway main-line power-supply systems in Europe (abbreviations of names of railway authorities cf. subchapter 15.2; *: CFL; **: MZ)

During the 1920s, Belgium, Italy, Spain and the Soviet Union, drawing on U.S. experience, established 3-kV DC long-distance networks, this system being adopted by Poland, northern Czechoslovakia, India, South Africa and Brazil after the Second World War. European areas using this system are narrowly dotted in Fig. 1.11. This system always used two drive motors in series until the three-phase drive technology superseded the commutator motor.

1.3.2 Single-phase alternating current railway systems

Fig. 1.11 shows the areas using the 1AC 15 kV/16 2/3 Hz alternating-current system for long-distance railways as chequered areas, including Sweden, Norway, Germany, Switzerland and Austria. This system has been in use since 1912.

Those regions utilizing 25-kV/50-Hz electrification are depicted using vertical hatch. Special notice should be taken of the 50/60-Hz high-speed or heavy-duty new lines in Japan, France, Spain and the Netherlands, which cut a swathe through vast areas of 1500-V DC-run railways (3 kV in Spain). A key of the abbreviations of the railway companies can be found in subchapter 15.2.

The various lengths of system network in 2003 were:

Table 1.1 Network line lengths and proportion of electrical railway systems (2003)

DC 1500 V	15,318 km / 9,497 miles	6.5 %
DC 3000 V	72,104 km / 44,704 miles	30.3 %
AC 15 kV/16 2/3 Hz	32,392 km / 20,083 miles	13.6 %
AC 25kV/50 (and 60) Hz	106,437 km / 65,991 miles	44.8 %
Others	11,349 km / 7,036 miles	4.8 %
Total	237,600 km / 147,312 miles	100.0 %

The 50-Hz system is experiencing the largest growth nowadays.

1.3.3 Three-phase three-conductor railway systems

The only three-phase public railway systems still in existence in Europe today are the Jungfrau-bahn and the Gornergrat-Bergbahn in central Switzerland. Apart from that, various “people mover” airport railways are operated as low-voltage three-phase three-conductor systems.

1.3.4 Standardized voltages of the train line

As electrification grew apace, the former vapour heating of passenger trains was replaced by electrical systems. Due to security reasons, it is obviously rather inappropriate to use the 15/25 kV supply voltage directly; thus, the main transformer branches off a lower voltage for the train line. The standardized overhead-line voltages have been allotted specified voltages for the train line according to UIC 550 (cf. Table. 1.2).

High-speed trains like the ICE use proprietary train lines of DC 500...700 V; this is favourable when considering inverter-fed compressor motors for air-conditioning equipment. If fed from a diesel-engine generator, trapezoid voltages AC may occur (cf. subchapter 9.1). In the U.S., three-wire systems using 3AC 480 V/60 Hz are common; those were introduced early on with regards to the power demand of train air conditioning, so-called Head-End Power systems.

Table 1.2 Train line voltages

Railway electrical system	Nominal voltage
AC 15 kV/16 ² / ₃ Hz	1AC 1000 V
AC 25kV/50 (and 60) Hz	1AC 1500 V, 3000V* in Eastern Europe
DC 1500 V	DC 1500V
DC 3000 V	DC 3000 V

*Due to ease of transition to the DC 3-kV used in Eastern Europe and the CIS, cf. Fig. 1.11!

1.3.5 State of electrification in selected countries

The state of electrification regards only the quota of electrified network length to total network length, NOT the quota of transport capacity.

Table 1.3 State of electrification in 1990

Country	State of electrification
Denmark	7 %
Germany	42 %
Switzerland	99 %
Europe (on average)	37 %
USA	1 %
Soviet Union	36 %
South Africa	36%

1.4 Comparison of traction systems

The following table 1.4 lists a number of advantages and disadvantages of electric traction when compared to diesel traction, for main-line traffic.

Table 1.4 A comparison of electrical and diesel-electrical traction

<p>Advantages of electric traction, compared to diesel traction</p> <ul style="list-style-type: none"> • In general, lower energy cost • Preservation of limited oil reserves • Usability of hydroelectric power and low-yield coal • Environment-friendly operation, lower noise • Possibility of energy recovery when braking, less wear of brake shoes (especially for three-phase drives!) • Higher partial efficiency (nominal efficiency off primary energy source is comparable!) • No need for carrying the power generator on the vehicle unit, thus more than double power at same weight (ca. 7 MW at wheel-rim with a four-axle locomotive of G = 85 t, compared to 3.5 MW at wheel-rim for a diesel-electrical locomotive of G = 130 t!) • Service speed over 200 kph and heavy mass transit only viable with electric traction • Possible overload of electrical machinery can be utilized • Lower maintenance cost • Higher number of operational hours due to easier maintenance and no need for pre- heating the engine • In total, cheaper traction units <p>Disadvantages</p> <ul style="list-style-type: none"> • High initial cost for catenaries and power-supply network <p>Rough guideline values for economic limits of track electrification</p> <ul style="list-style-type: none"> • Traffic work is $12 \cdot 10^6$ t/a, for a train of 1350 metric tons, per hour, on level routes; less in mountainous areas! • Energy consumption of about 300...400 MWh/(a·km), depending on price of diesel fuel
--

Figs. 1.12 and 1.13 show typical efficiencies of an electric line-fed locomotive and a diesel-electric locomotive, with the respective amounts of loss resp. partial efficiencies. It becomes obvious that electric traction does NOT offer a higher coefficient in itself, if the whole chain starting with the initial thermal energy of the primary fuel is considered. Recuperation is not taken into account, as it is extremely difficult to figure, being too dependent on too many different parameters.

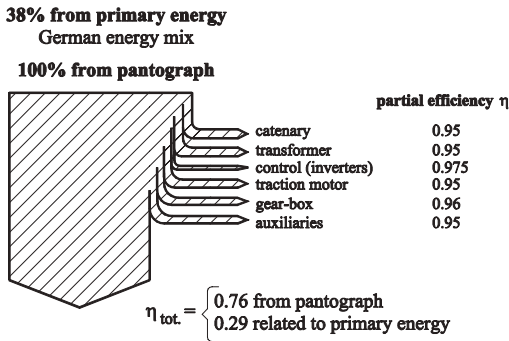


Fig. 1.12: Energy usage of a line-fed electric locomotive

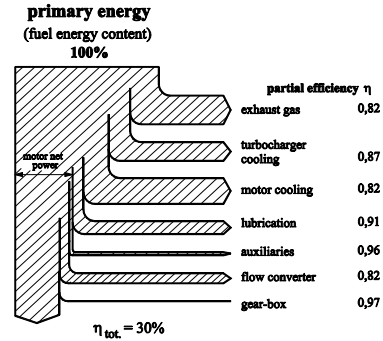


Fig. 1.13: Energy usage of a diesel-hydraulic locomotive [B18]

1.5 The European railway industry

Ever since the beginning of the 1990s, the European railway industry had to face constant change; the restructuring of the railway organisations (deregulation, privatization) led first to a decline in orders and in consequence to collapses and amalgamation; partially the production was transferred to low-wage countries, mainly East Europe.

Engineering industry divisions formerly responsible for the supply of the mechanical components of traction units (incl. Henschel, Krauss-Maffei, Krupp, and SACM) were integrated into the transportation divisions of the electrical large-scale industrial companies (like ABB, AEG, ALSTOM and Siemens), the latter now acting as leaders of system technology. In 2001, Bombardier, until then having their focus on coaches and aircraft engineering, acquired ADtranz from the Daimler-Chrysler Group.

In the big groups, factories concentrated their production portfolio on their “core competences”; so the bogie production of Bombardier Transportation was combined in Siegen (D), that of Siemens Transportation Systems in Graz (A), at the place of the former SGP.

As the railways gave away much of their former own technological competence, the way was now free for standard products, following “platform” strategies as known from automobile industrie. Much bigger lots could be produced then known from the seventies and eighties of the twentieth century. Corporate enterprises such as Mitsui Rail Capital Europe and Angel Trains entered the new business of leasing of rolling stock, eventually taking over e.g. the Siemens division “Dispolok” built up for that purpose in the late nineties. Table 1.5 provides a “snapshot” of the railway industry in 2006 (including some corporate history).

Table 1.5 European Traction Unit Manufacturers (2005/06)

	ALSTOM Transp. (FRANCE)	BOMBARDIER TRANSPORT.		SIEMENS TS (GERMANY)
		ADTRANZ (SWITZERLAND, GERMANY, SWEDEN)	BOMBARDIER (CANADA)	
Business volume (in billions of €) *)	5.1	5.0		4.5
Employees *)	26,000	28,600		18,865
Origins (selected!)	ALSTOM = Thomson-Houston + SACM Belfort; MTE Schneider, DeDietrich (F) FIAT Ferrov. (I) Linke-Hofmann-Busch (D) GEC Traction (UK) Until 1998: GEC-Alsthom	ABB-Henschel = ASEA (S) + BBC (CH, D, I) includ. Oerlikon, Sècheron (CH), TIBB (I) NEBB (N) + Henschel (GER) + BREL (UK) + AWTS (AEG incl. LEW Henningsdorf, MAN, MBB, Waggon-Union (D); Pafawag (PL); Westinghouse TS (USA) Matranovak (HU)	B. Mass Transit (CAN) B. Transit USA Talbot (D) DWA (D): Ammendorf Bautzen, Görlitz, Niesky (Management-Buy out in 2005) Division BN (B) ANF-Industrie (F) Bomb.-Wien (A) Prorail Ltd. (UK)	Siemens VT (TS) Krauss-Maffei Krupp VT DÜWAG Uerdingen (D) SGP (A) MATRA S.A. (F) VATech ELIN, (A)

*) World-wide)

Figs. 1.14 and 1.15 give an overview about the market situation; the whole railway product market is about 72 bn. €, that for rolling stock about 25 bn. €, and splits according to the diagrams into the following segments.

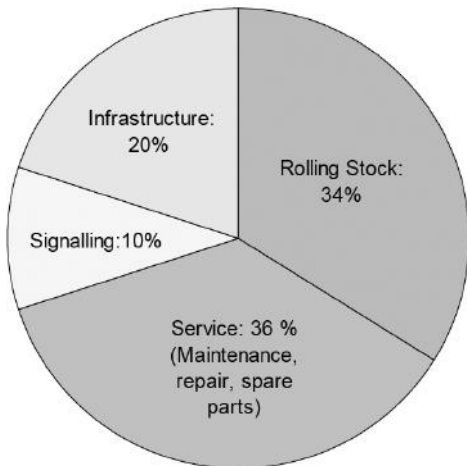


Fig. 1.14: Overall market volume of railway material, as of 2003-2005
(UNIFE-Study 2015)

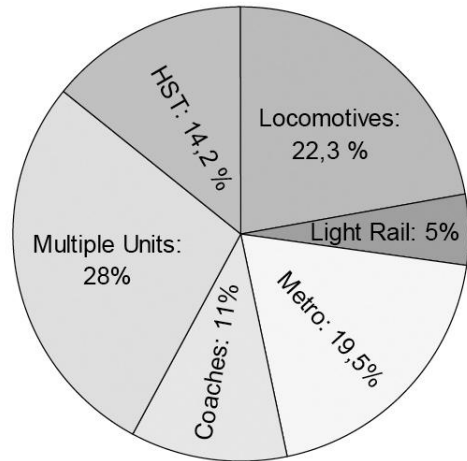


Fig. 1.15: Breakdown of rolling stock (2006-2015)
(UNIFE-Study 2015)

Table 1.7 Further manufacturers of traction units (in excerpt)

<p>Europe: AnsaldoBreda, Naples, Italy Balfour Beatty Rail GmbH – Power Systems, Frankfurt and Munich, Germany Brush Traction Ltd., Loughborough, UK Cegielski, Poznan, Poland Construcciones y Auxiliare de Ferrocarriles S.A (CAF), Beasain and Zaragoza, Spain ELIN EBG Traction, Vienna, Austria (Siemens) Ganz Tranelectro Traction (formerly Ganz-MAVAG), Budapest, Hungaria Riga Carriage Building Works, Latvia Skoda, Prague, with CKD Vagonka, Ostrava, Czech Republic Stadler Rail Group, Bussnang and Altenrhein/Switzerland; Pankow, Germany TALGO S.A., Spain Voith Turbo Lokomotivtechnik GmbH, Kiel Vossloh SFT (incl. MaK and Kiepe Elektrik, Düsseldorf; acquired the Valencia works for diesel-electric locomotives from ALSTOM in 2004), Germany Windhoff, Rheine; Schöma, Diepholz, Germany (small locomotives, special vehicles)</p> <p>Worldwide: General Electric (GE) Transportation Systems, Erie, Pa., U.S. General Motors, Electro-Motive Division (EMD), London/Ont., Canada; formerly also Lagrange, Ill., U.S.A. Hitachi, Kawasaki, Mitsubishi, Toshiba, Tokyo Denki, Japan Union Carriage & Waggon Co. (UCW), South Africa Daewoo, Hyundai, South Korea Chittaranjan, BHEL, IndiaZhuzhou, PRC</p>
--

Table 1.8 Leading associations/accords/authorities

UIC/IEV	Union Internationale des Chemins de Fer, Paris (International Railway Association)
ERRI OSShD	European Railway Research Institute (fm. ORE) Organisazija sotrudnitschestwa shelesnych dorog (Organisation for Cooperation of Railways (East European states, CIS and Iran)
RIC	Regolamento Internazionale delle Carrozze (Accord on the mutual use of passenger and luggage cars in international transport), January 1 st , 1950
RIV	Regolamento Internazionale delle Veicoli (Accord on the mutual use of cargo cars in international transport), January 1 st , 1958
TSI	Technical Specification on Interoperability. Guideline 96/48/EC of the European Council on Interoperability of the trans-European high-speed railway system. Official Journal of the E.C. No. L 235, September 17 th , 1996, p. 6 ff.
UNIFE VDV VDB	Union of European Railway Industries Association of German Transport Undertakings, Cologne Association of the German Rail Industry, Frankfurt/Main
EBA	Eisenbahn-Bundesamt, Berlin (technical supervision authority)

2 The mechanics of railway transportation

2.1 Principles of rail-guidance

2.1.1 Gauges

As mentioned in the historical overview, subchapter 1.2, the later European Standard Gauge of 1435 mm (distance between inner edges of rail tops) had been introduced by the railway pioneer George Stephenson. As early as the middle of the 19th century, it was adopted as the standard gauge for European railways. It is also found in the US and the PRC, Korea and Australia as well as on the new Japanese and Spanish high-speed mainlines.

“Standard gauge” (in the wider sense as compared to “narrow gauge”, discussed below) also includes the gauge range from 1524 mm to 1676 mm (5 ft and 5 ft 6 in, respectively), which were chosen as standard gauge in various countries. The 1524-mm gauge, widely called “Russian Gauge”, had been introduced in Czarist Russia due to strategical concerns. In Ireland, 1600-mm gauge was designated standard in the middle of the 19th century; from there, it proliferated to various Australian federal states and Brazil. 1665-mm gauge is mainly found on the Iberian peninsula, with the only fractionally larger gauge of 1676 mm being used in South America and the Indian subcontinent. Even larger gauges have been used on the North American Erie Railroad (New York-Great Lakes) and the Great Western Railway from London to Devon and Cornwall in the United Kingdom, those using 1800-mm and 2134-mm gauge, respectively. Both railways, however, had been converted to European standard gauge by the end of the 19th century to eliminate the drawbacks associated with using deviating gauges, most notably the impossibility of transfer for cars, thus requiring costly transshipping.

Besides the standard gauge railways, which have been most successful and numerous in the industrialized countries, various smaller gauges have seen use in various Third World countries and minor railways, the so called “narrow gauge”. “Metre Gauge” (of 1000 mm, or 3 ft 3 in) has been widely used in Europe for minor (secondary) railways and suburban lines, as well as in a number of former European colonies. 1067-mm gauge (3 ft 6 in) is common in various former British colonies in central and southern Africa, as well as in India, Indonesia, Japan and South America. The great success this gauge enjoyed in South Africa has given it the moniker of “Cape Gauge”. In contrast, the 1100-mm gauge of the Brunswick tramway must be regarded as exceptional.

Smaller gauges are commonly used on railways of minor importance, for example 600 mm (2 ft) with field and military railways, 750 mm and 760 mm with German or Austrian and former Yugoslav minor railways, respectively. 900 mm (2 ft 11 in) is a typical mine railway gauge, whereas 914 mm (3 ft) is common in Central and South America.

Narrow gauge railways have several advantages: Apart from considerably lower initial investment cost, they prove far easier to construct in difficult, rough and mountainous terrain. The

major drawbacks, however, are noticeably lower service capability and the easily underestimated cost of transshipping when using narrow gauge in conjunction with standard-gauge railways. As traffic volume increased, these transshipping costs regularly and quickly outweighed the low initial and maintenance cost that made narrow gauge so attractive.

A typical example is the re-gauging of the 760 mm Bosnia-Herzegovinian railway line from Sarajevo to Ploce on the Mediterranean, which was concluded in the 1960s.

As well as the various service capabilities inherent in the various gauges, various typical wheelset loads have been associated to these gauges. Whereas modern standard gauges (1435...1676 mm) can easily manage axle loads from 21 metric tons (Europe) to 35 metric tons (U.S.), for economic reasons, narrow gauges can only shoulder wheelset loads of 16 metric tons for meter gauge, dropping to some 9 metric tons for gauges of about 750 mm. Smaller field railways only served axle loads of only a couple (3.5 usually) metric tons.

Table 2.1 A selection of gauges

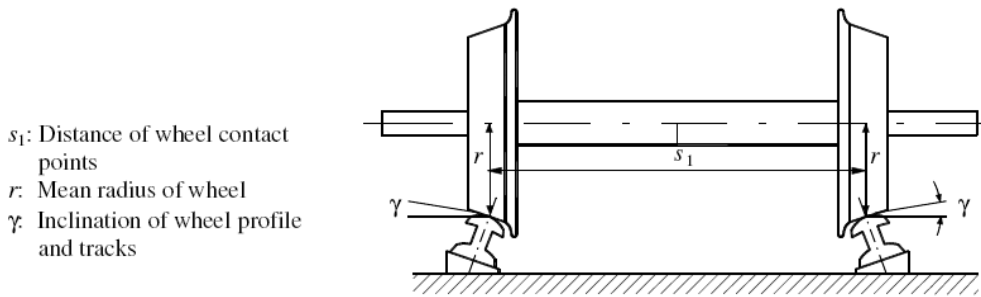
381 mm	Exhibition railways, some public railways in the UK
600 mm	Minor, field and military railways
750 mm	Minor railways
760 mm	Minor railways in Austria and former Yugoslavia (“Bosna Gauge”)
900 mm	Mining railways, for example in lignite strip mining
914 mm	Minor railways in Central and South America
1000 mm	Minor and colonial railways, “meter gauge”
1067 mm	Many railways in Central and Southern Africa, India, Indonesia, Japan; called “Cape Gauge” in South Africa
1100 mm	Brunswick tramway
1435 mm	“European standard gauge”, U.S., Northern Africa, Australia, China, Japanese and Spanish newly-constructed high-speed lines
1524 mm	CIS, Finland, Iran, Panama
1600 mm	Australia, Brazil, Ireland
1665 mm	Spain, Portugal
1676 mm	Argentina, India, Pakistan, Bangladesh, Sri Lanka, Chile

2.1.2 Guidance of wheelset in track

The system “wheel-track” that is key to railway technology has to meet three requirements:

- transmission of the vehicles’ weight to the rail
- transmission of traction power from the traction unit to the rail
- guidance of the vehicle in lateral direction both on straight and curved tracks

Wheelset loads were already mentioned in the previous section; subchapter 2.2 will discuss the transmission of traction power. This section shall discuss vehicular guidance (formerly, the term “axle” was common for “wheelset”, with some technical terms being derived from that).



s_1 : Distance of wheel contact points
 r : Mean radius of wheel
 γ : Inclination of wheel profile and tracks

Fig 2.1: Geometrical designations of the wheel set on track

As can be derived from Fig. 2.1, the wheels sport a conical running profile, which concurs to the horizontal at an angle of γ . Accordingly, the tracks are mounted at an angle of γ ($\tan \gamma = 0.025 \dots 0.04$).

When running through a curve, the wheelset, moved by centrifugal force, shifts outwards until the way covered on the larger reference circle diameter is equal to the longer way covered on the outer track, avoiding slip and thus wear of the wheel profile, at least in wide curve radii. Thus, railway vehicles can eschew the use of a differential gear which is indispensable for road vehicles.

If on a straight track the wheelset is shifted to the right, the right wheel moves upwards and runs on a larger reference circle diameter than the left, which in turn moves down, running on a smaller reference circle diameter, and vice versa. By revolving on the larger reference circle diameter, the right wheel experiences higher peripheral speed, resulting in a movement of the wheelset towards the centre of the track. This so called “sinusoidal running” was described in 1880 by Klingel [7], [8]; it has a typical wavelength, which results from the distance of the wheel contact points s_1 , the radius of the wheel r and the inclination of the wheel profile of $\tan \gamma$ at

$$\lambda = 2\pi \cdot \sqrt{\frac{s_1 \cdot r}{2 \cdot \tan \gamma}}, \tan \gamma = 0.025 \dots 0.04 \quad (2.1)$$

The conicity of the wheel thus results in automatic centering of the wheelset on the track.

On the other hand, this desirable reset causes oscillation of the wheelset, the strength of which is dependent on the speed of the vehicle. The frequency of the oscillation is at $f = v/\lambda$, v being the translatory speed of the wheelset. Thus it is imperative under all circumstances that this frequency does not incite the intrinsic oscillation of the wheelset. As is generally known, the resonance frequency of the mechanical pendulum is proportional to the root of the quotient of rigidity and mass. Heavy wheelsets further burdened by electrical motors result in lower frequency limits or higher spring rigidity, this in turn causing high recoil strength and high stress applied to the wheelset–track system; wear becomes inevitable. Thus, in order to reach high speeds, it is absolutely necessary to reduce the mass of the wheelset (e.g. by light construction and hollow axles) as well as using fully de-coupled drives (see subchapter 3.2), if one wishes to operate at low recoil strengths.

Greater wavelengths, and thus higher velocity limits, can practically not be achieved by using flatter wheel cones, since tire wear will quickly result in a S-shaped profile that has sequentially much higher conicity; this in turn results in a non-linear oscillation with, again, shorter dominant wavelength. To counter this effect, the Deutsche Bahn fits all vehicles with the so-called DB II-Wear Profile as standard. This system, derived from Prof. H. Neumann’s work [9] provides for a constant stable behaviour over the running time of the wheelset.

However, a traction unit uses more than one wheelset, which are mounted in a frame, bogies nowadays [B33]. Thus, coupled oscillations both of the wheelset and the bogie frame occur. To control these oscillations more easily, it has proven advantageous to de-couple them from one another. For this reason, a laterally-elastic spring suspension mates the wheelset to the bogie frame. Still, the sinusoidal oscillation and disturbances of the track alignment cause oscillations of the wheelset, and in turn, of the bogie – the latter being mainly rotary. In order to achieve higher speeds safely, a low moment of inertia is required.

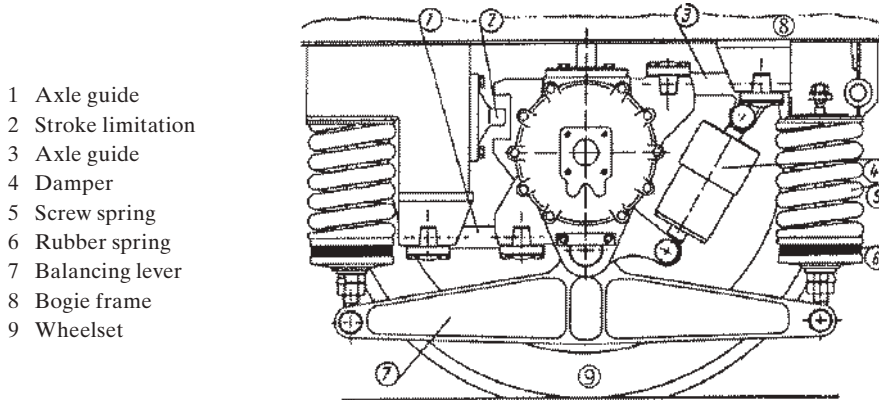


Fig. 2.2: Wheelset guidance including axle-guides and dampers (lemniscatic guidance)

Fig. 2.2 depicts a modern system of wheelset guidance, including axle-guides and dampers. The bogie frame (8) is mounted to the axle-bow cage via two Flexicoil screw springs (5) and a balancing lever (7), the springs forming the “primary suspension”. The stress of tractive and braking effort is transmitted via two axle guides (1 and 3) from the bogie to the axle-bow cage. This type of axle guidance is called “lemniscatic guidance”. The axle guides allow for a certain amount of lateral shift of the wheelset; the recoil strength for the lateral suspension is supplied by the screw springs, which are mounted fast to the bogie frame. For dampening of the vertical oscillations, a damper (4) and a rubber spring (6) are used; excessive movement is prohibited by the stroke limiter (2).

2.1.3 Frame and bogie

Fig. 2.3 shows the three translatory and the three rotary degrees of liberty that apply to a vehicle. Similar degrees of liberty apply to the wheelset and the bogie.

Up to the 1920s, electric locomotives of higher power output were constructed along the same principles as steam locomotives: A centrally placed high-power motor drove the wheelsets via parallel-crank drives and coupling rods (cf. subchapter 3.2).

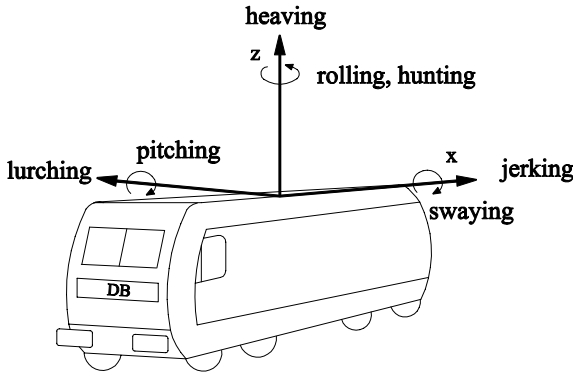


Fig. 2.3: Translatory and rotary degrees of liberty of vehicular movement and their denomination

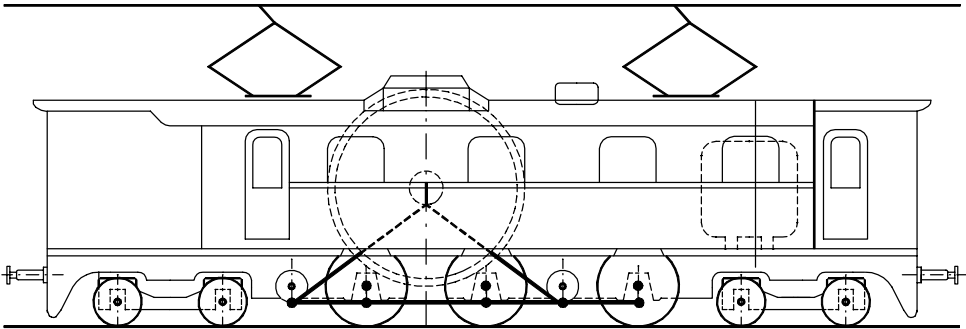


Fig. 2.4: Rigid-frame express locomotive Class E 06 of the DRG (1922)

See Fig. 2.4: To support the then considerable total weight of the electric equipment and to improve the running behavior at high speeds, idler wheelsets or bogies were used. Later on, the single-axle drive with high-speed motors and gears replaced the direct rod coupling.

The idler-free bogie system which is almost exclusively used today (Fig. 2.5) was first employed on tramways operating at low speeds. In the 1930s, this system was introduced with main-line locomotives of some 2 MW and speeds of 80 kph (50 mph). In the 1940s, the first high-speed high-performance locomotive was constructed in Switzerland; it reached a maximum speed of 120 kph (75 mph) and a nominal power of 3 MW (cf. subchapter 7.2). This engine must be considered the ancestor of all modern locomotives, which are able to attain speeds of up to 357 kph (220 mph).

A bogie combines two (seldom three today) wheelsets of the traction unit, the respective drive motors and the power transmissions (cf. subchapter 3.2). It revolves around a circular pivot mounted in the vehicle frame, allowing for rotation around the z and y axes and translating the resulting forces in the directions of x and y.

The weight force (z-axis) is transmitted via springs, the “secondary suspension”. Today, the voluminous pivot is often not physically existent, its tasks being fulfilled by coupling rods and the screw or spiral suspension springs (“Flexicoil”), which are mounted fixedly in the girder under-frame and the bogie frame, taking up the bogie rotation by torsion.

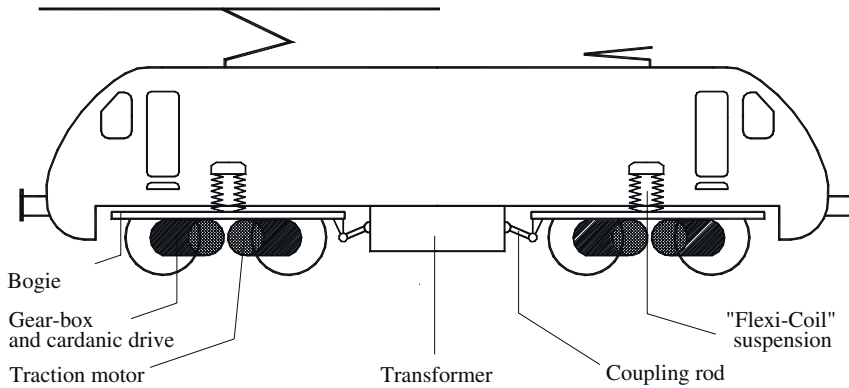


Fig. 2.5: Schematic illustration of a bogie locomotive with "Flexicoil" suspension

As has been proven with passenger carriages, bogies greatly improve running quality, since they halve the effects of track-induced thrusts in y- and z-direction on the vehicle and reduce the running resistance (cf. subchapter 2.2) in curves. Vehicles of short wheelbase (lengthwise distance of axles) have lower striking angles of the wheelset (i.e. wheelset group) and thus experience lower drag in curves; additionally, since the bogies align themselves radially towards the centre of the curve, the striking angle is further reduced.

The thrusts, however, do regularly cause inherent oscillation by the z- and y-axes, which proved the key problem hindering widespread introduction of the bogie for high-speed traction units; a striking example is the drive bogie of the express locomotive BR 103 of the DB (Fig. 2.6). At the time of construction (1965), to achieve the demanded power of 7 MW required the use of 6 motors of 1180 kW each, these being rigged as triple assemblies in two bogies. A single bogie weighed in at 31 metric tons, the wheelbase measuring 4500 mm. This resulted in a high axial moment of inertia, which led to low-frequency oscillations; due to the given wheelbase kinematics, these already occurred at speeds of just above 200 kph (125 mph) and could only be controlled by equipment of extra dampers.

The problem was effectively alleviated only by the introduction of the three-phase drive technology: due to higher number of revolutions, the power of the motor (while keeping the weight) was raised so rapidly, that outputs of 6–7 MW can be achieved by four drive motors, allowing for the use of twin-wheelset bogies. Fig. 2.7 shows the BR 120's bogie assembly: the weight is down to a mere 16.1 metric tons at a continuous output of 2 x 1400 kW.

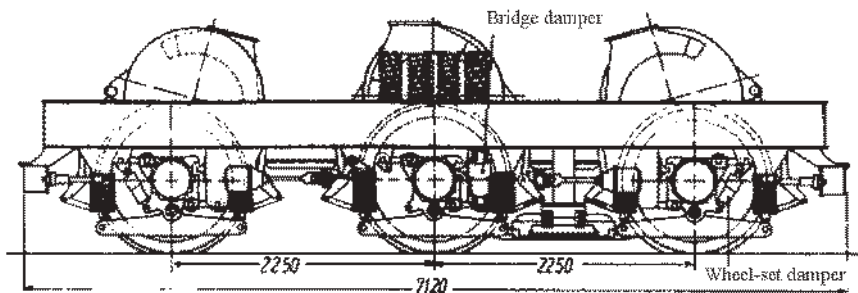


Fig. 2.6: Drive bogie of with three wheelsets (Class 103 DB), without central pivot

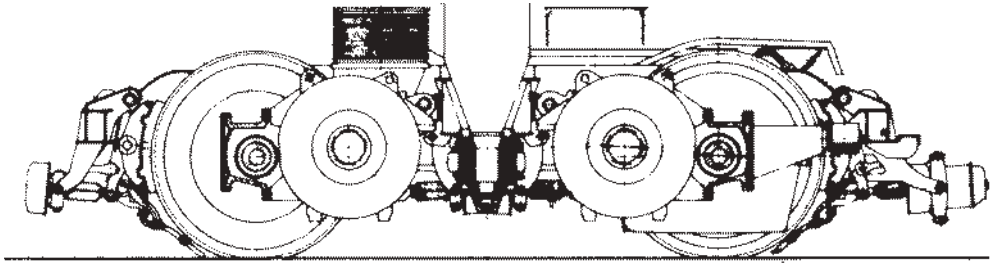


Fig. 2.7: Modern drive bogie with two wheelsets and a central pivot (Class 120 DB)

The relatively small traction motors can be mounted close to the pivot, the wheelbase is reduced to just 2.8 m (9 ft 1/5 in), thus greatly reducing inertia. Similar locomotives achieved speeds of 357 kph (225 mph, “Taurus” Class 1216 of ÖBB).

Even more advanced is the bogie model used on the French high-speed train TGV (Fig. 2.8). The drive motors have been removed totally from the bogie and are mounted laterally in the bridge girder, driving the wheelsets via cardan shafts. The weight of the bogie, while yielding 2 x 1100 kW, sank to 11 tons. On trials, such trains achieved speeds of 575 kph (360 mph). The German ICE HSTs use a similar drive concept, but with a concentric cardanic hollow shaft (subchapter 3.2).

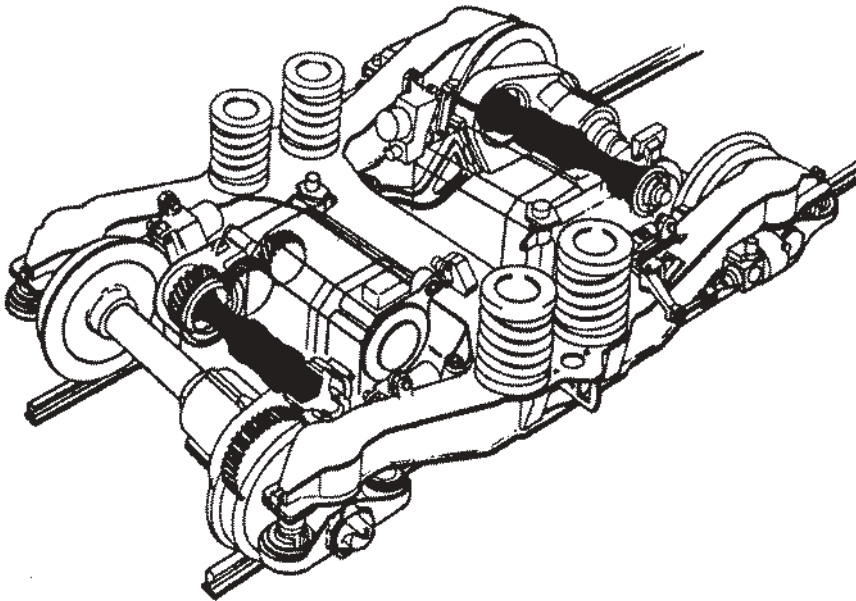


Fig. 2.8: Drive bogie of the TGV with traction motors mounted in the bridge girder

The “Integrated Complete Drive” is a compromise; it is discussed in detail in subchapter 3.2.

2.1.4 Bogies with self-steering wheelsets

On railways sporting a high number of small curve radii (e.g. in the Swiss Alps), high-speed locomotives increasingly use bogies with radially self-steering wheelsets. Fig. 2.9 (a) depicts a bogie with a rigid wheelbase. On the leading wheelset, a relatively big striking angle α leads to raised lateral friction of the wheels on the rail (and thus higher rolling resistance and wear). If using “soft wheelset guidance” (b), the striking angle causes the leading outer-curve conical wheel to run on a larger reference circle diameter and thus run faster; a force develops, forcing the wheelset radially towards the curve centre point (ditto on the rear inner-curve wheel).

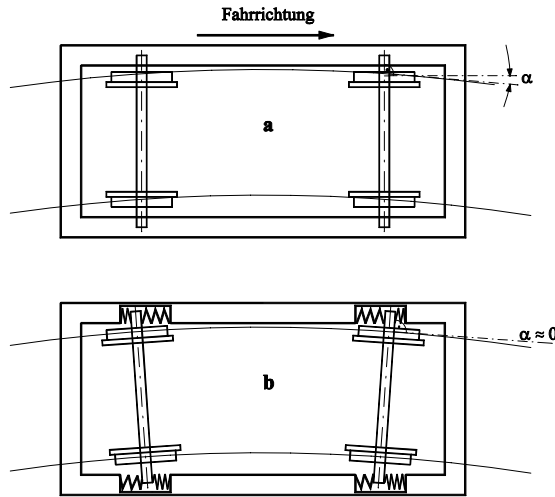


Fig. 2.9: Rigid bogie (a) and bogie using radially self-steering wheelsets (b) (EEW-TUD)

Fig. 2.10 shows the opposed-forced guidance of wheelsets in the bogie frame of the Swiss high-power locomotive Class 460 [113], which also transfers the lengthward (traction/braking) forces from the wheelsets to the bogie frame. The self-steering system reduces the screaming noise caused by the striking of the wheels and is therefore widely used in commuter traffic (subchapter 10.2).

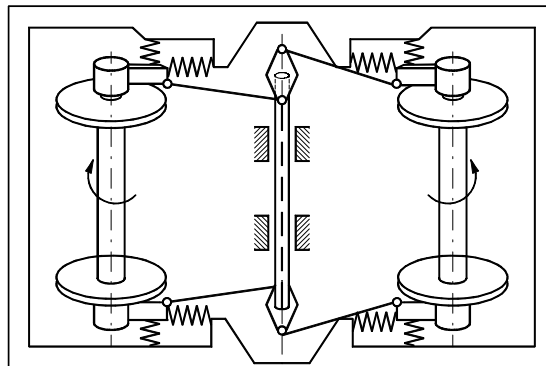


Fig. 2.10: Bogie using self-steering wheelsets of Class 460 SBB (EEW-TUD)

2.1.5 Curvature-dependant body-tilting equipment

A speed-enhancing system which is independent of track guidance is the curvature-dependant body-tilting equipment, also known as “Pendolino” system (after the first successful such vehicle in Italy [10]).

The maximum travel speed in curves is on one hand limited by the forces between wheel and track (causing wear), on the other hand, and more importantly, by the effect on the passengers’ comfort. The centrifugal acceleration, proportional to the square of the traveling speed,

$$a_y = \omega^2 \cdot R = v^2 / R \tag{2.2}$$

(v : traveling speed, R : radius of the curve)

proves to be a disturbance, especially to passengers moving inside the vehicle. To counter this, the outer rail is usually super-elevated, but due to safety requirements, this must be limited to a maximum value of \ddot{u} of 150 mm (ca. 6 inches).

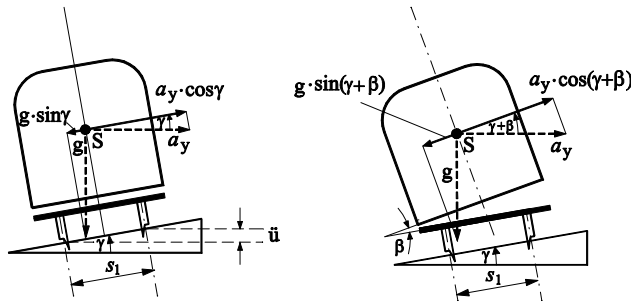


Fig. 2.11: Forces at the car body running through a curve

Due to these aspects of comfort, only a remaining centrifugal acceleration which is equal to a fictitious elevation of the outer rail of a further $\ddot{u}_f = 130$ mm (ca. 5.2 inches), the so-called “cant deficiency”, is allowed. Equating the component of the centrifugal acceleration parallel to rail level to the component of earth acceleration with opposite direction (cf. Fig. 2.11, left; g : earth acceleration = 9.81 m/s²; S : centre of gravity):

$$g \cdot \sin \gamma = \frac{v^2}{R} \cdot \cos \gamma \tag{2.3}$$

yields with

$$\tan \gamma = \frac{\ddot{u} + \ddot{u}_f}{s_1} \tag{2.4}$$

the admissible speed

$$v = 0,7s^{-1} \cdot \sqrt{R \cdot (\ddot{u} + \ddot{u}_f)} \tag{2.5}$$

or as a „tailored“ equation of quantities

$$\frac{v}{\text{kph}} = \sqrt{\frac{R / \text{m}}{11,8 \text{ mm}} \cdot \ddot{u} \cdot \ddot{u}_f} = 4.87 \sqrt{\frac{R}{\text{m}}} \tag{2.6}$$

This means that the maximum speed for a curve radius of 500 m may not exceed 110 kph (68 mph).

If the carbody is rotated by the the curvature-dependant body-tilting equipment by an additional angle $\beta = \arctan\{\delta\ddot{u}/s_1\}$ against rail level towards the centre of the curve, the admissible speed will – at same degree of comfort – be raised to

$$\frac{v_{\text{tilt}}}{\text{kph}} = \sqrt{\frac{R/\text{m}}{11.8} \cdot \left(\frac{\ddot{u} + \ddot{u}_f + \delta\ddot{u}}{\text{mm}} \right)} \quad (2.7)$$

e.g. with a maximal value of $\beta = 8^\circ$ corresponding to a fictitious track super-elevation of 210 mm to

$$\frac{v_{\text{tilt}}}{\text{kph}} = 6.45\sqrt{R/\text{m}} \quad (2.8)$$

The same curve of 500 m radius may now be travelled at $v_{\text{tilt}} = 145$ kph (90 mph), which is an increase of some 30%.

Tilting technology is divided into passive tilting technology, as used on the Spanish “Talgo” trains, which uses a rotating pole above the centre of gravity, which, however requires a space-consuming portal construction; and active tilting technology, which is e.g. used on the Italian “Pendolino”, the German diesel rail cars VT 611/612 or the 411/415 high-speed trains (cf. section 7.4.2), which use various means like hydraulic actuators or electric servo motors to rotate the carriage superstructure around a rotating pole beneath the centre of gravity [11]. The pendula may, as shown in Fig. 2.12, be mounted beneath the superstructure’s floor inside the bogies. Control of the servo system is derived from pendula and gyroscopes. Pantographs, however, must be reverted to true by using lateral pendula in order to achieve optimal contact with the catenary.

In addition, the tracks’ free-space area and maybe signal equipment must be modified for clearance, and one must remember that the forces at work between wheel and track increase by the square of the speed!

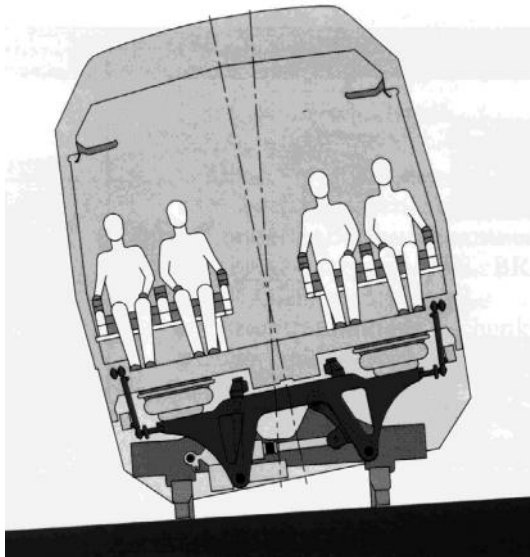


Fig. 2.12: Tilting equipment of diesel railcar VT 611/612 of DB AG (“Neicontrol-E“ with electric servo motor)

2.2 Train resistance

The train resistance W is the sum of all forces opposed to the driving movement, and can be separated into the following components [B3], [B5], and [B10]:

- Rolling resistance W_r
 - Curve resistance W_c
 - Gradient resistance W_g
 - Acceleration resistance W_{ac}
- $$W = W_r + W_c + W_g + W_{ac} \tag{2.9}$$

Usually it will be normalized to the weight force G_T of the train as $w = W/G_T$ and given in N/kN (or ‰).

2.2.1 Train rolling resistance

- DB, for passenger coaches (according to *Sauthoff*)

$$w_r = 1.0 + 0.0025 \cdot v + 4.8 \cdot \frac{n + 2.7}{G_T / \text{kN}} \cdot 0.0145 \cdot (v + 15)^2 \tag{2.10}$$

- DB, for express goods trains (acc. to *Strahl*): Roller bearings, homogenous pattern

$$w_c = 1.0 + 0.0002 \cdot v^2 \tag{2.11}$$

- DB, for mixed goods trains, with sliding bearings and inhomogeneous pattern

$$w_r = 2.5 + 0.0005 \cdot v^2 \tag{2.12}$$



Fig. 2.13: Train rolling resistance according to formulas used at DB (IC: 16 coaches)

2.2.2 Train resistance due to curves

Aligning the wheelsets in the curved track by the striking angle (cf. section 2.1.4) is connected with transversal slipping under friction; this will be taken into account by an additional train resistance component:

- At DB it is calculated according to Röckl (with curve radius R)

$$w_c = \begin{cases} \frac{650}{R/m-3} & \text{for } R \geq 300\text{m} \\ \frac{500}{R/m-55} & \text{for } R < 300\text{m} \end{cases} \quad (2.13)$$

- At SNCF:

$$w_c = \frac{800}{R/m} \quad (2.14)$$

2.2.3 Train gradient resistance

The specific gradient resistance w_g (in N/kN) equals the gradient s (in per mille):

$$w_g = s = \tan \alpha \cdot 1000 \quad (2.15)$$

Table 2.2 Gradients of various track types

Type of track	Gradient
Main lines in low mountain ranges	10...15 ‰
Main lines in the Alps (Gotthard, Brenner, v_{\max} 80 kph (50 mph)!	25...30 ‰
High-speed lines Paris-Sud-est and Cologne-Frankfurt/Main (multiple units only, no locomotive operation!)	35...40 ‰
Minor lines (drawn load max. 70% of adhesive load)	70 ‰
Most precipitous line (single car, Linz-Pöstlingsberg, brake cleaves!)	105 ‰
Mountain rack railway with vertical cog grip	250 ‰
Pilatus mountain railway with horizontal cog grip (to avoid climbing)	480 ‰

In the 19th century – due to the limited output of the locomotives of less than 2 kW per metric ton of train weight – it was customary to lengthen the tracks in hilly and mountainous regions intentionally by “excursions” into side valleys to reduce the gradients. This led to tight curvatures, which now oppose the increase of speed. Modern high-speed lines which are only used by high-speed multiple units of ca. 20 kW/metric ton and maximum speed in excess of 300 kph (200 mph) are usually built with maximum gradients of 35–40‰, but ample curve radii in excess of 3350 meters. At these gradients, maximum speed decreases to a “mere” 220–260 kph (135–160 mph).

2.2.4 Train acceleration resistance

Added to the train resistances at constant speed treated up to now an acceleration resistance will occur at changing speed. The accelerated train mass will be increased by the rotary moments of inertia, transformed by gear ratio and wheel diameter, which can be taken into account by the allowance for rotating masses ξ :

$$w_a = \frac{a}{g} \cdot \xi / 1000 (\text{N/kN}) \quad (2.16)$$

with: a : Train acceleration (in m/s^2)
 g : Constant of gravity (9.81 m/s^2)
 ξ : Specific allowance for rotating masses.

Typical values are given in Table 2.3.

Table 2.3 Allowance for rotating masses

Vehicle type	ξ
Coaches and goods carriages	1.03...1.04
Electric coaches	1.08...1.12
Electric locomotives	1.15...1.30
Mean value for locomotive-hauled trains	1.06...1.10
Electric rack railway cars (CH)	1.30...2.50

Typical acceleration values in service are:

Table 2.4 Typical acceleration values of trains

Train type	Acceleration a
Heavy goods trains	0.02...0.1 m/s^2
Normal goods trains	0.1...0.2 m/s^2
Passenger trains	0.3...0.4 m/s^2
Express long-distance trains	0.4...0.7 m/s^2
Suburban trains	0.8...1.2 m/s^2
Metro and Light Rail trains	1.0...3.0 m/s^2

2.2.5 Permanent and starting tractive efforts (F - v diagram)

To overcome the train resistance forces calculated in the previous subchapter the traction vehicle must deliver equivalent tractive efforts:

$$F = G_T \cdot w \quad (2.17)$$

The necessary nominal power will be defined by the product of F and the pertaining base speed, which will be called v_1 according to UIC (called speed at full notching, in times of contactor control). At speeds higher than v_1 the power will be kept constant, equal to nominal power; to that purpose the traction motors will generally be operated with weakened field. This is only possible to full extent with inverter-fed rotating-field machines; with series-wound commutator motors the allowable range of field weakening is limited due to commutation failure at fast

changes of the line voltage, as e.g. encountered at pantograph bouncing. Therefore the natural $1/n^2$ -characteristic at limited voltage without field weakening will prevail in traction vehicles with commutator machines.

Fig. 2.14 shows the tractive-effort vs. speed (F - v) diagrams of different locomotives of DB. With locomotives with commutator motors there is a discrimination between 1-h and 5-min-rated power (the latter for starting operation). The first value is determined by the thermal time constants of the motors (and/or transformer), the latter by the commutation limit. With interferred three-phase motor locomotives this difference is much smaller, due to the much smaller dominant time constant of the inverter cooling.

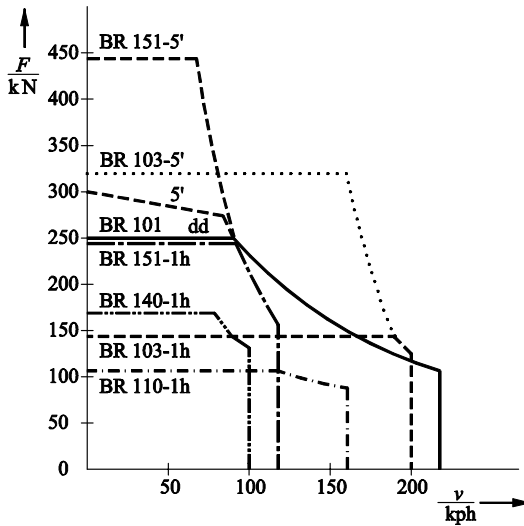


Fig. 2.14:
Continuous (1 h)
and starting (5')
tractive effort of different
loco-motives of DB

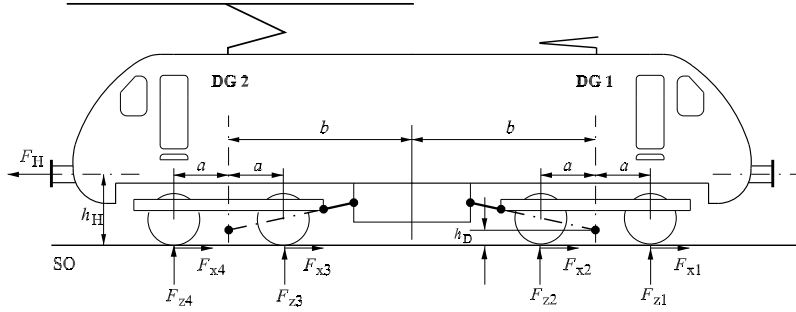
Classes (“BR”) 110 and 140 are identical AC-fed locomotives with about 3.5 MW rated power and $v_{\max} = 160$ and 100 km/h, respectively, by different gear ratios. Class 103 – the last high-speed locomotive with AC series-wound commutator motors – shows a permanent (1-h) rated power 7.1 MW (at $v_1 \approx 180$ km/h). Class 151 is the corresponding heavy goods-trains locomotive with $v_{\max} = 120$ km/h. The steep decrease of tractive effort beyond v_1 caused by the commutation limit is stunning.

Contrary to that the inverter locomotive Class 101 of DB AG with the so-called “universal characteristic” delivers its rated power of 6.4 MW over the broad range of about 90...220 kph (55... 140 mph). By that it is suited for express passenger trains as for fast goods trains as well; cf. Exercise 17.1: “ F - v Diagram of a Universal Locomotive”.

2.2.6 Load transfer

Before investigating the transmission of tractive effort from wheelset to rails in section 2.2.7 the reaction of the traction/braking force at the drawbar on the weight forces in the wheel contact points shall be looked at.

Fig. 2.15 represents in a schematic way a locomotive with two two-axle bogies with the acting forces and the relevant geometric distances.



2 · a	Wheel base	FH	Drawbar force
2 · b	Bogie centre distance	Fz1	Weight force of wheelset 1
hD	Force attack point in bogie over rail top	:	
hH	Height of drawbar over rail top (1030 mm)	Fz4	Weight force of wheelset 4

Fig. 2.15: Geometry and forces of a four-axle traction vehicle

$$\text{Loco weight force } G_{\text{Loco}} = F_{B1} + F_{B2} \quad (2.18)$$

$$\text{Assumption: } F_{x1} = F_{x2} = F_{x3} = F_{x4} = F_{xi} = F_H / 4 \quad (2.19)$$

$$\text{Bridge torque: } M_K = F_H \cdot (h_H - h_D) = (F_{zDG2} - F_{zDG1}) \cdot b \quad (2.20)$$

Bogie torques:

$$M_B = \frac{1}{2} F_H h_D = 2 \cdot F_{xi} \cdot h_D = (F_{z2} - F_{z1}) \cdot a = (F_{z4} - F_{z3}) \cdot a \quad (2.21)$$

Sum of contact forces in bogie:

$$F_{zB1} = \frac{1}{2} \left[G_{\text{Loco}} - F_H \left(\frac{h_H - h_D}{b} \right) \right] \quad (2.22a)$$

$$F_{zB2} = \frac{1}{2} \left[G_{\text{Loco}} + F_H \left(\frac{h_H - h_D}{b} \right) \right] \quad (2.22b)$$

Contact forces of wheelsets:

$$F_{z1} = \frac{1}{4} \left[G_{\text{Loco}} - F_H \left(\frac{h_H - h_D}{b} + \frac{h_D}{a} \right) \right] \quad (2.23a)$$

$$F_{z2} = \frac{1}{4} \left[G_{\text{Loco}} - F_H \left(\frac{h_H - h_D}{b} - \frac{h_D}{a} \right) \right] \quad (2.23b)$$

$$F_{z3} = \frac{1}{4} \left[G_{\text{Loco}} + F_H \left(\frac{h_H - h_D}{b} - \frac{h_D}{a} \right) \right] \quad (2.23c)$$

$$F_{z4} = \frac{1}{4} \left[G_{\text{Loco}} + F_H \left(\frac{h_H - h_D}{b} + \frac{h_D}{a} \right) \right] \quad (2.23d)$$

It can clearly be seen that a low force attack point in the bogie ($h_D \Rightarrow 0$, low pivot connection point or "deep-draft rods") reduces the load transfer from the leading to the rear wheelsets in the bogies.

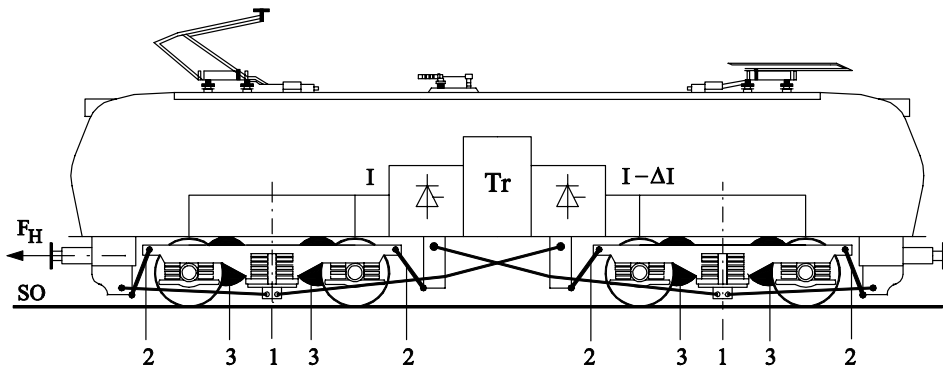
As an example for a rather low load transfer numerical values of the Swiss high-power locomotive Class 460 („Bahn 2000“) shall be given:

$$G = 82 \text{ t} \cdot 9,81 \text{ m/s}^2 = 805 \text{ kN}; F_H = 275 \text{ kN} (P = 6000 \text{ kW})$$

$$a = 1400 \text{ mm}, b = 5500 \text{ mm}, h_H = 1030 \text{ mm}, h_D \approx 250 \text{ mm}$$

$$\begin{aligned} F_{zDG1} &= 382 \text{ kN} = 402.5 \text{ kN} - 5 \% \\ F_{zDG2} &= 422 \text{ kN} = 402.5 \text{ kN} + 5 \% \\ F_{z1} &= 179.2 \text{ kN} = 201.25 \text{ kN} - 9.4 \% \\ F_{z2} &= 203.8 \text{ kN} = 201.25 \text{ kN} + 1.3 \% \\ F_{z3} &= 198.7 \text{ kN} = 201.25 \text{ kN} - 1.3 \% \\ F_{z4} &= 223.3 \text{ kN} = 201.25 \text{ kN} + 9.4 \% \end{aligned}$$

Different measures for counteracting the load transfer are exemplarily shown in Fig. 2.16 with the Austrian high-power locomotive Class 1044:



- 1 Weight transfer linkage by "deep-draft rods" ($h_D = 189 \text{ mm}$ over rail top)
 - 2 Electro-pneumatic wheelset balance with steel ropes
 - 3 Steep F - v characteristic by mixed excitation of traction motors
 - 4 Reduction of motor armature currents ($I - \Delta I$) in the leading bogie
- Tr: Main transformer

Fig. 2.16: Measures for counteracting the load transfer; example ÖBB Class 1044 [108]

Locomotives with inverter-fed three-phase drives (as Class 101 DB AG) mainly use measures 1 and 4; 3 is achieved by proper motor control (subchapter 6.3).

For thematic immersion, refer to Exercise 17.2: "Mechanical Design of a Universal Locomotive").

2.3 Adhesion, slip-and-slide control

As early as 1820 it became evident that, for general use, a nonpositive link was sufficient to transmit tractive forces from the driving wheelset to the rail; a positive-fit was only required in special cases like gradients over 60 ‰, in the form of rack-and-pinion railways.

Fig 2.17 displays forces and speed at the driving wheelset.

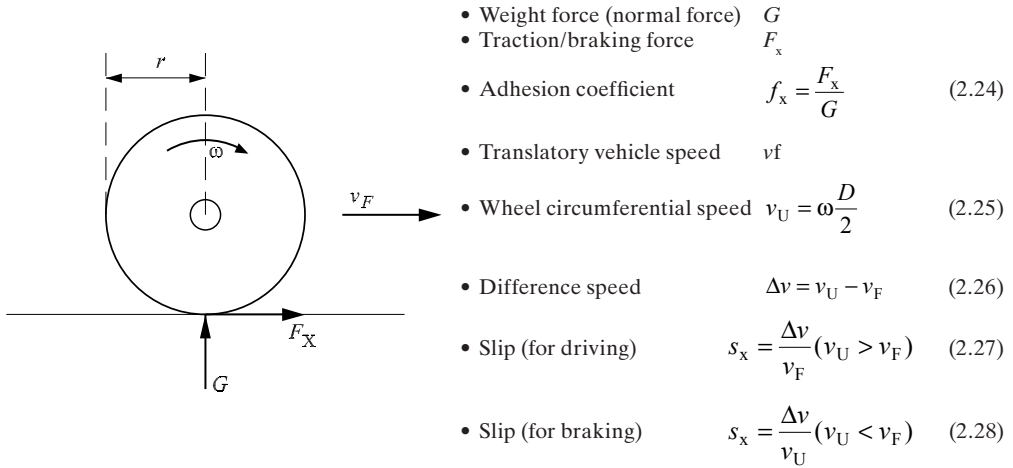


Fig. 2.17: Forces and speed at the driving wheelset (EEW-TUD)

Transferring forces via Coulomb (sliding) friction requires a difference speed between wheel circumference (v_U) and rail:

$$F_x = f_x (\Delta v, P_1 \dots P_n, v) \cdot G \tag{2.29}$$

The adhesion coefficient f_x mainly depends upon this difference Δv – shaped similarly to the torque characteristic of an induction machine with the maximum at Δv_{opt} – and further influences which may vary in a stochastic manner [12], [13], [14]. Fig. 2.18 gives examples of adhesion coefficient characteristics for dry ①, wet ② and greasy ③ rails.

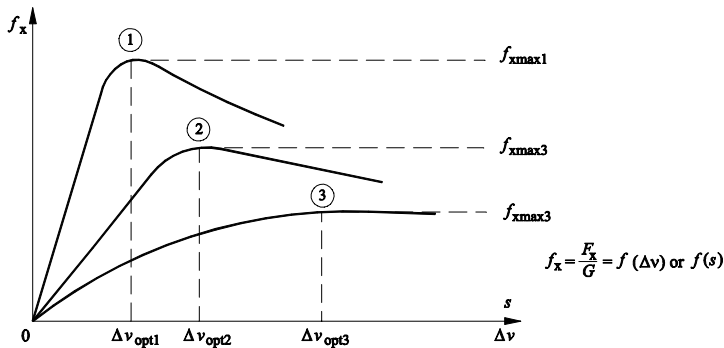


Fig. 2.18: Adhesion coefficient $f_x = f(\Delta v)$

Dominating parameters for $f_x, f_{xmax}, \Delta v_{opt}$ are:

- Coating (① dry; ② wet; ③ oily)
- Material quality
- Surface roughness
- Temperature

Typical values: $(0.05\dots) 0,1 \leq f_{max} \leq 0.4 (\dots,5)$
 $0.2 \% \leq s_{opt} \leq 6 \%$
 $0.05 \text{ m/s} \leq \Delta v_{opt} \leq 1 \text{ m/s}$

Additionally f_x will be reduced when negotiating curves as additional transversal slip occurs, and with rising absolute speed v . Furthermore there are dynamic changes of the wheel contact forces induced by the action of the wheelset, the bogie and the track as well and torque changes inevitable with classical camshaft control of the traction motor. In 1944 the scientists Curtius and Kniffler undertook measurements with the then high-power locomotive E 19 of DRG with individual wheelset drives, which could quantify the speed dependency – with ample scattering due to the other parameters (Fig. 2.19, [15]).

DB uses as mean regression curve:

$$f_x = \frac{7.5}{\frac{v}{\text{kph}} + 44} + 0.161 \tag{2.30}$$

It is most important how the electric drive reacts to the stochastic changes of the adhesion coefficient and thus to the load-torque changes. Fig 2.20 represents for an assumed tractive force characteristic $F(v_u)$ ① different control characteristics of the traction motor (equivalent to $M(n)$) and the appearing operating points:

② is the characteristic of a classical camshaft-controlled series-wound commutator motor at constant armature voltage (be it AC or DC). The big negative gradient ($M \sim 1/n^2$, cf. section 4.1.1) delivers the section point A always as a stable operation point.

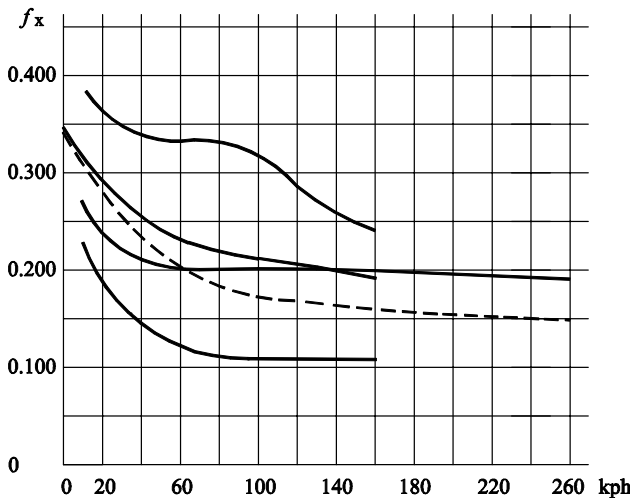


Fig. 2.19: Adhesion coefficients according to the measurements of Curtius and Kniffler [15]

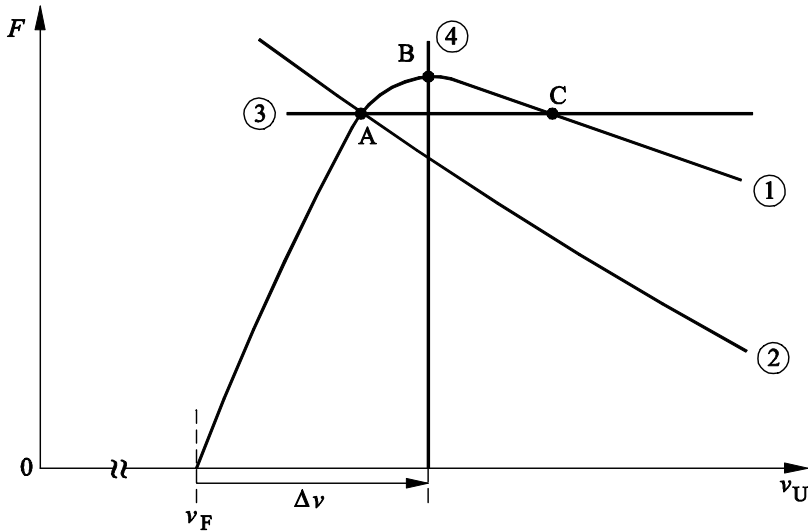


Fig. 2.20: Adhesion characteristic and motor characteristics

Torque-controlled motors ③, as fed by current-controlled DC choppers or converters with phase-controlled thyristors (subchapter 4.1) or three-phase inverters (subchapters 5.2 and 6.3) behave differently, however. When the operating point transgresses the maximum B by a short-time reduction of f_x , all operating points C become instable – the wheelset begins to slip (or to slide at braking operation at $F_H < 0$). A classical anti-slip-slide control reduces the torque set value dependent upon the speed rise rate dn/dt or dependent upon the speed difference of the individual wheelset from the mean value of all wheelsets.

A speed control according to characteristic ④ enables stable operation in each point of the adhesion characteristic (whether this makes sense in any case may be doubted since the friction loss power $F \cdot \Delta v$ quickly increases with the slip, with only a marginal gain of tractive effort in comparison with point A [20]). To obtain such a characteristic, a speed control loop is to be superimposed to the inner current (or torque) control loop of the drive. The speed set value must always be given by a value of Δv bigger than the actual translational speed v_F [17], which is necessary for the tractive effort.

To that purpose the true speed over ground may be measured – as in locomotive Class 101 of DBAG – by using radar equipment, while the optimal difference speed set value is determined depending upon the torque set value of the motors: $\Delta v_{opt} \cdot M_d / M_{dmax}$ ([18], feed-forward). As this dependence must reflect a mean adhesion coefficient (e.g. ① in Fig. 2.18) the result can only be suboptimal with actual adhesion conditions according to ② or ③ in Fig. 2.18.

Better results can be obtained by a "wheel-creep control" using a "search algorithm" like that developed by the Technical University of Darmstadt, which is explained in Fig. 2.21 [19], [20]. Starting from operation point (4) the speed set value will be increased; until the maximum value (1) of the adhesion coefficient characteristic the torque will rise, too. From now on with increasing v_{ref} the transmissible traction force sinks, the rotational speed rises, so that reaching point (2) the search direction will be inverted and v_{ref} will be reduced, until – via point (1) – again point (4) will be reached.

The lower parts of the figure show tractive effort, difference and absolute speed depending upon time. With decreasing f_x the search logic lowers the set value of the difference speed, until again the maximum of the actually transferable force will be found.

The method according to Hildenbrandt [21] finds the maximum of the adhesion coefficient by impressing a torque test signal, oscillating with 5...10 Hz, and evaluating the phase of the transfer function torque vs. speed at the motor. The phase changes in point 1 of Fig. from $< -90^\circ$ to $> -90^\circ$.

If only one wheel loses its contact with the rail, a relatively high-frequent (50...65 Hz) oscillation of both wheel discs against each other will be excited, which stresses the shaft extremely. This effect can be influenced positively by the wheel-slip control [22].

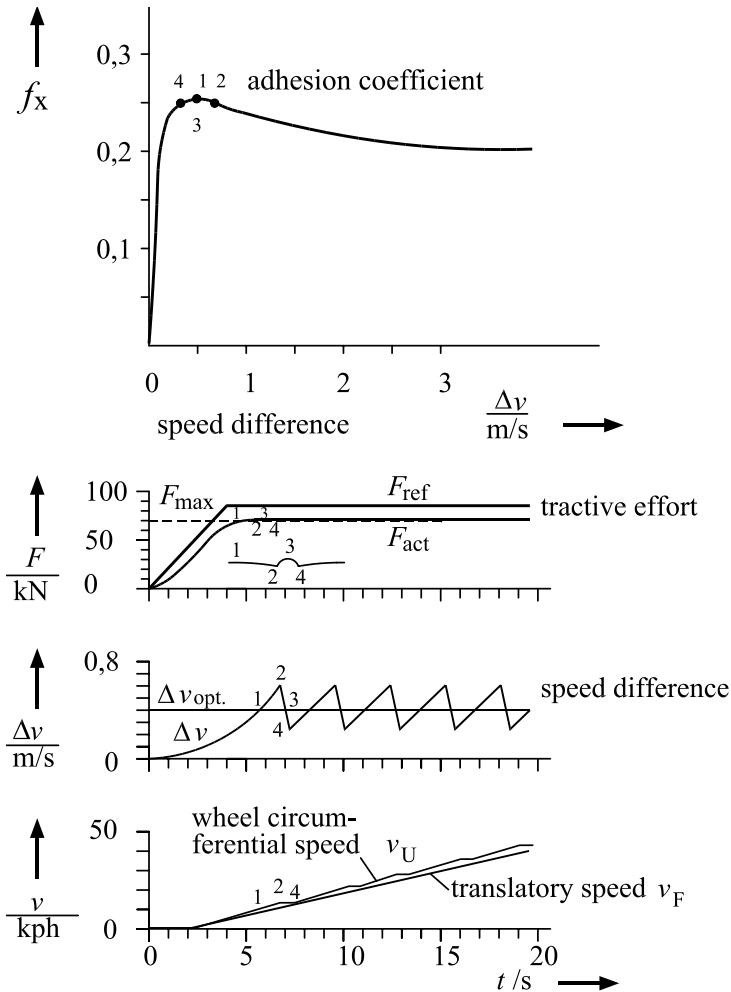


Fig. 2.21: TUD wheel-creep control – starting from standstill [19]

2.4 Traveling time loss by acceleration and braking

A vehicle starting with constant acceleration a_a to maximum (final) speed v_m takes the time $t_a = v_m/a_a$ and covers the distance $s_a = \frac{1}{2} v_m^2 / a_a$. For the same distance a vehicle running with constant speed v_m would only need the time $t_{v=const} = s_a/v_m$. Inserting s_a yields the time difference:

$$t_{vA} = t_a - t_{v=const} = \frac{1}{2} v_m/a_a. \tag{2.31}$$

This time is called "time loss at starting". The corresponding holds for the time loss at braking (Index b). The total traveling time over the distance s is then

$$t_{tot} = \frac{s}{v_m} + t_{va} + t_{vb} = \frac{s}{v_m} + \frac{v_m}{2} \left(\frac{a_a + a_b}{a_a \cdot a_b} \right) \tag{2.32}$$

To obtain the average traveling time the stopping time in the stations t_H must be added. So we obtain the average traveling speed as:

$$\bar{v} = \frac{s}{t_{ges} + t_H} \tag{2.33}$$

As an example, each regular stop on the Japanese high-speed lines produces a traveling time loss of about 5 min:

$v_m = 220 \text{ kph}$	$a_a = 0.34 \text{ m/s}^2$	$a_b = 0.30 \text{ m/s}^2$
	$t_{va} = 90 \text{ s}$	$t_{vb} = 100 \text{ s}$
	$t_H = 120 \text{ s}$	$\Sigma t = 310 \text{ s} \approx 5 \text{ min}$

Fig. 2.22 shows exemplarily tractive effort, speed and distance, depending upon time for the acceleration and braking period of a Metro train; the train resistance is assumed according to Sauthoff's formula (2.10). Cf. Exercise 17.3 "Average traveling speed of a Metro train".

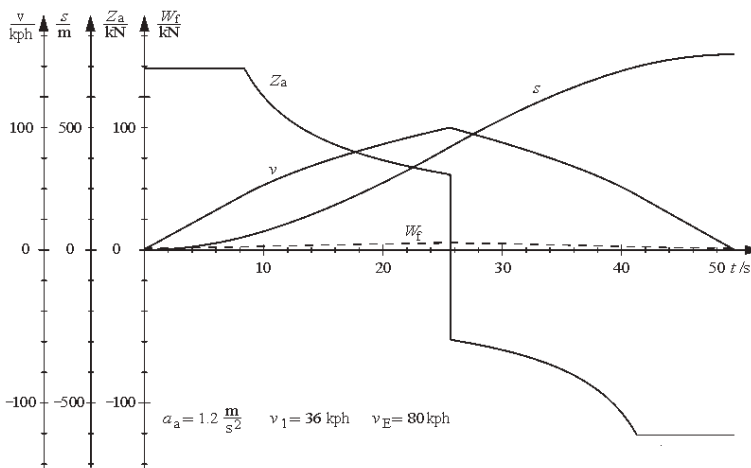


Fig. 2.22: Time characteristics of acceleration and braking of a Metro train.

3 Running gear and drive of traction vehicles

3.1 Classification of traction vehicles and wheel arrangement

3.1.1 Classification of traction vehicle types

- Locomotive
A locomotive is a traction vehicle which may be easily separated from the train assembly. It is generally not suited for the transportation of passengers and cargo. As a rule, an electric or a diesel locomotive can be used in both directions of travel (forward/reverse), yielding the same performance in either direction.
- Motor headcar
A motor or power headcar (“power head”) is an asymmetrical special locomotive which is permanently coupled to the train assembly. It has only one cockpit and can only be separated from the train assembly by using special equipment, a task only performed at railway depots, not during operation. Modern high-speed trains usually are equipped with one headcar on both front and rear ends, the rear headcar being remote-controlled from the frontal cockpit. If only one headcar is used on a high-speed train, as is the case with the Swedish X2 or the German ICE 2, a control trailer runs at the rear end.
- Motor coach (or motor car, rail car)
Motor coaches are traction vehicles suitable for transportation of passengers and cargo within the traction vehicle itself. Usually, a motor coach can be used to pull or push a number of transport cars and/or control trailers.
- Multiple-unit set
Multiple-unit sets are trains composed of one or more motor coaches or motor headcars, a number of cars and/or control trailers.
- Push-pull trains
A push-pull train consists of a locomotive, a number of passenger cars and a control trailer at the rear end of the train; using this control trailer, the train is steered during reverse-direction travel. This pattern offers several advantages, most notably shorter turnabout time in terminal stations, as well as greater flexibility of the placement of cars, compared to multiple-unit sets. Examples to be mentioned specially are various IC (Intercity) trains all over Germany.

3.1.2 Wheel arrangement

The modern classification system of wheel arrangement for traction units was specified and regulated in 1983 by the International Union of Railways (UIC):

UIC 612: Standard designation of wheel arrangement on locomotives and multiple-unit sets

In general, it concurs with the system of the Association of German Railway Administrations (VDEV) which has been in use since 1908.

- Wheelset arrangement within the main frame
The number of drive wheelsets is denoted by capital Roman letters (eg. A, B, C...). The number of trailing wheelsets (these being wheelsets only used for distributing the vehicle weight, but not transferring traction power from the motors) is denoted by Arabic letters (1, 2...). The nowadays predominant single-axle drive is indicated by a small 'o' (zero) on the line (eg. Bo).

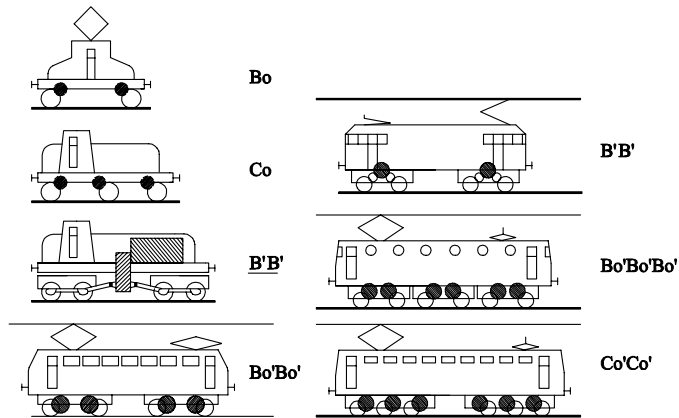


Fig. 3.1: Wheelset arrangements – examples (EEW-TUD)

Apart from that and alongside, there are various other systems, like the Anglo-American system of classification by key words like “Pacific” (2'C 1') or “Mikado” (1'D 1'), classification by fractional numbers and code prefixes for the main use of the traction vehicle (for example, the famous Bavarian steam express locomotive S 3/6, where ‘S’ denotes an express locomotive, ‘3’ the number of coupled drivers, ‘6’ being the total number of wheelsets, eg. 2'C 1'), similarly in Switzerland, and finally the Whyte system which denoted the number of wheels used (4-6-2 = 2'C 1'). The corresponding French denomination was 231.

- Wheelset arrangement in a segmented under-carriage
Modern traction vehicles of higher performance are generally constructed as bogie vehicles. Wheelsets which are flexible within the limits of the girder or wheelset groups, like bogies, are indicated by an apostrophe. The denomination of the wheelsets of a wheelset group is put in brackets if it consists of more than one numeral or one letter; no additional apostrophe is required if the group is flexible.

If all drive sets of a bogie-type traction vehicle are coupled both with one another and the motor (eg. by cardan shafts in the case of diesel-hydraulic locomotives), this is denoted by underlines. In the case of traction units which consist of separate sub-units without a common superstructure, the denominations of the components are linked by the symbol '+'. Fig. 3.1 gives various examples of electric and diesel-electric traction vehicles.

3.2 Mechanical components of power transmission

Power transmission is the key link between the drive engine and the drive wheelset. It fulfils the following tasks:

- It transmits the accelerative and decelerative torque from the drive motor via the driving wheelset to the rail
- It enables the relative movement of the spring-suspended driving wheelset in relation to the vehicle or bogie frame.

As we shall see, the dynamic quality of the drive is characterized by the share of components' mass directly joined to the drive wheelset.

Fig. 3.2 to 3.5 depict various drive systems from the “childhood days” of electrical traction, to elaborate the problem. Fig. 3.2 shows the so-called “Gearless” drive, which was introduced by Siemens in 1889 for the very first electrical traction vehicles of the London Underground, the famous “Tube”. While the motor is rigidly mounted in the vehicle girder, the rotor is fixed to the driving wheelset shaft, without any spring suspension or gears. Without any gears, the motor torque is equal to the wheelset torque, resulting in a correspondingly heavy motor. The drive is completely unsprung; the unsprung mass equals the vehicles weight, and all thrusts (of up to 40 times earth acceleration) are transmitted without attenuation from rail to drive. It is obvious that such a system only yields unsatisfactory drive behaviour and high rates of wear.

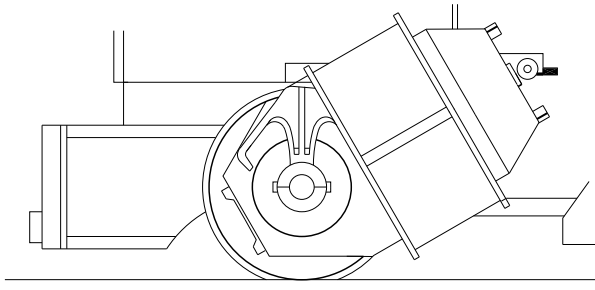


Fig. 3.2: Unsprung „Gearless“ drive (London Tube) 1889

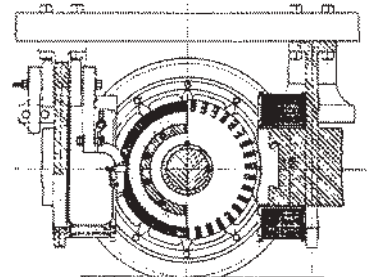


Fig. 3.3: „Bipolar“ Motor by Batchelder (GE) 1903; 410 kW.

In 1903, the so-called “bipolar motor” developed by A. Batchelder of General Electric proved itself to be a considerable advance. The rotor of the two-pole DC drive motor is still firmly joined to the wheelset shaft; the sprung wheelset, however, is able to move freely in vertical direction between the two pole shoes of the field-winding system. While considerably reducing the unsprung mass, however, this results in a low pole-pitch factor, poor magnetic return path and the imprecise electrical feed via the commutator.

During this period of time, European railway designers preferred a system derived from steam locomotive engines, using parallel cranks. Fig. 3.4 depicts such a system in use with the Royal Prussian State Railways (KPEV) in 1914. The 1925-kW drive motor is mounted upon the frame, driving two intermediate axles via low-speed parallel-crank gears. The intermediate axles, being affixed to the frame themselves, are mounted level with the drive wheelsets, driving the outer wheelsets via flexible coupling rods, allowing these being sprung. The main reason for the use of this crank drive was the unsatisfactory state of gearing technology at the time. Due to

unity transmission, the complete motor assembly was very heavy (example $G = 24$ metric tons, outer diameter 3,6 m (~12 ft)).

During the Great War, gearings of 1 MW rating became possible. Fig. 3.5 shows the Winterthur “inclined driving rod” system with primary gear transmission, which was developed by the Swiss Locomotive Factory (SLM) of Winterthur in 1922 for the 2nd series of “Krokodil”- type locomotives.

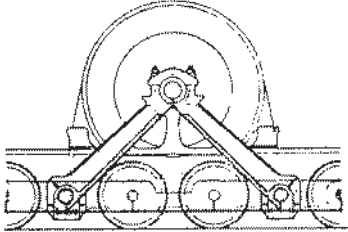
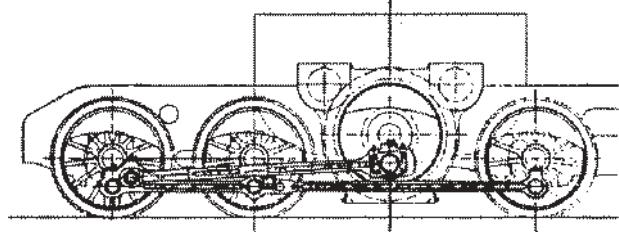


Fig. 3.4: Parallel-crank drive
KPEV 1914 Fig.



3.5: Winterthur inclined rod drive with primary gear 1922

Two drive motors provide torque via a primary gear transmission of about 1:3 to an intermediate driving axle which is mounted slightly higher than the driving wheelsets. It drives the outer drive wheelset via slightly inclined oblique driving rods, the inner wheelsets being driven by coupling rods from the outer sets. This system was used for slow locomotives of high tractive force until the 1960s; for example, the heavy “Dm” locomotives of the Lulea-Kiruna-Narvik iron-ore railway where equipped with this kind of drive.

From about 1930, the sprung single wheelset drive started to replace the previously predominant coupling-rod group drive. The oldest and most simple variant of the sprung drive is the axle-hung (or pin-and-nose) drive according to Sprague 1888 [24], Fig. 3.6. The great cogwheel is fixed firmly to the drive wheelset shaft. The motor, to whose shaft the pinion is attached, “leans” onto the drive-set shaft using two “paws” and assures thus the constant gear-centre distance. On the other side, the motor is spring-suspended to the frame. The unsprung mass of the drive is about half the motor’s weight plus the weight of the drive wheelset including the great cogwheel. Vertical thrusts from the rail are still transmitted to the motor, however alleviated by the levered relation. For these reasons, the axle-hung motor is now considered to be useful only for speeds up to 140 kph (87 mph).

Fig. 3.7 shows a bogie of the goods-train locomotive Class 152 of the DB AG (1999, [B17]), using two axle-hung drives with 1600-kW three-phase motors (2), rubber-suspended at the bogie centre bar (7). Please note the square bearing (1) of the revolving peg – the rotating ability of ca. $\pm 2.5^\circ$ is solely achieved by the use of rubber blocks! (6) are the Flexicoil springs of the secondary suspension. Further labelling numbers will be discussed in subchapter 11.1.

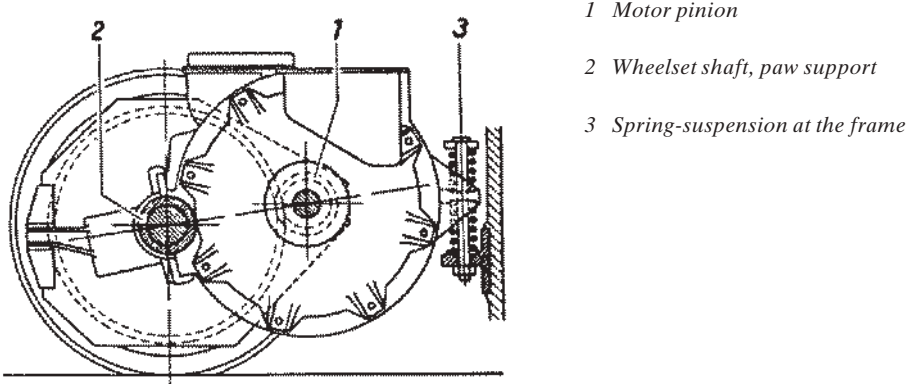


Fig. 3.6: Axle-hung motor drive [B1]

Definitive progress becomes visible in the SSW rubber circular-spring drive developed by Siemens after the Second World War (Fig. 3.9): The great cogwheel is mounted to a hollow shaft, which surrounds the drive wheelset shaft. The drive motor, being sprung to the bogie frame, leans now on the hollow shaft, thus ensuring correct grip of the gearing. On the great cogwheel, brackets (3) are mounted, which prop through holes in the wheel discs, transmitting the torque via rubber circular springs (4) to the drive wheel. At the same time, these springs transmit half the motor's weight to the drive wheelset. By using the rubber circular springs, the thrusts emitted from the rail and suffered by the motor are considerably reduced. However, the generally high unsprung portion of the axle-hung motor remains in full.

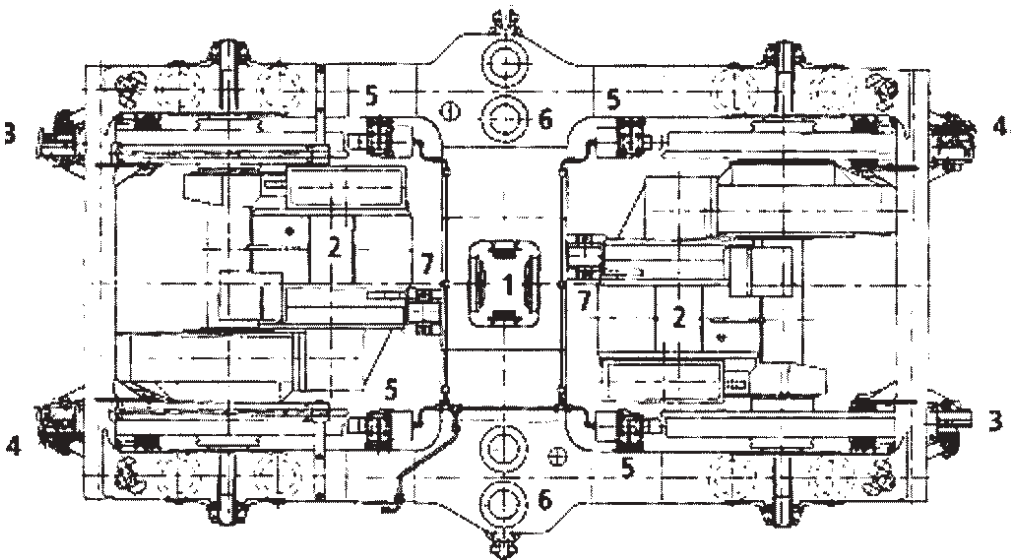


Fig. 3.7: Bogie of Class 152 of DB AG with axle-hung drives (Siemens AG, TS)

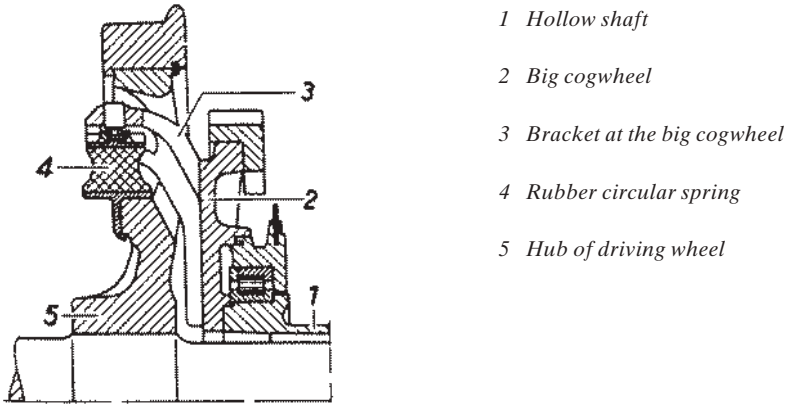
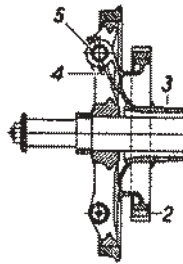
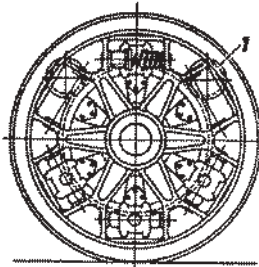
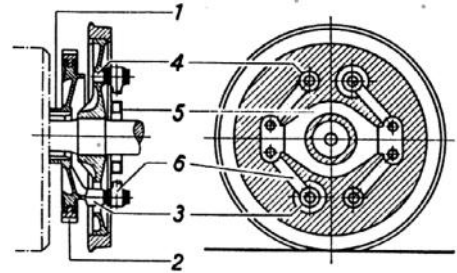


Fig. 3.8: SSW rubber circular-spring drive [B1]

True improvements could only be achieved by using a bogie drive decoupled from the wheelset as much as possible, the drive motor being mounted in the bogie assembly. Fig. 3.9 depicts the AEG-Kleinow helical spring-coil drive, developed from the Westinghouse drive in the 1920s. Drive motor and hollow shaft (3, with great cogwheel (2)) are firmly mounted to the bogie. Brackets (4) at the great cogwheel grip through the wheel spokes and transmit torque via helical springs-coils (5) to the driving wheel.



- 1 Motor pinion
- 2 Big cogwheel
- 3 Hollow shaft
- 4 Bracket at the big cogwheel
- 5 Spring coil in pot



- 1 Hollow shaft (quill)
- 2 Big cogwheel
- 3 Peg at big cogwheel
- 4 Peg at driving wheel
- 5 Guide frame ("dancing ring")
- 6 Coupling rods

Fig. 3.9: AEG-Kleinow spring-coil drive [B1]

Fig. 3.10: Alsthom quill drive with "dancing ring" [B1]

By using this helical spring-coil drive, the German express locomotive Class E 19 achieved maximum speeds of 225 kph (140 mph) by the year 1940. If the torque proved too big, the drive would be constructed double-sided.

A similar principle is found with the French Alsthom Hollow Shaft drive (Fig. 3.10). Actuator pegs (3), linked to the big cogwheel (2) mounted on the quill (1), grip coupling rods (6) through holes in the wheel disc, driving the guide frame (5), the so-called “dancing ring”. From this, the torque is transmitted via concurrent rods and pegs on the driving wheel (4) to the drive wheelset. In this case, free vertical adjustment of the driving wheelset in relation to the frame is possible, as well.

The “state of the art” used with almost all modern locomotives using three-phase drives is the BBC cardan hollow-shaft drive with rubber joints [26] (Fig. 3.11). Motor (1) with pinion (3) and big cogwheel (4) (both with herringbone gearing) are firmly mounted in the bogie frame.

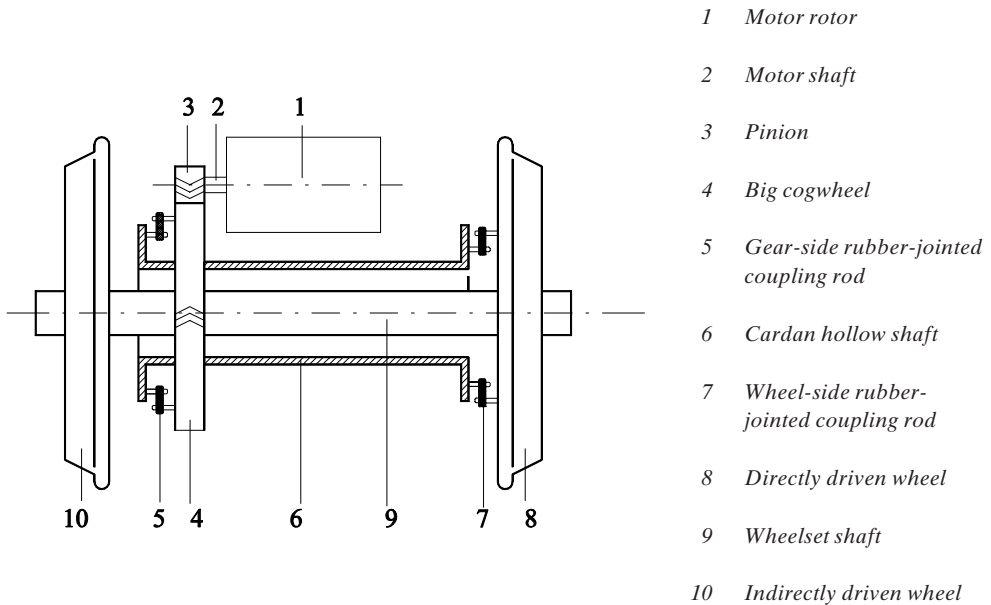
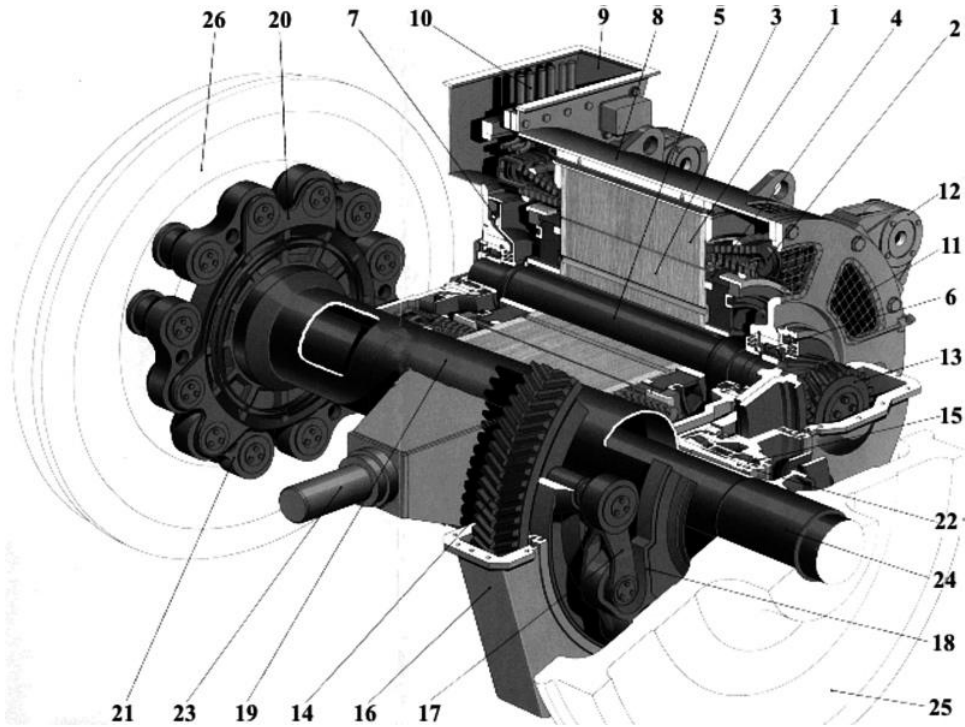


Fig 3.11: Basic representation of Cardan Hollow Shaft Drive with Rubber Joints

From the big cogwheel, torque is transmitted via six coupling rods (5) whose joints are embedded in rubber to a corresponding star on the left front side of the cardan quill (6). The cardan quill then transmits the torque via the star on the right side and identical coupling rods (7) to the right wheel disc (8); from thereon, the shaft drives the left wheel. Such coupling rods allow for vertical (sprung) movement of the axle in relation to the drive motor, as well as rotary flexibility of the wheelset on the x-axis (and the z-axis, in the case of radially-steered wheelsets). This provides optimal de-coupling of the inherent movements of wheelset and bogie. The drive motor is submitted to accelerative forces of merely ~ 5 g.

Fig. 3.12 shows exemplarily the drive of Class 120 of DB in a perspective cutaway.

**Motor**

- 1 Stator laminated core
- 2 Stator winding
- 3 Rotor laminated core
- 4 Squirrel-cage rotor winding
- 5 Shaft
- 6 cylinder roller bearing
- 7 Impulse encoder tooth wheel
- 8 Casing
- 9 Air inlet
- 10 Connection cables
- 11 Air exhaust
- 12 Fastening

Gear

- 13 Pinion
- 14 Big cogwheel
- 15 Bearing of big cogwheel
- 16 Protection box

Rubber-jointed cardan hollow-shaft drive

- 17 Rubber-jointed coupling rod
- 18 Hollow-shaft star
- 19 Hollow-shaft
- 20 Forked stark
- 21 Rubber-jointed coupling rod
- 22 Hollow-shaft casing
- 23 Suspension arm

Wheelset

- 24 Shaft of wheelset
- 25 Disc wheel
- 26 Disc wheel with drive pegs

Fig. 3.12: Motor, gears and hollow-shaft drive of Class 120

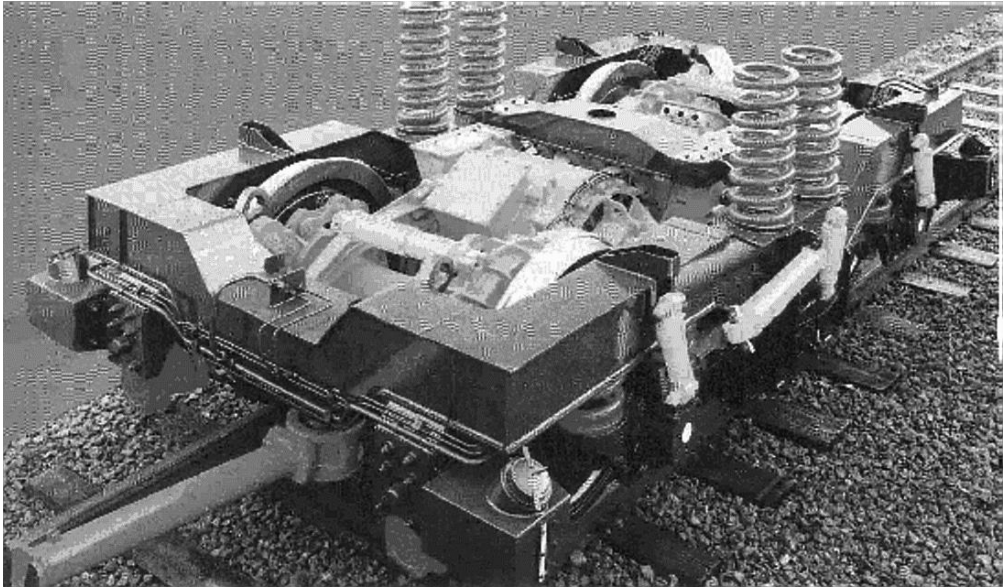


Fig. 3.13: Integrated Complete Drive in the bogie of Class 101 of DBAG (Bombardier Transportation)

An advanced version of mounting this quill drive into a bogie as seen on the Integrated Complete Drive (Integrierter Gesamtantrieb, IGA) of Adtranz/Bombardier is shown in Fig. 3.13. The drive motors are moved completely towards the vertical axis of the bogie. At this place, however, they are not mounted to the bogie frame, but to the vehicle frame. Thus, their portion of mass does not burden the bogie, and the moment of inertia of the bogie on the z-axis is considerably reduced, as well.

To the gearing, an intermediate wheel is added between pinion and great wheel, in order to increase the distance between motor axle and drive-set axle, thus providing more space for the inclusion of brake discs on the cardan quills. The drive motors are propped via brackets to the front and rear end girders of the bogie. The body weight is transmitted to the bogie frame via two sets of two Flexicoil spring elements which also transmit bogie lateral forces to the bridge. The traction forces are conducted from the lateral traverse of the bogie to the transformer box (and thus to the bridge) via coupling rods.

Fig. 3.14 illustrates Siemens' solution for the "Taurus" high-power locomotives ÖBB 1016/1116 ($P = 6300 \text{ kW}$), a high-performance drive with brake shaft ("Hochleistungsantrieb mit Bremswelle" HAB). The motors are mounted fixed within the bogie, the gearing does not have an intermediate wheel. The brake discs are mounted on a separate brake shaft, which is powered by an additional gear level (towards fast); thus, their mass is reduced. A locomotive of the subsequent three-system variant 1216 ÖBB attained a speed of 357 kph in 2006, without any major changes, demonstrating the excellent riding quality of this construction.

A rather simple form of bogie motor drive without quill is the so-called "axle-riding" pattern, which is used for vehicles of intermediate power (eg. commuter cars and the ICE 3, with only 500 kW per drive; Fig. 3.15). The gearing is fixed to the wheelset, flexible vertical adjustment is achieved only by an intermediate shaft with two curved-tooth couplings.

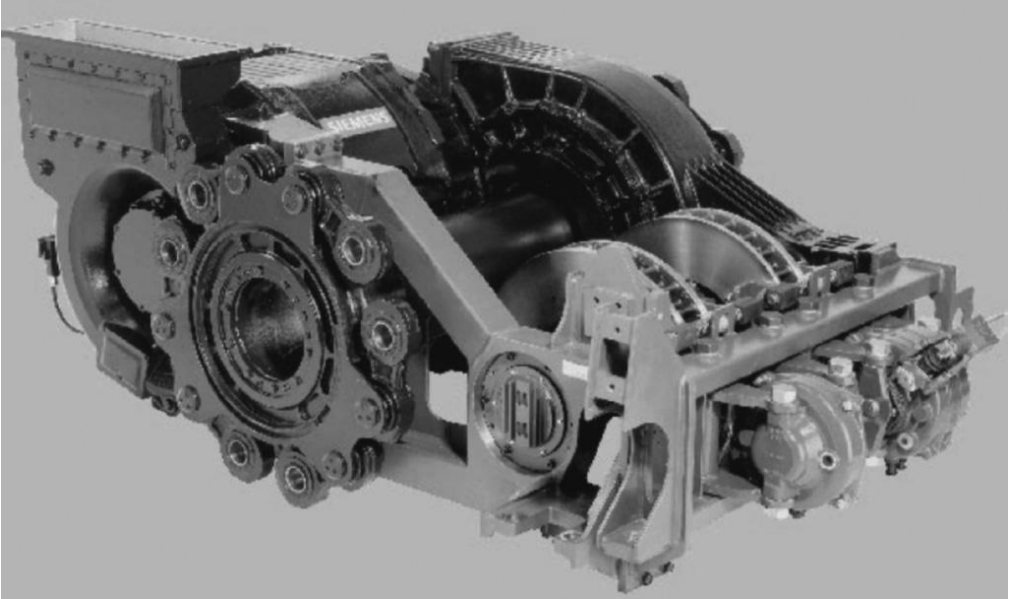


Fig 3.14: HAB quill drive of universal locomotive Class 1016 ÖBB (Siemens AG, A&D)

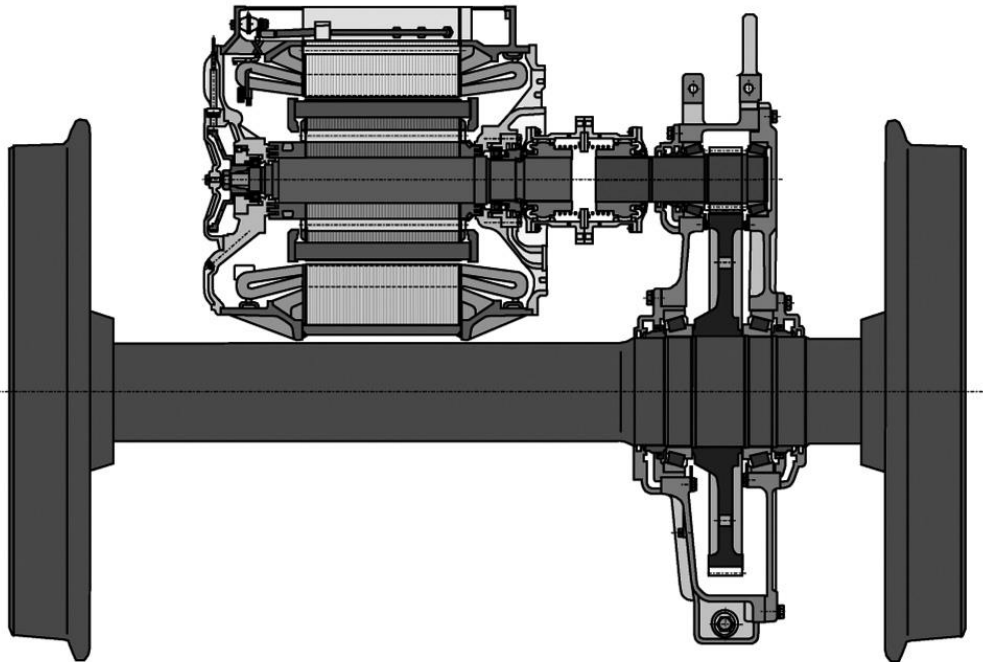
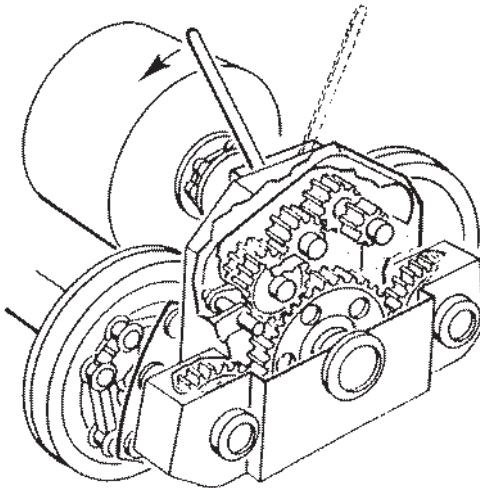


Fig. 3.15: Axle-riding gear and bogie-mounted 500-kW motor in ICE3 multiple unit Class 403 of DG AG

A specific French bogie pattern, the so-called Monomoteur drive (Alstom), is shown in Fig. 3.16. A high-mounted drive motor (DC commutator or synchronous motor) drives the wheelsets via a switchable spur-gear and “dancing-ring” couplings (Fig. 3.10). The switching option of this gearing (i_1 , i_2) is advantageous with DC drive motors to achieve two maximum speeds (v_1 , v_2) for express and cargo services, respectively. This pattern allows for a very short wheelbase (down to a minimum of 1.61 m / 5 ft 4 in) and thus minimal moment of inertia applied to the z-axis.



Shift transmission:

$$i_1 = 1.88 \rightarrow v_{max1} = 150 \text{ kph}$$

$$i_2 = 3.22 \rightarrow v_{max2} = 90 \text{ kph}$$

Fig. 3.16: Monomoteur bogie of SNCF

Finally, two special tramway drives shall be described. Fig. 3.17 depicts the classic DÜWAG twin-axle longitudinal drive from the 1950s. The longitudinal drive drives the two axle sets via bevel-gear gearings and rubber spring discs. Between the wheel discs and the wheel treads, additional rubber elements have been mounted to reduce noise and provide primary suspension (resilient wheels). A drawback of this longitudinal drive is (similarly as with the Monomoteur drive described previously) the rigid coupling of the front and rear wheelsets which may lead to tension warp in the drive on curved tracks, resulting in wear and increased noise.

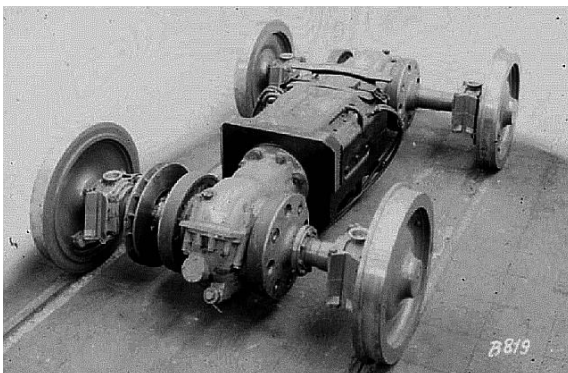


Fig. 3.17: DÜWAG Twin-Axle Longitudinal Drive for tramways (P ... 250 kW)

Therefore, in the 1990s, more modern variants using transversally-mounted individual motors and cardan-quill drives with rubber joints were devised. Fig. 3.18 shows the drive of the 70% low-floor tram by Siemens-DÜWAG (cf. subchapter 10.2). Only the left-hand, short part of the quill is used cardanically.

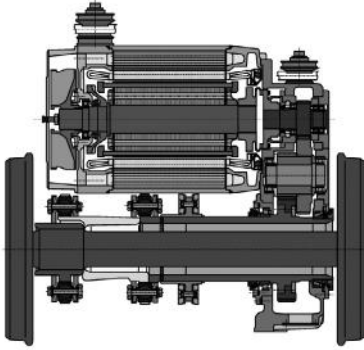


Fig. 3.18: Rubber-jointed hollow-shaft drive of the 70%-Low-Floor Tram NF6D by Siemens-DÜWAG 1993 (Siemens AG, A&D)

4 Commutator traction motors and their control

4.1 DC traction motor

4.1.1 DC commutator motor

Being the oldest electrical motor in existence (the first basics had been laid as early as 1830 by Ampère during lectures at the Sorbonne University in Paris), the DC commutator motor, using the subsequently described drum-type rotor pattern, was the predominant type of tractive motor until about 15 years ago.

Fig. 4.1 illustrates the general structure of a bipolar DC motor (number of pole pairs $p = 1$). The stator consists of the two magnetic poles, bearing the excitation windings and being mounted in a frame assembly that also serves as a return conduit for the magnetic flux (back, yoke). Pole shoes conduct this magnetic flux into the rotor, or anchor, resulting in an air gap beneath the poles of a constant width of just a few millimetres. Nowadays, poles, pole shoes and yoke are always laminated, similar to transformers, to ensure the flux follows the exciter-current value (or, in the case of series-wound motors, the armature current respectively).

The distance of two poles on the circumference is called *pole pitch* (τ_p), whereas the area of the circumference between the two poles is the *neutral zone*.

The level of induction in the airflow gap B_{lx} is dependant upon the local coordinate x of the circumference and is equal to:

$$B_{lx} = \frac{\mu_0}{\delta} \cdot I_E \cdot w_E \cdot \frac{1}{1 + \frac{l_{Fe}}{2 \cdot \delta \cdot \mu_r}} \quad (4.1)$$

with	δ	width of air gap
	μ_0	permeability constant $4\pi \cdot 10^{-7}$ Vs/Am
	I_E	field (exciter) current
	w_E	number of windings of one field winding
	μ_r	relative permeability (in general > 1000)
	l_{Fe}	average length of magnetic field lines in iron.

In general, the second summand in the denominator of the fraction can be disregarded in favor of the first. The flux density thus is inversely proportional to the air-gap width, resulting in the magnetic field within the neutral zone being about nil; beneath the poles, it has the value of B_L .

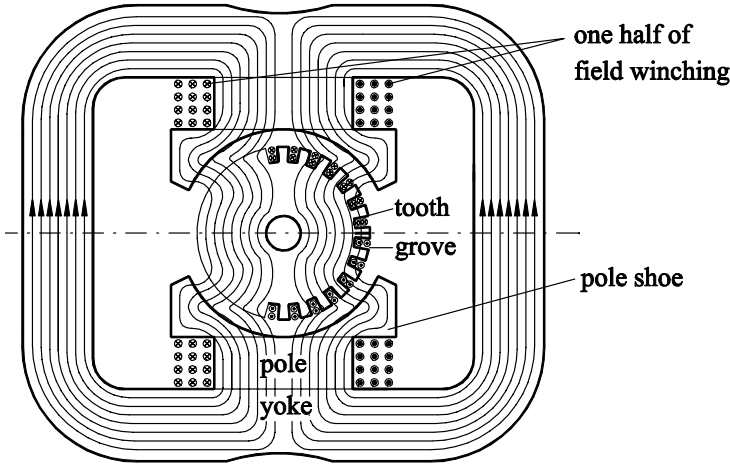


Fig. 4.1: Cross-section and exciter-field lines of a DC motor

N slots (N/p being an odd number) have been stamped into the sheet metal forming the cylindrical rotor lamination, which take up the rotor bars. At a speed of n , in each bar in the air gap (and, as can be shown, identically in each bar in a slot) voltage is induced as follows:

$$|u_i| = l_L \cdot r_L \cdot 2\pi \cdot n \cdot B_{Lx} \quad (4.2)$$

with

l_L length of lamination in axial direction
 r_L rotor radius.

Usually, two bars are arranged one over the other in every slot, called top-coil side bar and bottom-coil side bar, respectively (this being called a dual-layer winding). On one end of the rotor drum, a commutator (or collector) is affixed, which is a drum consisting of N insulated segments of copper and is firmly soldered to the bars. On the other end of the rotor, one top-coil side bar at a time is linked to one bottom-coil side bar via the end winding; the bottom-coil side bar is offset by about one pole pitch ($(N/p + 1)/2 =$ number of slots). Since the latter is always permeated by the opposite magnetic flux of the former, both bar voltages add up – at equal values – within the conductor loop. If the rotor revolves by one pole pitch, a voltage of inverse polarity is induced within the two bars of this loop. Fig. 4.2 illustrates the evolution of a loop winding for a rotor of $N = 11$ slots and serves to explain how the commutator achieves the serial connection of all bars under the same pole pitch, thus rectifying the induced loop AC voltages.

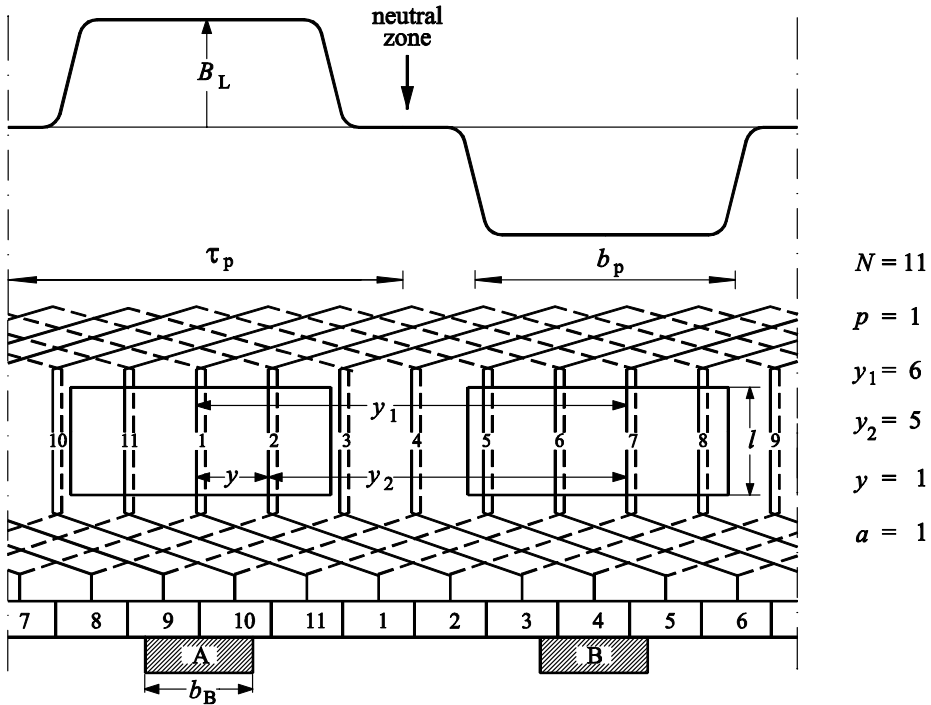


Fig. 4.2: Evolution of a dual-layer loop winding with $2p = 2$ and $N = 11$, on top peripheral exciter-field distribution

Starting with brush A which contacts segment #10, top-coil side bar 10 and bottom-coil side bar 5 (which is depicted dashed) form a loop; from bottom-coil side bar 5, one returns to segment #11 (= 10+1) and so on, until all $N = 11$ loops have been completed. The total voltage results from the series connection of the voltages induced in the top-coil side bars 10, 11, 1, 2 and 3, and the bottom-coil side bars 4, 5, 6, 7 and 9, respectively. In parallel, a second series connection is formed starting at brush A, segment #9, which series-connects to the right side of the bottom-coil side bars 3, 2, 1, 11 and 10 and top-coil side bars 9, 8, 7, 6, 5 and 4 respectively in reverse sense of circulation. In this chain, an identical voltage is induced, the number of parallel branches being $2a = 2$.

This results in all bars of the “upper” pole pitch (ie, above the dot-dashed line in Fig. 4.1, referred to the exciter-magnet system and the brushes) being connected in one direction, whereas all bars beneath the “lower” pole pitch are series-connected in the reverse direction. Accordingly, through all flowing half of the armature current I , the tangential forces (per bar)

$$F_x = 0.5 \cdot I \cdot l_L \cdot B_{lx} \tag{4.3}$$

form a uniform torque. When the rotor moves by one slot pitch, two new bars get inserted into the serial link, whereas two are removed from it. In the bars within the neutral zone, no voltage is induced, and they do not contribute to torque, either.

To sum up, the operational behaviour of the DC commutator motor can be described using the following three equations:

$$M_d = \frac{2}{\pi} \cdot I \cdot \Psi \quad (4.4)$$

$$u_i = 4 \cdot n \cdot \Psi \quad (4.5)$$

with flux linkage

$$\Psi = \frac{p \cdot N}{2 \cdot a} \cdot B_L \cdot \tau_p \cdot l_L = L_E \cdot I_E \quad (4.6)$$

B_L amplitude of flux density under pole
 L_E inductivity of field winding(s)

The bars of the “upper” rotor half, being linked in one direction, and the bars of the “lower” rotor half, being linked inversely, thus form a coil whose axis is indicated by the dot-dashed line in Fig. 4.1. When the armature current flows through the bars, an armature quadrature-axis field is excited, which is directed transversely towards the direction of the exciter field. By superposition of the two fields, parts of the rotor iron suffer from magnetic saturation; this results in inferior utilization and increased iron losses. Furthermore, the quadrature-field induces voltages in the bars within the neutral zone, which, until now, was field-free. This produces short-circuit currents over the segments short-circuited by the brushes.

Almost all railway traction motors, thus, are compensated. Fig. 4.3 depicts the compensation, or neutralizing winding, mounted in the pole shoes. The armature current is led through this winding and eliminates the armature quadrature-axis field beneath the poles. Additional commutation-pole windings also pervaded by the armature current cancel the voltages induced by the armature quadrature-axis field within the neutral zone and support the armature-current commutation by their own induced voltage in the loops crossing the neutral zone.

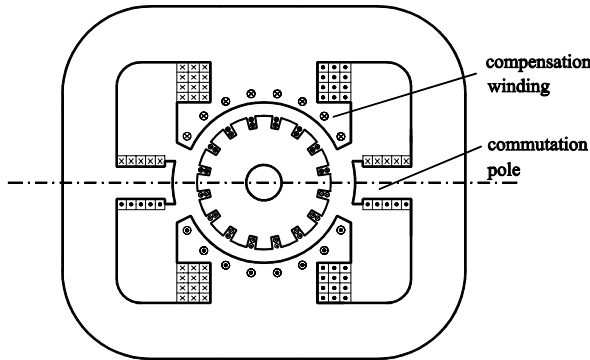


Fig. 4.3: Compensated DC commutator motor with commutation poles

Fig. 4.4 shows the Equivalent Circuit Diagram of a DC traction motor. The exciter field may be fed in various ways:

- The “classic” traction set-up is the so-called “series-wound motor”: The armature current flows through the excitation windings. Under a constant armature current, torque is about proportional to $1/n^2$; one receives an indulging, “soft” speed-torque characteristic, “naturally” adapted to the requirements of traction, with a high torque for starting and acceleration and a fast reduction of torque when speed increases; this has a stabilizing effect at slipping.

Field weakening, which is necessary for operation at constant power has to be brought about by resistors switched parallel to the excitation winding (3, “shunting”). For braking, the polarity of the excitation field must be reversed by contactors.

- Shunt or separate excitation is preferred for industrial motors, but is not widely used in classic technology due to the “hard” speed-torque characteristic; if so (“Sepex”), it requires controlled excitation converters, whose set value can be set as wished, for example, proportionally to the armature current, to emulate the characteristics of series excitation (“simulated series motor”). Field weakening and braking, however, are far easier executed.
- For Central European locomotives using thyristor-converter control, a mixed system of excitation (50/50 as the typical distribution) has proven successful [108].

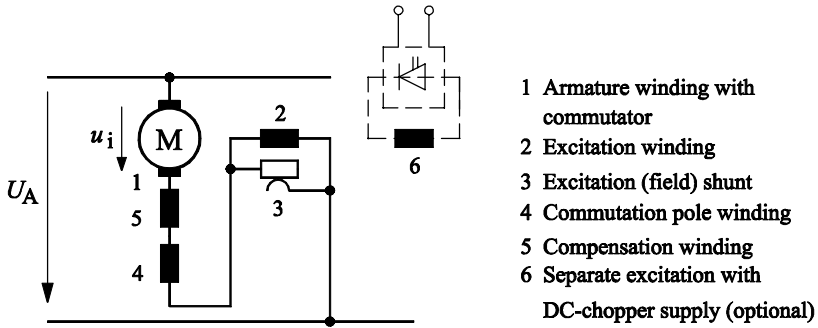


Fig. 4.4: ECD of a DC traction motor with mixed excitation

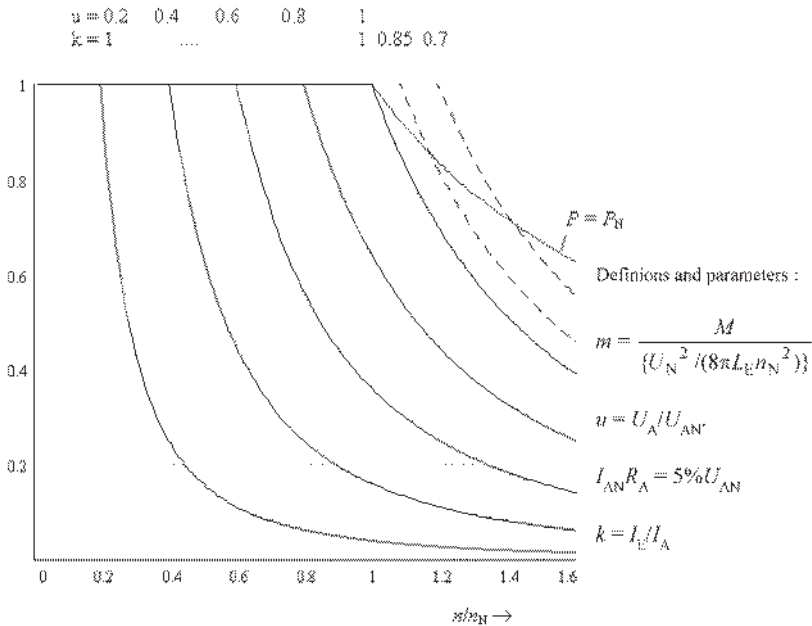


Fig. 4.5: Speed-torque characteristic of a series-wound DC commutator motor, with two shunt levels and the graph of constant(= nominal) power

Fig. 4.5 illustrates the speed-torque characteristic of a series-wound motor at constant terminal voltage (20, 40, 60, 80 and 100% U_{AN}) and $I_E = I$, as well as two levels of field-weakening (85% and 70%, dashed lines), and the graph of constant (= nominal) power. The attainable region of field weakening has to be limited in overhead-supplied traction vehicles with respect to safe commutation at pantograph bouncing (prevention of flash-over).

Fig. 4.6 shows (left) stator and (right) rotor of an eight-pole 810-kW DC commutator railway traction motor. The narrow commutation poles are clearly visible.

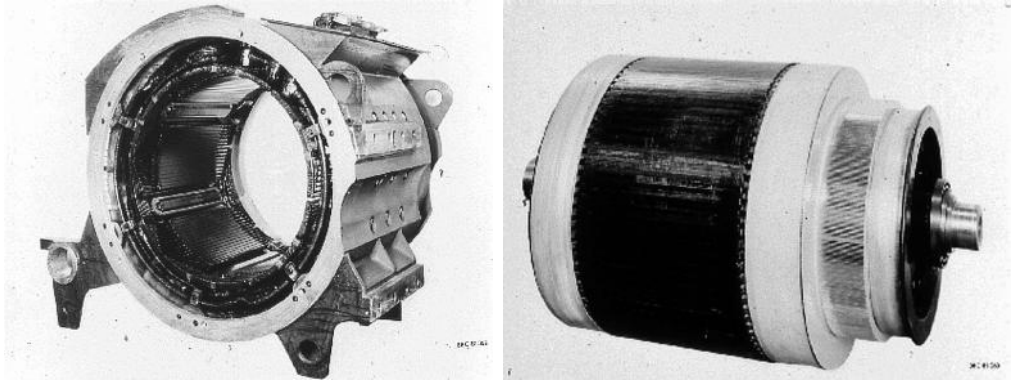


Fig. 4.6: Stator and rotor of a 3000-V/2 810-kW DC traction motor type MBg810 of locomotives Class 184 111, 112 of DB (Bombardier Transportation)

Railway motors are usually fitted with higher numbers of pole pairs ($2p = 8 \dots 14$), to reduce yoke flux and thus back thickness and overall diameter, while retaining the level of flux linkage. The highest motor power rating achieved so far is 1350 kW at a nominal revolution speed of 1100 min^{-1} (locomotive Class 1044 of ÖBB).

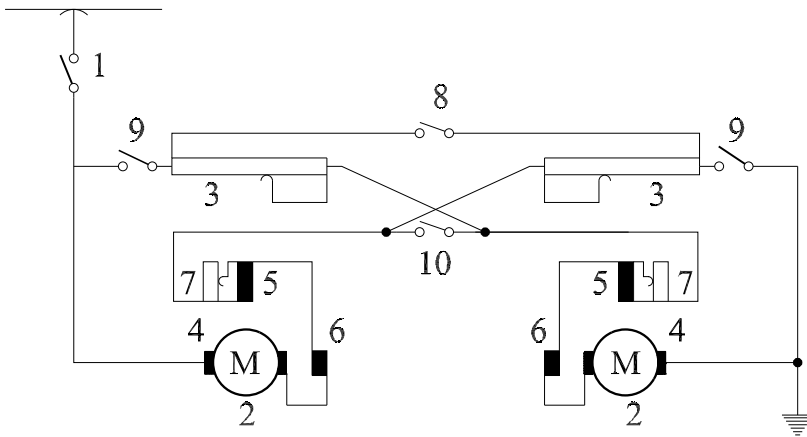
4.1.2 Variation of the terminal voltage by series resistors

Traditionally the actual terminal voltage of DC traction motors is varied by camshaft-controlled series resistors and by series-parallel regrouping of the even number of traction motors ($n = 2g$). Fig. 4.7 displays a simplified sample.

At starting the contactors 9 and 10 are open, 8 is closed; the motors are connected in series. At about half nominal speed, all resistors are short-circuited; with further increasing speed, contactor 10 is closed first, then the resistors are regrouped to maximal value, contactor 9 is closed and contactors 8 and 10 opened. Now the motor are in parallel connection. Beyond v_1 the exciter flux will be reduced by means of the field-weakening shunts 7. To avoid too big jerks in current and thus tractive effort, the starting-resistor steps must be chosen adequately small (typically 36...52 steps).

To enable braking the excitation windings have to be reversed first – as mentioned above – (which is not displayed in Fig. 4.7). The starting resistors serve as brake resistors.

As the greatest disadvantage of resistor control – besides tractive-effort sags and wear of contactors – remains low efficiency. Fig. 4.8 displays utilised and “lost” powers in dependence upon the speed in a schematic manner ($\eta_{\text{mot}} = 1$ is assumed).



- | | | | |
|---|--------------------|----|--------------------------|
| 1 | Main contactor | 6 | Commutation-pole winding |
| 2 | Traction motor | 7 | Field-weakening shunt |
| 3 | Starting resistor | 8 | Series contactor |
| 4 | Armature winding | 9 | Parallel contactor |
| 5 | Excitation winding | 10 | Bridge contactor |

Fig. 4.7: DC series-wound-motor drive with camshaft-controlled resistors [B1]

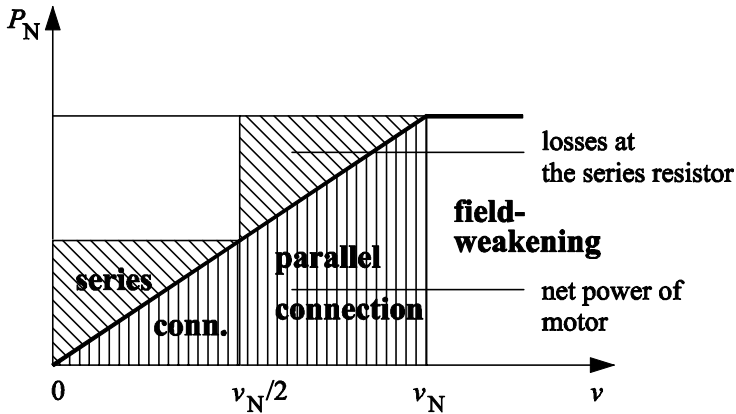


Fig. 4.8: Power balance for resistor control and series/parallel regrouping

4.1.3 Control of motor voltage in DC-supplied systems by means of a DC chopper

With thyristors with small hold-off time, so-called „fast“ devices, becoming available for self-commutated power electronic circuits in the 60es, first electric traction vehicles were equipped with DC choppers ([27], [28], [29]). Fig. 4.9 shows the main circuit diagram, together with the relevant time-dependent quantities.

As the inductive load maintains the current, a parallel or by-pass way must be offered to it, when T is to be turned off (the switch opened). This is done by a “free-wheeling” path with zero source voltage. As U_1 will not be reversed, a simple diode D is sufficient: When T is turned off, its voltage rises to $U_1 + \Delta$, Δ being a few volts; with that the voltage over D changes from $-U_1$ to $+\Delta$, D will start to conduct. At turn-on of T D will be extinguished by a circular current $U_1 - T - D$.

A controller varies a in such way, that at variable motor e.m.f. \bar{u}_2 ($= U_1$) the pre-set current average value \bar{i}_2 is kept. As the valve group consisting of T and D represents a lossless converter, the equation

$$P = U_1 \cdot i_1 = \bar{u}_2 \cdot i_2 \quad (4.8)$$

holds.

Consequently:

$$i_1 = a \cdot i_2 \quad (4.9)$$

In the 3rd line the voltage over the “smoothing reactor” L_2 , inserted between chopper and motor armature, is displayed:

$$u_{L2} = u_2 - \bar{u}_2 \quad (4.10)$$

The value of the inductivity has to be chosen in that way, that at given switching frequency f_z the output current peak-to-peak change Δi_2 (the double ripple value), driven by the time-integral Fu of the voltage over L_2

$$\Delta i_2 = Fu / L_2 = \frac{1}{L_2} \int u_{L2} dt = \frac{1}{L_2} \cdot \overline{|u_{L2}|} \cdot \frac{T}{2} = \frac{1}{f_z L_2} U_1 \cdot a(1-a) \quad (4.11)$$

does not exceed the admissible value, in regard of the commutator and the commutation-pole field of the DC motor (e.g. 20 ... 40 % of i_{2N}).

The 4th line displays output current i_2 and its partitioning into transistor current i_1 and diode current i_D , while the 5th line decomposes the chopper input current ($= i_1$) into its average value \bar{i}_1 and the alternating part, which must be delivered by the input filter capacitor C_1 , to keep the source current free from disturbant AC portions (cf. section 14.2.2). The (double) ripple value of the filter voltage is determined by the time-integral of the AC part of the chopper input current:

$$\Delta u_1 = \frac{Fi}{C_1} = \frac{1}{C_1} \int (i_1 - \bar{i}_1) dt = \frac{1}{f_z C_1} T_2 a \cdot (1-a) \quad (4.12)$$

Here the inductivity of the input filter choke L_1 is assumed as big enough, so that the resonance frequency

$$f_r = \frac{1}{2\pi\sqrt{L_1 \cdot C_1}} \ll f_z \quad (4.13)$$

will be sufficiently smaller than the switching frequency f_z of the chopper. The maximum ripple of output current and input filter voltage occurs at a duty cycle of 50% ($a = 0.5$).

To deepen the experience, Exercise 17.4 “DC traction motor fed by a DC chopper” is provided.

Operating m identical choppers with (equal) switching periods T staggered by T/m , the output current ripple as well as the input filter voltage ripple can be reduced considerably, as explained in section 14.2.2.

By regrouping transistor T and diode D , as shown in Fig. 4.10, the DC motor can recuperate its braking power into the DC line (regenerative braking, separate excitation or reversing the series-connected field provided): When the load is short-circuited by transistor T turned on via the inductor ($u_2 = 0$), the absolute value of the armature current rises. After turn-off of T the current flows via the separation diode D , which will now conduct, into the line against the higher source voltage U_1 , forcing the absolute value of the current to go back again. Turning on T again, the diode is turned off (“step-up chopper”, “boost converter”).

The voltage control factor is now

$$a = 1 - T_1/T, \tag{4.14}$$

the formulae for the current or input filter voltage ripple remain unchanged.

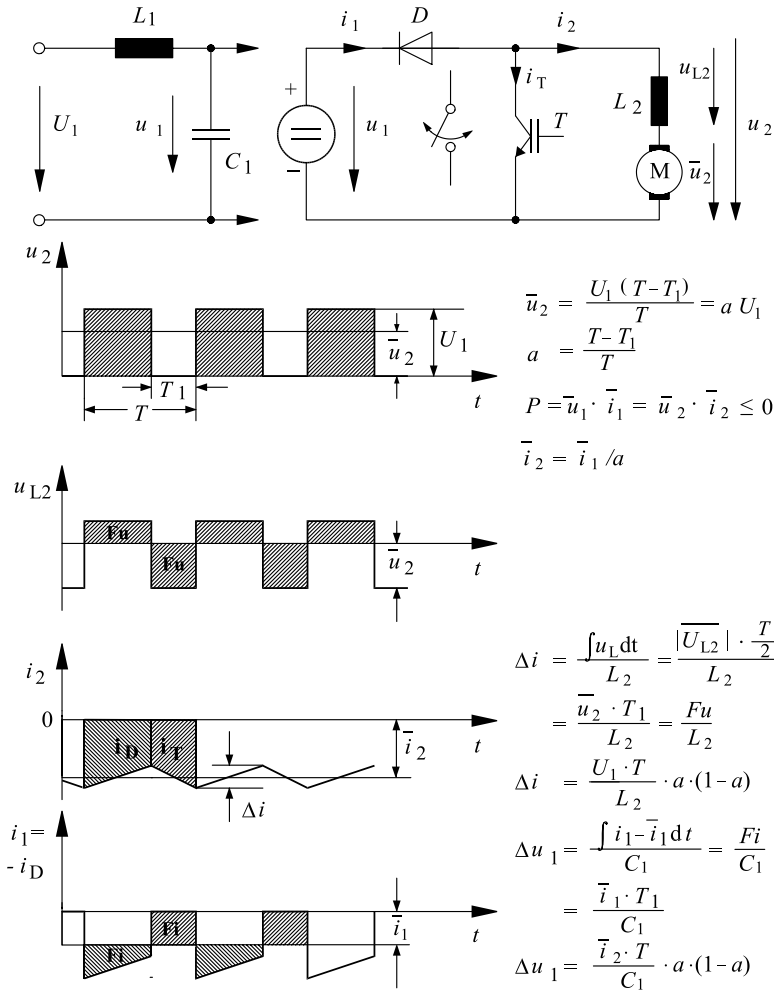


Fig. 4.10: DC chopper in step-up connection (regenerative braking operation)

Regrouping may be performed by contactors, Fig. 4.11, as e.g. in the tramcar M8C (Fig. 10.12); with decaying semiconductor price, two-quadrant choppers (for two directions of current) were increasingly used, cf. Fig. 4.12. (The thyristor symbol with two lines designates a thyristor with forced-commutation circuit (cf. section 6.6.1) or a GTO thyristor (section 6.6.2)).

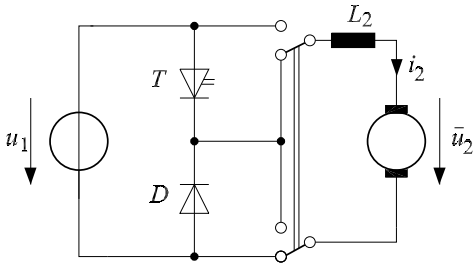


Fig. 4.11: Braking connection of 1-quadrant DC chopper with contactors

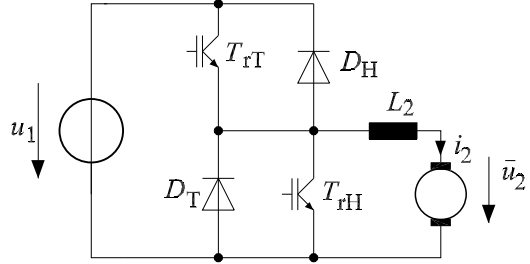


Fig. 4.12: 2-quadrant DC chopper for two directions of current

A braking resistor remains necessary in DC railway systems, as nearly all substation rectifiers are of the diode type, not capable of recuperation. In the beginning the resistor was connected only by simple contactors, later on via a controllable additional brake chopper, which controls the voltage over the input-filter capacitor to the value of $U_{1\max adm}$ (e.g. 900 V in 750-V light rail systems).

Fig. 4.13 shows the combined DC-chopper circuit, employed by BBC preferably, with “automatic field weakening“ (AFS).

Driving: In the active interval the armature current will be increased via D_1-T_2 , the excitation current being in free-wheeling status via D_2 . With blocking T_2 , the armature current is guided into the free-wheeling status via D_3 and the excitation winding, and forces armature and excitation current to be identical. Only with high duty cycle (short turn-off time) the field current is left behind the armature current and the field will be weakened. Q_1 serves as reversing switch group.

Braking: This operation is rather intricate in this circuit:

- 1 The direction of the exciter current remaining constant, the direction of the armature current is to be changed by Q_1 . T_2 remains blocked, in consequence D_1 , too.
- 2 Tramcars and Light Rail vehicles only applying this circuit need a braking effort equal to nominal tractive effort at maximum speed v_{\max} , to be compatible with brake deceleration values of about 3 m/s^2 of automobiles using the same traffic area². Thus the maximal braking power is bigger than motoring rated power by a factor of $v_{\max}/v_1 = 2.2...2.5$ (neglecting motor and chopper losses).
- 3 Brake resistor R_B and compound brake resistor R_V have to be designed for that demand, to be able to dissipate the peak brake power if the line is not capable of absorption. The motor e.g. is raised to $\sqrt{v_{\max}/v_1} = 1.5...1.6$ times nominal line voltage.
- 4 R_V will be chosen so that the nominal admissible line voltage $U_{F\max}$ (e.g. $1.2 U_{FN}$) drops at R_B . If the line is able to take over the brake power, T_3 can be turned off.

² In Germany 2.7 m/s^2 have to be guaranteed, by help of magnetic rail brakes (subchapter 11.2)

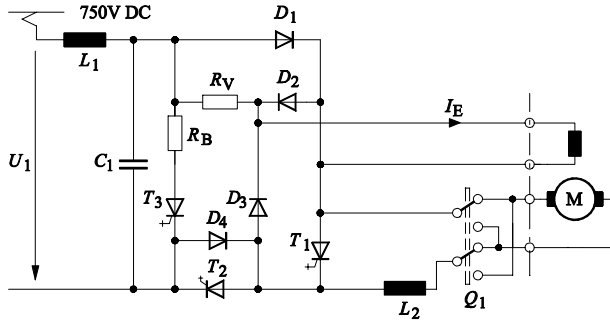


Fig. 4.13: Chopper control for driving and braking with Automatic Field Weakening (AFS)

- 5 In the speed range of $v_{\max} \geq v \geq \sqrt{v_{\max}/v_1} \cdot v_1$ the field must be weakened, so that the motor e.g. does not exceed the cited value. To that purpose the excitation current will be controlled via the duty cycle of T_1 , with D_2 acting as free-wheeling diode.
- 6 In the speed range of $\sqrt{v_{\max}/v_1} \cdot v_1 > v \geq v_1$ the brake power falls back to the value of $P_{N'}$, with full excitation current; the same holds for U_{ri} , falling back to U_{FN} . Subsequently in the range of $v_1 \geq v \geq 0$ U_{ri} is reduced proportional to v down to zero. At the same time the armature current drops to zero, while I_E – by a higher duty cycle of T_1 – will be kept on its nominal value.

4.1.4 Control of the motor voltage with AC systems by phase-control rectifiers

Commutator motors cannot be used with 50 Hz directly in the power range of traction motors, as it is possible with $16^{2/3}$ Hz, as treated in the following subchapter 4.2. To enable 50-Hz electrification (cf. subchapter 13.2) the simplest solution was the transformer with a tap-changer (similar as treated in section 4.2.2) and a diode bridge rectifier (Fig. 4.14), rendering heavy rotary converters obsolete, which were employed occasionally.

They came into service in Switzerland (BLS Ae 4/4 II), Sweden (SJ Rb1), Great Britain (Class 85...87) and Germany (Class 320 DB) in the sixties, when silicon diodes with suited rating became available. Due to their minor operational behavior as traction effort sags and wear of contacts, thyristors controlled by phase-angle delay were substituted for diodes and tap-changer, as soon as they were available. In the fifties already Ignitrons were used, as e.g. in the French locos shown in Fig. 1.5. Fig. 4.15 displays the most popular “two-pulse bridge in half-controllable connection of pairs of arms with sequential phase control”, with the pertaining voltage and current time-diagrams ($L_d \rightarrow \infty$, $u_K \rightarrow 0$, $w_{\text{sekI}} = w_{\text{sekII}}$, $U_{\text{sekI}} = U_{\text{sekII}}$). The basic features of sequential control are described in [V2], subchapter 4.6, or in [30], [31].

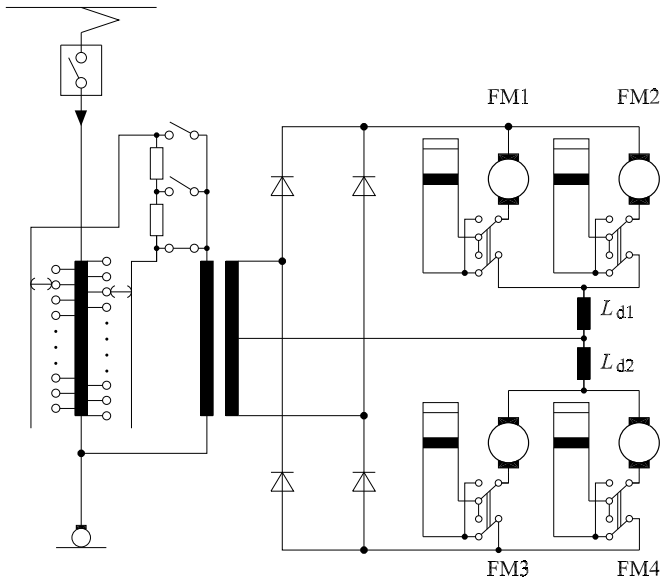


Fig 4.14: Circuit diagram of a „diode locomotive“ with high-voltage switch gear and undulating-current motors (BLS Ae 4/4 II)

The ideal no-load direct voltage (neglecting all resistive and transformer leakage voltage drops) is

$$\bar{u}_{di} = \frac{4 \cdot \hat{u}_{sek}}{\pi};$$

by sequential phase-angle control it is reduced to the controlled ideal no-load direct voltage

$$\bar{u}_{di\alpha} = \bar{u}_{di} \cdot \left\{ \frac{2 + \cos \alpha_I + \cos \alpha_{II}}{4} \right\} \tag{4.15}$$

$$\text{with } \left\{ \begin{array}{l} \pi > \alpha_I \geq 0, \quad \alpha_{II} = 180^\circ, \quad \text{for } a = \frac{\bar{u}_{di\alpha}}{4 \cdot \hat{u}_{sek}} \leq 0.5 \\ \alpha_I = 0, \quad 180^\circ > \alpha_{II} \geq 0, \quad \text{for } 0.5 < a = \frac{\bar{u}_{di\alpha}}{4 \cdot \hat{u}_{sek}} \leq 1 \end{array} \right\}$$

The real direct voltage – with respect to the inductive direct voltage regulation d_x , the resistive direct voltage regulation ($d_r = \frac{1}{\bar{u}_{di}} \sum R_i \cdot \bar{i}_d$) and the semiconductor threshold voltage ΣU_{T0} – is then

$$\bar{u}_d = \bar{u}_{di\alpha} - \bar{u}_{di} \cdot (d_x + d_r) - \Sigma U_{T0} \tag{4.16}$$

with the inductive and resistive direct-voltage regulation expressed by the corresponding transformer data and the operational conditions

$$d_{x,r} = u_{x,r} \cdot \frac{1}{\sqrt{2}} \cdot \frac{\bar{i}_d}{\bar{i}_{dN}} \cdot \frac{U_{sekN}}{U_{sek}}; \tag{4.17}$$

(for the two-pulse bridge circuit (B2)).

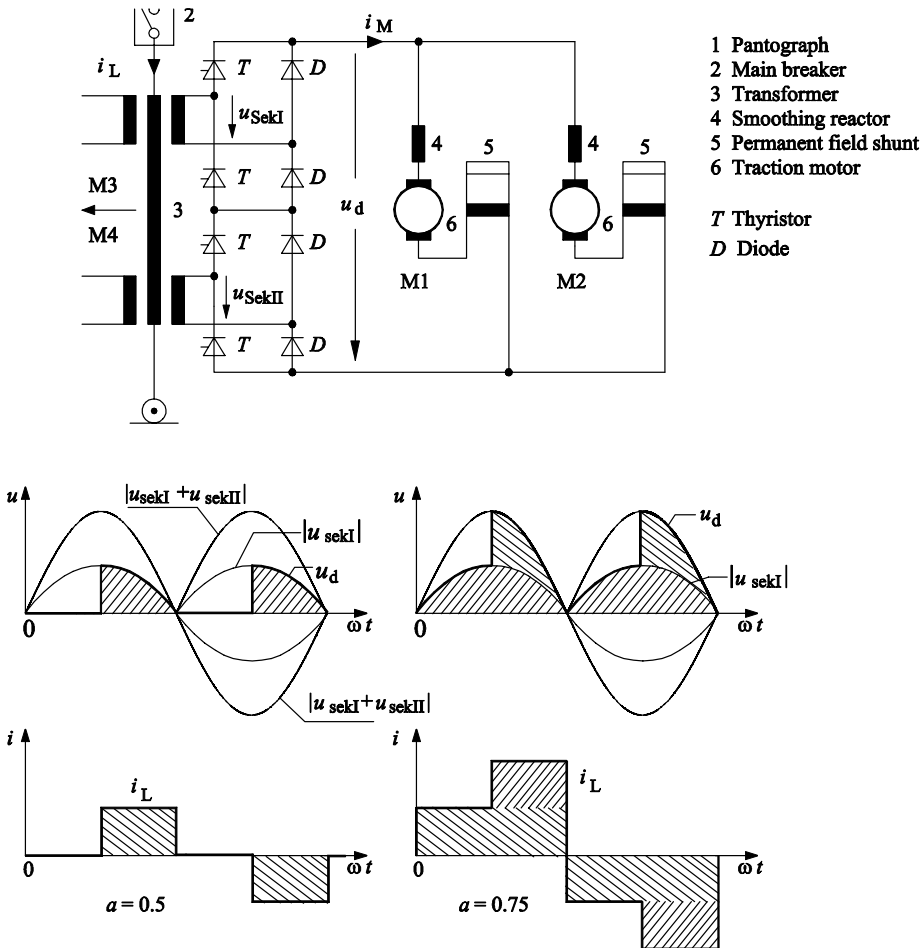


Fig. 4.15: Two-pulse bridge in half-controllable connection of pairs of arms with sequential phase control (EEW-TUD)

Regenerative braking by means of a bridge in fully-controllable connection enabling $\bar{u}_d < 0$ has rarely been used, as with respect to commutation failure at unreliable pantograph contact and subsequent conduction through the control angle has to keep a too big margin from 180° . But then the displacement factor $\cos \varphi_i$ is too poor ($\gg -1$).

The smoothing reactor limits Δi to 30...50 % i_N ; from that the denomination “undulating-current motor” is derived. In series-wound motors the voltage induced by this ripple of the excitation current in the rotor – which will be short-circuited by the brushes, cf. section 4.2.1 – is reduced by a resistive permanent shunt

The dimensioning of such a thyristor converter for a high-power locomotive is treated in Exercise 17.5 “Two-pulse bridge in half-controllable connection of pairs of arms with sequential phase control”.

The half-controllable connection reduces the fundamental reactive power considerably, to roughly $\approx 50\%$ of the value at full voltage yield; the same holds for the sequential control of two bridges (cf. [V2] and subchapter 4.3). But still the $\cos \varphi$ is far from unity [31].

In the late seventies the “quenchable” half-controllable bridge circuit (with the German acronym LUB, [32]) was developed by AEG. It complements the phase-angle control of the half-controllable connection of bridge I (delay angle α) by a quenching-angle control, by means of forced commutation for the thyristors T_L , cf. Fig. 4.16. The quenching angle is called β .

It can easily be seen that the quenching-angle control shifts the current block towards the maximum instantaneous value of the line voltage, attaining $\cos \varphi_i \approx 1$. But this circuit was used in few types only, as it became soon obsolete by the upcoming three-phase drive technology with voltage-source inverters.

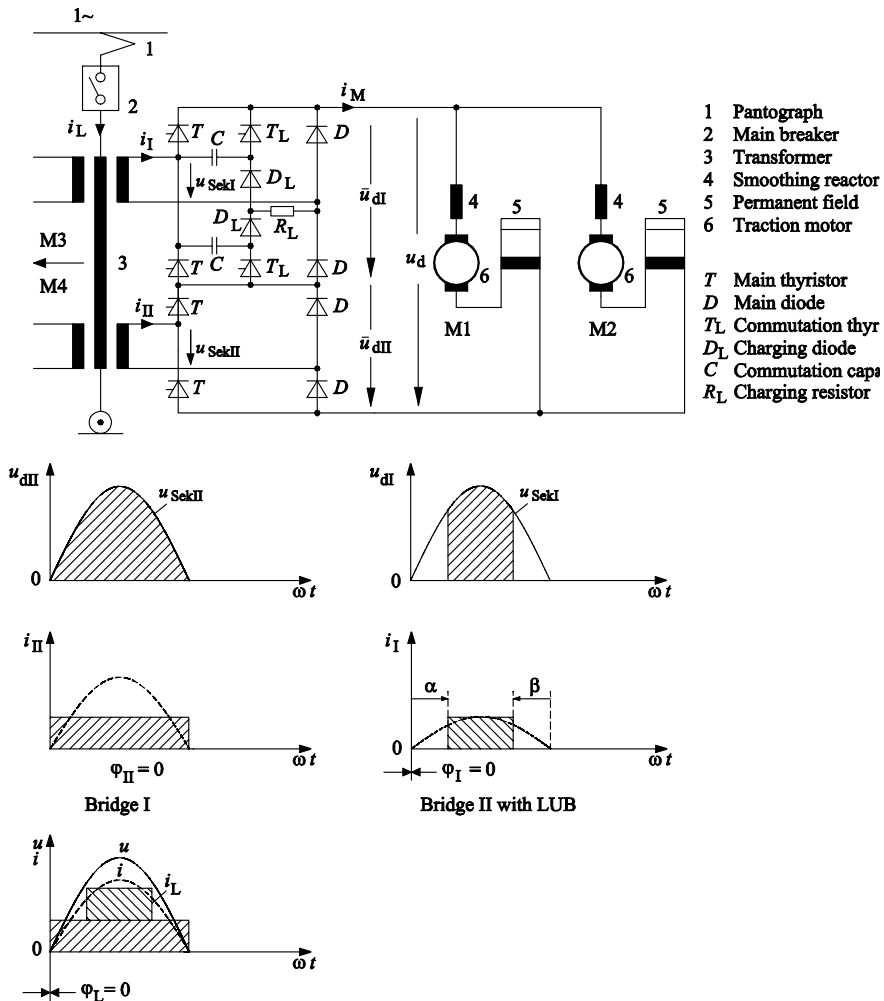


Fig. 4.16: Two-pulse bridge in half-controllable connection of pairs of arms with sequential phase control; bridge I quenchable (LUB) (EEW-TUD)

4.2 AC traction motor

4.2.1 AC commutator motor

As described previously, the wish to operate large long-distance railways with high nominal voltage and thus tolerable transmission losses efficiently was the impulse for AC electrification.

On principle, the commutator motor can be operated with AC, but only in series-wound connection, not in shunt connection, as the high inductivity of the shunt exciter winding would let the excitation current lag by nearly 90° , in respect to the armature voltage. But then an armature current with an aspired $\cos \varphi_1$ near unity would not deliver any torque.

The oscillating exciter field induces an AC voltage in the armature, the so-called transformer e.m.f., which will just be short-circuited by the brushes, as can be derived from Fig. 4.2. It drives a current, limited only by the small values of the resistance and the inductance of the rotor winding and the brush voltage; it is a heavy additional burden for the collector segments in the neutral zone. For that reason the induced voltage must be limited to

$$U_{i\sim} = \sqrt{2} \cdot \pi \cdot f_L \cdot \Phi_{\text{pol}} < 3 \text{ V}, \quad (4.18)$$

to reduce arcing. To limit this current decisively, the nominal value of the frequency of AC railway systems was selected to be $50 \text{ Hz}/3 = 16 \frac{2}{3} \text{ Hz}$ only (cf. page 10; 25 Hz was chosen in U.S.A. for the electrification of the Pennsylvania Railroad trunk line). Additionally a high number of poles ($2p = 8 \dots 14$) keeps the individual pole flux Φ_{pol} small, at an appropriate value of the flux linkage Ψ . But all these measures taken were not sufficient to establish operation with tolerable brush wear. Only the invention of the resistive shunts to the commutation-pole winding by H. Behn-Eschenburg 1903 fixed the problem: It shifts the phase of the commutation-pole flux, so that the induced voltage in the neutral zone is just compensated.

As the voltage induced by the AC field does not depend on speed, as the voltage induced by the commutation poles, an optimal compensation of $u_{i\sim}$ and thus a sparkless commutation is possible only in a small speed range. This is selected as about 70...80 % of rated speed n_1 , being the most important. Limiting the quadrature-axis voltage induced by the AC field renders a satisfying value of the $\cos \varphi_1$ near 0.95 – at least in the range of rated speed. In the starting region values of only ≈ 0.3 must be taken into account.

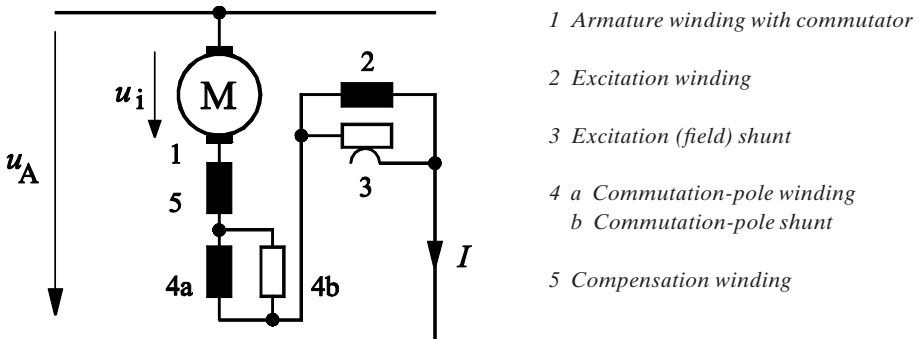


Fig. 4.17: Equivalent Circuit Diagram of an AC commutator motor

The AC traction motor has to be built with a fully laminated iron core and with compensation windings, due to the AC exciter flux. As exciter field and armature current oscillate with line frequency f_L , torque will pulsate with twice the line frequency. The amplitude of this pulsation exceeds the mean value, if $\cos \varphi_1 < 1$; negative instantaneous values occur. They lead to the lifting of the teeth of the toothwheels in rigidly coupled drives, and thus to noise and wear, which are tackled by a rotary-elastic coupling in the drive chain, as e.g. in the AEG-Westinghouse drive or the SSW rubber circular-spring drive (subchapter 3.2).

4.2.2 Control of motor voltage with the AC commutator motor

Generally, the motor voltage was varied by the tap-changer of the main transformer. Up to $P = 2,500$ kW the simple low-voltage control was applied; Fig. 4.18 gives a very early and simple example (Class 169 of DB, $P = 350$ kW, 1907).

The low-voltage taps (in most cases of an autotransformer) are connected alternately via camshaft-controlled contactors to two bus bars, which are connected by a further autotransformer ("current-divider reactor") with the motor terminals. This reactor limits the circular current at change-over, when both contacts lead current simultaneously for the necessary overlap, as interruption is not allowed in an inductive circuit.

With bigger power, the switch-gear will be too bulky and act too loud. It was substituted there for the high-voltage tap-changer switch-gear, commutating much smaller currents. Fig. 4.19 displays the schematic diagram of the control of the express locomotive Class 103 of DB. Since 1965, the main contactor in series to the tap-changer has been equipped with anti-parallel thyristors [33], which are only fired for the commutation of the tap currents.

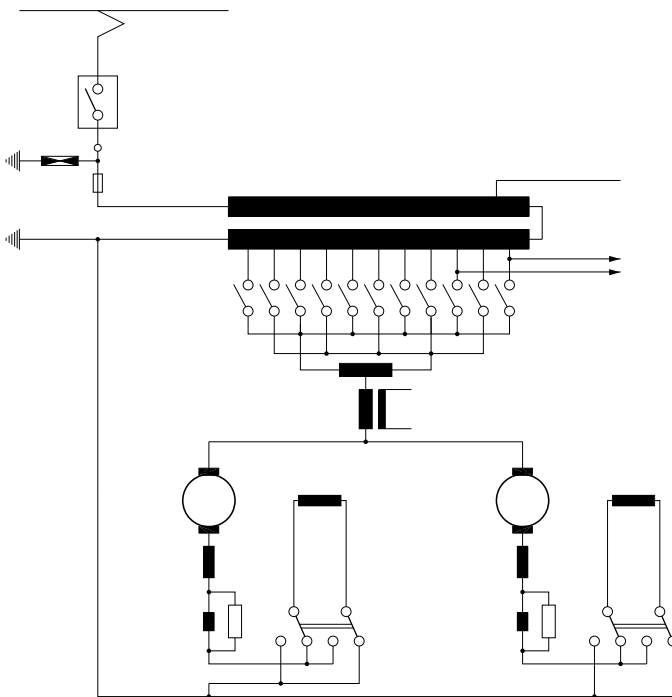


Fig. 4.18: Low-voltage tap-changer control of AC traction vehicles Schematic circuit diagram used with traction vehicles up to some 2500 kW

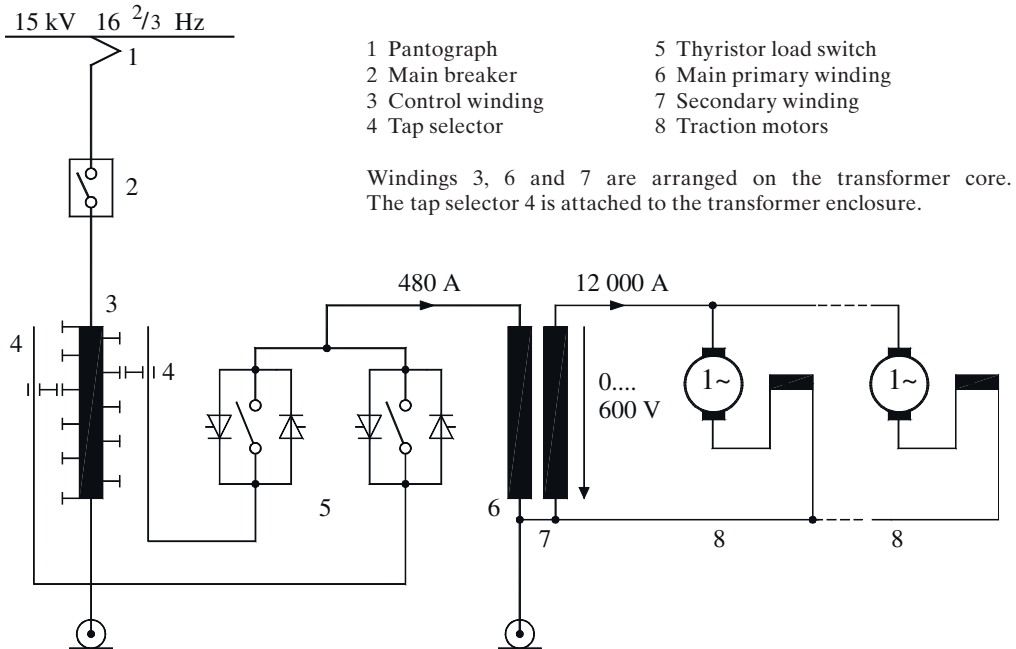


Fig. 4.19: High-voltage tap-changer control with thyristor switch

Thus the contactors leading the permanent current and the tap-changer contactors are opened without current and thus with minimal wear; a current-divider reactor is not needed anymore. In locomotive Class 103 the control winding has 39 steps, to minimize the sags of the traction effort at tap change-over.

The last stage of development in the control of the AC commutator motor is represented by the AC controller, brought into service by LEW Hennigsdorf in the locomotives Class 155/156 and 112/143 of DR (Deutsche Reichsbahn of former GDR) [34]. In contrast to the high-voltage tap-changer control with thyristor switch described before, the thyristors are now actuated in phase-angle delay control, gapping the voltage differences of the taps without any jerk in tractive effort; see Fig. 4.20.

In braking operation the tractions motors are supplied with separate excitation, e.g. with DC, working as DC generators on braking resistors; independence of line voltage will be reached by battery excitation. In the Alpine countries as Switzerland or Austria AC excitation enabling recuperation was preferred, shifting the phase of the excitation current suitably by special means, such as capacitors. The multitude of braking excitation circuits cannot be treated here, as being historic now; the interested reader's attention is called to the famous book of K. Sachs [B10], leaving no question open.

Modern locomotives with DC or AC traction commutator motors achieve now a constantly controllable tractive effort, without sags, but suffer from the rather heavy motor (e.g. 3,850 kg at 1250 kW rated permanent power and 1100 rpm), with no further potential of development and needing intensive maintenance.

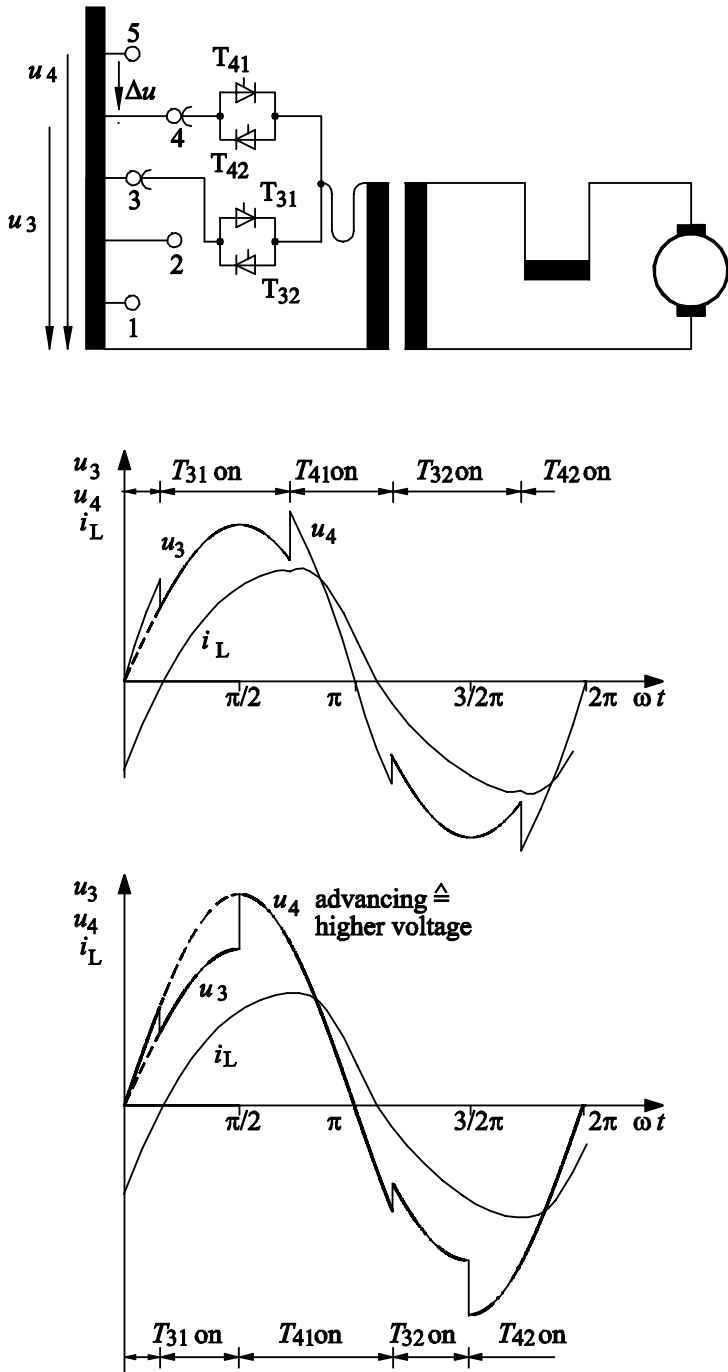


Fig. 4.20: LEW high-voltage tap-changer control with AC controller

5 Synchronous traction motors and their control

Electric machines based on the principle of rotating fields are widely known to be free from the limitation of the (root of the) product ($P \cdot n$), caused by the commutator [V1]. They can be built for highest power ratings (up to 2 GVA at 1500 min⁻¹) as well as for highest speeds (10,000 min⁻¹ in the multi-MW range). They can be subdivided into synchronous and asynchronous (or induction) machines. Thanks to the higher speed they have distinctly less mass than the commutator motor at same rated power, and they are – especially in the form of squirrel-cage induction motors (cf. chapter 6) – extremely robust and nearly free of maintenance [35].

In synchronous machines speed is tightly fixed to the supply frequency:

$$f_s = n \cdot p \tag{5.1}$$

Due to this fact the synchronous machine – apart from being used as generator in diesel-electric traction vehicles, using a rectifier – can only be applied as motor by means of a variable-frequency inverter in traction.

5.1 Synchronous motor

Generally, the stator bears a three-phase induction winding and the rotor a DC-excited winding, which is supplied by slip rings.

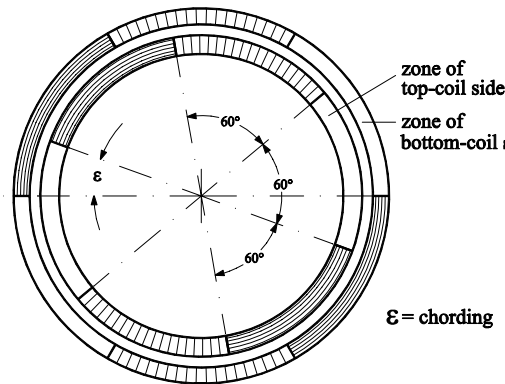


Fig. 5.1: Winding zones of a chorded dual-layer three-phase stator winding

Fig. 5.1 exhibits the winding zones of a two-pole dual-layer three-phase winding with two times six zones. Zones of top-coil and bottom-coil side bars belonging together are displaced not by an angle of π , but by $\pi - \epsilon$ ("chording"). This attenuates the harmonics of the voltage in the stator windings, induced by the rotor field of mainly trapezoidal spatial distribution. Fig. 5.2 shows one (of three) phase windings with $q = 3$ slots per phase and pole (concentric lap winding). The axes of the three-phase windings are displaced by $\pm 120^\circ$ in the electric phase-angle reference ($= 120^\circ/p$ mechanically) against each other. The turning rotor induces a symmetrical (balanced) three-phase voltage system, which is represented in the single-phase ECD by the phasor of the synchronously induced voltage (e.m.f.) \underline{E}_p .

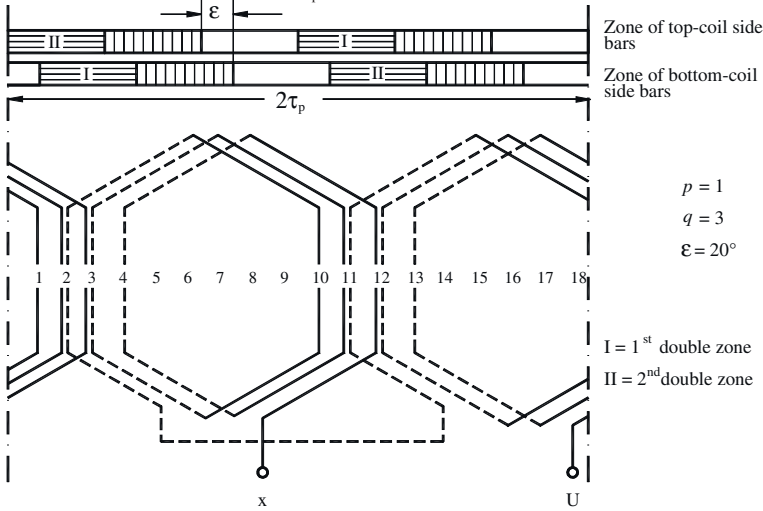


Fig. 5.2: One chord of a three-phase dual-layer concentric lap winding ($p = 1, q = 3, \epsilon = 20^\circ$)

A balanced three-phase current system impressed into the three stator windings excites a rotating field, running round with the angular frequency $\omega_s = 2\pi \cdot f_s = 2\pi \cdot n \cdot p$ with constant amplitude [V1]. If it leads the exciter field by 90° , the synchron machine works as a motor, with 90° phase lag as a generator. If both fields are in phase, the synchronous acts like a reactor ("synchronous compensator"), in counter-phase like a capacitor (consumer arrow system).

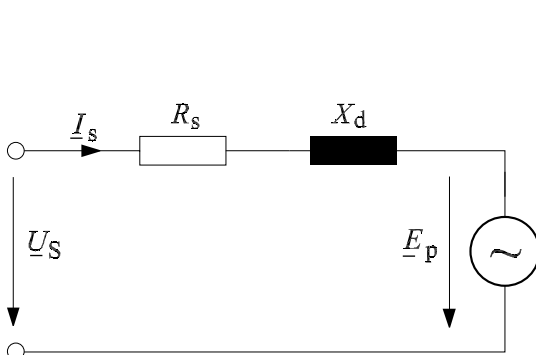


Fig. 5.3: Single-phase ECD of synchronous motor

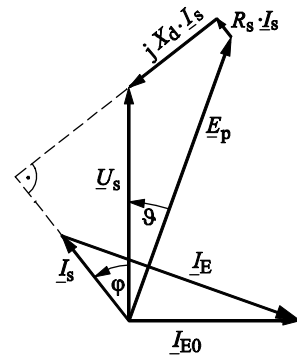


Fig. 5.4: Phasor diagram, over-excited motoring operation

The voltage induced by the stator field, which is proportional to the stator current, is represented in the ECD as voltage drop over the so-called “synchronous reactance” X_d . The main equations describing the operational behavior are (Fig. 5.3 and 5.4):

$$\underline{U}_s = R_s \cdot \underline{I}_s + jX_d \underline{I}_s + \underline{E}_p = jX_d \cdot \underline{I}_{EO} \quad (5.2)$$

$$\underline{E}_p = j \cdot \omega_s \cdot L_E \cdot \frac{k_E}{k_A} \cdot I_E = jX_d \cdot \underline{I}_E' \quad (5.3)$$

with ω_s : $2\pi \cdot f_s$
 L_E : Inductivity of exciter circuit
 I_E' : Equivalent exciter-three-phase rms phasor
 k_E/k_A : Winding transformation factor (rotor to stator system)

$$M_d = 3 \cdot \frac{U_s \cdot E_p}{\omega X_d} \cdot \sin \vartheta = P_{\text{mech}} \cdot \frac{P}{\omega} \quad (5.4)$$

with ϑ : Synchronous displacement angle

When a load impact retards the rotor in respect to the stator rotating field, the synchronous angle ϑ increases, and by that the delivered torque. This gives the synchronous machine an oscillatory behaviour, which is to be damped by the damper winding on the rotor. In addition, this attenuates all harmonic fields excited by spatial winding harmonics and stator-current harmonics [V1].

5.2 Feeding the synchronous traction motor with a load-commutated inverter

In the over-excited operation mode – as depicted in Fig. 5.4 – the synchronous motor can be fed by a simple thyristor bridge in the inverter mode with variable frequency and thus speed; the synchronous e.m.f. E_p acts as commutation voltage (“load-commutation”). In motor operation the converter is in the inverting mode with $90^\circ \leq \alpha \leq 150^\circ$, in braking operation in the rectifying mode with $0 \leq \alpha \leq 90^\circ$ (e.g. [V2], subchapter 4.7). Fig. 5.5 displays in the left upper corner the ECD of the circuit (which is often called “converter motor”), in the upper right corner the two quadrants in the M - n plain with positive speed and below the time-diagrams of the three-phase motor terminal voltage system and the three block-shaped stator currents i_1, i_2, i_3 ; first of all in generator or braking operation with $\alpha = 0$, then in motor operation ($\alpha = 150^\circ$). At the bottom line the pertaining DC-link voltage u_d can be seen. Its average value is delivered by a phase-angle controlled line single-phase bridge, with the smoothing reactor L_d taking up the different voltage-time integrals of machine-side and line-side bridges and keeping the DC-link current (nearly) constant. Torque contains a proportional ripple, with dominant sixfold stator frequency pulsation.

The firing pulses of the machine-side converter are synchronized with rotor angle by an impulse encoder mounted on the rotor shaft.

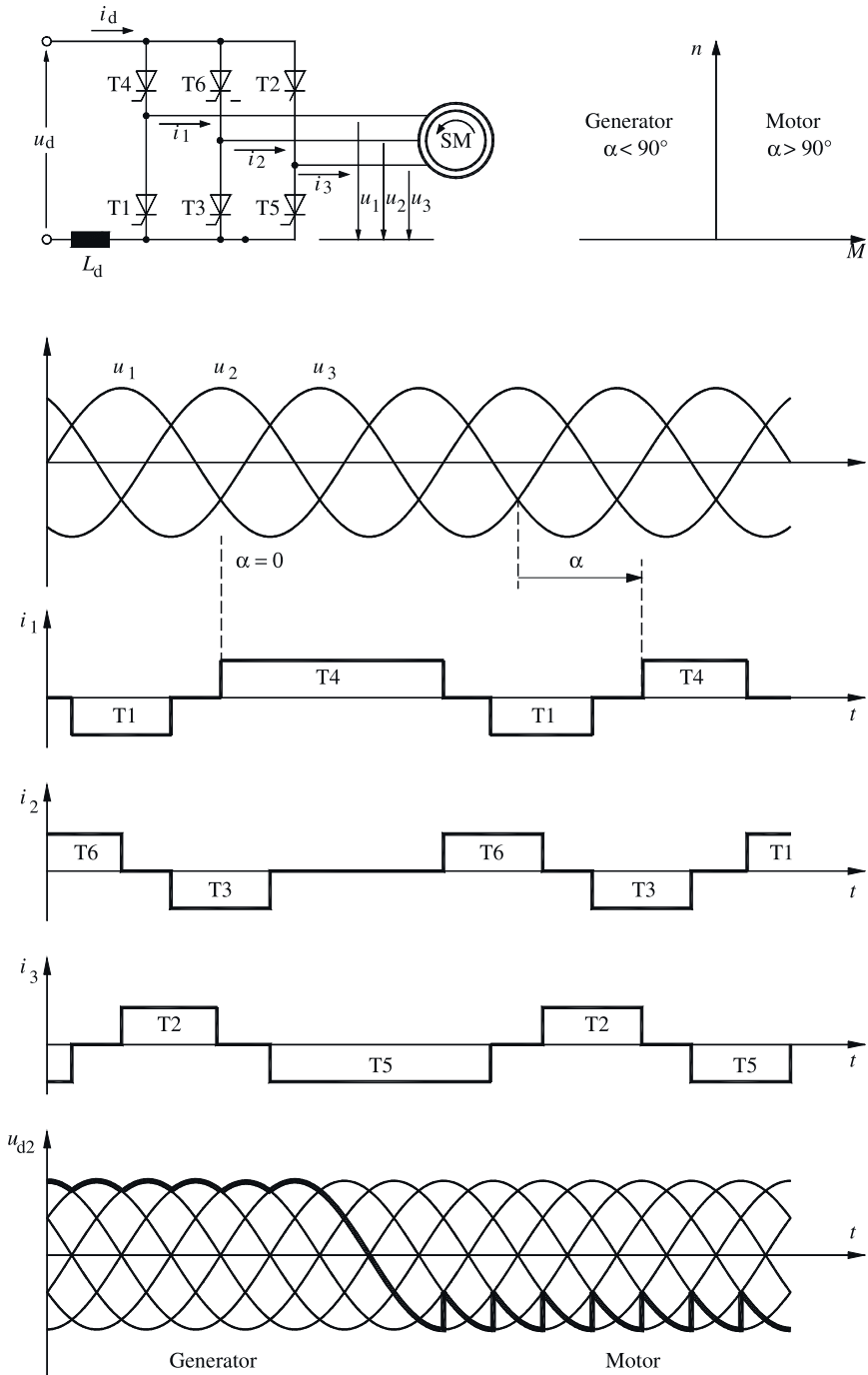


Fig. 5.5: Synchronous motor fed by load-commutated converter (EEW-TUD)

Fig. 5.6 shows the schematic circuit diagram of the French TGV-Atlantique two-system high-speed trains, later-on followed by the Thalys HSTs as a three-system variant, including 1AC 16 ²/₃ Hz, too. The two synchronous traction motors of each motor bogie in the motor headcars (same as Fig. 2.8), are equipped with six-pulse thyristor bridges (B6C) in series. In the 50-Hz power supply system they are supplied with DC power by two two-pulse bridges in half-controllable connection of pairs of arms with sequential phase control; thus recuperative braking is not possible. Under DC 1500 V the thyristor T_{CH} – a Gate-turn-off (GTO) thyristor (cf. section 6.6.2) is operated as a DC step-down chopper, with the diodes of the half-controllable connection acting as free-wheeling path. Switchable line filters F compensate the reactive power of the line converter [36], [37], [38].

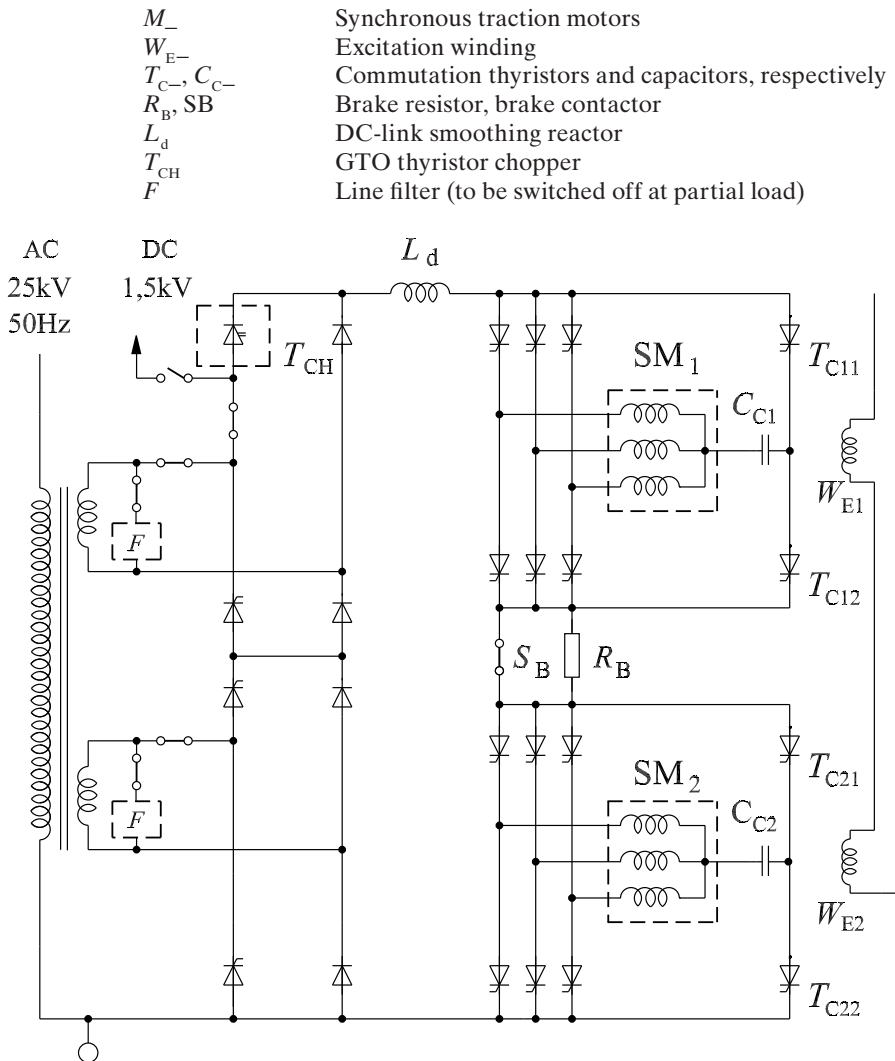


Fig. 5.6: Synchronous motor drive of TGV-Atlantique of SNCF

For braking the DC-link voltage is set to zero, the brake contactor S_B is opened and the brake resistor current is controlled via the phase-delay angle of the machine-side converter and the excitation (W_E). At low speed the synchronous e.m.f. E_p is too small to commutate the machine-side converter. This function must be taken over by a forced-commutation circuit via the star-points $C_c-T_{c1}-T_{c2}$, at $n < 4 \% n_1$. Due to the low frequency and the low motor e.m.f. the cost of this forced-commutation circuit is moderate.

A variant of this type of drive chain is used with the French dual-system high-power locomotives Class BB 26 000 “SYBIC” (Synchrone Bicourant, [39]), the schematic circuit diagram of which is represented in subchapter 8.2 (multi-system traction vehicles) as Fig. 8.3: The “Monomoteur” traction motor (cf. Fig. 3.16) with $P = 2800$ kW is equipped with two three-phase windings, with axes displaced spatially by 30° (“double-star motor”). It is fed by two thyristor bridge circuits connected in series, as with the TGV-Atlantique, controlled by firing pulses dephased by 30° in time. Thus the dominant torque pulsation is at twelve times stator frequency. The forced-commutation circuit for starting is common to both converters, situated between the two bridges commutating alternately. Current control is provided by the line-side DC chopper, which is fed in AC operation by an additional diode bridge rectifier.

The development potential of this technology is regarded as low [40], weight and losses of the DC-link reactor being a limit; recent French traction vehicles as locomotives (cf. section 7.4.1) or the Paris-East France-South-West Germany TGV apply induction machines, fed by IGBT inverters, too. It has to be seen as a transitory stage, to use the advantageous rotary-field motors even with not fully mastered VSI technology (1983). An important drawback is that due to the rigid dependency of frequency upon speed group supply of motors connected in parallel is not possible, respecting different diameters of worn wheels.

Recently new technologies for synchronous motors, like the permanently-excited type with rare-earth magnets (PM, [41]...[43]), both fed from individual IGBT inverters, are under test. As they offer a higher power-weight ratio than induction motors, they can do away with the heavy gear-box and enable an oil-free drive chain. In the Siemens INTRA prototype drive (500 kW, Fig. 5.7, [42]) the stator is mounted within the bogie frame, torque is transmitted via a cardan glass-fibre hollow shaft inside the rotor bore. In the SYNTEGRA drive (150-kW range for trams, Fig. 5.8, [43]) the rotor is fixed to the shaft of the wheelset, revamping W. v. Siemens’ simple gearless London Tube drive from 1889 with new technological means. Efficiency is claimed to be slightly higher than with IM drives, but special precautions must be taken to separate a faulty inverter from the motor, as the excitation cannot be terminated. Field weakening (for constant power operation) demands impression of demagnetizing (d) current components by the inverter; field-oriented control (cf. section 15.1.4) can be performed without rotor-position sensors now.

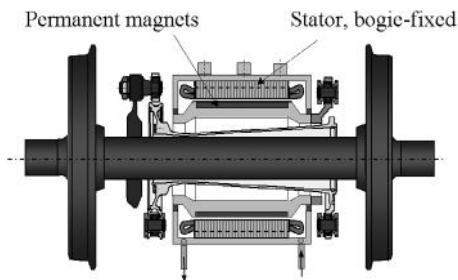


Fig. 5.7: INTRA gearless PM SM drive prototype 500 kW (Siemens AG, TS)

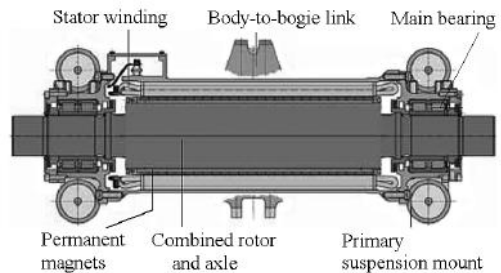


Fig. 5.8: SYNTEGRA integrated PM SM drive prototype (150 kW) (Siemens AG, TS)

6 Induction traction motors and their control

The asynchronous or induction motor – especially in the robust form with squirrel-cage rotor – has always been the “work-horse“ of electric drive technology and thus the ideal traction means for railway technical engineers. Brought to practical applicability in 1888 by M. Dolivo-Dobrowolski, it was used by Brown, Boveri & Cie. (BBC) in locomotives and motor cars for the first main line electrified with three-phase voltage of 750 V and 40 Hz between Burgdorf and Thun in Switzerland already in 1899. In the year 1903 the motor coaches on the test track between Marienfelde and Zossen south of Berlin reached a maximum speed of 210 kph, using squirrel-cage bogie-mounted motors and a three-wire catenary in vertical arrangement (Fig. 1.3). Subsequently several local lines in Upper Italy and then in 1908 the new Simplon Tunnel line were electrified with 3AC 3 kV/16 2/3 Hz conveyed by a horizontally arranged two-wire line (the third phase earthed with the rails).

But, however, the clumsy three-phase systems, which offered only a small number of few economic speeds, were outclassed by the new AC commutator motor system, since it required only a single overhead wire. With the exception of very few isolated local lines the last three-phase railways were retrofitted with AC or DC supply in the 1960s.

In the year 1971 the “second life“ of the induction traction motor started, and with much more success. Following the unlucky Hawk locomotive on trial in Great Britain the diesel-electric universal locomotive DE 2500, built by Henschel and BBC Mannheim (Fig. 1.8) could demonstrate the advantages of the frequency-variable operation of the induction motor by means of thyristor inverters. Since the mid-1990s all high-performance traction vehicles – high-power locomotives and high-speed trains – have employed induction motors, combining a high power-weight ratio ($> 1...1.5$ kW/kg) with robustness and low need for maintenance. The key factor has been the enormous increase of power of semiconductor devices and thus a corresponding decrease in inverter cost, achieved by the introduction of the self-turn-off devices Gate-Turn-Off (GTO) thyristor and recently the Insulated-Gate Bipolar Transistor (IGBT), which are described in subchapter 6.6 [44]...[50].

6.1 Construction and stationary behaviour of the induction machine

The stator of the induction machine (IM) carries a three-phase “rotating-field“ winding, as known from the synchronous machine (Fig. 5.1, 5.2). In the high-power range mainly dual-layer preformed windings are used. Fig. 6.1 shows the stator of the traction motor BQg4843 of Class 120 of DB (1400 kW, $p = 2$). The rotor may be equipped with a similar three-phase winding in

star connection, with the three free terminals made accessible via slip rings and brushes ("slip-ring rotor"); but most widespread is the squirrel-cage "winding" made of copper bars, inserted in rotor-drum slots and connected at both ends over short-circuit rings, as visible in the right part of Fig. 6.1.

Fig. 6.2 compares this motor by its size and weight to the AC commutator motor of Class 110/140 of DB, of 1950s' vintage (cf. Fig. 2.14).



left: Stator with casing



right: Rotor (A-side, with pinion)

$P_N = 1400\text{kW}$ $U_{\max} = 2200\text{ V}$ $I_N = 600\text{ A}$ $G = 2380\text{ kg}$
 $n_1 = 1778\text{ min}^{-1}$, $n_{\max} = 3600\text{ min}^{-1}$ (Bombardier Transportation)

Fig. 6.1: Three-phase traction motor BQg4843 of Class 120 DB (BBC)

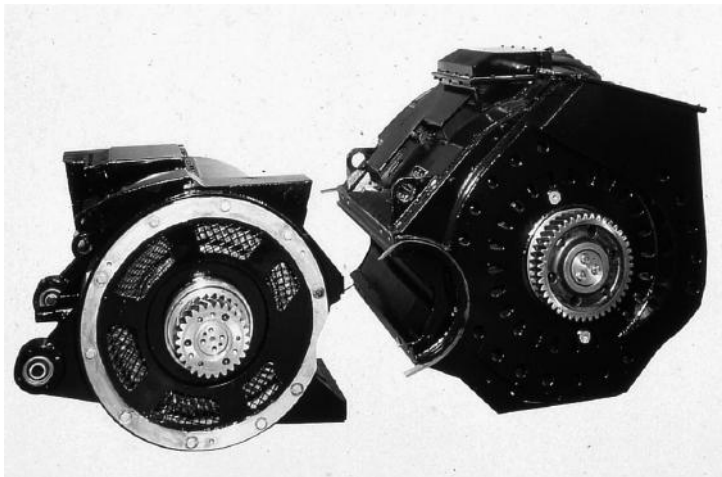


Fig. 6.2: Comparison of size of three-phase traction motor to AC commutator traction motor

left: QD 646 (prototype)
1400 kW / 2380 kg

right: WB 372-22
925 kW / 3500kg

(Bombardier Transport.)

To describe the working behaviour, the squirrel-cage winding is replaced by an equivalent three-phase winding with the same winding number (and winding factor) as the stator winding, so that the rated voltage ratio factor is unity (cf. [V1]). The machine is assumed symmetrical, only the fundamental-wave effects are taken into account. A balanced sinusoidal three-phase voltage system with the r.m.s. phasor U_s and the frequency f_s connected to the three terminals excites a rotating field of constant r.m.s. value, described by the phasor

$$\underline{\Psi}_s = \frac{U_s}{\dot{u}_s}. \quad (6.1)$$

This induces a three-phase voltage system (in the following abbreviated as „voltage“) in the rotor winding at standstill, described by the r.m.s. phasor $\underline{U}_2 = \underline{U}_s$. When the rotor turns in the same direction as the stator field with $\omega = \Omega_{\text{mech}} \cdot p = 2\pi \cdot n \cdot p$, the difference frequency is

$$\omega_r = \omega_s - \omega, \quad (6.2)$$

and a voltage oscillating with angular frequency ω_r

$$\underline{U}_2 = \underline{U}_1 \cdot \frac{\omega_r}{\omega_s} \quad (6.3)$$

is induced. The fraction ω_r/ω_s is commonly called “slip“.

Assuming the whole leakage inductivity concentrated in the rotor (L_σ) and a rotor winding resistance R_r (and if necessary an exterior resistor R_a , connected to the slip-ring brushes), the single-phase ECD for the rotor circuit in phasor representation is obtained (Fig. 6.3, left).

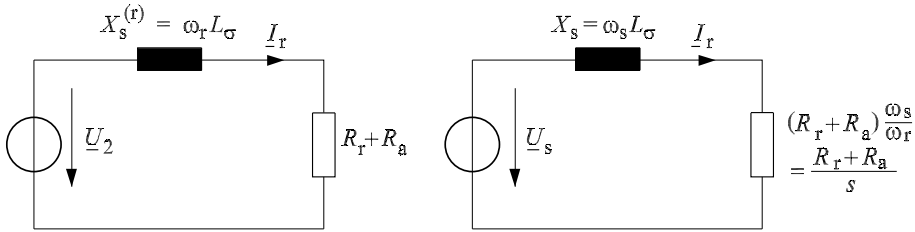


Fig. 6.3: Equivalent Circuit Diagram of rotor circuit on the left in rotor-fixed coordinates, on the right in stator-fixed coordinates

With all voltages, frequencies and impedances multiplied formally with ω_s/ω_r , the ECD will be transformed to stator-fixed coordinates, with all stator quantities oscillating with stator frequency ω_s and the rotor winding at standstill. All values of currents and flux linkages and the phase-angle relations remain unchanged.

The transformed winding resistance $(R_r + R_a)/s$ can be subdivided into the really existing part $R_r + R_a$ and into the remaining part $(R_r + R_a)/(1/s - 1)$, representing the delivered mechanical power. Applying AC theory, the power dissipated in $R_r + R_a$ is:

$$P_{\text{is}} = 3 \cdot s^2 \cdot U_s^2 \frac{R_r + R_a}{(R_r + R_a)^2 + s^2 X_s^2} \quad (6.4)$$

and from that the air-gap power

$$P_\delta = \frac{1}{s} P_{\text{is}} = 3 U_s^2 \frac{(R_r + R_a)/s}{\{(R_r + R_a)/s\}^2 + X_s^2} \quad (6.5)$$

Finally the mechanical (shaft) power is

$$P_{\text{mech}} = P_\delta \cdot (1 - s) \quad (6.6)$$

The current phasor locus describes the actual operation at fixed stator frequency, e.g. speed, torque and power. Additionally the magnetizing inductivity L_μ can be inserted in parallel to the

source \underline{U}_s . The stator winding resistance can be neglected, at least with high-power motors at frequencies beyond several Hz; thus the voltage exciting the magnetizing flux is identical to the terminal voltage, coupling the rotor and the stator equivalent mesh.

From Kirchhoff's 2nd law applied to the rotor mesh the rotor current phasor is derived:

$$\underline{I}_r = \frac{\underline{U}_s}{R_r/s + j\omega_s \cdot L_\sigma} = \underline{Y}_r \cdot \underline{U}_s \quad (6.7)$$

The rotor current is proportional to the admittance \underline{Y}_r of the rotor. The current phasor locus is found by inverting the impedance locus $\underline{Z}_r(\omega_r)$, which is a straight line parallel to the real axis in the distance $\omega_s L_\sigma$. The admittance locus is a circle, centred on the negative imaginary axis of the complex area and touching the origin, as can be seen in the left part of Fig. 6.4. Multiplication with \underline{U}_s and rotation of the diagram by $+90^\circ$ yields the conventional rotor current locus representation and – adding the magnetizing current phasor $\underline{I}_\mu = -j \cdot \underline{U}_s / (\omega_s L_\mu)$ – the stator current locus, known as Heyland Circular Diagram.

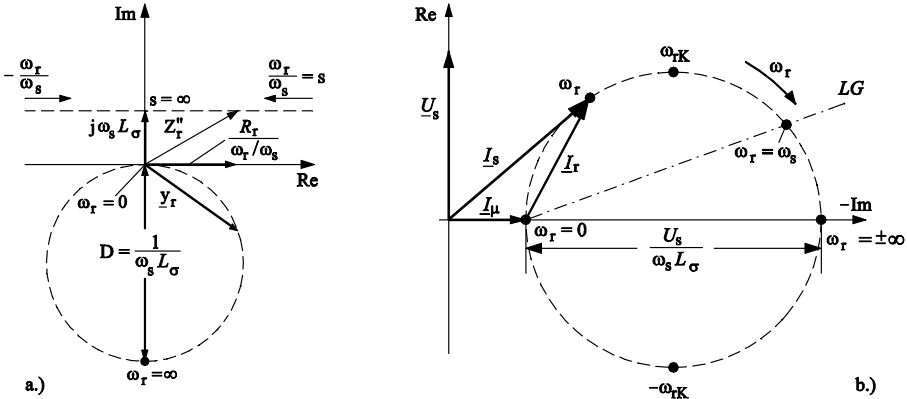


Fig. 6.4 Development of stator current locus of IM (Heyland Circular Diagram)

The component of the stator current parallel to the real axis, the active current, produces with $3 \cdot \underline{U}_s$ the active power

$$P = 3 \cdot U_s \cdot I_s \cdot \cos \varphi \quad (6.8)$$

which, divided by the mechanical synchronous angular frequency $\Omega_s = \omega_s/p$, yields the torque

$$M_d = P/\Omega = p \frac{P_\delta}{\omega_s} = 3 \cdot p \cdot \frac{U_s^2}{\omega_s} \frac{(R_r + R_a)/s}{(R_r + R_a)/s)^2 + X_s^2} \quad (6.9)$$

That is proportional to the distance of the working points on the locus from the imaginary axis; the distance of these working points to the dash-dotted straight line LG between the operating points $\omega_r = 0$ ($s = 0$) and $\omega_r = \omega_s$ ($s = 1$) is proportional to the shaft power. While the radius of the circle – representing the biggest torque available, the break-down torque – is dependent upon the inverse of the leakage inductivity L_σ , the actual working points on the curve are dependent upon the actual rotor winding resistance.

Outstanding working points are

- $\omega_r = 0$ ($s = 0$) Synchronous or no-load point
- $\omega_r = \omega_s$ ($s = 1$) Starting point
- $\omega_r = \pm \infty$ ($s = \pm \infty$) Ideal short-circuit point
- $\omega_r = \omega_{rK} = R_r/L_\sigma$ ($s = s_K = (R_r + R_a)/(\omega_s L_\sigma)$) Break-down point

With the break-down angular frequency ω_{rK} torque can be expressed as

$$M_d = 3p \cdot \frac{U_s^2}{\omega_s^2 \cdot L_\lambda} \cdot \frac{1}{\frac{\omega_{rK}}{\omega_r} + \frac{\omega_r}{\omega_{rK}}} \tag{6.10}$$

Its maximal value, the break-down torque, is:

$$M_{dK} = \frac{3}{2} \cdot p \cdot \frac{U_s^2}{\omega_s^2 L_\sigma} \tag{6.11}$$

Normalizing the actual torque to this maximal value, the so-called Kloss Formula is obtained:

$$\frac{M_d}{M_{dK}} = \frac{2}{\frac{\omega_{rK}}{\omega_r} + \frac{\omega_r}{\omega_{rK}}} = \frac{2}{\frac{s_K}{s} + \frac{s}{s_K}} \tag{6.12}$$

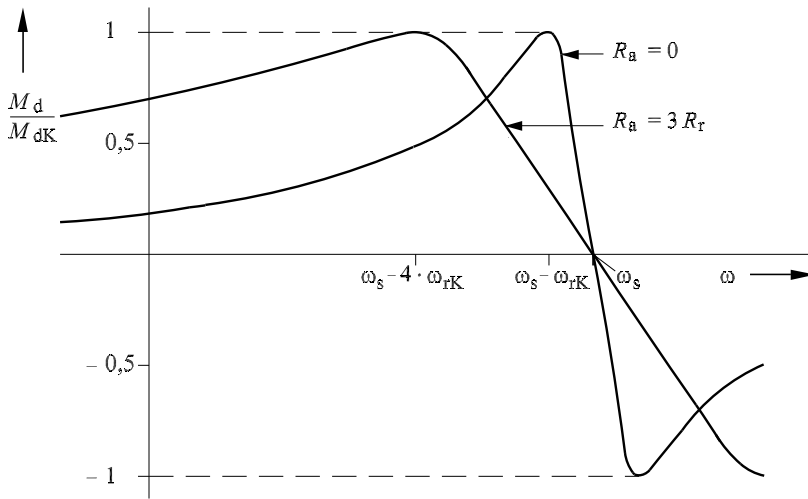


Fig. 6.5: Stator frequency-torque-characteristic of slip-ring induction motor with different rotor resistance values

With the rated torque of the motor being 40 % of break-down torque and $\omega_{rK} \approx 5...10$ % of rated angular frequency ω_{sN} (valid for machines with a rated power bigger than 100 kW), the starting torque at fixed stator frequency $\omega_s = \omega_{sN}$ and $\omega_r = \omega_s$ is only 10...20 % of M_{dK} , corresponding to only 20...40 % of rated torque M_{dN} . This proved insufficient for traction.

For that reason the induction traction motor had always to be equipped with a slip-ring rotor, as long as the stator frequency was fixed, equal to the line frequency. In the starting regime the

effective rotor resistance was increased by insertion of exterior “starting resistors”. Fig. 6.5 displays the torque function (6.12) in dependence upon angular frequency ω for the short-circuited rotor ($R_a = 0$) and for exterior starting resistors of $R_a = 3 \cdot R_r$. In the first case the maximum is found at $\omega = \omega_s - \omega_{rK}$, in the latter case at $\omega = \omega_s - 4 \cdot \omega_{rK}$. The starting torque in this case is four times the value with short-circuited rotor, here even bigger than rated torque.

In the region of small slip ($|\omega_s - \omega| \ll 1$) torque shows a steep, nearly linear characteristic, extending to the range of negative slip values, mirror-symmetrically to ω_s . Induction motors pass over immediately to the so-called supersynchronous braking operation with $\omega_r < 0$.

As long as inverters were not available to produce a proprietary supply with variable frequency, speed control and starting could be reached with only very few and imperfect technical means:

- The three-wire catenary of the first trial runs (cf. Fig. 1.3) was soon replaced by a two-wire system with horizontally-arranged wires, the third phase connected to the earthed rails. To bridge the necessarily long insulation gaps at switches and crossings two pantographs in a sufficiently wide distance were needed, as shown in Fig. 6.6.

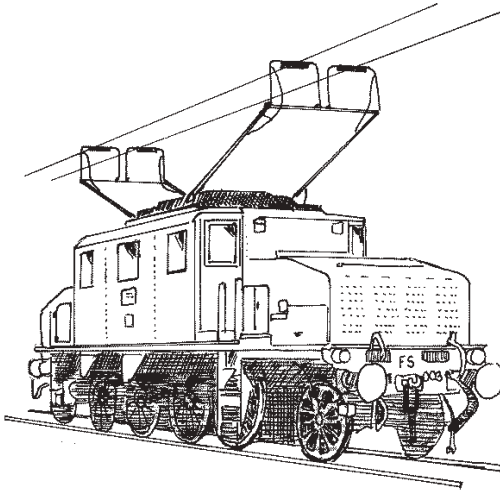


Fig. 6.6: Italian three-phase locomotive Class 431 (1920)

- The starting resistors were constructed as big iron sheets, hung into a solution of sodium carbonate, to be moved out or in by an auxiliary motor; when maximum speed was attained, the resistors were short-circuited at the brushes.
- Changing the number of pole pairs (e.g. $p = 4$ and $p = 6$) and by cascading the normally two motors (cf. Fig. 6.7) a few so-called synchronous speeds with a minimum of losses could be chosen. Cascading means, that the stator winding of the second motor is fed from the slip rings of the first motor; with both motors coupled mechanically, half speed is reached. With both means combined, four economical continuous speeds were possible, in this example in the ratio of 33.3 : 50 : 66.7 : 100. This rendered an “elastic” operation, especially compensating retards by slightly higher speed, impossible.
- Rotary converters changing the phase number and/or the frequency allowed to feed induction traction motors from a single-phase AC overhead system. They were in use in Hungary (Kando system [B10]), the United States and in France. But due to the extremely high weight the latter could only be used with slow and heavy goods locomotives with extreme starting effort, but limited power; as an example may serve the French Class 14000 (Co’Co’, of 2600 kW at 124 t) in the early 1950s.

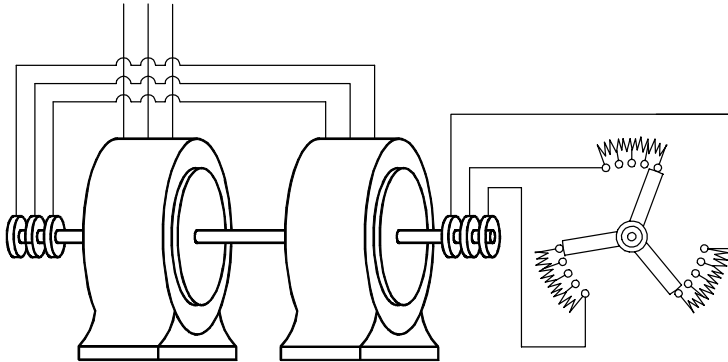


Fig. 6.7: Cascade connection of two slip-ring induction motors

Today pulse inverters allow to control the frequency f_s and the voltage r.m.s. value U_s of the produced three-phase voltage system freely and thus to utilize the advantages of the simple and robust squirrel-cage induction motor.

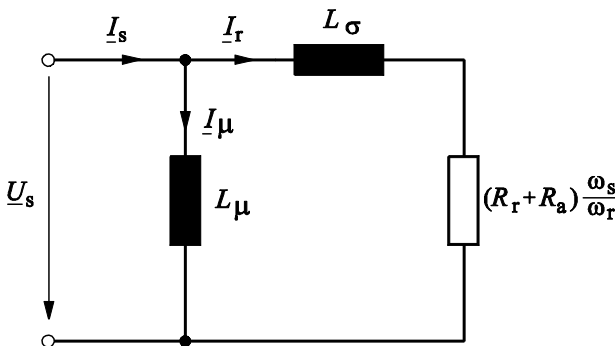


Fig. 6.8: Simplified „canonic“ ECD of IM

To investigate the operational behaviour, Fig. 6.8 shows the simplified “canonic” ECD (symmetrical motor, fundamental-wave ECD, $R_s = 0, R_{Fe} \rightarrow \infty$; “canonic” means, that the leakage inductance is concentrated either on stator or rotor side, not split as in the T-ECD).

With

$$\Psi_\mu = U_s / \omega_s = L_\mu \cdot I_\mu$$

the torque equation (6.10) will be transformed to:

$$M_d = 3 \cdot p \cdot \Psi_\mu^2 \cdot \frac{\omega_r / R_r}{1 + L_\sigma^2 \cdot (\omega_r / R_r)^2} \tag{6.13}$$

This form allows to formulate the control law clearly: The magnetizing flux Ψ_μ is to be kept on its rated value, by varying the voltage r.m.s. value proportional to angular frequency ω_s , as far as possible. The torque will then be controlled by setting the value of the rotor angular frequency ω_r ; in the lower range ($\omega_r < 0,25 \cdot R_r / L_\sigma$ and up to rated torque) torque is approximately proportional to the fraction ω_r / R_r .

There are the following operational ranges (cf. Fig. 6.9, [51], [52], [53]):

- Voltage control (formerly with camshaft control known as “notching”):
 $\Psi_\mu = \text{const} = \Psi_{\mu N}$, $M_d \approx k \cdot \omega_r / R_r$ ($\omega_r < 0,25 \cdot R_r / L_\sigma$).
 The motor voltage r.m.s. value U_s is to be varied proportional until
- Base speed:
 with $\omega_s = \omega_{s0}$, at which $U_s = U_{s\text{max}} = U_{sN}$ is reached. Further increasing the frequency,
- Field weakening:
 with $U_s = \text{const} = U_{s\text{max}}$ is entered, with $\Psi \sim 1/\omega_s$.

These definitions in regard of the *magnetic flux* are to be discerned from the following definitions, concerning the *drive power*:

- Point of constant power (point "1" acc. to UIC):
 From here on, $P_{\text{mech}} = P_{\text{mechN}}$ and $M_d = P_{\text{mechN}}/\Omega = P_{\text{mechN}} \cdot p/\omega$ hold. The most economical choice is to match base speed with the point of constant power, as known from the DC motor. To keep $P_{\text{mech}} = \text{const}$, it is necessary to increase ω_r with increasing ω_s , at the beginning proportionally; when ω_r is not small compared to $\omega_{rk} = R_r/L_\sigma$, more than proportional.

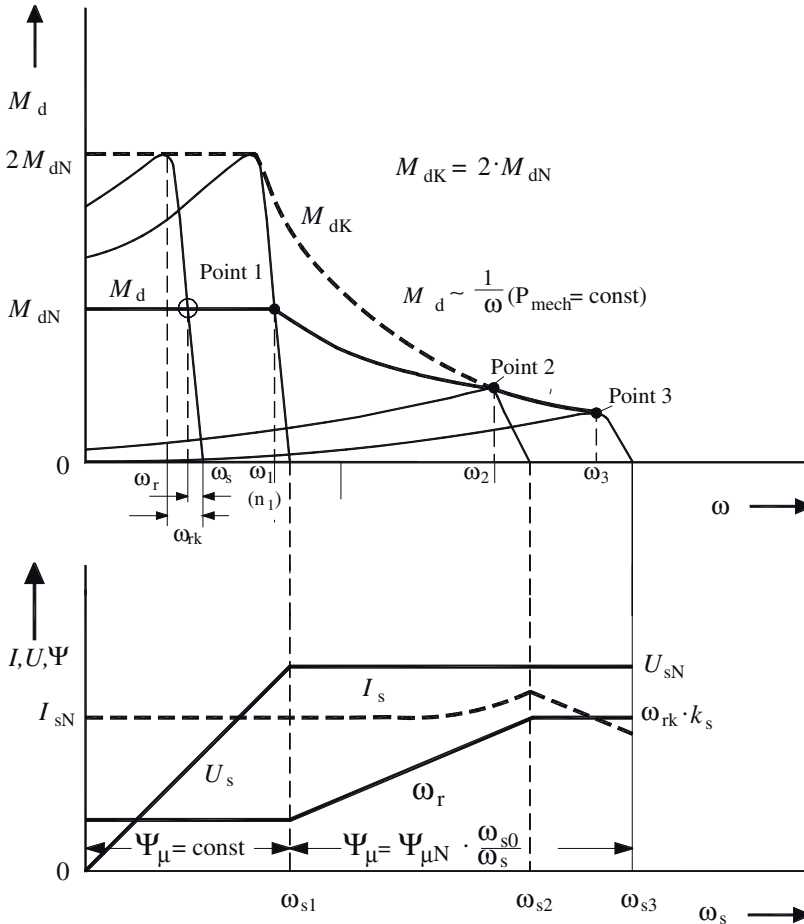


Fig. 6.9: Characteristics of torque vs. rotational angular frequency and of current, voltage and rotor angular frequency vs. stator angular frequency for the variable-frequency variable-voltage induction motor drive

- In the field-weakening range the break-down torque sinks according to $M_{dK} \sim 1/\omega_s^2$. Thus maximal frequency at rated power (point "2" according to UIC) will be reached, when M_d equals M_{dK} , with $\omega_r = \omega_{rK}$. From here onward speed can be raised further, if ω_r is limited to ω_{rK} , with power going back by $1/\omega_s$. Usually a safety factor $k_s (= 0.8...0.9)$ reducing ω_{rmax} to $k_s \cdot \omega_{rK}$ is introduced, as with the last tenths of normalized rotor frequency mainly the reactive current and thus the losses are increased, with only a very minor increase of torque.
- Point "3" is defined by the maximal overspeed of the motor, with respect to the maximum wheel-tire wear. The typical degree of field-weakening is about 1:2.5, which is possible with $M_{dN}/M_{dK} \approx 0.4$. This allows a good motor efficiency of $\eta \approx 95\%$. Shunt locomotives with high tractive effort, but limited power need an extended range of constant power. Field weakening should not exceed the value of 1:5.5, else the motor layout will be critical: The big value of M_{dK}/M_{dN} demands either an increase of the motor size or a very low leakage inductivity (equ. 6.11), which is obtained by low rotor bars, which in turn increase the rotor resistance and thus losses, only $\eta \approx 90\%$ being possible. If $f_{s(2)} > 5.5 f_{s(1)}$, the base frequency f_{s0} must be chosen bigger than the frequency of constant power $f_{s(1)}$, the magnetizing flux in the range of constant torque will be smaller than optimal. To compensate that, the stator current must be increased, compared to the minimal one, which is obtained at $f_{s0} = f_{s(1)}$. The power rating of the inverter is raised correspondingly.
- Regenerative braking is possible by changing the sign of the control quantity ω_r . The other sense of rotation (negative speed) is attained without switching of contactors, only by changing the sign of ω_s in the inverter control.

Exercise 17.6 "Three-phase induction traction motor for an Universal Locomotive with 6400 kW" is recommended here.

6.2 Voltage-source inverter (VSI)

Fig. 6.10 shows in its left part the schematic circuit diagram of a so-called three-phase voltage-source inverter (VSI) [44], [45], [46]), feeding an induction machine. The switching devices are Insulated-Gate Bipolar Transistors (IGBTs), dominating the traction inverter market up to 1 MVA power rating today; in parallel connection powers up to 1.6 MW at an input DC voltage of 3 kV can be handled. The DC-link storage element is the capacitor C . The standard inverter is of the "two-level" type, which means that the output terminals a, b, c are connected alternately with the positive or the negative bus bar of the DC link. In the right part of Fig. 6.10 the simplified ECD is displayed, in which the switching devices are replaced by two-way switches and the DC link is modeled by two identical voltage sources with $E = U_d/2$. The induction motor is replaced by three symmetrical impedances.

Fig. 6.11 depicts the three inverter output voltages u_{vM} ($v = a, b, c$) at square-wave or block modulation (the switching frequency is identical to the fundamental frequency of the three-phase voltage system to be generated), measured against the virtual mid-point M of the DC link; the difference voltage $u_{0M} = 1/3 \cdot \Sigma u_{vM}$, which is the zero-sequence portion of the three inverter output voltages, and finally the motor star voltages u_{v0} , containing no zero-sequence portions any more. The r.m.s. value U_s of the fundamental of the inverter output voltage is constant and equal to $0.45 \cdot U_d$, the value of the phase-to-phase voltage $0.78 \cdot U_d$, correspondingly. This type of voltage control is only suited for the field-weakening range, where U_s is equal to the maximal rated voltage.

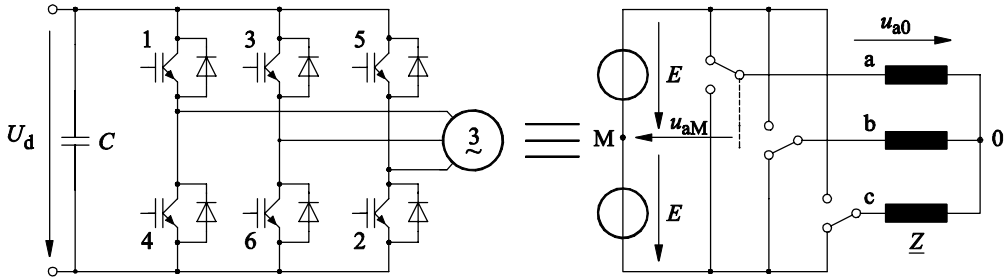


Fig. 6.10: IGBT two-level three-phase voltage source inverter with induction machine
 left part: Schematic circuit diagram
 right part: ECD with two-way switches and symmetrical three-phase load

The common way of voltage-amplitude control is "Pulse Width Modulation" (PWM) known already from the DC chopper: Within one pulse interval (or switching period) $T_z = 1/f_z$, which is short compared to the intended inverter-voltage fundamental period as well as to the motor short-circuit time constant $T_r = L_\sigma/R_r$ ($= 1/\omega_{rK}$) the output voltage is switched between the positive and the negative DC-link potential, so that its average value is equal to the average value of the intended sinusoidal voltage in this interval.

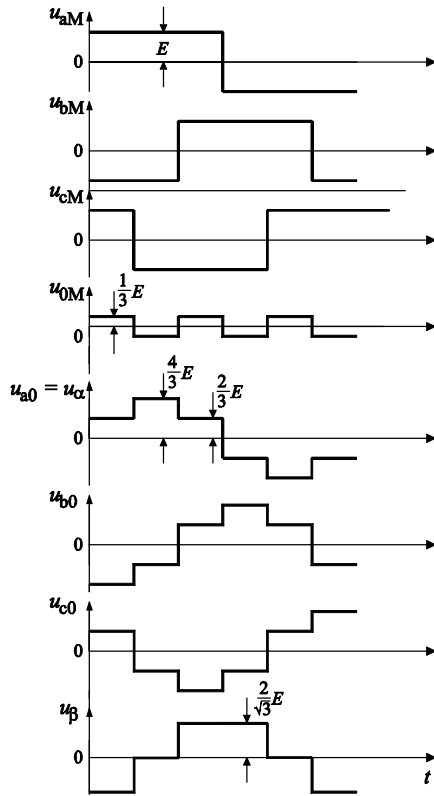


Fig. 6.11: Time functions of inverter output voltages
 u_{vM} ($v = a, b, c$),
 zero-sequence voltage u_{0M} ,
 motor star u_{v0} and sector numbers

Fig. 6.12 explains the procedure of the so-called “Symmetrized Sinusoidal Modulation“ now dominantly used (it produces the equivalent voltage pattern as the so-called “Space-Vector Modulation” with equal zero intervals), for a set of three sinusoidal balanced voltage set values: The instantaneous values of the three voltage set values u_{sv} ($v = a, b, c$) are superimposed by a modifying signal, calculated as the negative of the half of the set value with the smallest absolute value.

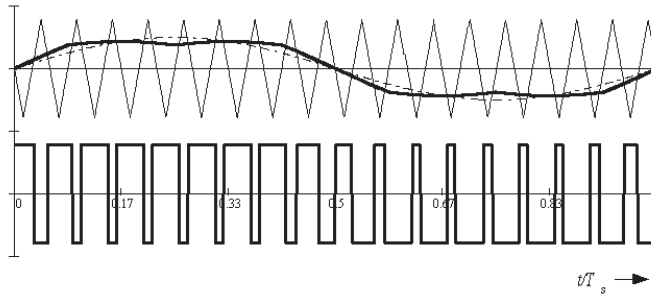


Fig. 6.12: Derivation of the voltage switching pattern at Symmetrized Sinusoidal Modulation

This being a zero-sequence system, the fundamental of the motor voltage will not be changed; but as the maximum duty cycle is reduced to 86% of that necessary for the original sinusoidal curve, the inverter can deliver a fundamental voltage increased by $1 - 1/86\% = 15\%$ at the same DC-link voltage. The new maximal value of the motor star voltage r.m.s. is $0.906 \cdot 0.45 \cdot U_d$.

Comparing the modified set value function f_v with the triangular compare function c_Δ of much higher frequency f_z (here the eighteenfold of the fundamental frequency), the pulsed inverter output voltage u_{vM} will be formed, as known e.g. from [57].

This type of pulse width modulation is suited, as long as f_z is at least ten to fifteen times the fundamental frequency f_s of the wanted output voltage. If the ratio is considerably smaller, disturbing low-frequent subharmonics in currents and torque will occur. Then it is preferred to select the switching frequency as an integer multiple of the fundamental frequency and synchronize both [58]. Generally, 120° -symmetry of the three output voltages and „sinusoidal symmetry“ ($f(x) = -f(-x)$; $f(x) = -f(x+\pi)$) is applied, when choosing the voltage pattern by definition of the switching angles. The switching ratios $N = 3, 5, 7, 9, 11 \dots$ are preferred. Patterns and switching ratios are selected obeying different criteria, as e.g. minimum current peak value, minimum current r.m.s. value or elimination of certain most disturbing low-order harmonics in the output voltage and subsequently in torque or DC-link current [217, 242]. In any case the switching frequency f_z of each semiconductor device ($= N_z \cdot f_s$ with synchronous switching patterns) must not exceed the admissible value, specified for the valve and its cooling system (cf. section 6.6.6).

Fig. 6.13 shows a sequence of inverter output-voltage waveforms with symmetrized sinusoidal modulation, optimized synchronous pulse patterns and square-wave modulation and the pertaining currents for different voltage control factors $a = U_s / U_{smax}$, corresponding to normalized stator frequencies $n_s = f_s / f_{s0}$ (at neglected stator resistance), for a base frequency $f_{s0} = 50$ Hz and a maximum switching frequency $f_z = 250$ Hz; the motor is loaded with rated torque $M_d = 40\% M_{dK}$, the leakage factor is assumed as 10%. The curves are normalized to the amplitude values of rated motor star voltage and rated current.

The inverter output currents (equal to the stator currents of the induction motor) can be calculated in the following way:

- For the fundamental, as described in the previous subchapter
- For the harmonics the harmonic voltage $u_{sh} = u_s - u_{s1}$ is calculated first. The harmonic currents are limited by an inductivity L_h , which is equal to the parallel connection of L_μ and L_σ . In ad-

dition it must be taken into account, that eddy-current effects reduce the value of the rotor leakage inductivity L_{σ} , the more the higher the rotor bars are. This is most important for high-power motors with high efficiency, which have to use high bars to attain a sufficient cross-section area of the rotor bars. With such bars, L_{σ} will be reduced to roughly $k_{1\sigma} L_{\sigma} = 70...75\% L_{\sigma}$. The influence on motors of shunt locomotives is less, as they have to use low bars (preferred of circular cross-section), to attain the necessary high ratio of break-down torque to rated torque, as explained above; L_{σ} will then only be reduced to some 90%, but the efficiency will only be some 90%, either!

$$L_{K.OS} = k_{1\sigma} \cdot L_{\sigma} (1 - \sigma). \quad (6.13)$$

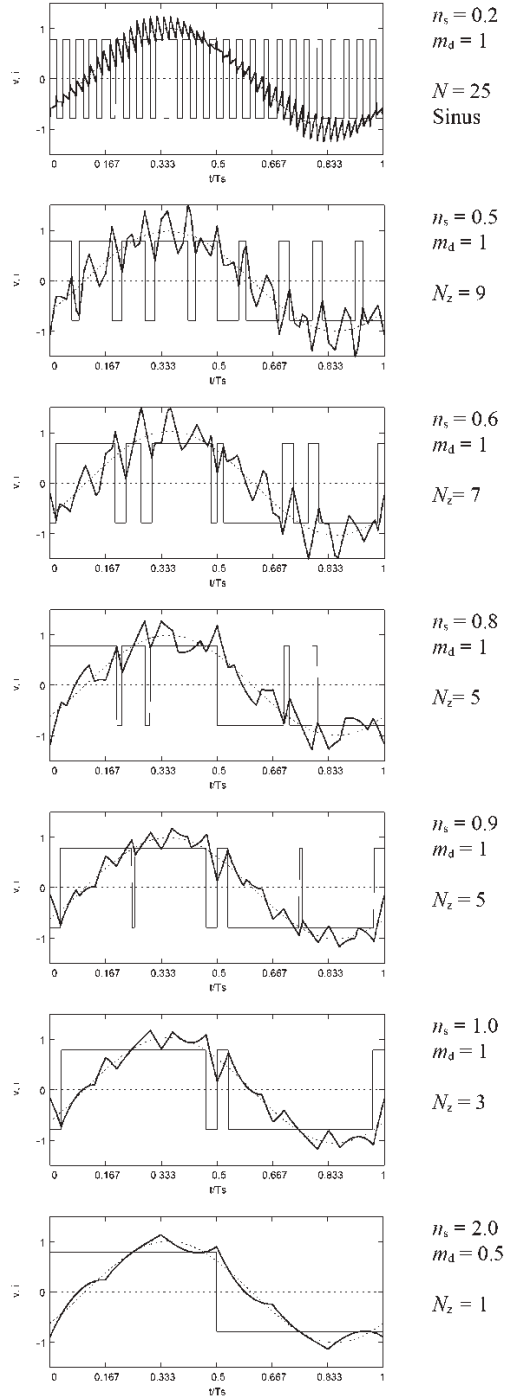


Fig. 6.13: VSI output voltage (thin lines) and stator current (bold lines) for different PWM patterns; dotted: Fundamental of stator current

6.3 Controlled operation of inverter-fed induction motor

Most widely used is

- U/f_s -characteristic control

It is mainly used for simple applications as pumps and ventilators, but it is not suited for traction, as – without additional, mainly model-based approaches – the torque can only be changed distinctly slower than the big magnetizing time constant L_μ/R_r (≈ 500 ms). This is by far not sufficient to cope with disturbing load changes, evoked by slipping or sliding, or with the loss of power supply by a bouncing pantograph.

- U/f_r -characteristic control with impulse encoder

The speed of the motor shaft is measured by means of an incremental impulse encoder (e.g. tooth wheel and magnetic sensor). The value of the rotor angular frequency set value ω_r^* , read out of pre-stored tables dependent upon actual speed and wanted traction effort, are added digitally to the measured the angular frequency $\omega = 2\pi \cdot n/p$, thus yielding

$$\omega_s = \omega + \omega_r^* \quad (6.14)$$

The voltage r.m.s. value will be controlled proportionally to ω_s ; at low speed and stator frequency a correcting value for the voltage drop over the stator winding will be added by means of pre-control. As this type of control is still strongly dependent on the knowledge of the motor parameters which may change seriously with operation conditions, it could not be solved sufficiently with the electronic means of the early seventies.

As protection of the semiconductor devices necessitates current measurement, very soon the so-called

- Slip-frequency-stator-current characteristics control

was introduced [57], [128]. This quasi-stationary control approach was state-of-the-art up to roughly the mid-1980s, when it was superseded by the dynamically superior so-called “field-oriented” methods as Vector Control (TRANSVEKTOR, Siemens AG, Japanese suppliers, ALSTOM) and Direct Self Control (DSC, BBC/ABB/Bombardier). With an impressed stator-current fundamental r.m.s. value I_s and a suited pre-set value of slip or rotor angular frequency ω_r , rotor-flux r.m.s. value Ψ_r and torque M are defined stationarily by the following equations:

$$I_\mu = \frac{\sqrt{\left(\frac{R_r}{s}\right)^2 + (\omega_s \cdot L_\sigma)^2}}{\sqrt{\left(\frac{R_r}{s}\right)^2 + \omega_s^2 \cdot (L_\mu + L_\sigma)^2}} \cdot I_s = \frac{\sqrt{1 + \left(\frac{\omega_r}{R_r} \cdot L_\sigma\right)^2}}{\sqrt{1 + \left(\frac{\omega_r}{R_r}\right)^2 \cdot (L_\mu + L_\sigma)^2}} \cdot I_s \quad (6.15)$$

$$M_d = 3p \cdot L_\mu^2 \cdot \frac{\frac{\omega_r}{R_r}}{1 + \left(\frac{\omega_r}{R_r}\right)^2 \cdot (L_\mu + L_\sigma)^2} \cdot I_s^2 = 3p \cdot \frac{L_\mu^2}{L_\sigma} \cdot \frac{\frac{\omega_r}{\sigma \omega_{rK}}}{1 + \left(\frac{\omega_r}{\sigma \omega_{rK}}\right)^2} \cdot I_s^2 \quad (6.16)$$

using

$$\sigma = L_\sigma / (L_\sigma + L_\mu). \quad (6.17)$$

The optimal set values for I_s and ω_r/R_r are pre-calculated dependent upon motor speed, taking into account e.g. the saturation characteristic of the motor, and stored in characteristic arrays. Fig. 6.14 gives as an example the torque characteristics dependent upon rotor frequency ω_r of the traction motor BQg4843 (Class 120 of DB, cf. Figs. 6.1, 6.2), for different stator-current r.m.s. values as parameter and a rotor temperature of 75°C . The maximum value appears at $f_r = \sigma\omega_{rK}/(2\pi)$.

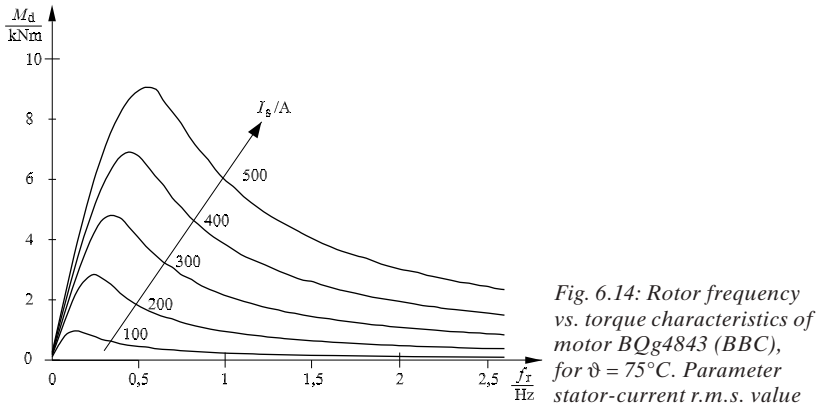


Fig. 6.14: Rotor frequency vs. torque characteristics of motor BQg4843 (BBC), for $\vartheta = 75^\circ\text{C}$. Parameter stator-current r.m.s. value

Fig. 6.15 shows (simplified) the stored characteristics of rotor (slip) frequency set value f_r^* and stator-current r.m.s. set value I_s^* , together with the underlying torque curves, in dependence upon rotational frequency f , with the load levels of 100%, 50%, 25% and no-load.

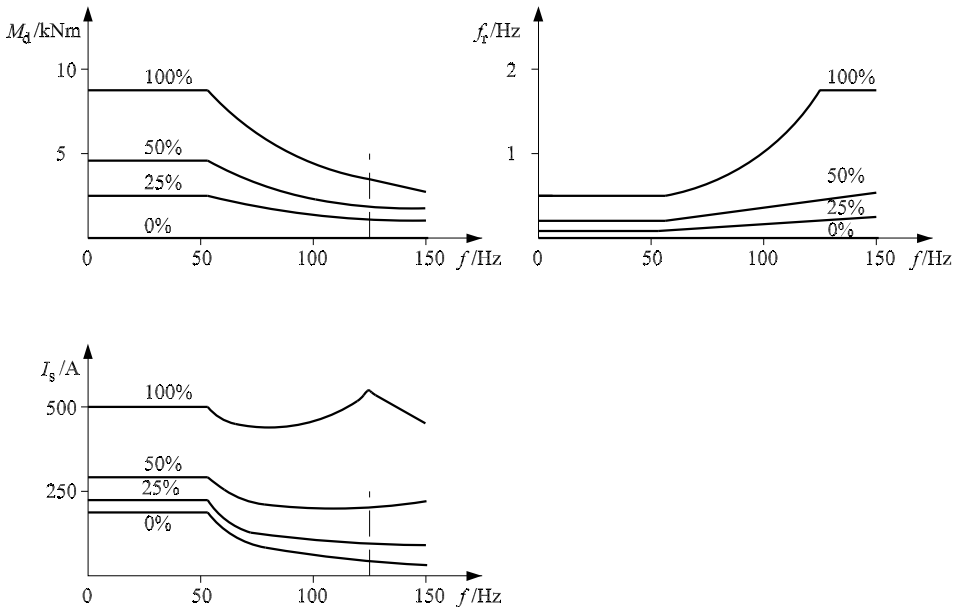


Fig. 6.15: Control characteristics for traction motor BQg4843 (BBC) in locomotive Class BR 120 of DB. $\vartheta = 75^\circ\text{C}$, $U_{dWR} = 2800\text{ V}$

The basic structure of the control is depicted in Fig. 6.16: The rotor (angular) frequency set value ω_r^* read from the array is corrected according to the actual motor winding temperature ϑ and added to the measured rotational frequency ω , yielding the stator = inverter frequency ω_s . The no-load magnetizing voltage U_{s0} is pre-set proportional to ω_s . The rectified and averaged value of the stator current $|I_s|$, roughly corresponding I_s^* , is compared to the set value I_s^* read from its characteristic array, in a PI controller.

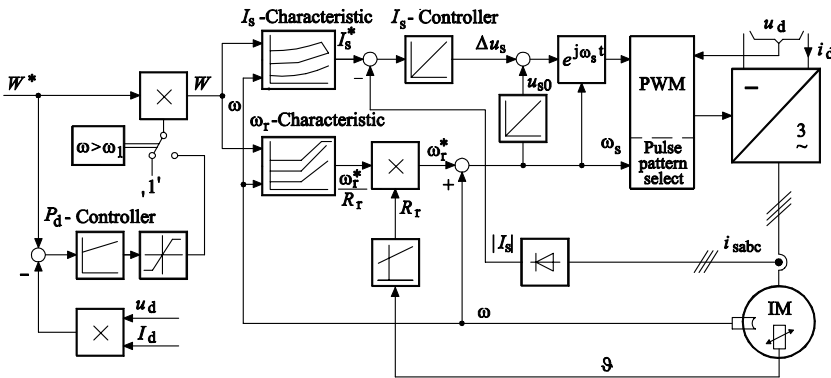


Fig. 6.16: Block diagram of slip-frequency-current-characteristic control (BBC)

It corrects the motor voltage according to the load. The controller output voltage is transformed in the Three-Phase Reference Source into the reference system, rotating with stator frequency ω_s and handed to the Pulse Width Modulator (PWM), which generates the firing commands for the inverter main and commutation thyristors (cf. section 6.6.1).

This type of control was used generally until the mid of the eighties, as being sufficient for the needs of the thyristor inverters. The drawback is found in the quasi-stationary approach: The torque is not allowed to change in shorter times, as three times the rotor short-circuit time constant $T_r = L_\sigma / R_r$ (30...50 ms). In the field-weakening range, the inverter is to be operated in square-wave modulation, as due to the low switching frequency f_{zadm} of under 200 Hz admissible then, even threefold switching ($N = 3$) is not allowed, for thermal reasons. This renders an independent current control impossible; torque can only be controlled via the slip frequency. But this control loop must be even distinctly slower than the current control loop, to limit strong and only lightly damped torque and DC-power oscillations with low frequency. To stabilize them, the power-control circuit shown left was introduced.

With the turn-off capability of the new power semiconductor devices GTO thyristor and – later – IGBT the power rating of the inverters could be increased; this raised the demand on the inverter control, to transmit powers of up to 1.75 MW at a wheelset load of only 21 t safely to the rails. A highly dynamical control strategy became inevitable, to exploit the available – and strongly variable – adhesion optimally, e.g. by wheel-creep control (cf. subchapter 2.3).

In industrial drives so-called “field-oriented” control systems had already been introduced in the early eighties. Now they were transferred to traction drives, too. The high computational power of Micro Processors (μP) and Digital Signal Processors (DSP) allowed much higher complexity than before. As a description *en détail* would go beyond the scope of this text-book, it is only possible to give the basic ideas behind. The interested reader is referred to subchapters 15.1 and 15.2 and the literature relevant to this subject.

- **Rotor-flux-oriented or Vector Control**
 Rotor-flux-oriented control [59]...[62] calculates by means of a machine model amplitude and phase of the rotor-field vector from measured values of inverter output voltages, stator currents and speed (or rotor position). It controls the components of stator current in reference to the rotor-field vector, so that the so-called „flux-determining“ component of the stator current (in phase with rotor-flux vector) magnetizes the motor optimally, whilst the quadrature “torque-determining” component regulates the torque according to its set value. Generally, this control is executed in a reference coordinate systems aligned to the rotor-flux vector, with the advantage of a mainly linear control plant and the use of linear PI controllers. But it is necessary to transform the current-component set values into this rotating reference system, and to transform back the controller outputs to the stator-winding-fixed reference system, in which the inverter PWM works. The torque response is similar to that of the torque-determining current component, typically few milliseconds. But with the low switching frequency of high-power inverters, the assumed free impression of current components is possible only with curtailments.
- **Direct Self Control (DSC)**
 This method [63], [64] calculates the instantaneous values of the stator-field in stator-winding-fixed coordinates and triggers directly the GTO thyristors/IGBTs, dependent upon the flux components crossing pre-set flux thresholds. By that the magnetizing status will be controlled according to its set value. Torque will be controlled via the mean peripheral speed of the stator-flux phasor on its trajectory, by means of a simple bang-bang controller. The control plant is highly nonlinear; this control is only to be mastered by a fully-digital control with DSPs. The hysteresis of the torque controller is adapted, so that the mean switching frequency per valve exploits the admissible value always fully. By that DSC is predestined for high-power inverters with very low switching frequency, in respect to the base frequency of the motor, but the variable switching frequency may be regarded as a drawback, when thinking of line interference. The dynamics of torque excels that of PWM used mostly with rotor-flux-oriented control by a factor of two. The method is extremely robust against power disturbances typical for traction, as bouncing of pantograph or slipping and sliding of wheels.
- **Indirect Stator-quantities Control (ISC)**
 ISC [65], [241] is used mainly in inverters with sufficient switching frequency, e.g. a ratio of f_z to f_{s0} of $> 10...15$. It combines the dynamic advantages of the DSC method with the benefits of PWM with fixed switching frequency; fluxes and currents are sinusoidal quantities. ISC enables extreme torque dynamics in the field-weakening range, same as DSC does, without any voltage margin, only by means of Dynamic Field Weakening. ISC is mainly employed in the starting range of traction vehicles with DSC and with Light Rail vehicles. It offers best starting position for further development, as e.g. the replacement of the rather sensible speed sensor by a speed observer, estimating speed from the electric quantities already available in the model-based control system [66], and subchapter 15.2.

6.4 Group supply of induction traction motors

If the power per drive unit (bogie) is not too big, e.g.:

- up to approx. 2.5 MW at a ratio of v_{\max}/v_1 less than 2.5 (full-electric locomotives)
- up to approx. 1.7 MW at $2.5 < v_{\max}/v_1 \leq 5.5$ (diesel-electric locomotives)
(based on inverters with $U_d = 2.8$ kV and 3-kA GTO thyristors)

group supply of motors connected in parallel is profitable due to cost degression of big GTO-thyristor inverters and due to the lower number of control units.

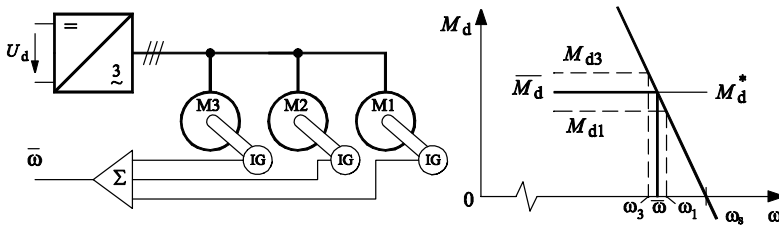


Fig. 6.17: Group supply of parallel-connected induction machines

The “speed” input for the controller e.g. as in Fig. 6.16 is the average value of the rotational angular frequencies of all motors (cf. Fig. 6.17). At a change of the individual tractive force of the wheelset by load transfer (section 2.2.6) and/or the stochastic changes of adhesion (subchapter 2.3) the sum of the tractive forces will be kept constant, slipping of single wheelsets is not possible. With the relief of the leading wheelset 1, ω_1 is slightly increased, due to the steep ω - M_d characteristic, while ω_3 is slightly decreased, assuming equal wheel diameters. The motors have to be dimensioned according to the higher load at load transfer [67].

Differences of the diameters of the wheels occur

- by wear of the wheel treads (typically 0.5 mm /10,000 km)
- by wear of the flanges in narrow curves and the subsequently necessary reprofiling of the entire wheel contour.

If wheelsets with different wheel diameters are fed by one common inverter, high torque and current differences will be the consequence, forcing to maintain narrow limits of the admissible wheel-tire diameter differences (the same deliberations hold for tireless monobloc wheels used in high-speed trains, of course).

The wheel-tires of one wheelset may have a positive difference δR with respect to the average value of all wheel pairs in the drive group. Then the following equations hold:

$$\omega = \frac{i \cdot v}{R + \delta R}; \quad M_d \approx 2 \cdot \frac{\omega_r}{\omega_{rK}} \cdot M_{dK}; \quad \omega_s = \bar{\omega} + \omega_r^* \tag{6.16–6.18}$$

The normalized rise of torque with respect to the average torque (equal to the torque set value) is then

$$\delta M_d / \bar{M}_d = \frac{\bar{\omega}}{\omega_r^*} \cdot \frac{\delta R}{R} \tag{6.19}$$

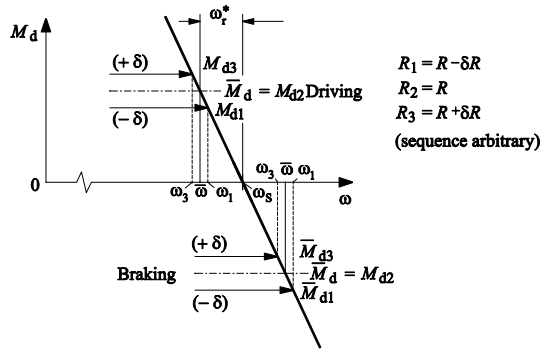


Fig. 6.18: Torque share of paralleled traction motors in a three-axle bogie with group supply, at driving and braking

In motoring operation the wheel with the bigger diameter delivers the bigger torque. The difference may be compensated by bigger wear, but in braking operation the wheelset with the smaller diameter will produce the bigger brake torque, as can be seen from Fig. 6.18!

The thermal loading of the motors rises approximately proportional to $\delta R / \bar{R}$, as the stator current r.m.s. value I_s is roughly proportional to $\sqrt{M_d}$; this must be taken into account, additionally to the possible overload by load transfer. This effect is the more distinct, the smaller the rotor break-down angular frequency $\omega_r = R_r / L_\sigma$ is, compared to the base-speed angular frequency $\omega_{s0} = 2\pi \cdot f_{s0}$, ergo with high-power locomotives with high motor efficiency (and thus small R_r). Diesel-electric locomotives, especially shunt locomotives, suffer less from this phenomenon, as R_r is bigger in relation to rated motor impedance. This is due to the high necessary break-down torque, achieved mainly by low rotor bars with smaller cross-section, as mentioned above. These locomotives can tolerate much bigger wheel-tire diameter differences, as can be seen from Table 6.1.

Table 6.1 Numeric examples of torque differences dependent upon wheel diameter differences

	DE locomotive 2,600 kW $\omega = 125 \text{ s}^{-1}$ (\approx base speed) $\omega_r^* = 6.3 \text{ s}^{-1}$	High-power loco 6,400 kW $\omega = 270 \text{ s}^{-1}$ (\approx base speed) $\omega_r^* = 5.4 \text{ s}^{-1}$ (150°C)
$\delta R / \bar{R}$	$\delta M_d / \bar{M}_d$	$\delta M_d / \bar{M}_d$
0.1 %	2 %	5 %
0.5 %	10 %	25 %
1 %	20 %	Prohibited!
2 %	(40 %)	„

In DE locomotives with three-phase bus bar up to 50 K temperature differences between single traction motors (out of six) have been measured!

To support understanding, Exercise 17.7 “Wheel-tire diameter differences at group supply of traction IM” is recommended.

6.5 Four-quadrant converter

Up to now, describing the VSI the constant input voltage with negligible source impedance was a prerequisite. In the first full-electric traction vehicles with three-phase induction motor drives [68] fed from 1AC supply the two-pulse bridge in half-controllable connection of pairs of arms with sequential phase control (Fig. 4.15) was employed. On principle, the power factor of this circuit is distinctly smaller than unity, due to

- the basically rectangular waveform of the current
- the superposed currents harmonics of the smoothing reactor with limited inductivity
- the fundamental phase shift by phase-angle control

(cf. subchapter 14.3).

Soon it became clear, that the massive application of high-power locomotives of 5...6 MW would lead to severe problems in the relative weak railway supply systems. In 1973, M. Depenbrock suggested a new pulse converter system [69], drawing a nearly sinusoidal line current in phase with line voltage and producing well-smoothed DC quantities at the same time. This being still of two-quadrant behaviour, it was soon developed to a "Four-Quadrant-Converter" or 4q-C [70], characterized by the following attributes:

The transformer secondary winding is connected to the outputs of two VSI pairs of arms, of same construction as those of the motor inverter (Fig. 6.19, left). Varying the duty cycle of both pairs suitedly, a bridge output voltage is generated, which – subtracted from line voltage – draws a line current, limited by the leakage inductance of the transformer, which is nearly sinusoidal – sufficient switching frequency provided – and in controllable phase in respect to the line voltage, preferably $\varphi_1 = 0^\circ$ (phasor diagram Fig. 6.19, centre) or 180° at braking.

Assuming a purely sinusoidal line voltage³

$$u_F = \hat{u}_{F1} \cdot \sin \omega_F t, \quad (6.20)$$

the 4q-C AC "input" (defined as per rectifier operation) voltage fundamental is defined as

$$u_S = \hat{u}_{S1} \cdot \sin(\omega_F t + \psi_1) = k_1 \cdot U_d. \quad (6.21)$$

The last term suggests to treat the 4q-C as a lossless transformer with a time-variant voltage ratio k_1 (< 1); then according to $p_s = u_s \cdot i_s = p_d = u_d \cdot i_d$

$$i_d = k_1 \cdot i_F \quad (6.22)$$

holds. The line current fundamental is set as:

$$i_F = \hat{i}_{F1} \cdot \sin(\omega_F t - \varphi_1). \quad (6.23)$$

With

$$k_1 = (\hat{u}_{S1} / U_d) \sin(\omega_F t + \psi_1) = \hat{k}_1 \cdot \sin(\omega_F t + \psi_1) \quad (6.24)$$

the 4q-C DC "output" current is

$$i_d = k_1 \cdot i_F = 0,5 \cdot \hat{k}_1 \cdot \hat{i}_{F1} \cdot \{\cos(\varphi_1 - \psi_1) - \cos(2\omega_F t - \varphi_1 + \psi_1)\} = \bar{i}_d + i_{d2} \quad (6.25)$$

³ Index, F' for 'line, feed' as mentioned in preface!

(Fig. 6.19, right); it contains the wished DC portion \bar{i}_d and a portion, oscillating with double line frequency, which is inevitable with any single-line power supply.

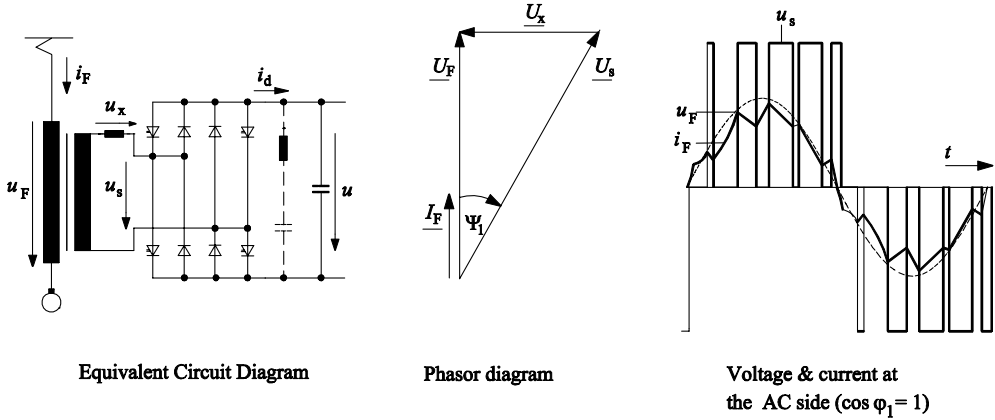


Fig. 6.19: Four-quadrant converter

Mostly (always with $f_F = 16 \frac{2}{3}$ Hz) the oscillating power is absorbed by a series-resonant "tank" circuit L_2, C_2 in parallel to the DC-link capacitor, tuned to $2 f_F$, producing a smooth DC-link voltage free of line-voltage-dependent harmonics.

Generally, the 4q-C is operated to take purely active power from the mains, or give back at braking. But it allows to draw additionally controllable reactive currents from the mains, according to the installed converter apparent power. This is useful to elevate the value of the line voltage at undervoltage by means of a capacitive current component or to lower the line voltage at high values, e.g. brought about by the own braking operation, by means of an inductive current component. As shown in [71], the transmittable power can be increased considerably at line voltages deviating from the nominal value.

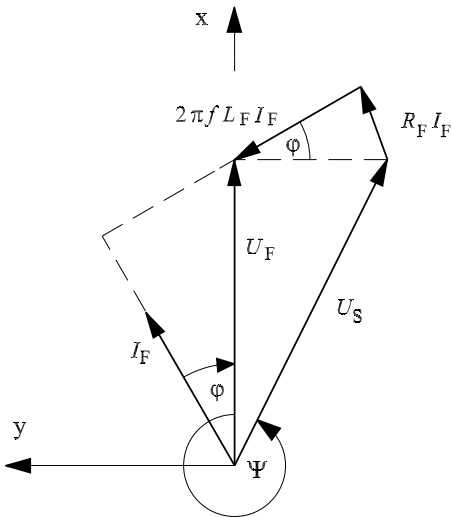


Fig. 6.20: Phasor diagram 4q-C for $\cos \varphi \neq 1$

With given DC-link power P_d , the stationary input power regarding the transformer winding resistance R_F is:

$$P_d + I_F^2 \cdot R_F = P_F = U_F \cdot I_F \cdot \cos \varphi_1 \quad (6.25)$$

The line current fundamental r.m.s. value is, at set line $\cos \varphi_1$:

$$I_F = \frac{U_F}{2 \cdot R_F} \cdot \cos \varphi_1 - \sqrt{\left(\frac{U_F}{2 \cdot R_F} \cdot \cos \varphi_1 \right)^2 - \frac{P_d}{R_F} \cdot \text{sign}(P_d)} \quad (6.26)$$

Now the converter-voltage fundamental-phasor diagram can be constructed:

$$U_{Sx} = U_F - R_F \cdot I_F \cdot \cos \varphi_1 + \omega_F \cdot L_F \cdot I_F \cdot \sin \varphi_1 \quad (6.27)$$

$$U_{Sy} = R_F \cdot I_F \cdot \sin \varphi_1 - \omega_F \cdot L_F \cdot I_F \cdot \cos \varphi_1 \quad (6.28)$$

and

$$U_S = \sqrt{U_{Sx}^2 + U_{Sy}^2} ; \psi_1 = -\arctan \left\{ \frac{U_{Sy}}{U_{Sx}} \right\}. \quad (6.29 \text{ a, b})$$

Table 6.2 Admissible tolerances of r.m.s. continuous value and frequency of line voltage (DIN EN 50163, Table 1; VDE 0115 pt. 102)

f_{FN}	U_N	δ_{u+}	δ_{u-}	δ_{f+}	δ_{f-}
$16^{2/3}$ Hz	15 kV	15 %	-20 %	2 %	-3 %
50, 60 Hz	25 kV	10 %	-24 %	2 %	-2 %

With the admissible tolerances of the r.m.s. value of the line voltage from the above Tab. 6.2 an equation for the appointment of the converter voltage and the nominal transformer no-load secondary voltage U_{FN} is obtained:

$$(1 + \delta_u) \cdot U_{FN} \leq \frac{U_{Smax}}{\sqrt{(1 \pm u_r)^2 + u_x^2}} \quad (6.30)$$

with the normalized values of resistive and inductive short-circuit voltage drop

$$u_r = \frac{I_{FN} \cdot R_F}{U_{FN}} \quad (6.31)$$

$$u_x = \frac{I_{FN} \cdot \omega_F \cdot L_F}{U_{FN}} \quad (6.32)$$

The pulsed converter input voltage u_s contains harmonics with the frequencies

$$f = [2h N_z \pm (2g - 1)] f_F \quad \text{for } g, h = 1, 2, 3, \dots \quad (6.33)$$

and the pulse number N_z (at $f_F = 16^{2/3}$ Hz and thyristors/GTO-thyristor equipment mostly 11 or 15) and line frequency f_F , sinusoidal PWM control provided.

The harmonics of the line current are limited by the transformer leakage inductance; but an increased leakage inductance means a bigger fundamental voltage drop, a bigger converter voltage will be necessary. Optimization of transmittable power found out, that the inductive short-circuit voltage is to be much bigger than known from standard locomotive transformers

for tap-changing or phase-control operation: E.g. $u_x \approx 30\%$ at $f_F = 16\frac{2}{3}$ Hz or $u_x \approx 50\text{--}70\%$ at $f_F = 50$ Hz, with $f_z = 183\frac{1}{3} \dots 250$ Hz for GTO thyristor equipment.

Each high-power traction vehicle contains 2 (or 3) four-quadrant converters per bogie (cf. subchapters 7.4 and 8.2), with parallel-connected DC links. As the two-phase bridge already cancels the pulse component with the switching frequency of each pair of arms (so-called “unipolar” switching used), the triangular compare function of the other (or two others) 4q-Cs in the bogie are phase-shifted by $\pi/2$ (or $\pi/3$, respectively); in addition, those of the 4q-Cs of the other bogie by $\pi/4$ (or $\pi/6$, respectively) against the first. So the pulse current “parcels” of low harmonic order cancel each others roughly, as described in section 14.3.4 more in detail. Finally only harmonics belonging to the eightfold (or the twelvefold) of the converter switching frequency are left, with consequently reduced line interference.

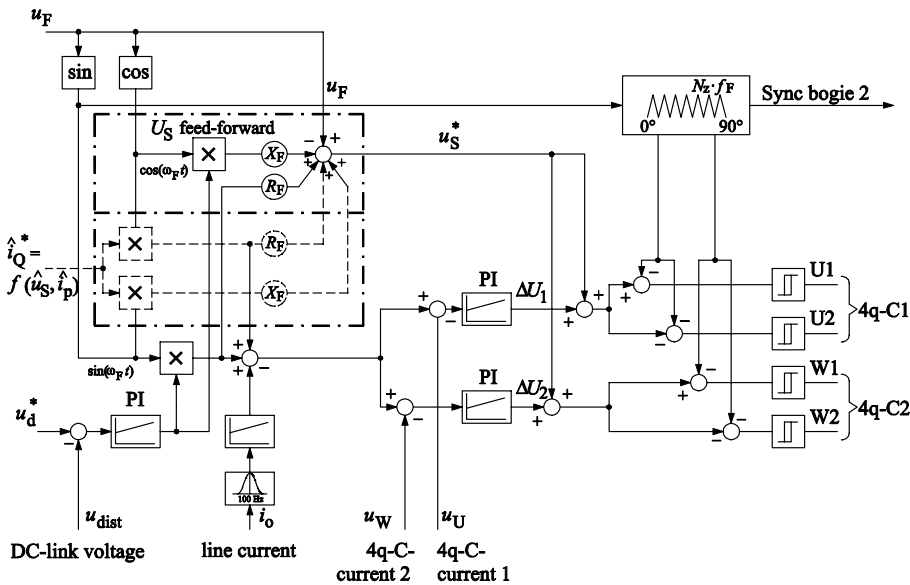


Fig. 6.21: Block diagram of analog four-quadrant-converter control (for one bogie)

Fig. 6.21 shows the block diagram of an analog solution of the four-quadrant-converter control for one bogie. The output of the superposed DC-link-voltage controller is the amplitude value of the active line-current set value. It is multiplied with a reference sinusoid, in phase with the line voltage, and yields the current set value for the PI current controllers of the 4q-Cs U1–U2 and W1–W2. Additionally, a U_s feed-forward modelling equation (6.28) supports the current controllers; a reactive line current set value \hat{i}_Q^* can be given. The controller outputs are compared to the respective triangular functions in the PWM blocks, with the second half-bridge receiving the inverted set value, to obtain “unipolar” switching. The suppression control for the 100-Hz line-current component is discussed in subchapter 14.7. A digital version is described e.g. in [72].

Fig. 6.22 displays the simulation of the main input and output-side quantities of a single 4q-C, together with the main PWM control signals, for $N_z = 15$ and $\cos \phi_1 = 0^\circ$.

Exercise 17.8 “Four-quadrant converter for Universal Locomotive 6400 kW with induction traction motors” shall deepen the understanding of this input circuit.

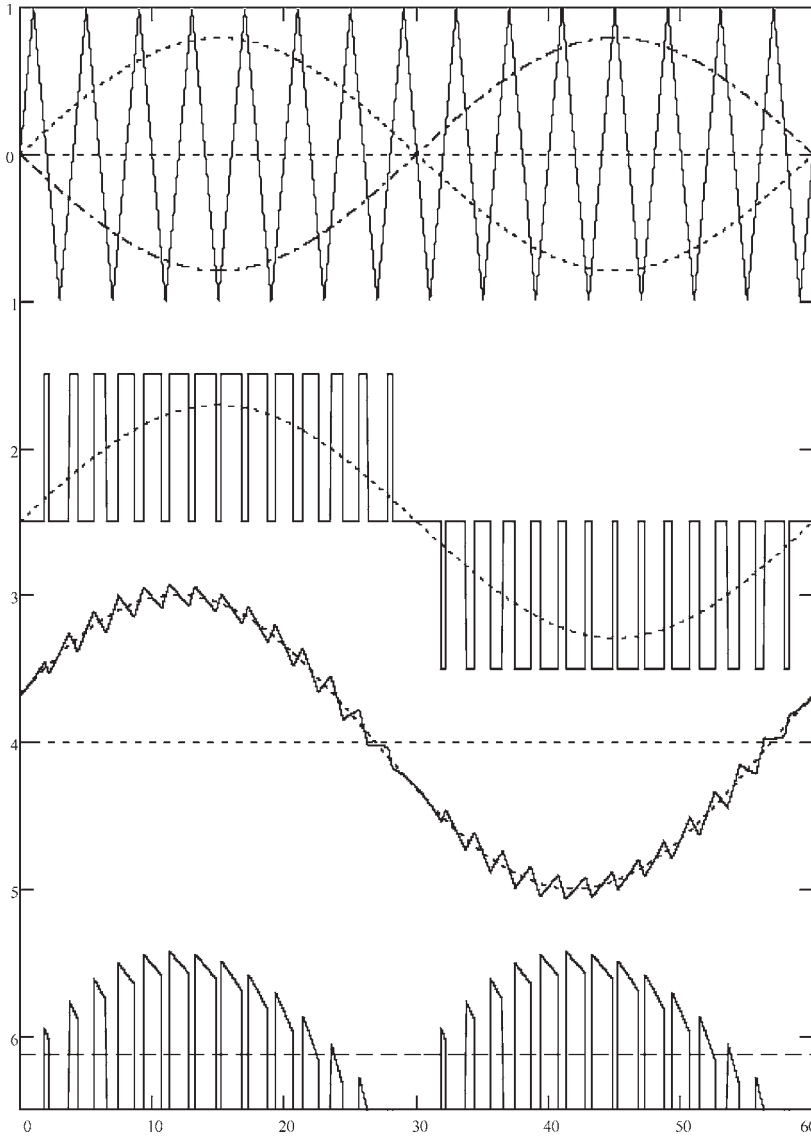


Fig. 6.22: Simulation of the main input-side and output-side quantities of a Four-Quadrant Converter Converter-voltage set values and triangular compare function

Converter input voltage and its fundamental (dotted), normalized to U_d

Converter input current and its fundamental (dotted), normalized to \hat{i}_F

Converter output current and its average value (dashed), normalized to \hat{i}_F

$P_d = 1832 \text{ kW}$, $U_F = 1558 \text{ V}$, $U_d = 2800 \text{ V}$, $f_F = 16^{2/3} \text{ Hz}$, $\cos \varphi_i = 1$, $\psi_i = 19.35^\circ$,

$f_z = 250 \text{ Hz}$, $T_{\min} = 200 \mu\text{s}$, $L_F = 4 \text{ mH}$, $R_F = 63 \text{ m}\Omega$, $I_F = 1238 \text{ A}$, $U_S = 1568 \text{ V}$

Phases refer to converter input voltage fundamental

6.6 Inverter circuit and construction technology

6.6.1 Forced-commutated thyristor voltage-source inverter

As long as power semiconductors, which could be turned off via their gate or base electrode, with sufficient power were not available (up to about 1980), pulse inverters could only be fitted with thyristors (formerly called Silicon Controlled Rectifiers, SCR). These were only able to block when the current was extinguished by exterior circuit force. “Forced-commutation” circuits took over this task, in traction mainly resonant circuits turned on by auxiliary thyristors and being automatically extinguished by the oscillation, having fulfilled their task.

Fig. 6.23 shows the circuit most widely used according to Erlach and Depenbrock [73]...[75], employed by BBC in over thousand traction vehicles with three-phase drive technology. The commutation circuit consists of the commutation capacitor C_K , the commutation reactors L_K and the auxiliary or commutation thyristors T_3 and T_4 .

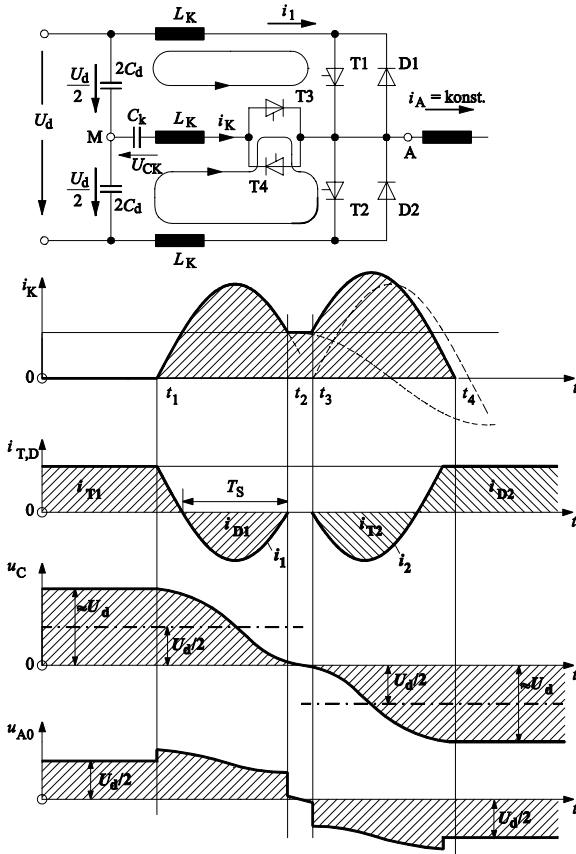


Fig. 6.23: Forced-commutated thyristor inverter with „blocking-voltage-free“ phase commutation circuit

⁴ Index, K' for communication', as mentioned in preface!

This resonant commutation circuit is connected to the mid-point M of the DC-link capacitors and the output of the thyristor/diode pair of arms of the VSI; resonant impedance and resonance frequency are, respectively:

$$Z_K = \sqrt{2 \cdot L_K / C_K} \quad (6.34)$$

$$\omega_K = \frac{1}{\sqrt{2 L_K \cdot C_K}} \quad (6.35)$$

The load current i_A is assumed flowing during the whole commutation period, as drawn by the big leakage inductance of the motor, in the beginning in main thyristor T_1 ; C_K is charged to $+U_d$ (after a proper starting sequence; $C_d \gg C_K$). Firing T_3 at t_1 , the commutation current oscillates with

$$i_K = \left(u_{CK}(t_1) - \frac{U_d}{2} \right) / Z_K \cdot \sin(\omega_K(t - t_1)) \quad (6.36)$$

the commutation capacitor swings with

$$u_c = \left(u_{CK}(t_1) - \frac{U_d}{2} \right) \cdot \cos(\omega_K(t - t_1)) + \frac{U_d}{2} \quad (6.37)$$

vs. zero, the main thyristor current is

$$i_{T1} = i_A - i_K \quad (6.38)$$

As soon as i_K exceeds i_A , T_1 is extinguished. The commutation-current oscillation is carried on via the anti-parallel D_1 . At t_2 i_{D1} equals 0, D_1 blocks; between the instant of $i_K = i_A$ and t_2 the small threshold voltage of the diode acts as blocking voltage at T_1 (so-called “blocking-voltage-free commutation“), the hold-off time T_s must be 1.5...2 times the recovery time T_H of the thyristors (under standardized conditions!), provided T_1 and D_1 are packed together with sufficiently low inductivity. From

$$\hat{i}_K = k_k \cdot i_{A \max} \quad k_k = 1.3 \dots 1.5 \quad (6.39)$$

and

$$T_s = k_q \cdot T_H \quad k_q = 1.5 \dots 2 \quad (6.40)$$

follow the values of the commutation-circuit elements

$$L_K = \frac{1}{2} \frac{T_s U_d}{k_k \hat{i}_{A \max} \arccos(1/k_q)}, \quad C_K = 2 L_K \left(\frac{k_k i_{A \max}}{U_d} \right)^2 \quad (6.41a, b)$$

T_H is between 35 μ s (thyristor blocking voltage $U_{DRM} = 1400$ V) and 60 μ s ($U_{DRM} = 2800$ V), typically.

As soon as D_1 blocks ($i_1 = 0$), the load current continues to flow via $C_K - L_K - T_3$ and discharges C_K linearly. At the instant t_3 T_2 is fired, the capacitor oscillates with

$$i_K = i_A \cos \omega_K t + \left(\frac{U_d}{2} - u_{CK}(t_3) \right) / Z_K \sin(\omega_K(t - t_3)) \quad (6.42)$$

and is charged with

$$u_{CK} = -\frac{U_d}{2} + \left(u_{CK}(t_3) - \frac{U_d}{2} \right) \cdot \cos(\omega_K(t - t_3)) \quad (6.43)$$

up to $u_{\text{CK}}(t_4) \approx -U_d$. Now it is prepared for the next commutation, taking place in the lower valve (“phase commutation”); this is necessary for negative load current i_A , whose polarity is not known to the commutation circuit. Advancing t_3 the value of $u_{\text{CK}}(t_4)$ can be increased. Such a “commutation control” has shown necessary for all high-power inverters with high resonant quality $Q = \omega_K \cdot 2 L_K / \Sigma R_K > 20 \dots 25$. If $u_{\text{CK}}(t_4)$ – e.g. under influence of a ripple in the DC-link voltage U_d – is too small, T_5 falls short of the rated value, T_1 fails to block and conducts again, a “shoot-through“ of the DC-link is initiated, as soon T_2 is turned on. The inverter is not controllable anymore. To limit the subsequent surge current amplitude

$$\hat{i}_{T-ST} = U_d \cdot \sqrt{C_d / (2 \cdot L_K)}, \quad (6.44)$$

the commutation reactance has to be split up in the inner and the outer part(s), as shown in Fig. 6.23. The commutation voltage drop over the outer parts can be seen as the “ears” of the output voltage u_A , with a peak value of $1.25 U_d$ at the main thyristors.

The commutation is – compared to alternative circuits – rather stable and well to be handled, as no „trapped“ energies have to be dissipated. A general drawback is the dependence of commutation capability upon the actual height of the DC-link voltage. The circuit element values have to be dimensioned always for U_{dmin} , but the peak current and thermal rating must be according to U_{dmax} ! This renders the layout of traction drives with variable input voltage difficult, as encountered with DC-supply systems and with diesel-electric drives at high tractive effort at low speed and thus low power, as treated more in detail in subchapter 9.2.

Apart from this, commutation capacitors and reactors are bulky and expensive anyway. Fig. 6.24 shows a “frequency thyristor“ (with small recovery time) and the pertinent gate-pulse transformer.

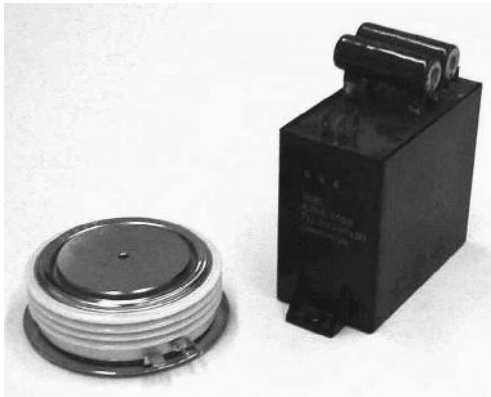


Fig. 6.24: Frequency thyristors with gate-pulse transformer (ABB)

6.6.2 Inverter with Gate-Turn-Off (GTO) thyristors

In the year 1977 the first 600-A Gate-Turn-Off (GTO) thyristors [76]) were presented by Toshiba. From about 1982 2000-A, 2500-V elements necessary for 1-MVA traction inverters with 1400...1500 V rated DC-link voltage were available. They were first used in Metro trains in Japan; in Europe the first locomotives with inverters employing these devices appeared in 1987 [77]). Meanwhile the 3000-A, 4500-V GTO as shown in Fig. 6.26 has developed as traction standard.

By a special interdigitated gate-cathode structure and a reduced turn-off gain at the cathode-side p-n junctions, a GTO thyristor can be turned off with a negative gate-current impulse of only 20% of rated anode turn-off current I_{TOM} . The current quenching under the cathode fingers

causes a critical current-density forcing the subsequent blocking-voltage gradient to be limited to values under 500 V/μs, to prevent destroying the device.

To that purpose capacitors in parallel to the device (“snubbers”) are necessary, which have to be discharged at each turn-on again, for periodic operation.

In addition series reactors are necessary, to limit the current fall in the anti-parallel diodes, which have to be de-magnetized after each turn-off [78]. Fig. 6.25 displays three widely-spread snubber circuits for VSI pairs of arms, equipped with GTO thyristors. Part a) shows the original RCD-LRD snubber circuit ([79], [77], [78]): Each GTO thyristor (V3, V4) has its own RCD turn-off snubber; the snubber capacitance value is defined by

$$C_s = \frac{I_{TQM}}{d_{uT} / dt_{adm}} \quad \text{with} \quad \left. \frac{du_T}{dt} \right|_{adm} \approx 500 \text{ V} / \mu\text{s} \quad (6.45)$$

C_s is discharged via R_s at the turn-on of the GTO thyristor. The turn-on inductivity is:

$$L_s = \frac{U_d}{di_T / dt_{adm}} \quad \text{with} \quad \left. \frac{di_T}{dt} \right|_{adm} \approx 250 \text{ V} / \mu\text{s} \quad (6.46)$$

L_s will be demagnetized via R_s , with the time constant being $T_L = L_s/R_s$; a consequence of this demagnetization voltage is the GTO overvoltage

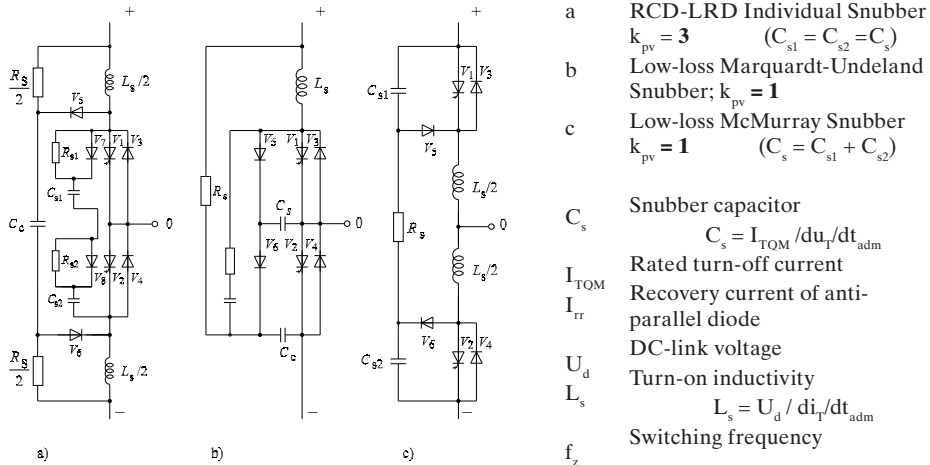
$$u_{Tmax} \approx U_d + R_s I_T. \quad (6.47)$$

At each turn-on and turn-off of one GTO thyristor the snubber capacitor of the opposite side is charged, too; in the loss formula (Fig. 6.25, bottom) the factor k_{pv} is to be set equal to 3.

Already at $f_z = 250 \text{ Hz}$, $U_d = 2800 \text{ V}$ and $I_{TQ} = 3000 \text{ A}$ (thus $C_s = 6 \mu\text{F}$) the losses cannot be dissipated reasonably. Consequently, “low-loss” snubber circuits have been developed.

• Marquardt-Undeland Snubber Circuit

There is only one snubber capacitor C_s , which snubs alternately V_1 and indirectly V_2 – via the storage capacitor C_c , charged to $\approx U_d$ [80], [81]. L_s limits the current rise, R_s dissipates the overcharge energy of C_s due to the demagnetization of L_s . In the loss formula k_{pv} is to be set to 1.



$$\text{Commutation power loss: } P_V = \left[k_{pv} \cdot \frac{1}{2} \cdot C_s \cdot U_d^2 + \frac{1}{2} \cdot L_s \cdot (I_{TQ}^2 + I_{rr}^2) \right] \cdot f_z$$

Fig. 6.25: GTO-VSI pair of arms with different snubber circuits

A drawback of this circuit is the unsymmetric topology and the high stress of the snubber diodes, when the GTOs are fired, as long as the snubber diodes are still conducting, e.g. shortly after a previous commutation in another branch. The mesh $C_5-V_2-C_C-V_6$ must be designed with extremely low inductivity, to prevent dangerous “needle” voltages at the device at turn-off with the typical high di/dt values of GTO thyristors ($> 2000 \text{ A}/\mu\text{s}$).

- McMurray Snubber Circuit

A symmetrical topology shows the snubber circuit going back to W. McMurray [82], [83]. During turn off of V_1 , C_{S2} is connected in parallel to C_{S1} via the DC-link source, so that $C_{S1} = C_{S2}$ can be chosen to $C_S/2$, only. By that k_{pv} is again $= 1$. A prerequisite is that the pair of arms is connected with sufficiently small inductivity to the low-inductive DC-link capacitor bank; typical values are 50 nH! This is a very demanding task.

6.6.3 IGBT Inverter

Insulated-Gate Bipolar Transistors (IGBT), being available since 1992 with sufficient power ratings, do not need any snubber circuits, as their switching gradients di/dt and du/dt can be controlled via the gate. They compare to vertical-structure Power MOSFETS, thus they are voltage-controlled. A supplementary, heavily-doped n layer at the drain side injects minority carriers and provides thus a low voltage drop at high current density [84].

Thyristors and GTO thyristors have been used in traction mostly as disc-type, pressure-contact devices in ceramic housings. IGBTs, in contrast, are mainly used as plastic-moulded modules (Fig. 6.27). On a common copper base plate and isolated by aluminum nitrid (AlN) or aluminum silicon carbide (AlSiC) DCB substrates⁵, the transistor and diode “chips“ (dimension $\approx 13 \times 13 \text{ mm}$) are mounted by anode-side soldering, connected in parallel. Cathodes and gates are contacted per wire-bonding. Life expectancy (number of thermal cycles withstood) is now regarded sufficient for traction (but still one decade smaller, than experienced with pressure-contact thyristors).

The standard module sizes are 1700 V, 2400 A (suited for Light Rail applications with DC 750 V); 3300 V, 1200 A (mass transit, fed by DC 1500 V, and AC via 4q-C with $U_{dN} = 1800 \text{ V}$; since 1996); 4500 V, 2000 A (main-line locomotives and high-speed trains for AC supply via 4q-S and finally 6500 V, 600 A for direct connection to DC 3 kV, since 2001).

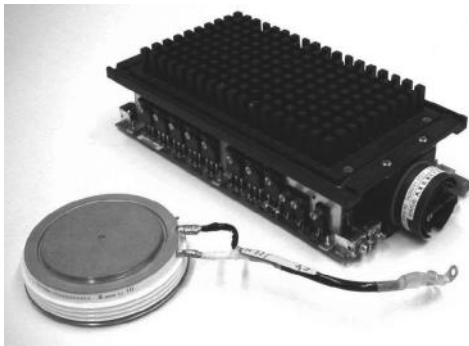


Fig. 6.26: GTO-Thyristor 3000 A, 4500 V with Gate Drive Unit (ABB)

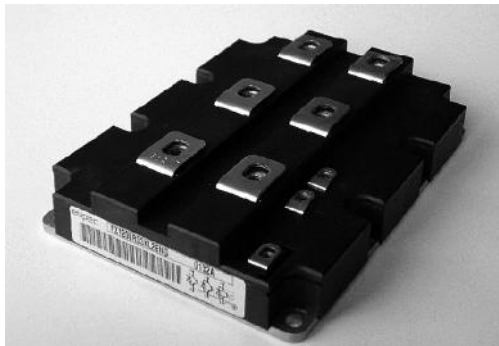


Fig. 6.27: IGBT 1200A, 3300 V (Infineon-EuPEC)

⁵ Direct Copper Bonded Substrate

Gate control must ensure the compromise between fast switching (to reduce switching losses) and admissible output du/dt (to limit the stress of the winding insulation of traction motors and transformers).

6.6.4 Three-level inverter

All voltage-source inverters addressed up to now are so-called two-level inverters, connecting either the positive or the negative potential of the DC link to the output terminals. During the late seventies several circuits were invented, which can also connect the output with the mid-potential M [85], to reduce the distortion of the motor currents and the height of the output-voltage steps, at low switching frequency of high-power thyristors and GTO thyristors.

But only the Neutral-Point-Clamped- (NPC-) concept with series connection of GTO thyristors (later of IGBTs, too) and additional “clamp” diodes to the centre tap M of the DC-link (Fig. 6.28, [86]) made the three-level inverter a candidate for traction. The main advantage is to be in the double value of DC-link voltage and thus power, enabling the direct use of 4.5-kV GTO thyristors at the 3-kV DC mains (cf. subchapter 8.2).

The mid-point potential is switched via D_5-T_2 to the output at positive output current, via T_3-D_6 at negative values.

Initially the interest in this circuit was lively; but now it recedes in traction as:

- Being no standard design, ergo low production numbers
- Alternative solutions with series connection of standard two-level inverters for multi-system locomotives favored (cf. subchapter 8.2)
- Output power available with standard GTO thyristors only adequate for bogie group drives, but uneconomical for single-wheelset drives preferred now
- Control state-of-the-art now [87], but still rather complex
- Inverters with 6.5-kV IGBT elements on market, for direct connection to DC 3 kV

Thus the three-level inverter is regarded as a solitary or transient solution in traction, useful as long as there are no devices with sufficient voltage blocking capability, to solve the task with the two-level inverter. 115 locomotives of type „Bahn 2000“ (Class 460 of SBB, with GTO thyristors, cf. subchapter 7.4), the E2 and E4 Shin-Kansen HSTs in Japan (with IGBTs) and some tramway drives with 1200-V IGBTs [145] were equipped with three-level inverters.

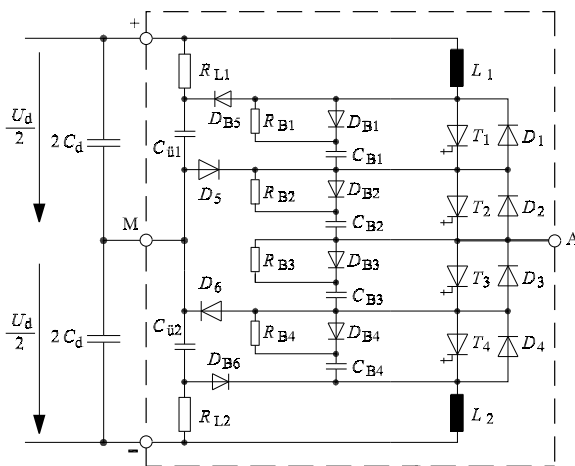


Fig. 6.28: Three-level NPC GTO-thyristor inverter with RCD snubbers (one pole)

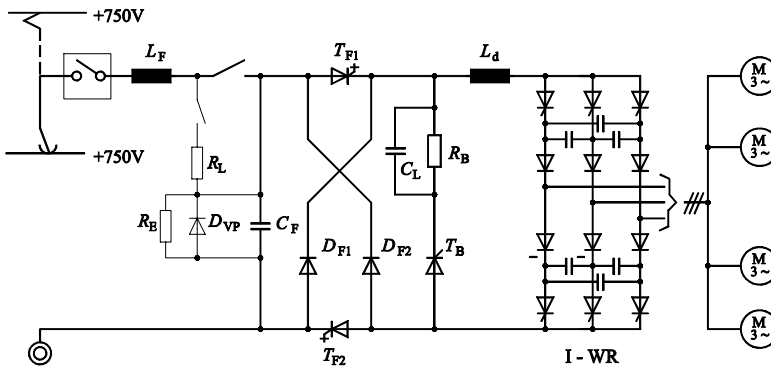
In contrast, very high-power inverters for line-power supply (section 13.1.3) and for Mag Lev (section 12.3.3) are successfully built using special Integrated Gate-Controlled GTO thyristors – but here the inverter power rating is beyond 5 MW!

6.6.5 Current-source inverter

In the 1980s the current-source inverter (CSI) was widely used in mass-transit application [88]. But they were outmoded by the fast development of the semiconductor devices towards asymmetric GTO-thyristor types and IGBTs optimized for VSI circuits, without reverse-blocking capability. The CSI needs this feature.

Similarly to the synchronous “converter” motor, a roughly constant direct current impressed by a line converter (the storing element of the DC link is a reactor) is distributed by the inverter in form of “block” currents cyclically to the three motor windings. As the induction motor needs to be magnetized always by the feeding supply (underexcited operation), it cannot commute a thyristor bridge, like the overexcited synchronous machine. This has to be performed by capacitors between the winding terminals, which are protected by separation diodes against discharging. Firing the thyristor next in the phase sequence, the previous is turned off; from that the name Autosequential Current-Source Inverter (ASCI).

Fig. 6.29 shows the main schematic circuit diagram of an ASCI of the last development stage [89], the current-regulating input and brake choppers equipped with GTO thyristors (1985–1990): T_{F1} (and D_{F1}) control the current in the driving mode, with T_{F2} conducting continuously. For regenerative braking (in step-up chopper mode) the brake current will be built up via T_{F2} – D_{F1} with T_{F1} blocked; after turn-off of T_{F2} the current flows via D_{F2} and D_{F1} against the source voltage into the DC grid. The brake chopper T_B – R_B controls the value of the filter voltage at braking to $U_{\text{max adm}}$, with T_B force-commutated by the GTO thyristor T_{F1} .



L_F	Line filter reactor	D_{F1}, D_{F2}	Free-wheeling/feed-back diodes
C_F	Filter capacitor	T_B	Brake thyristor
R_L, R_E	Charge/discharge resistors	R_B	Brake resistor
D_{VP}	Protection diode	C_L	Commutation capacitor
T_{F1}, T_{F2}	Chopper GTO thyristors	L_d	DC-link smoothing reactor

Fig. 6.29: Current-source inverter (ASCI) for metro and underground cars

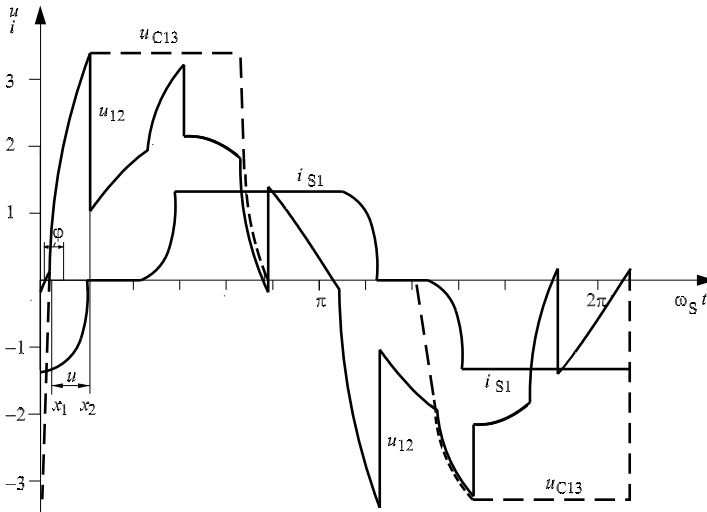


Fig. 6.30: Voltage and current waveforms of ASCI, motor operation

Fig. 6.30 displays the time functions of the motor phase-to-phase voltage u_{12} , the capacitor voltage u_{C13} and the winding current i_{S1} , in motoring operation. Clearly visible is the block form of the motor current, rounded by the commutation, and the mainly sinusoidal motor voltage, with superposed commutation peaks; the commutation capacitor shows a 120° trapezoidal voltage.

The block waveform of the current – and thus the six-pulse torque harmonics – can be mitigated by pulsing the DC-link current to and fro between the motor windings [90].

6.6.6 Cooling and constructional aspects

As explained above, all inverters with self-turn-off devices must be constructed with loops of minimal inductivity, to limit over-voltages from the high di/dt of these elements. The demand rises continuously from the forced-commutated thyristors (connection of the anti-parallel diode with $L_\sigma < 0.5 \mu\text{H}$) over the GTO thyristors (snubber circuit with $L_\sigma < 0.1 \mu\text{H}$) to the IGBT (DC-link interface with $L_\sigma < 20\dots30 \text{ nH}$). This is only feasible with a continuous reduction of all conductor distances and by great-area “sheet wiring“, as known from HF technology. These conductors and the devices themselves must be protected efficiently from pollution by dust, grease and humidity. In spite of the high efficiency ($\eta > 98\%$) of today’s inverters the spatial concentration of the power loss (up to 2 kW in semiconductors of only 75 mm silicon diameter) puts extremely high demand on the cooling system [56].

Air cooling is most appropriate for smaller power, as e.g. in Light Rail applications; it is robust and cheap. But the cooling airstream has to be kept strictly separate from the parts, electrically active [97]. Out of Europe air-stream cooling without ventilators is often demanded, which gives an increase to the radiator mass.

Liquid cooling is inevitable for high-power applications; it gives much more freedom to arrange the components within the vehicle and helps to avoid bulky airducts. Cooling “cans” – between which the semiconductors are pressed – in air or immersed in the cooling fluid (“immersed cooling“) are used. The current methods are explained, taking the cooling of GTO thyristors as example (Fig. 6.31).

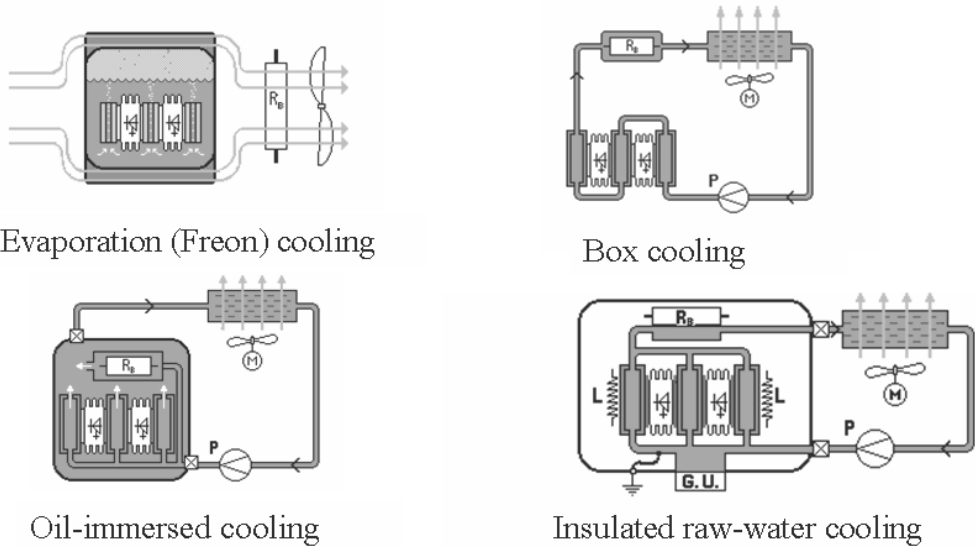


Fig. 6.31 Liquid cooling of high-power GTO-thyristor inverters

Evaporation cooling (Fig. 6.31a) allows an extremely high heat-flow density at minimum temperature difference and does not need pumps for the transport of the cooling liquid [91]. Initially the chlorinated fluoro-carbohydrogen Freon R113 was used, boiling at about 47°C (117°F) and a pressure of about 1 bar. The steam ascends by convection and is condensed at the inner ceiling of the vessel, from where heat will be dissipated finally to the ambient air via cooling fins or in a separate radiator, mounted on top of the vessel. Generally the snubber resistor – dissipating several kilowatts – is arranged outside the valuable volume of the vessel, as it does not demand low inductivity. According to the Montreal Agreement of 1988 Freon has been substituted for non-chlorinated fluoro-carbohydrogens [92].

Mineral oil is a cooling and insulating medium, familiar to railway technologists. Oil can cooling (Fig. 6.31b, [93]) in air has minimum weight, but immersed oil can cooling (Fig. 6.31c, [99]) protects all electrical components better from pollution and dew (“Simplon Tunnel suitability”). Pumps have to convey the hot oil to a central radiator, arranged in front of the transformer or diesel-motor radiator. Inflammability will be reduced by using silicon oils or esters (as used in locomotive classes 101/145 and 185 of DB AG, Fig. 6.39 and 6.40) [112].

Water cooling shows best performance regarding heat transfer, but problems arising from the (electrical) conductivity of water have to be solved. Either can cooling on HV potential, using de-ionised water [94], is applied or the cans have to be insulated by intermediate thin aluminium-nitride (AlN) discs from the devices on high potential (Fig. 6.31d, [95]). Then it is possible to earth the can and to use “raw” water, only mixed with anti-freeze glycol. ABB/ADtranz developed a special cooling can, only made from AlN [96].

IGBT modules are most easily to be mounted, due to the already isolated base plates; but these deteriorate the single-sided cooling even more. Most often the inverters are constructed thus, that at minor power yield direct air cooling of the common carrier plate is applied; only at high-power applications a water intermediate circuit is used. Pressure-contact IGBTs are available, but not used in traction, due to considerably higher cost.

Modularization of converters is an important issue. It can be seen – as in other technical areas, too – that with increasing maturity of technology the extent of the modules is increased. That may be explicated with several examples.

Fig. 6.32 presents the air-cooled 850-kVA thyristor inverter 13SG02a, built by BBC (Mannheim) in 1979 for diesel-electric shunt locomotives (subchapter 9.2). In the upper partition the “Plus drawer“ (T_1, D_1, L_K acc. to Fig. 6.23), the “commutation drawer“ (T_3, T_4, L_K) and the “Minus drawer“ (T_2, D_2, L_K) are arranged, one on top of the other, for the three pairs of arms side by side. Cabling is at the rear plane, down to the lower partition, where the commutation capacitors (small diameter) and the DC-link capacitors (big diameter) are housed. Critical in respect of inductivity is only the paralleling of thyristor and diode in the common heatsink.

Fig. 6.33 shows a “phase building block“ of the 1,870-kVA converter 13SG01a for locomotive Class 120 of DB (BBC 1979), with oil can cooling in air, Fig. 6.31b [93]. Each 2 times 4 power semiconductors are connected in series and pressed in one column, the (+) and (–) columns outwards, the commutation-thyristor column in the centre. Cooling oil is supplied from both sides and runs through the cans in countercurrent (the V-form oil connectors of each two anti-parallel semiconductors are visible), finally streaming through the snubber and balancing resistors grouped in the cooling boxes.



Fig. 6.32: Air-cooled thyristor inverter 13SG02a (BBC);
 $S_N = 850 \text{ kVA}$, $U_{dN} = 1 \text{ kV}$
 (Bombardier Transportation)

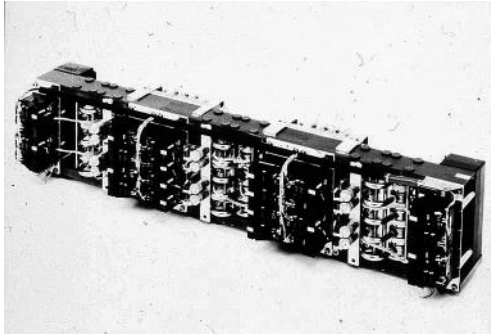


Fig. 6.33: Oil-cooled phase building block (Bombardier Transportation)

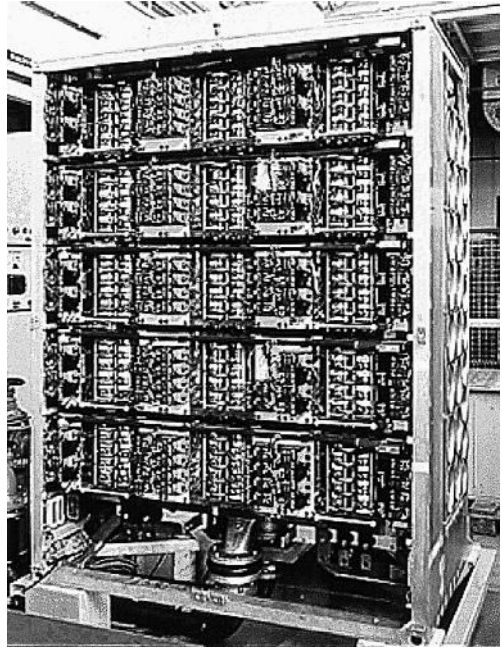


Fig. 6.34: Inverter 13SG01(BBC) for locomotive Class 120 of DB and first series of ICE 1- HST of DB; $U_{dN} = 2800\text{ V}$ (Bombardier Transportation)

In Fig. 6.34 the whole converter can be seen: Three phase building blocks (top, centre, bottom) make the inverter, two (situated in-between) the four-quadrant converter, which is equipped with bigger-diameter semiconductors, due to 50% more power per phase. The commutation and DC-link capacitors are arranged in the right and left rear partition; in-between them, all commutation reactors are housed in a vertical tube, cooled by oil, too. The resonant tank circuit, belonging to the 4q-C, is housed in another cabinet of same size.

Fig. 6.35 displays an evaporation-cooled GTO phase module, with Marquardt-Undeland Snubber (Fig. 6.25b), for a 3-MVA converter of ICE 1, 2nd series/ICE 2 (Siemens AG 1987, [97], [98]). Snubber and storage capacitors are accommodated together with all semi conductors in the evaporation vessel (as Fig. 6.31a), connected with minimum-inductivity sheets. Gate units (and gate-unit power supply) are mounted on the front lid.

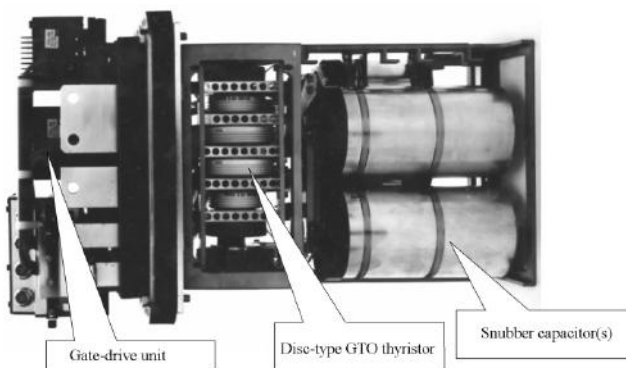


Fig. 6.35: Evaporation-cooled GTO-thyristor phase module (Siemens AG, A&D)

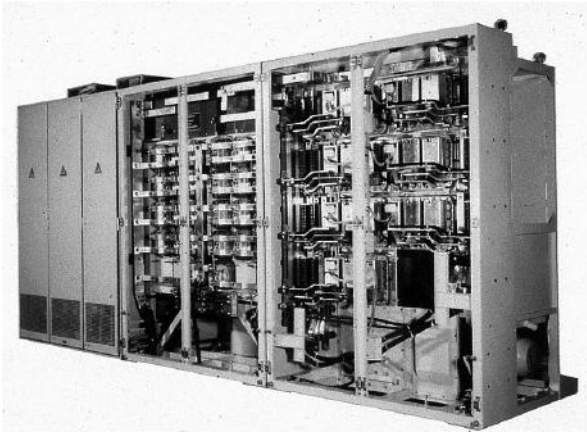


Fig. 6.36: Converter unit for one bogie of ICE 1, 2nd series/ICE 2; $U_{dN} = 2800\text{ V}$, $P_N = 2.4\text{ MW}$ (Siemens AG, A&D)

In Fig. 6.36 the complete converter unit of the ICE 1, 2nd series/ICE 2 HSTs for 2.4-MW traction power is to be seen. In the right cubicle the three inverter modules and 2 times 2 4q-C modules are arranged, below them the common snubber resistor and the converter blower, in the 2nd cubicle the DC-link capacitors and in the 3rd (left) cubicle the resonant tank circuit.

In contrast to evaporation technology, Fig. 6.37 shows the succeeding raw-water-cooled GTO-thyristor phase module, as sketched in Fig. 6.31d, using the McMurray snubber circuit (Fig. 6.25c), developed for upgrading the locomotive “EuroSprinter“ (Class 127 DB AG) and for the subsequent TAURUS locomotives) of Siemens AG. The snubber resistor is here arranged within the water-cooled module itself, due to the extreme demand on low-inductive connection; the DC-link capacitors arranged directly behind the modules are connected via low-inductive plugs and plate current bars.

Fig. 6.38 presents the pertaining converter frame-work (for one bogie, circuit acc. to Fig. 8.5). In five columns two times three inverter phase modules, two times two 4q-C modules and three overvoltage protection chopper modules are housed [95].

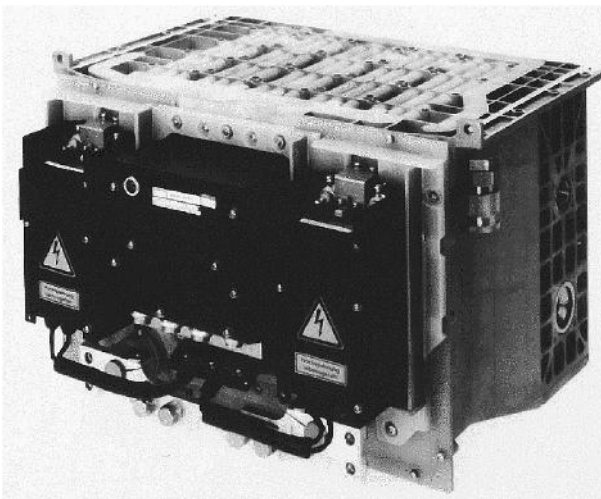


Fig. 6.37: Raw-water-cooled GTO-thyristor phase module (Siemens AG, A&D)

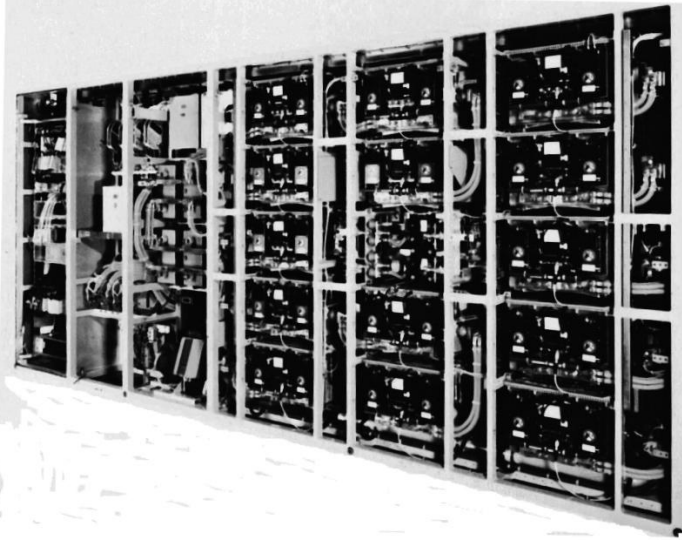
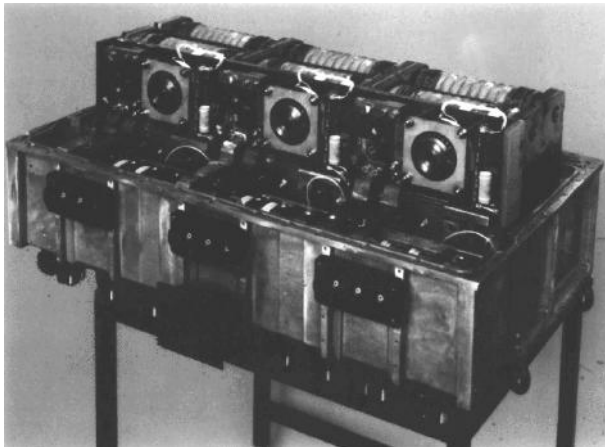


Fig. 6.38: GTO-thyristor converter scaffold for one bogie of “Euro-Sprinter” (Siemens AG, A&D)

A yet higher stage of modularization and an example of oil-immersion cooling can be seen in Fig. 6.39a, the so-called “large module” for 1.6 MW, housing all three phases of an inverter (type 13BH06a, ABB; [99]...[101]). All six GTO thyristors and their six anti-parallel diodes are clamped in one column (in front, lying crossways); before them the six coaxial gate-lead connectors. In the rear lower part the snubber and storage capacitors of the Marquardt-Undeland snubber circuits are arranged, on top of them the di/dt reactors (together with three crowbar thyristors, later on become unnecessary). Not visible are the three snubber resistors (each one for a phase).



a) Interior view (prototype)



b) Exterior view of the final product V1135 (Bombardier Transportation)

Fig. 6.39: Three-phase “large module“ 13BH06a

The cooling oil is led via self-closing couplings into the housing and guided first to the heat sinks of the semiconductors, leaving them for the outer part and cooling the other components. Due to the high power to be dissipated (about $3 \times 10 \text{ kW}$ at $f_z = 250 \text{ Hz}$) the snubber resistors have their own oil inlet.

Fig. 6.39 b exhibits the closed module; at the right side, the six gate units are fixed, at the left side the rolling contacts of the electric connection and the three output current transducers. Thus the module can be slid in or out rather quickly, but necessitating a crane to hoist it out through the opened roof in case of repair, weighing some 200 kg.

Fig. 6.40 displays the whole 3.1-MW converter group MITRAC TC 3100 (for one bogie of Class 101, e.g.). Left cubicle: Three-phase inverter large module on the left, the corresponding two-phase 4q-C module on the right side, above the common DC-link capacitors.

In the centre cubicle the resonant tank circuit is housed, with other auxiliary components and the whole “converter-near” control drawers. The inductors for the resonant circuit are accommodated within the main transformer casing, cf. Fig. 7.13.

With the IGBT converters, a similar development can be noted: While the first building blocks contained the IGBTs for one pair of arms, up to 5 IGBT modules à 300A in parallel, today seven or eight standard plastic-mould modules for the three phases and one or two brake choppers are found on a common cooling plate are found with all manufacturers of Light Rail equipment.

Fig. 6.41 displays an air-cooled 200-kW inverter, produced by Kiepe Elektrik for trolley buses ($U_F = 600 \text{ V}$, subchapter 12.2), with seven IGBT modules.

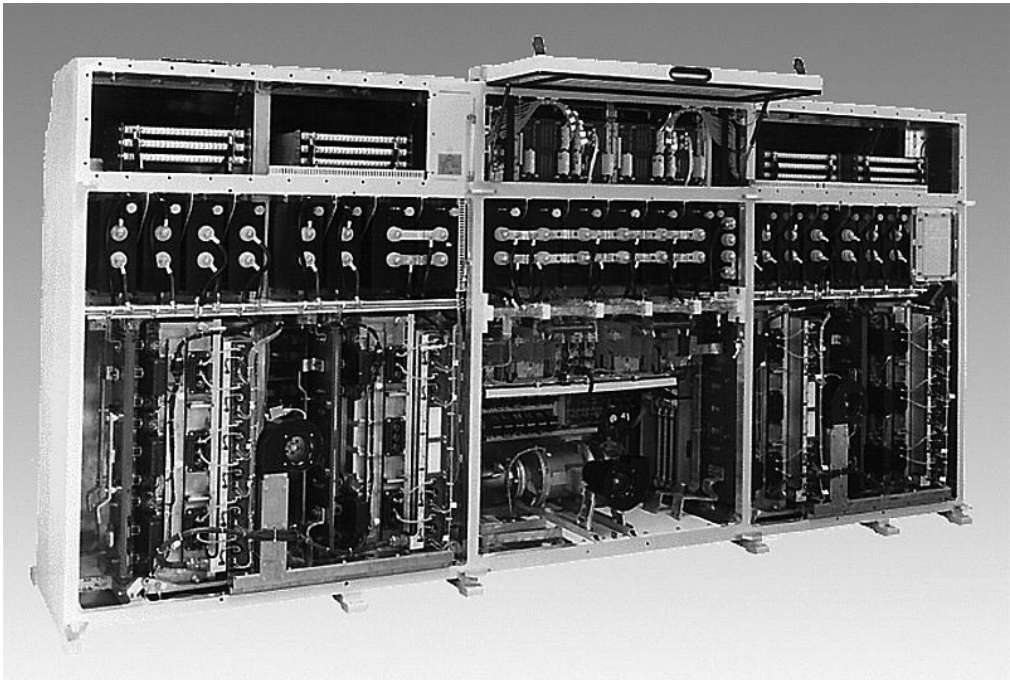


Fig. 6.40: Converter group MITRAC TC 3100 (Bombardier Transportation)

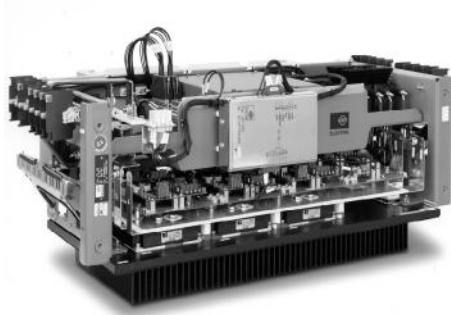


Fig. 6.41: 200-kW IGBT inverter DPU 409 $U_{dN} = 600\text{ V}$ (Kiepe Elektrik)

A proprietary (and somewhat isolated) solution called “Intelligent Power Module” (IPM) has been chosen by ADtranz Switzerland in the late nineties, with a current yield of 2,000 A, for high-power locomotives. The water-cooled ground plate (water plug seen left) houses 4.5-kV IGBT and diode chips and the gate units with additional supervision functions as known from other IPMs for industrial application, and is fitted with multi-contacts and fiber-optic connectors for control signal and status-reply signal (Fig. 6.42); [102].

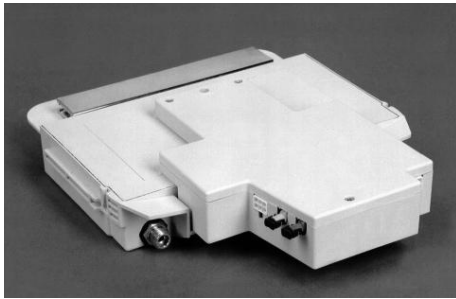


Fig. 6.42: “Intelligent Power Module” 4.5 kV, 2000 A (Bombardier Transportation)

Fig. 6.43 finally presents the water-cooled phase building block with 6.5-kV, 600-A IGBTs for the four-system locomotive Class 189 of DB AG (subchapter 8.2). In each phase building block two IGBT modules are mounted in parallel, in the 4q-C unit three. Three such building blocks make up an inverter rated at 1.6 MW.



Fig. 6.43: Water-cooled phase building block with 6.5-kV, 600-A IGBTs; $U_{dN} = 3\text{ kV}$ (Siemens AG, A&D)

7 Electric traction vehicles for main-line service

The examples will be treated in same sequence, as the technologies have been basically dealt with in the chapters 4, 5 and 6.

7.1 Electric locomotives with DC traction motors

7.1.1 DC chopper control

Fig. 7.1 gives (left) side and top elevation and (right) the main schematic circuit diagram of the universal locomotive Class E 632 of FS Italia for DC 3 kV, $P = 4,700$ kW, $v_{\max} = 160$ kph and $Z_A = 231$ kN (1985, [104]). The locomotive features three motor bogies with 1570-kW DC Monomoteurs (cf. Fig. 3.16) of $U_{A\max} = 2000$ V, fed by three-pulse DC choppers. Separate excitation is provided by an inverter in square-wave modulation from the 3-kV mains, transformer, rectifier and a controlling DC chopper ([105], [106]).

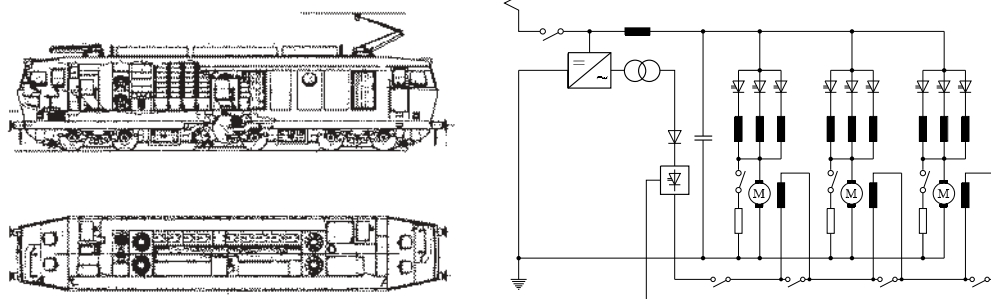


Fig. 7.1: Sketch of locomotive E 632 of FS Italia and main schematic circuit diagram

7.1.2 Thyristor phase-angle control

The locomotive Rc2/3 of the Swedish States Railway (SJ), built by ASEA, for AC 15 kV/ $16\frac{2}{3}$ Hz, was one of the pioneers of thyristor phase-angle control in 1970 (Fig. 7.2); $P_N = 3600$ kW, $v_{\max} = 130/160$ kph and $Z_A = 155/140$ kN (goods train/express train variant) [107].

Fig. 7.3 displays the main schematic circuit diagram, slightly simplified: Four times two two-pulse bridges in half-controllable connection of pairs of arms with sequential phase control (B2HZ) feed four traction motors separately. The field windings of the separately-excited traction motors are fed by M2 double-way rectifiers in anti-parallel connection.



Fig. 7.2: Locomotive Rc2 of SJ, with thyristor phase-angle control

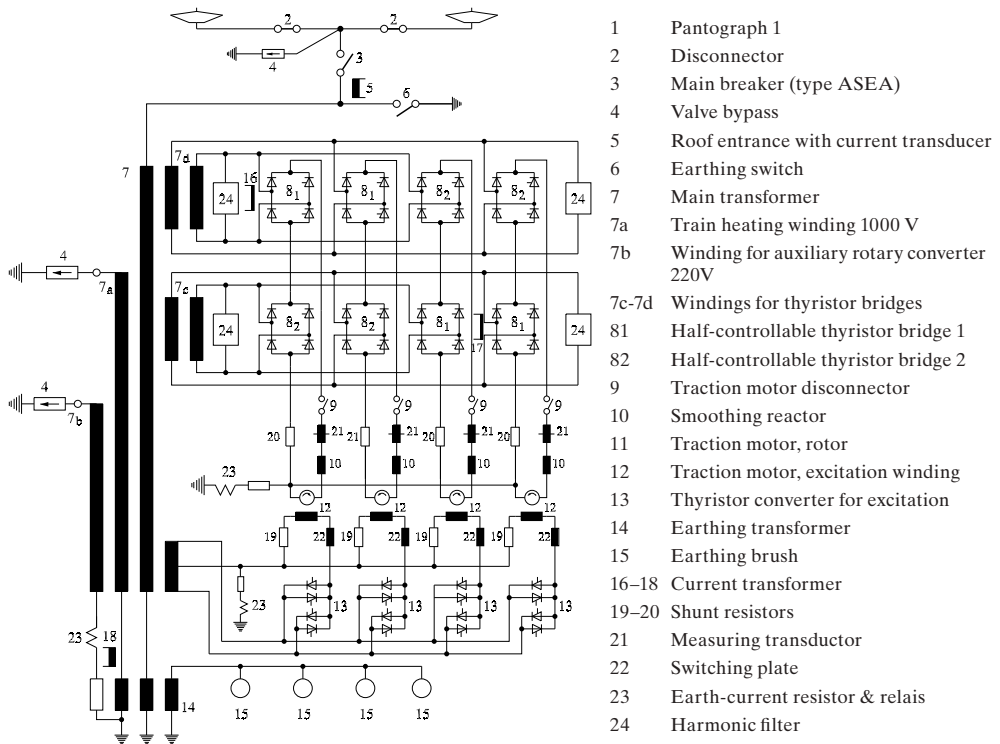


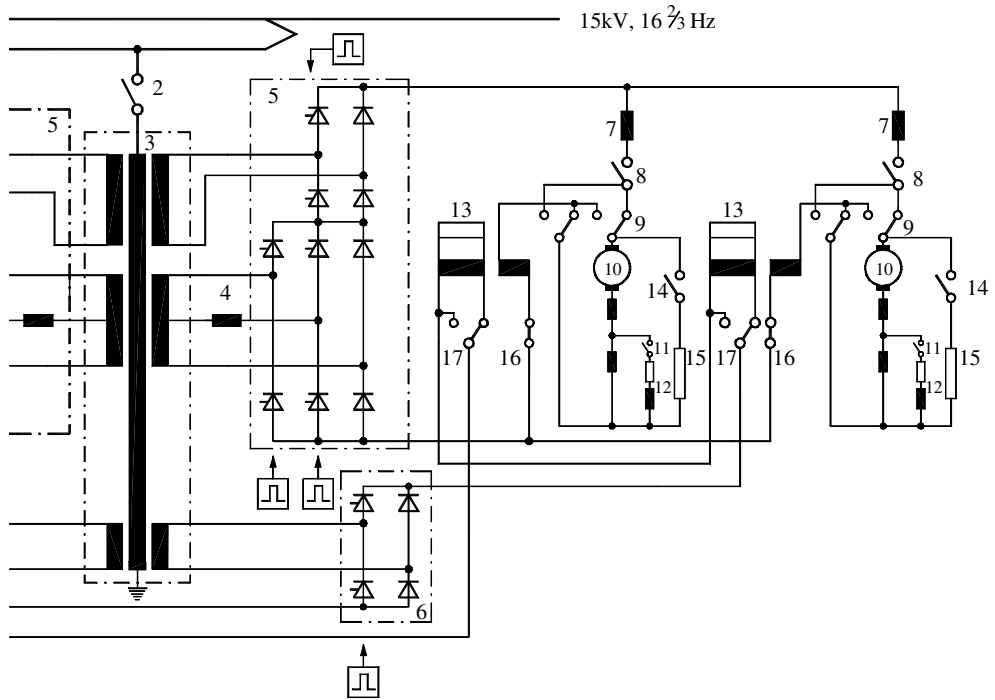
Fig. 7.3: Simplified schematic circuit diagram of locomotive SJ Rc2/3 (acc. to [107])

This locomotive type was very popular with different European railways. A descendant to be mentioned especially is the AEM-7 locomotive delivered by EMD and ASEA in 1979 to AM-TRAK, U.S.A., for the North-East Corridor service Boston–New York–Harrisburg, Pa. It operates on the 25 kV & 12.5 kV, 60 Hz and the 12.5 kV, 25 Hz systems as well and reaches a maximum speed of 200 kph (125 mph).

Fig. 7.4 shows the high-power locomotive Class 1044 of ÖBB (BBC, [108]), which was, in effect, the last – continental – development stage of the “thyristor locomotive” before the transition to three-phase drive technology; Fig. 7.5 the schematic circuit diagram. Here the converter feeds two traction motors in parallel; the lower bridge is extended by an additional pair of arms, connected via a commutation reactor to a tap of the secondary [31]. This allows to reduce the line interference at low output voltage, as the phase delay angle is smaller and the current rise slower (cf. section 14.3.2). The traction motors are equipped with mixed series-separate excitation (“simulated series motor”), typical for the German/Austrian/Swiss area. The one-hour power rating is 5,400 kW; $v_{\max} = 160$ km/h and $Z_{A\max} = 337$ kN (a “universal“ characteristic (cf. Fig. 2.16 and Exercise 17.5!))



Fig. 7.4: ÖBB Class 1044



- | | | | | | |
|---|----------------------|----|--------------------------|----|--------------------------|
| 1 | Pantograph | 8 | Disconnector | 13 | Shunt for separate field |
| 2 | Main breaker | 9 | Reversing switch | 14 | Brake contactor |
| 3 | Transformer | 10 | Traction motor | 15 | Brake resistor |
| 4 | Commutation choke | 11 | Commutation pole switch: | 16 | Armature disconnector |
| 5 | Armature converter | | Closed at $v > 90$ kph | 17 | Bypass contactor for |
| 6 | Excitation converter | 12 | Commutation pole shunt | | separate field |
| 7 | Smoothing choke | | | | |

Fig. 7.5: Schematic circuit diagram ÖBB Class 1044

7.2 Electric traction vehicles with AC commutator traction motors

The express-train locomotives for mountainous regions Class Ae 4/4 Nr. 251–254 of the Bern-Lötschberg-Simplon Railway (BLS) of 1944 are considered the first high-speed high-power locomotives without idling wheelsets ($P_N = 2,944 \text{ kW}$, $v_{\max} = 125 \text{ kph}$, $Z_A = 236 \text{ kN}$; Fig. 7.6). They feature deep-draft force attack in the bogies and an electro-pneumatic wheelset balance with steel ropes, to compensate for load transfer, as shown in Fig. 2.16. In the right part of the figure, the transformer and the high-voltage tap control is displayed (BBC, acc. to [B10]).

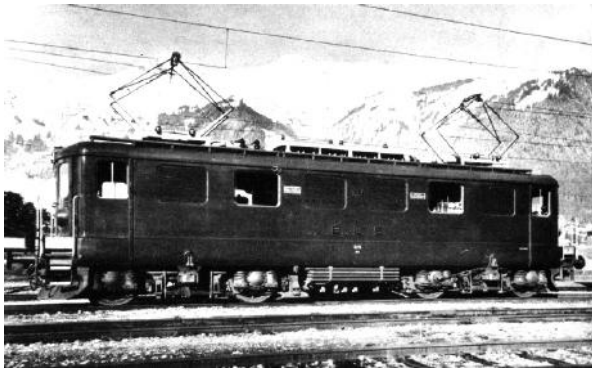
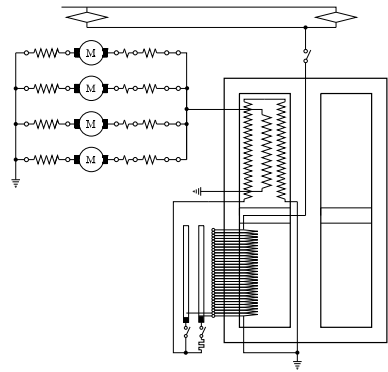


Fig. 7.6: BLS Ae 4/4 Nr. 251



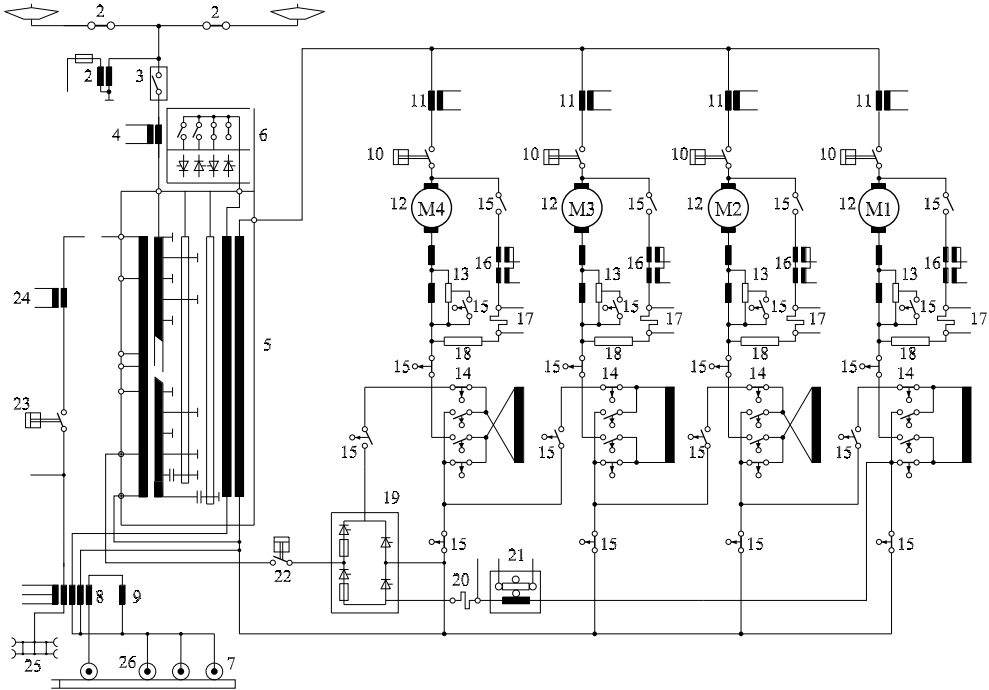
Transformer (shell-type, with radially-laminated core-column)

Fig. 7.7 represents the last locomotive with AC commutator motors put into operation by DB (apart from the locomotives taken over from DR and delivered subsequently until 1992, of Classes 112, 143 and 156 with LEW tap-changer control and thyristor controller, Fig. 4.20). It has been developed from the standard locomotives Class 110/140 from the mid-fifties: $P_N = 3,720 \text{ kW}$, $v_{\max} = 150 \text{ kph}$.



Fig. 7.7: BR 111 of DB AG (Bombardier Transportation)

The permanent power rating of the resistor brake has been raised to 2 MW, with the traction motors excited by a thyristor converter from the main transformer. Each motor has its own brake resistor; by this measure the tendency to slide is considerably reduced [109]. Schematic circuit diagram Fig. 7.8.



- | | | | |
|----|---|----|---|
| 1 | Pantograph | 14 | Reverser |
| 2 | Primary voltage instrument transformer | 15 | Traction-braking reverser |
| 3 | Main breaker | 16 | DC transducer |
| 4 | Primary current instrument transformer | 17 | Brake-current shunt |
| 5 | Main transformer | 18 | Brake resistor |
| 6 | High-voltage tap-changer switch gear | 19 | Excitation converter for electric brake |
| 7 | Earth contact for traction current | 20 | Brake-excitation current shunt |
| 8 | Compensated earth-current transducer | 21 | Brake torque calculation |
| 9 | Earthing reactor | 22 | Brake excitation switch |
| 10 | Traction motor disconnectors | 23 | Train heating switch |
| 11 | Traction motor current instrument transf. | 24 | Train heating current instrument transform. |
| 12 | Traction motor | 25 | Train heating coupling |
| 13 | Commutation pole shunt | 26 | Earth contact locomotive body |

Fig. 7.8: Circuit diagram Class 111 DB [109]

7.3 Electric traction vehicles with synchronous traction motors

Fig. 7.9 displays the high-speed train TGV-A (Train a Grand Vitesse-Atlantique) of SNCF, using the converter circuit according to Fig. 5.6. It is driven by a so-called power head, acc. to section 3.1.1. In Fig. 7.10 the faces of the evaporative-cooled converters [37], [110] are to be seen, containing a thyristor bridge each or a GTO chopper module.

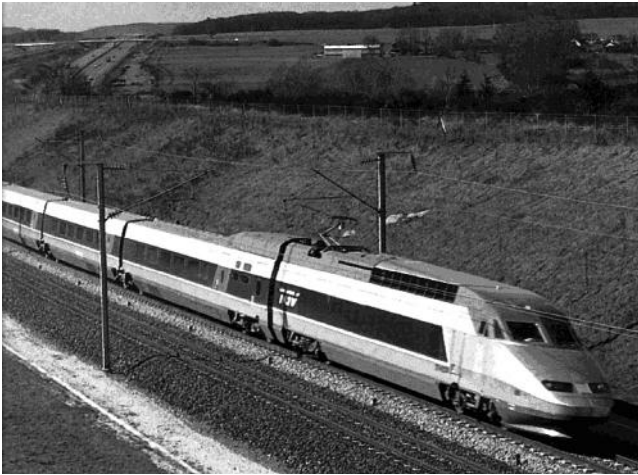


Fig. 7.9: High-speed train TGV-A of SNCF (Alstom Transports)

'Daughters' are the KTX HST for Korean National Railways (50 Hz) and the ACELA trains for AMTRAK (12.5 kV/25 Hz and 25 kV/60 Hz). The similar Thalys HST for Paris-Brussels-Amsterdam and Cologne (1996) are equipped for 15 kV, 16 2/3 Hz, too, at distinctly lower power (only 3,680 kW instead of 8,800 kW for 25 kV/50 Hz, due to transformer rating).



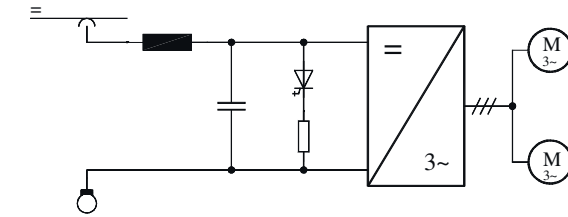
Fig. 7.10: Evaporative-cooled thyristor converters of TGV-A (Alstom Transports)

7.4 Electric traction vehicles with induction traction motors

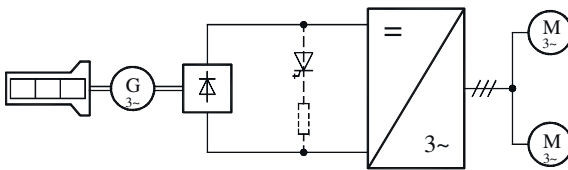
Three-phase drive technology with induction motors and voltage-source inverters allows to a degree not known before the standardization of vehicle drive technology, as Fig. 7.11 shall make clear: The drives differ only in the supply circuits for the DC links [45], [46], and [49]. This will be elucidated in subchapter 8.2 treating the multi-system traction vehicles.

This section shall present samples of locomotives and motor coaches with three-phase drives, the main components of which have already been treated in previous chapters.

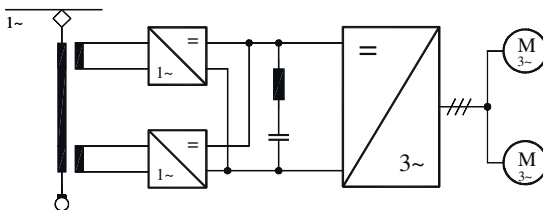
7.4.1 Locomotives



Light-rail vehicle directly fed from DC



Diesel-electric locomotive



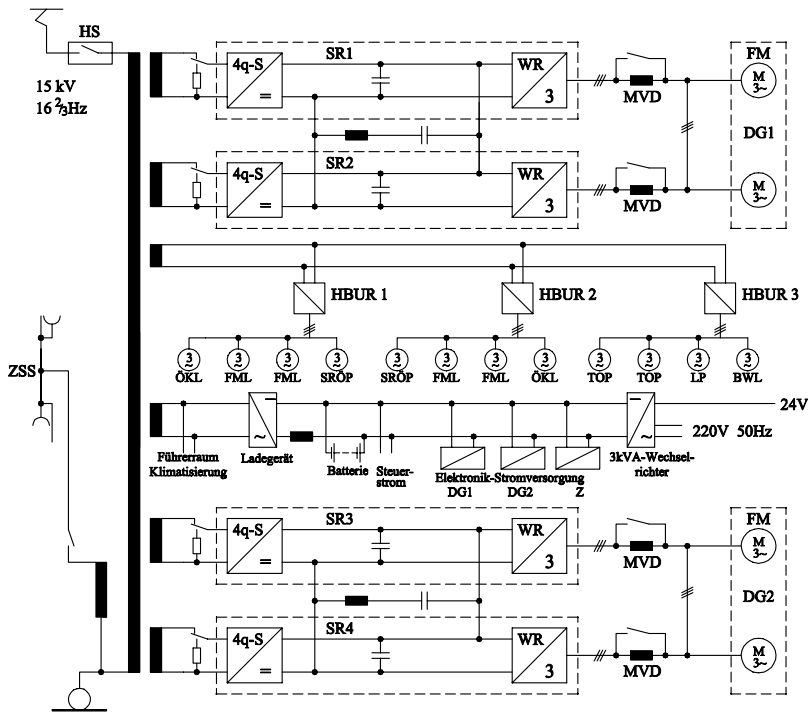
Vehicle fed from AC line with two 4q-C

Fig. 7.11: Schematic diagram of electric traction vehicles with three-phase drive technology

Vehicles fed from the DC line need a brake resistor/chopper, as – due to the diode rectifiers in the substations – the capacity of the grid to take up the brake energy cannot be taken for granted.

• Class 120 DB:

Fig. 1.9 has presented the exterior view of locomotive Class 120, Fig. 2.7 the bogie construction, Fig. 6.1 the traction motor (with the control characteristics given in Fig. 6.15) and Figs. 6.33 and 6.34 the phase building block and the converter; now Fig. 7.12 presents the main schematic diagram [93]. The two converters feeding the motors of one bogie are connected in parallel at the DC links; the resonant tank circuit is common. Due to the expenditure of control circuits then both inverters are controlled by one controller. To limit the harmonic motor currents, reactors (MVD) with some 50 % of the motor leakage inductance L_{σ} are connected in series, which are short-circuited at higher frequency ($> 0.5 f_{smax}$), when the motors have to produce full breakdown torque at maximum frequency.



BWL	Brake-resistor blower	ÖKL	Oil-cooler blower
FML	Traction-motor blower	SR	Converter
HBUR	Auxiliary converter	SRÖP	Converter oil pump
HS	Main breaker	TÖP	Transformer oil pump
LP	Compressor	ZSS	Train line
MVD	Motor series reactor		

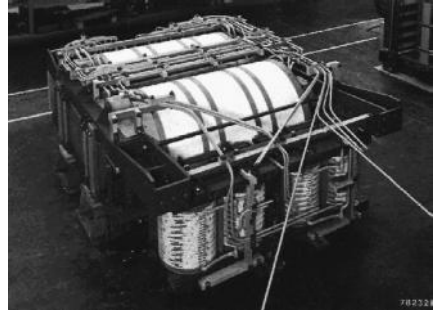
Fig. 7.12: Main circuit diagram Class 120 DB

Initially brake resistors had been provided, which were controlled by the 4q-C as a single-phase inverter; after short time they were removed, as it could be shown that the probability of the AC railway supply grid to fail is considerably lower than that of the brake contactors [111]. So now only the regenerative brake – together with the direct air brake (subchapter 11.1) – is used. In

the free space a 15-kV line filter to reduce the line interference (section 14.3.4) could be housed. The auxiliary converters (HBUR) 1 and 2 are controlled dependent upon demand with variable frequency, HBUR3 with fixed frequency.

The main transformer (Fig. 7.13) is built as a core-type transformer with four totally separated secondary windings and – concentrically arranged around them – the four primary windings, connected in series. The short-circuit voltage is $u_k \approx 33\%$.

Fig. 7.13: Transformer of Class 120
15000V / 4·1513V / 860 A
(in front the resonant tank
reactors are to be seen)
 $G_{ges} = 11.2\text{ t}$
forced oil cooling



The “stranded” conductors of the secondary windings are made from a multitude of flat, insulated partial conductors running in a screw line through all heights of the layer (Roebel-type winding), to reduce eddy-current losses. Outmost the train-heating and auxiliary windings are situated [93].

- Class 101

Fig. 7.14 shows the high-power locomotive Class 101 of DB AG, the successor of Class 120 for express trains (IC), Fig. 7.15 the main diagram ($P_N = 6,400\text{ kW}$, $v_{max} = 220\text{ kph}$, $Z_A = 300\text{ kN}$; [112]).

The GTO-thyristor converters (Figs. 6.39, 6.40) are again connected in parallel at their DC links, but the inverters are controlled separately (using DSC, subchapter 6.3 and 15.1.5), to be able to exploit adhesion maximally (bogies with Integrated Complete Drive, Fig. 3.13). Regrouping of the resonant circuit allows to maintain operation with 75% of rated power, if one inverter (or motor) fails. The line filter is connected to a 1000-V tertiary winding of the main transformer, for optimized lay out (cf. section 14.3.4). A derivate of this locomotive has been delivered to New Jersey Transit, U.S.A. in 24 units as Type ALP 46, for the 25 kV & 12.5 kV, 60 Hz and the 12.5 kV, 25 Hz systems [253].



Fig. 7.14: Locomotive Class 101 of DB AG

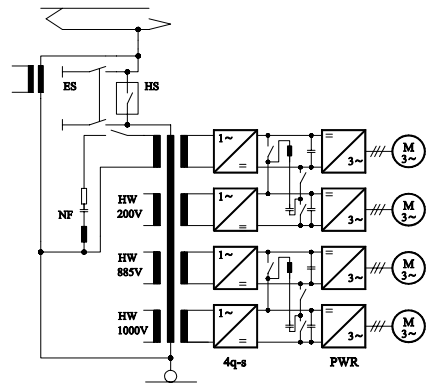


Fig. 7.15: Main circuit diagram of Class 101

- Class 460 of SBB

The locomotives of Class 460 of SBB (Fig. 7.16) are one of the few equipped with three-level GTO-thyristor converters [113]; Fig. 7.17 gives the schematic circuit diagram. The nominal DC-link voltage is 3,500 V, the rated power of one converter, equipped with standard 4.5-kV, 3-kA GTO devices, reaches 3,500 kW, so that only group supply of the two motors in each bogie was economically reasonable.



Fig. 7.16: SBB Class 460 Loco

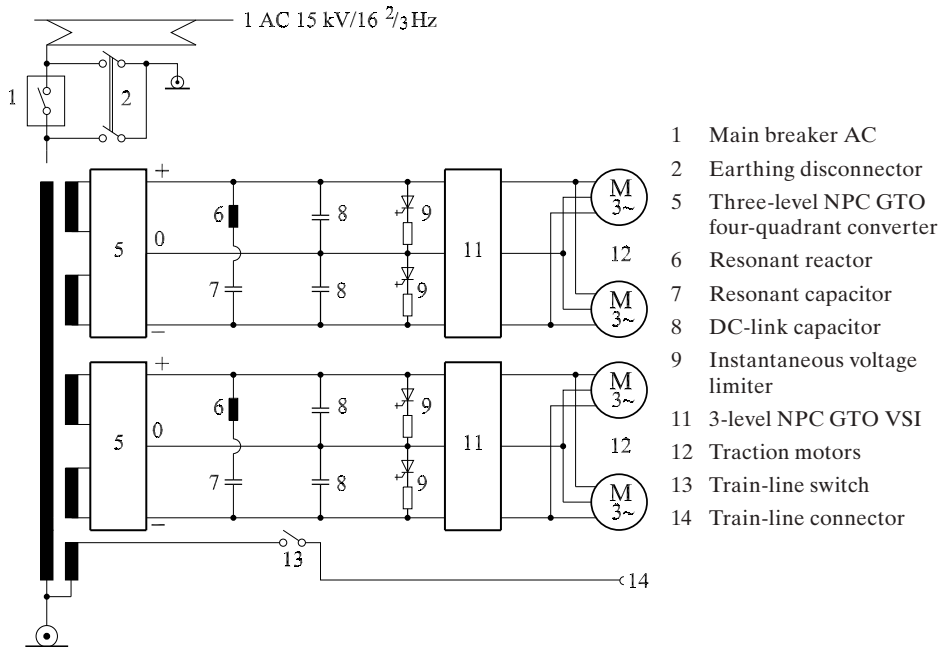


Fig. 7.17: Schematic circuit diagram SBB Class 460 with three-level NPC GTO inverter

The changes in the European railway landscape, mentioned in subchapter 1.1, such as liberalization and deregulation made the former “national” railways – now divided in transportation and infrastructure entities – dispense with the former multitude of individual varieties of locomotive types and turn to more general specifications. This development was supported by the upcoming of independent transport companies, often within bigger “logistics” groups, leasing their traction material from specialized enterprises as Dispolok (a Siemens TS division), Angel Trains (GB) or Mitsui Rail Capital Europe (MRCE), having agreed with Siemens to take over Dispolok in 2007.

Highly standardized and modularized “platform” traction vehicles evolved from this, allowing an optimization in technical and economical regard not possible before, known from the automotive and aviation industry, even including crash tests. An outstanding example is the TRAXX platform of Bombardier Transportation, built in more than 600 locomotives for DB AG, SBB or several leasing houses. They exploit the standardization potential offered by the three-phase drive technology (cf. Fig. 7.11) to an utmost degree. A power of 5.6 MW is delivered by two “seven-phase” traction blocks, three pairs of arms (phases) for the motor inverter and four for two four-quadrant converters, after 2005 equipped with IGBT modules in two-level technology dominantly [254], [255].

Fig. 7.18 shows the side elevation of DB AG Class 185.2 (TRAXX F140 AC2), the multi-purpose, two-frequency (15 kV, $16\frac{2}{3}$ Hz and 25 kV, 50 Hz) variant with $v_{\max} = 140$ kph and $Z_A = 300$ kN, Fig. 7.19 a photo of the equivalent MRCE type; please see subchapter 8.2, Figs. 8.11 and 8.13, too. Due to the relative low maximum speed, the drive is of the axle-hung type (sub-chapter 3.2). As for the diesel-electric locomotive, see subchapter 9.2, Figs. 9.23 and 9.24.

The same holds for the other industrial groups from Table 1.5; the PRIMA platform locomotive of ALSTOM Transports [256] is under delivery for SNCF (Class 437, Fig. 7.20) and the French Veolia Transports (E37.5). The Siemens TAURUS locomotives ES 64 U2...4 using the HAB quill drive (Fig. 3.14) has been delivered to ÖBB (Class 1016, 1116, 1216 [257]), DB AG (Class 182), the Slovenian SZ (Class 541) and e.g. Dispolok, for the full range of power supply systems (Fig. 1.11) and for diesel-electric operation with only minor differences in the mechanical construction. Fig. 7.21 shows locomotive ÖBB 1216.050 after its record trial, on which 357 kph were reached.

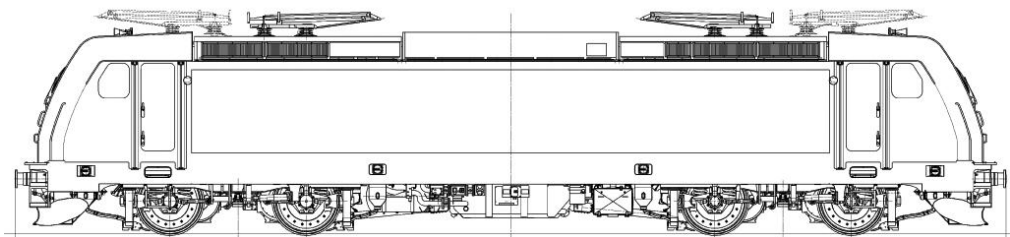


Fig. 7.18: Side elevation of locomotive Class 185.2 DBAG /TRAXX F140 AC2



*Fig. 7.19: TRAXX F140
AC2 MRCE 185 546
(equivalent to DBAG Class 185.2)
Signalling package for
German and France
(Bombardier Transportation)*



*Fig. 7.20: SNCF
Class 437 three-system
locomotive of the Alstom
PRIMA family (type 3U15)
(ALSTOM Transports)*



*Fig. 7.21: ÖBB Class 1216
("Taurus") three-system
locomotive (cf. Fig. 3.14, too)
(Siemens TS)*

7.4.2 High-speed trains

Since the introduction of scheduled high-speed Intercity connections in the thirties (in D, F, GB, I, U.S.A) the two concepts „Locomotive-hauled Train“ and High-speed EMU (cf. section 3.1.1) have been rivaling.

For the high-speed EMU, individual self-propelled units with multiple control, the following technical arguments speak in favour:

- The very high specific drive power ($P \sim v_{\max}^3$) of about 20 kW/t is distributed to many driving wheelsets. Thus it is feasible to keep wheelset loads under the value of 16...17 t, which is regarded necessary for reasons of stability and wear for $v_{\max} = 250...270$ kph/ 155...170 mph; wheelset loads of only 13...14 t necessary for $v_{\max} = 330$ kph/205 mph are only possible with motor coaches with at minimum 50 % driven wheelsets.
- Shorter trains, exploiting the limited station length better.
- Homogenous construction, thus lower train (air) resistance, lower total weight, especially if one bogie per each two car-ends is used (articulation, Jakobs' bogies).

Against high-speed EMUs and pro locomotive-hauled trains the following mainly economic and operational reasons are important:

- Only for small capacities the high-speed EMU is cheaper than the locomotive-hauled trains. It occurred nearly regularly that high-speed EMUs/DMUs had to be substituted for locomotive-hauled trains, when the transportation demand increased, due to the great attractiveness of these high-speed connections.
- The whole electric equipment of high power rating and thus volume has to be accommodated underneath the floor, which is technically more demanding.
- The capacity can only be adapted in rather rough steps (one or two MUs) to the actual demand.
- Individual trailers can be taken more easily out of the train compound, if repair becomes necessary; with multiple units that is only possible in the shops.
- Motor coaches need much more protection from noise and vibration.

Japan made its decision in favour of the EMU concept when introducing its Tokaido Line Shin-Kansen high-speed service in 1964 (cf. Fig. 1.6; [114]). The European railway authorities chose uniformly a compromise solution, the high-speed train with special streamlined trailer coaches and power headcars (cf. Fig. 7.22, top; [115]), e.g. in case of the French TGV (cf. Fig. 7.9), the German Intercity Express ICE 1/2 or the Italian Elettrotreno Rapido (ETR) 500.

The power headcar of the first series of ICE (Class 401, 1990, Fig. 7.23, [B20], [116]) corresponds to locomotive Class 120 of DB in its drive technology. The first 30 trains (with two headcars – cf. Fig. 7.22 top – each and 12...14 trailers) still being equipped with thyristor converters (as in Fig. 6.34, schematic diagram similar to Fig. 7.12), starting with headcar 61 (– 120) the evaporative-cooled GTO converter (Fig. 6.36) with seven phase modules was employed [98]. The drive is the BBC Cardan Hollow-Shaft Drive with Rubber Joints (acc. to Fig. 3.10); but the motor is totally fixed in the vehicle's bridge, to reduce the masses coupled to the bogie. Initially, the possibility to fix the drive to the bogie at low speed, to ease the negotiation of sharp curves (Umkoppelung des Antriebs, UM-AN), was provided; but this did not prove necessary and was abandoned.

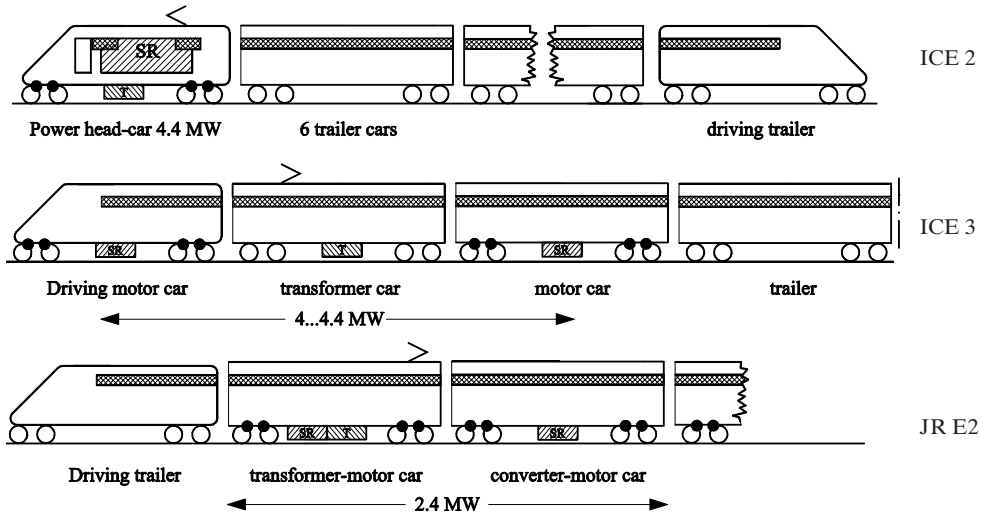


Fig. 7.22: Different concepts of High-Speed Trains

The prototype train Class 410 of ICE reached a speed of 407 kph in 1988. The second series, ICE 2 (Class 402, 44 trains) features one power headcar, six trailers and one control trailer. It enables the so-called “wing-train concept” which is especially suited for the German polycentric structure: The HSTs running united on the high-speed line can be easily split for two final targets, e.g. from Berlin to Düsseldorf via Essen or to Cologne via Wuppertal, with separation in Hamm.

As the ICE 1 trains with roughly one eighth of driven wheelsets are not able to start on ramps of more than 25 % gradient safely if one power headcar fails, it soon became clear that this concept was not suited for the newly planned High-Speed Line Cologne-Frankfurt (Fig. 7.24) with $s_{max} = 40\text{‰}$.

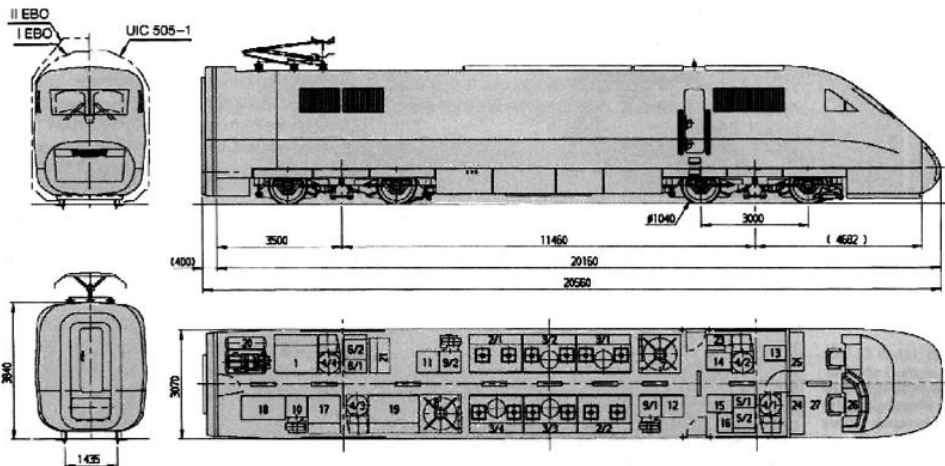


Fig. 7.23: Power Headcar of ICE 1, 2 ($P_N = 4.8 \text{ MW}$)



Fig. 7.24: High-speed line Cologne-Frankfurt

In addition, the planned scheduled maximum speed of 330 kph was not compatible with the axle load of 20 t of the Class 401 power headcars, either. Therefore a new multiple-unit high-speed train ICE 3 (Class 403, or 406 as multi-system vehicle for traffic to Benelux and France, cf. subchapter 8.2) with 50 % driven wheelsets and a wheelset load of only 16 t was developed (see Fig. 7.22, centre, only a half-train sketched); $P_N = 2.4$ MW. A photo of the train has been given in Fig. 1.10, the traction drive is as Fig. 3.15; the underfloor converters (cf. Fig. 7.25) with water-cooled GTO-thyristor modules as in Fig. 6.37, are housed in the 1st and the 3rd coach, the transformer ($G = 9.1$ t) in the 2nd coach.

From the ICE 3, Siemens developed an international “platform” HST VELARO [258], delivered to RENFE, RZD and the railways of Chinese People’s Republic (KZD).

A similar concept is underlying the ICE T, the high-speed train with curvature-dependant body-tilting equipment (section 2.1.5; see Fig. 7.26). With only $v_{\max} = 230$ kph it serves Enhancement Lines (“Ausbaustrecken”) in mountainous areas, not the high-speed lines. It uses the Italian “Pendolino” technology, with two traction motors of 500 kW mounted longitudinally in the motor coaches, driving each inner wheelset per bogie via cardan shafts and bevel gears. Here $6/20 = 30\%$ of the wheelsets of the five-piece Class 411 ($P_N = 3$ MW) or $8/28 = 28.6\%$ in the seven-piece Class 415 ($P_N = 4$ MW) are driven. The transformers are housed in the headcars, so the wheelset load is rather uniformly some 14 t.

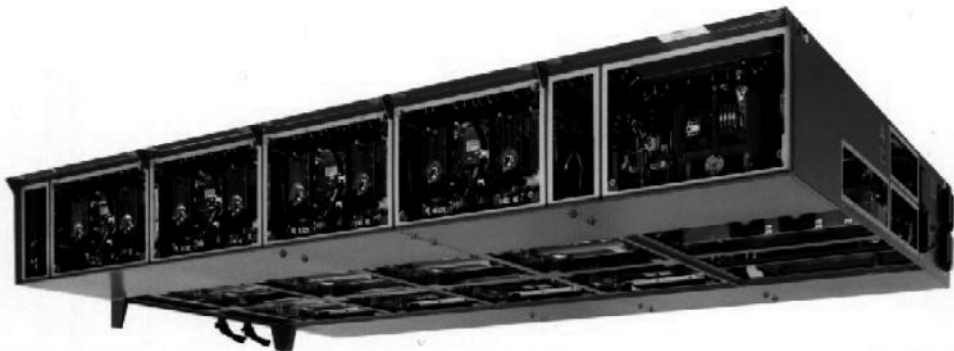


Fig. 7.25: Underfloor converter cubicle 2.2 MW for ICE 3, Class 403 (Siemens AG, A&D)

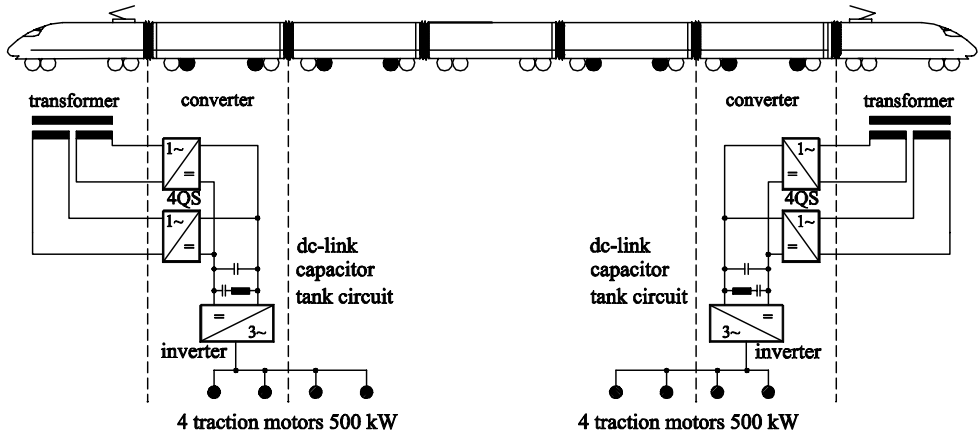


Fig. 7.26: General arrangement of traction equipment in ICE T (Cl. 415, acc. to [B 21])

This is necessary, to prevent the headcars being lifted by sidewinds (this was a problem with the control trailer of ICE 2, when leading). Fig. 7.27 gives a view of the ICE T train.

Fig. 7.22 has depicted (at the bottom line) the configuration of the recent E2-HST of Japan East RR. With IGBT-inverter-fed motors it features 75 % driven bogies. But it was necessary to give each headcar not motored a special “duck-bill profile“, which compensates – like a spoiler – the lessening wheelset load of the first bogie at high speed (Fig. 7.28, [114]). A similar solution had to be chosen with the new Talgo power headcars for Spain ($v_{max} = 350$ kph) by Krauss-Maffei/Bombardier.

A special problem arises with HSTs from current collection: The first pantograph excites long-wave oscillations of the catenary, which disturb the contact of the second one. Many HSTs use only one pantograph in service and feed the motor units via a HV connection cable in the roof (e.g. ICE 3, ICE T). The ICE 1 does not have such a connection line, for cost reasons; but this is admissible as the pantographs of both power headcars have a distance of about 400 m, in which the disturbing oscillations have died away already. The same holds for the French TGV.



Fig. 7.27: View of ICE T Class 411 DB AG



Fig. 7.28: Power headcar JR East E2 with duck-bill profile

8 Multi-system traction vehicles

8.1 Examples with DC commutator motors and synchronous motors

In the very early times of main-line electrification systems with different voltages and frequencies were strictly separated. So there was no demand of traction vehicles able to be operated on more than one power supply system. Times changed after World War II when

- in Western Europe traffic crossing the borders rose enormously as a consequence of the “Montan Union” and the Treaties of Rome (founding of EEC/EU) and
- in France the “new” 50-Hz AC system (north of the line Cherbourg–Paris–Basel) collided with the old 1500-V DC system at more and more nodes.

The most simple solution was chosen at the system change points between Belgium (DC 3 kV) and the Netherlands (DC 1.5 kV), by not using the upmost series grouping of the Belgian traction vehicles under 1.5 kV. Later, the 50-Hz AC system was included by using a transformer without a switch-gear and a diode (Ignitron) rectifier (cf. Fig. 8.1), controlling the motor voltage and thus the speed under both DC and AC systems by means of the resistor camshaft control. On principle the same technology was used with the German-Czech dual-system locomotives DB 180 / ČD 372 (AC 15 kV/16 ²/₃ Hz and DC 3 kV).

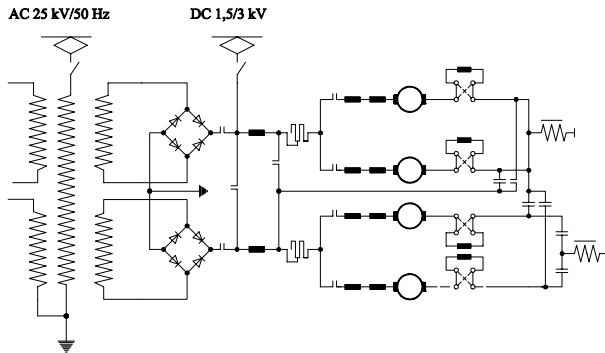
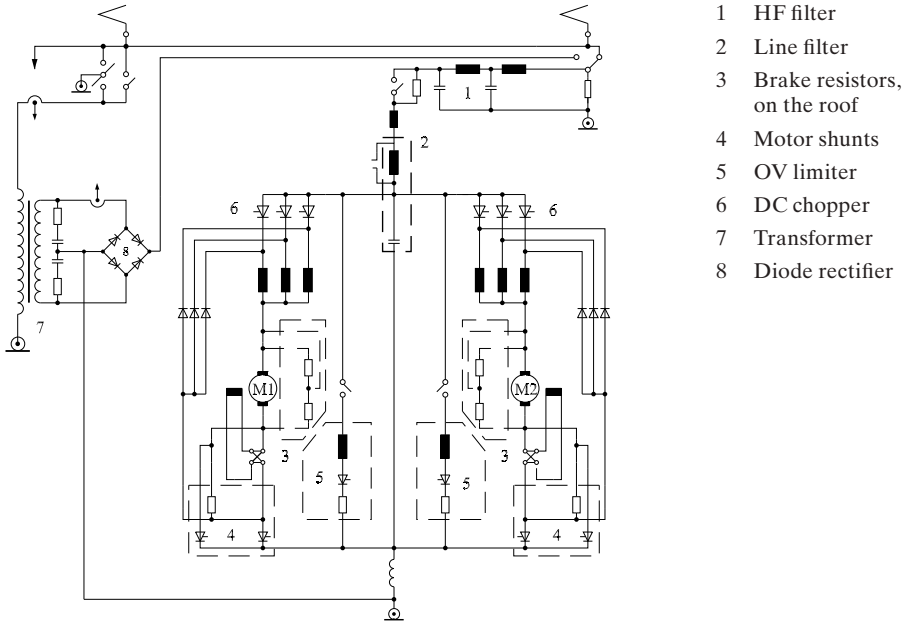


Fig. 8.1: Schematic diagram of three-system locomotive SNCB Class 1500 (1961)

In the “2nd generation”, the recently introduced DC-chopper technology was substituted for the traditional starting resistors. In the years 1971–76 the French SNCF developed three series of identical mechanical design and a nominal power of some 4,600 kW:

- Class 7 200 (DC 1.5 kV): Only DC-chopper control
- Class 15 000 (AC 25 kV/50 Hz): Only AC sequential phase control
- Class 22 200 (DC + AC): DC chopper control with additional transformer and diode rectifier for AC operation

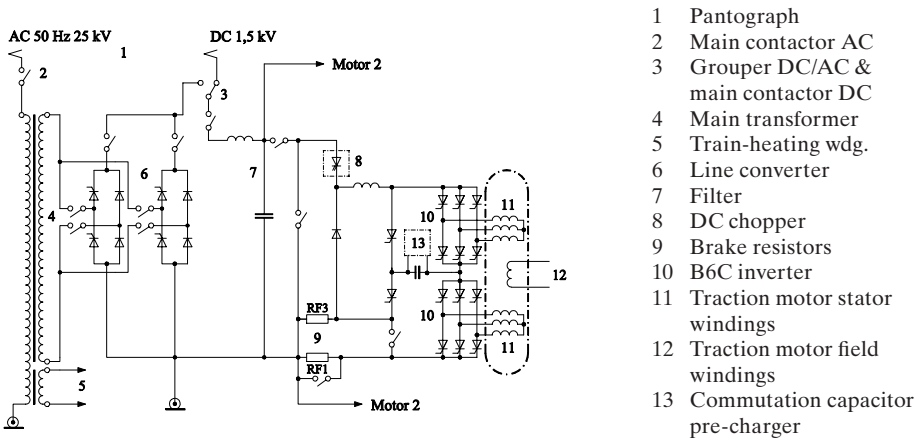
Fig. 8.2 displays the schematic diagram of the dual-system Class 22 200: Per bogie (with Monomoteur drive, cf. Fig. 3.16) three choppers are provided, the switchings staggered by 120° each. Electric braking is provided via chopper-controlled resistors.



- 1 HF filter
- 2 Line filter
- 3 Brake resistors, on the roof
- 4 Motor shunts
- 5 OV limiter
- 6 DC chopper
- 7 Transformer
- 8 Diode rectifier

Fig. 8.2: Schematic circuit diagram SNCF Class 22 200 with D- chopper control

Fig. 8.3 represents the successor SYBIC Class 26 500 (cf. subchapter 5.2): The DC commutator motor is substituted for the "12-pulse Converter Motor" (over-excited double-star synchronous motor and thyristor bridge inverter (2 x B6C)) [39].



- 1 Pantograph
- 2 Main contactor AC
- 3 Grouper DC/AC & main contactor DC
- 4 Main transformer
- 5 Train-heating wdg.
- 6 Line converter
- 7 Filter
- 8 DC chopper
- 9 Brake resistors
- 10 B6C inverter
- 11 Traction motor stator windings
- 12 Traction motor field windings
- 13 Commutation capacitor pre-charger

Fig 8.3: Schematic circuit diagram of SNCF Class 26 500 SYBIC with double-star synchronous converter motor

An extraordinary, but eventually not successful first attempt of self-commutated power electronics was the four-system locomotive Class E 410 (later 184.0) of DB, developed 1965 by AEG and Krupp (Fig. 8.4). The locomotive is equipped with four undulating-current traction motors of 800 kW, controlled permanently by bridge rectifiers in half-controllable connection. In DC mode the mains voltage is converted by a forced-commutated thyristor inverter into 110-Hz rectangular-block AC voltage and conveyed to the main transformer [117], [B25, pp. 300 f].

At DC 1.5 kV the inverter inputs are connected in parallel, at DC 3 kV in series connection. The AC systems selection between 15 kV, 16 ²/₃ Hz and 25 kV, 50 Hz is performed at the secondaries of the transformers, in the same way as with most dual-frequency locomotives, e.g. Class 181 of DB.

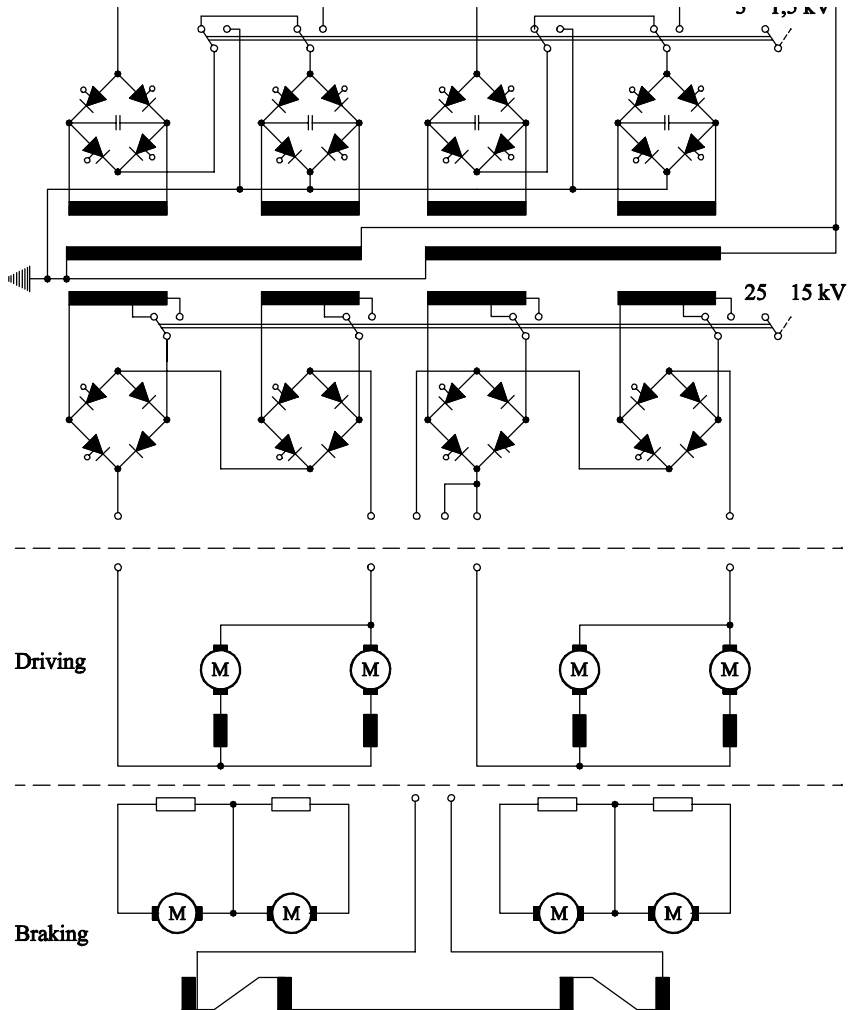


Fig 8.4: Schematic diagram of four-system locomotive Class 184 of DB, by AEG/ Krupp, of 1965.

8.2 Examples with inverter-fed induction motors

With the economical success of border-crossing Eurocity-(EC-) trains and High-Speed Trains like TGV and ICE and with the progressing deregulation and liberalization of European railway transport, the demand of high-performance traction units – now of course with three-phase drive technology – grew, able to cross the borders of the railway power supply systems without hindrance [118]. As a side remark: The roundabout 17 different train safety systems in Europe represent a much more severe obstacle today, which is going to be solved by superior computer-based and GSM-supported train control and safety systems as ETCS within the ETRMS.

In the times of GTO traction inverters the traction unit (locomotive, power headcar) with two bogies with independently controlled VSI drives could be regarded as the European standard high-performance concept [50]. The nominal DC-link voltage was 2400...2800 V, with both DC links paralleled via the two contactors shown centre-right in Fig. 8.5, and three four-quadrant converters with staggered pulsing, identical to the traction inverters. Three of them were necessary for two times 1.6-MW drive power in the 50-Hz AC system, for thermal reasons. The 4.5-kV GTO thyristors then only available did not permit direct operation off the 3-kV DC mains, due to line over-voltages exceeding 4.5 kV.

On principle it is possible to group the two inverters at 3-kV DC in series and at 1.5-kV DC in parallel and connect them via a filter choke with the catenary (provided the isolation level to earth is chosen suitably). But as the data of the traction motors have to be chosen for the dominant AC operation for a DC-link voltage of ~2.8 kV, the break-down torque and by that the power at maximum speed will be reduced too much at the actual DC-link voltage of only 1,500 V per inverter (cf. subchapter 6.1; [49]). This the customers will not accept.

With a DC-line voltage of 750...1500 V each pair of arms of the input four-quadrant converter can be re-grouped as a step-up two-quadrant converter [119]. The problem arises with the 3-kV operation. Two solutions chosen in the “GTO era” shall be represented:

$$U_F = 15\text{kV} / 16^{2/3} \text{ Hz} \& 25 \text{ kV}, 50 \text{ Hz}$$

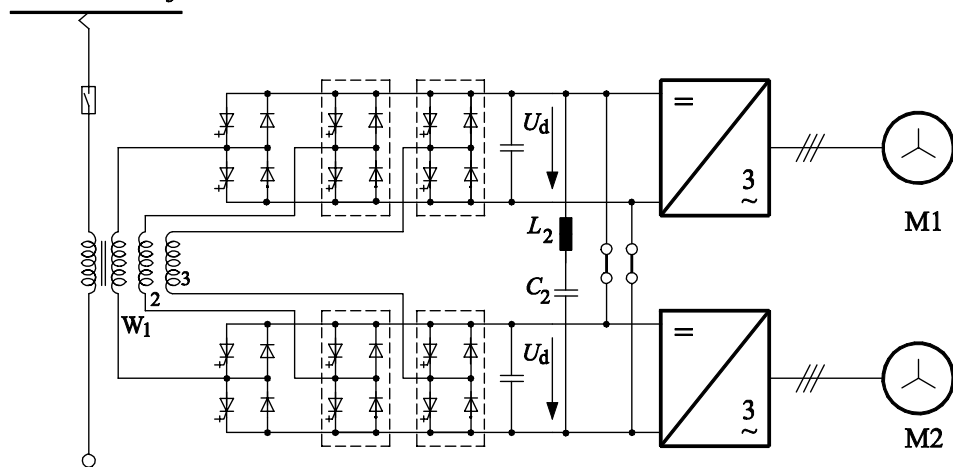


Fig. 8.5: Basic circuit diagram of one bogie of a high-performance dual-frequency traction vehicle in three-phase technology, as basis for a multi-system concept (voltage adaption not shown).

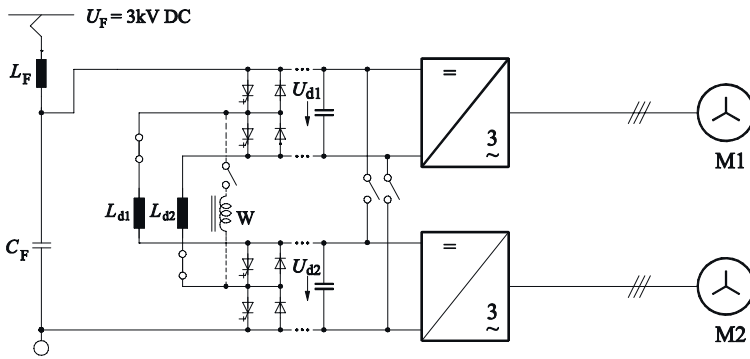


Fig. 8.6: Series connection of input 2q-chopper and DC link of the respective other drive

a) Each step-up chopper (from the re-grouping of the 4q-C pair of arms, as just mentioned) will be connected in series with the DC-link capacitor of the other converter (Fig. 8.6). Thus

$$U_F = U_{d1} + a_2 \cdot U_{d2} = U_{d2} + a_1 \cdot U_{d1} \tag{8.1}$$

holds. The input voltage U_F must always be greater than the nominal value of the DC-link voltage, else it and thus power would be reduced with lower line voltage. This solution has been chosen by Siemens TS for the Spanish locomotives RENFE S 252 [120] and the multi-system high-speed trains ICE 3 Class 406 [121] or by ALSTOM for the SNCF 36 000.

b) The additional smoothing reactors $L_{d1,2}$ may be regarded as a drawback, as increasing weight and losses. Adtranz developed for the three-system locomotives Class E 412 of Italian State Railways (FS) in 1993 a new Double-Star Connection (Fig. 8.7): The two inverters shown left are operated in AC mode (Germany, Austria 15 kV, 16 2/3 Hz or 25 kV, 50 Hz in South-East France) as three-phase four-quadrant converters, with paralleled DC links of $U_{dN} = 2700$ V; the two partial winding systems of the double-star motors are connected in series. In 3-kV DC mode both DC links are connected in series, the now separated motor partial winding systems (with a new star for the first by means of an additional contactor system) are fed by inverters from different DC links cross-wise. So even at different motor powers (cf. section 2.2.6) the two partial DC-link voltages remain balanced [122], [123].

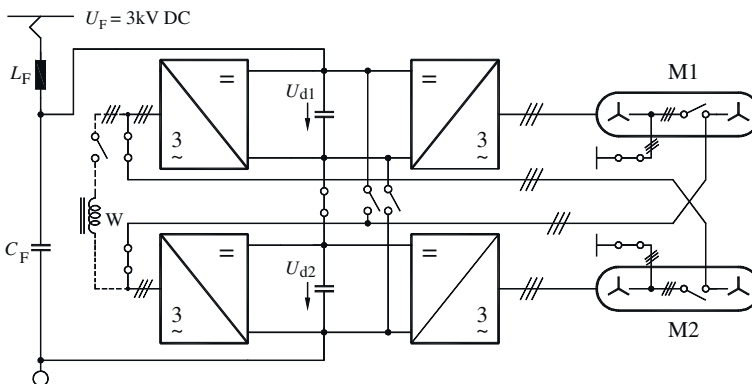


Fig. 8.7: Double-Star Connection (Adtranz, FS Italia Rh. E 412); 3-kV connection



Fig 8.8: RENFE S 252 (5.6 MW;
AC 25 kV 50 Hz and DC 3 kV)
(Siemens AG, TS)



Fig. 8.9: FS Italia Class E 412
(6 MW, AC 15 kV/16²/₃ Hz; 1.5 and 3 kV)
(Bombardier Transportation)

Both models are shown in the Fig. 8.8 and 8.9, respectively.

The dual-system locomotives Class 1822 of ÖBB (AC 15 kV/16²/₃ Hz and DC 3 kV), delivered by ABB and Siemens in 1993, are equipped with three-level inverters and 4q-Cs, similar to those of Class 460 of SBB with 4.5-kV GTOs (section 7.4.1). As they have a nominal DC-link voltage of 3.5 kV, direct operation off the 3-kV DC mains is possible. This has been a motive for adoption of the three-level GTO converter with 4.5-kV devices then [124].

In the long-term perspective all these solutions must be regarded as interim steps, which are going to be superseded by introduction of 6.5-kV IGBTs. It is already clear that the intermediate stage of 6.5-kV GTOs will be leapt over, apart from two specimen in Brazil and Slovenia [125]. Due to modularity and easier paralleling of the IGBT devices, there will be two 4q-Cs per bogie, in general.

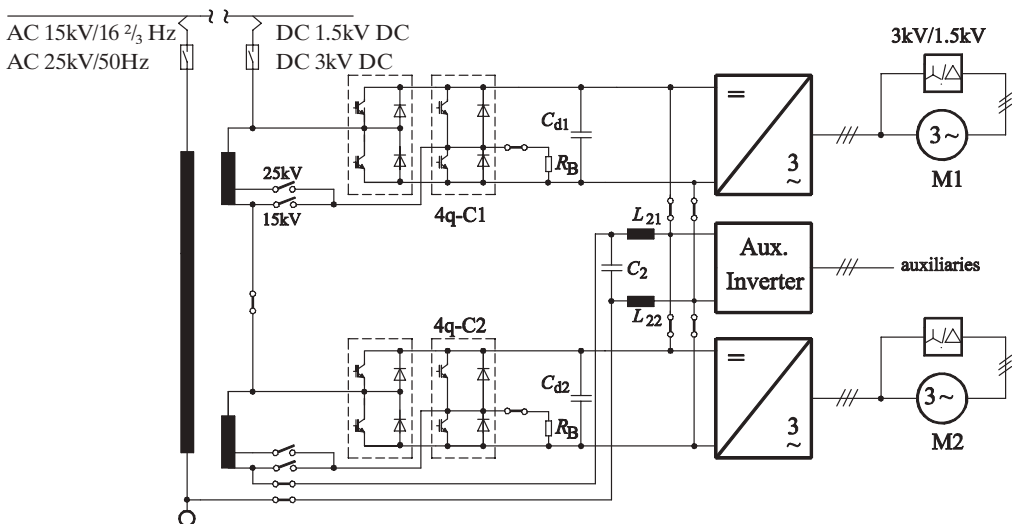


Fig. 8.10: Direct connection of 6.5-kV IGBT converters to the 3-kV DC mains in Class 189 DB AG

Fig. 8.10 shows the principle schematic diagram of the four-system locomotive Class 189 of DB AG, developed by Siemens TS, with 6.5-kV IGBT converters.

The contactors are shown in the 3-kV DC position only [127]. In DC mode the leakage inductivity of the secondary windings of the transformers serves as the first stage of the input filter, together with the resonant-circuit capacitor C_2 ; the respective resonant-circuit reactors L_{21} , L_{22} serve with C_{d1} , C_{d2} as second stage.

To adapt the traction drives (dimensioned for 3-kV DC-link voltage) to 1.5-kV DC operation, a star-delta re-grouping of the motor windings is used. This is possible, as at 1.5-kV DC only a reduced power of 4.2 MW is specified (AC: 6.4 MW, 3-kV DC: 6 MW). The break-down torque is then still $0,5^2 \cdot \sqrt{3}^2 \cdot 100\% = 75\%$ of the value at 3-kV operation (cf. Fig. 6.9). The ÖBB Class 1216 (Fig. 7.21) is delivered with the same inverter, but without the star-delta switch, as it needs not to serve 1.5-kV lines.

For all traction VSIs fed directly from the DC mains holds, that the minimal instantaneous value of the line voltage (e.g. -30% acc. to EN 50163 pt.1) determines the maximal motor leakage inductivity, to produce the break-down torque (equ. (6.11) necessary for the demanded power at maximal speed, as explained in subchapter 6.1, Fig. 6.9, and to be trained in Exercise 15.6. At maximum DC-mains voltage the harmonic losses of the motor will then be increased roughly by a factor of $[(1 + \delta_{U+})/(1 - \delta_{U-})]^2$, compared to a design with stabilized DC-link voltage.

These deliberations and the wish to use the same traction motors (without enhanced insulation) as in the standard AC TRAXX locomotives with $U_d \leq 2.8$ kV led Bombardier Transportation in the case of Class Re 484 for SBB to the following decision: At 3-kV DC operation the pairs of arms of the 4q-C are to be used as two-quadrant step-down pre-choppers for the traction inverter (Fig. 8.13, [127]). To that purpose the 4q-Cs (and inverters) are equipped with 6.5-kV IGBT modules. In the 1.5-kV DC operation mode the 4q-C is used as a step-up chopper. In both cases the leakage inductance of the transformer is used as filter, together with the re-grouped resonant-circuit capacitor C_{Saug} .

Finally, Fig. 8.11 offers a photo of locomotive Class 189 of DBAG, Fig. 8.12 of the Swiss Class Re 484.



Fig. 8.11: DBAG Class 189, with 6.5-kV IGBT inverters operated directly off the 3-kV DC mains (Siemens AG, TS)



Fig. 8.12: SBB Class Re 484 with 6.5-kV IGBT inverters operated with the 4q-C as pre-chopper in 3-kV DC mode (Bombardier Transp.)

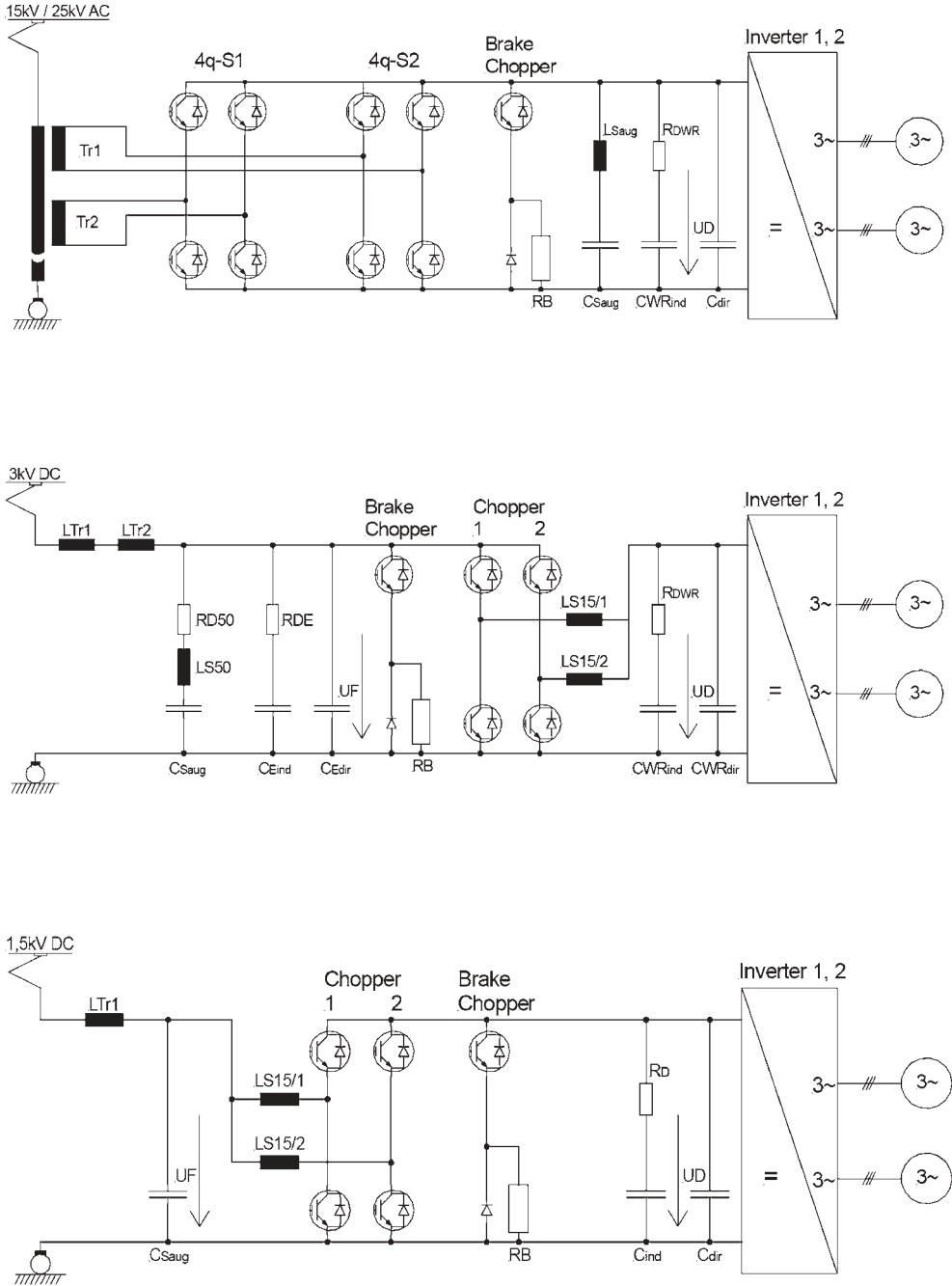


Fig. 8.13: Traction circuit for one bogie of SBB Re 484 in AC mode (top), 3-kV DC mode (centre) and 1.5-kV DC mode (bottom). (Bombardier Transportation)

9 Diesel-electric traction vehicles

9.1 Conventional technologies – hydraulic and electric drive chain

Traction vehicles with a diesel engine as primary energy source are necessary, when the line – due e.g. to minor capacity – has not been electrified, as treated in subchapter 1.4; the spark-ignition (Otto-cycle) engine and the gas turbine play only a peripheral role in railway traction.

Central problems when using a diesel engine in traction are

- its incapacity to deliver torque when starting, in contrast to the steam piston engine and the electro motor, and
- the rather fixed linkage of power and speed at minimum fuel consumption.

In street-bound vehicles these problems are overcome by

- the clutch, which allows to start the engine separately from the drive and which takes up speed differences at starting, and
- the change-speed gear, which can assign different speed-traction effort pairs to the same power of the diesel engine,

With rail-bound vehicles this is only possible at low power levels (e.g. with rail buses). The same holds true for the hydrostatic converter, known from excavators.

For rail traction vehicle of high power only at hand are

- the diesel-hydraulic power transmission with hydrodynamic (Föttinger) converter, which was and is extensively used in Germany, and
- the diesel-electric power transmission, either with DC commutator motors (“classical“ DE technology), or with inverter-fed induction motors.

Fig. 9.1 shows in a schematic way the hydro-dynamic converter according to H. Föttinger. The primary turbine wheel is driven by the diesel engine with constant speed n_1 and constant input torque M_1 (at given power) and accelerates as a centrifugal pump the oil. This is diverted by the (fixed) turbine guide wheel and drives the secondary (output) turbine wheel.

Fig. 9.2 gives the dependence of the output torque M_2 upon output speed n_2 ($m = M/M_1$). In principle, the Föttinger converter enables a variable speed ratio, similar to a $\dot{P} = \text{const}$ -characteristic. Yet the efficiency goes down to zero at $n_2/n_1 = 0$ and 1.

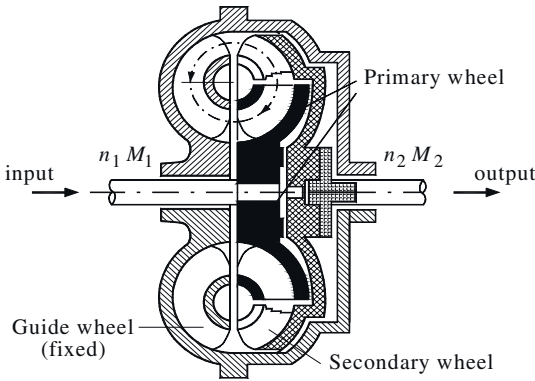


Fig. 9.1: Hydro-dynamic torque converter acc. to H. Föttinger

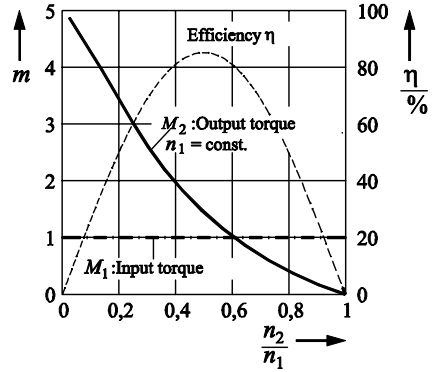


Fig. 9.2. Output characteristic of Föttinger hydro-dynamic converter; $n_1, M_1 = \text{const}$

Generally, several converter stages (3...4) with different gear ratios are used for the different speed ranges, which are filled or emptied successively and thus engaged. Small tractive forces at low speed, as e.g. needed in shunt operation, are reached by partial filling. If necessary, a switchable gear (express or goods train gear) is put behind which, in addition, allows reversing. In Fig. 9.3 an older three-converter gear with attached reversing gear can be seen.

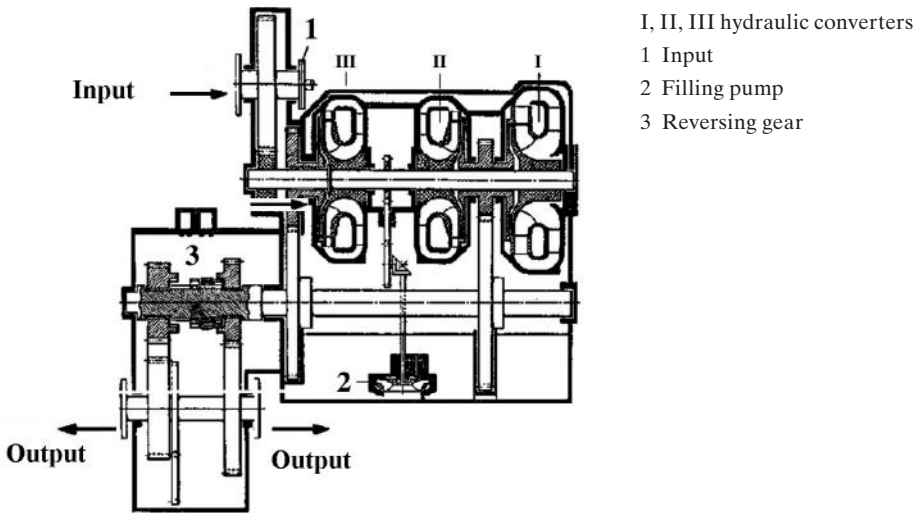


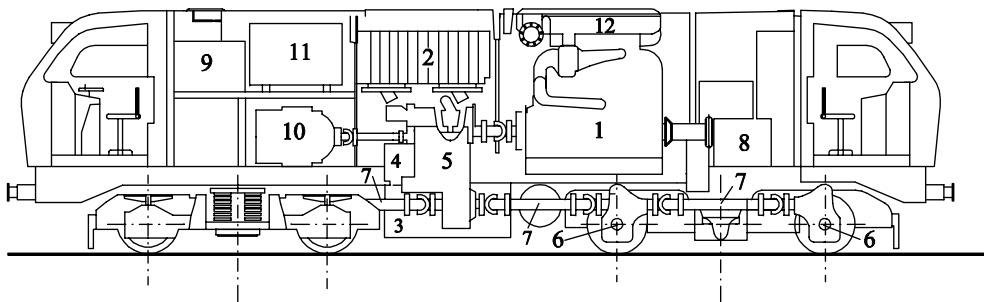
Fig. 9.3. Three-converter gear with attached reversing gear (Voith, [B1])

Diesel engine and hydro-dynamic converter can be drawn upon for braking vehicle and train, similarly as known from the resistor brake of electrically driven vehicles. The Voith vortex brake, attached to the turbo converter, is a hydraulic circulation with a throttle. Filling the circulation partially the brake power can be adapted. The losses of the hydro-dynamic converter and those of the brake circulation must be dissipated by a radiator.

The first successful diesel locomotive with hydro-dynamic converter of bigger power was commissioned in 1935 (DR V 140 with 1035-kW engine; Krauss-Maffei, MAN, Voith). After World War II DB developed a family of diesel-hydraulic traction vehicles, locomotives, motor coaches and rail buses with nominal powers from 180 up to 2850 kW.

Fig. 9.4 represents the most widespread 1,840-kW diesel locomotive Class 218 of DB. All four wheelsets are driven via cardan shafts (7) and bevel gears (6) from the central block (5), containing the converter, a two-stage gearbox and the reversing gear. A separate heating 3AC generator (10) is provided; its output voltage – with a frequency varying with engine speed – is converted by a cycloconverter (11), to feed the $16\frac{2}{3}$ -Hz, 1000-V train line.

Recently (2006) new 3,600 kW diesel-hydraulic prototypes ‘Maxima 40CC’ have been presented by Voith Turbo Lokomotivtechnik GmbH, Kiel.



- | | |
|-----------------------|---------------------------|
| 1 Diesel engine | 7 Cardan shaft |
| 2 Radiator + blower | 8 Starter-dynamo |
| 3 Diesel oil tank | 9 Starter battery |
| 4 Hydro-dynamic brake | 10 Heating generator |
| 5 Hydraulic converter | 11 Heating cycloconverter |
| 6 Wheelset bevel gear | 12 Exhaust sound-absorber |

Fig. 9.4: Diesel-hydraulic locomotive Class 218 of DB (1971) $P = 1840 \text{ kW}$, $v_{max} = 140/95 \text{ kph}$

The electric transmission with DC commutator traction motors was developed after World War I mainly in the U.S.A. by GM, GE and Westinghouse, in parallel by BBC Switzerland, from 1935 on. After World War II this technology got its way in the U.S.A. very fast as the one and only traction power. Initially DC generators were coupled to the diesel engine, which were substituted in the sixties by 3AC synchronous generators with diode rectifiers.

The traction motors are controlled via the generator excitation, with speed and power of the diesel engine set by the control lever, according to the "shell diagram", the plot of power vs. speed with diesel-oil consumption as parameter (Fig. 9.5). The characteristic shall run through the minima.

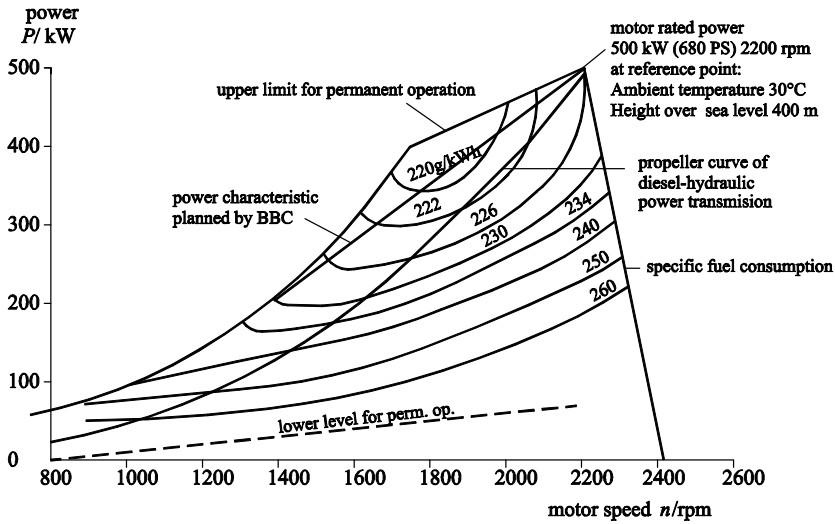
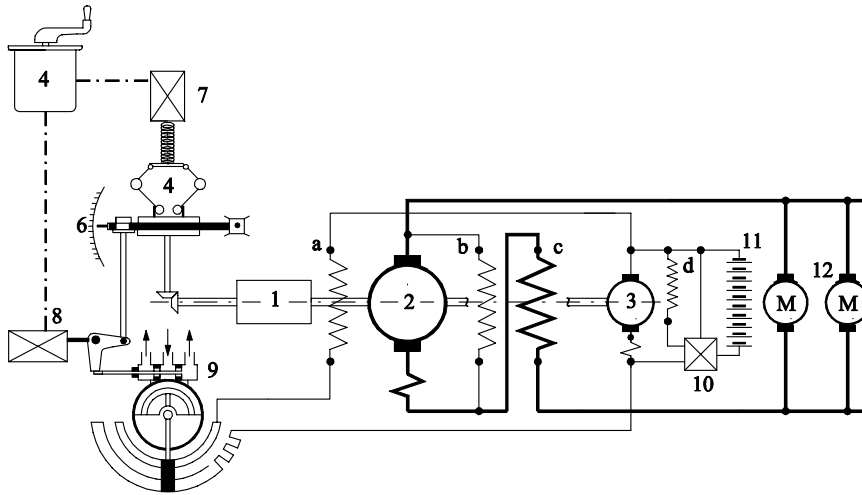


Fig. 9.5: *n-P characteristics of diesel engine MTU 6V 331 TC 12 (500 kW)*



- | | |
|---|--|
| 1 Diesel engine | 6 Fuel lever of diesel engine |
| 2 Main generator | 7 Electro-pneumatic speed controller |
| a Separate-excitation winding of main generator | 8 Torque control lever |
| b Shunt-excitation winding of main generator | 9 Servo-field controller |
| c Differential compounded series winding | 10 Combined battery-charge relay with voltage controller |
| 3 Auxiliary generator | 11 Battery |
| d Shunt-excitation winding of auxiliary generator | 12 Traction motors |
| 4 Control lever | |
| 5 Speed controller of diesel engine | |

Fig. 9.6: *Schematic diagram of BBC Servo-Field Controller [B1]*

Speed must not be “squeezed”; this was difficult to maintain, until electronic regulators became available. An example for the historic technology is the BBC Servo-Field Controller (Fig. 9.6): In the left part the operating point is set by a centrifugal controller, via the filling. The main generator (2) has windings for shunt, differential compounded series and separate excitation, the last controlled by an auxiliary generator via the servo-field controller [B 10].

An actual electronic control is depicted in Fig. 9.7. The control lever (1) gives the filling set value, matching the wanted throttle position. From that a characteristic (2) derives the optimal speed set value, which is compared with actual speed, measured by a tacho generator (6), in the controller (3). The output of (3) is the excitation-current set value, which is amplified in the excitation DC chopper (4) – leading the armature current I_A , measured in (8). So squeezing of diesel-engine speed is safely prevented.

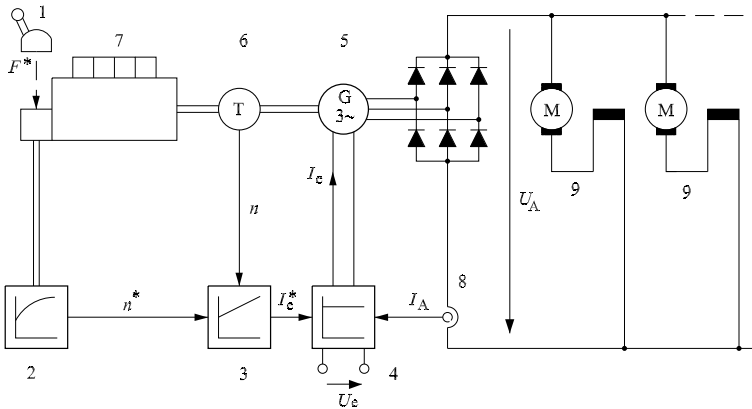


Fig. 9.7: Electronic generator control for diesel-electric traction vehicles with 3AC generator (EEW-TUD)

Today the AC generators are mostly equipped with brushless excitation (Fig. 9.8). The auxiliary excitation current I_c – controlled by a transistor chopper – feeds the fixed auxiliary excitation winding (1), inducing the voltages in the three-phase armature winding (2) on the rotor, which are rectified in a diode bridge (3) and supply the main excitation winding (4). (5) is the main three-phase stator winding system. Salient-pole as well as turbo rotors are found.

Electric transmission attains higher efficiency in the range of low speed than diesel-hydraulic transmission, but is heavier, in general.

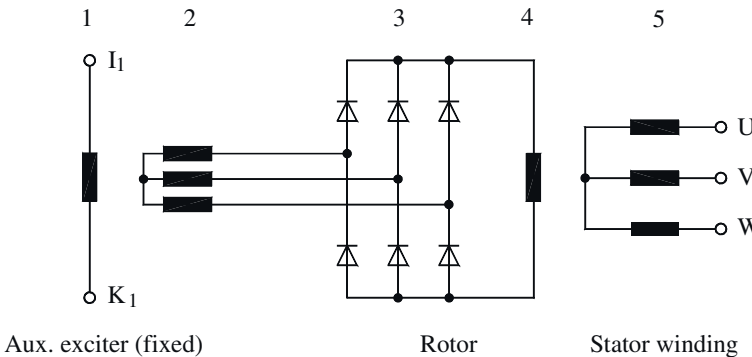


Fig. 9.8: Brushless synchronous generator for diesel-electric locomotives [B5]

9.2 Diesel-electric traction vehicles with three-phase drives

Though a mature technology, present on all world markets, diesel-electric transmission with DC motors comes to its bounds, resulting from the general limitation by the commutator and the need of maintenance – the same arguments in favor of the three-phase drive in line-fed high-performance traction vehicles.

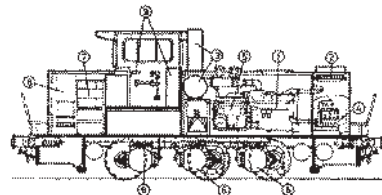
It was due to the simpler, line-independent power supply of the inverters that a diesel-electric locomotive was the first to be equipped in 1971 with the new three-phase drive technology, Class DE 2500 produced by Henschel and BBC (cf. Fig. 1.8, [128]). Subsequently many locomotives were delivered by BBC/ABB with this technology, characterized by

- Light-weight high-speed induction traction motors
- Thyristor voltage-source PWM inverter with phase commutation (cf. Fig. 6.23)
- Slip-frequency-stator-current characteristics control (subchapter 6.3).

As an example the 500-kW shunt locomotive type DE 501, built by BBC with MaK in 1979 [128], [130]) shall be described in detail. Fig. 9.9 shows the three-axle locomotive, Fig. 9.10 the side elevation with the arrangement of the main components, Fig. 9.11 the schematic circuit diagram. The speed-power characteristic of the diesel engine MTU 6V 331 TC 12 has been given in Fig. 9.5, the structure of the overall control is in Fig. 9.12.



Fig. 9.9: Diesel-electric shunt locomotive DE 501RAG



Diesel-engine plant	Electric part
1 Diesel engine	5 Generator
2 Radiator	6 Traction motors (pin-and-nose drive)
3 Exhaust	7 Apparatus frame
4 Brake compressor	8 Brake resistor
	9 Control

Fig. 9.10: Arrangement of components in DE 501 (Bombardier Transportation)

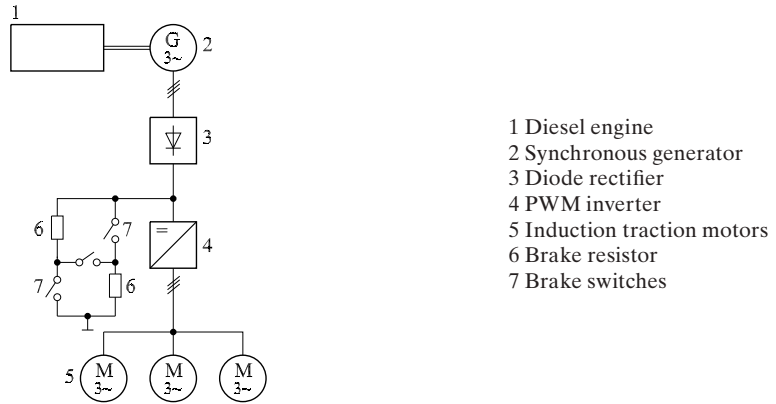


Fig. 9.11: Schematic circuit diagram of DE 501

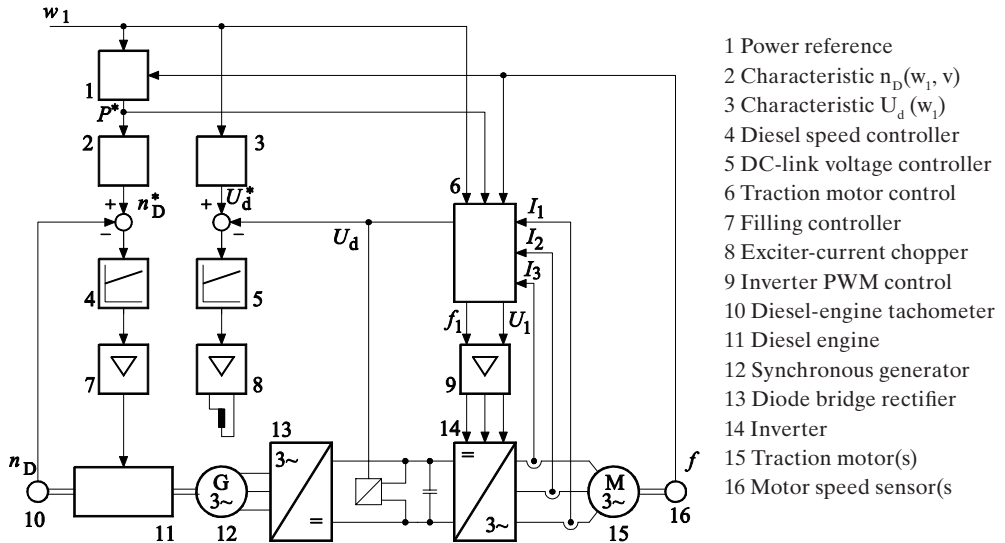


Fig. 9.12: Control structure of locomotive DE 501

The left column in Fig. 9.12 represents diesel-engine control with autonomous speed control, i.e. the diesel-motor speed error acts on the filling controller. Throttle position w_1 is the relative torque set value, which is understood beyond v_1 as the relative power set value.

The centre column contains the DC-link voltage control.

The right block is the genuine traction-motor control. According to the then state-of-the-art an 850-kVA thyristor inverter type 13SG02a (Fig. 6.32) with slip-frequency-current control (Fig. 6.16) was used. Fig. 9.13 gives the tractive/braking effort curves, depending upon speed, Fig. 9.14 the control characteristic of the traction motor, for $\vartheta = 130^\circ\text{C}$ and full-load. Table 9.1 sums up some important data of the locomotive.

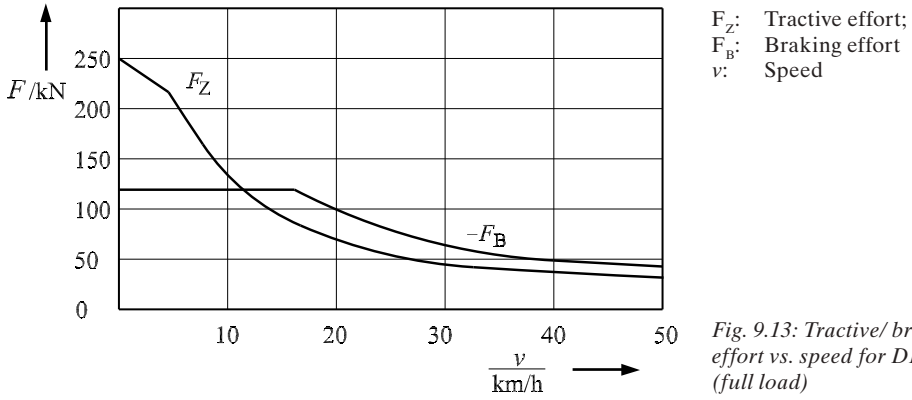


Fig. 9.13: Tractive/braking effort vs. speed for DE 501 (full load)

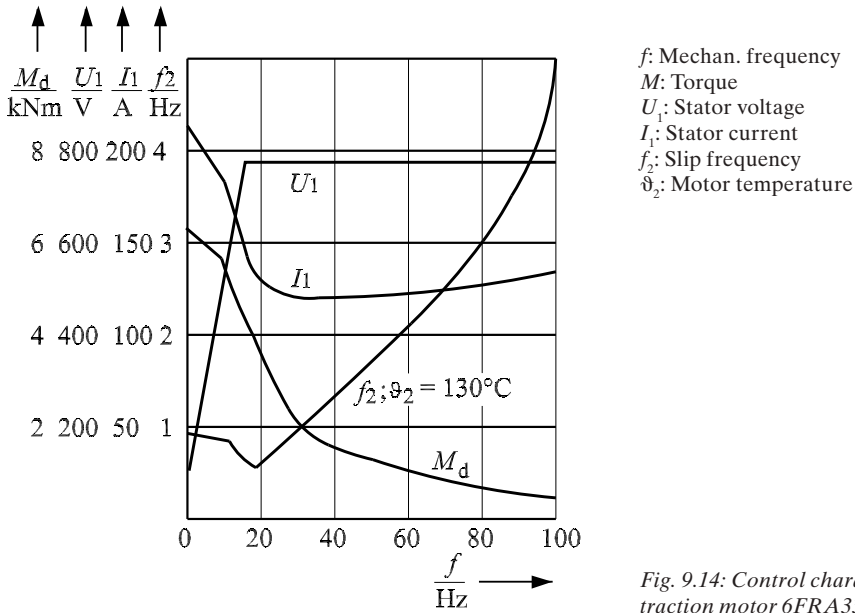


Fig. 9.14: Control characteristics of traction motor 6FRA3371 of DE 501

Table 9.1 Main data of DE shunt locomotive DE 501

Diesel engine	6 V 331 TC12 MTU
Diesel speed range	800 ... 2200 min ⁻¹
Rated power	500 kW
Weight in service	66 t
Gauge	1435 mm
Length over buffers	9470 mm
Maximum speed of locomotive	50 kph

The diesel engine of a shunt locomotive is to be operated always with optimal speed, i.e. that with minimum fuel consumption. For the dimensioning of the generator we start with the point of constant power (v_1 acc. to UIC, cf. Fig. 6.9). As the generator is always loaded with $|\cos \varphi| \approx 1$ by the diode rectifier, the rated synchronous e.m.f. E_{pN} at rated speed n_{DN} and nominal excitation is

$$E_{pN} = \sqrt{1 + x_{dN}^2} \cdot U_{SN} = \sqrt{1 + x_{dN}^2} \cdot 0.78 \cdot U_{dN} = \frac{x_{dN} \cdot I_{SN}}{U_{SN} / \sqrt{3}} \quad (9.1)$$

with the normalized synchronous reactance $x_{dN} = \frac{X_{dN} \cdot I_{SN}}{U_{SN} / \sqrt{3}}$ (cf. Figs. 5.3 and 5.4, $\varphi = \pi$ due

to consumer arrow system applied to the synchronous machine, $R_s \approx 0$). The starting point with rated tractive effort is regarded; here diesel engine and generator have to cover

- the losses of the traction motors and the inverter, equal to the rated losses of ≈ 55 kW
- the auxiliary power demand about 6 % P_{DN} ≈ 30 kW
- the generator losses ≈ 10 kW

roughly 100 kW. Thus the minimum speed n_{DE} acc. to Fig. 9.5 is $\approx 1100 \text{ min}^{-1} = 50 \% n_{DN}$.

To commutate the rated starting current amplitude of the traction motors, the forced-commutated inverter needs the full DC-link voltage U_{dN} , but only – due to the PWM principle – a very small input current, corresponding to the purely active power. Neglecting its voltage drop at the generator reactance, $E_p \approx U_{SN}$ holds, we obtain with the "oversize factors"

- k_{HG} for the main-generator iron cross-section
- k_{HE} for the auxiliary-generator iron cross-section

(the copper cross-section is not to be oversized!) the following dimension equation:

$$E_{pA} \approx \left(\frac{n_{DE}}{n_{DN}} \right)^2 \cdot k_{HG} \cdot k_{HE} \cdot E_{pN} = U_{SN} \quad (9.2)$$

and with

$$E_{pN} = E_{pA} \approx \left(\frac{n_{DE}}{n_{DN}} \right)^2 \cdot k_{HG} \cdot k_{HE} \cdot E_{pN} = U_{SN}$$

eventually

$$k_{HG} \cdot k_{HE} = \left(\frac{n_{DN}}{n_{DE}} \right)^2 \cdot \frac{1}{\sqrt{1 + x_{dN}^2}} \quad (9.3)$$

With an typical value of $x_{dN} = 1.5$ the product $k_{HG} \cdot k_{HE}$ must be 2.25, i.e. the iron cross-sections of both main and auxiliary generator must be oversized by some 50 %, the rated apparent power is about 750 kVA. This is considerably less than with a classical DC transmission, in which at a ratio of $v_2/v_1 \approx 8$ (as in Fig. 9.13) and a maximal field-weakening degree of 1:3 of the DC commutator motors the generator apparent power is roughly $8/3 = 2.7$ times the traction power.

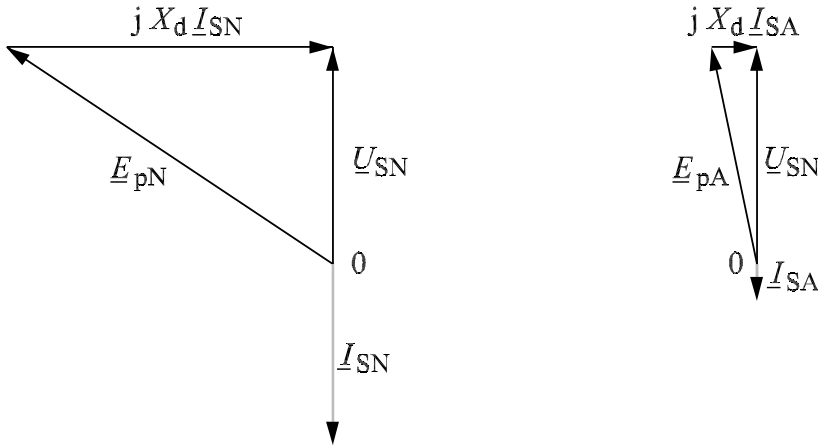


Fig. 9.15: Phasor diagram of generator quantities;
 a) Rated power

$x_{dN} = 1.5$ $U_{SN} = 0.78 U_{DN}$
 b) Starting operation ($n_{DA} \approx 0.5 n_{DN}$)

At partial load $0 \leq w_1 \leq 1$ the magnetic flux and the stator current of the traction motors are reduced proportionally to $\sqrt{w_1}$, to operate them with constant slip frequency f_s and thus with minimum losses. Is the DC-link voltage lowered according to a curve over $\sqrt{w_1}$, the commutation capability of the thyristor inverter is guaranteed with $U_d/U_{dN} \geq I_s/I_{sN}$.

In locomotive DE 501 the curve

$$U_d = U_{dN} \cdot (0.7 + 0.3 w_1). \tag{9.4}$$

was chosen; by that the commutation losses in the inverter and the current-harmonic losses in the motors are reduced distinctly at partial load. This is important as the motors have a high ratio of break-down torque to rated torque of about 5.5 (cf. Fig. 9.14) and thus a low leakage inductance, limiting the current harmonics.

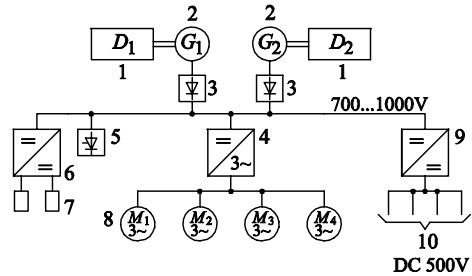
Main-line locomotives renounce generator oversizing, due to economic and weight reasons; instead of this the engine speed is raised in the starting region to the necessary value. The increased fuel consumption is of subordinate importance, due to the low share of starts at the total operation time.

From 1988 on, the GTO-thyristor technology was introduced, together with the new field-oriented control strategies. Fig. 9.16 shows locomotive DE 1003 of RAG, delivered by ABB and MaK. Two 500-kW diesel engines – switched on by demand – feed the 1400-V inverter with evaporation-cooled GTO-thyristor phase modules (2.5-kV, 2-kA devices), with water circulation and a separate radiator [131]. Fig. 9.17 give the main circuit diagram.

As the commutation capability of the GTO-thyristor inverter is not dependent upon the DC-link voltage, the main generator needs not to be oversized, at best the auxiliary generator to keep $U_d \sim n_D$ which can be suitable for the dimensioning of inverter and transformer of the train line (see below). Locomotive DE 1003 RAG was the first to apply the newly developed DSC (subchapter 6.3 or section 15.1.5).



Fig. 9.16: Diesel-electric locomotive DE 1003 of RAG (Bombardier Transp.)



- 1 Diesel engines 1, 2
- 2 Synchronous generators 1, 2
- 3 Diode rectifier 1, 2
- 4 GTO traction inverter
- 5 DC-link protection (crowbar)
- 6 GTO-thyristor brake chopper (2)
- 7 Brake resistors
- 8 Induction traction motors (pin-and-nose drive)
- 9 Auxiliary inverter
- 10 Auxiliary bus bar

Fig. 9.17: Main circuit diagram of DE 1003

In 1990 the step to the high-power class followed, in form of the ABB-MaK DE 1024 (Fig. 9.18), later Class 240 of DB AG, now with HGK; the diesel engine rating is 2,650 kW. Fig. 9.19 gives the main circuit diagram [132], [133]. Each GTO-VSI with $U_{DN} = 2,800$ V and evaporation-cooled GTO-thyristor phase modules with 4.5-kV, 3-kA GTO-thyristors (similar to Fig. 6.35) feed three traction motors of a bogie.

A single-phase inverter (two identical modules) supplies the train line (TL) with 1AC $16\frac{2}{3}$ Hz, 1000 V; $S_{TL} = 700$ kVA.



Fig. 9.18: Locomotive DE 1024 ABB-MaK
 $P_D = 2,650$ kW, $v_{max} = 160$ kph
 (Bombardier Transportation)

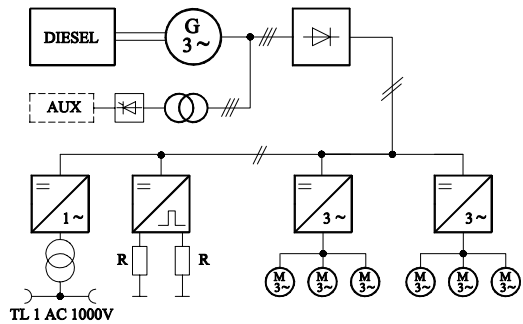


Fig. 9.19: Main diagram of DE 1024
 $P_{Traction} = 2,450$ kW, $S_{TL} = 700$ kVA

The most powerful locomotives with GTO inverters up to now were developed by GM-EMD for the North-American market; the inverters and traction motors are produced by Siemens. Fig. 9.20 shows a view of the 6000-HP variant of Union Pacific RR, Table 9.2 lists the main data. Fig. 9.21 gives the main circuit diagram of the locomotive: The generator has two separate three-phase winding systems, the nominal DC-link voltage is 2,800 V, the GTO-thyristor modules are evaporation-cooled [134], [135].



Table 9.2 Main data of SD 90 MAC

Wheelset arrangement	Co' Co'
Gauge	1435 mm
Service weight	190.5 t
Length over coupler	24,434 mm
Maximum speed	128 kph
Diesel engine	EMD „H-Engine“ 4476 kW at 1000 min ⁻¹
Starting tractive effort	890 kN
Permanent tract. effort	734 kN
Braking effort	510 kN

Fig. 9.20: Diesel-electric locomotive SD 90 MAC of Union Pacific RR, by GM-EMD and Siemens (Siemens AG, TS)

To make the American railroads accepting the parallel supply of three traction motors from a single inverter easier, the “HTCR” bogie was fitted with radially steerable wheelsets (Fig. 9.22), to reduce flange and tire wear and and take the edge off the wheel-diameter problem, as treated in subchapter 6.4.

General Electric (GE) in contrast chose for their diesel-electric locomotives with three-phase drives, the six-axle heavy-haul locomotives AC 6000 CW, AC 4400 CW or Blue Tiger (in Germany, together with ADtranz/Bombardier producing the mechanical part) and the four-axle passenger types “Genesis” and AMD-103, the alternative concept of individual air-cooled IGBT inverters, one per wheelset.

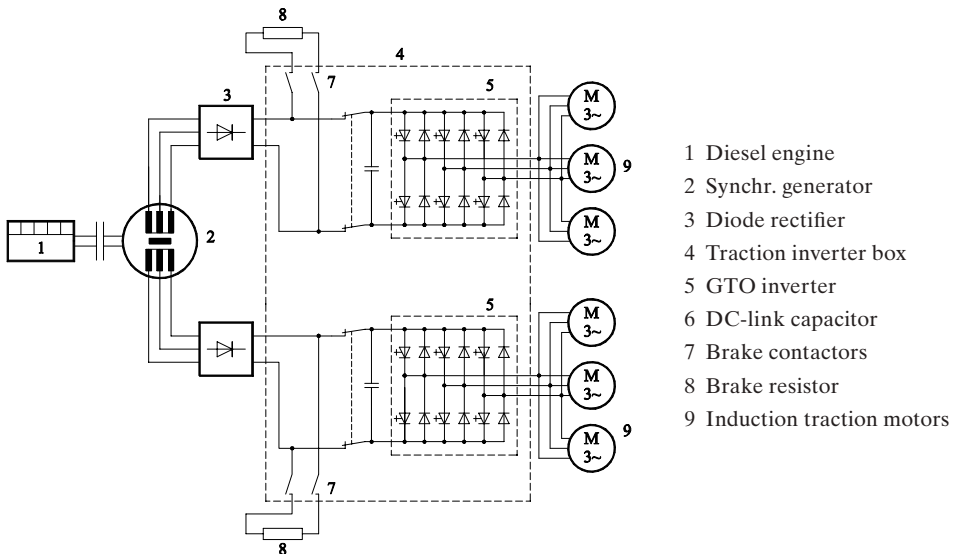


Fig. 9.21: Main circuit diagram SD 90 MAC (Siemens AG, TS)

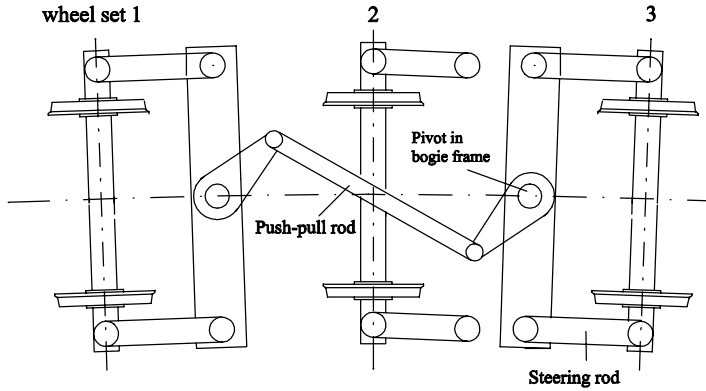


Fig. 9.22: Sketch of HTCR bogie with radially steerable wheelsets (acc. to Siemens AG, TS)

The most amazing outcome of the “platform” policy is the new TRAXX P160 DE of Bombardier Transportation [259] for LNVG (Class 246, Fig. 9.23), housing the “D-Power Package” consisting of the MTU diesel motor 16V 4000 R 41L with 2,200 kW and a 6-pole generator of VEM Sachsenwerk. The DC-link voltage is 1,800 V, chopper-controlled electric braking and a 500-kVA inverter-fed train line of 1000 V, 22 Hz are provided. The bogies are identical (including traction motors!) to those of the electric passenger locomotive Class 146.2. Bombardier claims that 75% of the parts are identical to those of the recent two-frequency locomotives TRAXX__AC2 [260]. For new multi-system locomotives, the corridor arrangement of the electric equipment in the car-bodies, typical for three-phase locomotives since Class 120, will be abandoned and replaced by an “E-PowerPackage”, as already demonstrated in the TRAXX F140DC2, the Angel Trains Cargo Class E 483 for 1.5 and 3 kV DC, in the centre aisle of the locomotive (Fig. 9.24).

Similarly ALSTOM produces (together with Siemens TS) a diesel-electric locomotive Class 475 on the basis of the PRIMA platform (cf. section 7.4.2).



Fig. 9.23: Diesel-electric locomotive TRAXX P160DE, Class 246 LNVG (Bombardier Transportation)

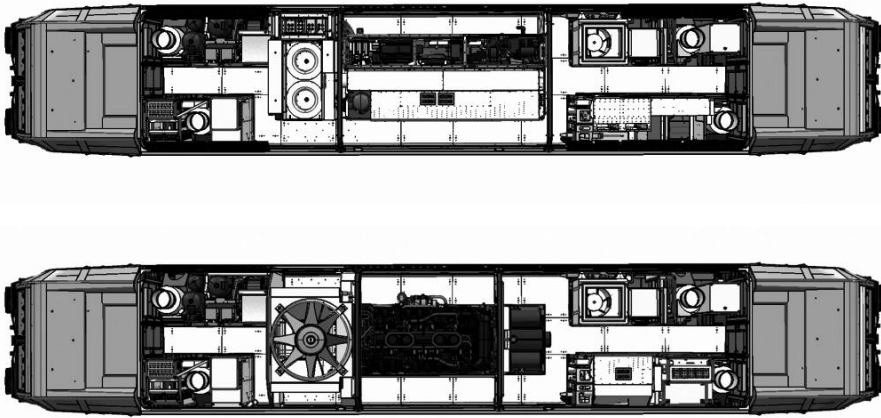


Fig. 9.24: Arrangement of equipment in a TRAXX locomotive with E-PowerPackage (top) and with D-PowerPackage (bottom) (Bombardier Transportation)

Diesel-electric motor coaches do not differ much from diesel-electric main-line locomotives, regarding the drive train, and do not need to be treated separately. As recent and innovative samples the ICE TD Class 605 of DB AG (with tilting equipment, four 560-kW diesel engines, $P_{N_Wheel} = 1700$ kW, $v_{max} = 200$ kph (Bombardier/ Siemens [B 22]), the regional DMU “Talent” Class 643 from Bombardier/ELIN [B24] and the Light Innovative Regional Express multiple unit “LIREX” by ALSTOM LHB shall be mentioned, the last having radially-steerable single-wheel running gears (KERF) and – for the first time – permanent-magnet synchronous generators, which are mounted together with the diesel engines on top of the train, to allow low-floor car bodies (cf. subchapter 10.2); $P_{N_Wheel} = 1700$ kW, $v_{max} = 200$ kph [136].

9.3 Dual-mode traction vehicles

Dual-mode traction vehicles operate purely electrically under the catenary (or at the third rail, cf. subchapter 13.4), whereas on not-electrified lines, they convey their energy from a diesel engine, coupled with a generator; besides that, battery storage is possible.

In the mining and iron industry locomotives are used, with the diesel engine power distinctly lower, than that of electric overhead operation [137]. An equivalent lay-out is to be found e.g. with the commuter-train locomotives Class FL9AC of Metro North Commuter Railroad (MNCRR), which are operated on lines towards New York diesel-electrically, in the city tunnels and especially in Grand Central Station with DC 650 V. ABB retrofitted 1990 15 of these cab-type locomotives, built originally by GM in 1959 as dual-mode locomotives, too [B 4], to three-phase drive technology [138]. Fig. 9.25 shows a photo of the locomotive (wheelset arrangement Bo’ (A1A)), Fig. 9.26 the main circuit diagram. In diesel-electric operation the engine ($P_D = 2,350$ kW) feeds via synchronous generator and diode bridge rectifier the DC link ($U_{dN} = 1400$ V).



Fig. 9.25: Dual-mode locomotive FL9AC of MNCRR (Bombardier Transportation)

From there two 1400-kVA GTO-inverters are feeding two traction motors of one bogie, each. In third-rail operation ($U_{FN} = 650\text{ V}$) two identical three-phase step-up DC choppers (as in Fig. 4.10), identical to the GTO inverters, feed the DC link or take brake power back to the grid; the switchings are interleaved by 120° . A fifth inverter supplies – as Head-End Power – the train line with 3AC 480 V, 60 Hz, ca. 1 MW; two additional GTO-thyristor phase modules control the dynamic brake power at the brake resistors.

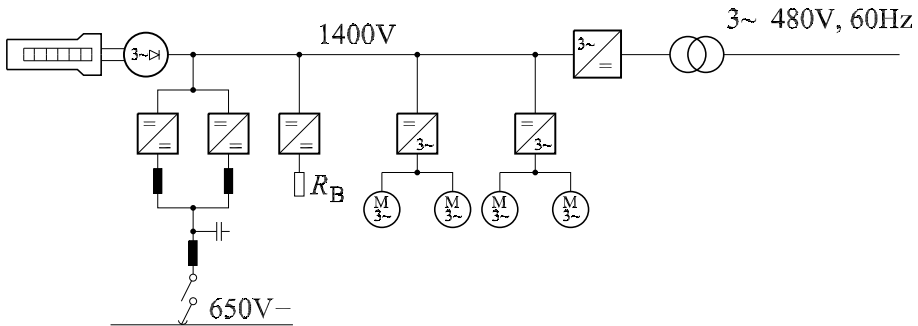


Fig. 9.26: Main circuit diagram of dual-mode locomotive MNCRR FL9AC

Finally Fig. 9.27 shows one of the new dual-mode Light Rail Trains 8NRTW-D for Regionalbahn Kassel (RBK), based on the CITADIS low-floor tramway platform of ALSTOM. Two diesel engines of 375 kW each are mounted on the roof top (2005/06).



Fig. 9.27: Dual-mode tramway RegioCitadis for Regionalbahn Kassel (RBK 751–760) (ALSTOM-LHB)

10 Suburban and Light Rail traction vehicles

The demand on public passenger transportation arose together with the growth of the first “modern” capital cities, such as London, Paris, New York, as a consequence of Industrial Revolution, mirroring the development of main-line rail transport. Thus in 1832 the first horse tramway took up service in New York; from 1862 on, the Metropolitan Railway connected – partially subterranean – the terminal stations in London. The railway societies started dense and fast commuter service alongside their main routes into the large cities and enabled the industrial population to live cheaper and healthier in newly arising suburbs.

In, 1881 W. v. Siemens presented the first electric tramway in Berlin-Lichterfelde; in 1889 the motive power of the London “Tube” suburban trains was equipped with electric drives, by Siemens too (cf. Fig. 3.2). In the same year F. Sprague introduced the tramway in Richmond/USA and thus created the first modern local traffic system, with many newly invented and pace-making system components as the axle-hung motor drive (Fig. 3.6), the multiple-unit control and the first reliable current pick-up from the overhead line, the rod collector (cf. subchapter 13.4). Underground and elevated railways came into existence for handling mass transit in the large cities, operated by the municipalities and not by the big railway societies any more.

Since the 1920s, individual transport and omnibuses have displaced many inner-city tramways and interurban lines; but as congestion of the inner cities threatened, public passenger transport – yet publicly subsidized – maintained their stronghold and could even extend it in recent time, as many new tramway and Light Rapid Transit systems arising e.g. in France and the U.S. demonstrate.

Table 10.1: Comparison of capability and economics of suburban transportation means

Transportation means	Metro	Under-ground	Light Rapid Transit	Light Rail (Tram)	Bus
Passengers per hour and direction	50,000	30...40,000	20...30,000	8...12,000	6...8,000
Stopping distance / m	> 1000	1000	800	500	300
Cost of investment per km line / Mio €	40...80	40...80	10...20	3...8	0...5
Revenue period / a	25	25	25	25	8
Number of passengers seated and standing	280	200	200	170	100
Mean transportation speed /kph	35...40	30...35	25...30	20...30	15...25
Primary energy consumption in Wh/km per seat	40...50	40...50	40...50	40...50	50...60
Economical threshold of number of inhabitants for public transport means	useful > 10 ⁶ necessary > 2 · 10 ⁶ inevitable > 3 · 10 ⁶		> 300,000	> 100,000	

So there is an optimal mission for each transportation means, as listed in Tab. 10.1, characterized by economic transport capacity and distance, with cost of investment and primary energy consumption pertaining to. Metro (“S-Bahn“ in the German-speaking countries) and Underground are counted to “mass transit”; they have their own Right of Way, separated from public streets and (mostly) from the main railway systems. Tramways (Light Rail Systems) and buses use the public traffic area, common with individual transportation; they feature low cost of investment, but impede each other more or less.

Light Rapid Transit (originating from Germany) is in-between mass transit and Light Rail, as being able to be operated in street level like a tramway and in concentration areas like an Underground. In special cases they use the AC main-line electrification, as described later.

10.1 Metro and Underground trains

The survey begins with Metro and Underground vehicles, which due to their high speed (up to 120 kph), high acceleration (up to 1.2 m/s^2) and consequently high specific power of $P' = 15...20 \text{ kW/t}$ can be compared to main-line coaches – even those for High-Speed Traffic (cf. section 7.4.2); [B23]; in Germany the Railway Construction and Operation order (EBO) is valid, same as for main-line services.

As long as they do not use jointly the main-line infrastructure with 1AC electrification, as in the Metro systems founded in the sixties and seventies in Munich, Frankfurt, Stuttgart, the Rhine-Ruhr area in Germany or in Zurich/Switzerland, metro and underground services are operated with DC 750...1200 V, from a third rail beside the track (cf. subchapter 13.4). DC overhead operation is only found if the track of a DC main line is to be used jointly, as tunnel lines need a much smaller clearance gauge with third rail and are thus much cheaper to build, at same vehicle cross-section as the main-line vehicle. DC offers lowest weight and expenditure for the vehicle equipment, at least with the conventional technologies, whereas the higher current transmission losses are only a minor factor, regarding the short distances. Generally, metro and underground coaches have standard gauge.

Today metro and underground trains sport a high percentage of driven wheelsets, as high acceleration is necessary; pure EMU operation is common, though metros with interurban character (greater stopping distances) use trailers, too. Multiple-unit control (all power switches or electronic controllers are to be actuated uniformly from all driving positions) allows in combination with automatic couplers a flexible train formation at minimal staff demand.

Fig. 10.1 shows, in the top line, the classical Berlin “S-Bahn-Viertelzug” ET/ES 165 (metro “quarter-train”, four twin-units consisting of a motor coach and a trailer make a “full train”), introduced in 1928. With $P = 4.90 \text{ kW}$ and $G = 66 \text{ t}$ (at full load) P' equals 5.5 kW/t , $v_{\text{max}} = 80 \text{ kph}$, DC 800 V. An automatic electro-pneumatic camshaft controller with current relays allowed setting of definite acceleration values ($< 0,5 \text{ m/s}^2$).

Fig. 10.1, lower line, depicts the 1AC-fed interurban train of DB Class ET 30 (BR 430), introduced in 1955 for the Ruhr-area rapid transportation scheme. Two traction motors are provided in the exterior bogies of each end car, $P' = 12 \text{ kW/t}$, $v_{\text{max}} = 120 \text{ kph}$, transformer tap-change control, as Fig. 4.18.

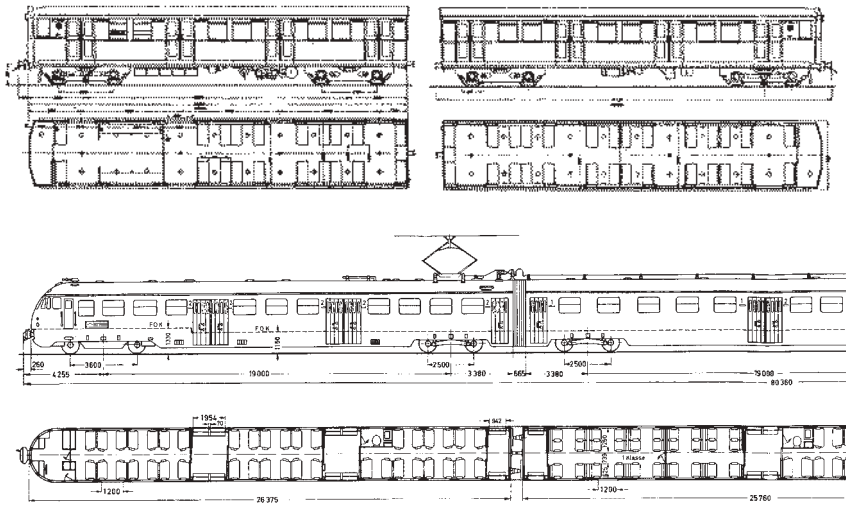


Fig. 10.1: Metro trains with camshaft control
 Top: S-Bahn Berlin 1928 (DC); bottom: DB ET 30 Ruhr area (AC 15 kV, 16 2/3 Hz)

Fig. 10.2 presents in a schematic way three general configurations of modern mass transit trains with power-electronic control [139]: On top the metro train Class 420, introduced for the 1972 Olympic Games in Munich, with 15 kV/16 2/3 Hz, all-axle drive, phase-delay-controlled “undulating-current” motors ($P = 17 \text{ kW/t}$, $v_{\text{max}} = 120 \text{ kph}$). In the centre line the very innovative train for Copenhagen Metro (DC 1500 V), the “S-Tog”, by ALSTOM-LHB and Siemens AG (1996, [140]); it does not have bogies, but radially steerable single-wheelset running gear (KERF), driven by four 215-kW induction motors, GTO inverter underfloor.

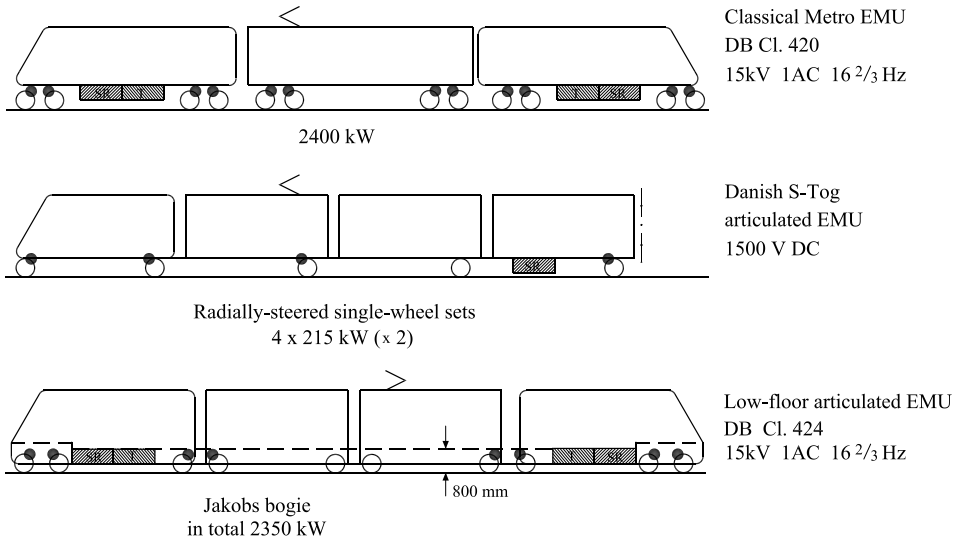


Fig. 10.2: Configurations of modern mass-transit trains

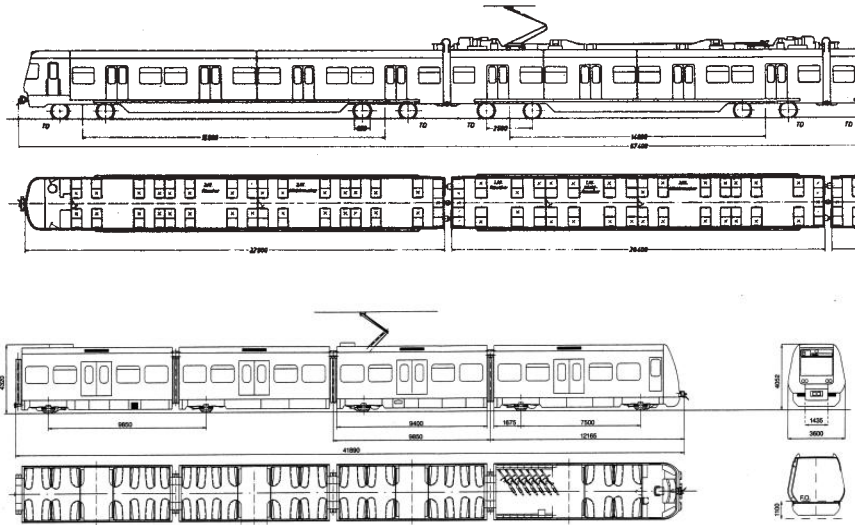


Fig. 10.3 Metro train Class 420 of DB and „S-Tog” Copenhagen in side and vertical elevation (Bombardier Transportation; ALSTOM LHB)

As the individual coaches are less than 10 m long, they can be built 3.6 m wide and allow two rows with three seats aside (only a half-train is shown).

The electric equipment (motors, drives and converters) is similar to that described in subchapter 4.1.3 and chapter 6, respectively. Fig. 10.3 shows both trains in side and vertical elevation, Fig. 10.4 and 10.5 the respective fotos.

Metro and underground systems as autonomous mass-transit systems are equipped with platforms of about 1 m height (over rail top), to ease and accelerate transfer of passengers. For supplementary mass-transit systems in “secondary” concentration areas as e.g. Hannover or Mannheim/Ludwigshafen in Germany, with distinctly less than 1 million inhabitants this was not feasible for economic reasons. The task was designing metro trains of comparable performance with a floor height of only 800 mm, which can be boarded from a standard platform of some 760 mm height fast and safely. Fig. 10.2 shows in the bottom line the new metro train Class 424 of DB AG with Jakobs’ bogies, for 1AC 15 kV/16 $\frac{2}{3}$ Hz [141]. It features 80% driven wheelsets with $D = 850$ mm only; $P' = 20.6$ kW/t and $v_{\max} = 140$ kph.



Fig. 10.4: Metro train Class 420 DB (Bombardier Transportation)



Fig. 10.5: „S-Tog” Copenhagen (ALSTOM LHB)

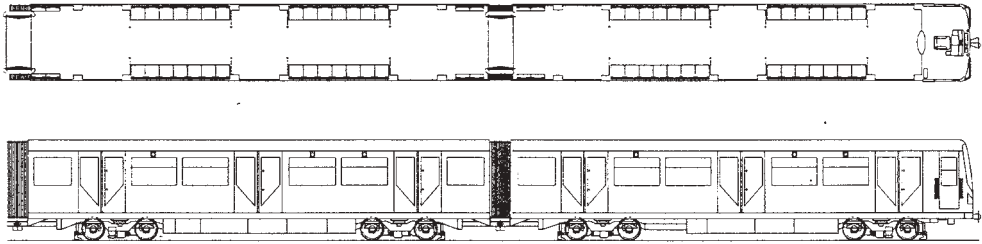


Fig. 10.6: Underground train series H of BVG, Berlin; IM drive similar to Fig. 3.18, ASCI (Bombardier Transportation)

Transformers and (water-cooled) GTO converters (Fig. 7.11, bottom line) of extra-low construction are mounted underfloor, the remaining equipment as air-conditioning in roof-mounted containers.

Modern mass-transit trains allow to ambulate freely through all coaches, raising the passengers' feeling of safety and thus the acceptance in the late night hours, as in the series H trains of Berlin Underground (BVG 1995, Fig.10.6): The whole six-coach train features an open passenger area; the 24 drives are controlled by ASCIs similar to Fig. 6.29.

Double-deck motive power is strongly desired for conurbations, as enabling shorter trains and thus nearly double capacity at same length of existing platforms. But the technical demand is extreme, as the electric equipment (transformers, converters) can be housed neither underfloor nor on the roof, but must be "hidden" somewhere in the passenger room, impeding free passage or lengthening the train. Rather new examples are the Czech commuter train Class 471/971 (DC 3 kV, CKD-Vagonka, Ostrava and Skoda, Plzen, Czech Republic) and the recent Zurich four-car "S-Bahn" EMU Class 514 (1AC 15 kV, 16 $\frac{2}{3}$ Hz; Siemens TS).

10.2 Light Rail and Light Rapid Transit vehicles, low-floor technology

After W. v. Siemens had, in 1881, started the first test operation of an electric tramway car in Berlin-Lichterfelde [1], more tests were performed with different drives schemes and with various current pick-up systems. It was only after 1892 that the advantages of Sprague's system with axle-hung motor drive and rod collector with roller were generally accepted. From 1895 on, one horse-towed or steam-operated tramway after the other was converted to electric service in Europe and the U.S.; e.g. in Germany the term "electric" was a synonym for tramways. The legal frame is set by rules different from those of railways and mass transit, in Germany by the BOSTrab, the decree on construction and operation of tramways.

10.2.1 Conventional tramway carriages and articulated trains

In Germany as well as in many other European countries the most simple two-axle car with similar trailers was favoured, using rigid wheelsets with a wheelbase of only 1.5...2.5 m to negotiate narrow curves in the old cities easily (Figs. 10.7, 10.8). In Great Britain they were built as double-deck cars, as trailer operation was not permitted. This simple type was preferred for economic reasons until after World War II, in spite of the well-known bad riding quality. The rod collector system was complicated, as it needs points in the catenary and reversing is clumsy; thus it was replaced by the simpler lyra bow collector and finally by the pantograph, today mainly as single-arm type (cf. subchapter 13.4).

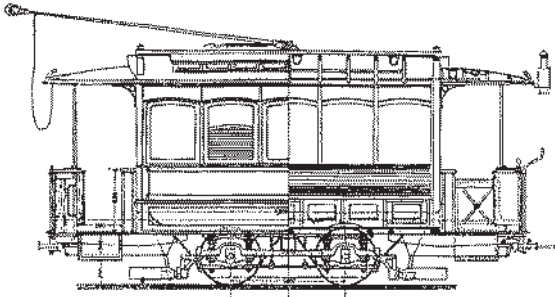


Fig. 10.7: Two-axle tramcar AEG-Herbrand 1895 (Klartext-Verlag)



Fig. 10.8: German war-time standard tramcar (KSW), 1942 (D. Höltge)

In the United States and some European countries as e.g. in Italy, the bogie car had asserted itself, in other countries as Germany only for Interurbans. In the twenties, passenger-flow systems were introduced (rear entry at the seated conductor; "PCC" cars, "Peter Witt" cars). After World War II the "four-axle" bogie car was introduced e.g. in Germany by DÜWAG and built in a number of some 900 cars.

But already in 1955 it was superseded by the six-axle articulated coach GTw6, wheel arrangement B' 2' B' with two driving bogies with two-axle longitudinal drive (Fig. 3.17, about 100 kW) and one trailing centre Jakobs' bogie supporting the articulation joint (cf. Fig. 10.9, top). It offered the same capacity as a high-capacity train of two four-axle coaches (240 seats), with only two instead of three persons staff. The width of the cars was – depending upon the tramway system – 2.2...2.35 m, the length some 20 m, 26 m in case of the subsequent doubly-articulated train GTw8, which became the most widespread type in Germany.

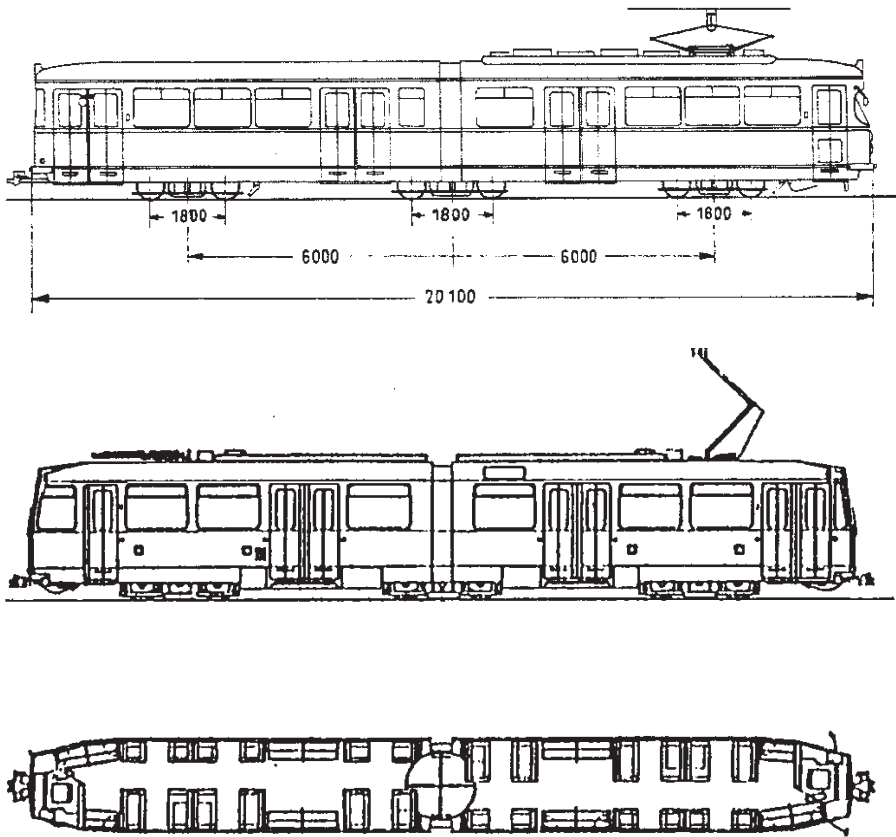


Fig. 10.9: DÜWAG articulated train GTw6 and M/N6 train

These trains were delivered in standard and in metre gauge and as uni- and bidirectional trains, the first needing turn loops at the end stations, allowing to dispense with doors on the left side. The passenger-flow system was replaced by conductor-less operation from 1970 on.

In the mid of the seventies the so-called M-cars were introduced for the – still metre-gauged – preliminary operation of Stadtbahn Ruhr (Light Rapid Transit; Fig. 10.9, bottom line, already equipped with DC choppers (Bochum M6C 1978) and with ASCIs and induction motors (Mülheim M6D 1982). This type was delivered in standard gauge, too (N6, N8).

In 1971, the German federal state Nordrhein-Westfalen initiated the development of the standard-gauge “Stadtbahnwagen Ruhr“ B 80/100, based on the same technical concept as the M/N cars, of 2.65 m width (Fig. 10.10). The DÜWAG two-axle longitudinal drives of $2 \cdot 235$ kW were originally camshaft-controlled, but later supplied with DC-chopper (‘C’) and with three-phase drives (ASCI with GTO-thyristor chopper, ‘D’). Similar constructions were used in other German cities as Frankfurt (Underground type U2) and delivered to new U.S. LRT schemes, later produced in the DÜWAG branch establishment in Sacramento. These Light Rapid Transit trains must be boarded – same as tramway cars – from street level, necessitating multiple automatic folding steps.

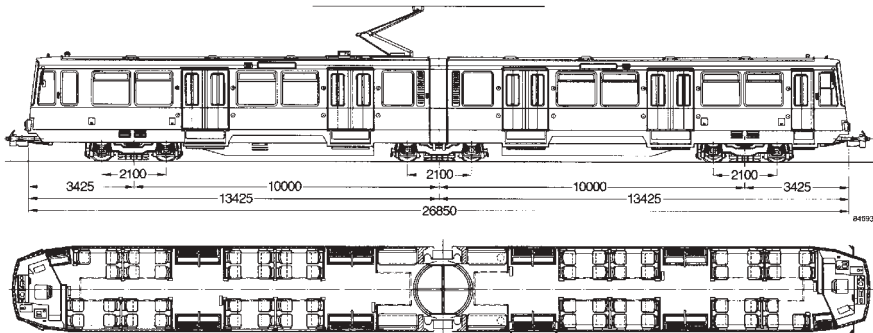


Fig. 10.10: B-LRT "Stadtbahn Ruhr" B 80/100 ($v_{max} = 80$ and 100 kph)
(Bombardier Transportation)

10.2.2 Dual-system Light Rapid Transit vehicles

Still a peculiarity are the dual-system LRT trains in the German cities of Karlsruhe, Saarbrücken and Kassel, which use the 15-kV, $16\frac{2}{3}$ -Hz lines of DB AG in an environment of some 150 km and revert to DC 750-V street-level operation, when approaching the very centres of these cities. This makes public transport more attractive, if the main station is far from the city centre. The main constructional difference between light rail vehicles obeying BOSTrab and railway vehicles – besides the smaller vehicle gauge – is the lesser resistance to longitudinal impacts of only 200...600 kN, compared to > 1500 kN acc. to EBO⁶. The "LRT guide-line" (1993) [B26] allows this, if a high brake deceleration and a limited maximum speed of the LRT vehicle is given, together with a maximum line speed of only 160 kph.

Fig. 10.11 depicts the main schematic circuit diagram of the Karlsruhe dual-system "Stadtbahn" train GT8-100C/2S (ABB-Siemens 1991), with DC traction motors and DC choppers with automatic field weakening (Fig. 4.13).

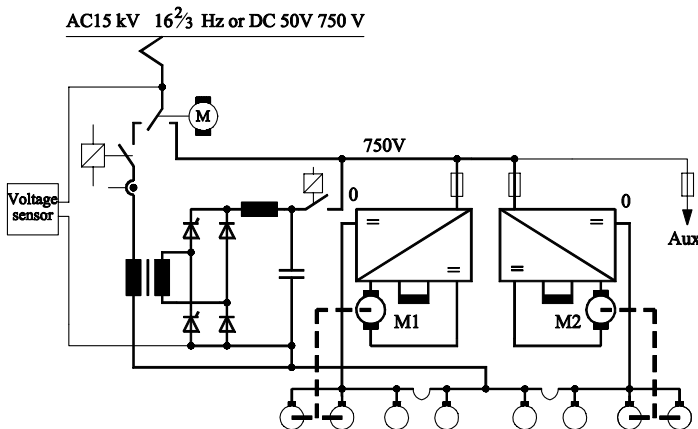


Fig. 10.11: Main circuit diagram of dual-system Light Rapid Transit train GT8-100C/2S Karlsruhe

⁶ Another difference is running at sight of tramways, while railway operation is controlled by signals



Fig. 10.12: Dual system Light Rapid Transit train GT8-100C/2S on 15-kV, 16 ²/₃ -Hz line (Bombardier Transportation)

The 570-kVA transformer with two-pulse bridge in half-controllable connection of pairs of arms is housed underfloor in the middle car of the doubly-articulated train, carrying the pantograph, too. Fig. 10.12 gives a view of the train on the main line. The subsequent generation GT8-100D/2S uses three-phase drive technology off the 750-V DC link, the AC-circuit is identical to that in Fig. 10.11. The trains series S 1000 for Saarbrücken from 1997, main circuit diagram Fig. 10.12, feature three-phase drive technology with two four-quadrant converters ($P = 960 \text{ kW}$, $G_{\text{max}} = 81 \text{ t}$, $v_{\text{max}} = 100 \text{ kph}$; Bombardier-Vienna, Kiepe Elektrik (inverters) and ELIN EBG Traction (4q-C).

Those new trains have a low-floor part of about 40 % (cf. subchapter 10.2). Similar “Tram Trains” have now been introduced in Paris (Siemens Avanto).

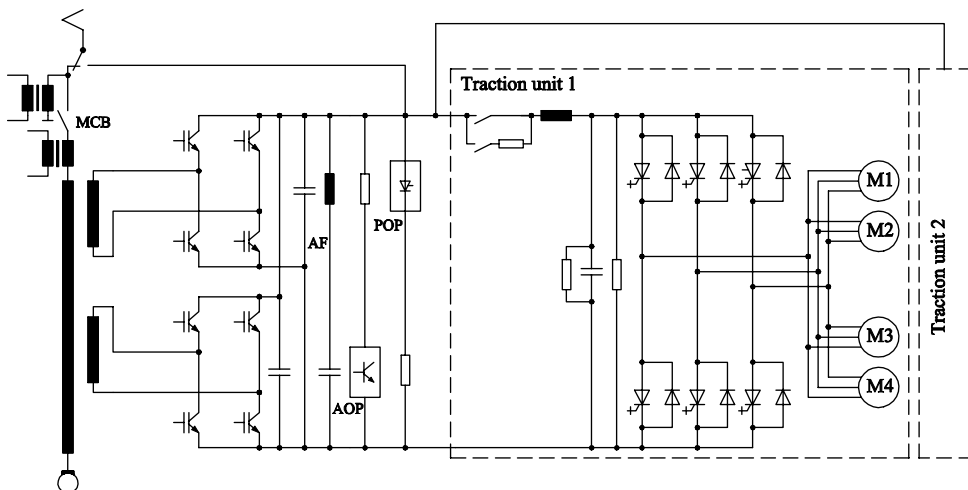


Fig. 10.13: Main circuit diagram dual-system LRT articulated train S 1000 Saarbrücken

10.2.3 Low-floor light rail vehicles

Common to all these light-rail vehicles is a floor height of 900 mm (with GTw₆ and M/N cars) to 1000 mm (with the B-type), which handicaps boarding from street level. In LRT operation corresponding high platforms have to be erected, which when over ground disturb the townscape. At the end of the eighties the LRV surge of enthusiasm in Germany eased off with decreasing public subsidies; new ways were to be found to make the classical tramway train more attractive and easy for the passengers.

In Grenoble/France a new tramway system with low-floor train had already been taken into service in 1987 by ALSTOM; in Germany the VDV initiated a common development by the carbuilders of a low-floor vehicle with only 300 mm floor height, which could be boarded from street level with only one step and from pedestrian islands directly. As driven wheels cannot be made much smaller than 550 mm (at speeds up to 80 kph) and the connecting shaft would have been in the passage area, single-wheel running gear was necessary.

In 1991, three prototypes with radially-steering single-wheel running gears (EEF) after the proposal of Prof. Frederichs, RWTH Aachen, were built with three-phase drive technology. Unfortunately they were not successful, since, at only slight wheel-tire wear, the steering geometry was not correct anymore and wear and noise increased intolerably. From these beginnings, an unexpected wave of different low-floor technologies was developed in the 1990s, which upset all unification strategies of VDV and led to an explosion of cost per seat from 15,000 to 30,000 Euro. But after a certain amount of consolidation, low-floor technology is the market leader. In the context of this book only the most important (and successful) development lines can be represented, referring to the relevant literature (e.g. [B26], [142]).

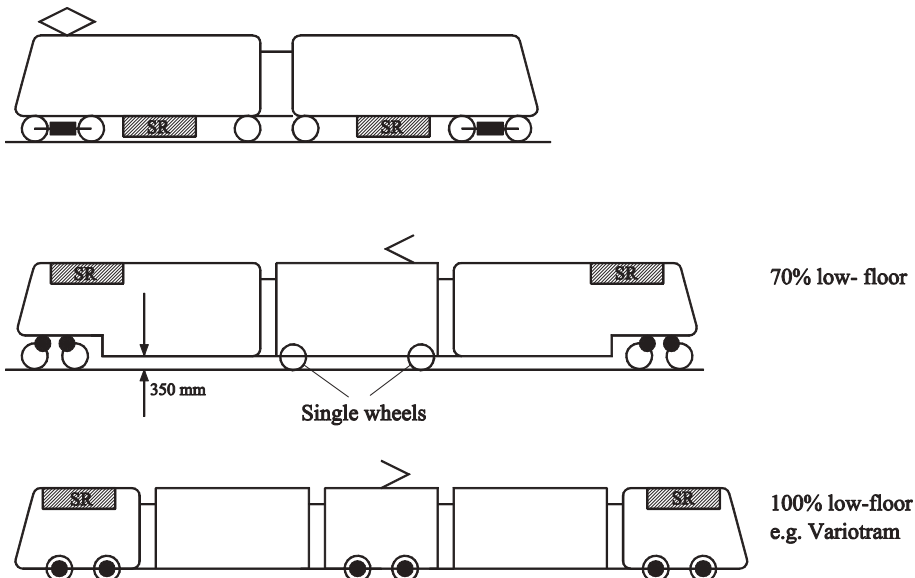


Fig. 10.14: Configurations of light rail vehicles

Fig. 10.14 may serve as an overview: On top the classical articulated train GTw₆ (or the M/N-car), with some 900 mm floor height, two-axle longitudinal (DÜWAG) drive and DC choppers

under floor. To circumvent the problems of small, individually driven single wheels, at first the so-called “70 % low-floor tram“ (centre line) with flat, but more or less conventional motor bogies under the high-floor end area was introduced, e.g. type M(N)F6D by DÜWAG/ Siemens (first application in Bochum 1992, Figs. 10.15 and 10.16). By space-saving induction traction motors and cardan hollow-shaft drives with rubber joints (cf. Fig. 3.18) the floor height is only about 700 mm. By steps the low-floor portion with 350 mm height (of some 70% of train length) is reached; the entry is only 290 mm over rail top. Radially-steered single-wheel trailing running gear (EEF) supports the centre car, on which the end-cars lean by means of a pivot joint. The air-cooled GTO inverters are mounted on roof-top.

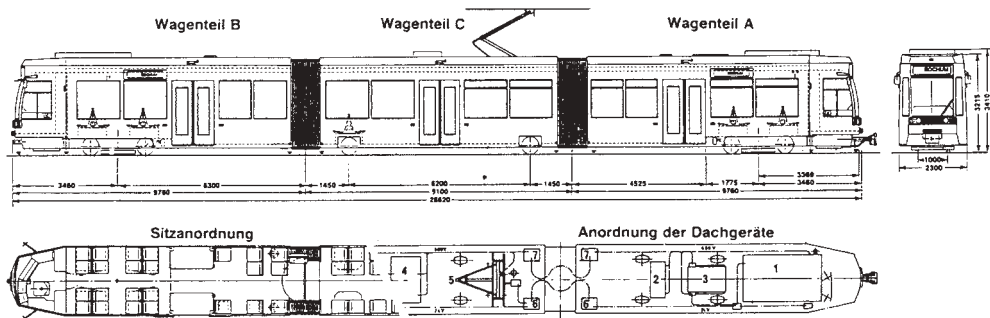


Fig. 10.15: 70 % low-floor tramway articulated train MF6D (Siemens AG, TS)

As the running behavior of the single-wheel running gear was not really satisfactory, this type was not ordered any more, after some 200 trains delivered. In the following time the trend was towards the so-called „100% low-floor tram“, as sketched in Fig. 10.14, bottom line.

The “Variotram” of ABB/ADtranz (prototype in 1993, series Chemnitz in 1998, Fig. 10.17) has four gearless hub motors à 40 kW, connected by rockers with the running gear (Fig. 10.18), which itself is connected by Flexicoil springs with the carbody (length 4.2 m, (2) in Fig. 10.19).



Fig. 10.16: MF6D Bochum (Siemens AG,TS)



Fig. 10.17: ADtranz Variotram Chemnitz (Bombardier Transportation)

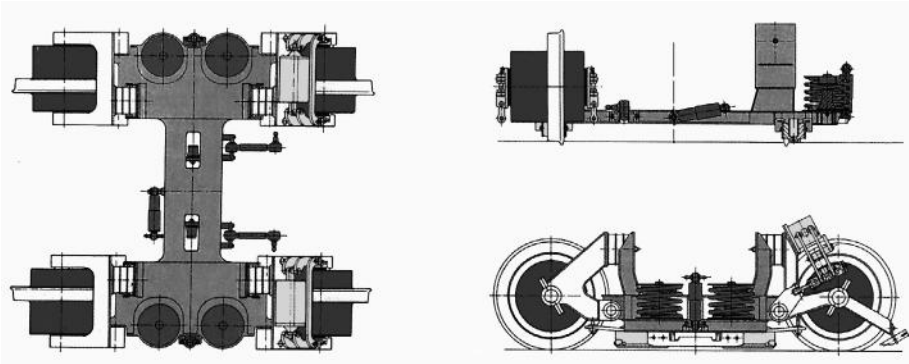


Fig. 10.18: Variotram running gear (Bombardier Transportation)

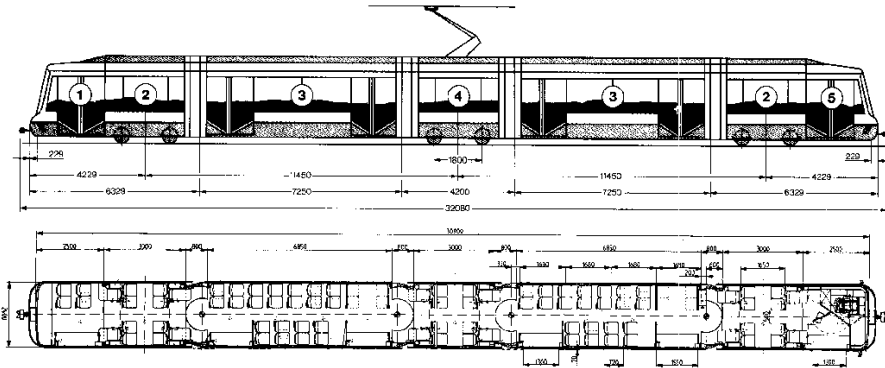


Fig. 10.19: Variotram articulated train 6MGT (Bombardier Transportation)

The – inner – stator is fixed, while the external hollow rotor is connected by rubber blocks directly with the wheel tires. Stator windings and IGBT inverters are water-cooled, the latter feeding each two motors of one side in parallel and secure by electrical means (constant torque control) running in straight and curved track. The passenger modules (Fig. 10.19, (3)) rest on the motored (2) or trailing (4) running gears, the riding quality can be compared to a bogie coach; height at entrance 290 mm, floor height 350 mm. Motored and trailing modules can be combined freely according to the demand, e.g. the seven-part tram for Mannheim (8MGT-LDE) shows the wheelset arrangement Bo+2+Bo+Bo.

MAN developed in 1990 (before being merged into AWTS and later ADtranz) a doubly-articulated 100 % low-floor vehicle GT6N for Bremen with three asymmetric (1A) bogies (with rotation limiter, Figs. 10.20 – 10.22). The driving wheels are connected by a primary gears with a deeply arranged connection shaft to a stiff “quasi wheelset“, which is driven via a bevel gear and a cardan shaft from a 84-kW induction traction motor, mounted longitudinally in the carbody. Due to the good running quality (on well-maintained track!) this type was at its time the most widespread low-floor tram in Germany, with 450 units, e.g. in Berlin, Bremen and Munich. The bogie concept was adopted by the later Bombardier ”Incentro“ tram; the ALSTOM CITADIS trams use running gears with similar drive concept, but with the motors mounted transversally.

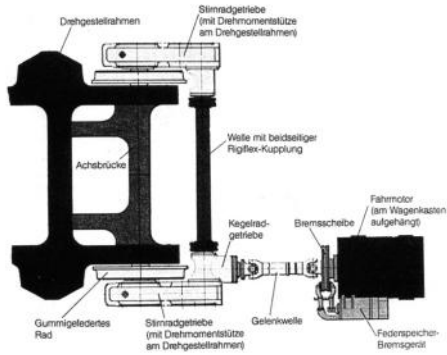


Fig. 10.20: Wheelset MAN-GT6N

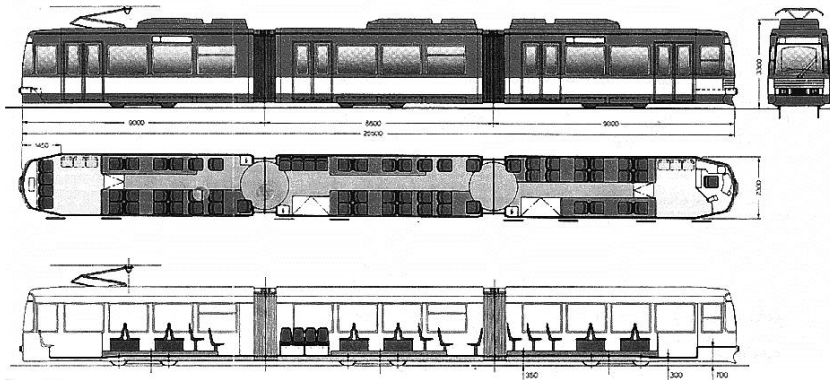


Fig. 10.21: 100 % low-floor articulated tramway GT6N (Bombardier Transportation)

DÜWAG and Siemens started in 1990 with a rather complex construction with driven single-wheel running gears, using hub motors with planetary gears, for the Frankfurt R-car, the first 100% low-floor tram in Germany. The electric circuitry was rather complicated, too, as 1700-V-IGBTs were not yet available to allow the direct connection to the 750-V DC mains; a pre-chopper similar to that in Fig. 8.6 had to be used [144]



Fig. 10.22: MAN-GT6N Bremen (Bombardier Transportation)



Fig. 10.23: 100 % low-floor multi-joint tram Combino (DÜWAG-Siemens)

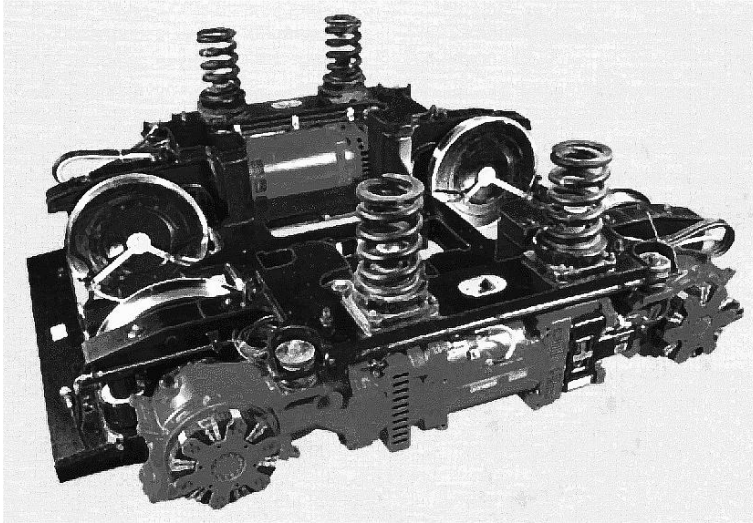


Fig. 10.24: Combino motor bogie with individual wheels and two longitudinal motors (Siemens AG, TS)

Later on Siemens-DUEWAG developed the “Combino” according to a strongly modularized concept, similar to that of Variotram. But the two single wheels of one side are driven commonly by one induction motor via hypoid bevel gears, which is mounted at the outside of the frame (Figs. 10.24, 10.25). After first orders in Basel/Switzerland, Potsdam/Germany and Amsterdam the Combino seemed to be well accepted by the market.

But with the beginning of the new century, cracks were detected in the roof girders of the aluminum carbody, which had to be attributed to an insufficient consideration of the cumulative load by the vertical thrusts, produced by the single-wheel running gear, in comparison with that of a true bogie. Severe reconstruction of all carbodies and parts of the joints was necessary, and several years no new trains were produced; now Combino Plus is under delivery. Similar damages were reported for steel-bodied vehicles of the MF6D type.

Thus, the beginning of the 21st century saw a renaissance of the bogie-type trams, with (outer) motor bogies similar to that of the 70% tramway, and (inner) trailing bogies with single wheels, allowing the unimpeded passage at low-floor height and hidden under landings carrying the seats, as e.g. the Bombardier Flexity Classic trains [143] (Fig. 10.25).

Fig. 10.26 compares the treated drives of tramways with 0, 70% and 100 % low-floor share.

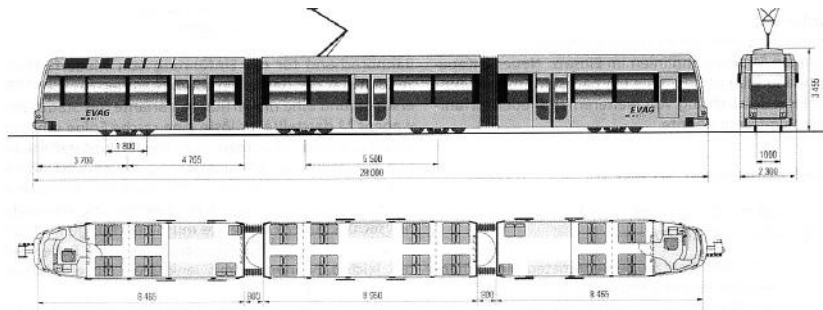


Fig. 10.25
EVAG M8D-NF
LF 2000 -
(Bombardier
Transportation)

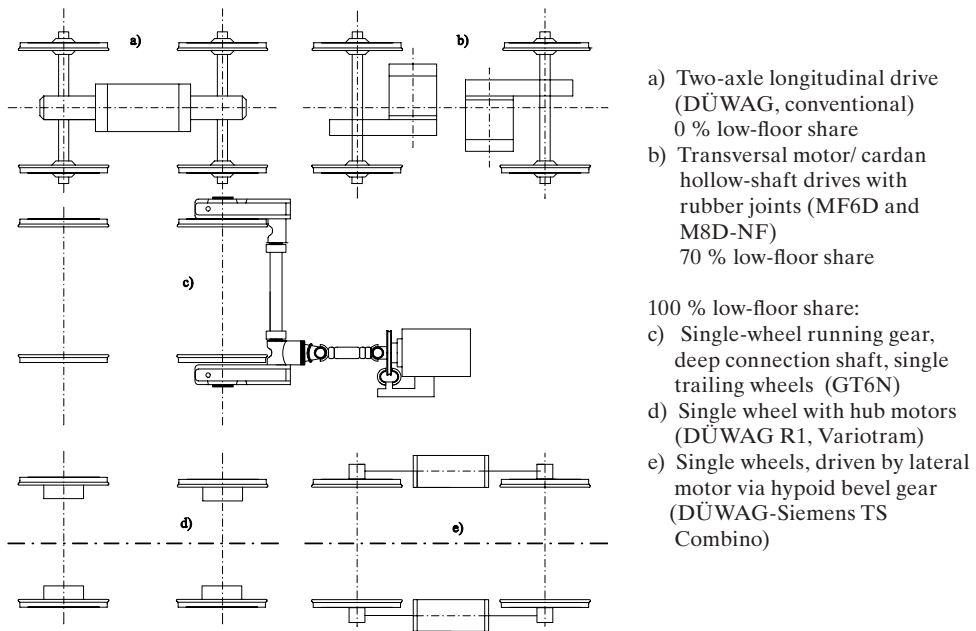


Fig. 10.26: Principal arrangements of different low-floor tramway drives

When dimensioning the drives of tramway and Light Rapid Transit vehicles, which have to obey e.g. the BOStrab, a constant deceleration of 2.7 m/s^2 from maximum speed down to zero speed is to be guaranteed, due to the coexistence with rubber-tired automobiles and buses in the public traffic area. This presupposes a magnetic rail brake, mainly independent of adhesion (cf. subchapter 11.2); but additionally the nominal torque value has to be available as brake torque at full speed v_{\max} , which means that the brake-power peak is roughly $v_{\max}/v_1 \cdot P_N \sim 2.5 \dots 3 \cdot P_N$ (cf. section 4.1.3, automatic field weakening).

With induction-motor drives the line voltage is raised to the maximal admissible value, e.g. $U_{FN} + 20\%$ (acc. to EN 50163); then the line switch is opened and the filter voltage is controlled by the brake chopper to a value of $U_{d\max} \approx \sqrt{(v_{\max}/v_1)} \cdot U_{FN}$; thus the limiting break-down torque reaches the necessary value for the brake-power peak and the motor currents need only to be raised to the same multiple of the nominal (permanent) traction value. Earlier concepts to take up the high motor e.m.f. by means of resistors, switched into the motor leads, similar as with the compound brake resistor of DC-motor drives, have not been followed.

As long as 1700-V-IGBTs were not yet available, several interim solutions had to be applied in 750-V DC systems, as GTO inverters, IGBT inverters with 1200-V devices and pre-choppers [144] and three-level IGBT inverters [145]. Today the standard two-level IGBT inverter has asserted itself [146]. Fig. 10.27a shows the typical main circuit diagram, with the one IM symbolic for one or more in parallel, Fig. 10.27b the construction of a roof-mounted converter (example 13SG44 of Bombardier Transportation, with water intermediate cooling).

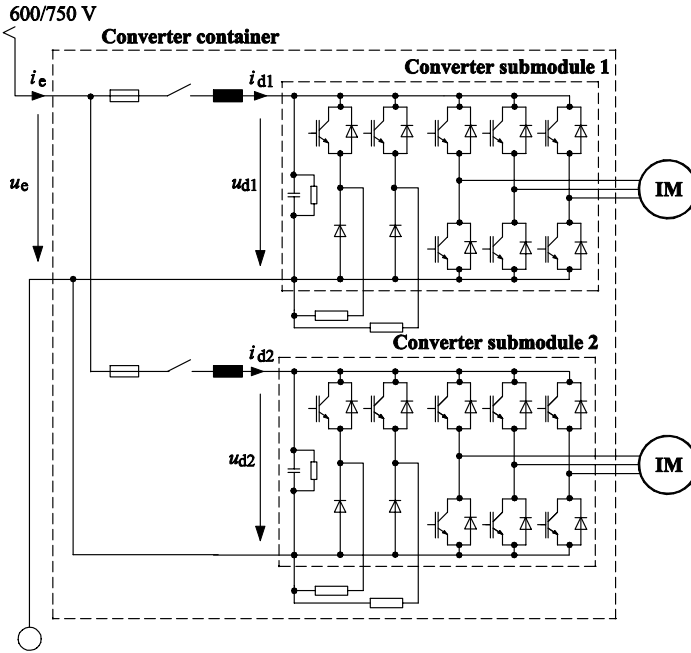


Fig. 10.27a: Main circuit diagram of a drive unit of a low-floor tramway vehicle (Bombardier Transportation)

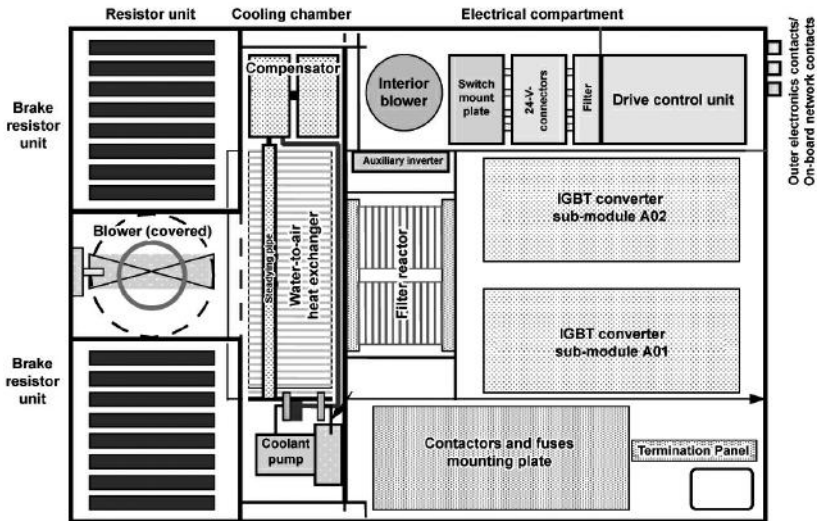


Fig. 10.27b: Construction of a roof-mounted converter 13 SG 44, containing two 300-kVA inverters (Bombardier Transportation)

10.3 Traction vehicles with energy storage

To derive benefit from electric traction on lines of low capacity, too, at the turn from the 19th to the 20th century storage motor vehicles with accumulators were developed, mainly in Germany. Most well-known were the Prussian motor coaches, type Wittfeld (Fig. 10.28a, [147], [148]), which were put to service from 1908 on, and were used later on by DR and DB, the last ones being scrapped in the sixties. They were equipped with lead-sulphuric acid accumulators under the front hoods, of initially two times 67 kWh capacity (at 3-h discharge) and two times 8 t mass, later increased to two times 147 kWh, 11 t, and had a radius of action of 100 to 180 km, respectively.



Fig. 10.28a: Accumulator motor coach ETA 177 of DB



Fig. 10.28b: Accumulator motor coach ETA 150 of DB (1953-57)

After World War II DB developed two new series, the prototype Class ETA 176 and Class ETA 150 of 232 motor coaches with four-axle control trailers (Fig. 10.28), with the storage batteries underneath the cars.

The main data of the subsequent types are displayed in Table 10.2, from [149]). Please note column 8, showing the development of the Figure of Merit “Weight G_D per product of floor space A_N times traveling speed v_{Tr} “, at increasing comfort (floor space A_N per seat, col. 9)

Table 10.2 German electric accumulator motor coaches and their main data

Nr.	1	2	3	4	5	6	7	8	9	10
Year Class DB Wheel arr.	Number of units	Weight G_D	Floor space A_N	Seats N_{Sp}	$v_{max}/$ v_{Travel}	$\frac{G_D}{A_N}$	$\frac{G_D}{N_{SP}}$	$\frac{G_D}{A_N \cdot v_T}$	$\frac{A_N}{N_{SP}}$	Weight Capac. (5h)
Units		t	m ²		kph	kg/m ²	kg	kg-h / (m ² ·km)	m ²	kg/kWh
1908-10 ETA 177 2A + A2	172	67	47	80	75 42	1,430 100%	838 100%	34 100%	0.6 100%	118 100%
1926-28 ETA 179 2A + A2	11	70	66	88	70 50	1,060 74%	795 95%	21.2 62%	0.75 125%	75 64%
1952 ETA 176 Bo' 2'	8	55	66	78	100 62	820 58%	705 84%	13.4 39%	0.85 141%	44 37%
1953-57 ETA 1501 Bo'2'	232	49	62	68 (59-86)	100 63	790 55%	720 86%	1.52 37%	0.91 152%	40 34%

- *Advantages* of the accumulator motor coach are – in analogy to Table 1.4 – saving of the then (until about 1955) expensive fuels as locomotive coal and diesel oil, the possibility to use cheap electricity, produced in the night, falling away of noise, smoke and preparation time. Electric motors can be overloaded, allowing higher acceleration, and the maintenance is much lower than with diesel engines.
- *Disadvantages* are the big weight of the accumulators (19...21 t in case of ETA 150) and the high cost, the expensive proprietary infrastructure of the charging stations (often operated by the battery supplier) and the limited radius of action (250 km without, up to 370 km with one recharging per day, at 400 kWh capacity of ETA 150). As it was not necessary to take line overvoltage into account, the motors could be operated economically with a high degree of field weakening, over a wide range of speed at constant power.

Motor coaches of Class ETA 176 were experimentally equipped in the very early sixties with the first DC choppers, including regenerative braking; one of the first inverter-fed induction motor drives of AEG was intended for use in an ETA 176 in 1964 [54]. But these new technologies were not introduced in series, the development of a new hybrid storage motor coach for 15kV, 16 ²/₃ Hz with induction traction motors (ETLO 528) was stopped in 1981; the last surviving motor coaches of Class ETA 150 (now 515) were discarded in 1995. In other countries accumulator motor coaches did not play a role at all; there is no glimpse of new coaches with accumulators, as with the still low price of diesel oil operation is not economical.

In 1928 DRG commissioned six dual-mode shunt locomotives Class E 80 with 248 kW for 15 kV, 16 ²/₃ Hz and a lead-acid battery of 417 kWh (at 5-h discharge), using two six-anode mercury-arc rectifiers of 140 kW and transformer tap-changer control. In 1956/57 E 80 01 was equipped with one of the very first experimental silicon diode rectifiers by SSW (for 800 kW!).

Still recently mining and track maintenance locomotives of minor power (< 50...100 kW) are equipped with accumulators, often as dual-mode locomotives (cf. subchapter 9.3); but they cannot be treated here.

In 2002 the first prototype of a mining locomotive using Proton-Exchange-Membrane-(PEM-) Fuel Cells was presented in Canada [150]. It has a peak power of 28 kW, at 14 kW continuous power of the fuel-cell stack; 3 kg of hydrogen are stored by means of metal-hydrid storages, enabling 8 hours of operation. A retrofit of a diesel-electric shunter with 1000 kW is announced for 2008.



Fig. 10.29: Mining locomotive prototype with PEM fuel-cell stack (www.fuelcellpropulsion.org)

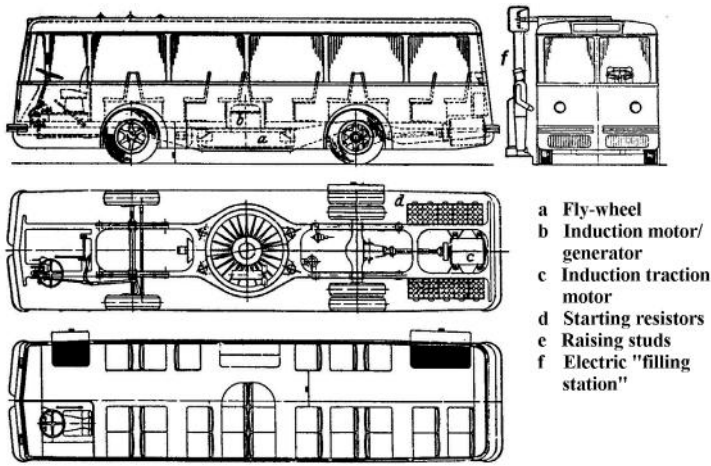


Fig. 10.30: Gyrobus MFO [151]

Besides electro-chemical storages (accumulators) rotating storages were used. In 1950 MFO's Gyrobus made its début and was delivered to Yverdon/Switzerland and to Leopoldville/then Belgian Congo [151], [152]. The steel flywheel of 1.6 m diameter and 1,500 kg weight (kinetic energy 8.3 kWh, used by 75%) was flanged together with the squirrel-cage rotor of a pole-changing induction motor-generator; the casing was filled with hydrogen to reduce friction losses. At each station the flywheel was accelerated to $3,000 \text{ min}^{-1}$ and fed subsequently the induction traction motor, which was of the pole-changing type, too. The control had seven steps, recuperation brake was possible. Investment for the five charging stations in Yverdon was claimed only 10 % of the catenary of a trolley bus (subchapter 12.3).

Today flywheel storages are tested in hybrid buses and e.g. in the experimental DMU LIREX of ALSTOM LHB [136], for intermediate storage of the brake energy and for relieving the diesel motor at acceleration, rated for the average power only. They are built of very strong carbon-fibre materials and driven by inverter-fed PM synchronous machines; the maximum attained speed is at 12,000 rpm, the usable energy 1.5...2 kWh. But as put in [152], the economic use is to be doubted, at recent fuel price. Cf. subchapter 13.3 und [204], too.

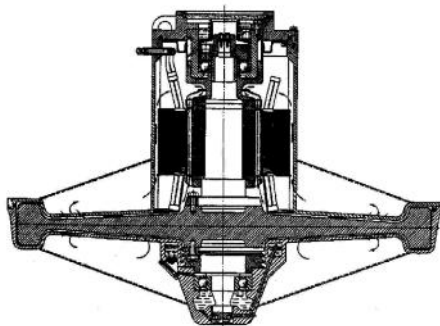


Fig. 10.31: Section through "Elektrogyro" [151]

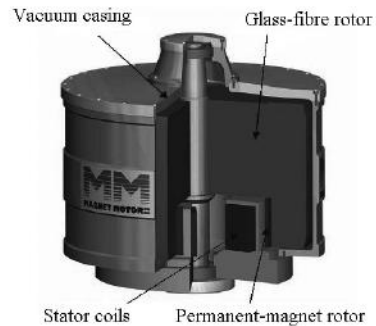


Fig. 10.32: Rotary storage 2 kWh/200 kW 12,000 rpm LIREX 2005 (ALSTOM-LHB)

11 Braking technology

Safe railway operation is most decisively determined by the quality and the reliability of the brakes. As early as 1917 the Kunze-Knorr-type continuous automatic air brake, based on the Westinghouse air brake, was introduced jointly by the German railway administrations, later with other European railways, too; it is still the dominant system. Rising speed and lightweight construction have made the demand increase, so that new, additional brake systems have been developed. Of course, only a very short overview can be given here.

11.1 Automatic air brake

The main brake pipe, going through the whole train, connects the brake equipment of all carriages with one another and with the locomotive; they are connected at the front-sides of the vehicles by shut-off cocks, flexible air-brake hoses and brake-hose couplings. In some automatic couplers as e.g. the Scharfenberg type, the brake-pipe coupling is integrated. The compressed air is produced in the motor vehicle and stored with some 8 bar in the main air reservoir (cf. Fig. 11.1); the pressure is reduced by the air-brake control valve to the operation pressure of 5 bars. It flows through the main brake pipe and the triple valves of the carriages to their auxiliary air reservoirs.

At 5 bars the brakes are released. Actuating the driver's brake valve the pressure in the main pipe is lowered by 0.4...1.5 bar (indirect brake), producing proportional brake force in the brake cylinders, which acts via the brake shoes to the wheel rims. If a brake hose is torn, or the driver reduces the pressure in the main pipe to zero by actuating the rapid-application position of the brake valve or the emergency brake valve, the so-called Ackermann valve, the emergency brake is actuated.

The impact of the brake can be set at the vehicles: Goods wagons feature a No-Load and a Load position (L-B), passenger carriages a G = Goods trains and a P = passenger-train change-over (slow/fast acting). High-speed goods wagons (to be used in passenger trains, too) usually are equipped with both changeovers.

Traction vehicles are equipped with a direct-acting air brake, in addition to the continuous indirect brake; both brakes act on the same brake cylinders. Fig. 11.2 shows the classical shoe brake and its rigging (example Class 151 of DB, year of origin 1956). While a steam locomotive only had one or two central brake cylinders, this locomotive is already equipped with 8 brake cylinders for 12 brake shoes (mostly made from grey cast iron). The parking brake acts purely mechanically on the same brake rigging. As the joints of this rod linkage need intensive and careful maintenance, today each brake shoe is actuated by its own brake cylinder.

The adhesion coefficient is dependent on many parameters in a nonlinear manner, as explained in subchapter 2.3. The whole deceleration energy $W = \frac{1}{2} m_{\text{Train}} \cdot \xi \cdot v^2$ is dissipated via the wheels and – to a lesser part – the brake shoes, endangering the fixation of the shrunk wheel tires; even monobloc wheels may be jeopardized.

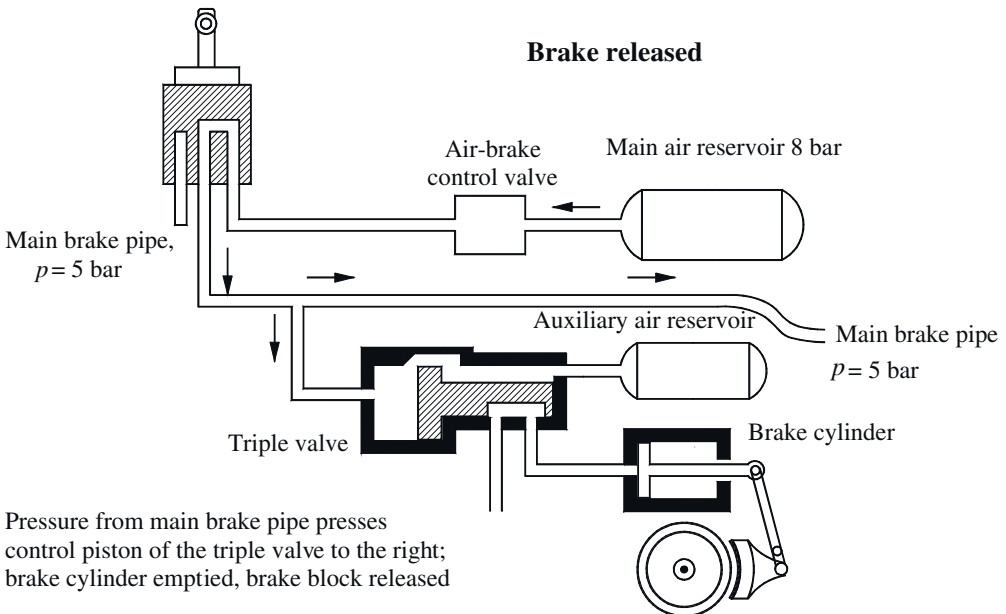
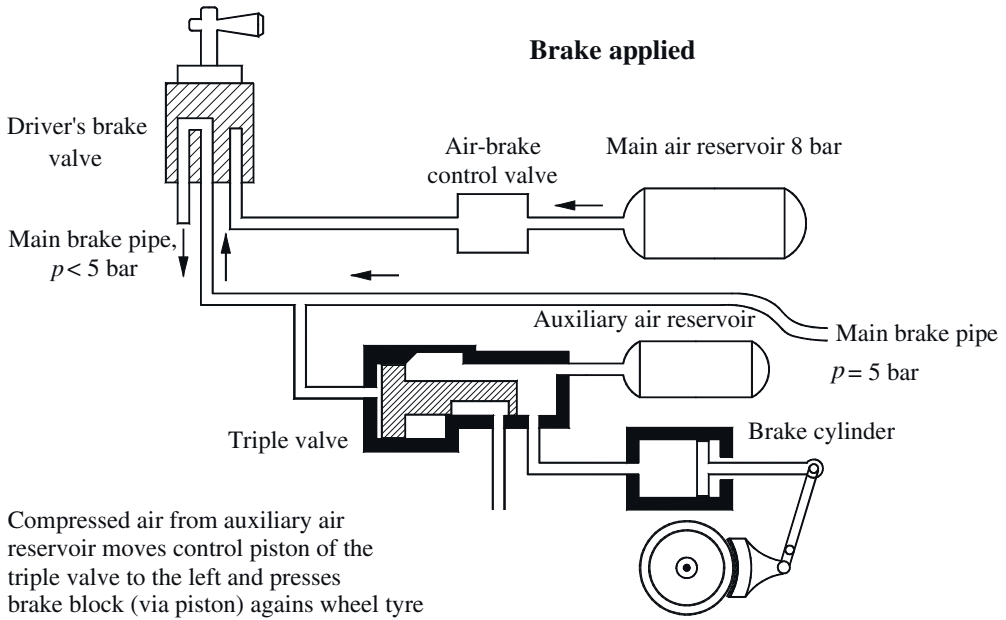


Fig. 11.1: Principle representation of automatic air brake

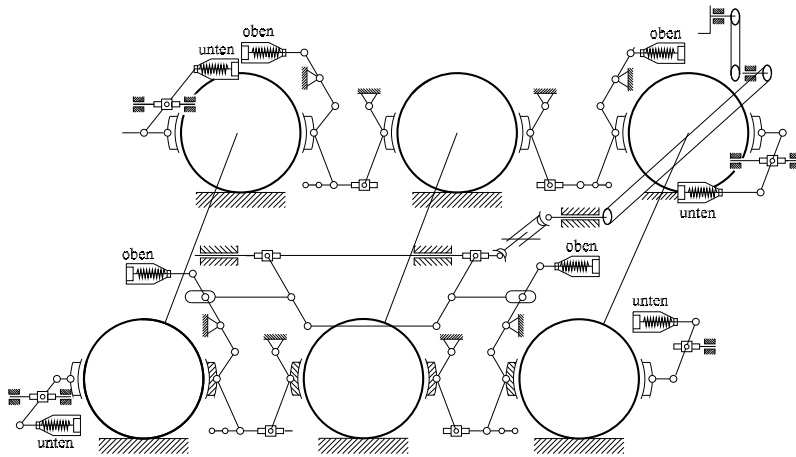


Fig. 11.2: Classical shoe brake with rigging (Class 151 of DB)

The disk brake keeps the deceleration energy away from the wheels, dissipating it directly to the ambient air. The brake adhesion coefficient is nearly independent of the speed and the pressure; the specific brake power can be raised considerably. The brake disks may be mounted either on the shafts (of carriage wheelsets), outside of the wheels (cf. Fig. 3.7, pos. 3 and 4), on the hollow shaft of the cardan drive, as employed with the IGA (Fig. 3.13) or on a separate hollow shaft, supported in the bogie frame as with the ICE 1 (cf. Fig. 11.3), or on a separate brake shaft, connected via a spur gear to the main drive, as in case of the HAB (Fig. 3.14). As the roughening effect of the brake shoe on the wheel rims is left out, the adhesion coefficient at the wheel-rail contact sinks, occasionally scouring braking are used (Fig. 3.7, pos. 5). This effect can be produced today by intentional driving with raised slip (wheel-tire conditioning, [16]).

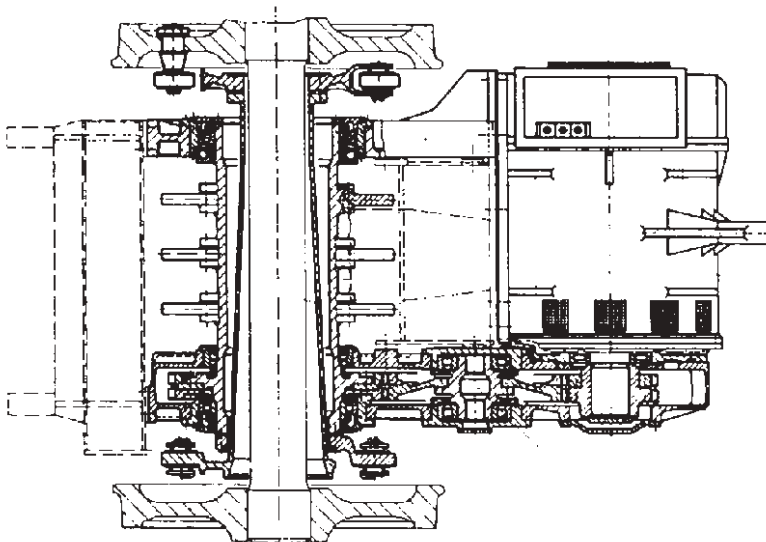


Fig. 11.3: Brake disks on a separate cardan hollow shaft of the ICE 1

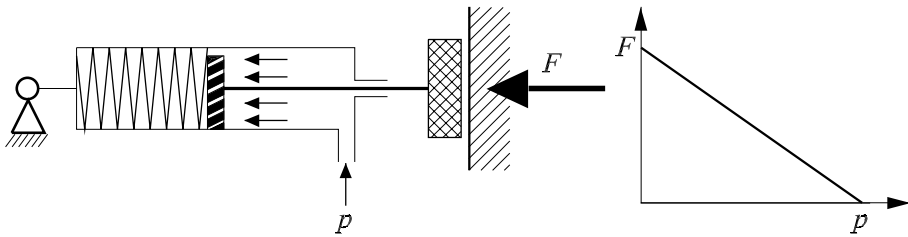


Fig. 11.4: Principal representation of a spring-storage brake

As modern locomotives and motor coaches with three-phase drive technology brake electrically with priority, the direct automatic air brake is only activated in the speed range over some 100 kph (range of constant power, 160 kph with ICE 3) or if there is a disturbance in the electric brake system. The automatic vigilance device or dead man’s handle (Sifa = *Sicherheitsfahr-schaltung* in German) checks the driver: If the button (or pedal) is not pressed in regular intervals (and released in-between!), the emergency brake is activated.

Modern constructions [153] integrate the parking brake as a spring-storage brake (Fig. 11.4) within the brake-cylinder block, replacing the spindle manual brake. The spring-storage brake is released by the pressure in the main brake pipe; when the air pressure is reduced, the spring delivers the braking force. “All-electric” tramways have spring-storage brakes operated by electric motors.

Fig. 11.5 depicts as an example the brake system of the universal locomotive prototype 12 X of AEG/ADtranz, together with all other devices operated by compressed air, as main circuit breaker, pantographs (subchapter 13.4) and signalling horns. The auxiliary compressor (centre) is used for rigging the vehicle, operated from the battery.

Fig. 11.6 shows the brake valve handles on the right side of the driver’s desk of a traction vehicle with three-phase drive technology.

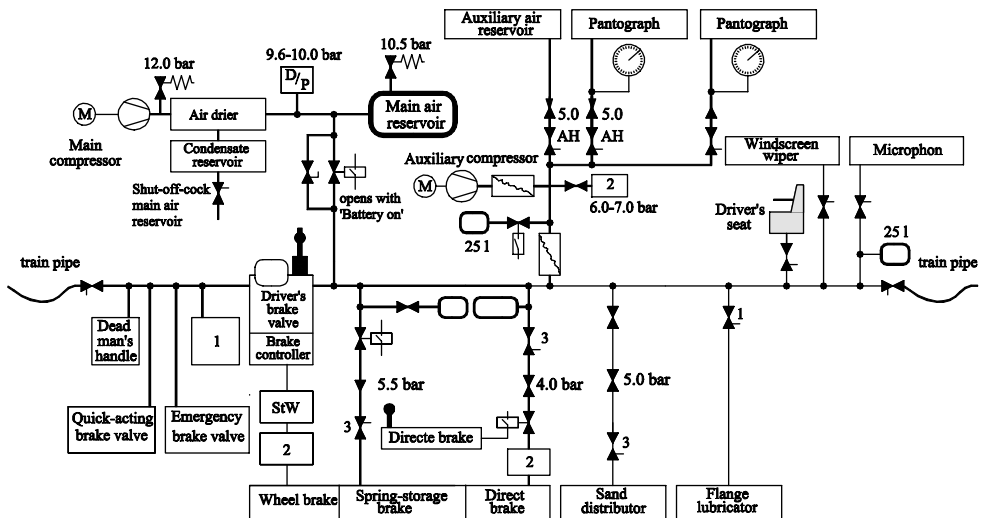


Fig. 11.5: Air-brake system of an electric locomotive with three-phase drive technology (example 12 X / Class 128 DB AG) (Bombardier Transportation)

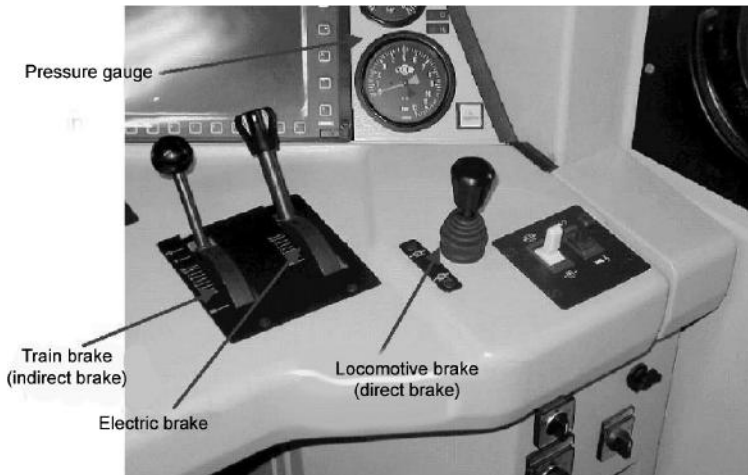


Fig. 11.6: Driver's desk of locomotive with three-phase drive technologie – operation of brakes (Bombardier Transportation)

11.2 Magnet rail brake

High-speed multiple units and light-rail vehicles demand higher brake deceleration, than transferable by adhesion only. For braking, f_{x-b} can be accounted to 0.15 only, for safety reasons. As $a_b = 2.7 \text{ m/s}^2$ is demanded by BOStrab for tramways and Light Rapid Transit trains, only $a = f_{x-b} \cdot g = 1.48 \text{ m/s}^2$ is feasible! Additional brake systems will be necessary, independent of the adhesion between wheel and rail.

The DC-excited, articulated magnet packets of the magnet rail brake (MRB) of 1...1.5 m length are mounted between the wheelsets and are lifted by springs by some 60...150 mm

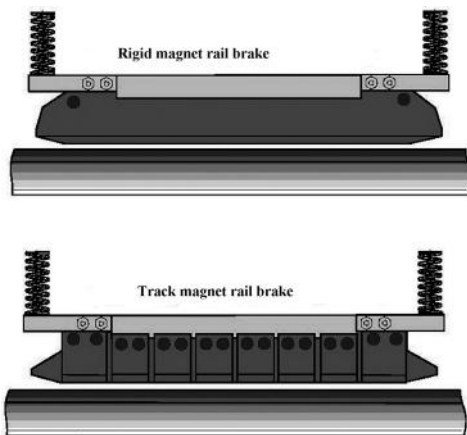


Fig. 11.7: Magnet rail brake (Siemens AG, TS)

over top of rail. When the emergency brake is activated, the MRB is lowered by compressed air, against the springs, and attracted to the rail by the exciting current.

Excitation of about 1.5 kW/m generates attractive forces of 65 kN/m and, with a braking adhesion coefficient of $\mu = 0.1$ a braking force of about 6.5 kN/m. The MSB decelerates the vehicle down to some 50 kph; braking down to standstill is taken over by the conventional air brake and the electric brake. The magnet rail brake is e.g. used with the ICE T (section 6.4.2) and the ICE TD (subchapter 9.2).

Exercise 17.9 “Stopping distance of a Light Rapid Transit Train with and without magnetic rail brake” works out the attainable stopping distances in dependence upon the applicable braking force.

11.3 Linear eddy-current brake

Disadvantages of the magnet rail brake are

- the wear of the brake shoes
- the variable adhesion coefficient.

They are overcome e.g. in case of the ICE 3 by the linear eddy-current brake, which is mounted in the trailing bogies. This brake is excited by DC, too, but with much higher power (cf. Fig. 11.8), and produces similar specific braking forces as the MRB by eddy-currents induced in the rails. The air gap is some 5...7 mm. The high exciting power is covered by an additional GTO or IGBT phase module, operated as step-down converter (section 4.1.3); [B 20]. At non-available line voltage, the traction motors maintain the value of the DC-link voltage by slight braking. Problems arose from possible interference with track circuits such as axle-counters by the strong magnetic field near to the rails, which could only be solved after time-taking experiments, by modifying the form of the coils and by special shielding. The very high brake power of high-speed trains warms up the rails considerably; this must even be taken into account when calculating the headway of the trains.

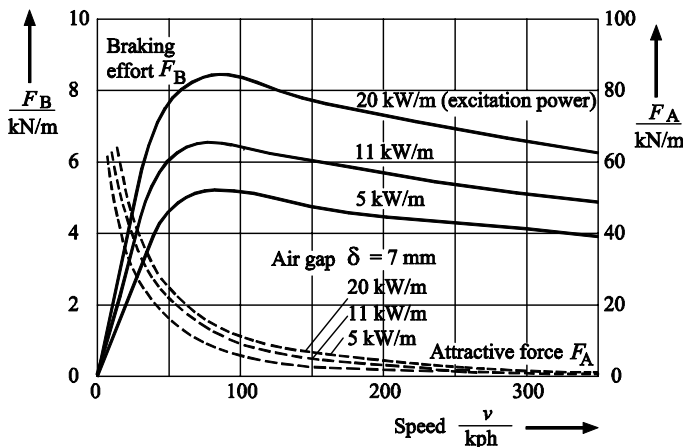


Fig. 11.8: Braking and attractive effort of a linear eddy-current brake (EEW-TUD)

12 Uncommon types of railways

We shall define “common” types of railways, as explained in section 1.1.1, as such railways operating on a twin-rail track (presumably of iron), using iron (or steel) wheels, the latter also providing for vehicle guidance and transmission of tractive power from the motor(s) to the rails; simply put, this would be the “classic rail-wheel system”. This system has a number of benefits, but also suffers from various limitations, for example reduced adhesive force and sinusoidal running.

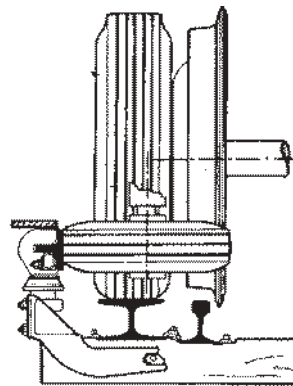
12.1 Track-guided railways on pressurized rubber-tire wheels

Quite frequently, underground railways have to negotiate considerable elevations, for example to evade other rail lines, shipping lanes or sewerage systems. This occasionally exceeds the available level of tractive and decelerative transmission afforded by adhesion, most notably if longer stretches of track are built as surface or elevated tracks and are thus exposed to rain and bedewing.

The *Métro* of Paris (RATP) had conducted trials of vehicles equipped with nitrogen-filled pressurized tire wheels, operating on wooden or concrete tracks, since 1956. From 1965 onwards, four lines were equipped with such vehicles (cf. Fig. 12.1 left; [B23]). Horizontal running wheels provide lateral guidance, thus reducing screaming of the wheels in tight curves. The steel flange wheels (Fig. 12.1, right) take over guidance when running over track switches (the running track being lowered in relation to the rails in this case) and in case of emergency. Current supply is provided by the two lateral guiding rails.



Fig. 12.1: Paris Métro train operating on pressurized rubber-tire wheels in an elevated station [B23]



Constructive principles of running, guiding and supporting wheels [B23]

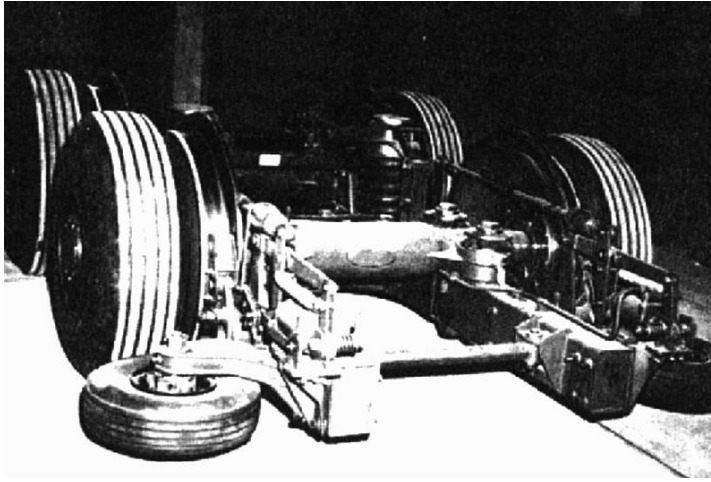


Fig. 12.2: Motor bogie of Paris Métro

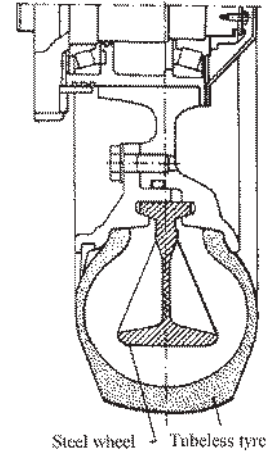


Fig. 12.3: Rubber tire with safety steel wheel

Fig. 12.2 depicts this type of bogie *en detail*, Fig. 12.3 illustrating a rubber tire with an integrated safety steel wheel (used in Sapporo, Japan, and Montreal, Canada).

A similar pressurized rubber-tire system is used with the fully automatic cabin railways of the French VAL pattern (véhicules automatiques légères, or light automatic vehicles, used in Lille, for example), as illustrated in Fig. 12.4. The wheelbase of the supporting wheels is 1880 mm (~ 6ft 1in), the distance of the two outer current-supply and guiding rails is 2130 mm (~ 6ft 11in). Two cars of 12.7 metres length each (~ 42ft) are articulated, wheelset arrangement being Bo + Bo; for further information, see caption of Fig. 12.4. Steering of the vehicle in track switches is achieved by using adjustable guide rails in the middle of the track, which direct a guiding wheel beneath the vehicles' floor.

A number of "people mover" systems operating on international airports are equipped with this or similar systems. For fully automatic operation, doors on the platforms' edges are required; these doors are exactly lined up with the train's doors and opened only after the train has come to a full halt.



Fig. 12.4: Automatic People Mover VAL 206 with pressurized rubber tires

Owner	TCL Lille
Supply current system	GS 750 V
Mass in service	30 t
Passengers	
seated/standing	68/208
Floor height over rail	900 mm
Rated power	4 · 120 kW
Maximum speed	80 kph

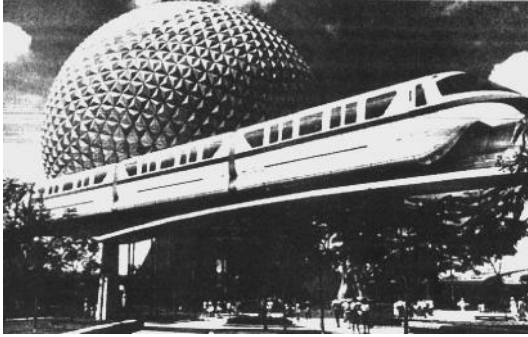


Fig. 12.5: Monorail girder railway (Alweg Railway)

The “Monorail”, “Girder Railway” or Alweg Railway, named after the inventor, Alfred Wennergren, who built a first trial line near Cologne in Germany in 1953 (cf. Fig. 12.5), runs on a central supporting and guiding girder rail of 700 mm width and 1200 mm height (2ft 4in and 4ft, respectively). The original requisites were higher speeds in tight curves, achieved by tilting the angle of the girder rail (which was usually mounted on pillars) towards the centre point of the curve. The most prominent disadvantage is the impeded or even inhibited transfer of passengers from one side of the vehicle to the other.

The Alweg Railway was mainly used in the leisure resorts of the Disney Corporation (Anaheim, CA and Orlando, FL) as well as a commuter conveyance for Haneda International Airport, Tokyo, Japan. Nonetheless, it has to be considered an isolated type of transport system and does not bear great potential for future use.

12.2 Suspension Railways

If the main level of traffic is inaccessible to rail-bound vehicles, either due to the dominance of individual transport or due to peculiar topographic circumstances (like extended stretches of water, or in mountainous areas), and if an underground railway would prove too costly in relation to the number of passengers (cf. Table 10.1), elevated railways like those used in Berlin, Hamburg or Chicago or suspension railways prove their worth. Of the vast number of proposed solutions, we shall only discuss the two most successful.



Fig. 12.6: Wuppertal suspension railway

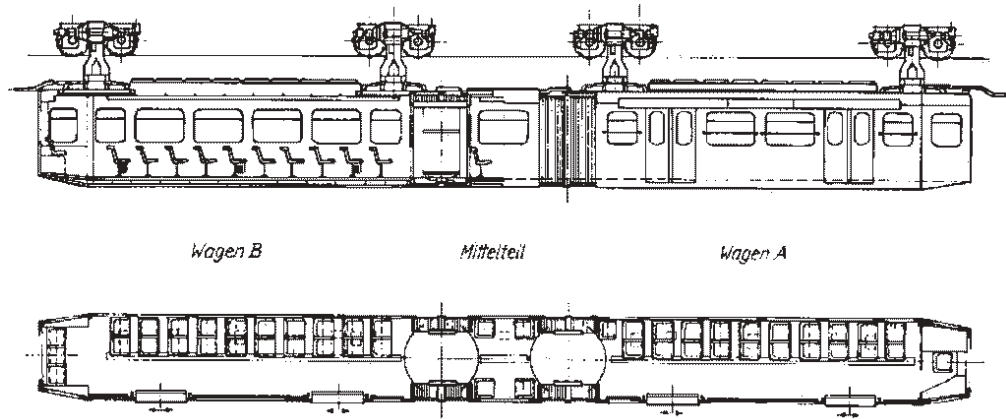


Fig. 12.7: Articulated motor-coach of Wuppertal suspension railway (1972)

The most popular suspension railway is arguably the Wuppertaler Schwebbahn (suspension railway) of Wuppertal, Germany). Based on the respective patent granted in 1893 to Eugen Langen and constructed during the years 1898 to 1903, this railway follows the course of the Wupper River between the districts of Vohwinkel and Oberbarmen, being suspended over the river on 470 supporting girders (cf. Fig. 12.6).

The drive and running wheels each have twin flanges; thus, there is no need for guiding rollers. When running through the minimum curve radius of 75 m at $v = 40$ kph (25 mph), the coach body tilts outward by 11° .

In the years between 1972 and 1974, Siemens and Kiepe Electric (with MAN as car-body contractor) delivered twenty-eight new trains (cf. Fig. 12.7), which were the first vehicles in Germany to be equipped with DC choppers by standard [154], [155]. Each articulated train has four drive motors of 50 kW each; $v_1 = 26$ kph (16 mph), $v_{\max} = 60$ kph (37 mph). Since 1997, the girder superstructure has been renewed.

Siemens' "H-Bahn" is a modular cabin suspension railway. After the prototype system used at Dortmund University from 1975 onwards proved successful, it is used under the name of "Sky-Train" at Düsseldorf International Airport, taking up full service in 2002. Fig. 12.8 shows, above, the twin-car train beneath the suspension girder; below, a side elevation.

Fig. 12.9 shows the running gear (with DC motors), Fig. 12.10 illustrates the track girders and running gear in cross-section, detailing the running area for the traction wheels and the contact-rail system (3 AC 400V, from both sides only being found at switches). The drive motors are fed from these contact rails via three-phase thyristor bridges.

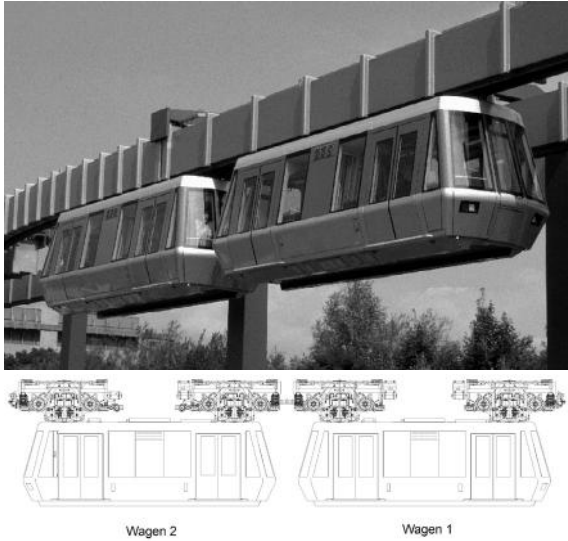


Fig. 12.8: Sky-Train
Düsseldorf Inter-
national Airport
(Siemens AG, TS TK, Berlin)

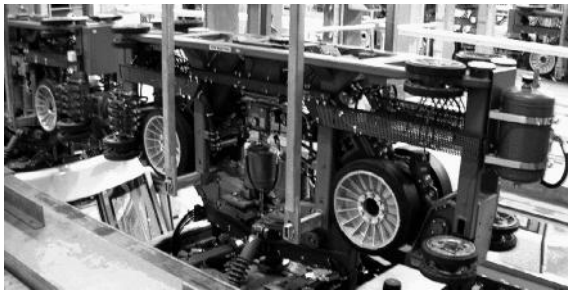


Fig. 12.9: Running
gear Sky-Train
(H-Bahn)

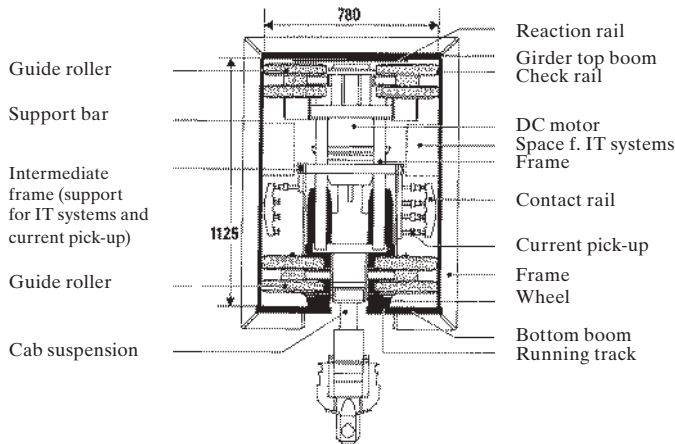


Fig. 12.10: Cross- section track girder and running gear (Siemens AG, TS TK, Berlin)

12.3 Trackless “railway” transportation systems

Trackless railways, in the strictest sense of the word, lack the basic element of track-bound guidance; but due to their dependence upon line-bound electric energy supply, they are still bound to specific “track” areas (cf. VDE 0115).

The best-known and most important trackless system is the overhead-fed trolley- or “O-“ bus. In 1901, the first Schiemann “O-Bus” took up service near Dresden (Fig. 12.11); however, it proved unable to stand up to the growing competition presented by combustion-engine buses and was withdrawn from service as early as 1906.

During the 1930s, more efficient trolley buses were developed, notably in Great Britain and Italy, as well as in Germany, where the big electric utility RWE became the main proponent of the system (Mettmann 1936). After the Second World War, a large number of ruined tramways were replaced by trolley buses, notably in small and medium-sized towns; the advent of the diesel bus in conjunction with continually sinking fuel prices, however, led to the almost complete demise of the trolley bus in many countries. In addition, initial cost for O-Bus systems are considerably higher than for diesel buses, due to the lower production numbers involved. Even the longevity of the electric systems, which were repeatedly installed in two or even three carbodies over the years, could not truly compensate for this.

Nowadays, there are three O-Bus systems still in operation in Germany, in the cities of Solingen, Essen and Eberswalde; in various Swiss, eastern European and Asian cities, large trolley-bus networks thrive, due to different political and economic circumstances (most notably the appreciation of the reduced pollution by exhaust gases).

Fig. 12.12 depicts a modern low-floor articulated trolley-bus type AG 300 T, built for the city of Arnhem, Netherlands, using three-phase traction technology manufactured by Kiepe Elektrik in 2000. Fig. 12.13 displays the main circuit diagram which corresponds to a recent tramway; $P_N = 156$ kW. A common feature of the system is a 55-kW diesel-motor driven generator, which serves as emergency backup and for free manoeuvring in depots. The IGBT inverter of 220 kVA (similar to that of Fig. 6.41) is air-cooled; line-recuperation braking is provided here, but often a diode-bridge commutator is attached to the input feed, which allows for simple operation of turn loops. Another point which shall only be cursorily noted are the special earthing specifications required to meet operator and passenger safety demands.

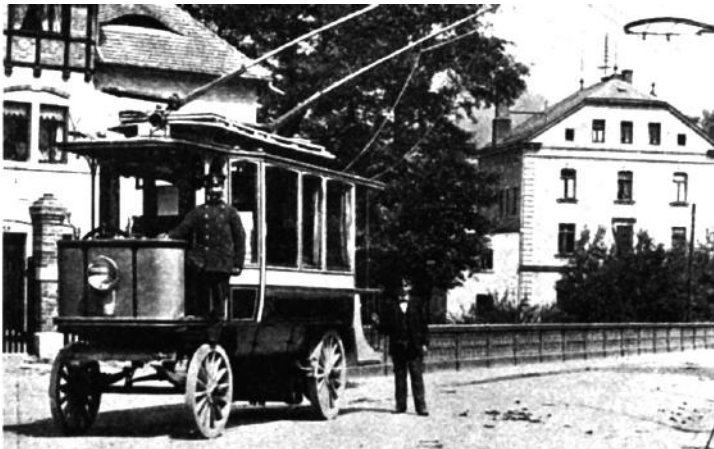
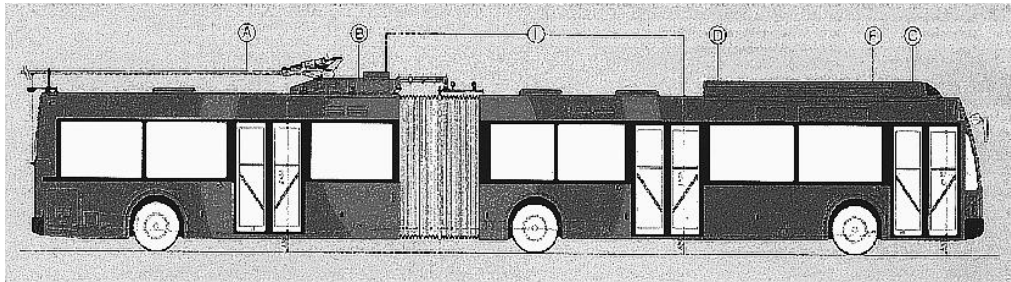


Fig. 12.11: Historic trolley bus, system Schiemann 1901



- | | |
|-------------------------|-------------------------|
| A Pantograph OSA | F Auxiliary inverter |
| B Main contactor | G Compressor |
| C Brake resistor | H Emergency drive |
| D Traction inverter DPU | I Heating |
| E Traction motor | J Isolation supervision |

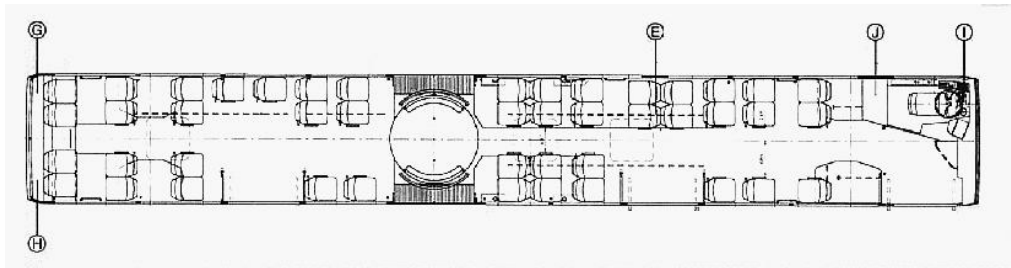


Fig. 12.12: Low-floor articulated trolley bus type AG 300 T for Arnhem/NL (Vossloh Kiepe GmbH)

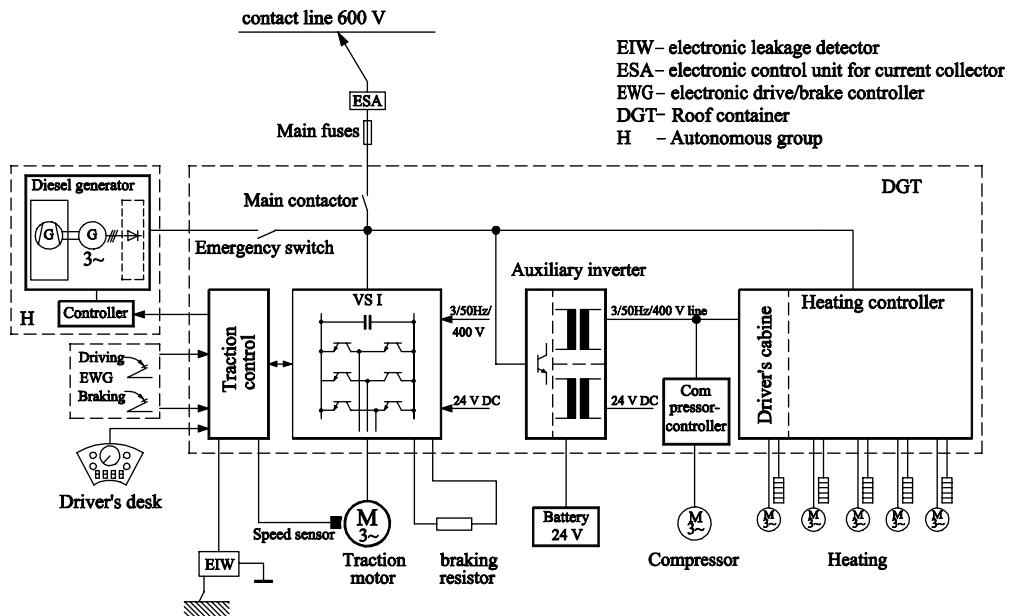


Fig. 12.13: Main schematic trolley bus type AG 300 T for Arnhem/NL. (Kiepe Elektrik GmbH)

Trolley buses equipped with full-power diesel-motor systems (177 kW), running between external guide-rails, are called dual-track bus (Duo-Spurbus) and have been used in Essen, for example [158], but since 1996 in diesel operation only, and in Adelaide/Australia.

The TVR doubly-articulated bus system, using a single central guide rail and a two-pole catenary, is manufactured by Bombardier and is used in Nancy/France [159].

In American and South African strip mines, diesel-electric haul trucks are used almost exclusively. The Haul Truck TI 272 manufactured by Siemens/Liebherr Mining Trucks (cf. Fig. 12.14) is a prime example of innovative chassis and traction technology [160]. Using two longitudinally-mounted asynchronous traction motors of 1.8 MW apiece which power one of the rear double wheels each, the truck is able to handle loads of up to 254 metric tons. The diesel engines' power peaks at a maximum of 1,650 kW (in respect to the wheels); the two generator windings (with a rated voltage of some 960 V) are series-connected via the diode rectifiers. To speed up the climb from the strip mine, the ramps feature electrical overhead contact lines (cf. Fig. 12.15), which supply electrical energy at levels of up to 2,600 V.

Fig. 12.16 shows the main circuit diagram of the new Haul Truck with Siemens three-phase drive technology. If fully using the installed inverter and motor power of 3.5 MW, speed on the respective 8% ramp rises from 14.3 kph (8.9 mph) under diesel power to 23.1 kph (14 mph) using the electrical overhead supply, while the truck is able to handle a payload of 327 metric tons of ore, at 230 metric tons vehicle weight and a traction resistance of $w_r = 2\%$; the generators are not excited. Furthermore, mixed or "booster" operation is possible: With older 1200...1600-V networks, which were previously operated by DC-motored dump trucks, the parallel-connected diode rectifiers are switched in series with the line voltage, resulting in $U_d = 2400...2600$ V. The GTO thyristor inverter with evaporation cooling corresponds to Figs. 6.35 and 6.36.

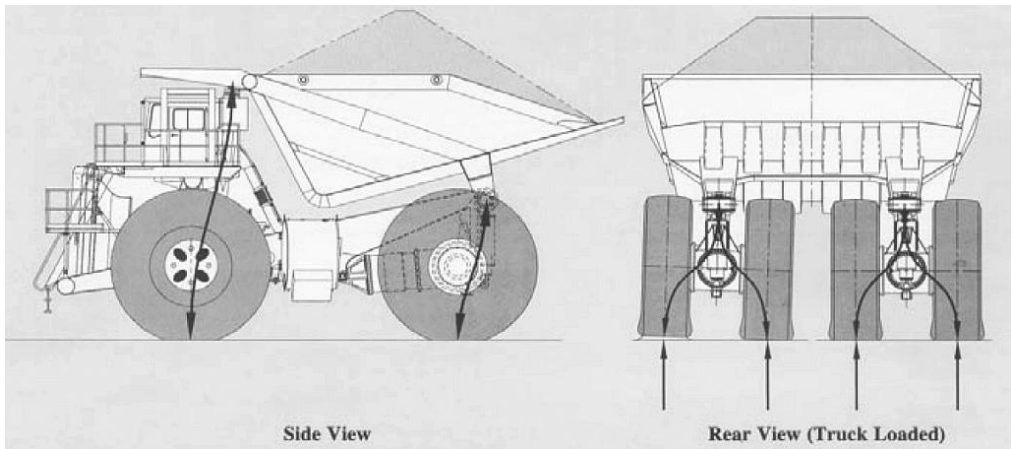


Fig. 12.14: Front and rear view of Haul Truck Liebherr TI 272 with two longitudinally-mounted induction traction motors (Siemens Energy & Automation, Inc.)



Fig. 12.15: 254-t Haul Truck Euclid-Hitachi R280 under overhead line (Siemens Energy & Automation, Inc.)

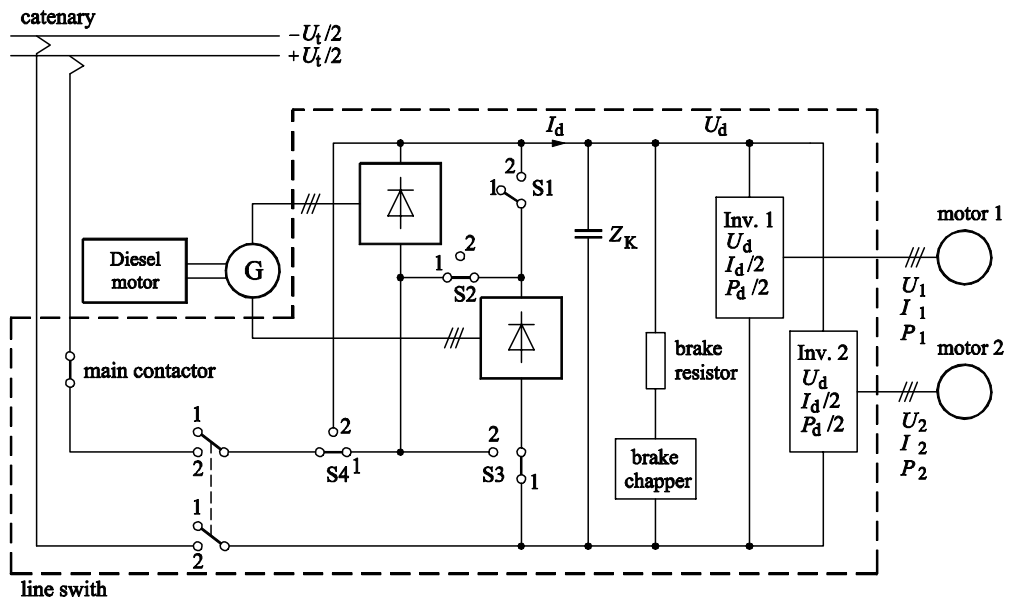


Fig. 12.16: Main circuit diagram of dual-power Liebherr Haul Truck: $P_{DN} = 2160 \text{ kW}$, $P_{invN} = 3.5 \text{ MW}$ at overhead line $U_{LN} = 2600 \text{ V}$, pay load 327 metric tons (acc. to [160])

12.4 Magnetic Levitation Railways (MagLev)

The triad inherent to the rail-wheel system, namely support – guidance – acceleration/deceleration, is limited today to speeds up to about 350 kph (217 mph). Above that, operation is hampered by various problems that cannot be solved economically anymore.

- The required power, which rises at the third power of speed (up to 20 MW at $v_{\max} = 500$ kph (310 mph) for a 300 metre-long (985 ft) train) results in the onboard drive system getting so heavy that the individual axle-loads of approx. 10 t required in respect to wear are transcended by far.
- Bogie oscillations, as excited by Klingel's Oscillations, are transformed into non-linear oscillations, which cannot be controlled any more. This problem also applies to motors mounted externally from the bogies, as described with the TGV in section 2.1.3. Wheel tires of flatter profile only have insufficient lifespan due to increased wear and lose quality at an alarming pace, so this is not a viable option.
- Train resistance, which increases by the second power of speed, cannot be overcome by respective tractive power due to the falling adhesion factor, even if using all-wheel drives.
- The wear of wheel and rail exceeds all economically sensible levels.

As early as 1935, H. Kemper [161], [162] proposed to provide support and guidance by use of “levitating” magnetic forces of attraction; he even displayed a working model of 210 kg of weight. For the drive, he proposed to use the synchronous travelling-wave linear motor with track-fixed three-phase (long-stator) windings – which is exactly the same pattern as chosen in the 1975 “Systementscheid” (System Decision) for the German TRANSRAPID system. This system took up trial operation in 1977 on the experimental track TVE at Lathen in the north-west of Germany, and has been in commercial use since 2003 on the Shanghai-Pudong Airport Line for the first time. Due to the constraints of this book, only a very concise overview of the very complex field of MagLev systems can be given; it is advisable to refer to works of specific technical literature (e.g. [163] – [167], [169] – [172]).

12.4.1 Support and Guidance

The so-called Electro-Magnetic Levitation (EML) depends on the forces of attraction which accrue when magnetic field lines emerge normally from the interface of areas of different permeability (cf. [V1]):

$$F = 1/2 \cdot A \cdot H^2 \cdot \mu_0 \cdot \mu_r^2 \quad (12.1)$$

with the cross-section A , the magnetic field strength H and μ_0 and μ_r acc. to section 4.2.2. Neglecting the excitation for the iron path (cf. equ. (4.1)), from

$$H \sim I_E \cdot w_E / \delta \quad (12.2)$$

follows that the attraction force, inversely proportional to the air gap, is unstable on principle; EML needs a (fast) stabilizing control, realized by 100-kHz DC choppers. The air gap is typically 8...12 mm, dependent upon speed.

Fig. 12.17 shows a cross-section of the TRANSRAPID TR 06 vehicle. The supporting magnets, which are also the exciter magnets for the long-stator motor (see below), are mounted inside the vehicle's levitation frame, gripping beneath the laminated iron packages of the stator. Fig. 12.8 gives a longitudinal section through the integrated support/drive-system. When the supporting magnets are switched off, the vehicle comes to rest on runners.

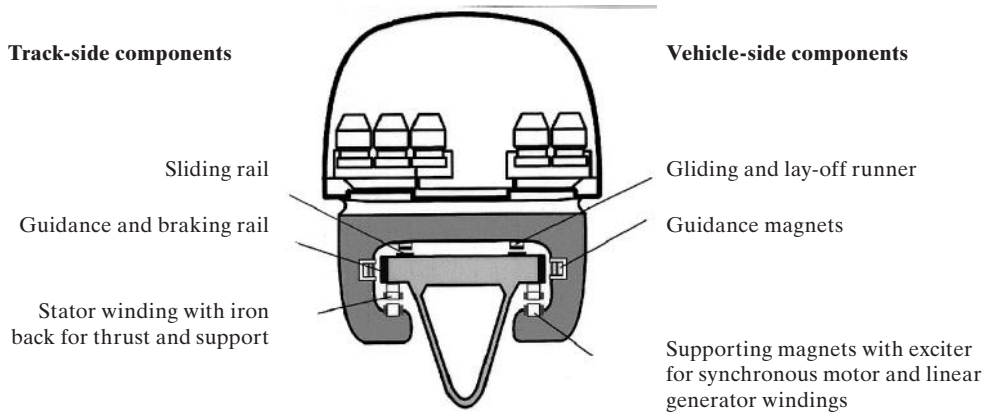


Fig. 12.17: Cross-section of TRANSRAPID TR 06 (acc. to [163])

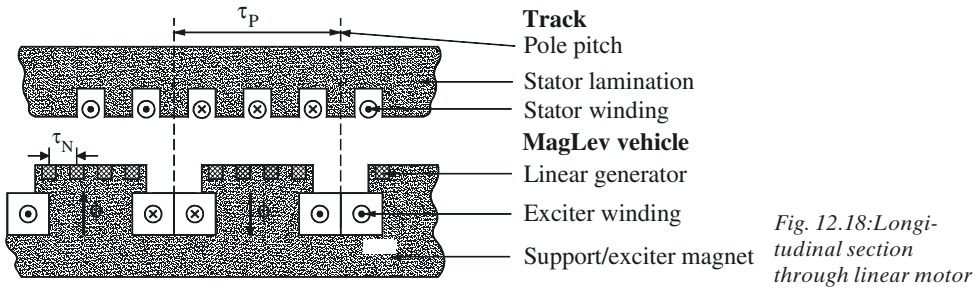


Fig. 12.18: Longitudinal section through linear motor

Guidance is achieved by similar, smaller magnets. The required power for support and guidance is about 1.75 kW per metric ton total weight.

Apart from the EML system, which is based on electromagnetic attraction, there is the Electro-Dynamic Levitation System (EDL), which is based on electromagnetic repulsive forces of the vehicular support (and exciter) field and the eddy currents induced by the supporting field itself in aluminum rail coils. It succumbed to the EML in the German System Decision, but is used in Japan for the MLX vehicles in service on the Yamanashi trial track [167]. The only economical way to generate the required strong vehicular magnetic fields (300 kA) is to use superconductive coils, thus requiring a high demand for cooling. The EDL system is inherently stable, but only weakly dampened and operates with air gaps of 100 mm (4 in); since the opposing fields in the rails only prove sufficient at speeds of more than 120 kph (74 mph), the vehicles have to start and stop using rubber-tire running gear.

Fig. 12.19 (taken from [167]) shows the train resistance forces caused by both supporting/guiding systems. The EDL system is only fully usable at speeds exceeding 400 kph (250 mph), whereas the EML system can also be used for local and commuter railways at lower speeds. The cooling requirements for the low-temperature superconductors of the EDL are comparable to the power requirements for support and guidance of the EML system.

Since 1975, AEG and Magnetbahn GmbH, Starnberg, have developed a variant of EML, using permanent magnets ("M-Bahn", [168]), and tested it between 1983 and 1991 on a derelict Berlin elevated subway line. The air gap is controlled in a purely mechanical way by means of casters and levers; the lateral guidance is taken over by rubber casters, too.

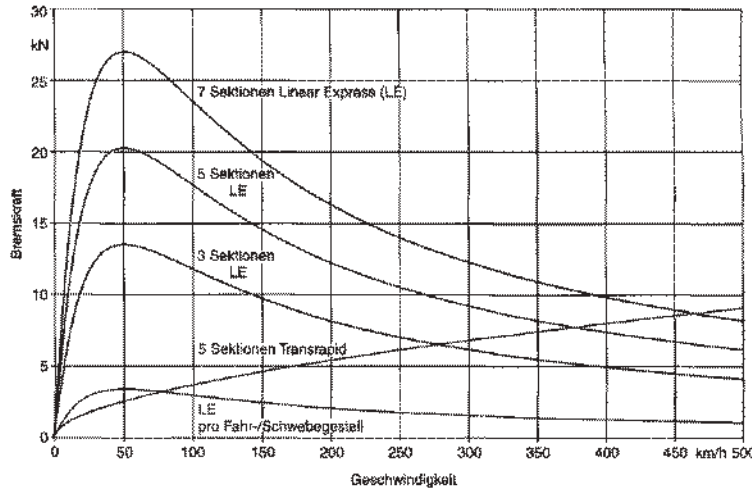


Fig. 12.19: Speed-dependent train resistance force due to eddy-current effects at TRANSRAPID (EMS) and Linear Express (EDS) [167]

Traction is provided by a linear synchronous long-stator motor, using the supporting magnets as exciter magnets.

12.4.2 Contactless transmission of traction force

The travelling-wave linear motor is comparable to a three-phase motor cut up and stretched. In the beginning, it was built as a so-called “short-stator induction motor” with the travelling-wave stator winding mounted inside the vehicle and a reaction rail made of aluminum (\rightarrow short-circuit rotor), which was affixed to the track; this system was used with various local transport systems. It fails, however, at higher traveling speed due to the weight of the inverters which have to be carried along by the vehicle; further more, the energy feed is a problem at $v > 300\text{...}350$ kph (200 mph). Thus, the long-stator motor turned the assembly upside down: The travelling-wave winding is connected with the track girder, hanging beneath it; its iron package is the return path for the supporting electromagnet, which itself works as the exciter field for the now synchronous travelling-wave motor (Fig. 12.17 and 12.18, [163]).

With the pole pitch of $\tau_p = 258$ mm used with the TRANSRAPID system, the stator winding must be fed at a frequency of $f = v/(2 \tau_p)$, for example 268 Hz at $v = 500$ kph (310 mph). Originally, the pole position was determined using search coils within the track and transmitted to the inverters in the substations (cf. section 12.4.3). Nowadays, the pole position is determined incrementally by sensors within the vehicle, which count the slots of the long stator, and are backed up by synchronizing with local balises. The field-oriented control method, as described in section 15.1.4, is used. Fig. 12.20 shows the basic assembly of the stator winding, table 12.1 collates the respective data.

In contrast to the usual inverter-fed synchronous drive (cf. subchapter 5.2)

- it is only the supporting function which defines the DC excitation current; there is no field weakening, which would not be useful in either way due to the rapidly rising train resistance, which is directly attuned to the dominant air resistance. Cf. Fig. 12.21.
- the propulsive and decelerative force is only controlled by amplitude and phase angle of the stator current
- the displacement factor $\cos \varphi$ is rather low at 0.7 and requires high inverter ratings.

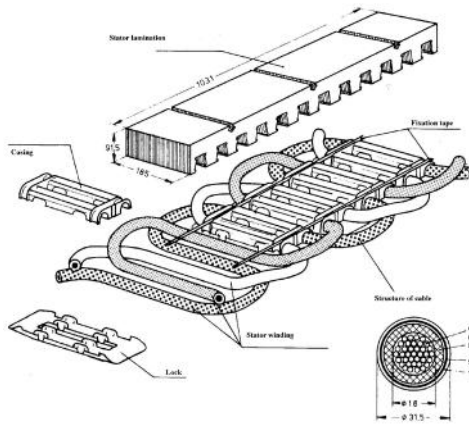


Table 12.1: Data of long-stator motor

Stator lamination	Width	185.0 mm
	Height	91.5 mm
	Length	1031.0 mm
	Pole pitch	258.0 mm
Winding cable	Material	Copper
	Cross-sect.	150.0 mm ²
	Diameter	32.1 mm
Supporting/ exciter magnet	Width	232 mm
	Height	190 mm
	Length	1318 mm
	Excitation	6000 A
Nominal air-gap width		10 mm

Fig. 12.20: Construction of stator winding system [163]

In order to limit the required magnetizing reactive power (which must be provided by the inverters) and the resultant losses, the stator winding is separated into sections of $L = 500 \dots 1500$ metres of length, which are only switched to the inverters by vacuum contactors if the train is currently running in the respective section.

Being independent of adhesion, MagLev allows for high acceleration right up to high speeds and high gradients of up to 10 %. The level of noise of the TRANSRAPID at 400 kph is about equal to that of ICE 3 at 300 kph. Since the levitation frames grip around the rail track, the TRANSRAPID cannot derail. In curves, higher superelevation and thus smaller radii than with conventional railways can be achieved, thus reducing cost for tracklaying in hilly terrain [171]. This, however, is roughly comparable to the gain offered by tilting technology (section 2.1.5), [171].

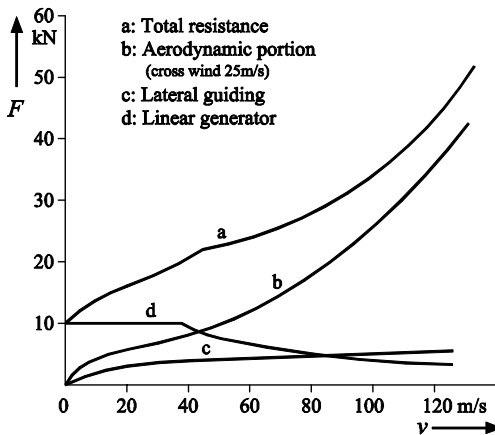
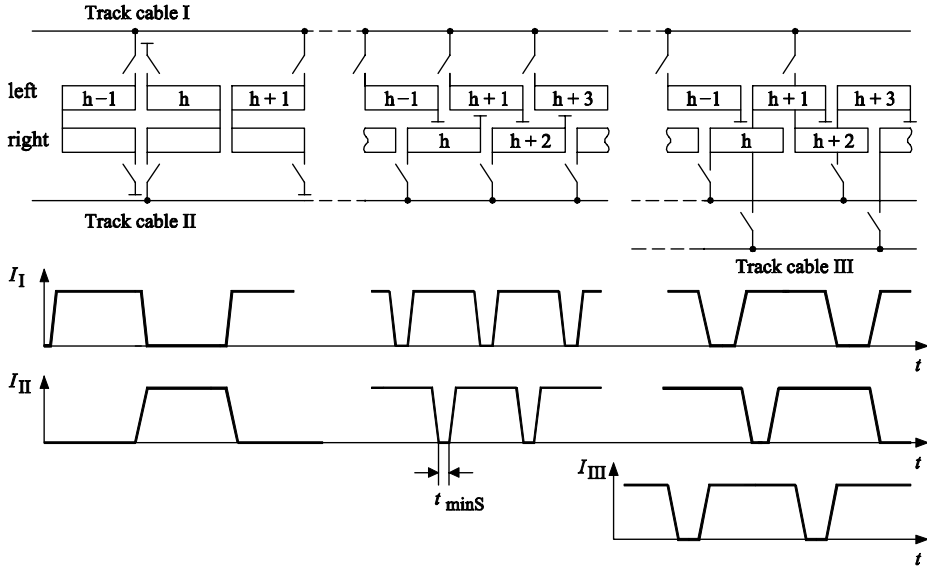


Fig. 12.21: Train resistance of TRANSRAPID TR06 [163]



Leap-frog procedure Alternating-step procedure Three-step procedure

Fig. 12.22: Section-change methods

A minimum of two inverters is required per substation; these must be capable of full power and require special control methods, as depicted in Fig. 12.22:

- “Leap-frog procedure”: The section ends are at the same height with the right and left motor part. The stator sections are attached to the two track cables in alternating sequence, the latter being fed by one inverter each. When the train tip reaches the end of the section, the stator current of the respective section is reduced linearly, whereas the stator current of the following section increases accordingly.
- “Alternating-step procedure”: The section ends of right and left motor part are offset by $L/2$. When changing from one stator section to the next, the current must be reduced to nil in the inverter/cable system currently online within an interval $t_{\min S}$, to ensure current-less switching of the substation vacuum contactors (to increase their lifespan). The tractive power decreases on an average and becomes unsmooth.
- “Three-step procedure”: Thus and due to concerns for comfort, the so-called triple step method is used in accelerative and decelerative sections, which requires a third inverter-and-track-cable system [169], [170]. At stator-section change, the previous and the new stator sections are fed by overlapping currents.

Due to economical reasons, the alternating-step method is preferred for areas run with steady speeds.

At track switches, however, the track girder must be bent into the desired direction by strong motors; thus, turn-around times in terminal stations are considerably longer than with conventional high-speed rail-wheel EMU operation.

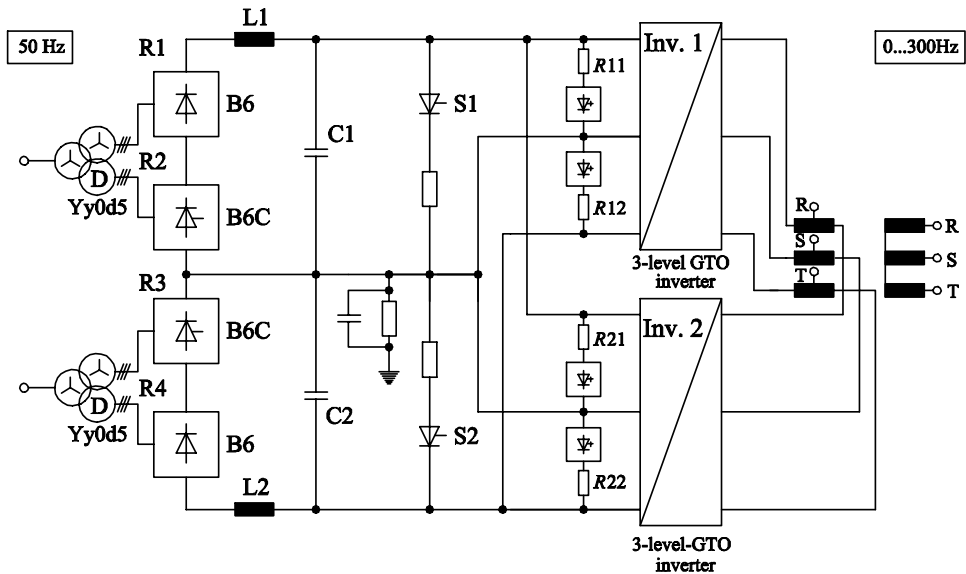


Fig. 12.23: High-power converter group with output transformer

12.4.3 Converter

For the very high inverter rating ranging from 12 MVA ($v_{\max} = 400$ kph) to 20 MVA ($v_{\max} = 500$ kph), group-connection of several three-level GTO-thyristor inverters is required (cf. Fig. 12.23 [169], cf. also [164]). At stator frequencies above 70 Hz (corresponding to 130 kph), two inverters, operated in square-wave modulation, feed the track windings via a transformer, achieving conductor-earth voltages of up to 10 kV. The phase offset of the two inverters (called the stair-case step width) is fixedly chosen in a way that reduces excitation of track resonances to a minimum; the voltage amplitude is then controlled by the DC-link voltage. The DC links are fed via twelve-pulse thyristor bridge circuits in sequential control and a DC-link reactor; these converters are fuseless, as known from High-Voltage DC transmission, to enable the valves to survive the surge currents in case of a winding short-circuit. At low stator frequency (and thus at low voltage amplitude and power) the two inverters operated with fixed DC-link voltage in pulsed operation are connected in parallel to the track cable, without a transformer.

For station and workshop operation, smaller IGBT inverters are used.

12.4.4 On-board power supply of vehicles

To feed the DC choppers for the support and guidance magnets as well as for overall on-board power supply, the linear-generator winding (within the vehicular iron package) as depicted in Fig.12.18 is used. It is fed from the harmonic-wave field of the open stator slots and transmits approx. 108 kW, from 100 kph upwards (TR 08). The voltage proportional to vehicle speed is rectified, controlled by DC choppers and supported by accumulators.

There are new proposals to use a high-frequency (20 kHz) transmission system in stations.

12.4.5 Application Pudong International Airport–Shanghai

The 31.5 km (19.5 miles) track from Pudong International Airport to Underground station Long Yang Road (Fig. 12.24; the top right part shows train TR 08 on the TVE) is traveled on at speeds of up to 430 kph (267 mph), resulting in a traveling time of approx. 7.5 minutes, with trains running at intervals of 10 minutes. The main track is split into four areas, with a mean stator-section length of 1.2 km (0.74 miles); the triple-step procedure is in service, using 12 GTO-thyristor inverters with a rated output of 15.6 MVA each. Two single three-level inverters of 7.5 MVA are used without output transformers in the transfer area in the rear terminal of Pudong. For the workshop, a low-power IGBT inverter is used.

Although the TRANSRAPID system has proven its technical feasibility and is successfully operating on the Shanghai line [170], it remains unclear if it is actually able to compete economically with rail-wheel high-speed systems, such as embodied by the ICE 3. This is especially important for tracks that are in direct competition to rail-wheel lines [171]. The systems' ability to provide cargo services is very small. For point-to-point links in long-distance traffic, parallel to congested railway lines, for airport commuter services and superposed public transports with average station distances greater than 15 km (9 miles), it might prove successful [171]. Both track and vehicles require distinctly higher initial cost than with conventional railways; maintenance costs, however, should prove to be lower.

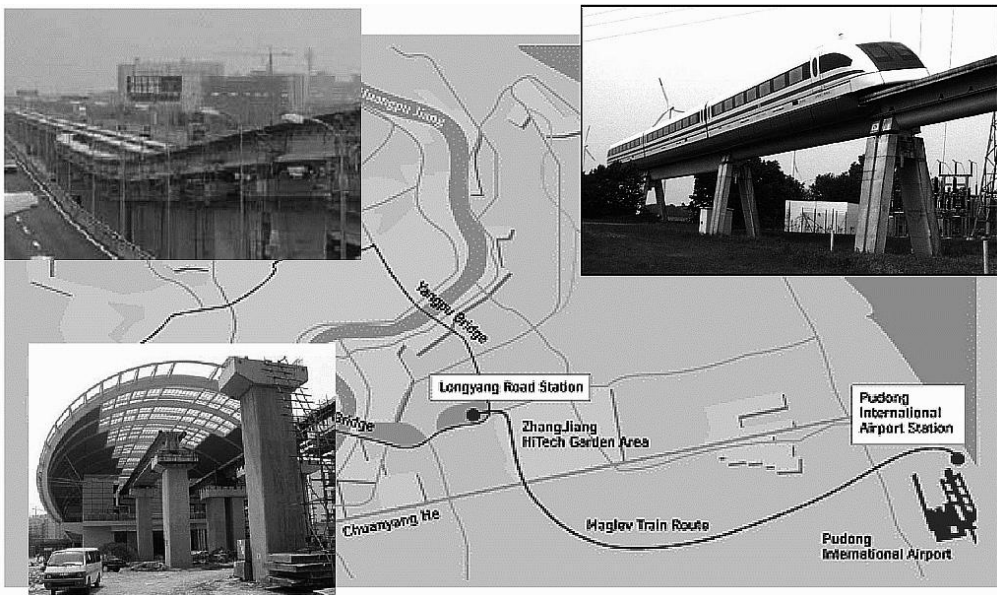


Fig. 12.24: TRANSRAPID line Pudong International Airport – Shanghai

13 Power supply of electric railways

13.1 AC railways operating at $16\frac{2}{3}$ (16.7) Hz

13.1.1 Centralized and decentralized supply in Germany

In 1912, with respect to the commutation of the AC commutator motor (cf. section 4.2.1), the “Central European” railway supply frequency was defined as one third of 50 Hz = $16\frac{2}{3}$ Hz (cf. also subchapter 1.2; from 1996 on, the nominal value is 16.7 Hz, cf. section 13.1.2). This decision required construction of a railway supply mains separate from the public mains; the generated/converted power of the railway mains nowadays is a mere 1.5% of the installed power of the German interconnected-operation mains. Fig. 13.1 illustrates the inclusion of the DB’s so-called “central mains” in the public 50-Hz, three-phase AC power supply net.

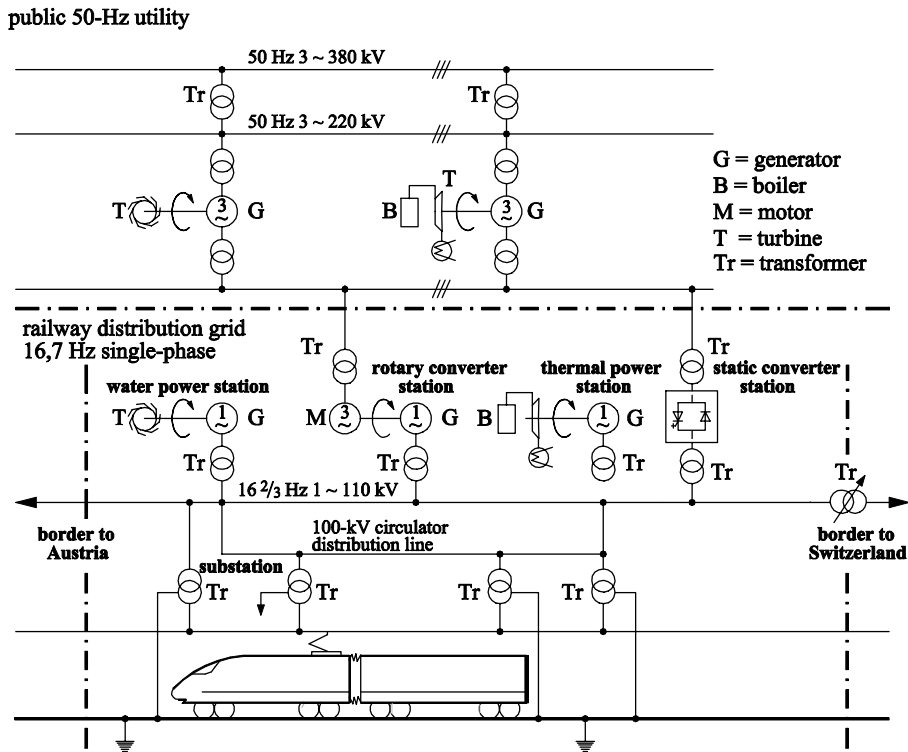


Fig. 13.1: Railway power supply in the central $16\frac{2}{3}$ -Hz mains of the DB

As the first “island railway mains” were established in Germany, Austria and Sweden prior to the outbreak of the First World War, power plants operated and owned by the railway companies were built as well. These include the hydroelectric plant at Kochel (Walchensee, from 1924) for the Bavarian mains, the thermal power station Muldenstein for the central Prussian mains and the hydroelectric plant at Porjus for the Kiruna railway in North Sweden (1915).

When, during the 1920s, electrification of railways could resume, it was resolved – analogous to the national 50-Hz supply – to construct a 2x55 kV transmission and distribution mains in southern Germany which would link power plants and substations. In 1942, the Bavarian and the Central German railway mains joined up at Saalfeld in Thuringia.

After the Second World War, the DB quickly re-established electrical operation in Bavaria and Baden-Württemberg, as well as re-initiating the electrification of new tracks. In the early fifties, a heated debate arose with respect to the Ruhr-area rapid transit “Ruhrschnellverkehr” whether to operate the railways with the general 50-Hz, which had been proven to be technically feasible by trials on the Höllental line. The DB decided, for continuity reasons and to maintain the option for a power-frequency-control system of its own, to keep to the $16\frac{2}{3}$ Hz supply system [173], and determinedly expanded the 110-kV transmission and interconnection mains. Furthermore, the electrification of the new high-speed line Cologne-Rhine/Main with $16\frac{2}{3}$ Hz underlined this decision [174], [175].

Following the complete dismantling of the electrical railway equipment in the Soviet Occupation Zone, later GDR, in 1946, locomotives, power plants and substation equipment were returned to the DR, successor of the Reichsbahn in the former GDR, only in 1956. The Soviet railway organisation SZD had run trials of the technology on the Workuta railway in Siberia, but found the system unsuitable for Soviet-Russian requirements. In 1958, the SZD started a program of 50-Hz electrification using French and (new) German technology.

In south Central Germany (Weimar-Leipzig-Dresden-Chemnitz), the old central mains was refurbished. For electrification of the northern lines to Berlin and from thereon to the Baltic Sea in the 1970s, the DR decided to use a decentralized power supply system with fixed-frequency synchronous-synchronous rotary converters, due to the lower initial cost (cf. section 13.1.2). In the 1930s, Norway and Sweden had also chosen decentralized supply for sparsely-populated areas. To avoid circular-current flow, the feeding sections must not be longitudinally coupled; thus, to make the system as fault-tolerant as possible, it is necessary to have a high converter spare and thus total rating, which results in the decentralized supply system becoming economically inefficient in the long run.

Following German re-unification in 1990, it was therefore decided to abandon the decentralized mains step by step. Initially, the Berlin area was tied up to the central mains at Wolfsburg and at Dessau; subsequently, the formerly separate mains were joined at Bebra and Saalfeld. The Prenzlau-Anklam line was converted to the autotransformer system (cf. section 13.2.2) in 2000, in order to replace cost-efficiently the old de-central converters.

Fig. 13.2 shows the current (2002) state of the DB Energie interconnected mains, together with the own power plants and the converter plants [177]. The 110-kV circuit length is about 7,650 km (4,743 miles). The transmission mains operate as a resonantly-earthed system with step-switched Petersen coils, at 15 substations distributed all over the mains. In 2003, the first converter for neutral-voltage displacement and residual earth-current control (due to detuning of the resonant circuit made up from the circuit capacities and the Petersen coils and due to harmonic currents produced by vehicles with power-electronic control, respectively) took up service in the converter plant Borken/Hessia.

Ties to the other $16\frac{2}{3}$ -Hz mains were established in Zirl and Salzburg towards Austria and at Etzwilen to Switzerland (there 132 kV, with the added option of power-flow control by a tap-changer transformer). The Swiss railway grid is earthed, in contrast to the German net.

Table 13.1 Power and energy statistics of the DB Energie transmission mains per 31.12.2000

Plants	Installed power		Source of energy	Energy	
	MW	%		GWh	%
Thermal power station	1475	46	Coal	3,861	34
			Nuclear	2,350	21
			Gas & oil	1,581	14
Hydro power station	209	7		1,223	11
Pump storage plant	150	5		–	–
Rotary converter, central	612	19		1,219	11
Rotary converter, decentral	608	19		840	7
Static converter, central	142	4		312	3
			Balance interconnected network	–96	–1
Sum	3,196	100	Consumption DBAG	11,300	100

Table 13.1 presents the most important statistics as of 2000 (the last year, in which the data were broken down in such detail). For comparison, the energy level of the German 50-Hz interconnected mains attains approx. 575 TWh/a, which is about 50 times as much! The total installed power of all traction vehicles is about seven times the installed generating power.

The (presumably) last railway-frequency generator sets of $P \sim 110$ MW for base-load coverage in the central mains of the “New Federal States” (ie former GDR) were constructed at Kirchmöser (near Berlin) and Schkopau (Saxony). From the 1950s onwards, however, single-phase rotary converters were installed to provide control peak power from the public mains in a more economic way (cf. section 4.1.2). Nonetheless, rotary converters run at similar cost as the specific railway power plants. After 1995, static converters are used for railway power supply (cf. section 4.1.3), which are far more cost-effective.

Fig. 13.3 shows, in comparison, the electrified 15-kV tracks of the DB AG which are operated by the DB subsidiary enterprise DB Netz AG. It includes approx. 19,100 km (11,780 miles) of overhead lines, which handle 85% of traffic. The lines are fed from the 110-kV mains via 178 substations of 20...40 MW nominal power, $u_k \sim 10\%$. Substation distances vary from 20 to 100 km (12 to 60 miles). During undisturbed operation, all supply sections as well as the overhead lines of both tracks are longitudinally and laterally coupled, which greatly enhances voltage quality (and, therefore, the acceptance of energy during recuperation). An isolated 50-Hz track in the Harz Mountains (Koenigshütte-Blankenburg) which had served as trial track for the GDR railway industry, too, was laid off in 2006. Hamburg and Berlin metro services are operated with 1,200 V and 850 V DC, respectively (see below); Lichtenhain-Cursdorf is a DBAG-owned tramway.

A compensation station has been installed in Munich-Pasing, to compensate centrally the reactive current of the phase-controlled Metro trains Class 420. Some countries as Norway use series compensation, to provide for better voltage in long lines in weakly-inhabited areas.



Fig. 13.2: 110-kV railway interconnected mains of DB Energie GmbH, as of 01.01.2007 [177]

- | | | | |
|------------|----------------------------|---|-----------------------------|
| Legend: == | 110-kV interconnected grid | ⊗ | Static converter, |
| □ | Nuclear power station | ● | Rotary converter, decentral |
| ● | Thermal power station | ○ | Substation |
| ⊙ | Hydro-power station | ⊙ | 110-kV station |
| ⊕ | Pump-storage plant | ▲ | 15-kV hydro-power plant |
| ◐ | Rotary converter, central | | |



Fig. 13.3: Electrified railway lines of the DB AG, as of 01.01.2007

- ① DC 1.5 kV
- ② DC 3 kV
- ③ 1AC 25 kV 50 Hz
- ④ DC 600 V

13.1.2 Rotary converters

As early as in 1912, the experimental electric service of the Badische Staatsbahn in the valleys of Wiese and Wehra near Basel used a rotary 1-MW machine converter.

Within the central mains, however, the converters have to operate flexibly at a varying frequency to allow for adjusted power-frequency control, independent from the inter-connected European mains, organized in UTCE. This is due to different load curves of general and rail-

way power demand. To that purpose, the (usually) four-pole single-phase synchronous generator (with ratings of up to 80 MW) is driven by a twelve-pole slip-ring induction motor. The negative-sequence rotary field of the single-phase load is alleviated as much as possible by using an especially strong damper winding. Nonetheless, the stator has to be suspended on rotary-spring supports, due to the remaining $33\frac{1}{3}$ Hz torque oscillations, evoking vibration and noise. Due to the single-phase character and the low frequency, the construction size of the generator is several times higher than that of a 3AC generator of equal nominal power.

The variation of the revolution speed by $+2\%/ -3\%$ (conforming to EN 50163/DIN 57 115, cf. Table 6.2) is achieved by slip-frequent supply of the rotor circuit. This uses thyristor cycloconverters which, accordingly, must have a rated power of approx. 3% of the rated output power of the converter set. In recent times GTO-thyristor inverters have been used.

Fig. 13.4 shows the main circuit diagram and the most important data of the two machine converters of the Community Power Plant (GKN) II of the present-day EnBW at Neckarwestheim/Germany, which took up service in 1988. They produce electric energy for DB and must be considered the largest machine converters in existence world-wide [178].

The 12.5-kV induction motor is directly connected to the 400-kV interconnected mains via a block transformer; from this 12.5-kV rail, the exciter-current converter (EC) of the 16 2/3-Hz current generator, the slip-power and starting cycloconverter (CC, $f_{\max} \sim 20$ Hz) and the station service demand (SSD) are fed. For start-up, the induction motor, with short-circuited stator circuit, is accelerated using the direct converter up to 180 min^{-1} (~ 18 Hz).

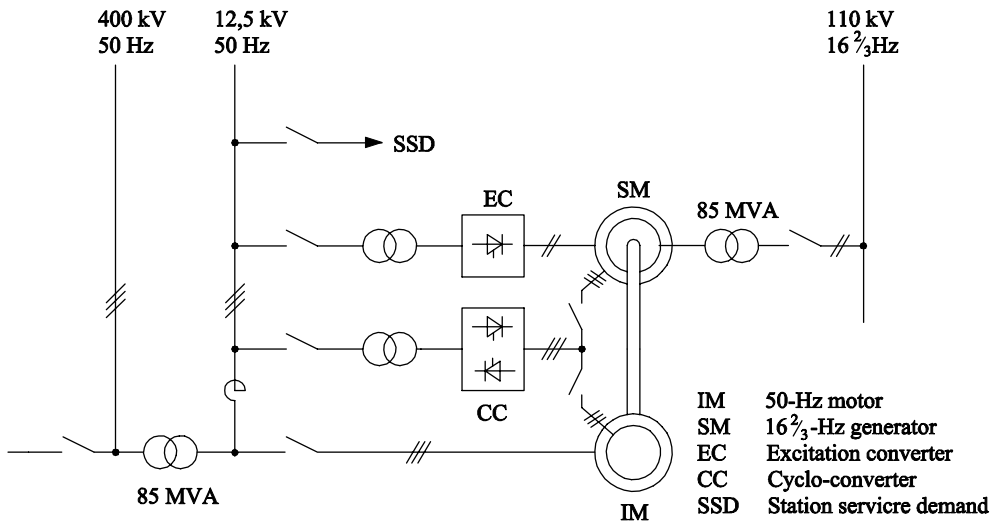


Fig. 13.4: Main schematic diagram of the 80-MW rotary converter 50-Hz/16 $\frac{2}{3}$ -Hz at GKN II

Subsequently, the cycloconverter is connected with two phases to the stator of the synchronous generator (SM), which is then accelerated at reduced field beyond the synchronous frequency. Finally, the rotor circuit of the IM is switched to the converter, the stator circuit of the IM is connected to the 3AC mains, and the synchronous motor is synchronized to the railway supply mains.

Fig. 13.5 shows the main schematic diagram and the waveforms of output voltage and current of a cycloconverter. During exactly synchronous operation, the output current of the direct

13.1.3 Static converters

The high initial and maintenance demand of rotary converters bred plans to use power electronics for its tasks. As early as 1936, the AEG constructed a “flexible frequency” 4-MW envelope-type cycloconverter at the Basel substation, which used mercury-vapor valves [181]. In Sweden, numerous fixed-frequency thyristor cycloconverters were built by ASEA during the 1970s. It must be noted, though, that the reactive power and the interharmonics of the cycloconverter on the 3AC side are a disadvantage.

From about 1990 onwards, GTO-thyristor technology was applied to railway supply converters, too [182], using initially a twelve-pulse thyristor bridge circuit instead of a GTO converter on the 3AC side for cost reasons. The single-phase side feeds the transmission system directly. The first such system was constructed by ABB at Giubiasco (Ticino, Switzerland) in 1992, with a rated power of $S_N = 20 \text{ MVA}$. Attached to the 2,650-V DC-link circuit are twelve GTO four-quadrant converters (4q-C), operated at phase-shifted square-wave (block) modulation. These feed the SBB 66/132-kV transmission system via six double-tier transformers. AEG and Siemens supplied similar plants to Germany ([183], [184]); an excellent overview is given in [185].

In Bremen, the five-fold rating was already attained in 1996 [186], using six GTO thyristors in series ($n+1$ pattern) per function place [Fig. 13.7]. This was the first time the Hard-Drive technology developed by ABB for directly series-connected GTO-thyristor systems [187] had been employed, which led to the innovation of the special “IGCT” element. The second of the two 50-MW converters at the railway converter station Munich-Karlsfeld [188] is equipped with IGCT elements.

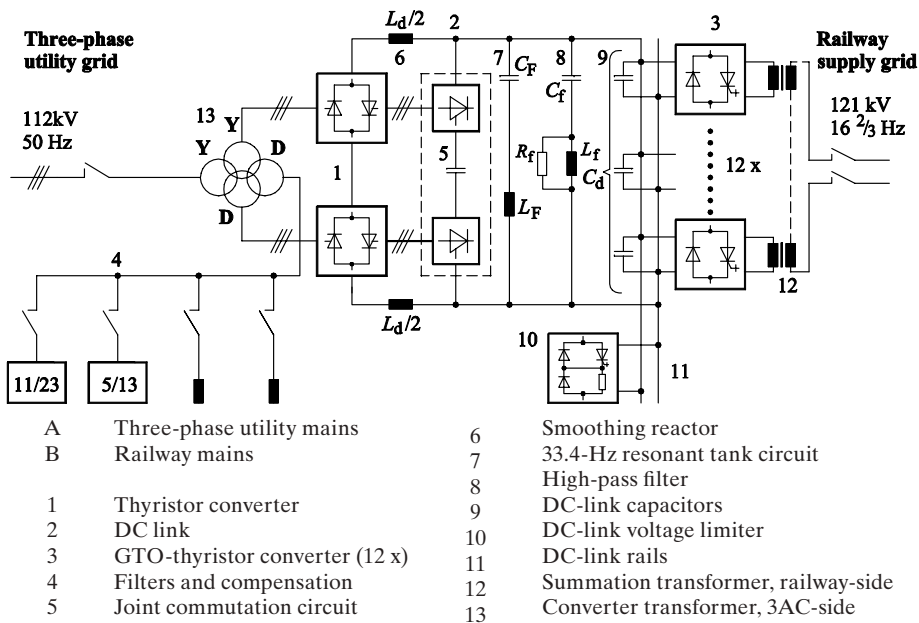


Fig. 13.7: Main circuit diagram of 100-MW railway supply converter at Bremen, ABB (ABB Switzerland AG).

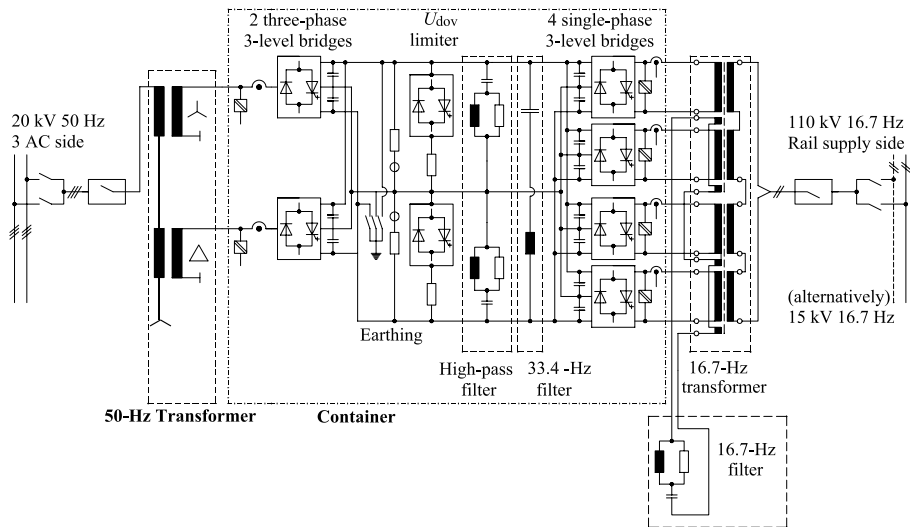


Fig. 13.8a: Main circuit diagram of 15-MW standard railway supply converter, using IGCT elements (ABB Switzerland AG)

Following these individually-manufactured large-scale plants, DB started development of 15-MW standardized converters [189], [190]. These use GTO and IGCT thyristors in a three-level pattern (cf. section 6.6.4), nowadays on the 50-Hz 3AC side as well. Fig. 13.8a is the main circuit diagram, Fig. 13.8b provides an external view of the ABB-built plant (the two 16.7-Hz transformers are visible to the right, the 50-Hz transformers between converter container and station building). At Limburg substation, eight such 15-MW converters provide for the 110-kV supply of the new high-speed line Cologne-Frankfurt.



Fig. 13.8b: 15-MW standard railway supply converter (ABB Switzerland AG)

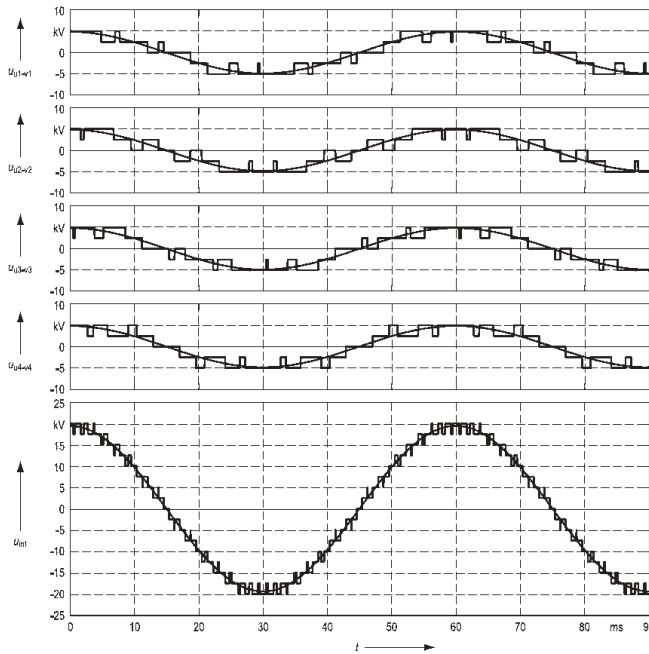


Fig. 13.9: Voltage waveforms at the transformer windings of the four 3-level H-bridges (top) and the sum of them (bottom) (ABB Switzerland AG)

Fig. 13.9 shows, how the $16\frac{2}{3}$ -Hz output voltage is composed of the voltages of the four three-level inverters [190a]. The switching frequency of each IGCT is 50 Hz, the resultant pulse frequency of the output voltage is $4 \cdot 2 \cdot 2 \cdot f_z = 800$ Hz.

13.2 AC railways operating at 50 Hz

13.2.1 Properties, and a comparison to the $16\frac{2}{3}$ -Hz system

As previously described, converters available in the 1950s (initially using Ignitrons, later silicon thyristors) allowed for eschewing the special railway-current frequency of $16\frac{2}{3}$ Hz and supplying the railway lines directly from the 50-Hz national supply mains. A number of countries operate national mains of 60 Hz, but in the following only 50 Hz is addressed, including 60 Hz without mentioning each time. In Japan, the whole high-speed line system is supplied with 60 Hz, as used in the south-western part. In the north-eastern part of Honshu island, where 50 Hz is public supply standard, the lines are supplied by converters, to have a uniform system and the full transformer power on the vehicles.

Using 50 Hz eliminated the considerable expense required for independent power generation (or conversion, respectively) as well as the need for separate interconnection lines. It features, however, a number of peculiarities which shall be discussed subsequently.

The triple frequency made an increase of the nominal voltage by a factor of $\sqrt{3}$ (in fact $25 \text{ kV} : 15 \text{ kV} = 1.667$) appear appropriate, which resulted in current levels smaller by the same factor and comparable voltage drops in the identical catenary at the same distance of substations. The inductivity per unit length is about $1.2 \dots 1.5 \text{ mH/km}$ (regardless of frequency) with single-track railway lines and $0.75 \dots 0.91 \text{ mH/km}$ with double-track lines (cf. also section 14.3.4).

At equal catenary height above rail top and equal clearance, the roof top must be lowered by approx. 25 cm (10in) due to the voltage distances involved, thus reducing the space available in the engine room.

The main problem, however, is the single-phase load applied to the 3AC medium-voltage mains, which is preferably used to feed the railway lines, for cost reasons. An asymmetry of the three line currents appears, which is described – using the symmetrical or Fortescue components [v1] – by a negative-sequence current system of same height as the positive-sequence current system, which supplies the required power. A negative-sequence voltage system occurs at the internal impedances of the supply mains which causes a counter-rotating field in rotary-field machines connected to the same mains, this resulting in brake torque, intense torque oscillations at double mains frequency and high ohmic losses [194].

These effects are particularly intense because a slip of $2-s$ ($s \ll 1$) is valid for a negative-sequence or counter system in induction machines, with only the leakage impedances limiting the currents. Thus it is required that the voltage negative-sequence system (superscript “ \ast ”) does not exceed 1% (long-time) or 3% (short-time) of the nominal mains voltage at the point of common coupling [195]; it can be calculated by

$$\frac{U^{\ast}}{U_N} = \frac{S_{N\text{-Singlephase}}}{S_K} \quad (13.1)$$

But the nominal short-circuit power

$$S_K = \frac{U_N^2}{X_K} \quad (13.2)$$

is below 5 GVA at 50% of the connection points within the 110-kV national mains, even in a highly industrialized country as Germany; in other countries the situation is often worse.

It is therefore essential that bordering railway feeding sections are supplied from different phases of the supply mains, to balance the asymmetries on average, at least. Fig. 13.10 illustrates various layouts. Nowadays it is general consensus to place the required phase separation within the substation area (second chart from the right). This segment has to be passed by traction vehicles in a powerless state, ie at open main circuit-breaker, which obviously complicates operation.

This compensation of asymmetry is only applicable on average, though. The Japanese Railroads had to install 200 MVA of converter power on the extremely burdened Tokaido high-speed line (Tokio-Osaka) to actively compensate for the asymmetry and the flicker due to the sudden changes of reactive power [196], [197]. A compensator is used with the Channel Tunnel, too.

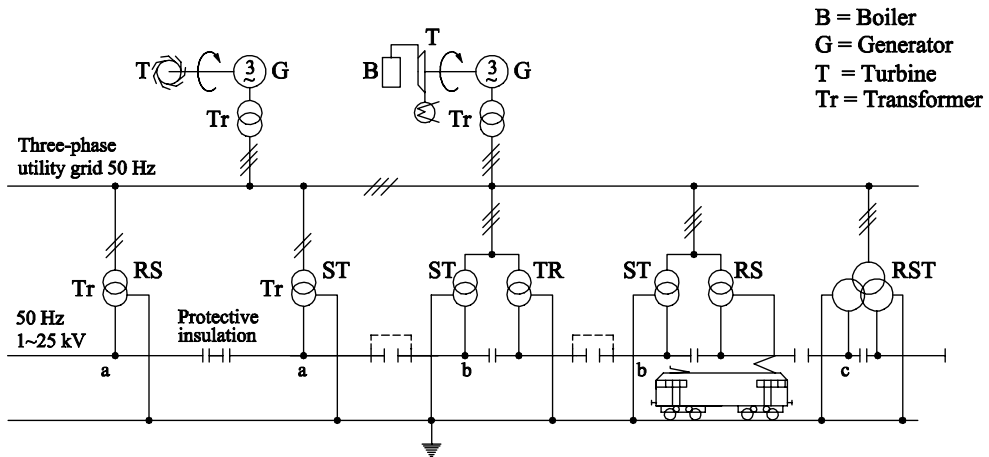


Fig. 13.10. Railway power supply from the 50-Hz public mains

Table 13.2 Comparison of 16 2/3-Hz and 50-Hz electrification

16 2/3 Hz	50 Hz
Nominal voltage 15 kV	Nominal voltage higher by 2/3, smaller vehicle profile
Heavy main transformer and smoothing reactors	Vehicle equipment (magnetic components) slightly lighter
Generation of energy requires complex special machinery (single-phase/low frequency) or converters; oscillating power at double line frequency must be provided	Negative-sequence voltage system in feeding 3AC system has to be limited to 1% U_N , requiring points of common coupling with high short-circuit power and/or balancing (F/GB, “Channel Tunnel”; in Japan, 202 MVA converter power for the Tokyo-Osaka line)
Catenary network is longitudinally and transversely coupled (since ca. 1970)	Phase separations (except for the very expensive coupling to a 380-kV mains)
Energy cost higher by some 0.03€/kWh; higher peak power and failure balancing, more independent from the public utilities	Notifiable power cost \approx 160% (due to required reserve), in Germany, no group accounting with various suppliers as e.g. in France, where EdF is only supplier!
Number of substations = 100%	Number of substations \approx 160% (network)
Transformer power = 100%	Transformer power \approx 160% for networks, up to 400% for isolated high-performance lines; further doubling if using autotransformer system, cf. section 13.2.2
Full recuperation capability (with traction vehicles using four-quadrant converters)	Limited recuperative capability due to separation segments and point feeding
Total capital expenditure = 100%	Total capital expenditure \approx 100%
Annual cost = 100%	Annual cost \approx 105%

Furthermore, the option of longitudinal coupling of feeding sections (as seen with the $16^{2/3}$ Hz mains) with its voltage-supporting effect is not available. To achieve comparable service security, a number of substation transformers more than 60% larger is required to be held at ready. This applies to regular railway mains; for isolated high-speed lines, even 300% of additional demand has been calculated. Thus, the lower energy cost (about 0.03 €/kWh less) is opposed to considerably higher power-dependent cost. The overall capital expenditure is roughly equal, but annual cost is about 5% higher than in the case of $16^{2/3}$ -Hz electrification (given German general circumstances).

Furthermore, electrical utilities often interdict the recuperation of the braking energy, which occurs irregularly; thus, one of the main advantages of modern three-phase drive technology cannot be gained, resulting in traction vehicles having to be equipped with brake resistors and choppers. Table 13.2 collects the pros and cons of the two power-supply systems in discussion.

13.2.2 Autotransformer system

In numerous countries or regions, especially such with low population density, the required powerful points of common coupling are not always available where a substation is to be built. Instead of upgrading the national mains or even construction new of new transmission lines, the operating voltage of the railway can be increased, thus reducing longitudinal impedance and voltage drop. To retain the nominal catenary voltage of 25 kV, autotransformers (AT) are used to generate a second voltage phase-shifted by 180° (“-25 kV”), which is then fed via a second (“feeder”) line to the catenary supports (“2AC”, cf. Fig. 13.11), [198]. For this, the reinforcement line which is often provided can be used.

At distances of approx. 10 km (6 miles), both the catenary and the feeder lines are linked using ATs of approx. $1/3$ of the substation transformer power. The impedance (as well as the voltage loss) drops to $1/4$. Within the active feeding sub-section, the return current divides (locally dependent) into $2I_b$ and $I_F - 2I_b$. Within all other sections, the rails are at zero current.

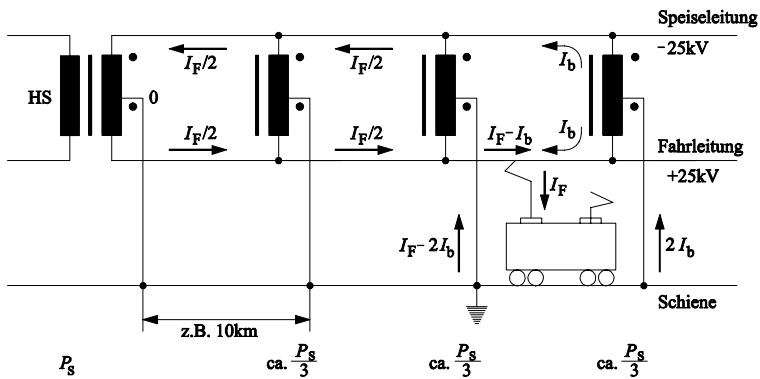


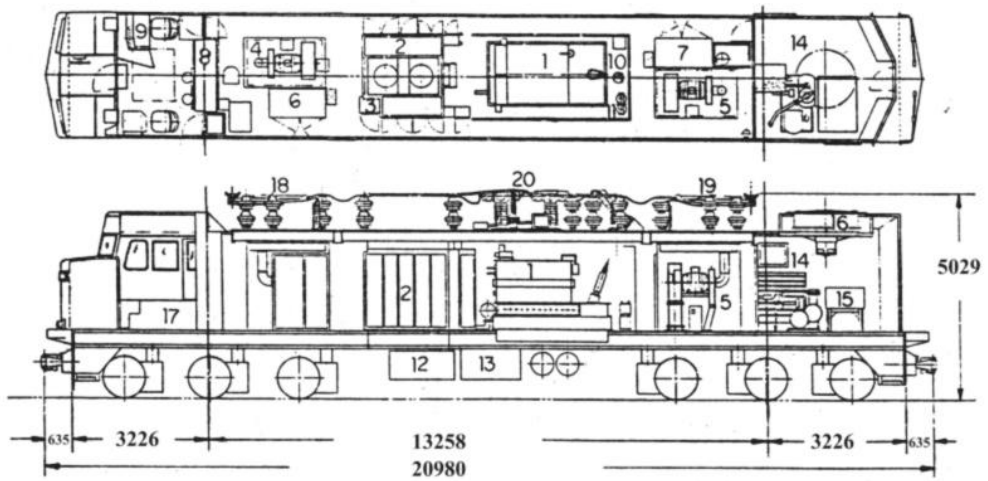
Fig. 13.11. Feeding a line using autotransformers (2AC system)

Due to the smaller distance of catenary and feeder (compared to the distance between catenary and rail), the coupling impedance with parallel information and signalling lines is reduced, thus alleviating communication interference problems (cf. subchapter 14.5).

Nowadays, the AT system is also used with $16^{2/3}$ -Hz railway lines within the decentralized mains of Eastern Germany, to replace scrapped rotary converters.

13.2.3 Increased operating voltage

Since ATs require quite a considerable expenditure (approx. four-fold transformer rating at 100 km/60 miles substation distance), isolated bulk material transport lines in sparsely populated areas, for example Canada, desert areas in the Western United States and South Africa, use a different, simpler system. The catenary operating voltage can be increased to 50 kV, as the traction vehicles do not have to transfer to other railways using standard voltage. Thus, substation distances of more than 120 km (75 miles) become feasible, using single-side feeding. The vehicles (cf. Fig. 13.12, the 3.8-MW locomotive of the British Columbia RR, Canada, using phase-angle delay control; data in Table 13.3) are constructed for nominal performance achieved at 50 % U_{FN} already [200], [201]. Please note the height of the isolators.



1	Transformer	8	Control cubicle	15	Compressor blower
2	Thyristor converter	9	Driver's desk	16	Brake resistor blower
3	Electronics cubicle	10	Grounding transformer	17	Air brake
4	Tr. motor blower bogie 1	11	Auxiliary transformer	18	Pantograph 1
5	Tr. motor blower bogie 2	12	Capacitor switchbox	19	Pantograph 2
6	Switchgear bogie 1	13	Reactors	20	Central hood
7	Switchgear bogie 1	14	Compressor		Dimensions in mm!

Fig. 13.12. 50-kV/60-Hz locomotive GF6C of British Columbia RR

Table 13.3 Railways operating at 50 kV nominal voltage

Railway Track Distances	Locomotive Wheelset formula P_N / v_{max}	Constructor Year of construction Vehicles built	Particularity
British Columbia RR / Canada Tumbler Ridge–Anzac L = 129 km / 80 miles, 1 substation at 112 km/70 miles from the mine; coal production shut down in 2000	GF6C Co'Co' 3,800 kW 90 kph /56 mph	GM Canada/ASEA 1983 7 locomotives scrapped in 2004	60 Hz Radar for slip protection
Black Mesa & Lake Powell RR / USA L=124 km / 77 miles, Substation at Navajo Power Plant	E 60 C Co'Co' 4,180 kW 116 kph / 72mph	GE 1973/76 6	60 Hz
South African Railway (SATS) Sishen–Saldanha Bay L=864 km / 536 miles	Class 9E Co'Co' 4,068 kW / ?	UC&WW/GEC 1878 31	50 Hz 1067 mm /3'6" Cape gauge

13.3 DC railways

Fig. 13.13 gives an overview of the basic layouts for supplying DC railways with nominal voltages $U_{FN} = 600 \text{ V} \dots 3 \text{ kV}$ from the public 3 AC medium-voltage mains. In the beginning, the contact line voltage had to be rather low ($< 1000 \text{ V}$), identical to the motor nominal voltage, then still rather low. In that form, main-line electrification was not economical.

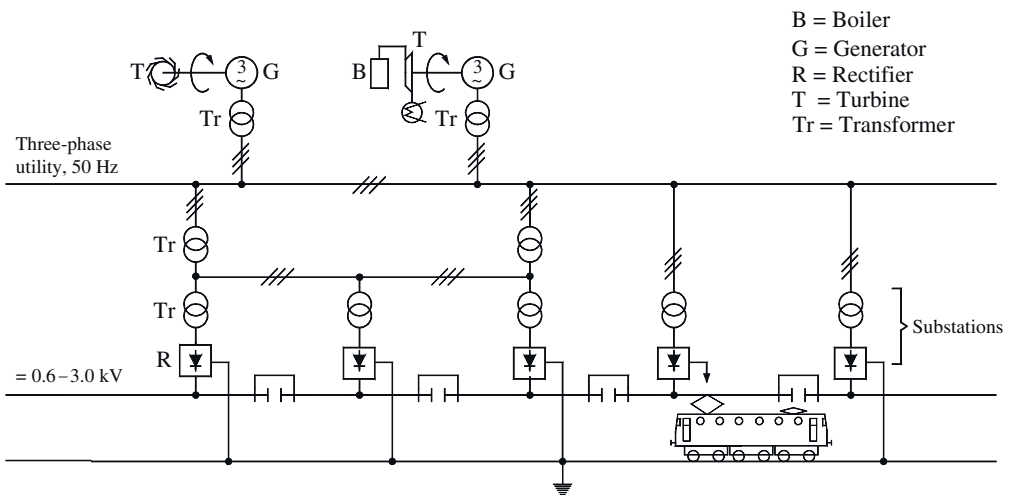


Fig. 13.13. Railway power supply of DC railways.

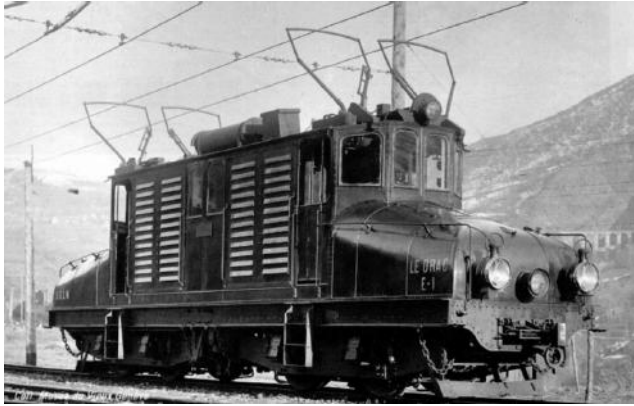


Fig. 13.14 Three-wire-DC locomotive of the Thury system

In 1903, R. Thury of Geneva applied the three-wire system (positive and negative contact line vs. earth, analogous to the AT system described in section 13.2.2), which was regularly used for urban power supply at that time, to the "La Mure" mineral railway south of Grenoble (2 x 1200 V, cf. Fig. 13.14, [201]). In the same year, F. Krizik introduced this system with the Tabor-Bechyn Railway in Bohemia (2 x 700 V). These systems were an intermediate step on the road to higher operating DC voltage. Both railways, however, changed to the conventional single-wire system as soon as motors and circuit breakers for higher DC voltage became available, due to the operational problems associated with a dual-pole catenary. 6-kV and 12-kV main-line DC systems have been in discussion in Russia and in Italy, to overcome the limitations of the 3-kV systems and the asymmetry problems of 50-Hz systems, but were eventually given up in favour of the conventional 25-kV 50-Hz system.

While railway-owned DC generators and rotary converters had been standard in the early years of the 20th century, rectifiers saw exclusive use from 1925 onwards. When using mercury-vapor rectifiers with common cathode and sheet-steel vessel, the latter is usually earthed, connecting the negative pole to the contact line (for example, with the Berlin S-Bahn, 800 V). Following their replacement by semiconductor/diode rectifiers, the negative pole is usually linked to the earthed rails today. Fig. 13.15 shows (in clockwise direction) a rotary converter, a mercury-vapor rectifier and a silicon-diode rectifier, as of 1960, in the Underground substation "Hallesches Tor" in Berlin; Fig. 13.16 depicts a current model, namely a non-ventilated diode bridge rectifier manufactured by Balfour Beatty Rail Ltd., Power Systems, available for 750...3000 V and 1130...4600 A.

Due to the high operating currents, large catenary cross-sections of (up to 2 x 120mm²) are required, and the substation distances are going down to 12 km (for example, within the French 1.5-kV long-distance railway network).

One of the main problem of DC railways is the undefined return of the operating current via earthed rails and earth itself (called "stray currents"). For safety reasons (touch voltage in case of short-circuit), certain minimum values (0.5 S/km for tramways, 2.5 S/km in commuter railways with separate tracks) are recommended for the leakance per unit length. Dependant upon the conductivity of the soil, more or less of the return current runs through the earth itself, causing corrosion to metal components such as cable jackets, gas and water tubes [202], [203]. In addition, the DC-excited magnetic field can influence physical measuring instruments, for example within university institutes, or medical diagnostic systems.

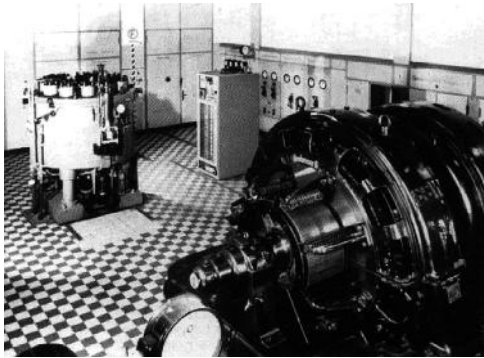


Fig. 13.15: (above): Underground substation in Berlin, from the front, clockwise: rotary converter, mercury-vapour rectifier, silicon-diode rectifier

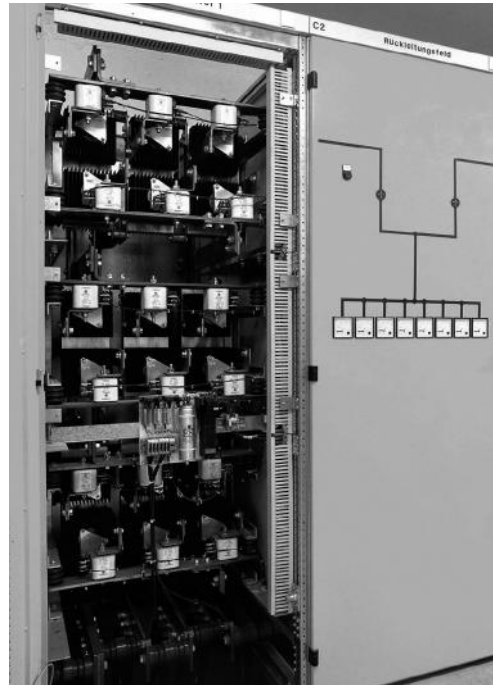
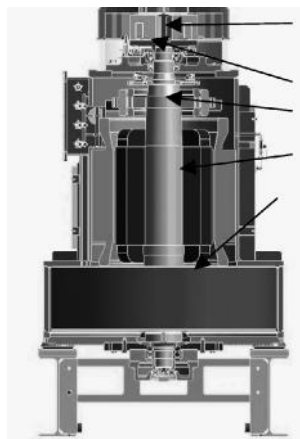


Fig. 13.16: (right) B6 diode bridge rectifier 2800 A, 750 V, 3 diodes in parallel, air-self-cooled; part of a B12 double bridge rectifier by means of star-star and star-delta transformers (Balfour Beatty Rail GmbH)

- Reduction of necessary investment in energy-supply infrastructure, lowering of energy cost
- Stored energy 4.6 kWh
- Maximal power 750 kW
- Nominal voltages 600 V – 750 V – 1500 V
- Speed range 1800..3300 rpm
- Savings 250...360 kWh/year, depending upon location
- Mature system, > 400 systems in operation world-wide



- Magnetic suspension
- Rotating diode bridge
- Exciter
- Synchronous machine
- Flywheel

Fig. 13.17: Rotary energy-storage system of Piller Power Systems GmbH.

In the case of railways operating at high and unsteady power demand and especially at brake-energy recovery, the use of a railway-operated 3AC bus bar is advisable, as is the case with the 30-kV 3AC system of the Berlin S-Bahn. Using internal balancing, this provides for an even total energy demand and, subsequently, lower power cost. Recuperating thyristor rectifiers are seldom used, since public utilities do mostly not recompense for returned power. Therefore, rotary [204] or static energy-storage devices with Double-Layer Capacitors [205] are used in increas-

ing numbers. Such devices store braking energy by measure of the installed storage energy, and furthermore, they help to reduce the voltage drop that occurs with modern high-performance vehicles at starting on existing older networks. [205] reports a 30% reduction of required energy and a rise of voltage by 4.3%, compared to original operation without a storage. Fig. 13.17 shows a rotary energy-storage system of Piller Power Systems in cross-section, including main data.

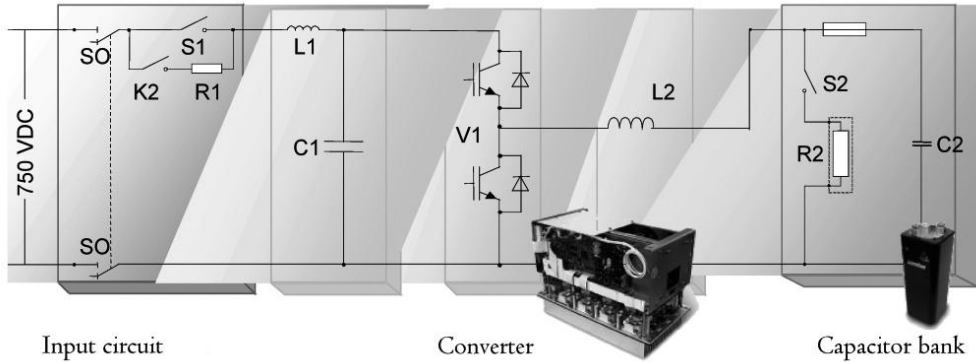


Fig. 13.18 Static energy-storage system SITRAS® SES using Double-Layer Capacitors (Siemens AG, TS)

Fig. 13.18 presents the coupling of a Double-Layer Capacitor storage device via a two-quadrant IGBT chopper to the DC line.

13.4 Contact lines and current collectors

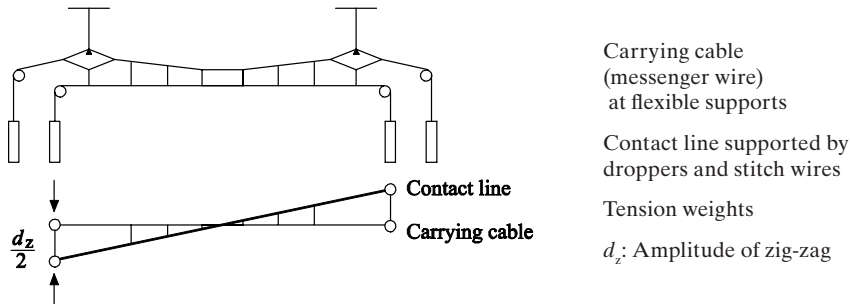
The simple single-wire contact line, which is supported by masts or transversal steel ropes, is to be used only with industrial railways and tramways operating at speeds less than 50 kph / 30 mph. With higher speeds, the sag and the inhomogeneity at the hard support points cause unacceptable losses of contact. In this case, catenaries are used, as depicted in Fig. 13.19; the contact line is kept at average height using droppers affixed to the carrying cable or messenger wire. For higher speed ($v_{\max} > 160$ kph/100 mph), stitch-wires are used at the support points, thus providing for constant flexibility of the catenary system. Further tension weights ensure constant tension force (≈ 120 N/mm²), thus giving an approximately constant eigenfrequency for the oscillations caused by the moving current collectors.

The lateral position of the catenary is varied within the straight direction by $d_z = 800$ mm (Germany) due to the so-called zig-zag placement; thus, an average wear of the 1000 mm-wide pantograph contact strip is achieved (the total collector head being 1950 mm wide). In Switzerland, the head width is a mere 1450 mm, to allow for smaller tunnel clearance, the zig-zag is accordingly narrower (550 mm). In curves, the allowed maximum lateral movement limits the distance of the catenary supports.

Another disturbance are old bridges which require a lowered height of the catenary; the standard value is 5.6 metres above rail top with standard-gauge railways. The extreme maximum speeds of 575 kph/360 mph (in France) and 407 kph/252 mph (in Germany) have been achieved

by greatly increasing the tension of the contact wire, thus raising the resonance frequency, and as there have not been old bridges on the newly built high-speed tracks, forcing the pantograph to large-scale vertical movement.

Within tunnels, the (fixed) overhead conductor rail with lower constructive height is increasingly used, since it greatly reduces both the complexity and the cost involved with enlarging the tunnel profile, required for electrification or for completely new construction of urban railway tunnels (Fig. 13.20).



Contact wire	Cross-section	Profile	Diameter	Weight	Resistance p. u. length E-Cu 20°C	Cd-Cu	Ag-Cu	Continuous current density
	mm ²		mm	kg/km	Ω/km	Ω/km	Ω/km	A/mm ²
Ri 80	80		10.6	710	> 0.220	0.25	0.22	ca. 4...5 (Ag-Cu+30%)
Ri 100	100		12	890	> 0.178	0.2	0.18	
Ri 120	120	13.2	1070	> 0.147	0.17	0.15		

Fig. 13.19: Schematic representation of high-speed catenary, with typical data



Fig. 13.20: Overhead conductor rail (left), transition to standard catenary, pantograph head with earthed horns (AVG Karlsruhe)

Following the first, reluctant trials with shuttle-type current collectors in slotted copper-tube contact lines (e.g. Frankfurt-Offenbach, 1884), Depole's rod current collector with roller (cf. Fig. 13.21) was the first fully operative solution to the problem of mobile contact (the return current is transferred via coal or copper brushes to the shafts of the wheelsets).

This system, however, has numerous disadvantages:

- High moment of inertia of the boom, which can be up to 5 metres long; this results in low inherent frequency in oscillations due to vertical disturbances of the contact line position, and thus poor contact at higher speeds
- High risk of “derailing” the roller at the breaks at the support points
- Necessity of catenary switches
- Cumbersome manual pass-around of the rod collector and “re-railing” necessary for change of direction of travel.

For these reasons, the rod collector is today only used with trolley buses (cf. section 12.3), as there is no viable alternative.

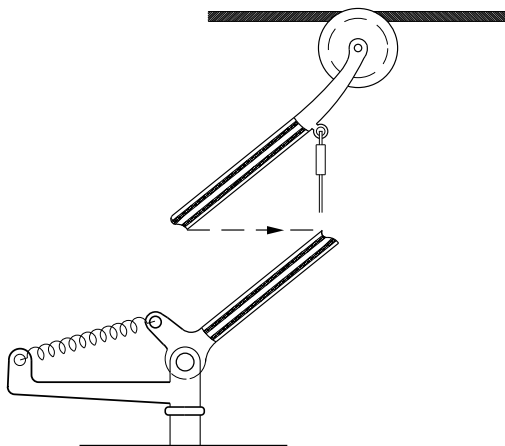


Fig. 13.21: Rod current collector

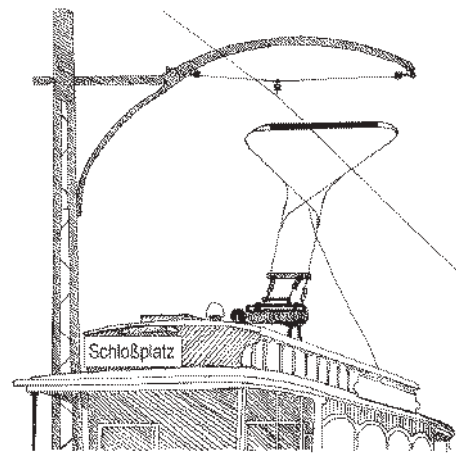


Fig. 13.22: “Lyra” bow collector

With railways, the course of development continued with the so-called “Lyra” or bow collector (Reichel/Siemens 1893, Fig. 13.22) with top-mounted contact strip made of copper or coal, see below; then, the “scissor-type” collector or pantograph, using a balancing double contact strip (Fig. 13.23), with opposed-force guidance of the lower scissors, culminating in the modern, almost exclusively-used “half-scissor” or single-arm pantograph (Fig. 13.24). This development was encompassed by a constantly reducing level of mass and thus improved contact properties at higher speed [B10], [206].

The pantograph is elevated by raising springs and pressed against the catenary with approximately constant force (120...150 N). It is lowered by the kinematics of the springs, resting in a low position. From this low position, a pneumatic cylinder or an electric motor (used with “all-electric vehicles”) raises it upwards to the working range, where the springs are acting upwards. Various patterns feature pneumatic quick-drop, to avoid damage to collector and catenary in case of longitudinal thrusts.

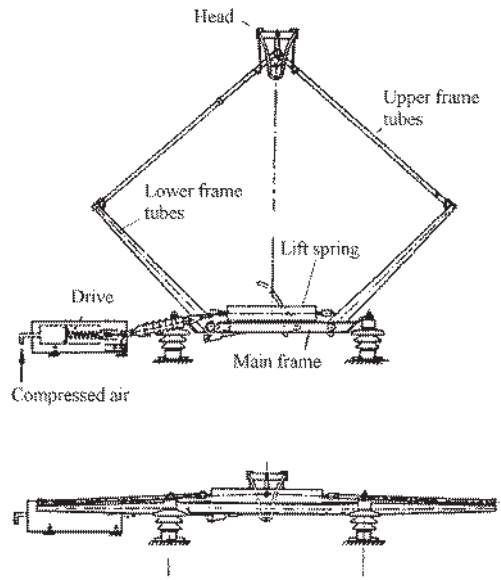
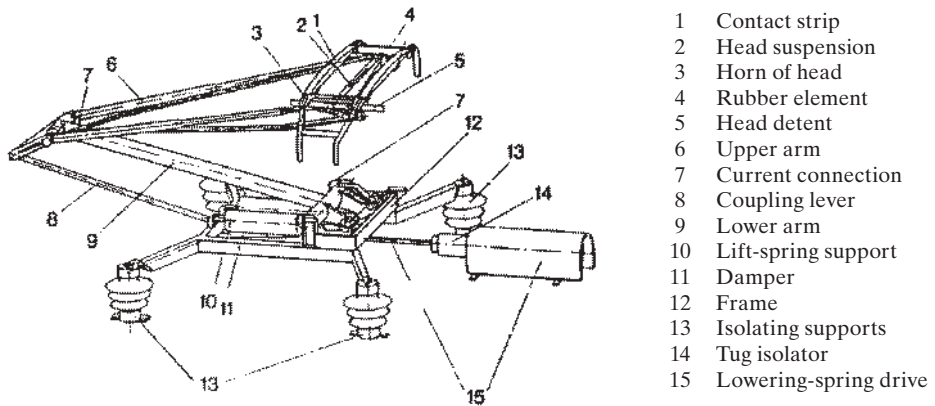


Fig. 13.23: Pantograph DBS 54 of the DB



- 1 Contact strip
- 2 Head suspension
- 3 Horn of head
- 4 Rubber element
- 5 Head detent
- 6 Upper arm
- 7 Current connection
- 8 Coupling lever
- 9 Lower arm
- 10 Lift-spring support
- 11 Damper
- 12 Frame
- 13 Isolating supports
- 14 Tug isolator
- 15 Lowering-spring drive

Fig. 13.24: Single-arm pantograph

Fig. 13.25 illustrates various contact strip material as well as the transferable current at given contact-line parameters. Please bear in mind that 6 MW rated input result in:

4000 A at $U_{FN} = 1.5$ kV
2000 A at $U_{FN} = 3$ kV
400 A at $U_{FN} = 15$ kV
240 A at $U_{FN} = 25$ kV

Carbon and copper (d) is preferably used with DC 1500 V, pure Cu with DC 3000 V (for example in Italy and Poland); carbon (a, b) is used with higher AC voltages. The “horns” are earthed.

Multi-system locomotives thus require a higher number of (up to four) pantographs, which is even enhanced by the different zig-zag widths in Germany and Switzerland.

For commuter railways using a track separated from road traffic, such as Metros and underground railways, lateral conductor rails (“third rails”) are generally used, due to the smaller size of the necessary clearance and, in consequence, lower cost of tunnel construction and bridge raising. Furthermore, maintenance is easier (even during short pauses of operation), since no tower wagon is required.

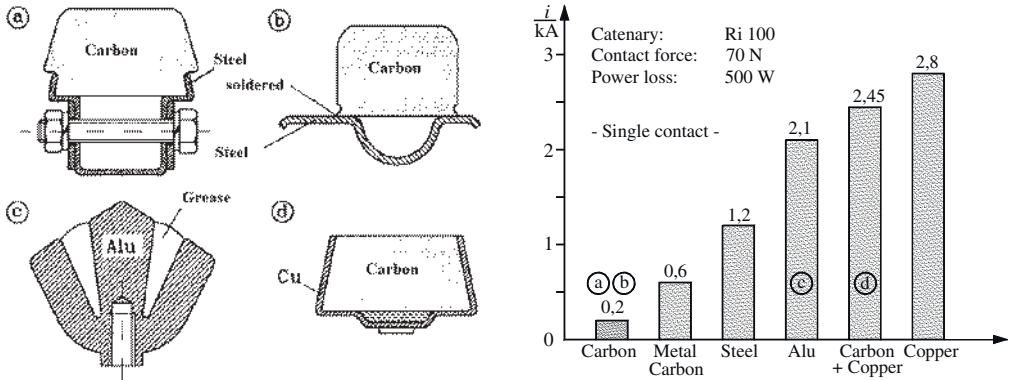


Fig. 13.25: Contact strip material and admissible load

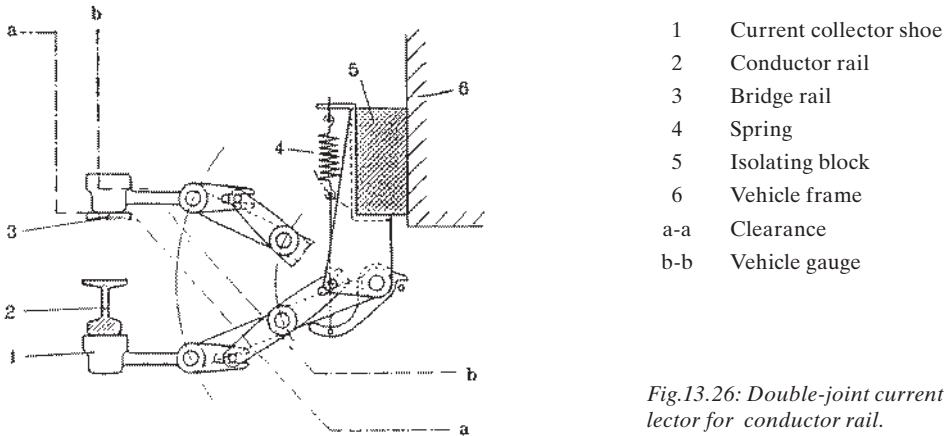


Fig.13.26: Double-joint current collector for conductor rail.

In former times, soft-iron running rails were used for conductor rails. Nowadays, high-performance commuter railways use aluminum-steel composite conductor rails [207], using a 6 mm-thick, geared high-grade steel strip, which is introduced when extruding the aluminum conductor rail; cross-section area is up to 4,830 mm² (7.5 sq. in.). Modern conductor rails are generally brushed from below; the collector, however, will interfere with the regular track clearance, this requiring such vehicles to be transferred only with the collectors removed. It is only with very early electrification schemes and old, narrow top-boom bridges that the conductor rail is brushed from above or from the side. Fig. 13.26 shows such a double-joint collector.

Due to track switches and both positions of platforms, the conductor rails have to be placed on both sides of the track, thus requiring collectors on both sides of the vehicle. On diamond

crossings (as well as road crossings in workshop areas), gaps in the conductor rails of up to 32 metres length are inevitable, which, fortunately, do only constitute a minor nuisance since collectors are usually mounted to every motor coach in the train. They forbid, however, the use of locomotives or single motor coaches in conductor-rail networks, unless energy-storage devices have been installed in these vehicles.

For decades, the subterranean power feed has been a thing of ages past, which was used for aesthetic reasons with various tramways operating in historic city centres, such as the crossing of the “Unter den Linden” boulevard in Berlin before World War I. Fig. 13.27 displays a cast-iron conduit beneath one of the rails [B28]; apart from that, there also were centrally-placed assemblies. Using dual-pole conductor rails, the problem of stray current was solved as well. Due to the complicated coupling and decoupling of the slip shoe attached to the tramway cars when changing from and to the regular overhead contact-line system, the complicated system of track-switches and unreliable operation in case of dirt, snow and ice, such systems fell out of favour, the last one being let up in Washington, D.C., in 1962.

- a Slotted rail
- b Contact rails
- c Cast-iron longitudinal sleeper
- d Isolator
- e Concrete filling

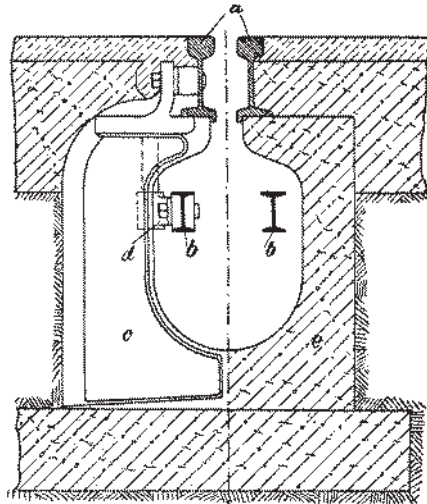


Fig. 13.27: Historic subterranean power feed using a slotted rail (pre-world-war I)

In 2003, the idea was revived by ALSTOM for the new Bordeaux tramway APS system. In the inner city there are conductor rails between the rails in the street surface, of some 7 m length, which are energized by solid-state switches only when a train (of considerably greater length) is over the contact section, so that endangering of pedestrians and animals is excluded. Fig. 13.28 shows (on the left) the tramway of the CITADIS family, and (on the right) the contact rail and the covers of the subterranean power switches. It took some time to find a really watertight and reliable construction of the switch-boxes; the APS infrastructure is reported to cost 300...400% more⁷ than a conventional catenary system, which is used outside the historic city anyway. Some cities in France (as Nice) use dual-mode vehicles with batteries (cf. subchapter 9.3) or rotating energy storage systems (subchapter 10.3).

⁷ DIE ZEIT 2007, Nr. 6, p. 24.



Fig. 13.28: Bordeaux APS tram (CITADIS) and power-enabling switches between the rails

14 Line interference

14.1 Survey

Already in the very early times of electric traction disturbing effects could be watched, being connected to the transport of electric energy via the contact rail to the traction vehicle and back to the power station via the rails. The high line voltage evoked inadmissibly high voltages in the telegraph and telephone lines parallel to the railway track, by electrostatic influence. The traction currents induced disturbing voltages, hampering data communication. This made installation of cable systems inevitable. A considerable portion of the return current flows via the earth and may cause dangerous voltages in metal pipes and cable sheets, crossing its way. In case of DC railways, electrolytic effects occur (cf. subchapter 13.3).

These unwanted secondary effects grew when in the 1930s the first converters were introduced in traction. This was – as mentioned before – to enable the use of 50-Hz current in traction, not to be dependent upon the expensive proprietary power-supply system with $16\frac{2}{3}$ Hz. First trial were undertaken in 1936 on the “Höllental“ secondary line in the Black Forest with several test locomotives of different technologies, mainly rectifiers. The discontinuous working of the converters caused disturbances in the line cables much stronger than known before; they were strongly dependent on the actual structure of the railway grid, what was interpreted by resonances [208].

Similar disturbances or interferences were observed with “standard“ converters in industry, too; they are today treated commonly under the term “Electro-Magnetic Compatibility“ (EMC). The interference investigation follows the scheme: Interference source (emission) – propagation medium – coupling – interference well (immission) [209], [210].

Interference sources are [211]

- the fundamental content of the line current (maybe with line frequency $f_N = 0$), which is modeled as a current source,
- the current harmonics of the converters on the traction vehicles, which can be regarded from the line-side as current sources, as there are DC choppers (section 4.1.3), phase-controlled converters (section 4.1.4), pulsed inverters (subchapter 6.2) and ASCIs (section 6.6.3), which can be modeled as current sources, too,
- the harmonics of the four-quadrant converters (subchapter 6.5) on board of the traction vehicles and the substation rectifiers, which are to be modeled as voltage sources,
- high-frequent ($f > 30$ kHz) interferences by the arc contact at the pantograph, the commutators of the DC traction motors and the switching edges of the power semiconductors and the microcomputer power supplies on board.

Looking at the propagation medium, the distributed impedances of the widely extended railway systems – when comparing to the frequencies in question – have to be taken into account. Besides that, filters on the vehicles and in the substation have a big influence.

If only looking at the voltage quality at the own pantograph (as the “PCC“ = „Point of Common Coupling“ of several consumers), the investigation can be finished here already. But when regarding interference at other places in the own supply system and in other networks as other AC or DC railways, public utility grids, telephone and general data communication networks or

special railway safety systems as e.g. track circuits or axle-counters, the coupling – galvanic, inductive, capacitive and radiation coupling – must be analyzed first, the input characteristics and the sensitivity of the interference wells.

Whilst these interference chains can be looked at monodirectional, there is an increasing part of disturbances arising from the cooperation and interaction of high-power traction vehicles with highly dynamical electronic control with components of the energy supply as catenary system, power stations and converters in a fed-back action [212]. The investigation of these effects is much more demanding, especially if quantitative results are expected.

For all interferences – which cannot be prevented totally, for economic reasons – reasonable limitations of the disturbance emission, immunity to interference and simple measures of the effects must be agreed upon, e.g. in the relevant norms as EN 50238, VDE 0228 [213].

14.2 Emission sources in DC railway systems

14.2.1 Voltage harmonics of the substation rectifiers

In substations, six-pulse diode rectifiers (B6) are used at minor power, twelve-pulse units (B12) at high power demand. Correspondingly, the frequencies of the interference voltage obey the following laws [V2]:

$$f = g \cdot 50 \text{ Hz}, g = 6 \cdot h, h = 1, 2, 3, \dots \quad \text{at B6} \quad (14.1)$$

$$f = g \cdot 50 \text{ Hz}, g = 12 \cdot h, h = 1, 2, 3, \dots \quad \text{at B12.} \quad (14.2)$$

The r.m.s. values of the harmonics of the rectifier output voltage are determined basically by the no-load law

$$\frac{U_g}{U_{diN}} = \frac{\sqrt{2}}{g^2 - 1}, \quad (14.3)$$

but additionally by the rectifier overlap at the commutation, due to the leakage impedance of the transformer. Table 14.1 lists the values, normalized to the ideal no-load direct voltage, for the normalized nominal short-circuit voltage $u_{xN} = 10\%$ and different loads (and thus overlap angles u), for six- and twelve-pulse diode rectifiers [214]. Mostly it is not necessary to know all individual harmonics; to assess the total disturbant effect, an 800-Hz equivalent voltage is defined as the frequency-weighted r.m.s. value of the individual harmonics, using the psophometric weighting p_f (described in detail in subchapter 14.5). The telephone harmonic form factor $t.h.f.$ is the mentioned r.m.s. value, normalized to the ideal no-load direct voltage:

$$t.h.f. = \frac{U_{Dist}}{\bar{u}_{diN}} = \sqrt{\sum_g \left[\frac{U_{dg} \cdot p_f(f_g) \cdot 800 \text{ Hz}}{\bar{u}_{diN} \cdot f_g} \right]^2}. \quad (14.4)$$

With 600- and 750-V tramways and underground railways, the impedances of substation and contact line can be taken as purely ohmic-inductive; with 1500-V- and 3000-V main lines cf. subchapter 14.4. As terminating impedances of the wells the input L-C filters of the traction vehicles can be assumed, with $C \rightarrow \infty$, in general [214].

The interference current in the substation is then

$$I_{\text{StU}} = \frac{t.h.f. \cdot \bar{u}_{di}}{2\pi \cdot 800 \text{ Hz} \cdot (L_N + L_F)} \quad (14.5)$$

with line inductivity $L_N > 0.5$ mH and filter inductivity L_F (L 's at 800 Hz!).

Table 14.1 AC portions U_{dg} and telephone harmonic form factor $t.h.f.$ of six-pulse and 12-pulse diode substation rectifiers, in dependence upon load

Overlap angle	u	0		12°		16,5°		26,5°		37°	
Inductive direct voltage regulation	d_x	0		0.01		0.02		0.05		0.1	
Norm. load current at $u_{xN} = 10\%$	I_d/I_{dN}	0		0.2		0.4		1		2	
Pulse number	p	6		12		6		12		6	
U_{d6} / \bar{u}_{di}		0.040	–	0.051	–	0.057	–	0.061	–	0.059	–
U_{d12} / \bar{u}_{di}		0.01	0.01	0.015	0.015	0.015	0.015	0.024	0.024	0.041	0.041
U_{d18} / \bar{u}_{di}		0.004	–	0.007	–	0.010	–	0.019	–	0.022	–
U_{d24} / \bar{u}_{di}		0.002	0.002	0.005	0.005	0.009	0.009	0.012	0.012	0.018	0.018
t.h.f. ($f_N = 50$ Hz assumed)		0.034	0.011	0.044	0.017	0.049	0.018	0.058	0.026	0.069	0.048

The interference current portion, caused by the harmonics of the substation rectifier voltage is of similar order of magnitude, as the portion due to vehicles with power-electronic control, which is treated in the next section..

14.2.2 Input-current harmonics of a step-down DC chopper

Converter having a big smoothing reactor on the load side (big in comparison to the line inductance), draw current blocks from the DC mains and are thus to be regarded as current sources (cf. Fig. 14.1); [215], [B25].

The r.m.s. values of the harmonics of the DC chopper input current are

$$I_{1g} = \frac{\sqrt{2}}{\pi \cdot g} \sin(g \cdot \pi \cdot a) \cdot \bar{i}_d, \quad g = 1, 2, 3 \dots \quad (14.6)$$

with $a = \bar{u}_2 / U_1$ (cf. section 4.1.3).

The frequencies are according to

$$f_g = g \cdot f_z. \quad (14.7)$$

Fig. 14.2 gives the spectra of normalized input current (and output voltage, as well!).

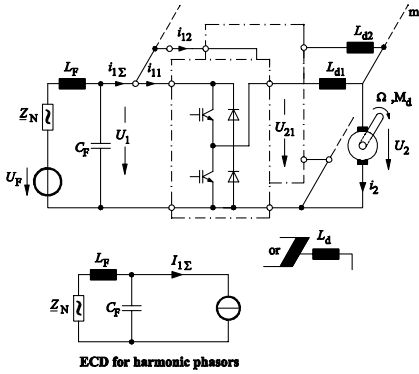


Fig. 14.1: Traction converter with current-source line-side behavior and ECD valid for harmonics

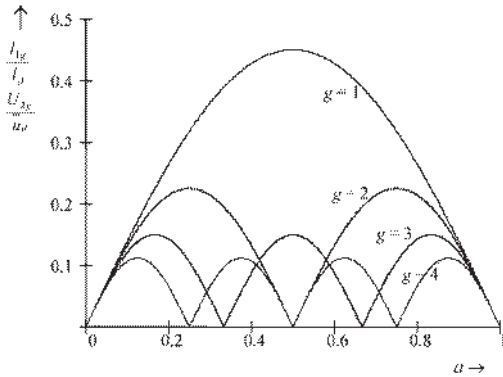


Fig. 14.2: Spectra $I_{1g}/\bar{i}_2, U_{dg}/\bar{u}_1 = f(a)$ of the step-down DC chopper

If m (equal) DC choppers are paralleled and switched with an “interleaving“ of $1/(m \cdot f_z)$, using triangular compare functions, phase-shifted by this value (cf. Figs. 7.1 and 8.2, both with $m = 3$), they can be replaced by an equivalent current source

$$I_{1\Sigma\Sigma} = \frac{\sqrt{2}}{\pi \cdot g \cdot m} \sin(g \cdot \pi \cdot m \cdot a) \cdot \bar{i}_d, \quad g = 1, 2, 3. \tag{14.8}$$

The resulting frequencies are now:

$$f = g \cdot m \cdot f_z, \tag{14.9}$$

The harmonic frequencies compare to those of a chopper with m -fold switching frequency, i.e. all harmonics with $g \neq k \cdot m$ ($k = 1, 2, 3$) disappear. The same holds for the harmonics of the chopper output voltage u_2 . The m smoothing reactors can be replaced by $m - 1$ interphase reactors (autotransformers) and one common smoothing reactor of comparably smaller inductivity (analog to [V2]).

14.2.3 Input-current harmonics of an ASCI

The six-pulse rectified motor e.m.f. acts – in analogy to section 14.2.1 – as a harmonic voltage source, driving current portions with $6 \cdot g$ -fold frequency through the big smoothing reactor. The amplitudes of these currents are attenuated by the input DC chopper with the (direct) voltage control factor; the frequencies remain unchanged, representing the main disturbance. Besides them, modulations products of the harmonics of the chopper switching function with the inverter DC-link current harmonics appear. They show the frequencies

$$f_{dv} = g \cdot f_z \pm k \cdot 6 \cdot f_s, \tag{14.10}$$

but fortunately with rather small amplitudes [209], [216]

If the motor inverter is pulsed, to make the motor current more sinusoidal (trapezoidal, to be precise), the $6 \cdot g$ -multiples of the stator frequency will be attenuated, and pulse-frequent portions dominate.

14.2.4 Input-current harmonics of a VSI

At the DC rail between valve group and DC-link capacitor, the current harmonics of a VSI can be regarded as impressed by the – in comparison – big motor leakage inductances. Their spectral content is mainly determined by the pulse pattern (cf. subchapter 6.2, Fig. 6.13) and the voltage control factor [217], [242].

With sinusoidal modulation (Fig. 6.12, 6.13 top) the dominating frequencies are:

$$\begin{cases} 2 \cdot g \cdot f_z \pm 2 \cdot k \cdot f_s & g = 1, 2, 3 \dots \quad k = 0, 1, 2, 3, \dots \\ (2 \cdot g - 1) \cdot f_z \pm (2 \cdot k + 1) \cdot 3f_s & g = 1, 2, 3 \dots \quad k = 0, 1, 2, 3, \dots \end{cases} \quad (14.11a, b)$$

In Fig. 14.3, first line left, the waveform of the DC-link current is displayed, with same operating conditions (centre column) as in Fig. 6.13, top; on the right side the spectrum is shown. All values are normalized to the fundamental amplitude of the inverter output current. The $2 \cdot N_z = 50$ th harmonic is dominating. Harmonic lines with harmonic order $v = 25 \pm 3 = 21$ and 28 are clearly to be seen, too; in general the line with lower order is more disturbing, as of lower frequency.

In all synchronous pulse modes (with the symmetry conditions named in subchapter 6.2) only harmonic frequencies

$$f_v = g \cdot 6 \cdot f_s, \quad g = 1, 2, 3 \dots \quad (14.12)$$

occur, as the side-band frequencies coincide with the 6-g-fold order [217], [242].

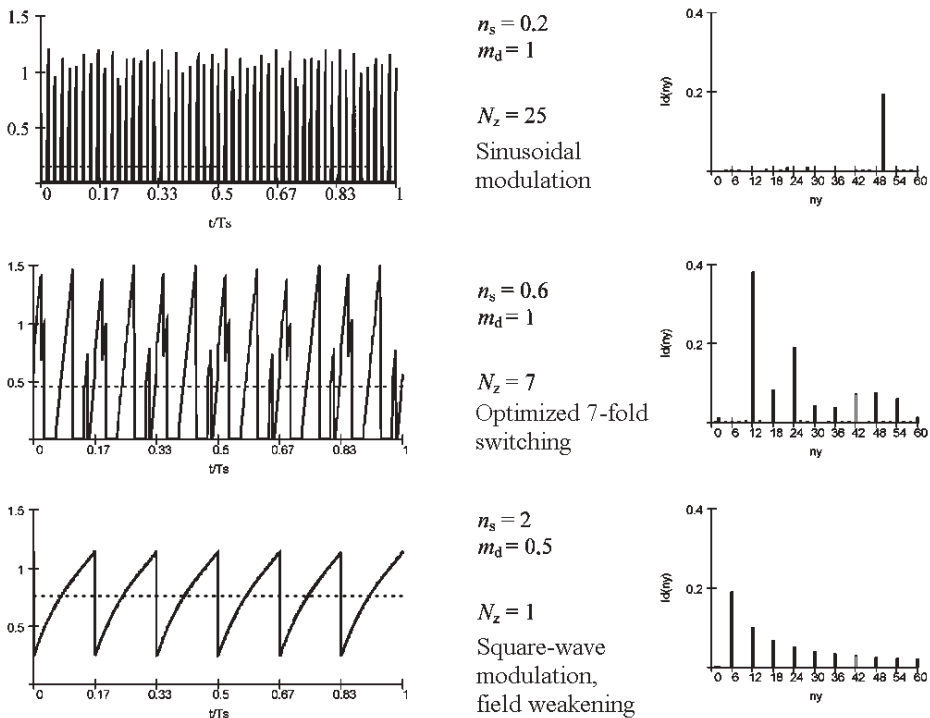


Fig. 14.3: Waveforms and r.m.s. spectra of DC-link current of a VSI under different pulse patterns (subchapter 6.2, Fig. 6.13)

Fig. 14.3, 2nd line, represents optimized sevenfold switching, corresponding to Fig. 6.13, 3rd line. The most important DC-link current harmonic is the twelfthth.

At square-wave modulation (Fig. 14.3, bottom line, same as Fig. 6.13, lowest line) the frequencies of the DC-link current harmonics are as:

$$f_v = g \cdot 6 \cdot f_s, \quad g = 1, 2, 3 \dots, \quad (14.13)$$

The sixth harmonic is that with the biggest amplitude.

According to the Equivalent Circuit Diagram in Fig. 14.1, bottom line, these current harmonics are fed into the parallel connection of DC-link filter capacitor (and additional transversal filter branches, if existing) and the series connection of filter inductivity L_F and line impedance Z_N . DC railways of greater extension with 1.5 or 3 kV and catenary may need a more accurate network modelling, as treated for AC lines in subchapter 14.4.

14.3 Emission sources in AC railway systems

14.3.1 Voltage harmonics of the power supply

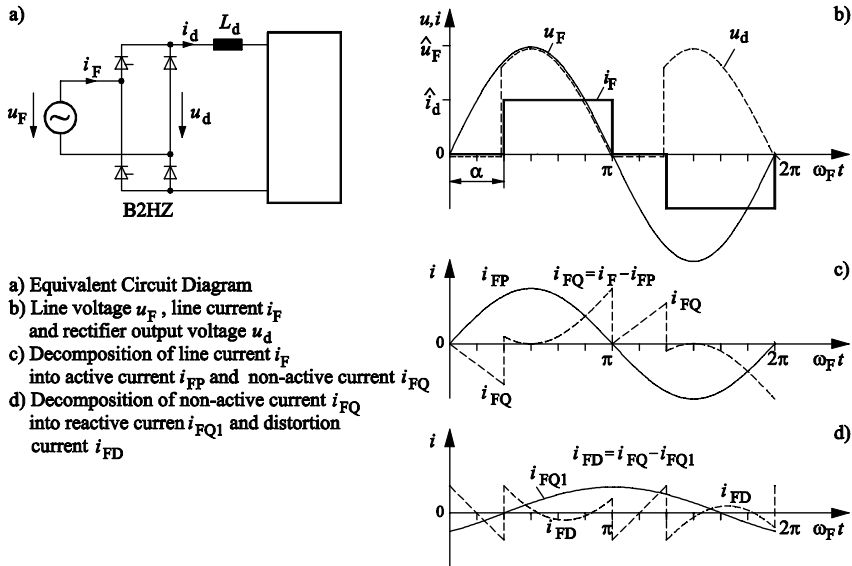
Voltage harmonics of synchronous generators can be neglected. With inverter supply, in some cases special filters tuned to the resultant pulse frequency of the series-connected inverters (as in Fig. 13.8) may be necessary; in other systems (as e.g. in Switzerland) filters may be banished, to avoid any resonances.

14.3.2 Input-current harmonics by phase-angle control

As it is well known, an AC traction vehicle with power-electronic control does not take in the “ideal“ line current, which is just necessary to produce the demanded power. With sinusoidal line voltage, the ideal current is sinusoidal, too, and in phase with the line voltage.

The relations under “real“, not idealized conditions, shall be exemplified at the two-pulse bridge in half-controllable connection of pairs of arms, the basic circuit of the classical thyristor-converter locomotive (cf. section 4.1.4). Fig. 14.4a shows the Equivalent Circuit Diagram: The line voltage u_F is rectified by the “B2HZ“ bridge and conveyed via the smoothing reactor L_d to the DC motor for undulating current or to the DC link of an inverter.

For the basic investigation, the impedance of the line and the main transformer is set to zero, and the inductivity of the smoothing reactor is assumed as infinite.



a) Equivalent Circuit Diagram
 b) Line voltage u_F , line current i_F and rectifier output voltage u_d
 c) Decomposition of line current i_F into active current i_{FP} and non-active current i_{FQ}
 d) Decomposition of non-active current i_{FQ} into reactive current i_{FQ1} and distortion current i_{FD}

Fig. 14.4: Line current of the two-pulse bridge in half-controllable connection of pairs of arms; decomposition into active and non-active components ($L_d \rightarrow \infty$)

The trigger delay α of the thyristors of the left branch sets the average value of the direct voltage. As most of these locomotives do without recuperation, the two other valves are diodes. At the zero crossing of the line voltage u_F (π in Fig. 14.4b), they take over the current from the thyristor and let it by-pass the transformer, until at $\pi + \alpha$ the next thyristor is fired. In this interval the bridge output voltage equals zero; the line current i_F has a block-like waveform.

This current can be decomposed into the following components ([218], [211], [V1], [V2]):

- Active current i_{FP} (Fig. 14.4c), the portion of i_F with same frequency as u_F and in phase with u_F , producing with u_F the active power of the drive
- Nonactive current $i_{FQ} = i_F - i_{FP}$; this can again be decomposed to (Fig. 14.4d)
- Reactive current i_{FQ1} , the portion of i_F with same frequency as u_F and phase-shifted by 90° , and the remaining
- Distortion or harmonic current i_{FD} .

The r.m.s. values of these three orthogonal components, I_{FP} , I_{FQ1} and I_{FD} , can be added geometrically to the r.m.s. value of the line current I_F :

$$I_F = \sqrt{I_{FP}^2 + I_{FQ1}^2 + I_{FD}^2} \tag{14.14}$$

The product

$$S = U_F \cdot I_F \tag{14.15}$$

is defined as “apparent power“ and determines e.g. the rating of the transformer and the losses of the power distribution.

The ratio

$$\lambda = U_F \cdot I_{FP} / S \quad (14.16)$$

is called “power factor”; its reciprocal value figures the higher load of the line, compared to the active power. It can be written as the product

$$\lambda = g \cdot |\cos\varphi_1| \quad (14.17)$$

of fundamental factor

$$g = \sqrt{I_{FP}^2 + I_{FQ1}^2} / I_F \quad (14.18)$$

and the absolute value of the fundamental displacement factor

$$\cos\varphi_1 = I_{FP} / \sqrt{I_{FP}^2 + I_{FQ1}^2} \quad (14.19)$$

The free-wheeling of the half-controllable bridge advances the centre of the current blocks and reduces the reactive current by this. The disturbing effects of the reactive current remain restricted to the railway supply system. According to the reciprocal value of the power factor the generators and the transmission system have to be oversized, the transmission losses will be increased and the on-board transformer will be heavier.

The voltage drop in the supply grid rises, decreasing the possible load power. Interference with signalling and communication systems in the vicinity of the electric railway system is of less importance, as it will be clear from subchapter 14.5.

The distortion current can be decomposed by means of the Fourier Series Expansion into an infinite sum of components with frequencies equal to integer multiples of the line frequency, the so-called harmonics. All even harmonics disappear with symmetrical converter control ($i(x + \pi) = -i(x)$). The r.m.s. values of the line current harmonics can be calculated as (at neglected transformer leakage impedance and $L_d \rightarrow \infty$):

$$I_{lg} = \frac{\sqrt{2}}{\pi \cdot g} \sin\left(g \cdot \frac{\pi - \alpha}{2}\right) \cdot \bar{i}_d \quad g = 1, 3, 5, \dots \quad (14.20)$$

Traction vehicles with three-phase drive technology produce in addition current components with frequencies, which are not integer multiples of the line frequency, but dependent on the variable inverter output frequency and the switching frequency (cf. sections 14.2.3, 14.3.3), the so-called “interharmonics”.

Treating the distortion current, it is advisable to distinguish between low-frequent (up to 100 Hz), medium-frequent (100 Hz up to some 10 kHz) and high-frequent components.

Low-frequent components are important from the energetic point of view, reducing the fundamental factor by some 10 %. Further-on, they may distort the voltage waveform to such a degree, that inadmissible overvoltages are produced, jeopardizing other devices or overloading protection devices, or that additional zero crossings are generated, disturbing the synchronizing function of power electronics, which are not equipped with special filters.

In Fig. 14.5, curve 2 is the typical dependency of the power factor λ of the two-pulse bridge in half-controllable connection of pairs of arms with sequential phase control; on an average, it is below 0.65, distinctly less than the AC commutator motor (curve 1).

Though sequential phase control reduces the line reactive power, it remains considerable, mainly at low output voltage. Phase-shifting capacitors can be employed: With condensed traffic,

as e.g. with Metro service on AC railway systems, it is preferred to install them concentratedly in the substations (section 13.1.1).

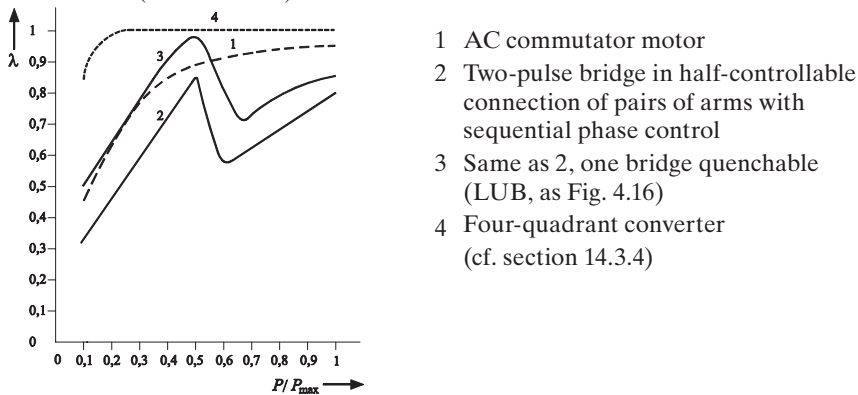


Fig. 14.5: Power factor λ of AC traction vehicles

With long feeding sections, the decentral implementation on-board of the traction vehicles is more economical, as it reduces the voltage drop on the traction vehicle (Sweden, France). The capacitor rating (in kVAr) may be up to one third of the vehicle rating (in kW). In any case, the capacitor is complemented by a reactor to a resonant tank circuit, tuned to roughly the third harmonic, to suppress oscillations. Often the filter capacitors can be switched off by thyristors (e.g. Fig. 5.6).

In the early seventies, quenchable half-controllable bridges had been developed (Fig. 4.16); cutting off and thus centring the current block in relation to the line voltage, the reactive power is reduced to zero, with less expense as using compensation capacitors. In Fig. 14.5, curve 3 represents the course of the power factor of such an equipment. Except for prototypes tested temporarily on DB lines, this circuit was only used in the 3-MW, 50-Hz locomotives Class 7E, delivered by German electrical industry to South African Transportation Systems.

Medium-frequency current harmonics of the two-pulse bridge in half-controllable connection of pairs of arms with sequential phase control can be reduced by the following provisions [31]:

- Higher number of steps: Looking at the limited voltage of DC motors (< 1500 V) and the available voltage rating of thyristors, more than three series-connected bridges do not make sense. Then AC-side sequential control with autotransformer connection may be advantageous, as described below, together with an
- Increased leakage inductance of the main transformer: An increase of the overlap reduces the distortion currents and thus the interference to a high degree. A suitable connection of the commutation reactor is possible with the AC-side sequential control, as shown in Fig. 7.5, item '4'). The commutation reactor is only effective at low output voltage and does not reduce the yield at full direct voltage. Yet at partial yield, the power factor is decreased. This circuit was used with the most powerful locomotive with phase control and undulating-current motors, Class 1044 of ÖBB (Figs. 7.4, 7.5).
- Reduction of the inductivity of the smoothing reactor: The rising DC-current ripple reduces the current to be commutated and by that the interference currents. A limit is set by the deterioration of the commutation of the DC motor itself, so that a ripple of 40% peak-peak is not exceeded, at rated current.
- Line filters: The compensation filters described above reduce harmonics of an order >3 .

- Pulsed line converters for DC-current links have been discussed widely in literature, but were not used in traction vehicles. Due to the development of semiconductor devices, it is not likely that there will be a change in near future.

High-frequency portions of the distortion current interfere with the communication services of railways and public providers (subchapter 14.5) and with the audio-frequency track circuits of railways (subchapter 14.6).

14.3.3 Input-current harmonics by inverter input current

The input current of a step-down DC chopper (equ. (14.6)), of the thyristor bridge of the load-commutated synchronous motor or of the ASCI contains current harmonics with the frequency f_{dv} and an amplitude $k \cdot \bar{i}_d$. They are modulated by the fundamental-frequency time-dependent current transformation ratio of the half-controllable bridge (as an example):

$$\frac{I_{1g}}{\bar{i}_d} = \frac{\sqrt{2}}{\pi} \sin\left(\frac{\pi - \alpha}{2}\right) \quad (14.21)$$

(cf. equ. (14.18)) as two side-bands with half amplitude and the frequencies

$$f_{dv} \pm f_F \quad (14.22)$$

into the line current with the r.m.s. values:

$$I_{1g}(f_{dv} \pm f_F) = \frac{1}{2} \cdot \frac{\sqrt{2}}{\pi} \sin\left(\frac{\pi - \alpha}{2}\right) \cdot k \cdot \bar{i}_d \quad (14.23)$$

Additionally, modulation products with the harmonics of that time-dependent current transformation ratio are observed, but which shall not treated here, as being of much smaller amplitude than those of equ. (14.23).

14.3.4 Input voltage harmonics of the four-quadrant converter

The two-quadrant DC step-up chopper, working on the DC-link capacitor, as basic element of the four-quadrant converter is to be seen as a voltage source, as the di/dt reactors in the chopper are much smaller than the line reactance. The line currents are obtained by dividing the voltage harmonics of the chopper by the sum of transformer impedance (in case of the 4q-C), the filter reactance and line reactance, taking in regard the transversal branches of the filter, as treated later. Fig. 14.6 displays the circuit diagram of m parallel two-quadrant step-up choppers, with switching interleaved by $1/(mf_{ez})$, and below the ECD for the harmonics.

The r.m.s. values of the equivalent chopper input voltage harmonics $U_{\Sigma g}$ are (dually to equ. (14.8)), cf. Fig. 14.7:

$$U_{\Sigma g} = \frac{1}{m} \cdot \sum_{\mu} U_{s\mu} = \frac{\sqrt{2}}{\pi \cdot g \cdot m} \sin(g \cdot \pi \cdot m \cdot a) \cdot \bar{u}_d \quad (14.24)$$

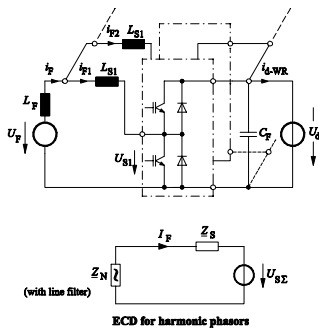


Fig. 14.6: Traction converter (two-quadrant step-up chopper) with impressed voltage and ECD for marionics

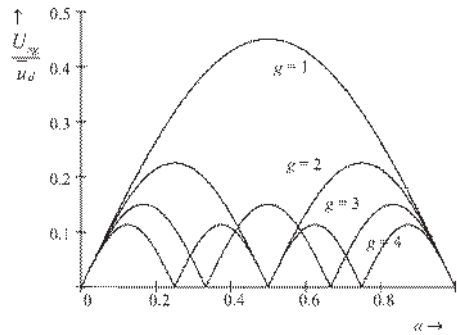


Fig. 14.7: Spectra $U_{sg}/u_d = f(\alpha)$ of the two-quadrant step up chopper

In a four-quadrant converter circuit (subchapter 6.5) the transformer secondary winding is connected between the outputs of two two-quadrant choppers (similar to the inverter phase modules). With the usual (unipolar) PWM control with two inverse reference functions (cf. Fig. 6.22, top line), the pulsed bridge voltage u_s contains harmonics with the frequencies

$$f = [2 \cdot h \cdot N_z \pm (2g - 1) \cdot f_F] \quad \text{for } g, h = 1, 2, 3, \dots \quad (14.25)$$

with the pulse number N_z (at 16 $\frac{2}{3}$ Hz mostly 11 or 15 for GTO-thyristor converters) and line frequency f_F ; the amplitudes can be described approximately [219] as:

$$\hat{u}_{S2kN \pm (2m-1)} = \mp U_d \left\{ \frac{4 N_z}{\pi(2 h N_z \pm (2g - 1))} \right\} \cdot J_{\pm(2m-1)} \left\{ 2 h N_z \pm (2g - 1) \cdot \hat{k}_1 \cdot \frac{\pi}{2 N_z} \right\} \quad (14.26)$$

(J_v is the Bessel function of order v). The harmonics of the line current are limited by the leakage inductivity of the transformer and the line impedance.

A traction vehicle is equipped with at least two 4q-Cs, with locomotives often 2 or 3 per bogie. As defined in equ. (14.24), the converter equivalent voltage is calculated as the average value of the m converter voltages; the effective inductivity is the m^{th} part of the leakage inductivity of each transformer winding.

The switchings of the 4q-Cs of one bogie group are phase-shifted by $\pi/2$ or $\pi/3$, respectively; in addition those of the other bogie group by $\pi/4$ or $\pi/6$, respectively, against the other (cf. subchapter 6.5). By that the pulse parcels of low order cancel each other, and finally only those around eightfold (or twelvefold) switching frequency remain. To present that graphically, a 50-Hz, 25-kV application with fivefold switching ($f_z = 250$ Hz) is chosen as an example; the normalized short-circuit voltage of the transformer is 44 %, that of the line is neglected [216].

Fig. 14.8a shows the spectra of the converter voltage and of the line current (on the primary side of the transformer) of 4q-C Nr. 1. The dominating spectral lines in the vicinity of $2 \cdot f_z = 500$ Hz can be easily recognized. The interference current r.m.s. value (with psophometric weighting, cf. subchapter 14.5, Fig. 14.11) I_{pe} is about 6 A, with a line-current fundamental of 55 A.

Due to the symmetries, only sinus components occur in the spectrum. Those with phase 180° can now be drawn negative. Fig. 14.8b gives the spectral lines of the converter voltages of 4q-C 1 and 2 (the latter dashed) of bogie group 1. The lines around $2 \cdot f_z = 500$ Hz and the lines around $3 \cdot 2 \cdot f_z = 1500$ Hz have opposite phases and cancel each other, when added to the converter

equivalent voltage. I_{pc} is still some 5 A; this is a consequence of the high psophometric weighting valuation of the unchanged lines at $2 \cdot 2 f_z = 1000$ Hz, cf. Fig. 14.13).

Fig. 4.5.8c depicts the spectral lines of the bogie group 1 (solid); as dashed lines those of 4q-Cs 3 and 4 of bogie group 2 are attached. It can clearly be seen, how the lines around $4 \cdot f_z = 1000$ Hz cancel each other. Fig. 14.8d shows converter equivalent voltage and line current spectra, with the dominating bundle around 2 kHz (please note changed scale of ordinate!).

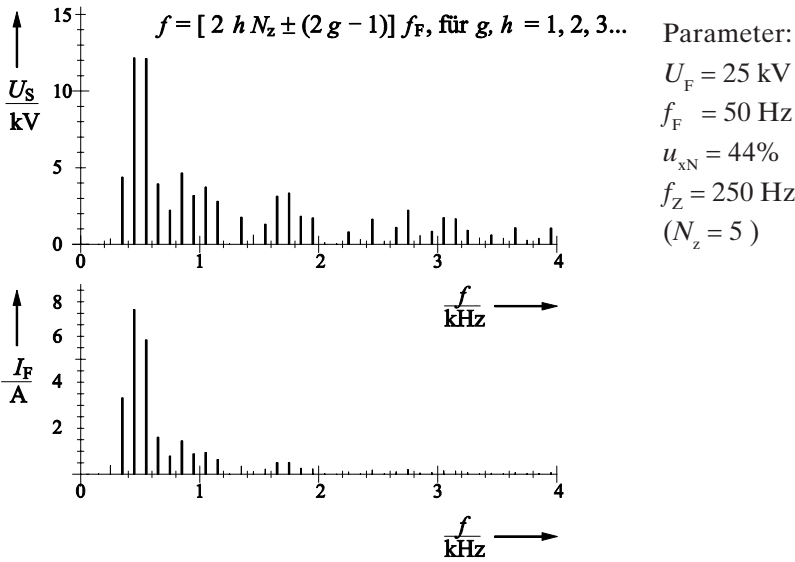


Fig. 14.8a: Spectra of voltage U_s and of line current I_F of 4q-C 1 (r.m.s. values)

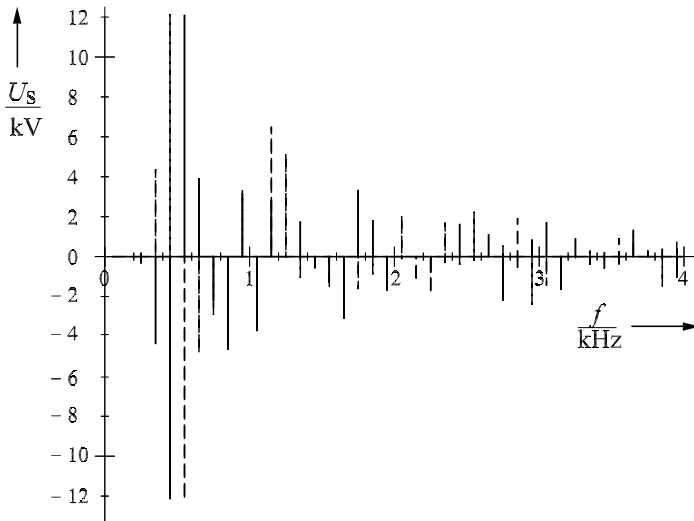


Fig. 14.8b: Spectra of U_s of 4q-C 1 and 4q-C 2 (switching staggered by $\pi/2$ vs. bogie group 1 (dashed lines))

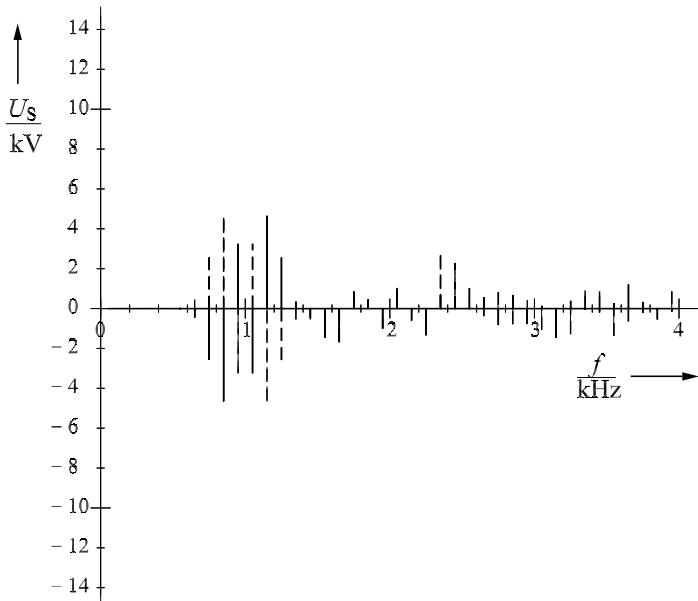


Fig. 14.8c: Spectra of U_{s1} (bogie group 1) and U_{s2} (bogie group 2), switching phase-shifted by $\pi/4$ (and $3\pi/4$, respectively, against $U_{s,p}$, dashed lines)

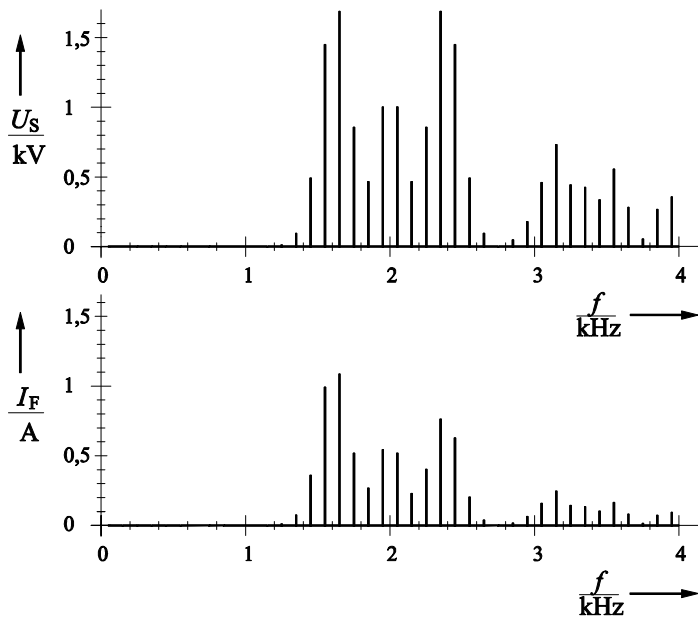


Fig. 14.8d: Spectra of equivalent voltage $U_{s\sigma}$ of all four $4q$ -Cs and of pertaining line current (changed ordinate scales!)

I_{pe} is now reduced to 1.6 A, at a line current r.m.s. of 220 A; the power factor reaches the value 0.999 in this example. Unfortunately the elimination of low-order harmonics is not so perfect, as shown in this example; at different bogie drive powers (e.g. by load transfer compensation, section 2.2.6) and slightly different DC-link voltages not-negligible portions with low frequencies occur. Additionally the emergency operation with only one bogie drive must not be lost sight of.

A low-pass filter on the high-voltage side of the transformer (Fig. 14.9, [220], [221], [222]) can reduce the interference current to roughly 50%. The filter rating is much smaller, compared to that of a thyristor locomotive. A disadvantage of all filters is, that they act like a "vacuum cleaner" on all distortions in the line voltage; by that they draw distortion currents in similar magnitude, as those of the 4q-C itself, in analogy to section 14.2.1.

An improvement is the connection of the filter to a tertiary winding of the transformer (Figs. 7.15 and 14.10, [223]). By adapting the coupling between primary, secondary and tertiary winding both the "sucking in" of distortions from the line and the own interference emission can be optimized. The filter elements can be dimensioned rather freely for convenient voltages of some 1000 V (and not 15 or even 25 kV). The converter rating is much smaller, as now half the leakage inductance is between filter and line, which makes the transverse branch much more effective. The filter of Class 101 DB AG shown in Fig. 14.10 (dashed frame) is tuned to a series resonance at $4 \cdot f_z = 1000$ Hz, the dominating harmonic frequency in emergency operation, when only one bogie group is active. The dominating lines in normal operation around $8 \cdot f_z = 2000$ Hz are still sufficiently damped.

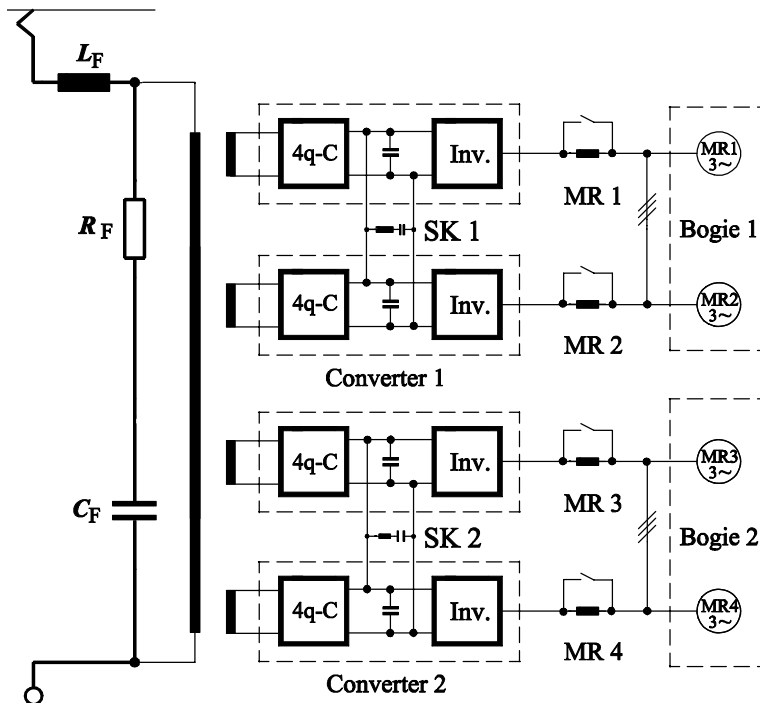


Fig. 14.9: High-voltage input filter of locomotive Class 120 DB

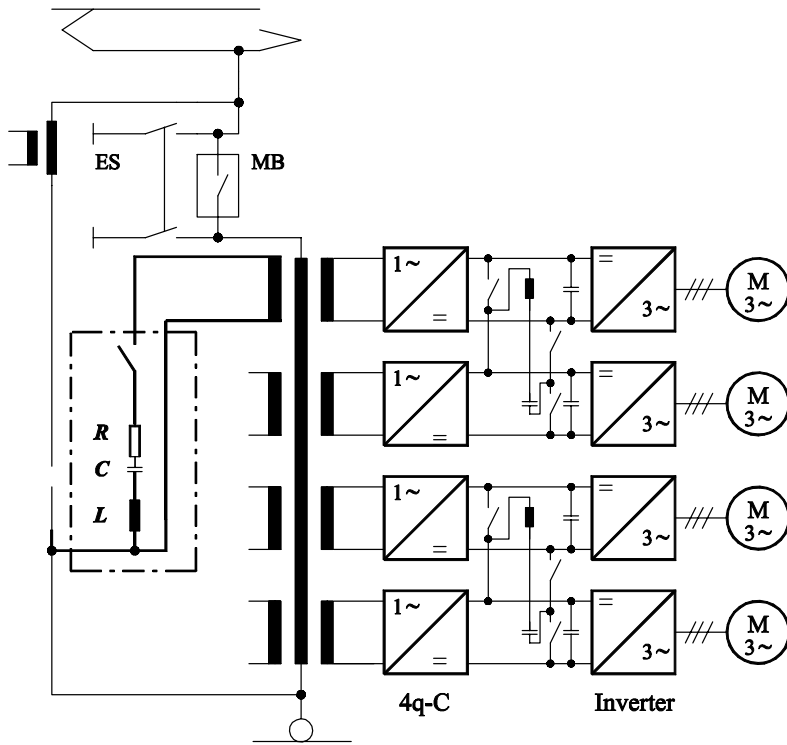


Fig. 14.10: Line filter, connected to the transformer tertiary winding, Class 101 DB AG

14.3.5 Modulation of VSI input-current harmonics by the four-quadrant converter

The input-current harmonics of the traction voltage-source inverter cause a ripple of the DC-link voltage at the impedance of the DC-link (C_d parallel to resonant tank circuit L_2-C_2). According to equ. (6.21) harmonics of the direct voltage with frequency f_x , and r.m.s. value U_{dx} are modulated into the converter voltage U_s (small-signal behavior) and cause line current harmonics [211] with the frequencies

$$f_{Fx} = f_x \pm f_F \tag{14.27}$$

and the r.m.s. values

$$I_{Fx} \approx 0.5 \cdot k_1 \cdot U_{dx} \cdot [f_F / (f_x \pm f_F)] \cdot P_N / (u_{xN} \cdot U_{FN}^2). \tag{14.28}$$

Given a maximal DC-link voltage ripple (peak-peak) of 3.5 % U_{dN} at $f_x = 83.3$ Hz, currents of about 0.14 % of rated current with 66.6 Hz and 100 Hz appear, i.e. ~ 0.5 A in case of a 5.6-MW/16 $\frac{2}{3}$ -Hz locomotive. This must be taken into account when assessing the critical low-frequency signaling interference (subchapter 14.6).

14.4 Impedances of the railway power-supply system

It was an early observation, made soon after the introduction of the first rectifier locomotives on the Höllental line, that the disturbance currents and especially the interference voltages are not only dependent upon the emission of the rectifiers, but are strongly influenced by the actual lengths of lines and the position of the disturbing traction vehicle on the line [208]. Some 35 years later, an amplification of the psophometric interference current of locomotives with 4q-Cs was observed on the Straubing–Plattling line of DB, which is rather critical.

This amplification vs. the calculated value (which could be measured on shorter “normal“, inductive line sections) was

- by a factor of 2 with 2 four-quadrant converters,
- by a factor of 4 with 4 four-quadrant converters operating [210].

This becomes clear, when taking into account that railway overhead lines are not to be regarded as short, in comparison with the wavelengths of the interfering harmonics, produced by the converters. Railway overhead lines are normally modelled by the two-wire theory. Contact line and carrying cable are concentrated in one equivalent conductor, the rails in another equivalent conductor, additionally taking into account the participation of the earth [224]. In the same manner, two-track lines are described by one equivalent conductor pair.

The impedances per unit length are drawn from several publications, mainly [224] and [219], and listed in Table 14.2. From these the characteristic wave impedance

$$\underline{Z}_w = \sqrt{(r' + j\omega \ell') / (g' + j\omega c')} \tag{14.29}$$

and the propagation constant

$$\underline{\gamma} = \sqrt{(r' + j\omega \ell') \cdot (g' + j\omega c')} = \alpha + j\beta \tag{14.30}$$

can be calculated.

Table 14.2 Characteristic values of single-phase railway networks

Configuration	ℓ'	c'	r'
one track, one catenary	1.2...1.5 mH/km (2.1 mH/km)*	11...14 nF/km	0.28 / 0.47 Ω/km **
two tracks, two catenaries	0.75...0.91	18...20 nF/km	0.09 / 0.28 Ω/km **
* Norwegian State Railway NSB			
** 1 st value for 16 ² / ₃ Hz ... 50 Hz, 2 nd value for 1 kHz			

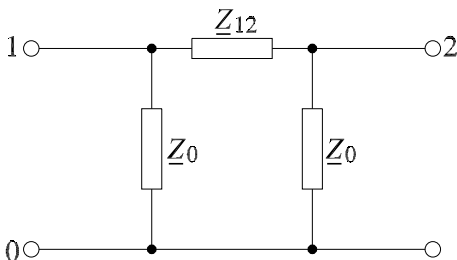


Fig. 14.11 π-ECD of a line segment

The ohmic part of the transverse conductance, g' , is rather small, in general; it can be used to consider stationary consumers, such as switch heating along the line.

Voltage and current at the beginning and the end of a line segment not too long can be represented by a π -ECD (Fig. 14.11); we obtain (with the length l of the segment)

$$\underline{Z}_{12} = Z_w \cdot \sinh(\gamma l) \quad (14.31)$$

$$\underline{Z}_0 = Z_w \cdot \tanh(\gamma l/2). \quad (14.32)$$

In [219] a relatively simple equivalent model for 16 $^{2}/_3$ -Hz railways was developed, consisting of three neighboring sections of 40, 50 and 60 km length, fed by three substations of 20 MVA each. The locomotive as disturbance source moves along the central 50-km section (Fig. 14.12a). The following parameters were assumed:

Table 14.3 Parameters for line modeling (two-track line)

$\ell' = 0.75$ mH/km	$r_0' = 95$ m Ω /km	$L_u = 13$ mH
$c' = 20$ nF/km	Increase with $r' = r_0' \cdot \left\{ 0.15 \cdot \frac{f}{50\text{Hz}} + \left(\frac{f}{50\text{Hz}} \right)^{0.07} \right\}$	$R_u = 0.5$ Ω

Fig. 14.12b shows the impedance of this line, seen from the pantograph, in amplitude and phase vs. frequency, for the three vehicle positions $S1 = 0, 25$ and 50 km. The typical sequence of parallel and series resonances in the range of 1.2...2 kHz can be clearly seen, the region in which the spectrum of the 4q-C equivalent sum voltage has the strongest lines ($f_z = 11 \cdot 16^{2}/_3$ Hz, $f_{\text{dist}} = 2 \cdot 4 \cdot f_z = 1467$ Hz), situated at different frequencies according to the position of the locomotive. Please take into account that for $f = 2$ kHz the wavelength is only 150 km, which is not really big (\sim factor 10) against the lengths of the sections, so that it is only a rough estimation.

Fig. 14.12c finally shows the transfer function I_F/U_{SS} , seen by the equivalent 4q-C. For comparison, the corresponding function values neglecting the line capacitances ($c' = 0$) are entered as thin lines. Disturbing harmonics may be amplified or attenuated, in comparison with the (hypothetic) purely ohmic-inductive supply system. As the maxima cover the whole range between 1.3 and 2 kHz, dependent on the position of the vehicle, it is not really viable to improve the situation much by merely changing the switching frequency of the line converter.

In [219] several proposals were investigated, to identify the resonance behaviour of line filter and line and to correct the pulse patterns of the 4q-C in such way, that the concentration of spectral lines in bundles according to equ. (14.25) is avoided, if these coincide with detected line resonance frequencies. The procedure was viable on principle [225], but has not been introduced since.

If the railway supply voltage is distorted by high-power locomotives with phase-angle control, producing strong low-order harmonics (3rd, 5th and 7th), as e.g. observed in the eighties in Norway, the existing 4q-C control with a sinusoidal voltage control factor $k_1 = k_{\wedge} \cdot \sin(\omega t + \psi_1)$ according to equ. (6.21) produces in the DC-link voltage by modulation acc. to equ. (6.25) strong current components with double, fourfold and sixfold line frequency. Those with double line frequency will be taken up by the resonant tank circuit without any DC-link voltage component; but those of 4 and 6 times line frequency meet a rather low DC-link admittance, caused by the parallel resonance of the resonant tank circuit and DC-link capacitor and – maybe – the inverter control at certain motor frequencies. This may produce inadmissible voltage oscillations in the DC link, which can be compensated by a suited frequency-selective and load-dependent phase-shifting feed-forward of measured 3rd or 5th line voltage harmonic on k [226].

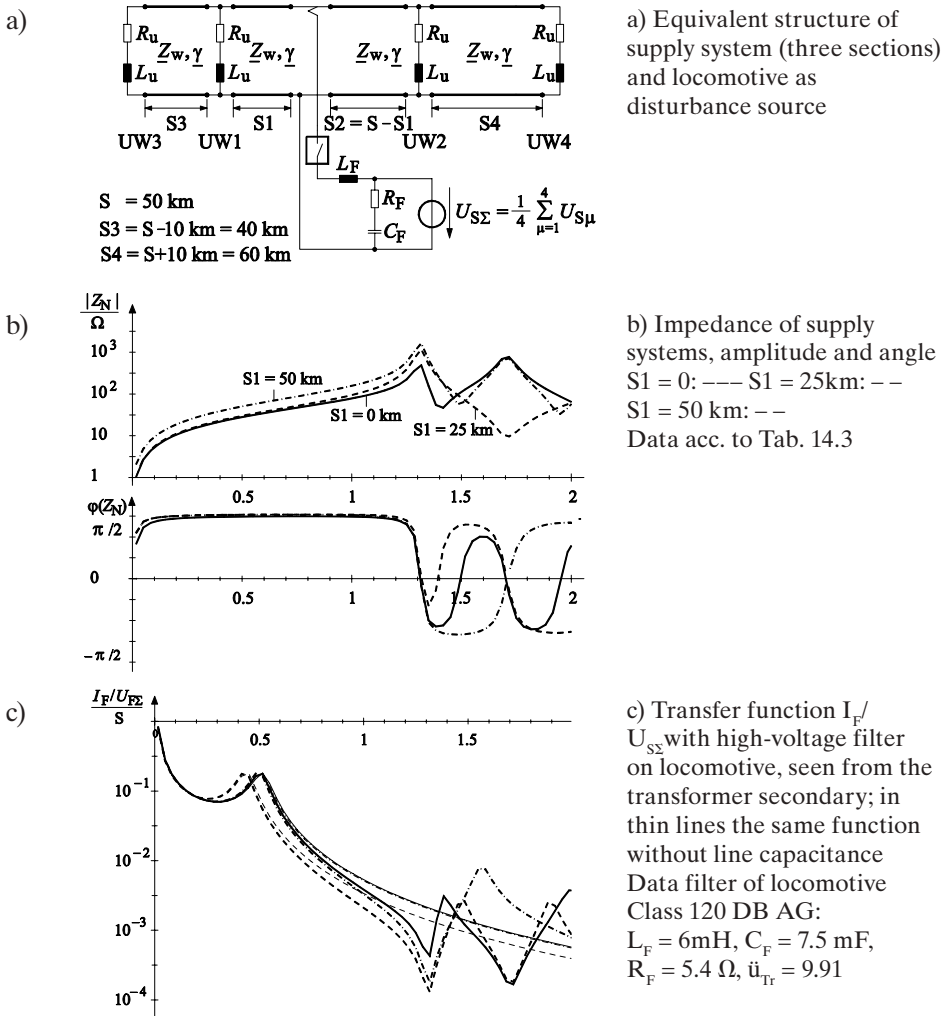


Fig. 14.12: Resonance in the railway supply system

Besides these voltage resonances, which can be regarded as impressed by quasistationary sources, several new effects have arisen in the last two decades, which can be attributed to the interaction of several vehicles with four-quadrant converters (and filters) between each other and with the line and the line supply (generators and power-electronic converters). In some frequency ranges the input admittance of the vehicle can exceed a critical negative real value, so that the control may become unstable. This has lead already to a collapse of the Swiss railway supply system in 1995 [212].

A lot of different types of power supplies (railway power stations, rotary and static converters) and transmission lines and filters has to be regarded; traction vehicles are delivered by different manufacturers in concurrence, applying different technologies which they do not want to reveal in detail. But as the free access of railway operators must be guaranteed without discrediting by the power system operator, the necessary compatibility should be secured by a formal compatibility process, as proposed in the draft for EN 50388 [227].

14.5 Mechanisms of coupling, psophometric interference current

Very often power and signal lines (track circuits, telecontrol links, telephone and telegraph circuits) of the railways themselves and of third parties are lying tightly parallel over a long distance with electrified railway lines, leading to mutual coupling and interference.

The mutual interference of public 50-Hz lines and 16 ²/₃-Hz railway supply lines and of DC and AC railway supply lines cannot be treated here; please refer to the relevant literature (e.g. [228], [229]). The scope of this book shall be limited to the interference of railway power lines with signal lines in the narrower sense, as it is important for the safety of railway transport and is strongly related to power-electronic control, the central topic of this book.

Coupling between railway power lines and signalling circuits is possible on a galvanic, inductive, capacitive and radiation way. The inductive coupling is the most important in the scope of this chapter. Coupling is always proportional to length and proximity of parallel laying, the so-called length of exposed section. Already 16 ²/₃-Hz lines with tap-changer-controlled traction vehicles forced to abandon the classical open-wire telephone lines parallel to the railway track and to cabling of these communication lines. The harmonics produced by converters induce much higher disturbance voltages, due to higher frequency [230], [231].

To assess the interference with telecommunication equipment globally, the "psophometric interference current" was introduced. It is an equivalent current with a frequency of 800 Hz, composed of the r.m.s. values of the individual current harmonics according to

$$I_{pe} = \sqrt{\sum_f (h_f \cdot p_f \cdot I_{Ff})}, \quad (14.33)$$

with h_f the coupling factor, p_f the noise weighting and I_{Ff} the current harmonic for the f -th harmonic frequency.

The coupling factor h_f is dependent upon many influencing variables. To assess the emission of disturbant currents by the traction vehicle globally, the interference current is measured with constant coupling $h_f = 1$ on the vehicle itself, according to e.g. VDE 0228 [213]. The noise weighting p_f has been defined according to the response of the telephone system and the frequency-dependent sensibility of the human ear in the "psophometric weighting function p_f " (e.g. VDE 0228), cf. Fig. 14.13.

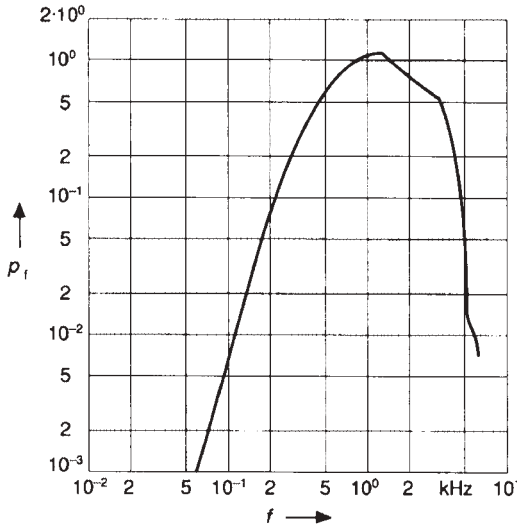


Fig. 14.13: Psophometric weighting factor p_f

This function has the unity value at 800 Hz and its maximum at 1.2 kHz. It results – as mentioned before – in a strong penalizing of the typical frequency content of four-quadrant converters in the 1...2-kHz range.

The influence of the line resonances described in the previous subchapter increases the interference current portion with (parallel) resonance frequency more than proportionally and in consequence the psophometric interference current – especially for pulse-converter traction vehicles – considerably. It may be even higher in locations far from the emitting source, e.g. in substations, or at other vehicles with input filters. These resonances have to be taken into account suitably when selecting and evaluating the different measures to be taken on the vehicle, to reduce the interference currents.

A probable means, used with many railways, to reduce the fundamental inductive voltage drop and the coupling for the harmonics is the booster transformer (Fig. 14.14). It forces the return current out of the rails into a return wire near to the contact wire; only in this section, where the traction vehicle actually is situated, the return current flows through the rails. This reduces the loop formed by contact wire and return conductor distinctly, the self-inductance and the coupling are reduced. In a similar way, the autotransformer circuit (section 13.2.2) lowers the impedance and the interference field intensity to roughly 1/4.

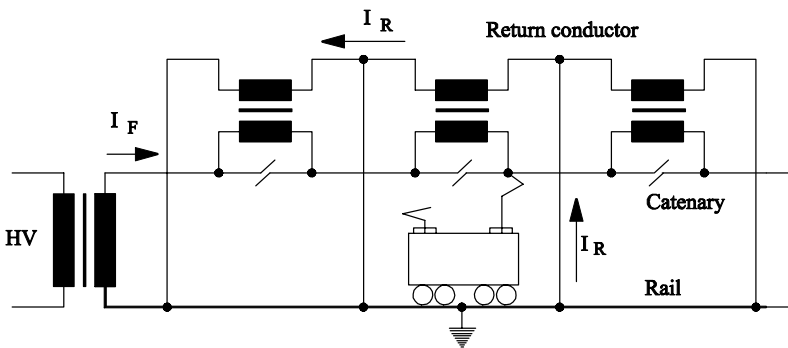


Fig. 14.14: Booster transformer circuit

14.6 Track circuits

Many railways use track relay circuits with AC of frequencies different from that of the power system, typically between 42 and 450 Hz, to detect occupancy or freedom of a track section. They can be disturbed by low-frequent traction current components.

Fig. 14.15 shows an elder 100-Hz track circuit with insulating joints in both rails, as used with DB on the open track [209], [210], [211], [231]. The block voltage is fed at the one end and measured at the other end of the surveyed section by a two-phase motor block relay. A wheelset in this section short-circuits this voltage and makes the relay drop out. The traction return current bypasses the insulating joints via common-mode transformers.

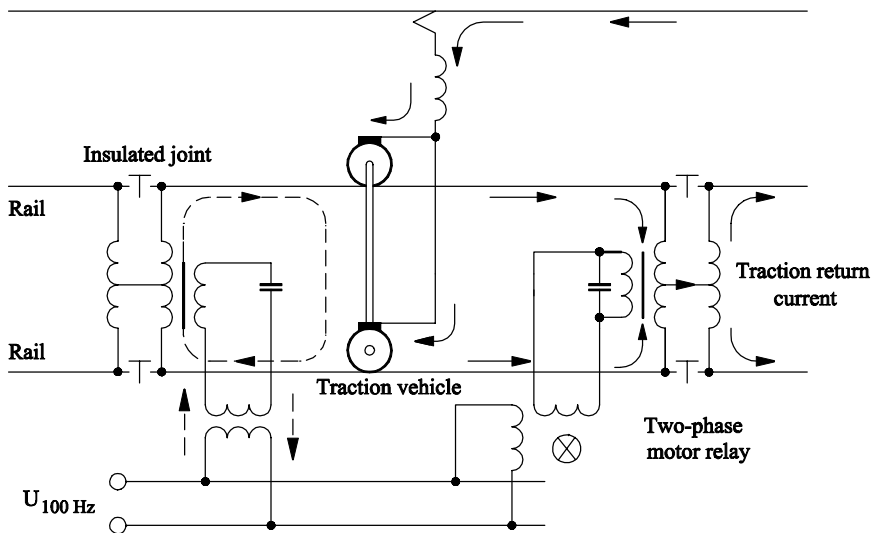


Fig. 14.15: 100-Hz track relay circuit with double-side insulating joints and track transformers

To make the motor relay pick up and produce a wrong “free” signal, the symmetrical flow of the return current must be interrupted e.g. by a broken rail or joint and the produced rail voltage drop must have the “right” amplitude and phase and persist for a minimum time. DB admits 2 A of 100 Hz for 0.5 s, to allow transients e.g. at magnetizing the transformer.

The operating principle of a recent audio-frequency track circuit is displayed in Fig. 14.16. In contrast to the 100-Hz circuit, it does not need insulating joints; to separate the detection sections, short-circuiting connections between the rails are used. Capacitors at the transmitting and receiving devices tune the rail inductivity to a resonant circuit for the audio-frequency of 9.5...14.5 kHz. The wheelsets in this section detune the resonant circuit by bridging the rail inductivity and make the voltage drop. These circuits use sensitive electronic amplifiers; traction return current components of some 20 mA are admitted in the audio-frequency range. More and more such circuits are coded, to increase immunity.

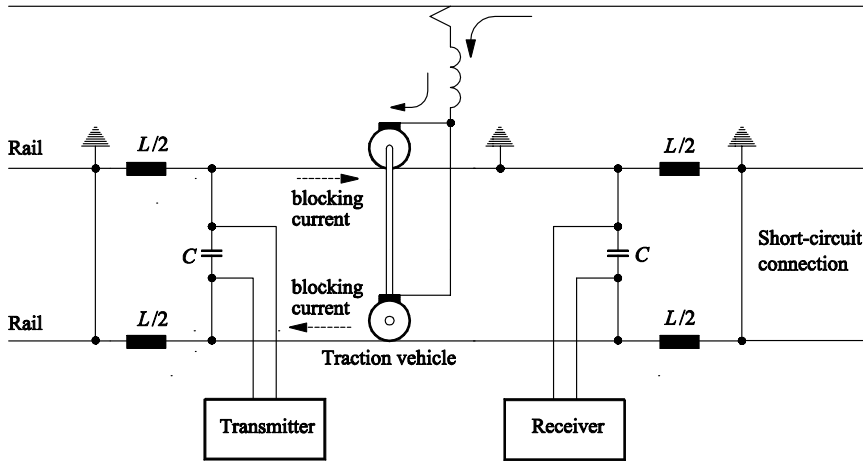


Fig. 14.16: Audio-frequency track circuit

14.7 Suppression of low-frequent interference currents of power-electronic converters

The four-quadrant converter does not produce even harmonics, if the DC-link voltage is smooth and the Pulse Width Modulation (PWM) meets the symmetry conditions. Nevertheless, on locomotive Class 120 100-Hz currents of up to 5 A have been measured in the initial phase [210]. These currents can be caused

- by unsymmetrical magnetization of the main transformer, e.g. at switch-on or at short interruptions by pantograph bouncing (“rush effect”) or by DC components produced by errors of PWM control,
- by modulation of harmonics of the DC-link voltage (section 14.3.5). As mentioned before, a DC-link voltage ripple (peak-peak) of 3,5 % U_{dN} at $f_x = 83.3$ Hz produces currents of about 0.14 % of rated current with 66.6 Hz and 100 Hz, i.e. ~ 0.5 A with a 5.6-MW/16 $\frac{2}{3}$ -Hz locomotive.

It can be seen that the influence of the magnetizing current is dominating.

For locomotive Class 120 of DB an “anti-control” was developed [233], [215]. It measures the 100-Hz component in the line current by means of a band-pass filter; this component is attenuated and added to the control of the 4q-C voltage (cf. Fig. 6.21, input “line current”). The 100-Hz line-current component can be limited to values under 0.5 A, as the 4q-C has enough control gain at an equivalent summed switching frequency of 1...2 kHz (section 14.3.4).

Similar methods were used with DC traction vehicles, to extinguish critical interfering current components by means of pre-choppers, used in the early times of three-phase traction [215]. Today these pre-choppers are out of use with light rail and mass transit equipment, but used occasionally again in multi-system locomotives (cf. subchapter 8.2).

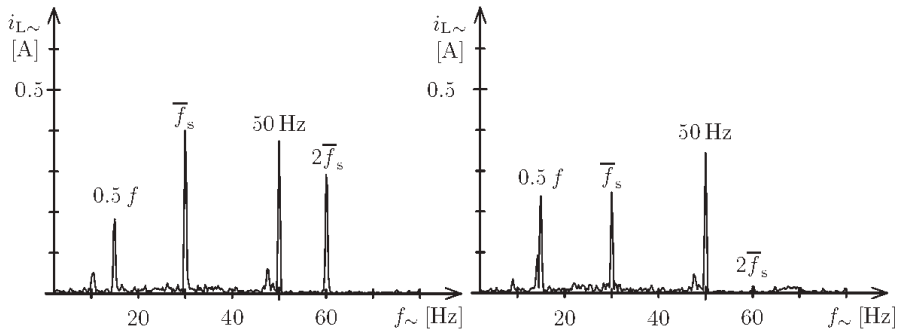


Fig. 14.17: Spectra of DC 750-V line current of a 120-kW drive without and with suppression of unwanted line-current portions (here: $2 \cdot f_s = 60$ Hz) via the torque set value

New highly dynamic torque control methods as e.g. field-oriented control or DSC and ISC (subchapter 6.3) have enough bandwidth of gain to impress DC-link current components in the wanted frequency range via torque control in counter-phase to the disturbant current component, so that the limits are kept. Fig. 14.17 demonstrates the method (which is in use with several LRT vehicles) by lab measurements of a 120-kW 4-pole IM drive, fed from a 750-V DC line. In the left part the original spectrum is shown, with lines at half, single and double IM stator frequency, due to imperfect symmetry of the PWM ($f_z = 2$ kHz), and at 50 Hz, due to asymmetry of substation rectifiers. In the right part, the anti-control for 60 Hz is active and suppresses the $2 \cdot f_s$ -line from 290 mA to less than 20 mA, which is more than -25 dB [234].

So called "active filters" have been discussed much in literature (e.g. [235]), as they are used in utility grids. They are inverters with high switching frequency, injecting current components in parallel to the input filter, compensating the interference currents. As the proof of reliability is difficult, they have not been used in traction. The first method is accepted, as the vehicle cannot be operated (and does not produce interference), if the inverter control fails.

14.8 High-frequent disturbance

High-frequent disturbances are of minor importance with AC railway systems; they are mainly produced by corona discharge at the isolators of the catenary and sporadically by arcs at the pantograph head. Rather seldom they are produced by the converters of the traction vehicles, only in case of unlucky resonances. Recently, the steep switching transients of IGBTs and occasionally the switching frequency of microcomputers and their switched-mode power supplies step forth. These disturbances are mainly coupled by radiation.

15 Appendix

15.1 Control strategies for traction induction motor drives

Revised version of the paper:

Steimel, A.: Control of the induction machine in traction. *Elektrische Bahnen* 96 (1998), Nr. 12, pp. 361–369 [65].

15.1.1 Demands by railway traction

While in traction the dynamic demand on the response to set-point changes is low due to reasons of comfort, the dynamic demand on disturbance behavior is rather high due to disturbances by input power interruptions as pantograph bouncing or loose of adhesion and slip-slide control. With the capability of the new power semiconductors GTO thyristor and IGBT, the rated powers of the inverter could be increased, and by that the demand on the control grew. A power of 1,750 kW had to be transferred to the rails at a wheelset load of only 21 t safely. This made a highly dynamic control inevitable, to exploit the available adhesion maximally, e.g. in form of wheel-creep control, operating near to the instability limit introduced by the maximum of the adhesion coefficient curve (subchapter 2.3).

For that reason the so-called "field-oriented" control strategies already introduced with industrial drives were applied with traction drives in the mid of the eighties. The high calculation power of Micro Controllers and Digital Signal Processors made such sophisticated control schemes possible. With the very high powers of locomotive and power head-car drives, the low switching frequency posed a special problem, initiating special solutions [49].

15.1.2 Space-phasor representation of three-phase systems

To be able to describe three-phase systems under dynamical conditions and with nonsinusoidal waveforms effectively, the so-called Space Phasor Theory was developed in the late fifties by *Kovacs* and *Racs* in Budapest [236]. It offers great advantages, especially if the three-phase quantities have the zero-sum quality. This is generally the case for the current in machines and networks with a free star point; for voltages it is fulfilled, if the voltages are measured against the zero point, which is defined by $\sum u = 0$. Then only two quantities are linearly independent; to treat them, the complex representation is most suited, facilitating graphical representation. Three pertaining (three-phase) time-dependent quantities $z_a(t)$, $z_b(t)$, $z_c(t)$, with z being a current, voltage or flux linkage quantity, form a space phasor $\underline{\underline{z}}$ (marked by an arrow under the symbol), as depicted in Fig. 15.1:

$$\underline{z}(t) = \frac{2}{3} \cdot \{z_a(t) + \underline{a} \cdot z_b(t) + \underline{a}^2 \cdot z_c(t)\} = z_\alpha(t) + j \cdot z_\beta(t) \tag{15.1}$$

with $\underline{a} = e^{j120^\circ}$. (If the z_v are not zero-sum quantities, the zero-sequence system

$$\underline{z}(t) = \frac{1}{3} \cdot \{z_a(t) + z_b(t) + z_c(t)\}$$

has to be treated separately; this is generally the case with PWM methods).

From a space phasor the three-phase quantities are regained by projection on the three coordinate axes a , b and c , shifted by 120° , as shown in Fig. 15.1, right:

$$z_a(t) = \text{Re}(\underline{z}(t)), \quad z_b(t) = \text{Re}(\underline{z}(t) \cdot \underline{a}^2), \quad z_c(t) = \text{Re}(\underline{z}(t) \cdot \underline{a}), \tag{15.2}$$

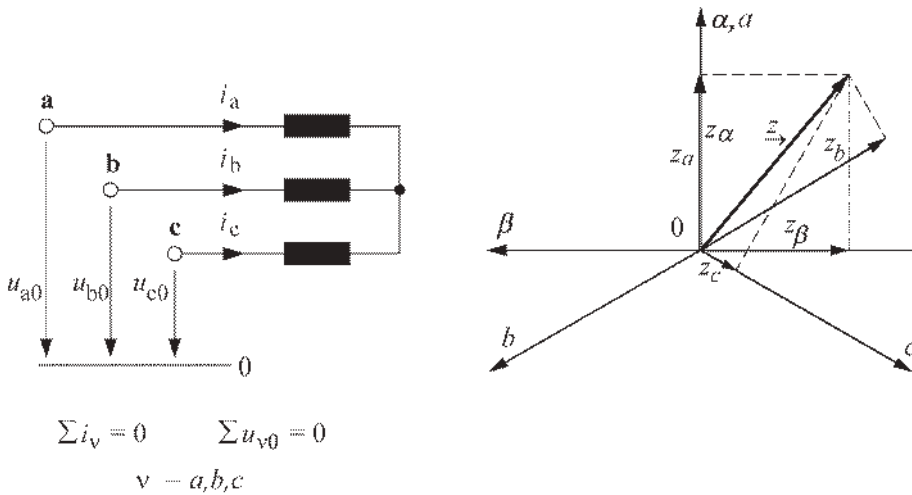


Fig. 15.1: Space-phasor representation of three-phase quantities

Calculations with space-phasor quantities are very similar to those with conventional electric quantities; in a coordinate transform between two rotating reference systems the law of sequential differentiation has to be obeyed (cf. textbook to lecture [V3] or [237]).

15.1.3 Dynamical equivalent circuit diagram of an Induction Machine

Fig. 15.2 shows the space-phasor ECD of an induction machine, which is fully valid in the dynamical case, too, in a reference system rotating with arbitrary frequency ω_B against the stator reference system. “Canonic” means that there are only two inductances connected to the upper star point, not three as in the T-ECD. The preconditions are:

- Symmetrical construction
- Windings distributed sinusoidally around the stator circumference
- Only fundamental-wave quantities regarded
- Constant parameters, i.e. no saturation or skin effects
- All rotor parameters already transformed to the stator side

For a detailed derivation, please refer to [V3].

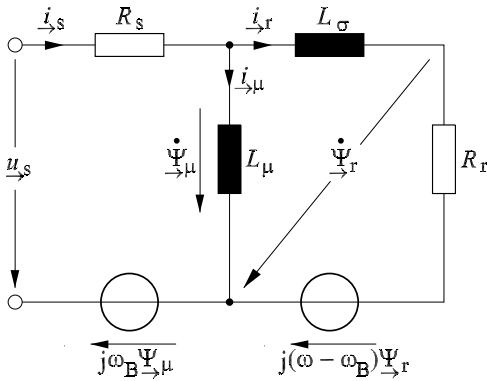


Fig. 15.2: Canonic Γ -ECD of an IM in a reference system rotating with ω_B against the stator reference system

The differential equations of the state variables stator and rotor flux linkage space phasors are:

$$\underline{\dot{\Psi}}_{\mu} = \underline{u}_s - R_s \cdot \underline{i}_s - j \cdot \omega_B \cdot \underline{\Psi}_r \tag{15.3}$$

$$\underline{\dot{\Psi}}_r = R_r \cdot \underline{i}_r + j \cdot (\omega - \omega_B) \cdot \underline{\Psi}_r \tag{15.4}$$

The stator-current space phasor will be obtained as:

$$\underline{i}_s = \underline{i}_{\mu} + \underline{i}_r = \left[\frac{1}{L_{\mu}} + \frac{1}{L_{\sigma}} \right] \cdot \underline{\Psi}_{\mu} - \frac{1}{L_{\sigma}} \cdot \underline{\Psi}_r \tag{15.5}$$

Torque can be calculated with the following two equations:

$$M_d = \frac{3}{2} \cdot p \cdot \text{Im} \left\{ \underline{\Psi}_{\mu}^{**} \cdot \underline{i}_s \right\} \tag{15.6}$$

$$M_d = \frac{3}{2} \cdot p \cdot \frac{1}{L_{\sigma}} \cdot |\underline{\Psi}_{\mu}| \cdot |\underline{\Psi}_r| \cdot \sin \vartheta \tag{15.7}$$

with p : number of pole pairs and

$$\vartheta = \delta(\underline{\Psi}_{\mu}) - \delta(\underline{\Psi}_r) \tag{15.8}$$

15.1.4 Field-oriented control

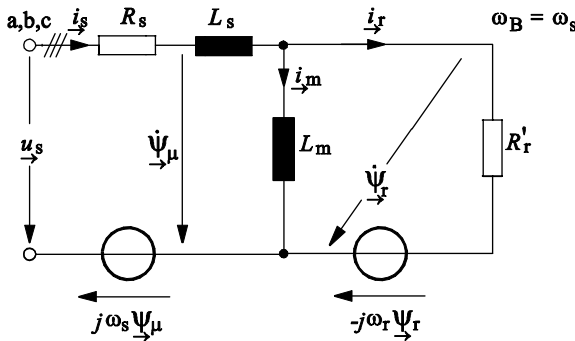
- **Basic idea**

From industrial control it was known already, that a nearly ideal control behavior results if the stator current is not controlled as a scalar quantity only (by its r.m.s. value, as e.g. in Fig. 6.16),

⁸ ** means the conjugate-complex value!

but vectorially, oriented at the machine flux-linkage space phasor. This principle of “field orientation” was developed in the late sixties; *Hasse* [238] showed that both stator and rotor flux linkage could be used. But as the equations for rotor-flux orientation are simpler due to linearity this approach was realized first and is now known as Field Orientation or Vector Control.

Fig. 15.3 depicts the so-called Inverse- Γ -ECD of the IM; it is most suited for analysis, if the stator current can be regarded as impressed. The reference coordinate system is assumed as rotating with the rotor-flux space phasor ($\omega_B = \omega_s$).



Conversion of parameters from Γ - to Inverse- Γ ECD:

$$R_r' = (1 - \sigma)^2 \cdot R_r \tag{15.9}$$

$$L_m = (1 - \sigma) \cdot L_\mu \tag{15.10}$$

$$L_s = (1 - \sigma) \cdot L_0 \tag{15.11}$$

Fig. 15.3: Canonic Inverse- Γ -ECD of an IM in the rotor-flux-fixed reference system

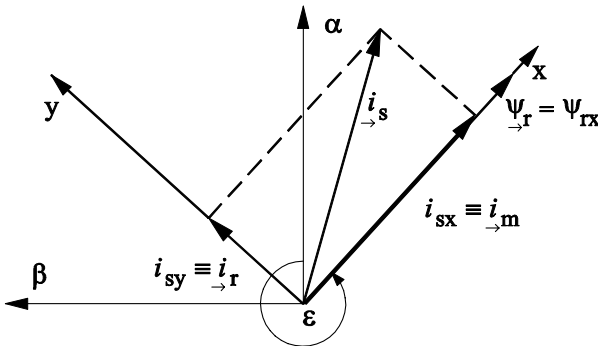


Fig. 15.4: Orientation of stator current and rotor flux in the α, β and x, y reference systems

In Fig. 15.4 the pertaining space-phasor diagram can be seen: The x axis of the reference system coincides with the direction of the rotor flux space phasor; its angle against the stator-fixed α, β reference system is ϵ . The stator-current space phasor i_s is decomposed by projection onto the x axis in a flux-determining component $i_{sx} = \text{Re}\{i_s\} = i_m$ and an orthogonal, torque-determining component $i_{sy} = \text{Im}\{i_s\} = i_r$. The last conception implies, that the rotor flux is always controlled to a constant amplitude. Both quantities are subjected to linear control as known from the DC machine, as being constant quantities in the quasi-steady state.

Now there are three main tasks:

- To identify the position of the rotor flux in the stator-winding-fixed reference frame, even at standstill
- To do the necessary computations, especially the coordinate transformations, in “real time”
- To impress the current as demanded by control with an high-power inverter with restricted switching frequency

• **Direct Field Orientation**

If the speed is not too low rotor flux is best calculated from measured stator voltages and currents by a real-time machine model. This is now known by the term “Direct Field Orientation” and has been developed originally by *Blaschke* [239]. See Fig. 15.5:

The machine or flux model consists of the integral equation

$$\underline{\Psi}_r = \int (u_s - R_s \cdot i_s) \cdot dt - L_s \cdot i_s + \underline{\Psi}_{r0} \tag{15.12}$$

The so-called “Vector Analyzer” VA calculates the modulus of the rotor-flux space phasor

$$|\underline{\Psi}_r| = \sqrt{\Psi_{r\alpha}^2 + \Psi_{r\beta}^2} \tag{15.13}$$

and the transformation angle between stator-fixed and rotor-fixed reference system

$$\varepsilon = \arctan [\Psi_{r\beta} / \Psi_{r\alpha}] \cdot (1 - \text{sgn} [\Psi_{r\alpha}]). \tag{15.14}$$

The “Vector Rotator” VR calculates the x, y coordinates of i_s , referring to $\underline{\Psi}_r$:

$$i_s^{x,y} = i_s^{\alpha,\beta} \cdot e^{-j\varepsilon(t)} \tag{15.15}$$

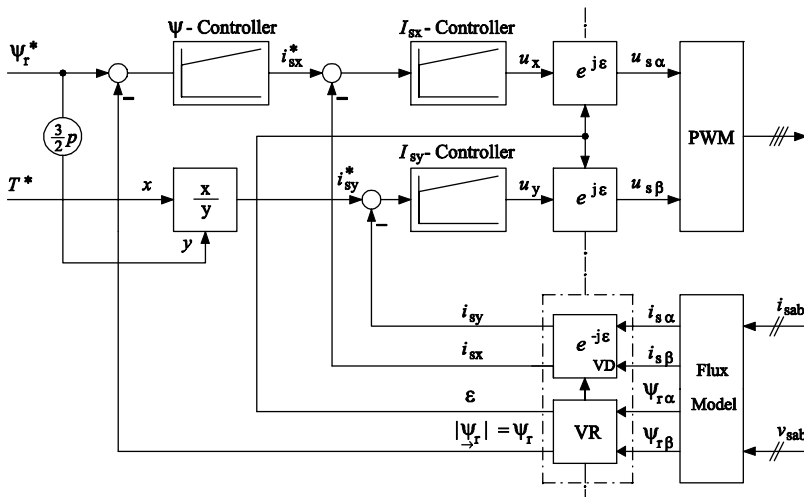


Fig. 15.5: Principle of Direct Field Orientation (DFO)

The set value of rotor flux (space-phasor modulus) is compared with the actual value, delivered by the Vector Analyzer, in a linear PI-type controller, yielding the set value of the flux-determining component i_{sx}^* . The set value of the torque-determining component i_{sy}^* is calculated from torque set value and rotor-flux-modulus set value:

$$i_{sy}^* = \frac{M_d^*}{3/2 \cdot p \cdot \Psi_r^*} \tag{15.16}$$

These two set values are compared with the respective actual values, delivered by the Vector Rotator. The outputs of these controllers are transformed back to the stator-winding-fixed ref-

erence system by an angular rotation by $\exp \{j\varepsilon(t)\}$ and handed to the Pulse Width Modulator. This control is independent of the value of the rotor resistance and does not need a temperature pick-up. But it cannot perform starting, as the open integration drifts away. To compensate that, high-pass filters have to be added, worsening the behavior at low stator frequency.

• **Indirect Field Orientation**

This problem does not occur with Indirect Field orientation, as introduced by *Jötten* and *Hasse* [238]. Please refer to Fig. 15.6: The rotor position angle

$$\xi(t) = \int \omega \cdot dt \tag{15.17}$$

is calculated from the integration of the pulses delivered by an incremental encoder. As already assumed, the rotor flux is controlled constantly in the rotor-flux-fixed reference system, so that $\Psi_{ry} = 0$ and $d\Psi_{rx}/dt = d\Psi_r/dt = 0$ hold. Then the rotor equation is formulated as:

$$\omega_r \cdot \underline{\Psi}_r = \underline{i}_r \cdot R_r = \omega_r \cdot L_m \cdot \underline{i}_m \tag{15.18}$$

Using the torque equation

$$M_d = \frac{3}{2} \cdot p \cdot L_m \cdot |\underline{i}_m| \cdot |\underline{i}_r|, \tag{15.19}$$

the rotor-frequency set value

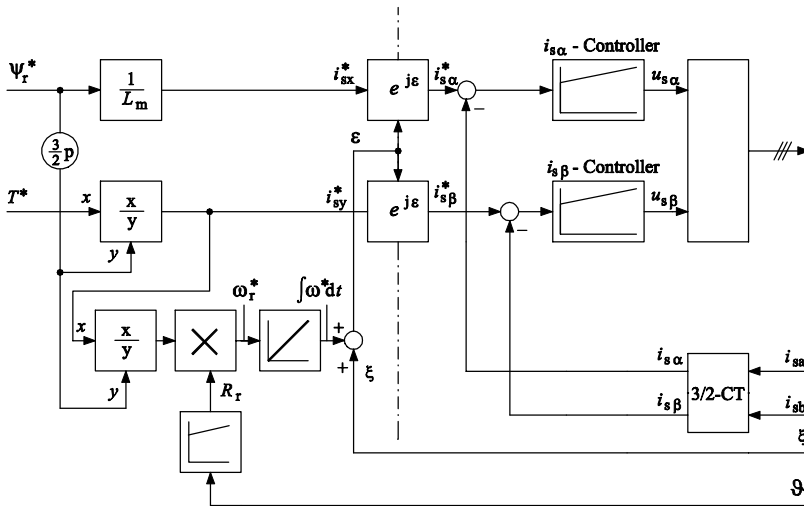


Fig. 15.6: Principle of Indirect Field Orientation (IFO)

$$\omega_r^* = \frac{R_r}{\frac{3}{2} \cdot p \cdot |\underline{\Psi}_r|^2} \cdot M_d^* \tag{15.20}$$

is calculated from the torque set value M_d^* . This quantity is again integrated and added to the rotor position angle $\xi(t)$, delivering the angle $\varepsilon(t)$, necessary for transformation.

The x, y components of \underline{u}_s are computed in the Decoupling Unit which compensates the strong mutual inductive coupling by L_s . They are then transformed into α - β coordinates and handed to the PWM unit producing the asynchronous or the synchronized optimized pulse patterns at low or medium frequency, respectively.

Rotor-field orientation has proved a very efficient control strategy for all kinds of induction motor drives, from servo drives to cycloconverter-fed mill drives or to the TRANSRAPID linear-motor drive. Advantageous is the linearization of the control loop by the coordinate transformation, the torque response is as good as the current response. A modern solution using 32-bit DSPs is described in [61].

Certain drawbacks may be seen when this rotor-flux orientation scheme is applied to high-power VSI-fed traction drives:

- Synchronized PWM exploits the low switching frequency (≤ 250 Hz) insufficiently, only in few operating points: E. g. at the change-over from five-fold to three-fold switching the switching frequency after the change is only 60% of the allowed value, with increased torque ripple, peak current and DC-link interference [74, 217].
- The time-triggered generation of pulses in the range of optimized pulse patterns makes the drive sensitive to swift changes of the input voltages, typical for railway applications.
- The calculation of the current set values in the field-weakening region is complicated and time-consuming; the torque response achieved up to now is several 10 ms, compared to some 3 ms in the region of constant flux.

15.1.5 Direct Self Control

A new control strategy overcoming these drawbacks is Direct Self Control (DSC) invented by *Depenbrock* in 1984 [63], [64], [240]. It calculates flux and torque as instantaneous values directly in the stator-fixed reference frame and controls both by simple two-level controllers, giving directly the firing signals for the inverter valves. This asynchronous control exploits the low switching frequency fully; phasor transformations with trigonometric functions are not necessary.

As DSC starts with impressed voltages, not currents, we choose the Γ -ECD (Fig. 15.8) with the leakage inductivity concentrated in the rotor mesh, to have the stator circuit as simple as possible; the reference systems is stator-winding-fixed, accordingly ($\omega_B = 0$).

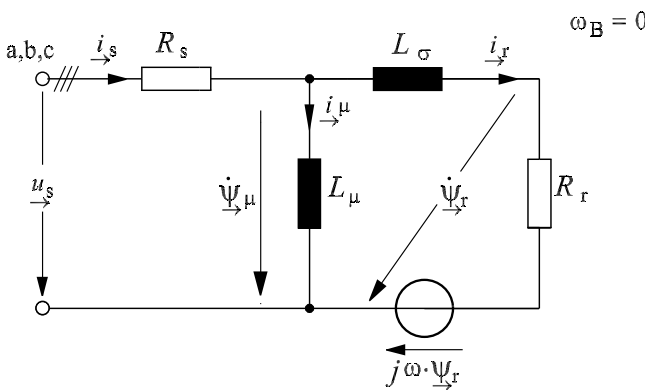


Fig. 15.8: Γ -ECD of IM in stator-fixed reference system

• **Operation at rated speed, Flux Self Control**

We start analysis at rated speed (point ‘1’ acc. to Fig. 6.9). The stator-voltage space phasor \underline{u}_s (Fig. 15.9) can only occupy the discrete six outer positions $v = 1$ to 6. The stator-flux space phasor $\underline{\Psi}_\mu$ follows according to the integral of the magnetizing voltage.

$$\underline{\Psi}_\mu = \int (\underline{u}_s - R_s \cdot \underline{i}_s) \cdot dt + \underline{\Psi}_{\mu 0} \tag{15.24}$$

on a hexagonal track curve if the six space phasors are switched cyclically.

This is already known from square-wave modulation. The new idea is not to command a time-dependent voltage pattern but to let the flux decide at the corners of the hexagon which stator voltage space phasor to turn on for the next sector. The projections of the flux space phasor onto the β axes $\beta_a, \beta_b, \beta_c$ give the necessary information. These β -flux coordinates showing trapezoidal waveforms are compared with the control threshold Ψ_μ^* .

In the rotor mesh (Fig. 15.8) the equation

$$\dot{\underline{\Psi}}_r = j\omega \cdot \underline{\Psi}_r + \frac{R_r}{L_\sigma} \cdot (\underline{\Psi}_\mu - \underline{\Psi}_r); \tag{15.25}$$

holds; integrating this delivers the space phasor of the rotor flux which runs approximately on a circular track curve, and can only be changed obeying the rotor short-circuit time constant L_σ/R_r .

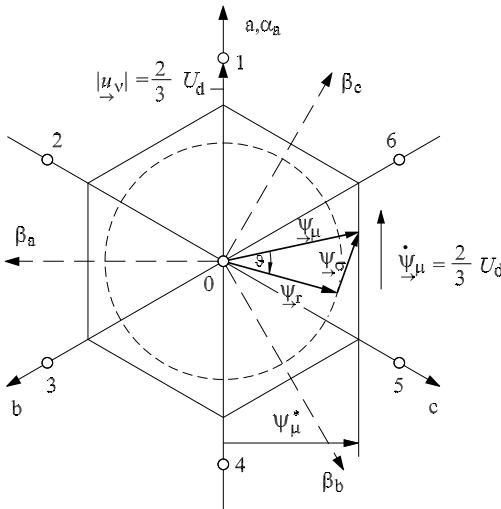


Fig. 15.9: Space phasors of inverter output voltages and of stator flux

Torque is obtained either by

$$M_d = \frac{3}{2} \cdot p \cdot \{ \Psi_\alpha \cdot i_{s\beta} - \Psi_\beta \cdot i_{s\alpha} \} \tag{15.26}$$

or

$$M_d = \frac{3}{2} \cdot p \cdot \frac{1}{L_\sigma} \cdot |\underline{\Psi}_\mu| \cdot |\underline{\Psi}_r| \cdot \sin \vartheta. \tag{15.27}$$

To increase the torque the flux threshold Ψ_{μ}^* has to be lowered by a linear controller, to increase the angular velocity of the stator-flux space phasor at given track speed ($\sim U_d$) by a shorter track curve, which increases the load angle ϑ and thus the torque M_d .

• **Control of Inverter Voltage Amplitude**

If a speed lower than rated speed is demanded at rated flux, the mean speed of the stator-flux space phasor on its trajectory must be reduced to obtain a revolution in a longer time period. As the tracking speed $d\Psi_{\mu}/dt$ is constant, equal to $2/3 \cdot U_d$, this must be performed by inserting zero-voltage states at which the stator-flux space phasor halts, which is equivalent to pulsing.

How often and how long the zero states have to be inserted is decided by a two-level torque controller: If the actual torque is bigger than the set value M_d^* , increased by half the hysteresis width ε_m , the angle ϑ has to be decreased by inserting the zero state, and vice versa. The torque is free from low-order harmonics, its rise-time is highest possible with given DC-link voltage and leakage inductivity (2 ... 3 ms).

• **Practical Implementation in Traction Drives**

Fig. 15.10 shows the basic structure of the DSC implemented on the GTO-thyristor inverter traction equipment of ABB/ADtranz in Germany and Switzerland, in now more than 2000 locomotive and metro applications.

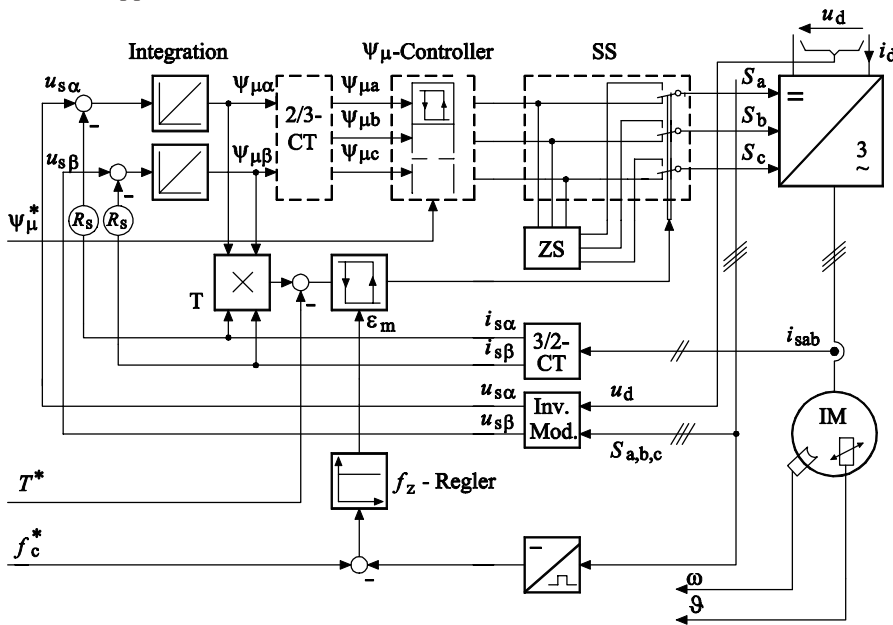


Fig. 15.10: Structure of Direct Self Control (DSC)

The stator mesh model (top left) computes the α, β stator-flux coordinates; the 2/3-Coordinate Converter 2/3-CT forms the three $\beta_{a,b,c}$ fluxes, which are compared with the set value Ψ_{μ}^* in the Flux Controller. Stator voltages need not to be measured, but are modeled from DC-link voltage and the switching signals in the Inverter Model.

Torque is computed in block T from the stator-flux and the stator-current components and compared in a Schmitt Trigger acting on the Signal Select SS choosing either the voltage space

phasor preselected by flux self control or the zero state; Zero Select ZS chooses that zero state which can be reached with only one switching.

Exactly six switchings are necessary to lead the flux space phasor once around the hexagon; the remaining switchings are used for keeping the torque within the band. So the pulse frequency is nearly 50% greater than with sinusoidal PWM. The switching frequency f_z keeps always the allowed value by controlled adaption of torque hysteresis. Thus motor and DC-link current harmonics and torque ripple are at least equivalent, mostly lower than with synchronized PWM with same maximum switching frequency [217], [242]. By processing always instantaneous values DSC is very robust against DC-link voltage disturbances.

The calculations in the machine and inverter models and the controllers are rather simple, as no trigonometric functions are needed; the necessary speed for direct two-level control is achieved by use of the DSP Texas Instruments TMS 320C50. A whole cycle is calculated in 50 μ s.

Fig. 15.11 shows a simplified simulation of the most important quantities of DSC at mean speed ($a = 0.5$ at $R_s = 0$). In the top line the torque, normalized to rated torque) is displayed, shifted by +1, oscillating within its tolerance band; it is free from low-frequent harmonics.

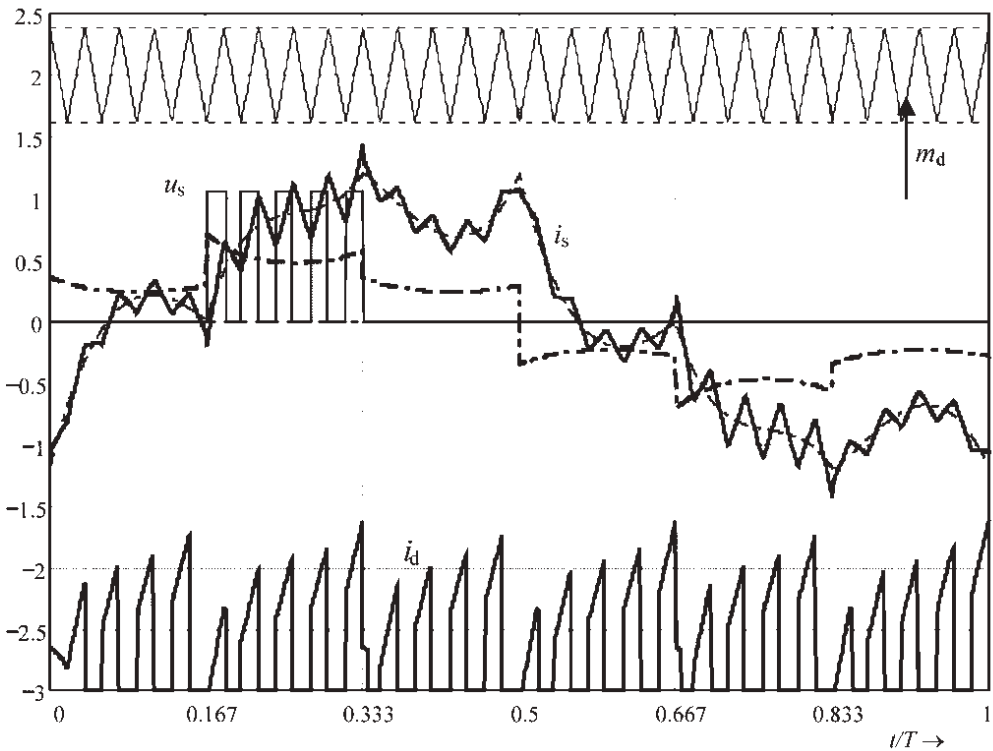


Fig. 15.11: Torque, phase voltage, phase current and DC-link current
 $a = 0.5$, $m = M_{dN}/M_{dK} = 0.4$; $\sigma = 10\%$. $f_z = 5 f_{s0}$

Below the ideal average value of the phase voltage per pulse period is displayed as a dash-dotted line, and the pulsed phase voltage – to improve clearness only in the 2nd sector, the “active” sector, in which the torque controller acts directly on this voltage (same in the 5th). As a bold line the

phase current is shown, with its typical six-pulse “garland” distortion; thin-dashed is the average value per pulse period. At the bottom line, the DC-link current is to be seen.

- **Dynamic field weakening**

In the field-weakening range optimal dynamic behavior is obtained by the so-called Dynamic Field Weakening, which is very easily applied to stator-flux-oriented control. At a demanded torque rise the flux is weakened by a short-cut A–B–E of the flux trajectory instead of the stationary track A–B_{stat}–E_{stat} (Fig. 15.11). With the distances A–E and A–E_{stat} being equal, the flux angle (and thus torque) is increased very fast by $\Delta\vartheta_E$ [240]. Torque is reduced similarly by decreasing the flux angle ϑ by inserting zero-voltage states. Thus DSC reaches a similar dynamic torque response time in the field-weakening range as in the voltage control range, of about one third of the base period (e.g. 3 ms at $f_s = 100$ Hz).

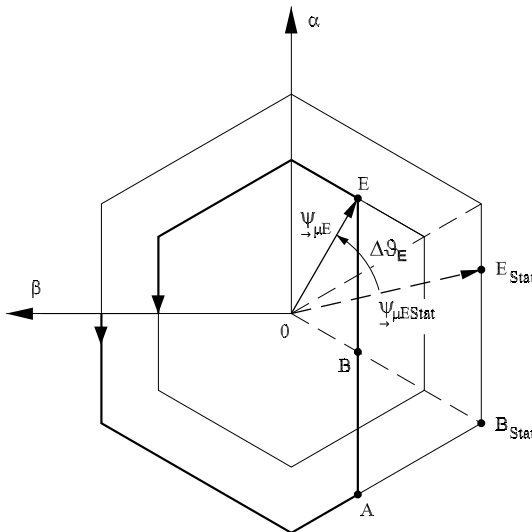


Fig. 15.12: Stator-flux trajectory at Dynamic Field Weakening

- **Operation in the starting region**

At very low frequencies two problems arise:

- The error due to the resistive stator voltage drop deflects the flux track curve inwards, the six controlling actions at the corners are not enough any more, the flux will be weakened. Flux hysteresis control needs additional switchings, similar to asynchronous PWM.
- At low speed the integration of the stator mesh equation only is not sufficient anymore, as mentioned with Direct Field Orientation. The machine model must be extended by the rotor mesh, and change its character to a current-rotor-frequency model.

A PWM scheme with stator-flux-derived reference values, the Indirect Stator-quantities Control (ISC), guiding the stator flux space phasor on a circular track, can do this simpler, while the advantages of stator-flux orientation, especially the robustness, remain.

As ISC used with high-power GTO inverters in the starting region is very similar to that used for fast-switching IGBT inverters in the whole speed range, it shall be described commonly in the form used for the latter, as this is more important for future applications [241].

15.1.6 Indirect Stator-quantities Control

The stator mesh model known from DSC is completed by the rotor model using rotor speed and temperature. The model stator currents are compared with the measured stator currents to compensate model-flux errors; the gain of this observer has to be decreased adaptively at higher speed.

To lead the stator-flux space phasor on the wanted circular track the radius (the flux space-phasor modulus) is set by the linear flux controller via k_ψ , the angle increment $\Delta\chi_{\mu}$ (χ_{μ} is the angle of stator flux in α - β coordinates) by the PI torque controller, backed by an ω_s -feed-forward control. With k_ψ and $\Delta\chi_{\mu}$ the stator-flux increment in period n , $\Delta\Psi_{\mu}(t_n)$ is predicted from the stator-flux space phasor of the previous pulse period t_{n-1} in a dead-beat fashion by

$$\Delta\underline{\Psi}_{\mu}(t_n) = [(1 + k_{\psi}) \cdot \exp(j\Delta\chi_{\mu}) - 1] \cdot \underline{\Psi}_{\mu}(t_{n-1}) \tag{15.28}$$

This flux change, divided by the pulse period T_m and corrected by the resistive stator voltage drop $R_s \cdot i_s$ gives the stator-voltage space phasor u_s , to be executed by PWM. While with slow-switching GTO inverters the PWM algorithm still can be calculated during the minimum off-time of the devices in the DSP itself [12], with IGBT inverters an additional PWM chip, e. g. a FPGA, is necessary.

The practical implementation is shown in Fig. 15.13: The left part of the figure displays the completed machine model, while in the top the torque control is shown. Torque set and actual value are transformed to rotor frequencies by multiplication by $R_r / (\frac{3}{2} \cdot p \cdot \Psi_r^2)$, which simplifies ω_s -feed forward and break-down protection (region '2'...'3' in Fig. 6.9!). Multi-lication with pulse period T_m yields the angle increment $\Delta\chi_{\mu}$.

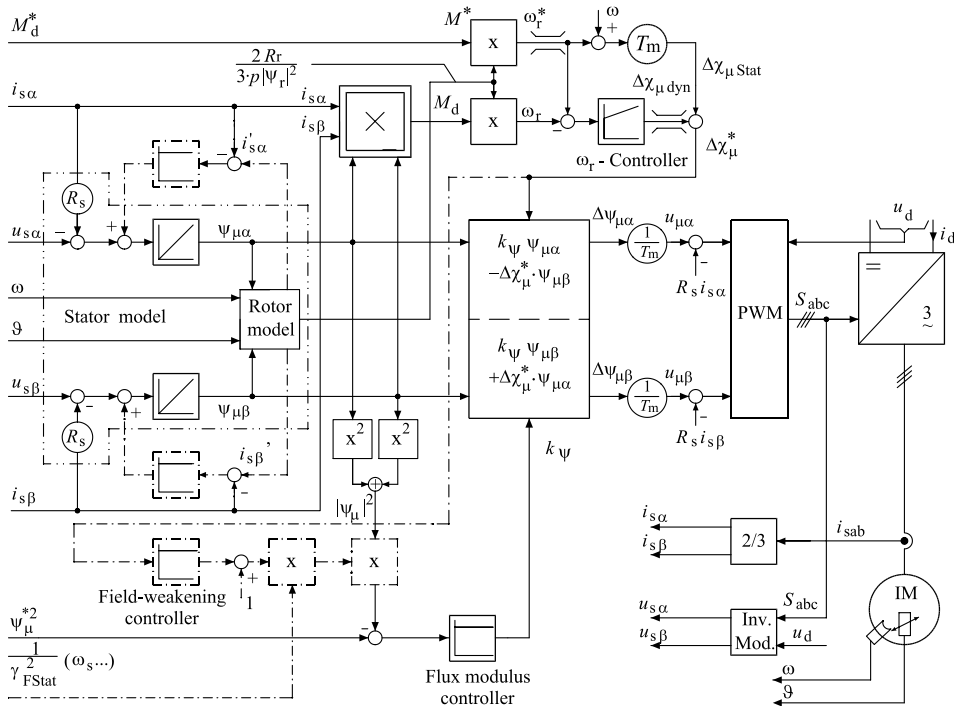


Fig. 15.13: Structure of Indirect Stator-Quantities Control (ISC)

In the lower part the flux-modulus controller is to be seen; manipulation of squares avoids calculation of the roots which is time-consuming in DSPs. In the voltage-control range the whole torque dynamic is produced via change of the voltage only, while the flux modulus stays at its rated value. In the field-weakening range the demanded angle increase cannot be obtained anymore, as the voltage is already at its maximum value. The stationary flux weakening γ_{stat}^2 is calculated as a feed-forward; its inverse increases the actual flux feed-back and achieves in this way field weakening.

The uncompensated output $\Delta\chi_{\text{st}}$ of the rotor-frequency controller is used to reduce the stator-flux modulus dynamically to the value necessary for fast torque response, via increase of the feed-back (dash-dotted lines).

Fig. 15.13 shows the torque response of an IGBT-inverter test drive at step changes of the torque set value, together with the corresponding square of the flux modulus and the voltage control ratio $|a|$; torque is normalized to break-down torque, flux to rated flux: At a positive step of M_d^* the voltage stays at the maximum value, while the stator flux is reduced considerably. Thus a torque rise time of about 6 ms (one third of the base period of about 19 ms) is achieved [241]. The dynamics of the negative torque step are mainly achieved by voltage variation, while the stator-flux modulus follows slowly the stationary demand, as to avoid over-currents due to fast changes of the leakage flux as the difference of stator flux and the slowly changing rotor flux.

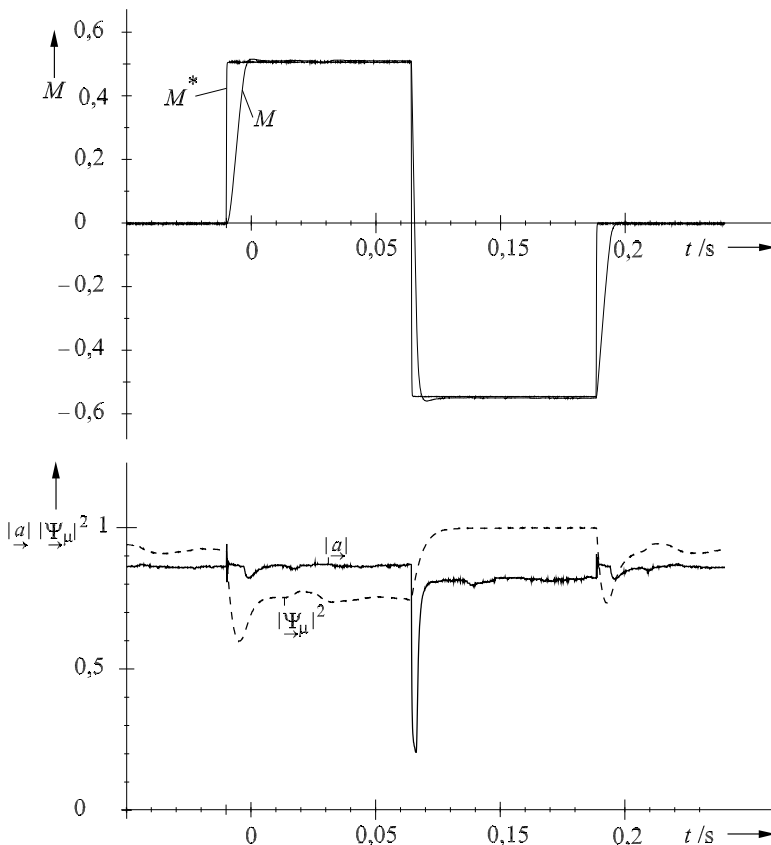


Fig. 15.14: Torque response with ISC range in the field-weakening range ($\omega = 1.05 \omega_0$)

15.1.7 Conclusion

Three control schemes used most widely for traction induction-motor control are examined and compared with the preceding slip-frequency-current-characteristic control, described in subchapter 6.3:

Slip-frequency-current-characteristic control impresses the stator current r.m.s. value together with the necessary slip frequency, which is then added to measured rotational speed. This gives good steady-state behaviour, but torque response and disturbance behavior are poor as in the transient the angular relations are rather undefined. For new equipment it is not state-of-the-art anymore.

Rotor-Field Orientation impresses the stator current in the correct phasorial relation to the rotor flux in the dynamic case, too. The flux- and the torque-determining current components are controlled by (originally) linear PI-controllers. The dynamic response is good, except for very low switching frequency as the current controller cannot impress the current in the expected way, and in the field-weakening range as tedious calculations are necessary to calculate current set values satisfying the voltage limitation. In addition synchronized Pulse Width Modulation “wastes” the restricted switching capability of the inverter.

That was the incentive for Direct Self Control. It leads the stator-flux space phasor on a preferably hexagonal track curve which economizes the switching capability best; the revolution speed on this track curve is governed by the two-level torque controller directly, no additional PWM is necessary. The modelling of the machine is more complex but with customary Digital Signal Processors all calculations can be solved quick enough for simple two-level control. Direct stator-flux control can improve the dynamic performance in the field-weakening range decisively by so-called Dynamic Field-Weakening; the drive is very insensitive against abrupt input-voltage changes typical for traction applications.

If restricted switching frequency is not the first issue (as with IGBT inverters for light rail applications) the principle of instantaneous stator-flux-orientation introduced with DSC can be used with PWM very well, too, in Indirect Stator-Quantities Control (ISC). The flux is then led on a circular track curve, the torque is controlled by its average over the pulse period only, not directly; hence the name. Dynamic field-weakening gives the same unprecedented dynamic torque response in the field-weakening range as in DSC, without any need for a voltage control margin, which is of eminent importance for highly-exploited traction drives. ISC is provided for the starting region of GTO-inverter DSC drives, too, avoiding problems with inverter dead-time of direct two-level control.

15.2 Speed-sensorless stator-flux-oriented control of induction motor drives in traction

Adapted version of the paper:

Depenbrock, M.; Foerth, Ch.; Hoffmann, F.; Koch, S.; Steimel, A.; Weidauer, M.: Speed-sensorless stator-flux-oriented control of induction motor drives in traction.

Communications – Scientific Letters of the University of Zilina 2–3/2001, pp. 68–75 [66]

Abstract: Indirect Stator-Quantities Control (ISC) combines the principle of stator-flux orientation proven successful in Direct Self Control (DSC) with Pulse-Width Modulation (PWM). High torque dynamics and robust behavior against input voltage disturbance are achieved in the whole operation range including field weakening. After careful correction of inverter-voltage errors and DC portions in the stator fluxes and currents not necessary for the actual operation point, the difference of the stator-current space phasors in the machine and in the controlled model is employed for speed and stator-resistance estimation, allowing to dispense with speed sensors. A special flux management allows infinitely slow change between driving and braking.

15.2.1 Introduction

In the eighties of the last century Vector Control of induction machines already successful with industrial drives was introduced in traction, too [65]. As well known it impresses the components of the stator-current space phasor in orientation to the rotor-flux space phasor by means of control. In traction drives with high power this approach was limited, as the switching frequency is in general too low to impress the currents sufficiently well.

In 1984 M. Depenbrock proposed ([63], [65]) to orient the space phasor of the stator voltage directly at the space phasor of the stator flux, which is obtained in a very simple manner as the integral of the magnetizing stator voltage, according to Faraday's Law. In Direct Self Control (DSC) the stator-flux components activate the suited next voltage switching when they reach predetermined thresholds. Thus flux guides itself on its trajectory symmetrical to the origin and controls the magnetization of the machine. Torque is controlled by varying the track speed, in DSC simply by a torque hysteresis controller which actuates pulsing and makes a separate Pulse Width Modulator unnecessary. Flux Self Guidance makes the drive insensitive to input-voltage disturbances met typically in traction, as e.g. by pantograph bouncing. Asynchronous pulsing exploits the limited switching frequency best compared to synchronized pulse patterns [217], [242] used elsewhere.

In the nineties IGBT inverters superseded GTO-thyristor inverters in the range of low and medium powers as typical for Light Rail and Metro applications, allowing distinctly higher switching frequencies. In the first years of this century the same happened with inverters for locomotives and high-speed trains. The question arose how to transfer the advantages of Direct Stator Flux Control to these new inverters, which made some of the old restrictions obsolete. With a sufficient ratio of switching to stator base frequency, sinusoidal PWM can be used without drawback, making the traction drive easier to adapt to severe line harmonic limitations. It has been already employed with DSC-controlled GTO-thyristor inverters in the starting region [64], where DSC shows some complications [65].

As stator-flux oriented control uses the complete machine model already it can be well applied for estimation of speed from the terminal quantities. As often additional broadband volt-

age sensors are not wanted, careful compensation of the inverter-voltage errors is to be applied when the voltage is modelled from measured DC-link voltage and switching commands. Then robust estimator schemes can be applied to estimate two parameters, e.g. rotational speed and stator resistance, from the difference of the space phasors of machine and model currents. As the model is of the linear fundamental-wave type, the system is unobservable at stator frequency being permanently zero. Nevertheless a special management of the flux magnitude enables the drive to operate permanently at any speed around and at zero.

15.2.2 Model of the induction machine

Each highly dynamic flux-oriented control needs a model of the induction machine as exact as possible to calculate the non-measurable fluxes. On the other hand it must be calculable in sufficiently short time on a Digital Signal Processor (DSP). Space-phasor notation (section 15.1.2, [236]) is used for description, denoted by arrows under the letter symbols. For stator-flux orientation the "canonical" Γ -Equivalent Circuit Diagram (ECD), with the leakage inductance L_σ concentrated in the rotor mesh, using the stator-winding-fixed reference system is most convenient (Fig. 15.15), as already explained in subchapter 15.1.

It describes the fundamental values of all quantities correctly. Saturation of the main inductance L_μ is measured off-line and taken into account by a characteristic dependent on stator-flux magnitude. The stator resistance R_s must be identified on-line.

The state equations can be derived according to this ECD:

$$\underline{\dot{\psi}}_\mu = \underline{u}_s - R_s \cdot \underline{i}_s \tag{15.29}$$

$$\underline{\dot{\psi}}_r = R_r \cdot \underline{i}_r + j \cdot \omega \cdot \underline{\psi}_r \tag{15.30}$$

The stator current is:

$$\underline{i}_s = \underline{i}_\mu + \underline{i}_r = \left[\frac{1}{L_\mu} + \frac{1}{L_\sigma} \right] \cdot \underline{\psi}_\mu - \frac{1}{L_\sigma} \cdot \underline{\psi}_r \tag{15.31}$$

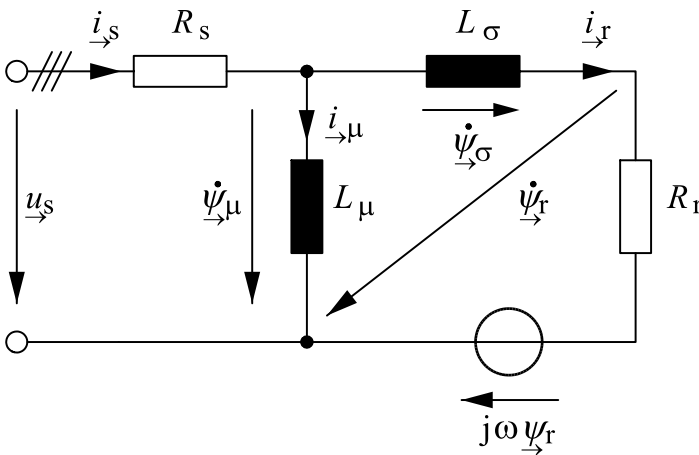


Fig. 15.15: Equivalent Circuit Diagram of induction machine in space-phasor notation, stator-fixed reference frame

Torque can be calculated by the two equations

$$M_d = \frac{3}{2} \cdot p \cdot \text{Im} \left\{ \underline{\Psi}_\mu^{**} \cdot \underline{i}_s \right\}^9 \tag{15.32}$$

$$M_d = \frac{3}{2} \cdot p \cdot \frac{1}{L_\sigma} \cdot |\underline{\Psi}_\mu| \cdot |\underline{\Psi}_r| \cdot \sin \vartheta \tag{15.33}$$

with $\vartheta = \chi(\underline{\Psi}_i) - \chi(\underline{\Psi}_r)$ and p number of pole pairs. The first equation is used within the DSP program, the second is better suited for basic deliberations. It is well known from the synchronous machine, and it will be taken to illustrate the basic idea of torque control.

15.2.3 Stator-flux oriented control

The basic task of machine control is to produce the demanded torque and to keep the (stator) flux intensity on its demanded value.

Stator-flux orientation leads the tip of the stator-flux space phasor on a predetermined trajectory, in the case of high switching frequency a multi-corner polygon, nearly a circle ([63], [243]. The radius of the ideal trajectory will be defined by control of the modulus of the stator-flux space phasor. The tracking speed – in the sampled system expressed by the angular increment per sampling period – results from the output of a linear torque controller [241].

In the following we assume that the modulation period T_m equal to the half switching period is small against the rotor leakage time constant $T_\sigma = R_r / L_\sigma$ and the fundamental period T_s . Fig. 15.16 shows the stator-flux space phasor at the beginning and the end of a modulation period T_m (equal to processor cycle); in the most general case the stator flux is stretched by $k_\psi(v)$ and rotated by $\Delta\chi_\mu(v)$:

$$\underline{\Psi}_\mu(v) = \left\{ (1 + k_\psi(v)) \cdot e^{j\Delta\chi_\mu(v)} \right\} \cdot \underline{\Psi}_\mu(v-1) \tag{15.34}$$

and thus changed by

$$\Delta\underline{\Psi}_\mu(v) = \underline{\Psi}_\mu(v) - \underline{\Psi}_\mu(v-1) = \left\{ (1 + k_\psi(v)) \cdot e^{j\Delta\chi_\mu(v)} - 1 \right\} \cdot \underline{\Psi}_\mu(v-1). \tag{15.35}$$

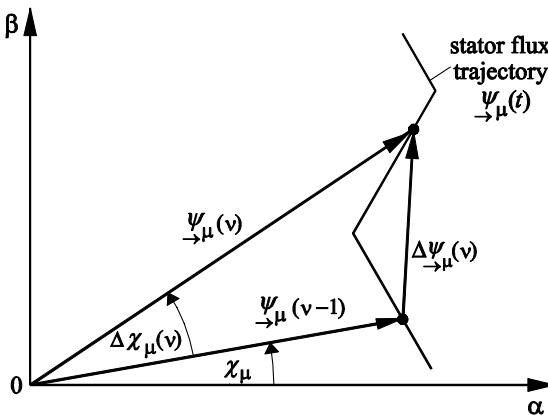


Fig. 15.16: Stator-flux trajectory and stator-flux increment $\Delta\underline{\Psi}_\mu(v)$

⁹ **means the conjugate-complex value

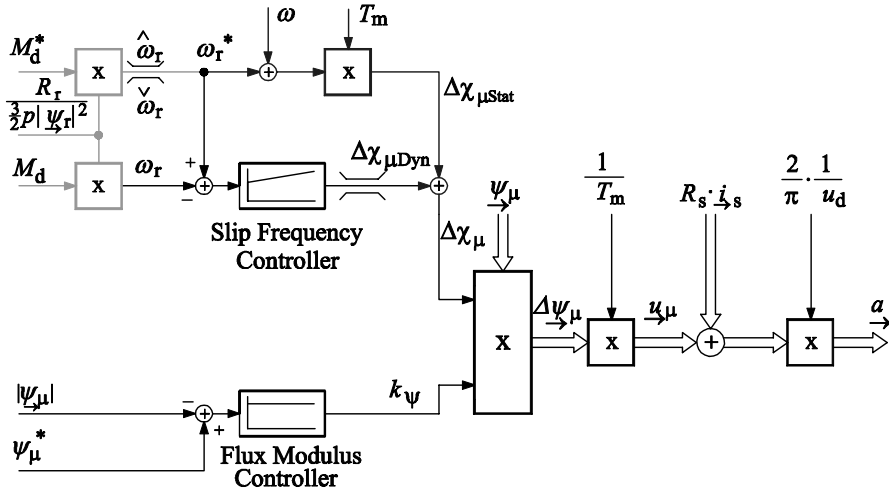


Fig. 15.17: Basic structure of Indirect Stator-Quantities Control (ISC)

Fig. 15.17 shows the basic structure of the controller; all quantities are mean values per sampling period. The stretching factor $k_{\Psi}(v)$ is delivered by a P-type flux-modulus controller. Torque set value M_d^* and actual value M_d are first transformed to rotor angular frequencies by multiplication with $R_r / \left(\frac{3}{2} \cdot p \cdot \Psi_r^2\right)$. Thus break-down can be easily prevented by limiting the set value of ω_r^* . Then both angular frequencies are compared in a PI-type controller delivering the dynamic part of the angular increment, $\Delta\chi_{\mu Dyn}$. The integral channel will be relieved by a stationary feed-forward

$$\Delta\chi_{\mu Stat} = (\omega + \omega_r^*) \cdot T_m \quad (15.36)$$

The following block calculates $\Delta\Psi_{\mu}(v)$ by developing equ. (15.34) in a Taylor series, broken after the third power:

$$\Delta\Psi_{\mu}(v) = k_{\Psi}(v) \cdot \left\{1 - \frac{1}{2} \cdot \Delta\chi_{\mu}^2(v)\right\} \cdot \Psi_{\mu}(v-1) - j \cdot \left\{\Delta\chi_{\mu}^2(v) - \frac{1}{6} \cdot \Delta\chi_{\mu}^3(v)\right\} \cdot \Psi_{\mu}(v-1) \quad (15.37)$$

The stator-flux-increment space phasor will then be multiplied with $1/T_m$ yielding the magnetizing voltage u_{μ} , to which the resistive stator voltage drop $R_s \cdot i_s$ will be added. Finally division by $u_d \cdot \pi/2$ delivers the voltage-control space phasor a handed to the PWM unit [241], [244]. Please note that there are no underlaid current-component controllers anymore.

Now the issue of low frequencies shall be addressed in detail. The stator flux in the model will always be controlled correctly, even at zero frequency. But at low frequency the correspondence of model and real machine currents will be insufficient, mainly due to errors of the temperature-dependent stator resistance and of the inverter voltages modelled from the measured DC-link voltage u_d and the switching signals.

Fig. 15.18 shows the complete machine model acc. to equ. (15.29)...(15.31). The very left blocks, in dashed lines, are current-balancing controllers comparing measured ($i_{sc(\beta)w}$) and model current ($i_{sc(\beta)}$) coordinates, to correct these errors in a Luenberger observer structure. The gain has to be decreased with increasing speed, so that the model works as an i - n -model at low and as a u - i -model at high speed [243].

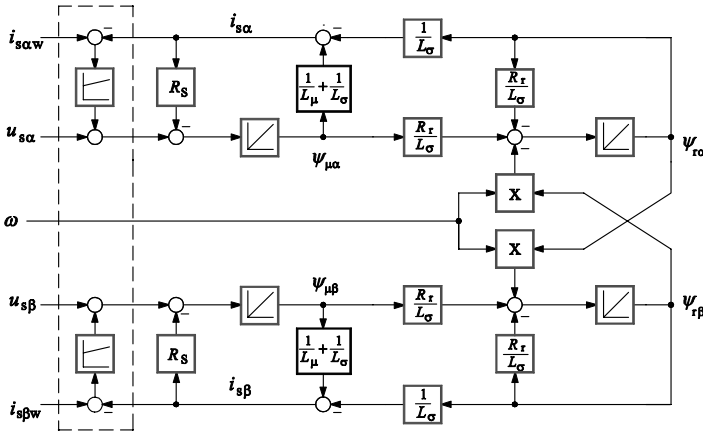


Fig. 15.18: Complete IM model (with current-balancing controllers)

If as shown the stator-voltage drop is calculated with the model currents, the control acts only on the model, the true machine will only be "chained" to the model by the current-balancing controllers. This enables e. g. testing of the control without powering the real drive.

15.2.4 Field-weakening operation

For high power traction drives the limitation of output voltage by sinusoidal PWM to less than 90% of the maximum possible value of the fundamental at square-wave modulation is disadvantageous, as the break-down torque at high speed will be limited to less than 80%. By means of suited overmodulation schemes [244] some 95% can be reached, with comparable dynamics. But finally the transition to square-wave modulation is inevitable. When the maximum voltage – it may be sinusoidal, "overmodulated" or square-wave – has been reached, the torque (constant power range) can only be controlled by field weakening.

Fig. 15.19 shows the completion of the control structure by a field-weakening controller.

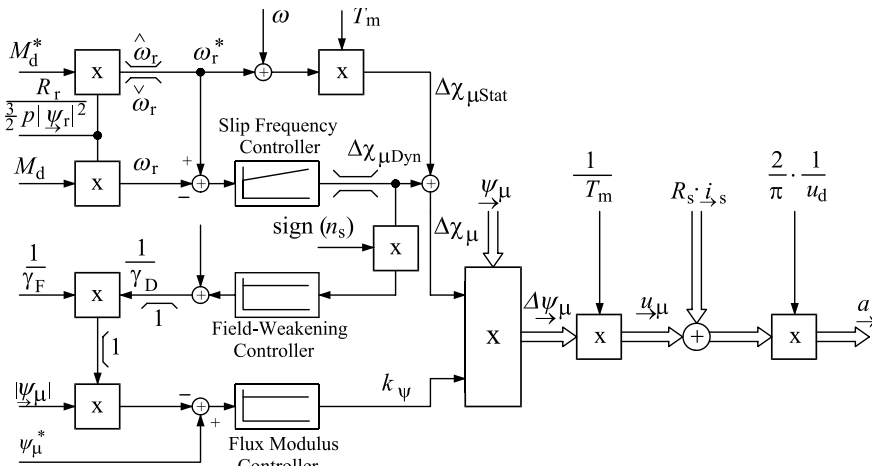


Fig. 15.19: Structure of ISC with Field-Weakening Controller

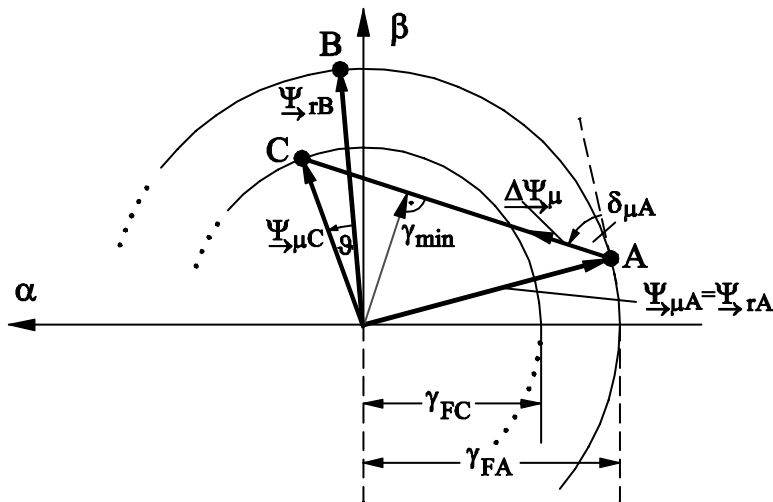


Fig. 15.20: Trajectories of stator and rotor-flux space phasor at Dynamic Field Weakening

The stationary field weakening via the factor $1/\gamma_F$ ($\gamma = \psi_\mu / \psi_{\mu rated}$; left part) works in feed-forward mode by amplifying the flux modulus feed-back. The angular increase $\Delta\chi_\mu$, necessary for torque increase cannot be gained as before as the voltage is already at its maximum. Here Dynamic Field Weakening developed for DSC (section 15.1.5) [65] is helpful again [241].

Fig. 15.20 shows the transient for a torque step out of idling operation, connecting the two stationary circular flux trajectories with radii γ_{FA} (before) and γ_{FC} (after the step). For short time the rotor-flux space phasor moves further-on on the trajectory with the radius γ_{FA} , while the stator-flux space phasor takes the "cut-off" trajectory AC having the same length as AB, weakening the stator-flux modulus intermediately to γ_{min} . The angle ϑ is increased from zero to the stationary value in the fastest possible way.

The command for the dynamic field-weakening $1/\gamma_D$ is derived from the dynamic response of the slip-frequency controller, $\Delta\chi_{\mu Dyn}$, increasing the flux feedback additionally. A torque increase is thus performed in less than $1/3$ of the base period, without any voltage margin! At a negative torque step dynamics are achieved only by variation of the control factor \underline{a} . Subsequently, the stator-flux modulus is guided rather slowly (taking into account the rotor leakage time constant) to the new stationary value, to avoid excessive leakage flux and thus overcurrent.

15.2.5 Correction of inverter-voltage errors

Each model-based control structure is as good as the quality of the modeled quantities and the parameters. The major source of uncertainty is the modeling of the stator voltage from the measured DC-link voltage and the switching signals (to circumvent measuring).

Errors are due to

- Voltage drop of semiconductor devices
- Differences in the switching-delay times
- Different influence of the interlocking time, dependent on the sign of the inverter output (= stator) current

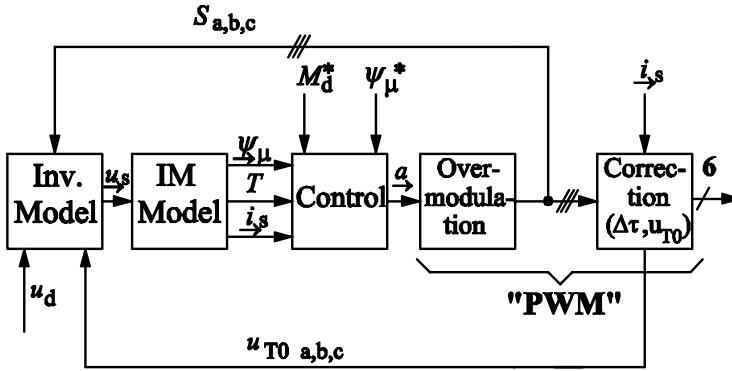


Fig. 15.21: Correction scheme for inverter-voltage errors in recent ISC

These errors depend mainly on the value and the sign of the inverter output current. In the structure described up to now the current-coordinate balancing controller will compensate them, but only to that degree limited by the stability of the control.

Fig. 15.21 shows the block structure of the correction system applied with ISC today [244], [246]. Control hands the set value for the (normalized) stator-voltage space phasor \underline{a} to the Overmodulation block, where the zero-sequence system for Symmetrized Sinusoidal Modulation (subchapter 6.2, Fig. 6.12) is added and overmodulation is performed, if needed.

In the Correction block the switching-time errors are corrected and the device-voltage drops are compensated, based on the model stator-current space phasor. Now the stator-voltage average value per pulse period will be identical with the ideal one. The demanded switching commands $S_{a,b,c}$ are given back – together with the correcting voltage drops – to the Inverter Model calculating the model stator-voltage average value per pulse period identical to that of the real motor.

It is now possible to operate the drive without the previously necessary current-balancing controllers. The information set free by this can now be used to estimate e.g. the speed. The most important ECD parameter at low frequency is stator resistance, as it influences the stator current severely. It must be estimated on-line for high performance drives.

15.2.6 Sensorless identification of speed

Speed sensors in traction induction motors have always been a bottleneck as spoiling the robustness and/or control performance of the simple squirrel-cage motor: Either they are robust – then the angular resolution is limited and the signal delay at low speed is high. Or they have high resolution and good dynamic response, but then they are sensitive to shock and hazard.

In the last years the demand on the speed sensors grew, e.g. for the aforementioned speed feed-forward $\Delta\chi_{\mu\text{Stat}}$ or for speed control as part of adhesion control systems. In low-floor Light Rail Vehicles sensors increase the volume of the individual small motors reasonably. Cost is not negligible, for the sensor itself and for planning, mounting (cabling) and commissioning, and is an important component of Life Cycle Cost (LCC).

Open-loop speed estimation schemes are already widely introduced in industrial application. They are extremely dependent upon parameters. Much more robust are observer schemes, as e.g. that described in [245], which has been extended and especially improved by the following scheme ([244], [246], [247]).

Basis is the linear fundamental-wave model used already in ISC; no parasitic effects as slotting or saliency are used. The real machine is described by an identically structured ECD; the quantities in the real machine shall be designated by the index ‘w’. The differences are

$$\Delta x = x - x_w. \tag{15.38}$$

If as supposed both machine and model are fed with identical voltage average values per pulse period and show no difference in the parameters, the same current would flow in each. If the difference of the stator-voltage drops due to different currents is not too big, both current space phasors can be described in steady-state by the same Heyland circle diagram (Fig. 15.22), assuming an identical, constantly rotating stator-flux space phasor.

It is obvious that different speeds lead to different slip values and thus to different stator currents. If all other parameters are identical, this difference can be employed for speed estimation. From the figure it can be seen that e.g. the component of Δi_s being perpendicular to the stator-flux space phasor Ψ_μ will be suited as indicator under the conditions assumed.

At the critical point of stator frequency being zero, speed identification is not possible in the stationary state: The whole DC stator voltage drops over the stator resistance, the rotor mesh is short-circuited by the magnetizing inductance. Only a change of flux or speed can induce a current difference which may be evaluated for speed identification.

The mathematical analysis of the stator-current difference leads to a space-phasor differential equation of second order. To make it more compact some abbreviations and normalizations shall be introduced before, the time-constant factor

$$\rho = \frac{L_r / R_r}{L_s / R_s} = \frac{L_\sigma + L_l}{L_l} \cdot \frac{R_s}{R_r} \tag{15.39}$$

and the leakage factor

$$\sigma = \frac{L_\sigma}{L_\sigma + L_\mu} \tag{15.40}$$

The angular frequency is normalized to rotor break-down value $\omega_{rk} = L_\sigma / R_r$ and designated by ‘n’, time is normalized to the inverse of ω_{rk} . The derivatives to the normalized time are marked by \dot{x} .

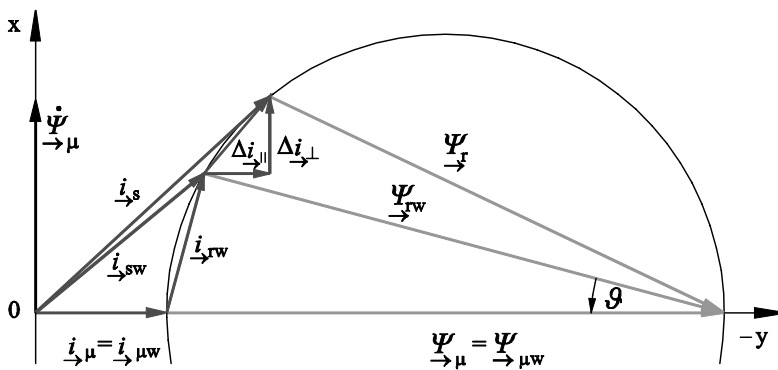


Fig. 15.22: Heyland Circle Diagram for real machine (x_w) and model (x) at identical stator flux space phasor

Then the differential equation can be written as:

$$\underline{\overset{\circ}{\Delta i_s}} + (\rho + 1 - j \cdot n_w) \cdot \underline{\overset{\circ}{\Delta i_s}} + \rho \cdot (\sigma - j \cdot n_w) \cdot \underline{\overset{\circ}{\Delta i_s}} = j \cdot \frac{1}{L_\sigma} \cdot \left(\Delta n \cdot \underline{\overset{\circ}{\Psi_r}} \right) \quad (15.41)$$

The excitation of the system and by that the stator-current difference vanishes if the following conditions are fulfilled:

- The speed difference or the rotor flux are permanently equal to zero (trivial case)
- The derivatives of both quantities are zero

The last condition marks the case that speed identification fails at stator frequency zero.

In the stationary case under symmetrical sinusoidal conditions the first and second time-derivative of the stator current difference can be expressed by the difference itself and the normalized stator frequency n_s :

$$\underline{\overset{\circ}{\Delta i_s}} = j \cdot n_s \cdot \underline{\overset{\circ}{\Delta i_s}}, \quad \underline{\overset{\circ}{\Delta i_s}} = -n_s^2 \cdot \underline{\overset{\circ}{\Delta i_s}} \quad (15.42)$$

Then the solution of the differential equation for stationary operation is given by

$$\underline{\overset{\circ}{\Delta i_s}} = \frac{n_s}{\left[\rho \cdot \sigma - (n_r + \Delta n) \cdot n_s \right] + j \cdot \left[\rho \cdot (n_r + \Delta n) + n_s \right]} \cdot \frac{\Delta n}{L_\sigma} \cdot \underline{\Psi_r} \quad (15.43)$$

This is a rotating space phasor containing the information about the speed difference. After multiplication with the conjugate-complex rotor-flux space phasor $\underline{\Psi_r}^{**}$ ¹⁰, the leakage inductivity L_σ , an additional suited working-point-dependent complex factor \underline{K} and normalization by multiplication with $1/\Psi_r^2$ a resting (DC) quantity is obtained (in steady-state). The real part is parallel and the imaginary part perpendicular to the product of $\underline{\Psi_r}$ and \underline{K}^* :

$$\text{Im} \left\{ \frac{\underline{\Psi_r}^{**}}{\underline{\Psi_r}^2} \cdot \underline{K} \cdot \underline{\overset{\circ}{\Delta i_s}} \cdot L_\sigma \right\} = G_{i_2} \cdot \Delta n \quad (15.44)$$

The perpendicular component to be used for speed identification in an observer structure is proportional to the speed difference and a function of the machine and operating parameters and shall be summarized in a factor G_{i_2} . In nearly the whole operation range the factor \underline{K} is chosen equal to

$$\underline{K} = (1 + j \cdot n_r) / \sqrt{1 + n_r^2}, \quad (15.45)$$

showing a rather uniform negative gain. Only in the range of *very small stator frequency with opposite signs of torque and speed* the indicator would change its sign [241] and defeat a stable control. The factor is then to be chosen as shown in [247] to

$$\underline{K} = (1 + j \cdot n_r / \sigma) / \sqrt{1 + (n_r / \sigma)^2} \quad (15.46)$$

The corresponding gain is depicted in Fig. 15.23, dependent upon stator frequency n_s , up to about double rated speed, with the normalized rotor frequency n_r as main parameter.

At the critical stator frequency zero the gain G_{i_2} vanishes, the machine is unobservable. Outside this point the left part of equ. (15.44) can be used as error function for a PI-controller, ad-

10 **means the conjugate-complex value

justing the speed signal in the observer. The practical settling time is about one third of the rotor leakage time-constant T_σ [246].

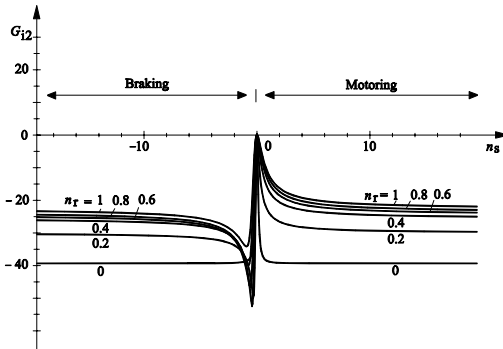


Fig. 15.23: Factor $G_{12} = f(n_s, n_r)$, using equ. (15.46)

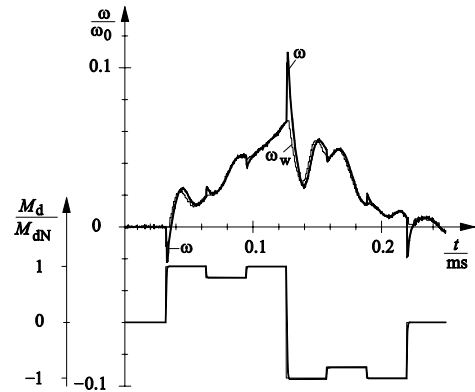


Fig. 15.24: Estimated ω and measured speed (ω_w) at acceleration and braking with up to 100 % rated torque

The excellent quality of this speed observer scheme shall be demonstrated by experimental results of a 120-kW traction induction motor fed from a 500-kVA IGBT traction inverter with a nominal DC-link voltage of 750 V.

Fig. 15.24 shows speed estimation under dynamic conditions. A torque set value step sequence is given on the induction machine coupled with a DC machine, speed follows mainly in a triangular fashion. Real speed ω_w (measured with an incremental encoder with 2000 pulses/rev. and pulse quadrupling) and estimated speed ω are shown, together with the torque functions. Estimated speed follows the measured speed astonishingly exactly, including the oscillation of the two-masses-and-spring system.

The peaks visible in ω when the torque changes very fast are due to current displacement effects in the rotor bars reducing $L_{\sigma w}$. So the real rotor currents rise faster than those in the model, which cannot take care of this effect due to limited calculation time. It will be interpreted by the speed estimator as a negative speed error. But it has no vital consequence on the quality of speed estimation as set value and actual torque differ anyway during such extremely fast transients.

With such a scheme speed reversals with a change rate of $24 \text{ min}^{-1}/\text{s}$ and permanent full load operation at a minimum stator frequency of only 0.33 Hz can be safely managed. But it must be kept in mind that at still lower values or rates of change the scheme will fail. An escape of the problem will be given in section 15.2.9.

15.2.7 Stator-resistance estimation

An indispensable prerequisite is exact on-line identification of the stator resistance which changes severely with temperature. Obviously thermal sensors are not wanted. Both stator and rotor temperature can be identified at standstill unequivocally, but not at speed.

The same change of temperature in stator and rotor shall be assumed as first approach. So the value of ρ is not changed, when R_s changes. Then an equation similar to (15.43) can be found for the appertaining stator-current space-phasor difference $\Delta \underline{i}_s$ caused by the difference ΔR_s [248]. For small ΔR_s and $\rho = \rho_w$ this equation can be written as

$$\underline{\Delta i_{sR}} = \frac{n_r^2 - \sigma^2 - j \cdot 2 \cdot \sigma \cdot n_r}{\underline{Z}} \cdot \frac{\Delta R_s}{L_\sigma \cdot R_r} \cdot \underline{\Psi_r} \tag{15.47}$$

with

$$\underline{Z} = [\rho \cdot \sigma - n_r \cdot n_s] + j \cdot [\rho \cdot n_r + n_s] \tag{15.48}$$

Multiplying the sum of equ. (15.43) and equ. (15.47) with the conjugate-complex rotor-flux space phasor $\underline{\Psi_r^{**}}$, further with L_σ , the complex (mainly imaginary) factor \underline{Z} and $1/\Psi_r^2$ yields again a resting quantity (in steady state). The imaginary part of this is only proportional to ΔR_s :

$$\text{Im} \left\{ \frac{\underline{\Psi_r^{**}}}{\underline{\Psi_r}^2} \cdot \left(\underline{\Delta i_s} + \underline{\Delta i_{sR}} \right) \cdot L_\sigma \cdot \underline{Z} \right\} = G_{Rs} \cdot \frac{\Delta R_s}{R_r} \tag{15.49}$$

In steady state Δn has no influence on the result, as it is contained only in the real part. As the stator resistance changes only slowly, an integral controller will be used for identification; the left side of equ. (15.49) multiplied with the sign of n_r is its input. This method is independent of the speed-identification scheme for small differences of speed and stator resistance.

Fig. 15.25 shows that speed estimation at very low stator frequency needs correct values of R_s . The drive (same as used in Fig. 15.24) operates at standstill with 100% rated torque (= 35% of breakdown torque M_{dK}). The model stator-resistance value is initialized to 80% of its nominal value. Due to this mismatch the estimations of stator flux and correspondingly of speed are wrong. The ripple frequency is six times stator frequency due to malfunctioning of the inverter-voltage correction circuit (Fig. 15.21) by a severe difference between $\underline{\Delta i_s}$ and $\underline{\Delta i_{sw}}$. The initial error in speed is 1% of rated speed. At $t = 1.9$ s the identification of R_s starts, the actual value of $1.018 \cdot R_{s20^\circ C}$ is found within 2...3 s. Simultaneously all state variables converge to their correct values, the ripple vanishes and speed reaches the correct value zero. The method operates well in the range of small frequencies, where the influence of the stator resistance is relevant and where this identification is necessary.

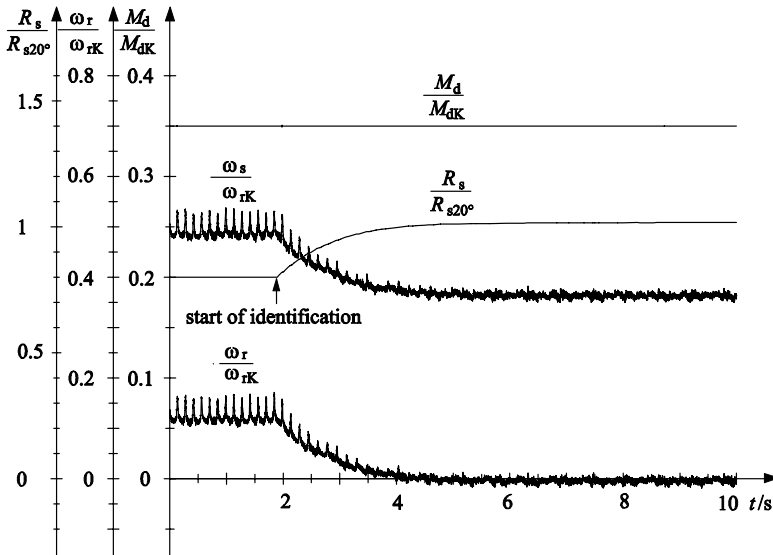


Fig. 15.25: On-line identification of stator resistance at standstill

15.2.8 Suppression of parasitic DC voltages

As in the ISC structure only the mathematical model in the DSP is controlled, unwanted DC components in voltage and fluxes are of only numerical order and can thus be neglected. As will be shown later there are possible operation points in which – under steady-state conditions – DC portions must be allowed in the stator fluxes and stator currents, which the control must handle without problems. But in spite of all sophisticated parameter identification and compensation of inverter-voltage errors in the real inverter drive, parasitic DC-voltage portions cannot be prevented. In standard field-oriented control schemes the DC portions of the *measured* motor voltages and (sometimes) wrongly the stator fluxes have to be cancelled by high-pass filtering, setting a considerable minimum operation frequency.

In ISC another way has been found: In a rather quick-acting circuit the DC portions in the stator-current differences are detected. To that purpose the stator-current-difference space phasor is sampled at time intervals corresponding to e.g. about 5° of χ (see Fig. 15.26). The DC-portion space phasor is then approximately [249]

$$\underline{\Delta i_{\rightarrow}} \approx \left[\frac{1}{2} \cdot \left(\underline{\Delta i_{s2}} + \underline{\Delta i_{s1}} \right) + j \cdot \frac{1}{\Delta \chi} \cdot \left(\underline{\Delta i_{s2}} - \underline{\Delta i_{s1}} \right) \right] \quad (15.50)$$

and given as input to two PI-controllers, whose outputs are acting as correcting input voltages $\underline{\Delta u_{s-}}$ of the stator-flux integrator inputs, compensating any *parasitic* DC difference between the model voltages and the real inverter voltages, but not suppressing *necessary* DC portions in the stator fluxes or the stator currents.

15.2.9 Operation with infinitely slow change between driving and breaking

The speed of a linearly modeled induction machine cannot be observed at zero stator frequency without injecting test signals, providing a change of flux. Test signals are often not wanted as they may disturb e.g. signaling circuits, or they cannot be injected sufficiently with the low switching frequency of high-power inverters.

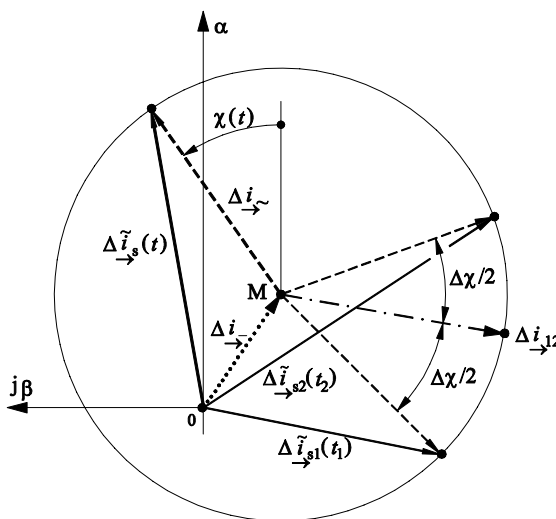


Fig. 15.26: Space phasor of stator-current differences caused by a parasitic DC voltage, at speed identification

As it has been shown slow passings through the region of very small stator frequency can be safely managed. The question is whether an operation mode is possible which simply avoids stationary working in the region below 0.4...0.5 Hz, a value that can safely be mastered with the described control structure.

To that purpose a scheme has been proposed and successfully implemented [248] which avoids operation with too low stator frequency by manipulating the modulus of the stator-flux space phasor. For a given (non-zero) torque a reduction of the rotor flux modulus raises the necessary slip (angular) frequency:

$$\omega_r = \frac{2 \cdot R_r}{3 \cdot p \cdot \Psi_r^2} \cdot M_d \tag{15.51}$$

The function of the operation management is explained for a reversing of speed at constant torque. Fig. 15.27 shows the normalized rotor frequency n_r as a function of normalized speed n ; in the diagram working points with constant normalized stator frequency n_s are straight lines with gradient -1 . Speed identification works safely for stator frequencies with an absolute value $\geq n_{smin}$. Thus the drive must not work stationarily in the region between the lines $n_s = -n_{smin}$ and $n_s = +n_{smin}$ in Fig. 15.27.

Starting at point A, the machine brakes with negative speed and positive (non-zero) torque and rotor frequency; the absolute values of speed and stator frequency decrease. At point B the stator frequency reaches the limit $-n_{smin}$. Now there are two choices to produce the wanted torque: With full flux, minimal slip frequency and negative stator frequency (point B) or with reduced flux magnitude and a rotor frequency increased by $\Delta n_r = 2 n_{smin}$ (point C), where the stator frequency is already positive and $+n_{smin}$.

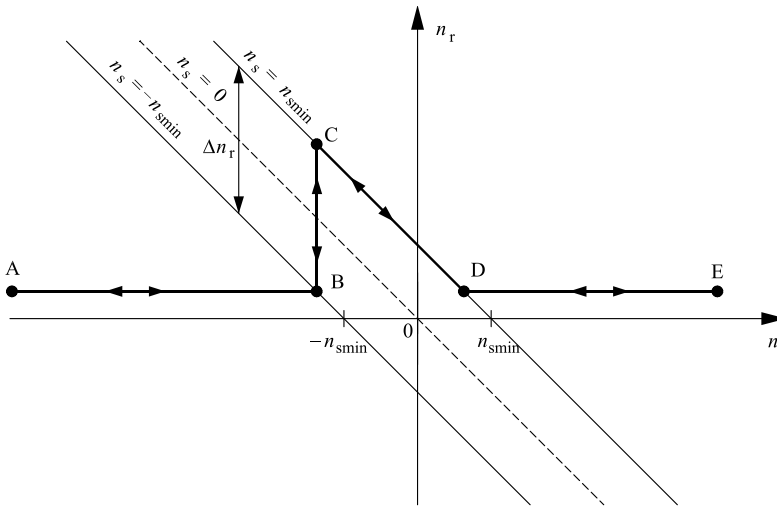


Fig. 15.27: Normalized rotor frequency n_r vs. normalized speed n at constant torque

The operation management decides to decrease the flux such that the crossing of the stator frequency through the „forbidden zone” is sufficiently fast. On the other hand the transition must be slow in regard to the rotor leakage time constant T_{σ} , to avoid an inadmissible dynamic increase of the leakage flux and thus stator current.

As speed changes further, the operation point moves along the line $n_s = +n_{smin}$ towards D, while the flux is continuously increasing again, so that the drive is operated at $n_s = n_{smin}$ with maximum permissible flux and minimum stator current. This is done by stator-frequency control. At

D normal motoring operation with full flux and constant rotor frequency is reached again and maintained until E.

The opposite reversing starts at point E in motoring mode. With decreasing speed point D and $n_s = +n_{s\min}$ is reached. For further decreasing speed the flux must be decreased continuously to keep the stator frequency at its upper limit $+n_{s\min}$. The control supervises whether the torque can be produced with full flux and negative stator frequency $\leq -n_{s\min}$, too. When at point C the condition is fulfilled, the drives changes sharply to B.

In practical operation an additional hysteresis avoids jittering. Fig. 15.28 shows the time functions of such a very slow speed reversal, measured at the 120-kW drive. The DC load machine is speed-controlled and impresses the triangularly changing speed; the IM is torque-controlled. The two upper traces show stator-flux modulus and torque, the middle trace the observed stator frequency and the lower traces the nearly perfectly coinciding values of true and observed speed. For $M_{dr} = 0.35 M_{dk}$ the slip angular frequency is $0.187 \cdot \omega_{rk} = 2\pi \cdot 0.89 \text{ s}^{-1}$, which is more than two times the above-mentioned minimum frequency of $\omega_{rk} = 2\pi \cdot 0.33 \text{ s}^{-1}$. The frequency hysteresis is $0.02 \cdot \omega_{rk}$, stator flux is reduced down to 50%. [248] shows how at practical no-load condition safe transition is reached by switching-on a minimum torque of less than 3.5% of rated torque. [250] reports on practical tests on a Combino low-floor tram-car; it shows that vehicles running down a slope can be smoothly stopped, held at zero speed and accelerated in the opposite direction, without speed sensors.

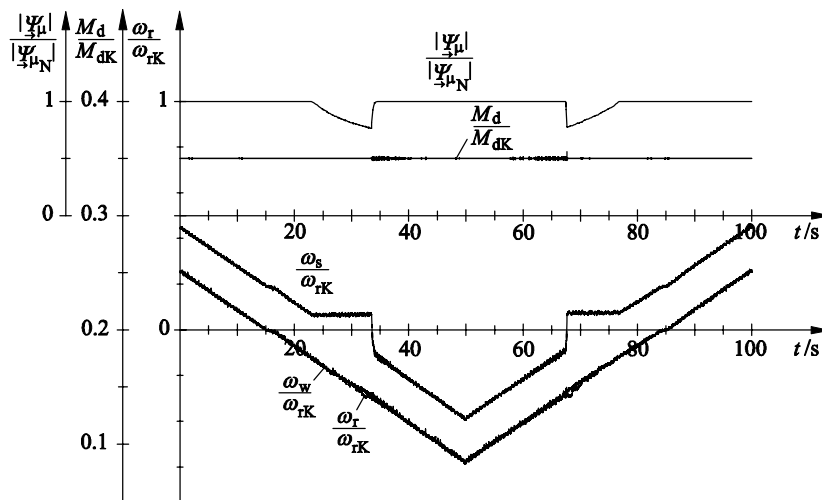


Fig. 15.28: Very slow speed reversing operation with rated torque. 120-kW motor.

[251], [252] finally report on the successful implementation of a speed-sensorless system, based on the described one, in the new SITRAC Siemens traction control and intensively tested in different light-rail and Metro applications in Spain, China, Japan (Fig. 15.31) and Taiwan. The new Underground trains for Oslo, Norway will – after tests in revenue operation since end of 2005 – already be delivered without speed sensors in the motors (2007).

15.2.10 Difference of Indirect Stator-Quantities Control and Direct Vector Control

Fig. 15.29 shows in an overview the whole control system of speed-sensorless Indirect Stator-Quantities Control (ISC). In the Control block stator-flux modulus and torque reference values are computed together with the actual values of stator-flux and stator-current space phasors and torque, delivered by the IM model (sections 15.2.3, 15.2.4). The normalized output-voltage space phasor \underline{a} is transformed in the PWM block to the switching commands for the inverter (voltage-error correction (section 15.2.5) indicated only by the input arrow to the inverter block). From the switching commands and the DC-link voltage the stator-voltage space phasor is calculated in the inverter model and handed to the IM model. The necessary speed and stator-resistance information for the u - i - n -model are obtained from the comparison of the manipulated stator-current space phasors of model and machine (section 15.2.6). Finally the Δi_{s-} -block suppresses parasitic DC portions in the stator voltages (section 15.2.7).

As claimed in section 15.2.8 there may be operation points where DC portions in the stator fluxes and currents *must* be admitted. Such a point is depicted in Fig. 15.30: The (very low) speed reference is modulated with – mainly – stator frequency 0.65 Hz. In stator flux and stator current DC portions are clearly visible. The slight 50-Hz oscillation in the speed signal is due to such an unsymmetry in the armature current of the DC load machine, which demonstrates on the other hand the excellent resolution of the speed identification scheme.

This operation is not allowed with Direct Vector Control systems, as described in section 15.1.4, suppressing all DC portions in the measured stator voltages and perhaps the stator flux, as those cancel the *necessary* DC portions too.

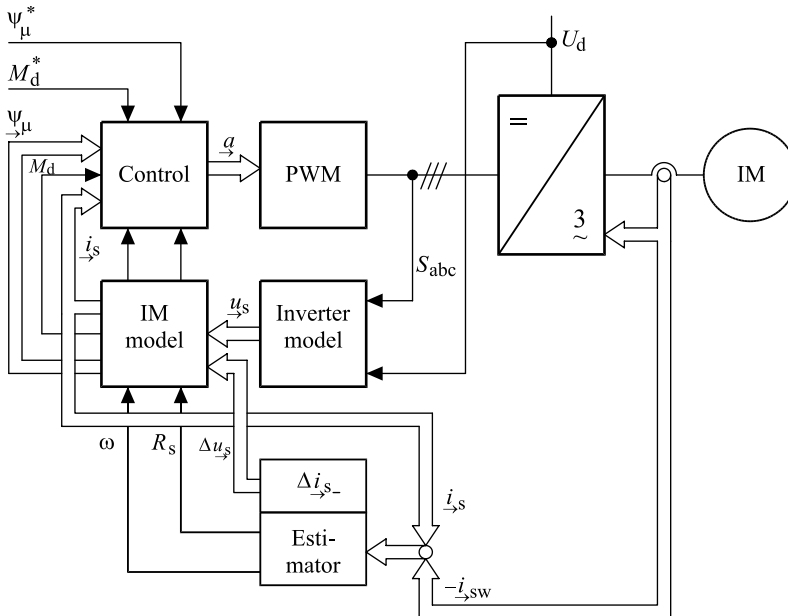


Fig. 15.29: Overall block structure of speed-sensorless ISC

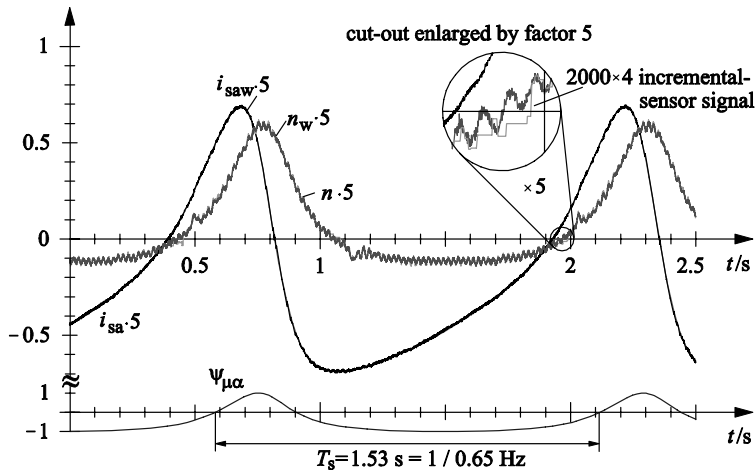


Fig. 15.30: Operation with stator-frequency-modulated speed reference. Stable operation in spite of DC portions in stator fluxes and currents

Though this may be regarded a somewhat hypothetical working point, it makes clear the extended operation possibilities of Indirect Stator-Quantities control, compared with usual Direct Vector Control at very low speeds. With field-oriented traction drives, this disadvantage is overcome by using Indirect Field Orientation, as described in section 15.1.4.

15.2.11 Conclusion

Indirect Stator-Quantities Control (ISC) unifies the advantages of stator-flux orientation proven successful in Direct Self Control, with Pulse Width Modulation well suited for fast-switching IGBT inverters. Using the signals available in the model-based control the motor speed can be estimated so that no speed sensors are needed anymore. Careful feed-forward correction of inverter-voltage errors and especially the on-line cancelling of any unwanted parasitic DC portions in the stator currents is indispensable for safe operation in the zero-speed zone with unrestricted speed reference. Additional work not described here has been necessary on automatic identification procedures of machine and inverter parameters and on procedures for magnetizing the machine with unknown speed and residual flux without speed sensor.



Fig. 15.31: Keihin Kyoko Tokyo N 1000 series with speed-sensorless drives, in revenue service since 2005 (Siemens TS)

15.3 Unified Notation of Carriages of UIC and OSShD

(Cipher 3 und 4 of carriage number)

Nr.	Railway	Abbrev.	Nr.	Railway	Abbrev.
1			52	Bulgarian State Railways	BDZ
2			53	Nat. Soc. of Romanian Railways	SNCFR
3			54	Czech Railways	CD
4			55	Hungarian State Railways	MAV
5			56	Slovakian Railways	ZSR
6			57	Azerbaijani Railways	AZ
7			58	Armenian Railways	ARM
8			59	Kirgizian Railways	KRG
9			60	Irian Transport Comp.	CIE
10	Finnish Rys	VR	61	Korean National Railways	KNR
11			62	Swiss Cargo Cars Association	SP
12			63	Bern-Lötschberg-Simplon (CH)	BLS
13			64	Nord-Milano Ry.	FNM
14	Int. Sleeping-Car & Tourism Comp.	CIWLT	65	Rys. of the Rep. Macedonia	MZ
15			66	Tadzhikistan Railways	TZD
16			67	Turkmenian Railways	TRK
17			68	Bentheimer Eisenbahn AG	BE
18			69	Eurotunnel	
20	Russian Rys.	RZD	70	English, Welsh & Scottish Ry.	EWS/RT
21	Byelorussian Rys.	BC	71	Nat. Admin. of Spanish Rys.	RENFE
22	Ukrainian Rys.	UZ	72	Formerly Yugoslavian Ry.	JZ
23	Moldavian Rys.	CFM	73	Hellenic Railways Organization	OH
24	Lithuanian Rys.	LG	74	Swedish State Railways	SJ
25	Latvian Rys.	LDZ	75	Turkish State Railways	TCDD
26	National Estonian Rys.	EVR	76	Norwegian National Railways	NSB
27	Kazakhian Rys.	KZH	77	-	
28	Georgian Rys.	GR	78	Croatian Railways	HZ
29	Uzbekistan Rys.	SAZ	79	Slovenian Railways	SZ
30	Rys. of Dem. P.R. Korea	KRZ	80	German Railways Deutsche Bahn	DB
31	Rys. of Mongolia P.R..	MTZ	81	Austrian Federal Railways	ÖBB
32	Vietnam Rys.	DSVN	82	Nat. Ry. Comp. of Luxemburg	CFL
33	Rys. of Chinese Peoples Republic.	KZD	83	Italian State Railways	FS
34	Not assigned		84	Netherlands Railways	NS

Nr.	Railway	Abbrev.	Nr.	Railway	Abbrev.
..	“		85	Swiss Federal Railways	SBB
39	“		86	Danish State Railways	DSB
40	Ferrocarril de Cuba	FC	87	Nat. Ry. Comp. of France	SNCF
41	Albanian Rys.	HSH	88	Nat. Ry. Comp of Belgium	SNCB
42	East Japan Railway Company	EJRC	89	Rys. of Bosna and Herzegovina	ZBH
43	Gyor-Sopron-Ebenfurti Vasut	GySEV	91	Nat. Tunisian Rys.	SNCFT
44	Budapest Transport Company	BHEV	93	Nat. Office of Maroc Railways	ONLFM
45	Not assigned		94	Portuguese Railways	CP
46	“		95	Israel Railways	IR
47	“		96	Rys. of the Islamic Republic Iran	RAI
49	“		97	Syrian Railways	CFS
50	Rys. of Serpska Republic, Bosnia	ZFHB	98	Nat. Rys. of Lebanon	CEL
51	Polish State Railways	PKP	99	Iraqi Republic Railways	IRR

15.4 Symbols and Abbreviations

Symbols

a	Acceleration; half of wheelbase; control factor	ii	Rail superelevation
a, b, c	Terminals of an IM	v	Speed
A	Area of cross-section	w, W	Train resistance; no. of windings
B	Induction	X	Inductance
b	Half of bogie centre distance	x, y, z	Coordinate axis
C	Capacity	Y	Admittance
c	Capacity per unit length	Z	Impedance
E	Induced voltage; half DC-link voltage of inverter	Φ	Magnetic flux
f	Frequency; adhesion coefficient	ϑ	Rotor displacement angle; temperature
F	Force	Ψ, ψ	Flux linkage
Fi	Current-time area	α	Phase delay angle
Fu	Voltage-time area	$\alpha, \beta,$	angles
g	Constant of gravity (9.81 m/s ²); counting index; conductivity per unit length	γ, ξ	
G	Weight force	δ	Air-gap widthfundamental con-
h	Height; counting index	ε	Chording angle
H	Magnetic field intensity	γ	Inclination of wheel surface
i	Gear ratio; current	η	Efficiency
k	Factor; degree of field-weakening	φ, ψ	Phase angle
L	Inductivity	λ	Wave length of „Sinusoidal Running“; power factor; scale factor
l	Length; inductivity per unit length	μ	Permeability
m	Mass	v	Numbering index of arms
M	Torque	σ	Leakage factor
M	Mid-point of inverter DC link	τ	Pole pitch
n	Number; speed	ω	Angular frequency
N	Number of windings; switch. ratio	ξ	Specific extra factor for rotating masses
p	Number of pole pairs		
p_F	Interference weighting factor		
P	Power		
q	Number of slots per phase winding and pole		
r	Radius (of wheel); resistivity per unit length		
R	Curve radius; resistance		
s	Distance; gradient; slip		
s_l	Distance of wheel contact points		
T	Time period; time constant		
t	Time instant		
u	Voltage; normalized voltage		

Prefixes

Σ	Sum quantity
δ, Δ	Difference quantity

Superscripts

'	Transferred to primary side; specific
*	Reference value
**	Conjugate-complex value
..	Negative-sequence system
...	Zero-sequence system

Underscripts

\rightarrow	Space phasor
—	Complex number, vector

Subscripts

0	Related to zero point
1	Belonging to point 1, UIC
1, 2, ..	Numbering index
A	Starting-; armature-; output- ; initial value
a	Acceleration; starter,
adm	Admissible
B	Braking; belonging to snubber
c	Capacitor...; in the curve
d	DC quantity; belonging to DC link; synchronous (synchr. masch.)
D	Pivot...; diesel...; distortion
dyn	Dynamic
E	Exciter circuit...; end value
F	Line...
Fe	Belonging to iron circuit
H	Drawbar..., stopping...-
h	Harmonic
L	Length of rotor packet; loading
K	Short-circuit...; commutation...
max	Maximal
mech	Mechanic(al)
min	Minimal
N	Nominal value; switching ratio of inverter
opt	optimal
P	Active part
p	To synchronous internal voltage
pol	Belonging to pole
Q	Nonactive part
x	Inductive portion
r	Rotor-; resistive part; rated value; relative
R	Resonance
s	Stator...
S	Chopper input...; snubber...,
sek	Secondary-side quantity
ST	Shoot-through...
stat	Stationary
T	Transformer...
TQ	Turn-off...
V	Loss...
x, y, z	To coordinate axis
z	Switching-
δ	To air gap
σ	Leakage...
μ	Magnetizing...

Notation of time-dependent quantities

x	General time-dependent quantity
X	r.m.s. value; constant DC quantity
\hat{x}	Amplitude
\bar{x}	Average (mean) value
x	Modulus, absolute value

Abbreviations (Railways cf. 15.2)

ABB	Asea Brown Boveri Railway business → ADtranz
AEG	Allgemeine Elektrizitäts- Gesellschaft; Railway business → AWTS
AlSiC	Aluminum Silicon Carbide
AlN	Aluminum Nitride
AP	Anti-parallel
APS	Alimentation par le sol (subterranean power supply)
ASCI	Autosequentially-commutated Current-Source Inverter
ASEA	Allmänna Svenska Elektriska Aktiebolaget → ABB
AT	Autotransformer
AVG	Albtal-Verkehrs-Gesellschaft mbH, Karlsruhe
AWTS	AEG-Westinghouse Transpor- tation Systems → ADtranz
A&D	Automation and Drives
B	Boiler
BBC	Brown Boveri & Cie → ABB
BVG	Berliner Verkehrs-Gesellschaft (Berlin municipal transport)
C	Capacitor
CIS	Community of Independent States (former USSR)
CSI	Current-Source Inverter
D	Diode
DE	Diesel-electric
DB	Deutsche Bundesbahn (.. 1994)
DB AG	Deutsche Bahn AG (> 1994)
DR	Deutsche Reichsbahn (GDR)
DRG	Deutsche Reichsbahn (1920–45)
DSP	Digital Signal Processor
DSC	Direct Self Control
DÜWAG	Düsseldorfer Waggonbau-AG
EBO	Eisenbahnbau- und Betriebs-Ordnung
ECD	Equivalent Circuit Diagram
EdF	Electricité de France

EEW	Institute for Electrical Energy Conversion, TU Darmstadt	RAG	Ruhrkohle-Aktiengesellschaft
e.m.f.	Electro-motive force	RATP	Régie autonome des transports Parisiens (Paris métro)
EnBW	Energieversorgung Baden-Württemberg	RBK	Regionalbahn Kassel
ERTMS	European Railway Transport Management System	RWE	Rheinisch-Westfälische Elektrizitätsgesellschaft (utility)
ETCS	European Train Control System	RWTH	TU Aachen
EVAG	Essener Verkehrs-AG	Ry., Rys.	Railway, railways
FPGA	Free-programmable field array	SM	Synchronous machine
G	Generator	SSW	Siemens-Schuckert Werke
GE	General Electric (USA)	StraBO	Straßenbahn-Bau- und Betriebs-Ordnung
GEC	General Electric Corp. (GB)	T	Thyristor; tachometer; turbine
GTO	Gate-Turn-Off (thyristor)	Talgo	Tren articulado ligero Goicoechea Oriol (light articulated train Goicoechea and Oriol)
HEP	Head-End Power System	TGV	Train à Grande Vitesse → HST
HF	High frequency	Tr	Transistor
HGK	Hafen und Güterverkehr Köln (Harbour & Cargo Transport, Cologne)	TL	Train line
HST	High-Speed Train/Traffic	TS	Transportation Systems
ICE	Inter-City Express	TUD	TU Darmstadt
IGBT	Insulated-Gate Bipolar Transistor	TVE	TRANSRAPID Versuchsstrecke (test line) Emsland
IGCT	Integrated Gate-Commutated Thyristor	UCTE	Union for the Coordination of Transmission of Electricity
ISC	Indirect Stator-Quantities Control	UC&	Union Carriage & Waggons Works Co, Cape Town, ZA
L	Reactor, inductivity	WW	Works Co, Cape Town, ZA
LNVG	Landesnahverkehrsgesellschaft Niedersachsen	V	Valve
LRT	Light Rapid Transit	VAL	Véhicules automatiques légères (Lille people mover system)
M	Mid-point of DC link; motor	VDV	Association of German Transport Undertakings, Cologne
MAN	Maschinenfabrik Augsburg-Nürnberg	VSI	Voltage-source inverter
MRCE	Mitsui Rail Capital Europe		
NEBB	Norsk Elektrisk Brown Boveri		
OV	Over-voltage ...		

16 References

16.1 Books

- [B1] Henschel Lokomotiv-Taschenbuch, Edition 1960. VDI-Verlag GmbH, Düsseldorf
- [B2] Bäßold, D.; Rampp, B.; Tietze, Ch.: Elektrische Lokomotiven deutscher Eisenbahnen. Alba-Verlag Düsseldorf 1993.
- [B3] Filipovic, Z.: Elektrische Bahnen – Grundlagen, Triebfahrzeuge, Stromversorgung. Springer-Verlag Berlin–Heidelberg–New York–London–Paris–Tokio 1995 (3rd edition).
- [B4] Hollingworth, B.; Cook, A.: The Great Book of Trains. 1987 Salamander Books Ltd.
- [B5] Müller, Siegfried: Elektrische und dieselektrische Triebfahrzeuge – Leistungsfähigkeit, Wirtschaftlichkeit, Arbeitsweise. Birkhäuser-Verlag Basel-Boston-Stuttgart 1979, out of print, still available via Minirex AG, CH-6002 Luzern.
- [B6] Mehlretter, J. M. (editor): Elektrische Triebfahrzeuge – Entwicklungen der DB seit 1970 und ausländische Lösungen. Motorbuch-Verlag Stuttgart 1986.
- [B7] Rossberg, R. R.: Geschichte der Eisenbahn. Sigloch Service Edition Künzelsau 1977 / Stürtz-Verlag Würzburg 1977.
- [B8] Repetzki, K. R. (editor): Elektrische Schienenfahrzeuge in Glasers Annalen 1909–1929 (Vol. 1); Elektrische Schienenfahrzeuge in Glasers Annalen 1930–1953 (Vol. 2); Steiger Verlag Solingen 1990 (Transpress-Reprint).
- [B9] Rotter, R.; Petrovitsch, H.: Triebfahrzeuge österreichischer Eisenbahnen. Alba-Verlag Düsseldorf 1990.
- [B10] Sachs, K.: Elektrische Triebfahrzeuge. Ein Handbuch für die Praxis sowie für Studierende in drei Bänden. Springer-Verlag Wien-New York 1973 (2nd edition)
Vol. 1: Allgemeine Grundlagen und Mechanischer Teil. Vol. 2: Elektrischer Teil und Spezialfahrzeuge. Vol. 3: Tabellen und Tafeln.
- [B11] Stockklausner, H. K.: 50 Jahre Diesellokomotiven – Gesamtentwicklung 1913-1945/Entwicklung seit 1945 in Europa. Birkhäuser Verlag Basel-Stuttgart 1963
- [B12] Stockklausner, H. K.: 50 Jahre Elektro-Vollbahnlokomotiven (15 kV, 16 ²/₃ Hz) in Österreich und Deutschland. Special print “Eisenbahn“, Ployer-Verlag, Wien 1952
- [B13] 120 – Elektrische Lokomotive in Drehstromtechnik der Deutschen Bundesbahn. Special print of journal “Elektrische Bahnen“.
R. Oldenbourg, Munich 1984 (out of print).
- [B14] Electrification of Railways – International Conference. 11. – 14. November 1991, Würzburg. Sonder- und Vorabdruck aus „Elektrische Bahnen-eb“. R. Oldenbourg, Munich 1991.
- [B15] 2. International Conference Electric Railway Systems. 23. – 25. 03. 1999, Berlin. ETG-Fachbericht 74. VDE-Verlag Berlin-Offenbach 1999.
- [B16] Baur, K. G.: Baureihe 101 – Die neuen Lokomotiv-Stars der Deutschen Bahn. GeraMond Munich, 2000

- [B17] Baur, K. G.: Baureihe 152 – Geballte Kraft für schwere Züge. GeraMond Munich, 2001
- [B18] Doleschal, E.; Gerl, H.; Petrovitsch, H.; Saliger, W.: Triebfahrzeuge österreichischer Eisenbahnen – Diesel-Lokomotiven und Diesel-Triebwagen. Eisenbahn-Fahrzeug-Archiv A3. Alba-Verlag Düsseldorf, 2. Aufl. 1999
- [B19] Bendel, H., u. a.: Die elektrische Lokomotive. Transpress Berlin, 1994
- [B20] Martinsen, W.O.; Rahn, T. (editors): ICE – Zug der Zukunft. Hestra-Verlag Darmstadt 1997
- [B21] Kurz, H.; Weschta, A. (editors): ICE T, BR 411, 415 und 605. Hestra-Verlag Darmstadt, 2000
- [B22] Messerschmidt, W.: Ellok-Raritäten – Kuriositäten und Besonderheiten elektrischer Lokomotiven. Franckh, Stuttgart 1976
- [B23] Schleife, W. u. a.: Metros der Welt – Geschichte – Technik – Betrieb. Transpress, Berlin, 2nd edition 1992
- [B24] Riechers, D.: Regionaltriebwagen. Neue Fahrzeuge für Deutschlands Nahverkehr. Transpress, Stuttgart 1998
- [B25] Mohan, N.; Undeland, T.; Robbins, W.: Power Electronics - Converters, Applications and Design. John Wiley & Sons, New York, 2nd edition, 1995
- [B26] VDV, BMVBW: Light Rail in Germany. Alba Fachverlag GmbH + Co KG, Düsseldorf 2000
- [B27] Biesenack, H.; George, G.; Hofmann, G.; Schmieder, A.: Energieversorgung elektrischer Bahnen. Teubner, Wiesbaden 2006
- [B28] Boshart, A.: Straßenbahnen. Sammlung Göschen 559, 2nd edition, Berlin and Leipzig 1920
- [B29] Dettmar, G.: Die Entwicklung der Starkstromtechnik in Deutschland, Teil 1: Die Anfänge bis etwa 1890 (Kap. 11). ETZ-Verlag, Berlin 1940 – 2nd edition (Reprint) vde-verlag gmbh, Berlin-Offenbach 1990
- [B30] Baur, K. G.: Die Geschichte der Drehstromlokomotive. EK-Verlag, Freiburg 2005
- [B31] IEC: International Electrotechnical Vocabulary online database <http://std.iec.ch/iec60050>
- [B32] UIC (editors): UIC Railway Dictionary. I: Deutsch-English-Francais. MAV Rt., Budapest 1995
- [B33] Baur, K. G.: Drehgestelle – Bogies. EK-Verlag, Freiburg 2006
- [V1] Lecture „Grundlagen der Energietechnik (Basics of Electrical Power Engineering)“, Institute for Electrical Power Engineering and Power Electronics, Ruhr-University Bochum 2006
- [V2] Lecture „Leistungselektronik (Power Electronics)“, Lehrstuhl für Erzeugung und Anwendung Elektrischer Energie, Institute for Electrical Power Engineering and Power Electronics, Ruhr-University Bochum 2006
- [V3] Lecture „Raumzeigerbasierte Regelung für Power Quality und Induktionsmaschinen (Space-vector-based control for Power Quality and Induction Machines)“, Institute for Electrical Power Engineering and Power Electronics, Ruhr-University Bochum 2006

16.2 Journals

- [Z1] Elektrische Bahnen – eb. R. Oldenbourg Verlag München.
- [Z2] ZEV+DET Glasers Annalen – Die Eisenbahntechnik. G. Siemens Verlagsbuch-handlung Berlin.
- [Z3] Eisenbahntechnische Rundschau ETR. Hestra Verlag Darmstadt
- [Z4] Eisenbahn-Revue International. Verlag Minirex AG Luzern.
- [Z5] eisenbahn magazin. Alba Publikation Düsseldorf.

16.3 Selected papers from journals and conferences

- [1] Schoen, L.: 100 Jahre elektrische Bahnen.
Etz Bd. 100 (1979), Nr. 12, pp. 630–633
- [2] Kill, E.: Elektrische Bahnsysteme – heute und morgen.
Etz Bd. 101 (1980), Nr. 16/17, pp. 938–943
- [3] Sachs, K.: Vergangenheit, Gegenwart und Zukunft der elektrischen Traktion in der Schweiz. Bull. SEV 34 (1943), Nr. 20, pp. 587–612
- [4] Ernst, A.: Hundert Jahre elektrische Eisenbahn: Rückblick aus schweizerischer Sicht auf die Entwicklung der elektrischen Eisenbahn.
Bull. SEV/VSE 70 (1979), Nr. 9, pp. 423–431
- [5] Rotter, R.: 150 Jahre Eisenbahn in Österreich, Teil III: Die elektrische Zugförderung im Jubiläumsjahr 150 Jahre Eisenbahn in Österreich.
Elektrotechnik und Maschinenbau 104 (1987), pp. 309–331
- [6] Gladigau, A.: Historische Entwicklung und Stand der Bahnstromsysteme.
Elektrische Bahnen 85 (1987), Nr.12, pp. 383–390
- [7] Klingel, _: Über den Lauf der Eisenbahnwagen auf gerader Bahn.
Organ für die Fortschritte des Eisenbahnwesens XX (1883)
- [8] Koffman, J. L.: Hundert Jahre Klingels Formel.
ZEV-Glas. Ann. 108 (1984), Nr. 2, pp. 54–56
- [9] Weber, H. H.: Prof. Heumanns Arbeiten auf dem Gebiet der Spurführung im Zeichen der heutigen Rad/Schiene-Technik.
ZEV-Glas. Ann. 102 (1978), Nr. 7–8, pp. 201–213
- [10] Kottenhahn, V.: Schneller Fahren auf vorhandenen Strecken – Die gleisbogenab-hängige Wagenkastensteuerung.
ETR- Eisenbahntechnische Rundschau 36 (1987), Nr. 11, pp. 705–711.
- [11] Koschinski, K.; Krolop, M.: Neigetchnik in Europa. Eisenbahn-Journal Special Print 4/2001. Hermann Merker Verlag, Fürstfeldbruck
- [12] Kalker, J. J.: On the rolling contact of two elastic bodies in the presence of dry friction.
Diss. TU Delft (1967)
- [13] Krettek, O.: Wo stehen wir in der Erforschung des Kraftschlusses?
ZEV-Glas. Ann. 97 (1973), Nr. 1, pp. 19–28, p. 157
- [14] Fiehn, H.; Weinhardt, M.; Zeevenhooven, N.: Drehstromversuchsfahrzeug der Niederländischen Eisenbahnen – Adhäsionsmessungen.
Elektrische Bahnen 77 (1979), Nr. 19, pp. 329–338

- [15] Curtius, E. W.; Kniffler, A.: Neue Erkenntnisse über die Haftung zwischen Treibrad und Schiene. *Elektrische Bahnen* 20 (1944), Nr. 2, pp. 25–29; Nr. 3, pp. 51–57
- [16] Lang, W.; Roth, G.: Optimale Kraftschlußausnutzung bei Hochleistungs-Schiene-fahrzeugen. *Eisenbahntechnische Rundschau* 42 (1993), Nr. 1–2, pp. 61–66
- [17] Bauer, H.-P.; Pfeiffer, R.; Hahn, K.: Optimale Kraftschlußausnutzung durch selbst-adaptierende Radschlupfregelung am Beispiel eines Drehstrom-Lokomotivantriebes. *Elektrische Bahnen* 84 (1986), Nr. 2, pp. 43–57
- [18] Weinhardt, M.: Erkenntnisse und Maßnahmen zur Hochausnutzung des Kraftschlusses auf modernen Triebfahrzeugen. *Archiv für Eisenbahntechnik* 42, pp. 119–144
- [19] Buscher, M.; Pfeiffer, R.; Schwartz, H.-J.: Radschlupfregelung für Drehstromloko-motiven. *Elektrische Bahnen* 91 (1993), Nr. 5, pp. 163–178
- [20] Engel, B.; Beck, H.-P.; Alders, J.: Verschleißreduzierende Radschlupfregelung mit hoher Kraftschlußausnutzung. *Elektrische Bahnen* 96 (1998), Nr. 6, pp. 201–209
- [21] Schreiber, R.; Kögel, R.; Häse, P.; Hildenbrand, P.: Regelung zur optimalen Kraftschlußausnutzung bei Drehstromlokomotiven auf der Basis der Steigung der Kraftschlußkennlinien. *Elektrische Bahnen* 93 (1995) Nr. 5, pp. 157–163
- [22] Jöckel, A.; Pfeifer, R.: Regelungstechnische Bedämpfung der Reibschwingungen im Antriebsstrang von Drehstromtriebfahrzeugen. *Elektrische Bahnen* 93 (1995), Nr. 5, pp. 151–157
- [23] Kilb, E.: Antriebe für elektrische Triebfahrzeuge. *Elsners Taschenbuch für den maschinentechnischen Fahrdienst*. Tetzlaff-Verlag Frankfurt, 1965, pp. 212 ff.; 1966, pp. 61 ff.
- [24] Koffman, J. L.: Der Tatzlager-Motor, eine Erfindung von F. J. Sprague, und die Auswirkungen auf den Oberbau. *Lok-Magazin* 88 (1978), pp. 15–22
- [25] Kloß, G.: Der SSW-Gummiringfederantrieb. Zur Entwicklung der abgefederten Tatzlagermotoren. *Elektrische Bahnen* 51 (1953), Nr. 10, p. 256ff.
- [26] Koch, W.: Der neue BBC-Gummi-Gelenk-Kardantrieb für schnellfahrende Lokomotiven. *Elektrische Bahnen* 61 (1963), Nr. 5, pp. 98–109
- [27] Abraham, L., Heumann, K., Koppelman, F., Patschke, U.: Pulsverfahren der Energieelektronik elektromotorischer Antriebe. *VDE-Fachberichte* 23 (1964), pp. 239–252
- [28] Heintze, K.; Wagner, R.: Elektronische Gleichstromsteller zur Geschwindigkeitssteuerung von aus Fahrleitungen gespeisten Gleichstrom-Triebfahrzeugen. *ETZ-A* 1966, Nr. 5, pp. 165 ff.
- [29] Knapp, P.: Der Gleichstromsteller zum Antrieb und Bremsen von Gleichstrom-fahrzeugen. *Brown-Boveri Mitteilungen* 1970, Nr. 6/7, pp. 252 ff.
- [30] Skudelny, H.-Ch.: Stromrichterschaltungen für Wechselstrom-Triebfahrzeuge. *ETZ-A* 1965, Nr. 8, S. 249–259
- [31] Winter, P.: Netzverhalten von Wechselstromtriebfahrzeugen mit Mehrfachfolgesteuerungen in Stromrichtersparschaltung. *ZEV-Glasers Annalen* 96 (1972), Nr. 2/3, pp. 87 ff.
- [32] Förster, J.: Löschbare Fahrzeugstromrichter zur Netzentlastung und –stützung. *Elektrische Bahnen* 43 (1972), Nr. 1, pp. 13–17
- [33] Stein, W.: Lichtbogenfreie Lastumschaltung mit Siliziumstromtoren bei Stufentransformatoren. *Elektrische Bahnen* 34 (1963), Nr. 9, p. 204 ff.
- [34] Fechner, W.; Dusin, M.: Einsatz und Erprobung der neuen LEW-Lokomotive Baureihe 212/243. *Elektrische Bahnen* 84 (1986), Nr. 2, pp. 57–63

- [35] Rentmeister, M.: Grenzen der Leistungsfähigkeit elektrischer Triebfahrzeuge. *Elektrische Bahnen* 77 (1979), Nr. 8, pp. 220–226
- [36] Brun, D.: Why the French chose synchronous motors. *Railway Gazette International* Feb. 1985, pp. 130–134
- [37] Coget, G.: The new generation of SNCF high-speed rolling stock: The TGV-Atlantique train. *Rail Engineering International* 1986, Nr 3, pp. 15–18
- [38] Runge, W.: Bahnantriebssysteme mit synchronen Fahrmotoren; Wirkungsweise, Eigenschaften und Besonderheiten gegenüber Asynchronantrieben. *Elektrische Bahnen* eb 85 (1987), Nr. 7, pp. 205–217
- [39] Boutonnet, J.-C.: Lokomotive Baureihe 26000 SYBIC der Société Nationale des Chemins des fer Français. *Elektrische Bahnen* 92 (1994), Nr. 1/2, pp. 38–47
- [40] Bonifas, J.: La Traction Asynchrone des TGV de Nouvelle Generation, *Int. Symp. on Technological Innovation in Guided Transport*, Lille 1994
- [41] Andresen, E.; Blöcher, B.; Heil, J.; Pfeiffer, R.: Permanent erregter Synchronmotor mit maschinenkommutiertem Frequenzumrichter. *etz-Archiv* 9 (1987), pp. 399–402
- [42] Jöckel, A.; Koch, Th.; Binder, A.: Getrieblose Antriebe für den ICE der nächsten Generation. *VDE-Kongress 2002, Fachtagung 2: Zukunftsweisende Bahntechnik*.
- [43] Weh, H.: Permanenterrregte Synchronmaschine hoher Kraftdichte nach dem Trans-versalflussprinzip. *Etz Archiv* 10 (1988), Nr. 5, pp. 143–149
- [44] Steimel, K.: Die elektrische Energietechnik der Schienen- und Straßenfahrzeuge *ETZ A* 89 (1968), Nr. 24, pp. 658–669
- [45] Körber, J.: Drehstromtechnik für elektrische und dieselelektrische Triebfahrzeuge – Erfahrungen und Ausblick. *ZEV-Glasers Annalen* 100 (1976), Nr. 2/3, pp. 58–64
- [46] Teich, W.: Drehstromantriebstechnik in Schienenfahrzeugen – Versuchseinheiten, Prototypen, Serien. *ZEV-Glasers Annalen* 101 (1977), Nr. 8/9, pp. 371–382
- [47] Müller-Hellmann, A.; Skudelny, H.-Ch.: Übersicht über den Stand der Drehstromantriebstechnik bei Bahnverwaltungen in der Bundesrepublik Deutschland. *Elektrische Bahnen* eb 79 (1981), Nr. 11, pp. 374–379; Nr. 12, pp. 418–422
- [48] Horstmann, D.; Wagner, R.; Weigel, W.-D.: 100 Jahre Entwicklung der Antriebstechnik für elektrische Bahnen. *Elektrische Bahnen* 101 (2003), Nr. 6, pp. 255–270, and Nr. 7, pp. 338–345
- [49] Depenbrock, M.; Steimel, A.: High Power Traction Drives and Convertors. *Electrical Drives Symposium EDS '90, Capri 1990*, pp. I 1–9
- [50] Steimel, A.: Electric Railway Traction in Europe. *IEEE Industry Applications Magazine*, Vol. 2, Nr. 6, Nov./Dec. 1996, pp. 6–17
- [51] Largiadèr, H.: Gesichtspunkte für die Bemessung umrichter gespeister Asynchronmotoren für die Traktion. *Brown Boveri Mitteilungen* 57 (1970), Nr. 4, pp. 152–167
- [52] Teich, W.: Grundsätzliche Abhängigkeiten der Fahrmotor- und Wechselrichter-Dimensionierung beim Asynchronantrieb. *ETR Eisenbahntechnische Rundschau* 1975, Nr.1/2, pp. 44–50
- [53] Moritz, W.-D.; Röhlk, J.: Drehstrom-Asynchronfahrmotoren für elektrische Triebfahrzeuge. *Elektrische Bahnen* 50 (1979), Nr. 3, pp. 65–71
- [54] Steimel, K.; Heumann, K.: Kommutatorloser Bahnmotor mit Pulswechselrichter für Akkumulatortriebwagen. *AEg-Mitteilungen* 55 (1965), Nr. 3, pp. 220–226
- [55] Hochbruck, H.; Kocher, E.; Körber, J.; Teich, W.: Drehstromtechnik mit Asynchronfahrmotoren – ein neues Antriebssystem für Bahnen. *BBC-Nachrichten* 57 (1975), Nr. 5/6, pp. 348–359

- [56] Steimel, A.: GTO-Umrichter mit Spannungszwischenkreis. ETG-Fachtagung 23 „Abschaltbare Elemente der Leistungselektronik und ihre Anwendungen“ (1988), pp. 333–343
- [57] Schönung, A.; Stemmler, H.: Geregelter Drehstrom-Umkehrantrieb mit gesteuertem Umrichter nach dem Unterschwingungsverfahren. BBC-Mitteilungen 1964, pp. 555–577
- [58] Müller, E.; Ricke, F.: Die Auswirkung verschiedener Steuertechniken des Unterschwingungsverfahrens auf die Wechselrichter-Ausgangsspannung. Brown Boveri Mitteilungen 60 (1973), Nr. 1, pp. 35–44
- [59] Blaschke, F.: The principle of field orientation as applied to the new TRANS-VECTOR closed-loop control system for rotating machines. Siemens Review (1972), pp. 217–226
- [60] Gedeon, G.; Klausecker, K.; Lang, W.: Mikrocomputer-Ansteuerung für ICE. Elektrische Bahnen 86 (1988), Nr. 7, pp. 229–235
- [61] Horstmann, D.; Stanke, G.: Die stromrichternahe Antriebsregelung des Steuergeräts für Bahnautomatisierungssysteme SIBAS 32. Elektrische Bahnen 90 (1992), Nr.11, pp. 344–350
- [62] Bonifas, J.; Marchand, J.: A New Traction System for the Paris Metro. 4th Europ. Conf. on Power Electronics, Florence 1991
- [63] Depenbrock, M.: Direct Self-Control (DSC) of Inverter-Fed Induction Machine. IEEE Transactions on Power Electronics, vol. 4, pp. 420–429, 1988
- [64] Jänecke, M.; Kremer, R.; Steuerwald, G.: Direct Self Control (DSC), A Novel Method Of Controlling Asynchronous Machines in Traction Applications. Elektrische Bahnen 88 (1990), No. 3, pp. 81–87
- [65] Steimel, A.: Control of the induction machine in traction. Elektrische Bahnen 96 (1998), Nr. 12, pp. 361–369
- [66] Depenbrock, M.; Foerth, Ch.; Hoffmann, F.; Koch, S.; Steimel, A.; Weidauer, M.: Speed-sensorless stator-flux-oriented control of induction motor drives in traction. Communications – Scientific Letters of the University of Zilina 2–3/2001, pp. 68–75
- [67] Feldmann, U.; Löwe, H.-J.; Piepenbreier, E.: Schieflast auf Schienen. Der Nahverkehr 1990, H. 2, S. 44–51. Siemens A19100-V500-B343
- [68] Maiss, K. J.; Teich, W.: Elektrische Lokomotiven für 15 kV 16 2/3 und 50 Hz mit BBC-Drehstromantriebstechnik für schweren Industrieinsatz. Elektrische Bahnen 48 (1977), Nr. 4, pp. 95–103
- [69] Depenbrock, M.: Einphasen-Stromrichter mit sinusförmigem Netzstrom und gut geglätteten Gleichgrößen. ETZ-A 94 (1973), Nr. 8, pp. 466–471
- [70] Kehrmann, H.; Lienau, W.; Nill, R.: Vierquadrantensteller – eine netzfreundliche Einspeisung für Triebfahrzeuge mit Drehstromantrieb. Elektrische Bahnen 45 (1974), Nr. 6, pp. 135–142
- [71] Appun, P.; Lienau, W.: Der Vierquadrantensteller bei induktivem und kapazitivem Betrieb. etzArchiv 6 (1984), Nr. 1, pp. 3–8
- [72] Seger, T.; Wächter, M.: Direct Digital Control of Four-Quadrant Power Converter. 2nd Europ. Conf. on Power Electronics, Grenoble 1987, pp. 123–128
- [73] Depenbrock, M.: Selbstgeführte Wechselrichter mit lastunabhängigem Kommutierungsschwingkreis. BBC-Nachr. 46 (1964) 12, pp. 669–673
- [74] Brenneisen, J., Schönung, A.: Bestimmungsgrößen des selbstgeführten Stromrichters in sperrspannungsfreier Schaltung bei Steuerung nach dem Unterschwingungsverfahren. ETZ-A 90 (1969), Nr. 14, pp. 353–357

- [75] Appun, P.; Futterlieb, E.; Kommissari, K.; Marx, W.: Die elektrische Auslegung der Stromrichterausrüstung der Lokomotive 120 der Deutschen Bundesbahn. *Elektrische Bahnen* 80 (1982), Nr. 10, pp. 290–294 and Nr. 11, pp. 314–317
- [76] Gerlach, W.: Abschaltbare Bauelemente der Leistungselektronik. *ETG-Fachtagung 23 „Abschaltbare Elemente der Leistungselektronik und ihre Anwendungen“* (1988), pp. 1–27
- [77] Runge, W.; Skrabo, B.: Application of GTO Thyristors in Motive Power Converters. ABB Publication CH-VT1360E
- [78] Runge, W.; Steimel, A.: Some Aspects of the Circuit Design of High-Power GTO Converters, 3rd Europ. Conf. on Power Electronics, Aachen 1989, pp. 1555–1560
- [79] Ohashi, H.: Snubber Circuit for High-Power Gate Turn-Off Thyristors. *IEEE Transactions on Industrial Applications* 19 (1983), Nr. 4, pp. 655–664
- [80] Marquardt, R.: Untersuchung von Stromrichterschaltungen mit GTO-Thyristoren. Ph. D. Dissertation TU Hannover 1982
- [81] Undeland, T.; Jensen, F.; Steinbakk, A.; Røgne, T.; Hernes, M.: A snubber configuration for both power transistors and GTO PWM inverters. *IEEE PESC Conference* 1984, pp. 42–53.
- [82] McMurray, W.: Efficient Snubbers for Voltage-Source GTO Inverters. *IEEE PESC Conference Record* 1985, pp. 20–27
- [83] Wagner, J.: Thyristorbeschaltung für stromkommutierte Wechselrichter. German Patent DE 2128454
- [84] Sittig, R.: Hochleistungsbauelemente für die Traktion. *Elektrische Bahnen* 97 (1999), Nr. 9, pp. 300–305
- [85] Holtz, J.; Stadtfeld, S.; Lammert, P.: An economic very high power PWM inverter for induction motor drives, Europ. Conf. on Power Electronics, Brussels 1985, 3.75
- [86] Nabae, A.; Takahashi, I.; Akagi, H.: A New Neutral-Point-Clamped PWM Inverter. *IEEE Trans. Ind. Appl.* 17 (1981), Nr. 5, pp. 518–523
- [87] Steinke, J. K.: PWM Control Of A Three-Level Inverter Principles and Practical Experience. Proc. of the IEE-PEVD, London 1990
- [88] Waidmann, W.: Drehstromantrieb für Gleichstrombahnen. *Siemens-Zeitschrift* 50 (1976), Nr. 7, pp. 493–497
- [89] Falk, P.; Sauer, H.: Die elektrische Ausrüstung der neuen Triebzüge 480 der Berliner S-Bahn. *Eisenbahntechnische Rundschau (ETR)* 35 (1986), Nr. 9, pp. 607–617
- [90] Lienau, W.; Müller-Hellmann, A.: Möglichkeiten zum Betrieb von stromeinprägenden Wechselrichtern ohne niederfrequente Oberschwingungen. *ETZ-A* 97 (1976), pp. 663–667
- [91] Wiegner, G.: Siedekühlung für Fahrzeugstromrichter. *ZEV-Glasers Annalen* 109 (1985), Nr. 2/3, pp. 103–113
- [92] Jomard, T.; Eckes, U.; Lallemand, M.: Two-Phase Cooling Evolution of High Power Semiconductors, 4th Europ. Conf. on Power Electronics, Florence 1991, pp.491–496
- [93] Gammert, R.: Die elektrische Ausrüstung der Drehstromlokomotive Baureihe 120 der Deutschen Bundesbahn. *Elektrische Bahnen* 77 (1979), Nr. 10, pp. 272–283
- [94] Jung, M.: Hochleistungsstromrichter für Bahnen. *Elektrische Bahnen* 91 (1993), Nr. 3, pp. 87–93
- [95] Führer, W. M.; Marquardt, R.; Papp, G.: Water-cooled High Power GTO Converters for Electric Traction, 5th Europ. Conf. on Power Electronics, Brighton 1993, pp. 294–298

- [96] Baumann, H.; Lienau, W.: Kühlverfahren für Drehstromantriebssysteme im leichten und schweren Nahverkehr. ETG-Fachbericht 50 „Elektrische Antriebe für Fahrzeuge des öffentlichen Nahverkehrs“, pp. 87–109
- [97] Marquardt, R.: GTO-Hochleistungsstromrichter für Bahnen. ETR 41 (1992), Nr. 1/2, pp. 41–46
- [98] Marquardt, R.: High Power GTO Converters for the New German High Speed Train ICE. 3rd Europ. Conf. on Power Electronics, Aachen 1989, pp. 583–588
- [99] Bendien, J.; Krämer, W.: A 3-Phase High- Power GTO-Converter for Locomotive Drive Systems. 4th Europ. Conf. on Power Electronics, Florence 1991, pp. 579–582
- [100] Rappenglück, W.; Gammert, R.; Geier, W.: Eine neue Stromrichter- und Leitetchnik- generation zur Erprobung bei der DB. ETR 40 (1991), Nr. 10, pp. 641–648
- [101] Lienau, W.; Runge, W.: Development Trends of High Power Traction Converters. 4th Europ. Conf. on Power Electronics, Florence 1991, pp. 583–588
- [102] Herbst, I.: Status and future trends of propulsion systems for rolling stock and their correlation to power semiconductors. 2001 International Symposium on Power Semiconductor Devices & ICS, Osaka
- [103] Bakran, M. M.; Eckel, H.-G.: Traction Converter with 6.5kV IGBT modules. 9th Europ. Conf. on Power Electronics, Graz 2001
- [104] Ferrazzini, P.: Die elektrischen, mit Gleichstromsteller ausgerüsteten Vollbahn-lokomotiven der Reihen E 632/E 633 der Italienischen Staatsbahnen, Teil 2: Elektrischer Teil. ZEV-Glas. Ann. 107 (1983) Nr. 8/9, pp. 288–296
- [105] Framba, B.; Morisi, L.; Varini, A.; Vittadini, G.: Le locomotive a chopper Gr. 652 ed E 453/454 delle F.S. 1°, in Convegno Internazionale: Le ferrovie nei trasporti degli anni 2000, Bologna 1989
- [106] Gomisel, G.; Romano, R.: L'equipaggiamento elettrico dell' elettronico ETR 450. La Tecnica Professionale No. 5, 1989
- [107] Björklund, B.: Thyristorlokomotiven Reihe Rc 2 und Rc 3 der Schwedischen Staatsbahnen. Elektrische Bahnen, Nr. 6 (1971), pp. 122–130
- [108] Kühner, F.; Mojzis, K.: Die österreichische Thyristorlokomotive ÖBB Reihe 1044. Eisenbahntechnik 10 (1975), Nr. 3, pp. 71–83
- [109] Katzer, G.: Die elektrische Ausrüstung der Lokomotive Baureihe 111 der Deutschen Bundesbahn. ZEV-Glasers Annalen 99 (1975), Nr. 12, pp. 351–353
- [110] Schönfisch, J.: Hochgeschwindigkeitszüge in Frankreich. Elektrische Bahnen 100 (2002), Nr. 1/2, pp. 68–74
- [111] Badstieber, J., Kommissari, K.: Energierückgewinnung bei Bremsvorgängen. Etz 103 (1982), Nr. 7/8, pp. 373–378
- [112] Still, L.; Hammer, W.: Auslegung und elektrischer Leistungsteil der Lokomotive Baureihe 101 der Deutschen Bahn. Elektrische Bahnen 94 (1996), Nr. 8/9, pp. 235–247
- [113] Gerber, M.; Drabek, E.; Müller, R.: Die Lokomotiven 2000 Serie 460 der Schweizerischen Bundesbahnen. Schweizer Eisenbahn-Revue 10/1991, pp. 321–377
- [114] Petrovitsch, H.: Das Shinkansen-Hochgeschwindigkeits-Netz in Japan. Eisenbahn-Revue 7/2002, pp. 320–330, 8-9/2002, pp. 372–379
- [115] Rappenglück, W.: Die Antriebskonzeption von Triebfahrzeugen für den Schnellverkehr. Elektrische Bahnen 49 (1978), Nr. 12, pp. 306–320
- [116] Winden, R.: Three-Phase Drive System from Brown Boveri for the Intercity Experimental Trainset of German Federal Railways. Brown Boveri Review 12/86, pp. 680–688

- [117] Tietze, C.: Die elektrische Ausrüstung der Viersystemlokomotive 184 (Bauart AEG) der DB mit Thyristor-Leistungsstromrichtern. *Elektrische Bahnen* 37 (1966), Nr. 11, pp. 259–265
- [118] Appun, P.; Reichelt, E.: Mehrsystemlokomotiven – heutige technische Möglichkeiten der Realisierung. *Eisenbahntechnische Rundschau (ETR)* 38 (1989), Nr. 4, pp. 195–200
- [119] Zimmermann, C.: Die Zweisystemlokomotive Class 92 für Güter- und Nachtreisezüge durch den Kanaltunnel und in Großbritannien. *Eisenbahn-Revue* 3/1997, pp. 84–91
- [120] Distelrath, V.; Martin, A.: The S 252 Dual-System AC Electric Locomotive with Three-Phase Drive for Spanish Railways. *Elektrische Bahnen* 88 (1990), Nr. 5, pp. 224–235
- [121] Weschta, A.: Die elektrische Ausrüstung der Schnellverkehrstriebzüge ICE 3 und ICT der Deutschen Bahn AG. *ZEV-DET Glasers Annalen* 119 (1995), Nr. 9/10, pp. 425–435
- [122] Ketteler, K.-H.: Multisystem Propulsion Concept on the Basis of the Double Star Concept. 6th Europ. Conf. on Power Electronics, Sevilla 1995, pp. 2.159–2.166
- [123] Morisi, L.; Sezenna, F.; Mantica, L.; Oberti, M.: High Performance Multisystem Locomotive E 412 for Italian State Railways. 6th Europ. Conf. on Power Electronics, Sevilla 1995, pp. 2.066–2.071
- [124] Jahn, P.; Leichtfried, H.: Traktionsausrüstung der ÖBB-Zweisystemlokomotive Reihe 1822. *ABB-Technik* 4/92, pp. 15–22
- [125] Fuchs, A.; Friedrich, T.; Marquardt, R.: Advanced multi-system locomotives using 6.5 kV power semiconductors. 8th Europ. Conf. on Power Electronics, Lausanne 1999
- [126] Kießling, B.; Thoma, Ch.: Europalokomotive BR 189 – Die Mehrsystemlokomotive für den europaweiten Einsatz. *ZEVrail Glasers Annalen* Nr. 126 (2002), Nr. 9
- [127] Gerster, C.; Skarpetowski, G.; Sommer, H.; Still, L.: Advanced multi-system traction chain for locomotives and power heads. 10th Conf. on Power Electronic and Motion Control (EPE-PEMC), Riga 2004
- [128] Brenneisen, J.; Futterlieb, E.; Müller, E. and Schulz, M.: A New Converter Drive System for a Diesel-Electric Locomotive with an Asynchronous Traction Motor. *IEEE Trans. on Industrial Application*, Vol. IA-9 (1973), Nr. 4, pp. 482–491
- [129] Kampschulte, B.; Steimel, A.: PWM-Inverter-fed AC Drive for Diesel-Electric Shunt Locomotives. *IEEE/IAS International Semiconductor Power Converter Conference (ISPCC)*, 1982, pp. 137–144
- [130] Teich, W.: Wesentliche Systemunterschiede zwischen der Drehstromantriebstechnik und der hydraulischen Übertragung. *Elektrische Bahnen* 81 (1983), Nr. 4, pp. 124–131
- [131] Steimel, A.: Application of Evaporative cooled GTO Inverters and Transistor Auxiliary Inverters on a Diesel-Electric Locomotive. 3rd Europ. Conf. on Power Electronics, Aachen 1989, pp. 1575–1580
- [132] Tretow, H.-J.: DE 1024 – eine schwere Diesellokomotive für universellen Einsatz. *Eisenbahntechnische Rundschau (ETR)* 38 (1989), Nr. 9, pp. 569–574
- [133] Gratzfeld, P.: Moderne dieselelektrische Lokomotiven mit GTO-Wechselrichtern. *Eisenbahntechnische Rundschau (ETR)* 38 (1989), Nr. 12, pp. 745–750
- [134] At Burlington Northern's: Diesel AC Gets Started. *Siemens/AEG Transportation Systems Special Aug.* 1993, pp. 32–33
- [135] Wagner, R.: Drehstrom-Antriebstechnik für Diesellokomotiven in Nordamerika. *ZEV-DET Glasers Annalen* 1994, Nr. 2/3

- [136] Lenhard, D.; Engel, B.; Langwost, J.; Söffker, C.: Elektrische Ausrüstung des Triebzuges LIREX Baureihe 618/619 für DB Regio. *Elektrische Bahnen* 98 (2000), Nr. 8, pp. 279–288
- [137] Kuhn, W.; Schulz, M.: Zweikraftlokomotive mit Drehstromtechnik. *BBC-Nachrichten* 60 (1978), Nr. 4, pp. 135–141
- [138] Sachse, D.: Drehstromantriebstechnik für nordamerikanische Diesellokomotiven. *ZEV-DET Glasers Annalen* 1989, Nr. 4, pp. 431–443
- [139] Müller-Hellmann, A.: Drehstromantriebe auf Fahrzeugen des Schienen-Nahverkehrs. *Der Nahverkehr* 4/84
- [140] Dompke, T.; Brunnecker, U.: S-Bahn-Triebzug Kopenhagen – innovatives Konzept für die Zukunft. *ZEV+DET Glasers Annalen* 122 (1998), Nr. 4, pp. 125–137
- [141] Falk, P.: Triebzugfamilie Baureihen 423 bis 426 für DB Regio. *Elektrische Bahnen* 98 (2000), Nr. 5–6, pp. 163–173
- [142] – : Fünf Jahre ÖPNV-Niederflur-Schienenfahrzeuge. *Stadtverkehr – Fachzeitschrift für den öffentlichen Personen-Nahverkehr*, special/1993. EK-Verlag Freiburg, 1993
- [143] Ahlbrecht, H.; Dreps, M.; Int-Veen, M.; Kochte, R.: Niederflur-Straßenbahnen MD8-NF in Essen – Baustein der Fahrzeugfamilie LF 2000. *Elektrische Bahnen* 101 (2003), Nr. 7, pp. 330–337, and Nr. 9, pp. 429–436
- [144] Weschta, A.: Power Converters with IGBTs for the new Light Rail Vehicle for the City of Frankfurt. *5th Europ. Conf. on Power Electronics*, Brighton 1993, pp. 229–234
- [145] Schütze, Th.; Strönisch, V.: Low Floor Trams with IGBT 3-level-inverters. *4th Europ. Conf. on Power Electronics*, Florence 1991
- [146] Bakran, M.; Eckel, H. G.: The Evolution of IGBT Converters in Mass Transit Applications. *IEEE-IAS Annual Meeting 2000*, Rome, CD-Rom
- [147] Wittfeld, G.: Elektrische Speicher. *Glasers Annalen* 1922, Nr. 12, pp. 166–171 (in [B8])
- [148] Troche, H.: Die Akkumulator-Triebwagen Bauart Wittfeld der Preußischen Staatsbahn. *Jahrbuch 10/1978 der Dt. Ges. f. Eisenbahngeschichte*, pp. 5–114
- [149] Wilke, G.: Elektrische Energiespeicher in ihrer Verwendung für Speichertriebwagen der Deutschen Bundesbahn. *Eisenbahntechnische Rundschau* 1953, Nr. 10, pp. 508–512; Nr. 11, pp. 542–548
- [150] – : Brennstoffzellen-Lokomotive erfolgreich getestet. *Elektrizitätswirtschaft* 101 (2002), Nr. 19, pp. 11 and www.fuelcellpropulsion.org
- [151] Schulze-Manitius, H.: Der Gyrobus. *Kraftfahrzeugtechnik* 1 (1951), Nr. 9, pp. 208–210
- [152] Müller, S.: Schwungrad-Energiespeicher auf Bahn und Bus gestern und heute. *Eisenbahn-Revue International* 2001, Nr. 11, pp. 512–515; Nr. 12, pp. 563–567
- [153] Jungkind, E.: Die Druckluftbremse der elektrischen Lokomotive Baureihe 120 für die Deutsche Bundesbahn. *Elektrische Bahnen* 78 (1980), Nr.3, pp. 67–70; in [B13]
- [154] Raschl, A.: Moderne Gelenkwagen für die Wuppertaler Schwebebahn. *Elektrische Bahnen* 45 (1974), Nr. 5, pp. 102–109
- [155] Biel, W.; Biontino, S.: Elektrische Ausrüstungen mit Thyristor-Gleichstromsteller-Steuerung für die neuen Gelenkwagen der Wuppertaler Schwebebahn. *Elektrische Bahnen* 45 (1974), Nr. 5, pp. 110–115
- [156] Müller, S.: H-Bahn – Systementwicklung für den Schienennahverkehr von morgen. *ETZ* Bd. 102 (1981), Nr. 14, pp. 758–761
- [157] Petersen, H.-J.; Klein, S.: Die Automatisierungstechnik der neuen Kabinenbahn am Flughafen Düsseldorf. *ZEV+DET Glasers Annalen – Die Eisenbahntechnik* 2001, Nr. 4

- [158] Ahlbrecht, H.: Das Duo-Spursystem in Essen. *Elektrische Bahnen* 90 (1992), Nr. 4, pp. 153–160
- [159] Naumann, T.: Nancy: König Fahrgast ist am Zug – oder am Bus? *Stadtverkehr* 9/02, pp. 32–36
- [160] Brown, G. D.; Ebacher, B. J.; Koellner, W. G.: Increased Productivity with AC Drives for Mining Excavators and Haul Trucks. IEEE Industrial Application Society (IAS), 35th Annual Meeting 2000, Rome
- [161] Kemper, H.: Schwebende Aufhängung durch magnetische Kräfte: Eine Möglichkeit für eine grundsätzlich neue Fortbewegungsart. *Elektrotechnische Zeitschrift (ETZ)* 59 (1938), p. 391 ff.
- [162] Kemper, H.: Schwebebahn mit räderlosen Fahrzeugen, die an eisernen Fahrschienen mittels magnetischer Felder schwebend entlang geführt werden. German Patent DRP 643 316, filed 11.08.1934
- [163] Parsch, C. P.; Ciessow, G.: Die Antriebsausrüstung des TRANSRAPID 06 mit eisenbehaftetem Langstatormotor. *Elektrische Bahnen* 79 (1981), Nr. 8, pp. 290–295
- [164] Dreimann, K.; Betz, H.; Leistikow, R.: Die Stromversorgung für den Antrieb des TRANSRAPID 06. *Elektrische Bahnen* 79 (1981), Nr. 8, pp. 296–301
- [165] Lingaya, S.; Wiechens, H.: Die Streckenschaltanlage für den Antrieb des TRANSRAPID 06. *Elektrische Bahnen* 79 (1981), Nr. 8, pp. 302–307
- [166] Gibson, J. P.; Klocker, P.; Mrha, W.; Salomon, B.: Steuerung und Regelung für den Antrieb des TRANSRAPID 06. *Elektrische Bahnen* 79 (1981), Nr. 8, pp. 307–311
- [167] Mnich, P.; Rogg, D.; Witt, M.: Stand und Vergleich der Magnetschnellbahnsysteme in Deutschland und Japan. *Elektrische Bahnen* 97 (1999), Nr. 12, pp. 410–420
- [168] Heidelberg, G.; Pleger, J.: Die M-Bahn – ein magnetisch getragenes Nahverkehrsmittel. *Eisenbahntechnische Rundschau (ETR)* 33 (1984), Nr. 6, pp. 515–518.
- [169] Hellinger, R.; Nothhaft, J.: Energieversorgung und Antriebssystem für TRANSRAPID-Anwendungsstrecken. VDE-Congress 2002, Special Conf. 2 „Zukunftsweisende Bahntechnik“, 3.4.
- [170] Henning, U.; Hellinger, R.: Antriebsausrüstung des Transrapid. *Elektrische Bahnen* 101 (2003), Nr. 1–2, pp. 81–90
- [171] Breimeier, R.: Die Magnetschwebbahn – die Eisenbahn der Zukunft? *Eisenbahn-Revue International* 11/2001, pp. 515–519
- [172] Breimeier, R.: Transrapid-Diskussion mit geschönten Daten? *Eisenbahn-Revue International* 3/2002, pp. 154–157
- [173] Kilb, E.: Die unsymmetrische Belastung des Drehstromnetzes durch Einphasenwechselstrombahnen 50 Hz. *Elektrische Bahnen* 22 (1951), Nr. 10, pp. 263–267 and Nr. 11, pp. 285–293
- [174] Bischof, W.: Untersuchung über die optimale Energieversorgung einer Referenzstrecke Frankfurt-Köln. *Elektrische Bahnen* 87 (1989), Nr. 6, pp. 168–172
- [175] Tietze, C.: Bahnstrom wieder im Gerede. *Eisenbahn-Magazin* 9/96, pp. 38–42
- [176] Eberling, W.; Levermann-Vollmer, D.; Klinge, R.; Martens, G.: Oberleitungskonzepte und Autotransformersystem bei der Deutschen Bahn. *Elektrische Bahnen* 100 (2002), Nr. 7, pp. 259–265
- [177] – : Elektrischer Betrieb bei der Deutschen Bahn im Jahre 2006. *Elektrische Bahnen* 105 (2007), Nr. 1/2, pp. 4–44
- [178] Putz, G.: Die 70-MW-Umformersätze des GKN II. *Elektrische Bahnen* 87 (1989), Nr. 3, pp. 83–86
- [179] Granzer, R.: Die dezentrale Bahnenergieversorgung bei der Deutschen Reichsbahn. *Elektrische Bahnen* 89 (1991), Nr. 1, pp. 36–39 and Nr. 2, pp. 62–65

- [180] Wechmann, W.: Bahnstrom aus der öffentlichen Elektrizitätsversorgung unter Berücksichtigung der neuesten Technik. World Power Conference Stockholm 1933, pp. 11–121
- [181] Tröger, R.: 4000-kVA-Umrichter für das Reichsbahn-Unterwerk der Wiesentalbahn. Elektrische Bahnen 10 (1934), pp. 15–19
- [182] Gaupp, O.; Linhofer, G.; Lochner, G.: Leistungsstarke statische Frequenzumrichter für den Bahnverkehr durch die Alpen. ABB Technik 5/1995, pp. 4–10
- [183] Zimmert, G.; Scheuring, J.; Werth, L.; Koeltzsch, W.; Niehage, H.; Tadros, Y.: Umrichterwerk Jübek. Elektrische Bahnen 93 (1995), Nr. 3, pp. 85–92
- [184] Fieber, E.; Hühmer, H.-G.: Statischer Umrichter Muldenstein. Elektrische Bahnen 93 (1995), Nr. 1/2, pp. 43–48; Nr. 3, pp. 94–97
- [185] Lönard, D.; Northe, J.; Wensky, D.: Statische Bahnstromumrichter – Systemüber-sicht ausgeführter Anlagen. Elektrische Bahnen 93 (1995), Nr. 6, pp. 179–190
- [186] Gaupp, O.; Dähler, P.; Bärlocher, E.; Werninger, J.: Vollstatische 100-MW-Frequenzkupplung Bremen. ABB Technik 9/10 1996, pp. 4–17
- [187] Grüning, H.; Lönard, D.: Leistungshalbleiter und Schaltungstechnik für Bahnstromanwendungen der Zukunft. Elektrische Bahnen 97 (1999), Nr. 1/2, pp. 42–48
- [188] Fister, V.; Kreitmayer, S.; Jergas, E.; Niessen, M.; Lönard, D.; Northe, J.: Bahnstromumrichter Karlsfeld der Bayernwerk AG. Elektrische Bahnen 93 (1995), Nr.1/2, pp. 43–48; Nr. 3, pp. 94–97
- [189] Baumeler, H.: 15-MW-Standardumrichter für DB Energie. Elektrische Bahnen 98 (2000), Nr. 10, pp. 358–363
- [190] Dicks, H.; Janning, J.: Standardumrichter Typ BAUM für DB Energie. Elektrische Bahnen 98 (2000), Nr. 10, pp. 364–373
- [191] Schäfer, H.- H.: Problematik der Stromversorgung von 50-Hz- und 60-Hz-Bahnstrecken. Elektrische Bahnen 50 (1979), Nr. 2, pp. 41–90
- [192] Kiwit, W.: Bahnstrom aus der öffentlichen Energieversorgung. Elektrische Bahnen 85 (1987), Nr. 12, pp. 416–424
- [193] Schäfer, H.- H.: 50 Hz für Bahnstrom – eine Frage des Umfelds! Elektrische Bahnen 85 (1987), Nr. 12, pp. 433–438
- [194] Palecek, J.: Belastungsunsymmetrie bei 50-Hz-Bahnen. Elektrische Bahnen 96(1998), Nr. 11, pp. 355–357
- [195] EN 50 160: Merkmale der Spannung in Öffentlichen Elektrizitätsversorgungsnetzen. Nov. 1994
- [196] Hirakawa, M. et al.: Application of Self-Commutated Inverters to Substation Reactive Power Control. CIGRE Report 23-205, 1996
- [197] Xie, J. : Symmetrierumrichter für 50-Hz-Bahnen. Elektrische Bahnen 97 (1999), Nr. 1/2, pp. 49–55
- [198] Braun, E.; Klinge, R.; Zimmert, G.; Hofmann G.: Mehrspannungssysteme in der Bahnenergieversorgung im Vergleich. Elektrische Bahnen 93 (1995), Nr. 3, pp. 67–73
- [199] Hertel, U.: Elektrifizierung in Kanada – die Tumbler-Ridge-Bahn. Elektrische Bahnen 84 (1986), Nr. 9, pp. 266–277
- [200] Rao, N. U.: The GM GF6C Electric Locomotive. IEEE Transactions on Industrial Application Vol. 22 (1986), Nr. 3, pp. 502–511
- [201] Hübener, W.: Elektrische Schmalspur-Güterzuglokomotive für 2400 V Gleichstrom für die Bahn St. Georges de Commiers-la Mure. Elektrische Bahnen 1906, Nr. 4, pp. 185–192
- [202] Röhlig, S.: Streuströme bei DC-Bahnen und elektrotechnische Anforderungen an den Gleisbau. Elektrische Bahnen 99 (2001), Nr. 1/2, pp. 84–89

- [203] DIN EN 50 122-1: Bahnanwendungen – Ortsfeste Anlagen, Schutzmaßnahmen in Bezug auf elektrische Sicherheit und Erdung. 1997-12
and -2: Bahnanwendungen – Ortsfeste Anlagen, Schutzmaßnahmen gegen Auswirkung von Streuströmen verursacht von Gleichstrombahnen, 1999-05.
- [204] Gunselmann, W.; Höschler, P.: Energiespeichereinsatz bei den Kölner Verkehrsbetrieben. *Elektrische Bahnen* 98 (2000), Nr. 11–12, pp. 463–468
- [205] Halfmann, U.; Hein, G.; Olsen, H.; Röhlig, S.: Wirtschaftliche Optimierung von Stadtbahnen durch Nutzung der Bremsenergie in Energiespeichern. VDE-Congress 2002, FT 2 „Zukunftsweisende Bahntechnik“, 1.3
- [206] Blaschko, R.; Jäger, K.: Hochgeschwindigkeits-Stromabnehmer für den ICE 3. *Elektrische Bahnen* 98 (2000), Nr. 9, pp. 332–338
- [207] Mier, G.: Stahl/Aluminium-Stromschienen für S- und U-Bahnen. *Elektrische Bahnen* 89 (1991), Nr. 7, pp. 212–215
- [208] Jötten, R.: Über die Belastung von Fahrleitungsnetzen durch Stromrichterlokomotiven. Ph. D. Dissertation TH Darmstadt 1953
- [209] Bethge, W.: Die elektromagnetische Verträglichkeit (EMV) elektrischer Triebfahrzeuge mit Nachrichtenanlagen. *Elektrische Bahnen* 81 (1983) Nr. 7, pp. 216–226
- [210] Bethge, W.: Die Lokomotivbaureihe 120 – Beeinflussungsuntersuchungen bezüglich der Fernmelde- und Sicherungsanlagen. *Elektrische Bahnen* 81 (1983), Nr. 7, pp. 216–226
- [211] Steimel, A.: Netzbelastung durch Wechselstrom-Triebfahrzeuge mit leistungselektronischer Steuerung. *etz Archiv* 12 (1990), Nr. 3, pp. 69–79
- [212] Meyer, M.; Schöning, J.: Netzstabilität in großen Bahnnetzen. *Eisenbahn-Revue* 7–8/1999, pp. 312–317
- [213] DIN VDE 0228 Teil 3/09.88: Beeinflussung durch Wechselstrom-Bahnanlagen. VDE-Verlag Berlin-Offenbach
- [214] Runge, W.: Netzrückwirkungen bei Fahrzeugen an der Fahrleitung. ETG-Special Report 50: Elektrische Antriebe für Fahrzeuge des öffentlichen Nahverkehrs, pp. 215–233
- [215] Runge, W.: Niederfrequente Netzrückwirkungen von Bahnfahrzeugen mit Drehstromantriebstechnik. *Elektrische Bahnen* 90 (1992), Nr. 10, pp. 319–325
- [216] Steimel, A.: Line Interference by A.C. Traction Material Controlled by Power Electronic Systems. KAIST-Workshop “New Transportation Systems”, 1993, Taejon/ Korea, pp. 30–37
- [217] Steimel, A.: Steuerungsbedingte Unterschiede von wechselrichtergespeisten Traktionsantrieben. *Elektrische Bahnen* 92 (1994), Nr. 1/2, pp. 24–36
- [218] Fryze, S.: Wirk-, Blind- und Scheinleistung in elektrischen Stromkreisen mit nicht-sinusförmigem Verlauf von Strom und Spannung. *ETZ* 53 (1932), pp. 596–599, 625–627, 700–702
- [219] Klein, H.-J.: Entstehung, Ausbreitung und Wirkung der Störströme von Pulsstromrichtern auf Bahnfahrzeugen mit Wechselspannungseinspeisung. Ph. D. Dissertation Wuppertal 1987
- [220] Reichelt, E.: Leichte Universallokomotive El 17 der Norwegischen Staatsbahn mit Drehstromantriebstechnik. *Elektrische Bahnen* 80 (1982) Nr. 7, pp. 207–214
- [221] Fischer, J. W.; Löbel, W.: Gesichtspunkte für die Bemessung von Netzfiltern bei Stromrichterfahrzeugen im Wechselspannungsnetz. *Elektrische Bahnen* 85 (1987), Nr. 5, pp. 148–153

- [222] Kristiansen, H.; Lang, A.: Lokomotiven in Drehstromtechnik El 17 für die Expreßzüge der Norwegischen Staatsbahn – Zweite Bauserie. *Elektrische Bahnen* 85 (1987) Nr. 6, pp. 173–181
- [223] Runge, W.: Control of Line Harmonics due to Four-quadrant-converter in AC Tractive Stock by means of Filter and Transformer. 7th Europ. Conf. on Power Electronics, Trondheim 1997, 3.459–3.464
- [224] Krittian, F.: Messung und Berechnung der Fahrleitungsimpedanz elektrifizierter Eisenbahnstrecken. *Elektrische Bahnen* 42 (1971) Nr. 7, pp. 151–157
- [225] Holtz, J.; Kraha, J.: Adaptive optimal pulse width modulation for the line-side converter of electric locomotives. *Elektrische Bahnen* 88 (1990), Nr. 3, pp. 116–121
- [226] Hüchelheim, K.; Mangold, Ch.: Novel 4-quadrant converter control method. *Elektrische Bahnen* 88 (1990), Nr. 3, pp. 122–125
- [227] CENELEC: EN 50388 (2005): Power supply and rolling stock – Technical criteria for the coordination between power supply and rolling stock to achieve interoperability – M/275
- [228] Vennegeerts, H.; Haubrich, H.-J.; Schaarschmidt, J.; Kox, A.: Parallelführung von Bahnstrom- und Drehstrom-Freileitungen. *Elektrische Bahnen* 98 (2000), Nr. 3, pp. 100–104
- [229] Buckel, R.: Elektrische Schutzmaßnahmen an Untergrundbahnen mit Gleich- und Wechselstrombetrieb. *Schienen der Welt* 1970, Nr. 1
- [230] Buckel, R.: Elektromagnetische Umweltbeeinflussung durch Triebfahrzeuge mit An-schnittsteuerung. *Elektrische Bahnen* 45 (1974), Nr. 1, pp. 19–21 and Nr. 2, pp. 39–45
- [231] Buckel, R.: Beeinflussung von Fernsprechanlagen durch Oberschwingungen im Fahr-leitungsnetz von Gleichstrombahnen. *Elektrische Bahnen* 82 (1984) Nr. 4, pp. 123–133
- [232] Henning, U.; Petersen, A. J.; Würfler, D.; Staudt, V.; Pozzobon, P.: Elektrische System-kompatibilität im europäischen Bahnnetz – Ergebnisse des Projekts ESCARV. *Elek-trische Bahnen* 99 (2001) Nr. 6/7, pp. 284–291
- [233] Gemmeke, K.: Suppression of narrow-band harmonics in the input current of traction vehicles. 3rd IFAC-Symposium, Lausanne 1983, pp. 627–634
- [234] Würflinger, K.; Foerth, C.; Steimel, A.: Reduction of interference currents in dc traction inverter drives using the highly dynamic torque control. 10th Europ. Conf. on Power Electronics, Toulouse 2003
- [235] Van der Weem, J.: Ein neues Konzept zur Minderung der Beeinflussung von 50-Hz-Gleisstromkreisen. *Elektrische Bahnen* 90 (1992), Nr. 10, pp. 328–332
- [236] Kovacs, K.P.; Racs, I.: *Transiente Vorgänge in Wechselstrommaschinen*. Verlag der Ungarischen Akademie der Wissenschaften, Budapest 1959
- [237] Steimel, A.: Stator-flux-oriented high performance control in traction. Tutorial H-4, 35th Annual Meeting IEEE IAS Industry Application Society, Rome 2000
- [238] Hasse, K.: Zum dynamischen Verhalten der Asynchronmaschine bei Betrieb mit vari-abler Ständerfrequenz und Ständerspannung. *ETZ-A* 89 (1968), pp. 77–81
- [239] Blaschke, F.: Das Verfahren der Feldorientierung zur Regelung der Asynchronma-schine. *Siemens Forschungs- u. Entwicklungs-Berichte* 1 (1972), Nr. 1, pp. 184–193
- [240] Depenbrock, M.; Skrotzki, Th.: Drehmomenteinstellung im Feldschwächbereich bei stromrichter-gespeisten Drehfeldantrieben mit Direkter Selbstregelung (DSR). *Etz-Archiv* 9 (1987), Nr. 1, pp. 3–8

- [241] Jänecke, M.; Hoffmann, F.: Fast Torque Control of an IGBT-Inverter-Fed Three-Phase A.C. Drive in the Whole Speed Range – Experimental Results. 6th Europ. Conf. on Power Electronics, Sevilla 1995, Vol. 3, pp. 399–404
- [242] Steimel, A.: Direct Self Control and Synchronous Pulse Techniques for High-Power Traction Inverters in Comparison. IEEE Transactions on Industrial Electronics Vol. 51 (2004), No. 4, pp. 810–820
- [243] Baader, U.: Hochdynamische Drehmomentregelung einer Asynchronmaschine im ständerflussbezogenen Koordinatensystem. *EtzArchiv* 6 (1989), H. 1, S. 11–16
- [244] Hoffmann, F.: Drehgeberlos geregelte Induktionsmaschinen an IGBT-Pulsstromrichtern. Ph. D. Dissertation, Ruhr-Universität Bochum, Germany, 1996.
- [245] Kubota, H.; Matsuse, K.; Nakano, T.: DSP-based speed adaptive flux observer of induction motor. IEEE Transactions on Industry Applications, 1993, No. 2, pp. 344–348
- [246] Depenbrock, M.; Hoffmann, F.; Koch, S.: Speed Sensorless High Performance Control for Traction Drives. 7th Europ. Conf. on Power Electronics, Trondheim 1997, Vol. 1, pp. 1.418–1.423
- [247] Hoffmann, F.; Koch, S.: Steady State Analysis of Speed Sensorless Control of Induction Machines. Industrial Electronics Conference (IECON), Aachen 1998, Vol. 3, pp. 1626–1631
- [248] Depenbrock, M.; Foerth, C.; Koch, S.: Speed Sensorless Control Of Induction Motors At Very Low Stator Frequencies. 8th Europ. Conf. on Power Electronics, Lausanne 1999
- [249] Foerth, C.: Traktionsantrieb ohne Drehzahlgeber mit minimiertem Messaufwand. Ph. D. Dissertation, Ruhr-Universität Bochum, Germany, 2001
- [250] Frenzke, T.; Hoffmann, F.; Langer, H.-G.: Speed Sensorless Control of Traction Drives – Experiences on Vehicles. 8th Europ. Conf. on Power Electronics, Lausanne 1999
- [251] Amler, G.; Sperr, F.; Hoffmann, F.: Highly dynamic and speed sensorless control of traction drives. 10th Europ. Conf. on Power Electronics, Toulouse 2003
- [252] Gerl, B.: Schienenverkehr – Antriebe mit Zugkraft. Siemens Pictures of the World, Spring 2006. <http://www.siemens.de/pdf>
- [253] Schwendt, L.: Eine neue Lokomotive für die Neue Welt – die ALP 46 für New Jersey Transit (USA). *Eisenbahn-Revue* 4/2002, pp. 180–185
- [254] Schreiber, R.; Papritz, M.: Baureihe 185 – Weiterentwicklung einer bewährten Plattform. *Eisenbahn-Revue* 8-9/2004, pp. 358–363
- [255] Vitins, J.; Landolt, M.: Elektrische Lokomotiven für den internationalen Güterverkehr. *Eisenbahn-Revue* 4/2006, pp. 170–175
- [256] – : Neue 6-MW-Prima-Lokomotive von Alstom. *Eisenbahn-Revue* 10/2004, pp. 449–451
- [257] Schurig, J.: Die Mehrsystem-Lokomotive ES 64 U4 (ÖBB-Reihe 1216). *Eisenbahn-Revue* 5/2005, pp. 220–228, 6/2005, pp. 268–274 and 7/2005, pp. 333–335
- [258] Möller, D.; Schlegel, C.: Velaro – Further Development of the ICE for Worldwide Use. *Elektrische Bahnen* 104 (2006), Nr. 5, pp. 258–263.
- [259] Baur, K. G.: TRAXX DE – Die neue Diesellokomotive von Bombardier. *Eisenbahn-Kurier* 1/2007, pp. 66–71
- [260] Buscher, M.; Köck, F.; Trotsch, P.; Bikle, U.: TRAXX: Integrale Plattform zur Steigerung der Wettbewerbsfähigkeit des Schienenverkehrs. *ETR – Eisenbahntechnische Rundschau* 9/2006,

17 Exercises with exemplary solutions

17.1 F-v-Diagram of a Universal Locomotive

The specification of a high-power universal locomotive provides – in a simplified manner – the three following load cases for permanent speed ($a = 0$), which shall define the corner points of the F-v-Diagram (weights in metric tons):

1. Intercity train	Mass (with locomotive)	m_1	570	t
	Number of coaches	n_1	15	
	Speed	v_1	220	kph
	Gradient	s_1	5 ‰	
2. Express goods train	Mass (with locomotive)	m_2	2200	t
	Speed	v_2	120	kph
	Gradient	s_2	5 ‰	
3. Mixed goods train	Mass (with locomotive)	m_3	2000	t
	Speed	v_3	75	kph
	Gradient	s_3	10 ‰	

The rolling resistances are to be calculated according to the DB formulas according to *Sauthoff* (for 1.; the locomotive is to be regarded as an additional coach) or acc. to *Strahl* (2. or 3., respectively) according to section 2.2.1. The curvature resistance needs not to be regarded as the ruling gradient shall take this already into account (“compensated curves“). Load case 3 shall define the nominal tractive effort, which shall be assumed in the starting region as well.

- Calculate the nominal power P_N and the nominal starting tractive effort F_A !
- At which speed v nominal power P_N will be reached?
- Sketch the necessary traction forces F (in kN) 1..3 depending upon speed. Carry in the limit tractive effort curve $F = f(P_N, v)$ as well as the maximum transmittable tractive effort of the locomotive according to Curtius-Kniffler (equ. 2.30), assuming a locomotive weight of $G = 84$ t!
- Give the values of the starting acceleration on level track ($s = 0!$) in the three load cases!

Normalized train resistance: $w = w_r + w_c + w_g + w_a$; here $w_a, w_c = 0$

$$w_{r1} \text{ acc. to Sauthoff: } w_{r1} = 1 + 0.0025 \cdot v + 4.8 \cdot \frac{n_1 + 1 + 2,7}{G_z / \text{kN}} \cdot 0.0145 \cdot (v + 15)^2;$$

$$\text{with } v = 220 \text{ kph} \quad w_{r1} = 13,7 \text{ ‰}$$

$$w_{r2,3} \text{ acc. to Strahl: } w_{r2} = 1 + 0,0002 \cdot v^2 = 3,9 \text{ ‰}$$

$$\text{Gradient resistance: } w_s = s \quad w_{s1} = 5 \text{ ‰} \quad w_{s2} = 5 \text{ ‰} \quad w_{s3} = 10 \text{ ‰}$$

Train resistance	$w_1 = 18,7\text{‰}$	$w_2 = 8,9\text{‰}$	$w_3 = 15,3\text{‰}$
Necessary tractive effort:: $F_i = w_i \cdot m \cdot g$	$F_1 = 105 \text{ kN}$	$F_2 = 192 \text{ kN}$	$F_3 = 300 \text{ kN}$
→ Selected as nominal tractive effort:			$F_{AN} = 300 \text{ kN}$
Nominal power: $P_i = F_i \cdot v_i$;	$P_1 = 6.4 \text{ MW}$	$P_2 = 6.4 \text{ MW}$	$P_3 = 6.25 \text{ MW}$
→ Selected as nominal power		$P_N = 6.4 \text{ MW}$	
Speed at nominal power:	$v = \frac{P_N}{F_{AN}} = \frac{6400 \text{ kW}}{300 \text{ kN}} = 21.3 \frac{\text{m}}{\text{s}} = 77 \text{ kph}$		
Acc. to Curtius-Kniffler:	$f_x = \frac{7.5}{v/\text{kph} + 44} + 0.161$ (sketch!)		
$F_\mu = f_x \cdot m \cdot g$; with $m = 84 \text{ t}$: $F_\mu(v=0) = 273 \text{ kN}$			$F_\mu(v=220 \text{ kph}) = 156 \text{ kN}$
Acceleration at level track: $w_s = 0$			
At standstill: $v=0$	$w_1 = 1.05\text{‰}$	$w_2 = 1\text{‰}$	$w_3 = 2.5\text{‰}$
Starting resistive force:	$F_1 = 5.9 \text{ kN}$	$F_2 = 216 \text{ kN}$	$F_3 = 49 \text{ kN}$
It holds: $a_i = (Z_A - F_i) / m_i$;	$a_1 = 0.52 \frac{\text{m}}{\text{s}^2}$	$a_2 = 0.13 \frac{\text{m}}{\text{s}^2}$	$a_3 = 0.13 \frac{\text{m}}{\text{s}^2}$

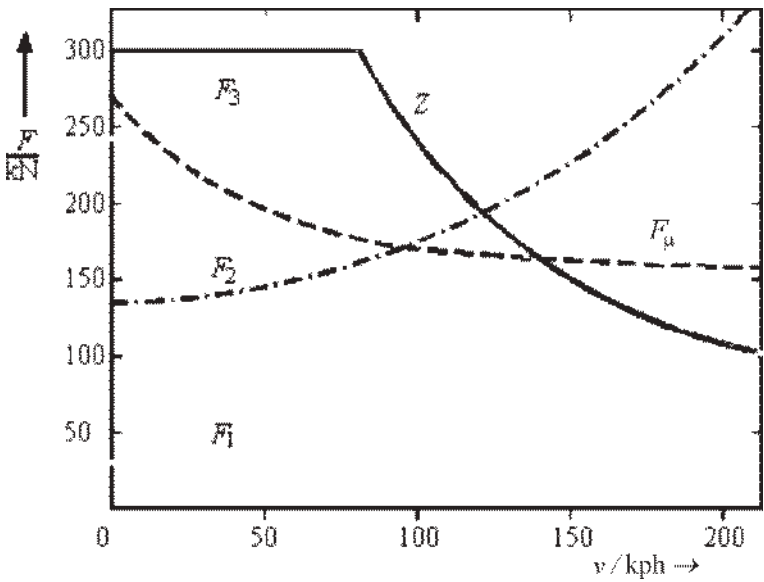


Fig. 17.1: Traction force vs. speed

17.2 Mechanical design of a Universal Locomotive

In Exercise 17.1 the power and the tractive effort of a Universal Locomotive has been defined. It shall be constructed as a four-axle bogie locomotive with a service mass (weight) of 84 t (metric tons). Additional data:

- Wheelbase in bogie $2a = 3000$ mm
- Distance of bogie centers $2b = 9900$ mm
- Tractive force at drawbar $F_H = 300$ kN
- Height of drawbar over rail top $h_H = 1030$ mm

What is the maximal height h_D of the force attack point in the bogie over rail top, so that the resulting sum of the weight forces of the front bogie does not fall below 95 % of the static weight forces, when starting with nominal starting tractive effort (from 17.1)?

Calculate the weight forces of all four wheelsets when starting with nominal starting tractive effort and the load transfer (in %)!

Continuing the design the following data are selected:

- Wheel diameter (new) $D_0 = 1250$ mm
- Maximum wheel wear $\delta R = 40$ mm

What is the gear ratio i (= ratio of motor to wheelset shaft speed) under the conditions that at

- $v_{\max} = 220$ kph, fully-worn wheels and neglected (mechanical) slip s_x the admissible maximum motor speed of
- $n_{\text{Mot, max}} = 3950$ min⁻¹

will not be exceeded?

How big is then – assuming ideal single-wheelset control with torque reference proportional to the wheelset weight force – the torque of the most heavily loaded motor with new wheels (D_0)? The efficiency of the gear shall be assumed as

- $\eta_G = 0.98$.

First let's have a look at the forward bogie (1), which will be relieved by the drawbar tug:

$$F_{zB1} = \frac{1}{2} \cdot \left[G_{\text{Loco}} - F_H \cdot \frac{h_H - h_D}{b} \right]$$

The static weight force per bogie is: $F_{B\text{-stat}} = \frac{1}{2} \cdot G_{\text{Loco}}$

The condition is: $F_{zB1} \stackrel{!}{>} 0.95 \cdot \frac{1}{2} \cdot G_{\text{Loco}}$

From that follows: $\frac{1}{2} \cdot \left[G_{\text{Loco}} - F_H \cdot \frac{h_H - h_D}{b} \right] \stackrel{!}{>} 0.95 \cdot \frac{1}{2} \cdot G_{\text{Loco}} \Rightarrow h_D \stackrel{!}{>} 350$ mm

Numbering the wheelsets from 1 to 4 from front to rear; the attack of the drawbar force is behind wheelset 4.

Wheelset weight forces:

$$F_{z1} = \frac{1}{4} \left[G_{\text{Loco}} - F_H \cdot \left(\frac{h_H - h_D}{b} + \frac{h_D}{a} \right) \right] = 178.2 \text{ kN} \quad F_{z2} = \frac{1}{4} \left[G_{\text{Loco}} - F_H \cdot \left(\frac{h_H - h_D}{b} - \frac{h_D}{a} \right) \right] = 213.2 \text{ kN}$$

$$F_{Z3} = \frac{1}{4} \left[G_{\text{Loco}} + F_H \cdot \left(\frac{h_H - h_D}{b} - \frac{h_D}{a} \right) \right] = 198.8 \text{ kN} \quad F_{Z4} = \frac{1}{4} \left[G_{\text{Loco}} + F_H \cdot \left(\frac{h_H - h_D}{b} + \frac{h_D}{a} \right) \right] = 233.8 \text{ kN}$$

With $F_{\text{ref}} = \frac{1}{4} \cdot G_{\text{Loco}} = 206 \text{ kN}$ follows the relative load transfer (in %): $E_{Zi} = 100 \cdot \left(1 - \frac{F_{Zi}}{F_{\text{ref}}} \right)$

Bogie 1: $E_{Z1} = 13.5\%$ (relieved) $E_{Z2} = -3.5\%$ (burdened)

Bogie 2: $E_{Z3} = 3.5\%$ (relieved) $E_{Z4} = -13.5\%$ (burdened)

With worn wheels the maximum motor speed n_{max} rises at given maximum speed v_{max} .

$$D_{\text{min}} = D_0 - 2 \cdot \delta R = 1170 \text{ mm}$$

$$i = \frac{n_{\text{Motor}}}{n_{\text{Wheelset}}}; \quad n_{\text{Wheelset}} = \frac{v_{\text{max}}}{\pi \cdot D_{\text{min}}} = 1000 \text{ min}^{-1} \quad \rightarrow i \leq 3.96$$

Assuming constant circumferential force the motor torque will decrease with decreasing wheel diameter, $M \sim F \cdot R$. The maximum torque occurs with new wheels at wheelset ,4' with highest absolute value of F_Z :

$$F_{\text{max}} = \frac{1}{4} \cdot F_H \cdot \frac{F_{Z4}}{F_{\text{ref}}} = 85.1 \text{ kN} \quad M_{\text{dMotor}} = \frac{1}{i} \cdot \frac{1}{\eta} \cdot F_{\text{max}} \cdot \frac{D_0}{2} = 13.7 \text{ kNm}$$

17.3 Mean traveling speed of a Metro train

A Metro train with a weight (mass) of $m_T = 90 \text{ t}$ shall maintain a starting acceleration of $a_a = 1.2 \text{ m/s}^2$ up to nominal speed $v_1 = 36 \text{ kph}$ under rated conditions; the allowance for rotating parts is $\xi = 1.11$. From v_1 to maximum speed $v_m = 80 \text{ kph}$ the power is to be kept constant, the tractive effort is reduced inversely to speed. For braking a symmetrical behavior is to be assumed; the train resistance shall be neglected.

- 1 Calculate the nominal starting tractive effort F_{AN} and the nominal power P_N .
- 2 Calculate the instants t_1 and t_m , at which the speeds v_1 and v_m , respectively, are attained, starting from $t = 0$! The solution of the differential equation $\frac{dv}{dt} = \frac{K}{v}$ is $v = \sqrt{2 \cdot K \cdot t + C}$.

- 3 How big are the distances s_1 and s_m at the instants t_1 and t_m , respectively?

$$\int \sqrt{a \cdot x + b} \, dt = \frac{2}{3 \cdot a} \cdot \sqrt{(a \cdot x + b)^3}$$

- 4 Calculate the total time loss at starting and braking t_v .

- 5 Calculate the average traveling speed \bar{v} , with a mean distance of stations $L = 1000 \text{ m}$ and a mean stopping time in each station of $t_H = 20 \text{ s}$, depending on the number n of stops and for $n \rightarrow \infty$?

Exemplary solution:

$$1. \quad F_{AN} = m \cdot \xi \cdot a_a = 120 \text{ kN} \quad P_N = Z_{AN} \cdot v_1 = 1200 \text{ kW}$$

2. Energy balance:

$$\text{at instant } t_1: \quad W_{\text{kin}1} = \frac{1}{2} \cdot m_T \cdot v_1^2$$

$$\text{at instant } t_m: \quad W_{\text{kin}m} = \frac{1}{2} \cdot m_T \cdot v_m^2$$

In the speed region beyond v_1 $P = P_N = \text{const}$ holds; with $P = \frac{dW}{dt}$ follows:

$$P = \frac{W_{\text{kin}m} - W_{\text{kin}1}}{t_m - t_1} \quad \rightarrow \quad t_m = \frac{v_m^2 - v_1^2}{2 \cdot a \cdot v_1} + t_1$$

$$t_1 = \frac{v_1}{a} = 8.3 \text{ s}$$

$$t_m = 24.7 \text{ s}$$

$$3. \quad s_1 = \frac{1}{2} \cdot a \cdot t_1^2 = 41.6 \text{ m}$$

$$s_2 = s_1 \cdot \int_u^e v dt; \text{ with } P_N(t) = \frac{\frac{1}{2} \cdot m_z \cdot (v^2 - v_1^2)}{t - t_1} \quad \rightarrow \quad v = \sqrt{2 \cdot a \cdot v_1 \cdot (t - t_1) + v_1^2}$$

$$s_m = 41.6 \text{ m} + 276.84 \text{ m} = 318.5 \text{ m}$$

As the braking is assumed to be symmetrically, i.e. with opposite force, the braking time is

$$t_B = 24.74 \text{ s}$$

and the whole braking distance

$$s_m = 41.6 \text{ m} + 276.84 \text{ m} = 318.5 \text{ m}$$

$$4. \quad \text{At } v = v_m = \text{const} \text{ the train covers the distance of } s_m = 318.5 \text{ m in } \Delta t = \frac{s}{v_E} = 14.3 \text{ s.}$$

The total time loss per acceleration and braking period is

$$t_v = t_m - \Delta t = 10.4 \text{ s}$$

5. The distance between two stations, covered at speed v_m , is:

$$s_E = L - s_2 - s_B = 363 \text{ m}$$

For that distance the time

$$t_E = \frac{s_E}{v_E} = 16.35 \text{ s}$$

is needed. The average speed, dependent on the number n of stoppings, is

$$\bar{v} = \frac{(n-1) \cdot L}{n \cdot t_H + (n-1) \cdot (t_2 + t_E + t_B)}$$

and finally

$$\bar{v}(n \rightarrow \infty) = 11.7 \frac{\text{m}}{\text{s}} \approx 42 \text{ kph}$$

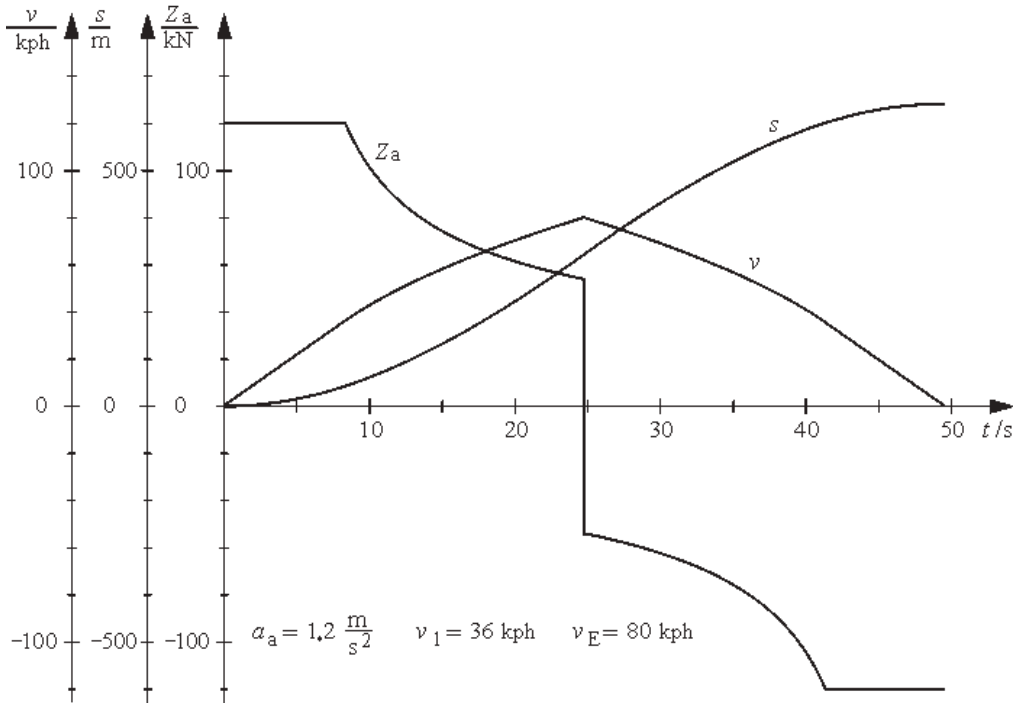


Fig. 17.2: Speed v , distance s and tractive/braking effort F vs. time

17.4 DC traction motor fed by a DC chopper

A separately-excited DC motor of a Metro train drive with a nominal voltage of $U_{AN} = 750$ V and a nominal power of $P_N = 300$ kW is to be controlled via a DC chopper with a switching frequency of $f_z = 500$ Hz from the 750-V DC line. All losses are to be neglected.

- 1 Calculate the necessary inductivity L_2 of the (linear) smoothing choke, so that the normalized armature current ripple (peak-to-peak) $\Delta i_2 / \bar{i}_2$ does not exceed the value of 40 %!
- 2 Calculate the necessary capacity C_1 of the input filter (the inductivity L_1 of the line filter choke is to be assumed infinitely), so that the normalized filter voltage ripple (peak-to-peak) $\Delta u_1 / \bar{u}_1$ does not exceed the value of 10 %!
- 3 Display the normalized (peak-to-peak) ripples $\Delta i_2 / \bar{i}_2$ and $\Delta u_1 / \bar{u}_1$ in one diagram, depending on the control factor a of the chopper!
- 4 The resonance frequency of the filter is now to be assumed as $f_c = 35$ Hz. Calculate the value of the inductivity L_1 , if C_1 from 2. is used and the inductivity of the catenary/3rd rail and the rectifier substation can be neglected.
- 5 Calculate the component of the line current with switching frequency $I_{N(250\text{Hz})}$, with the values of above. What is the value of $\Delta u_1 / \bar{u}_1$ now (only the component with switching frequency needs to be taken into account)?

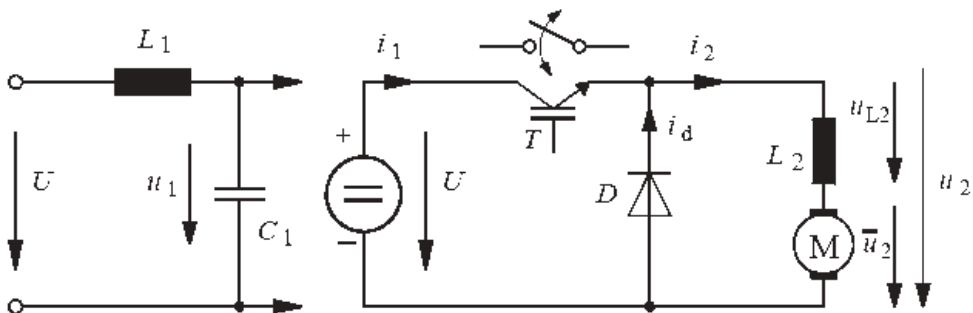


Fig. 17.3: ECD of DC chopper

1. The maximum current ripple is at $a = 0.5$, that is $T_1 = T / 2$

$$\Delta i_2 = \int_0^{T_1} u_{L2} dt = \int_{T_1}^T u_{L2} dt \quad \frac{\Delta i_2}{\bar{i}_2} \leq 0.4$$

In the interval $T - T_1$ $u_{L2} = \bar{u}_2$ holds:

$$L_2 = \frac{\bar{u}_2 \cdot (T - T_1)}{\Delta i_2} = \frac{\frac{1}{2} \cdot U_1 \cdot \frac{1}{2} \cdot T}{\Delta i_2}$$

With $\bar{i}_2 = \frac{P_N}{U_{AN}} = 400$ A $\Delta i_2 \leq 0.4 \cdot \bar{i}_2 = 160$ A holds. Then

$$L_2 = \frac{U_1}{4 \cdot f_z \cdot \Delta i_2} \geq 2.35 \text{ mH}$$

2. $\Delta u_1 \stackrel{!}{<} 0.2 \cdot \bar{u}_1$

$$\Delta u_1 = \frac{1}{C_1} \int (i_1 - \bar{i}_1) dt = \frac{F_i}{C_1}$$

$$C_1 = \frac{F_i}{\Delta u_1} = \frac{F_i}{0.1 \cdot u_1}$$

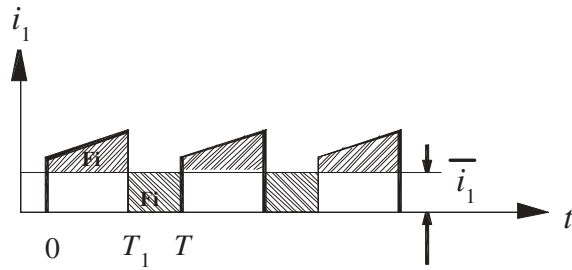


Fig. 17.4: DC chopper input current

Δu_1 will be maximal, if F_i is maximal, that is at $a = 0.5$ or $T_1 = T / 2$

$$\bar{i}_1 = a \cdot \bar{i}_2 = 0.5 \cdot \bar{i}_2 \rightarrow F_i = \frac{1}{2} \cdot I_{IN} \cdot \frac{1}{2} \cdot T = \frac{I_{IN}}{4 \cdot f_z} \rightarrow C_1 = \frac{I_{IN}}{0.1 \cdot u_1 \cdot 4 \cdot f_z} = 2.67 \text{ mF}$$

3. $\Delta i_2 = \frac{U_1 \cdot T}{L_2} \cdot a \cdot (1-a)$; with $L_2 = \frac{U_1}{0.4 \cdot \bar{i}_2 \cdot 4 \cdot f_z}$ and $f_z = \frac{1}{T}$

$$\frac{\Delta i_2}{\bar{i}_2} = 0.4 \cdot 4 \cdot a \cdot (1-a)$$

$$\Delta u_1 = \frac{\bar{i}_2 \cdot T}{C_1} \cdot a \cdot (1-a); \text{ with } C_1 = \frac{\bar{i}_2}{0.1 \cdot u_1 \cdot 4 \cdot f_z} \text{ and } f_z = \frac{1}{T}$$

$$\frac{\Delta u_1}{u_1} = 0.1 \cdot 4 \cdot a \cdot (1-a)$$

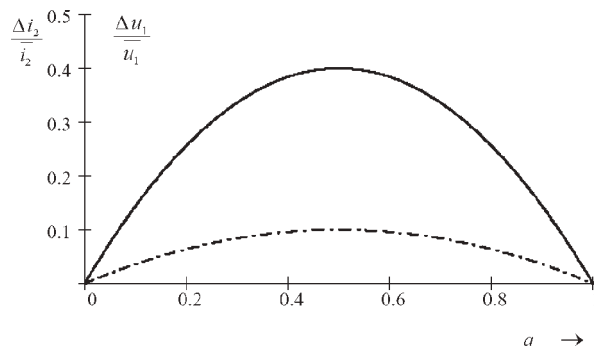


Fig. 17.5: Normalized output/input filter ripple (peak-to-peak values)

4. $f_e = \frac{1}{2 \cdot \pi \cdot \sqrt{L_1 \cdot C_1}} = 35 \text{ Hz}$; with $C_1 = 2.67 \text{ mF}$ $L_1 = \frac{1}{4 \cdot \pi^2 \cdot f_e^2 \cdot C_1} = 7.74 \text{ mH}$

5. $a = 0.5$
current gradient neglected

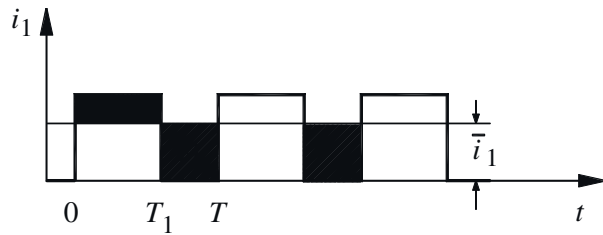


Fig. 17.6: DC chopper input current, simplified

Fourier Series Expansion of input current:

$$\hat{i}_{1(250\text{Hz})} = \frac{4}{\pi} \cdot \frac{I_{2N}}{2} \quad I_{1(250)} = \frac{1}{\sqrt{2}} \cdot \hat{i}_1 = 180 \text{ A}$$

The line current passing the filter can be calculated with the current divider equation

$$\left| \frac{I_{N(250)}}{I_{1(250)}} \right| = \frac{\frac{1}{j\omega C_1}}{j\omega L_1 + \frac{1}{j\omega C_1}} = \frac{1}{1 - v^2}$$

with the normalized frequency

$$v = 2\pi \cdot f_z \cdot \sqrt{(L_1 \cdot C_1)} = 14.3 \quad \underline{I}_{1(250)} = 180 \text{ A} \cdot 0.5\% = 0.9 \text{ A}$$

$$U_{1(250\text{Hz})} = I_{1(250\text{Hz})} \cdot 2\pi \cdot L_1 = 21.4 \text{ V}$$

$$\frac{\Delta u_I}{u_1} = \frac{2 \cdot \sqrt{2} \cdot U_{1(250\text{Hz})}}{u_1} = \frac{60.5 \text{ V}}{750 \text{ V}} = 8\% < 0.1!$$

17.5 Two-pulse bridge in half-controllable connection of pairs of arms with sequential phase control

A high-power locomotive (following the example of ÖBB 1044) for single-phase AC 15 kV/ 16 2/3 Hz is equipped with four DC traction motors with the following data:

$$P_N = 1350 \text{ kW} \quad U_N = 1015 \text{ V} \quad n_N = 1150 \text{ rpm}$$

Each two motors of a bogie are fed by a two-pulse bridge converter in half-controllable connection of pairs of arms with sequential phase control acc. to Fig. 4.15; the smoothing chokes are provided for each single traction motor.

- 1 What is the necessary value of the transformer secondary (partial) voltages U_I and U_{II} (with $U_I = U_{II}$) under the condition, that nominal power has to be supplied with a line

voltage reduced by 8%, related to the nominal value, and the following data are valid:

Normalized inductive transformer voltage drop	$u_{xN} = 5\%$
Normalized ohmic transformer voltage drop	$u_{rN} = 5\%$
Resistance of motor and smoothing choke	$R_A = 30 \text{ m}\Omega$
Inductivity of smoothing choke assumed with infinitive value	
Threshold voltage per valve (thyristor, diode)	$U_T = 1 \text{ VD2.}$

- Determine the control characteristic $\bar{u}_{di\alpha} = f(\alpha_I, \alpha_{II})$ and display in a graph the control (trigger delay) angles $\alpha_I, \alpha_{II} = f(a)$ for sequential phase control ($a = u_{di\alpha} / u_{di}$)
- Determine the r.m.s. value of the line current in dependence upon α , at $L_d \rightarrow \infty$, as given above, and neglecting all voltage drops! Calculate the power factor $\lambda(a)$ and enter the quantities into the diagram in dependence upon a !
- Ascertain now the value of the inductivity of the smoothing choke (which is to be assumed as linear) in each motor branch under the simplifying assumptions of item 3, if the double DC current ripple factor (peak to peak) is demanded as 40%!
Hint: The maximal voltage-time area is at $\alpha_I = 0^\circ, \alpha_{II} = 50\%$.

1. Regard the DC Equivalent Circuit Diagram of the series connection of two bridges:

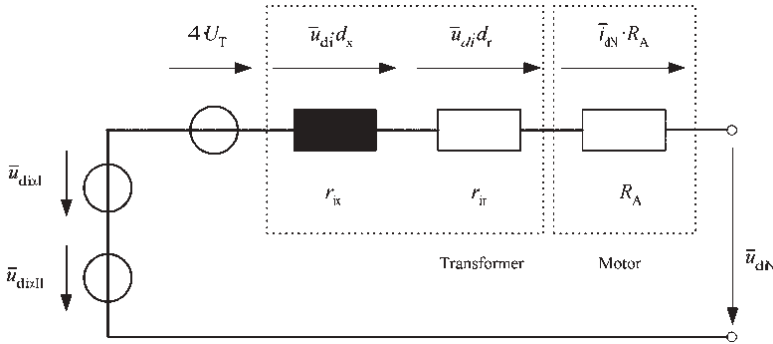


Fig. 17.7 ECD of transformer, converter and motor

$$u_N = \bar{u}_{diN} = 2 \cdot \bar{u}_{di\alpha N} - 4 \cdot U_T - R_A \cdot \bar{i}_{dN} - \bar{u}_{di} \cdot d_x - \bar{u}_{di} \cdot d_r$$

$$\bar{u}_{di} = 2 \cdot \bar{u}_{di\alpha} = 2 \cdot (1 - 0.08) \cdot \frac{2}{\pi} \cdot \sqrt{2} \cdot U_1;$$

with
$$\bar{u}_{di} = \frac{2}{\pi} \cdot \sqrt{2} \cdot U_S$$

$$\rightarrow \bar{u}_{diN} = 2 \cdot (1 - 0.08) \cdot \frac{2}{\pi} \cdot \sqrt{2} \cdot U_1 \cdot (1 - d_x - d_r) - 4 \cdot U_T - R_A \cdot \bar{i}_{dN}$$

$$d_{xN} = z_e \cdot u_{xN} = \frac{1}{\sqrt{2}} \cdot u_{xN} \quad \rightarrow \quad d_x = d_{xN} \cdot \frac{I_d}{I_{dN}} \cdot \frac{U_{\sim N}}{U_{\sim}}$$

$$d_{rN} = z_e \cdot u_{rN} = \frac{1}{\sqrt{2}} \cdot u_{rN} \quad \rightarrow \quad d_r = d_{rN} \cdot \frac{I_d}{I_{dN}} \cdot \frac{U_{\sim N}}{U_{\sim}}$$

$$\rightarrow d_x + d_r = \frac{I_d}{I_{dN}} \cdot \frac{U_{\sim N}}{U_{\sim}} \cdot (d_{xN} + d_{rN}) = \frac{I_d}{I_{dN}} \cdot \frac{U_{\sim N}}{U_{\sim}} \cdot (u_{xN} + u_M) \cdot \frac{1}{\sqrt{2}}$$

For $P = \text{const}$: $I_d = \frac{I_{dN}}{(1-0.08)}$ at $U_{\sim} = (1-0.08) \cdot U_{\sim N}$

$$\rightarrow \bar{u}_{diN} = 2 \cdot (1-0.08) \cdot \frac{2}{\pi} \cdot \sqrt{2} \cdot U_1 \cdot \left(1 - \frac{\frac{1}{\sqrt{2}} \cdot (u_{xN} + u_{rN})}{(1-0.08)^2}\right) - 4 \cdot U_T - R_A \cdot \bar{i}_{dN};$$

with $\bar{u}_{diN} = U_N$

$$\rightarrow U_1 = \frac{U_N + 4 \cdot U_T + R_A \cdot \bar{i}_{dN}}{2 \cdot (1-0.08) \cdot \frac{2}{\pi} \cdot \sqrt{2} \cdot \left(1 - \frac{\frac{1}{\sqrt{2}} \cdot (u_{xN} + u_{rN})}{(1-0.08)^2}\right)} = 700 \text{ V}$$

$$\frac{U_1}{U_{\text{prim}}} = \frac{700 \text{ V}}{15000 \text{ V}} = \frac{1}{21.4}$$

$$2. \quad \bar{u}_{di\alpha} = \underbrace{\frac{1}{\pi} \int_{\alpha_1}^{\pi} \hat{u}_I \cdot \sin \omega t \, d\omega}_{\text{Bridge I}} + \underbrace{\frac{1}{\pi} \int_{\alpha_{II}}^{\pi} \hat{u}_{II} \cdot \sin \omega t \, d\omega}_{\text{Bridge II}} = \frac{\hat{u}_I}{\pi} \cdot (1 + \cos \alpha_1) + \frac{\hat{u}_{II}}{\pi} \cdot (1 + \cos \alpha_{II})$$

with $\hat{u}_I = \hat{u}_{II}$: $\rightarrow \bar{u}_{di\alpha} = \frac{\hat{u}_I}{\pi} \cdot (2 + \cos \alpha_1 + \cos \alpha_{II})$

i.e.: Trigger delay angle $\alpha_i = 0^\circ$: Maximum bridge output voltage
 $\alpha_i = 180^\circ$: Minimum bridge output voltage

a) Keep $\alpha_{II} = \text{const} = 180^\circ$ first and vary α_1 in the region of 0° to 180° then:

$$\bar{u}_{di\alpha} = \frac{\hat{u}_I}{\pi} \cdot (2 + \cos \alpha_1 - 1) \quad \rightarrow \quad \alpha_1 = \arccos \left(\pi \cdot \frac{\bar{u}_{di\alpha}}{\hat{u}_I} - 1 \right)$$

b) Keep $\alpha_1 = \text{const} = 0^\circ$ and vary α_{II} in the region of 180° to 0° .

$$\bar{u}_{di\alpha} = \frac{\hat{u}_I}{\pi} \cdot (2 + 1 + \cos \alpha_{II}) \quad \rightarrow \quad \alpha_{II} = \arccos \left(\pi \cdot \frac{\bar{u}_{di\alpha}}{\hat{u}_I} - 3 \right)$$

Define the control factor $a = \frac{\bar{u}_{di\alpha}}{\bar{u}_{di}}$, with $\bar{u}_{di} = \bar{u}_{di\alpha}(\alpha_1 = \alpha_{II} = 0^\circ) = \frac{4}{\pi} \cdot \hat{u}_I$

$$\Rightarrow a = \frac{\overline{u_{\text{di}\alpha}}}{\hat{u}_1} \cdot \frac{\pi}{4}$$

$$\text{Thus } \alpha_{\text{I}} = \begin{cases} \arccos(4 \cdot a - 1) & 0 \leq a \leq 0,5 \\ 0^\circ & 0,5 \leq a \leq 1 \end{cases} \quad \text{and}$$

$$\alpha_{\text{II}} = \begin{cases} 180^\circ & 0 \leq a \leq 0,5 \\ \arccos(4 \cdot a - 3) & 0,5 \leq a \leq 1 \end{cases} \quad \text{hold.}$$

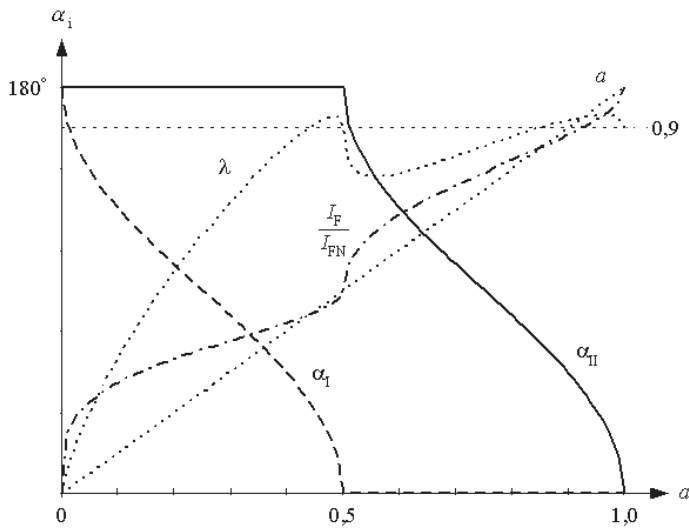


Fig. 17.8: Characteristics of two half-controllable bridges in sequential phase control

3. For $0 \leq a \leq 0.5$:

$$I_{\text{sek}}^2 = \frac{1}{\pi} \cdot \int_{\alpha_1}^{\pi} \bar{i}_{\text{dN}}^2 d\omega t = \frac{1}{\pi} \cdot \bar{i}_{\text{dN}}^2 \cdot (\pi - \alpha_1)$$

$$\Rightarrow I_{\text{sek}} = \bar{i}_{\text{dN}} \cdot \sqrt{1 - \frac{\alpha_1}{\pi}}$$

$$I_{\text{prim}} = \frac{u_{\text{sek}}}{u_{\text{prim}}} \cdot \bar{i}_{\text{dN}} \cdot \sqrt{1 - \frac{\alpha_1}{\pi}}$$

 For $0.5 \leq a \leq 1$:

$$I_{\text{sek}}^2 = \frac{1}{\pi} \cdot \int_0^{\alpha_{\text{II}}} \bar{i}_{\text{dN}}^2 d\omega t + \frac{1}{\pi} \cdot \int_{\alpha_{\text{II}}}^{\pi} (2 \cdot \bar{i}_{\text{dN}})^2 d\omega t$$

$$I_{\text{sek}}^2 = \bar{i}_{\text{dN}}^2 \cdot \left(\frac{\alpha_{\text{II}}}{\pi} + 4 \cdot \frac{\pi - \alpha_{\text{II}}}{\pi} \right)$$

$$\Rightarrow I_{\text{sek}} = \bar{i}_{\text{dN}} \cdot \sqrt{\frac{\alpha_{\text{II}}}{\pi} + 4 \cdot \left(1 - \frac{\alpha_{\text{II}}}{\pi}\right)}$$

$$I_{\text{prim}} = \frac{u_{\text{sek}}}{u_{\text{prim}}} \cdot \bar{i}_{\text{dN}} \cdot \sqrt{\frac{\alpha_{\text{II}}}{\pi} + 4 \cdot \left(1 - \frac{\alpha_{\text{II}}}{\pi}\right)}$$

$$\lambda = \frac{|P|}{S} = \frac{\bar{u}_{\text{dix}} \cdot \bar{i}_{\text{dN}}}{U_S \cdot I_F} \quad \text{with} \quad U_S = \frac{1}{\sqrt{2}} \cdot \hat{u}_1$$

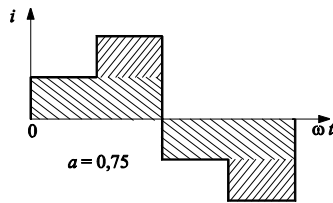
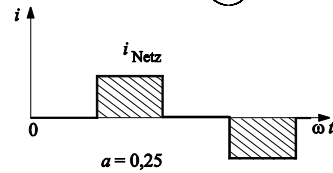
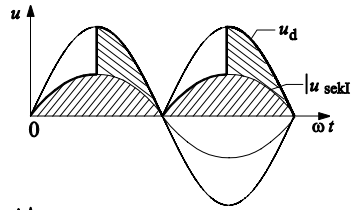
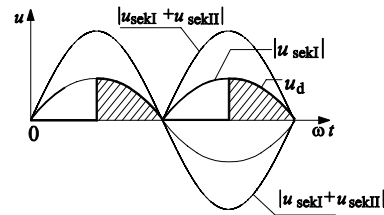


Fig. 17.9: Principal voltage and current waveforms

 a) Only α_1 variable ($0 \leq a \leq 0.5$): \Rightarrow

$$\bar{u}_{\text{dix}} = \frac{\hat{u}_1}{\pi} \cdot (1 + \cos \alpha_1)$$

$$\lambda = \frac{\frac{\hat{u}_1}{\pi} \cdot (1 + \cos \alpha_1) \cdot \bar{i}_{\text{dN}}}{\frac{1}{\sqrt{2}} \cdot \hat{u}_1 \cdot \bar{i}_{\text{dN}} \cdot \sqrt{1 - \frac{\alpha_1}{\pi}}} = \frac{\sqrt{2}}{\pi} \cdot \frac{1 + \cos \alpha_1}{\sqrt{1 - \frac{\alpha_1}{\pi}}}$$

 b) Only α_1 variable ($0.5 \leq a \leq 1$): \Rightarrow

$$\bar{u}_{\text{dix}} = \frac{\hat{u}_1}{\pi} \cdot (3 + \cos \alpha_{\text{II}})$$

$$\lambda = \frac{\frac{\hat{u}_1}{\pi} \cdot (3 + \cos \alpha_{\text{II}}) \cdot \bar{i}_{\text{dN}}}{\frac{1}{\sqrt{2}} \cdot \hat{u}_1 \cdot \bar{i}_{\text{dN}} \cdot \sqrt{\frac{\alpha_{\text{II}}}{\pi} + 4 \cdot \left(1 - \frac{\alpha_{\text{II}}}{\pi}\right)}} = \frac{\sqrt{2}}{\pi} \cdot \frac{3 + \cos \alpha_{\text{II}}}{\sqrt{\frac{\alpha_{\text{II}}}{\pi} + 4 \cdot \left(1 - \frac{\alpha_{\text{II}}}{\pi}\right)}} = \frac{\sqrt{2}}{\pi} \cdot \frac{3 + \cos \alpha_{\text{II}}}{\sqrt{4 - 3 \cdot \frac{\alpha_{\text{II}}}{\pi}}}$$

$$4. \quad \bar{u}_{\text{dix}} = \frac{\hat{u}_1}{\pi} \cdot (3 + \cos 50^\circ) = 1.16 \cdot \hat{u}_1$$

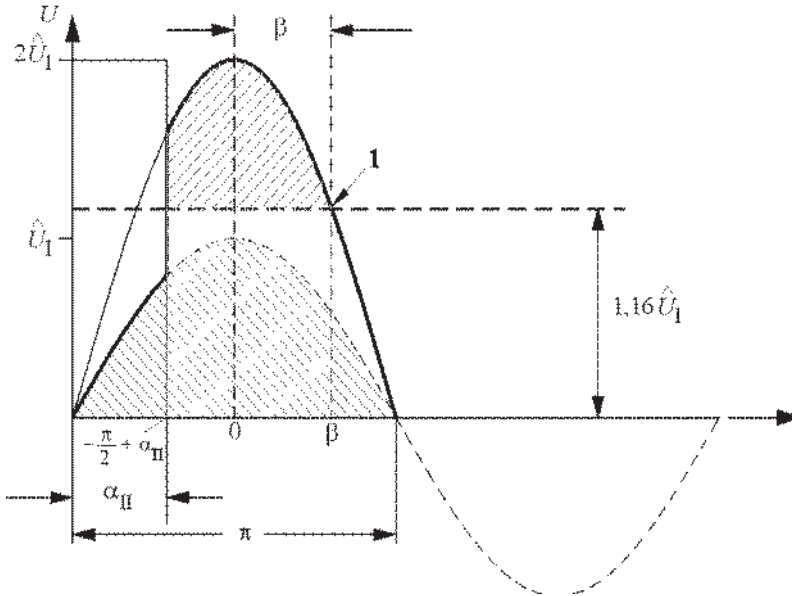


Fig. 17.10: Voltage-time areas of half-controllable bridge

For point 1 holds:

$$2 \cdot \hat{u}_1 \cdot \cos \beta = \bar{u}_{\text{dix}} \quad \rightarrow \quad \beta = \arccos \frac{\bar{u}_{\text{dix}}}{2 \cdot \hat{u}_1} = 54.6^\circ$$

Calculate the voltage-time area above the line \bar{u}_{dix} :

$$\int u_L dt = \underbrace{\int_{(-\frac{\pi}{2} + \alpha_{II})/\omega}^{\beta/\omega} 2 \cdot \hat{u}_1 \cdot \cos \omega t dt}_{\text{area II}} - \underbrace{\bar{u}_{\text{dix}} \cdot \left(\frac{\pi}{2} - \alpha_{II} + \beta \right) / \omega}_{\text{rectangular area}} = 9.5 \text{ Vs}$$

$$\text{with } \frac{\Delta i_d}{i_{dN}} = 0,4 \quad \rightarrow L = \frac{\int u_L dt}{\Delta i_d} = 17.9 \text{ mH}$$

The averaged value of the rectified inductor voltage is:

$$\overline{|u_{L-}|} = \frac{\omega}{\varepsilon} \cdot \int u_L dt = \frac{2 \cdot \pi \cdot 16 \frac{2}{3} \text{ Hz}}{\pi/2} \cdot 9.5 \text{ Vs} = 634 \text{ V} \quad \text{with } \varepsilon = \hat{\text{half conduction angle}}$$

17.6 Three-phase induction traction motor for a Universal Locomotive with 6,400 kW

The Universal Locomotive with a nominal power of 6400 kW defined and laid out mechanically in the Exercises 17.1 and 17.2 is to be equipped with three-phase squirrel-cage induction traction motor, the key electrical data of which shall be determined in this exercise. Only fundamental r.m.s. values have to be regarded.

- 1 Calculate the maximum rotary angular frequency ω_1 at the nominal point $v_1 = 77$ kph with new wheels/wheel tires ($D_0 = 1250$ mm, $i = 3.96$) for a four-pole motor design.
- 2 The leakage inductivity is determined by the demand, that the motor produces the torque which corresponds to nominal power + 5% (to compensate the load transfer from Exercise 17.2 at individual wheelset control) at maximum speed corresponding to maximum loco speed and fully-worn wheels/wheel tires ($\delta R = 40$ mm) just equates the break-down torque. The nominal DC-link voltage of the inverter is 2,800 V, the inverter is to be operated at this frequency in square-wave or block modulation.

What is the value of the rotor angular break-down frequency ω_1 at constant (maximum) terminal voltage? The rotor short-circuit time constant L_σ/R_r is 50 ms, at maximum rotor temperature; the influence of the stator resistance shall be neglected.

3. The magnetizing inductivity L_μ (which can be assumed linear) is to be calculated from the predefined leakage factor $\sigma = 10\%$.
4. In the starting region the motors are to be operated with minimum stator current (for minimal losses); what is the necessary rotor angular frequency ω_{r4} , if the magnetizing inductivity L_μ can be assumed linear? Calculate the stator current I_{s4} and the magnetizing current $I_{\mu4}$ to be impressed for the nominal torque M_{dmax} of 13.7 kNm from 17.2 and the value of the stator flux $\Psi_{\mu4}$! Draw the Heyland Circular Diagram with $\lambda_1 = 200$ A/cm). What is the value of the fundamental displacement factor $\cos \varphi_1$?
5. At the nominal point the flux which is optimal for the starting point cannot be maintained, due to the increased iron losses. The nominal point (100 % terminal voltage, square-wave modulation, from item 2) shall coincide with the point of constant power acc. to Exercise 1 (77 kph). Determine the r.m.s. value of the stator flux fundamental $\Psi_{\mu5}$ (using ω_{r4} from item 4 as first guess), then the pertaining magnetizing current $I_{\mu5}$, the rotor angular frequency ω_{r5} and the stator current r.m.s. value I_{s5} . Enter these values in the diagram; read the value of $\cos \varphi_{15}$?
6. Calculate the values of the stator-current r.m.s. I_{s6} , of stator flux $\Psi_{\mu6}$ at maximum stator frequency and power acc. to item 2! Enter these values in the diagram, and read the value of $\cos \varphi_{16}$!

$$1. \quad \omega_1 = 2 \cdot \pi \cdot p \cdot n = 2 \cdot \pi \cdot \frac{v_L}{\pi \cdot D_0} \cdot i = 270 \text{ s}^{-1}$$

$$2. \quad D = D_0 - 2 \cdot \delta R \text{ mm} = 1170 \text{ mm}$$

$$P_{\max} = \frac{1}{4} \cdot 1.05 \cdot P_N = 1680 \text{ kW per motor}$$

$$M_d = 3 \cdot p \cdot \frac{U_S^2}{\omega_S^2} \cdot \frac{\frac{\omega_r}{R_r}}{1 + \omega_r^2 \cdot \left(\frac{L_\sigma}{R_r}\right)^2} \quad \text{In the break-down point: } \omega_r = \omega_{rK} = \frac{R_r}{L_\sigma} = \frac{1}{T_\sigma} = 20 \text{ s}^{-1}$$

$$L_\sigma = \frac{3}{2} \cdot p \cdot \frac{U_S^2}{\omega_{SK}^2} \cdot \frac{1}{M_{dK}}; \quad U_S = U_{S\lambda} = \frac{\sqrt{2}}{\pi} \cdot U_d = 1260 \text{ V}$$

$$M_{dK} = \frac{M_{dRadmax}}{i} = \frac{F_{Rad}}{i} \cdot \frac{D}{2} = \frac{P_{max}}{v_{max} \cdot i} \cdot \frac{D}{2} = 4060 \text{ Nm}$$

$$\omega_{SK} = \omega_{rmax} + \omega_{rK}; \quad \omega_{rmax} = 2 \cdot \pi \cdot p \cdot \frac{v_{max}}{\pi \cdot D} \cdot i = 827 \text{ s}^{-1}$$

$$\rightarrow L_\sigma = 1.63 \text{ mH}$$

$$3. \quad \sigma = \frac{L_\sigma}{L_\mu + L_\sigma} \rightarrow L_\mu = L_\sigma \cdot \left(\frac{1}{\sigma} - 1\right); \quad \text{with } \sigma = 0.1 \rightarrow L_\mu = 9 \cdot L_\sigma = 14.7 \text{ mH}$$

$$4. \quad M_{dmax} = 3 \cdot p \cdot \frac{U_S^2}{\omega_S^2} \cdot \frac{\frac{\omega_r}{R_r}}{1 + \omega_r^2 \cdot \left(\frac{L_\sigma}{R_r}\right)^2} \quad \text{with } \frac{R_r}{L_\sigma} = \omega_{rK}, \quad \frac{U_S}{\omega_S} = \Psi_\mu$$

$$M_{dmax} = 3 \cdot p \cdot \frac{\Psi_\mu^2}{L_\sigma} \cdot \frac{\frac{\omega_r}{\omega_{rK}}}{1 + \left(\frac{\omega_r}{\omega_{rK}}\right)^2} \quad \text{with } \Psi_\mu = L_\mu \cdot I_\mu, \quad I_\mu = I_S \sqrt{\frac{1 + \left(\frac{\omega_r}{\omega_{rK}}\right)^2}{1 + \left(\frac{\omega_r}{\sigma \cdot \omega_{rK}}\right)^2}}$$

$$M_{dmax} = 3 \cdot p \cdot \frac{L_\mu^2}{L_\sigma} \cdot \frac{\frac{\omega_r}{\omega_{rK}}}{1 + \left(\frac{\omega_r}{\sigma \cdot \omega_{rK}}\right)^2} \cdot I_S^2 \rightarrow I_S^2 = \frac{M_{dmax}}{3 \cdot p} \cdot \frac{L_\sigma}{L_\mu^2} \cdot \frac{1 + \left(\frac{\omega_r}{\sigma \cdot \omega_{rK}}\right)^2}{\frac{\omega_r}{\omega_{rK}}}$$

$$I_S \text{ will be minimal, if: } \frac{d}{d\omega_r} \left[\frac{1}{\omega_{rK} \cdot \sigma^2} \cdot \frac{\omega_{rK}^2 \cdot \sigma^2 + \omega_r^2}{\omega_r} \right] = 0 \rightarrow \omega_r = \sigma \cdot \omega_{rK} = 2 \text{ s}^{-1}$$

$$I_S = 587 \text{ A}$$

$$I_\mu = 417 \text{ A}$$

$$\rightarrow \Psi_\mu = 6.13 \text{ Vs}$$

$$2. \text{ The wheel diameters are } D_x = 2 \cdot (\bar{R} + \delta R) \quad \text{with} \quad \bar{R} = \frac{1}{3} \cdot \sum_{x=1}^3 \frac{D_x}{2} = \frac{1112.5 \text{ mm}}{2} = R_3!$$

Looking at the individual wheelsets:

$$\delta R_1 = \frac{D_1}{2} - \bar{R} = 2.75 \text{ mm} \quad \delta R_2 = \frac{D_2}{2} - \bar{R} = -2.75 \text{ mm} \quad \delta R_3 = 0 \text{ mm}$$

Insert $f = p \cdot n$ into the table.

$$\text{With } \omega_x = 2 \cdot \pi \cdot p \cdot n_x \text{ and } n_x = \frac{v}{\pi \cdot D_x} \cdot i \text{ follows } \omega_{rx} = \frac{p \cdot v \cdot i}{D_x/2}$$

$$\text{Wheelset 1: } M_{d1} = 2 \cdot M_{dK} \cdot \frac{\omega_{r1}}{\omega_{rK}} \quad \text{Wheelset 2: } M_{d2} = 2 \cdot M_{dK} \cdot \frac{\omega_{r2}}{\omega_{rK}}$$

$$\text{From identical supply frequency } \omega_s = \omega_1 + \omega_{r1} = \omega_s = \omega_2 + \omega_{r2}$$

$$\text{follows } \omega_{r1} = \bar{\omega} + \omega_r^* - \omega_1 \quad \text{and} \quad \omega_{r2} = \bar{\omega} + \omega_r^* - \omega_2$$

$$\text{and} \quad M_{d1} = 2 \cdot M_{dK} \cdot \frac{\bar{\omega} + \omega_r^* - \omega_1}{\omega_{rK}} \quad M_{d2} = 2 \cdot M_{dK} \cdot \frac{\bar{\omega} + \omega_r^* - \omega_2}{\omega_{rK}}$$

$$\text{with } \omega_s = \bar{\omega} + \omega_r^* \quad \bar{\omega} = \frac{1}{3} \cdot (\omega_1 + \omega_2 + \omega_3), \quad \text{here } \bar{\omega} = \frac{1}{2} \cdot (\omega_1 + \omega_2)$$

$$M_{d1} = \frac{M_{dK}}{\omega_{rK}} \cdot (\omega_2 - \omega_1 + 2 \cdot \omega_r^*) \quad M_{d2} = \frac{M_{dK}}{\omega_{rK}} \cdot (\omega_1 - \omega_2 + 2 \cdot \omega_r^*)$$

$$\text{Replacing } \omega_1 = \frac{p \cdot v \cdot i}{R + \delta R} \quad \omega_2 = \frac{p \cdot v \cdot i}{R - \delta R}$$

$$M_{d1} = \frac{M_{dK}}{\omega_{rK}} \cdot \left(2 \cdot \omega_r^* + \frac{p \cdot v \cdot i \cdot 2 \cdot \delta R}{\bar{R}^2 - \delta R^2} \right) \quad M_{d2} = \frac{M_{dK}}{\omega_{rK}} \cdot \left(2 \cdot \omega_r^* + \frac{p \cdot v \cdot i \cdot (-2 \cdot \delta R)}{\bar{R}^2 - \delta R^2} \right)$$

and with $\delta R \ll \bar{R}$

$$M_{d1} \approx 2 \cdot M_{dK} \cdot \frac{\omega_r^*}{\omega_{rK}} \cdot \left(1 + \frac{p \cdot v \cdot i \cdot \delta R}{\omega_r^* \cdot \bar{R}^2} \right) \quad M_{d2} \approx 2 \cdot M_{dK} \cdot \frac{\omega_r^*}{\omega_{rK}} \cdot \left(1 - \frac{p \cdot v \cdot i \cdot \delta R}{\omega_r^* \cdot \bar{R}^2} \right)$$

$$M_{d1} \approx 2 \cdot M_{dK} \cdot \frac{\omega_r^*}{\omega_{rK}} \cdot \left(1 + \frac{\delta R}{\bar{R}} \cdot \frac{p \cdot v \cdot i}{R} \cdot \frac{1}{\omega_r^*} \right) \quad M_{d2} \approx 2 \cdot M_{dK} \cdot \frac{\omega_r^*}{\omega_{rK}} \cdot \left(1 - \frac{\delta R}{\bar{R}} \cdot \frac{p \cdot v \cdot i}{R} \cdot \frac{1}{\omega_r^*} \right)$$

$$\text{and with } \bar{\omega} = \frac{p \cdot v \cdot i}{R}:$$

$$M_{d1} \approx 2 \cdot M_{dK} \cdot \frac{\omega_r^*}{\omega_{rK}} \cdot \left(1 + \frac{\delta R}{R} \cdot \frac{\bar{\omega}}{\omega_r^*} \right) \quad M_{d2} \approx 2 \cdot M_{dK} \cdot \frac{\omega_r^*}{\omega_{rK}} \cdot \left(1 - \frac{\delta R}{R} \cdot \frac{\bar{\omega}}{\omega_r^*} \right)$$

From that the torque deviations, related to \bar{M}_d , follows:

$$\rightarrow \frac{\delta M_{d1}}{M_d} = \frac{M_{d1} - \bar{M}_d}{\bar{M}_d} = \frac{\delta R}{R} \cdot \frac{\bar{\omega}}{\omega_r^*} \quad \rightarrow \frac{\delta M_{d2}}{M_d} = \frac{M_{d2} - \bar{M}_d}{\bar{M}_d} = \frac{\delta R}{R} \cdot \frac{\bar{\omega}}{\omega_r^*}$$

Enter these values into the table with $\frac{\bar{\omega}}{\omega_r^*} = \frac{f}{f_r}$

$$3. P_{tot} = 2 \cdot \left(\sum_{x=1}^3 M_{dx} \cdot \bar{\Omega} \right) = 2 \cdot \sum_{x=1}^3 M_{dx} \cdot \frac{2 \cdot \pi \cdot f}{p}$$

$$v = \frac{2 \cdot \pi \cdot n \cdot \bar{R}}{i} \quad \rightarrow \text{into table}$$

n/min^{-1}	0	337	666	1480	3190	3435
M_d^*/Nm	15,000	15,000	7,620	3,430	1,590	1,370
f_r/Hz	0.4	0.4	0.3	0.66	1.2	1.2
f/Hz	0	11.2	22.2	49.3	106.3	114.5
M_{d1}/Nm	15,000	17,083	10,410	4,700	2,290	2,015
$\delta M_{d1}/\bar{M}_d$	0	0.14	0.37	0.37	0.44	0.47
M_{d2}/Nm	15,000	12,917	4,830	2,160	890	725
$\delta M_{d2}/\bar{M}_d$	0	-0.14	-0.37	-0.37	-0.44	-0.47
M_{d3}/Nm	15,000	15,000	7,620	3,430	1,590	1,370
$\delta M_{d3}/\bar{M}_d$	0	0	0	0	0	0
P_{tot}/kW	0	3,175	3,190	3,190	3,187	2,957
v/kph	0	13.6	26.9	59.9	129.0	138.9

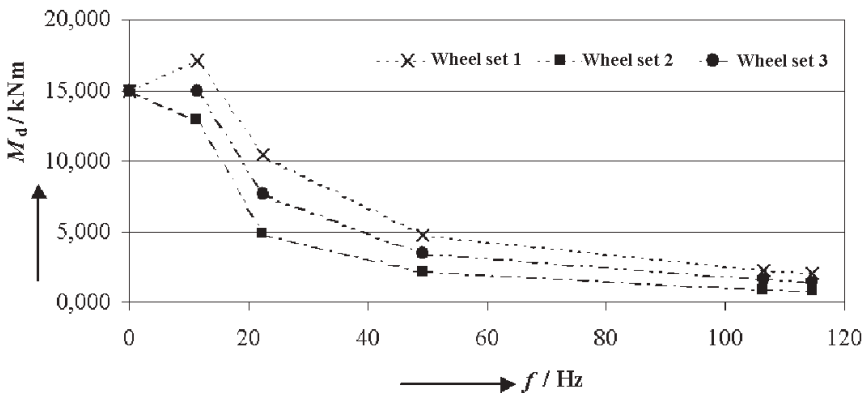


Fig. 17.12: Wheelset torques at different tire wears vs. rotational frequency

17.8 Four-quadrant converter for a Universal Locomotive 6,400 kW

The Universal Locomotive with a nominal power of 6400 kW with squirrel-cage induction traction motors laid out in Exercises 17.1, 17.2 and 17.6 shall be supplied by each two four-quadrant converters per bogie from the $16\frac{2}{3}$ -Hz/15-kV railway supply grid.

1. Calculate the input power of one four-quadrant converter (4q-C) at the nominal (tractive) power of 6400 kW at wheel rim with the addition of 5% per leading bogie from Exercise 7.2, assuming the following global efficiencies:

$$\begin{aligned} \eta_{\text{Gears}} &= 0.98 \\ \eta_{\text{Motor}} &= 0.95 \\ \eta_{\text{Inverter}} &= 0.985. \end{aligned}$$

The losses of the 4q-C and the resonant tank circuit shall be neglected!

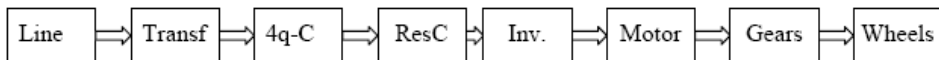
2. The main data of the 4q-C are:

$$\begin{aligned} U_{\text{dN}} &= 2800 \text{ V} \\ f_z &= 250 \text{ Hz} \\ T_{\text{min}} &= 200 \text{ } \mu\text{s} \end{aligned}$$

Calculate the maximal converter input voltage U_{Smax} (r.m.s. value of fundamental)!

3. With $u_{\text{xN}} = 0.333$ und $u_{\text{rN}} = 0.05$ the secondary transformer no-load output voltage U_{T2N} is to be determined such that at a line voltage of 115% nominal value and $\cos \phi_1 = +1$ the maximal converter input voltage U_{Smax} from 2. will not be exceeded. Regard that u_{xN} and u_{rN} are defined for U_{T2N} (at nominal power)!
4. Calculate for nominal line voltage the converter input current I_{T2} (r.m.s. value of fundamental) and from that the absolute values of transformer leakage inductivity and transformer winding resistance. Calculate U_s and ψ_1 !
5. What are the values of the 4q-C output DC current \bar{i}_d and the resonant tank circuit r.m.s. current $I_{\text{d(2)}}$. Select the values of C_2 and L_2 , so that the amplitude of the AC component of the tank capacitor voltage u_{C2} does not exceed the value of 800 V!
6. What is the r.m.s. value of the harmonic portion of the 4q-C input current, due to pulse width modulation?
7. Calculate I_{T2} , U_s , ψ_1 , \bar{i}_d and $I_{\text{d(2)}}$ for regenerative braking at nominal line voltage with a braking power at the wheels identical to the negative value of the nominal tractive power!
8. In braking operation and maximal line voltage $1,15 \cdot U_{\text{T2N}}$ a (fundamental) displacement angle of 164° has been found necessary to keep the value of the maximal converter input voltage (by taking up inductive current the transformer voltage drop is to be subtracted from the line voltage). Calculate I_{T2} , ψ_1 , \bar{i}_d and I_{d2} and show that $U_s \leq U_{\text{Smax}}$!

1. With $\eta_{\text{SK}} = \eta_{4\text{q-S}} = 1$



$$P_{4\text{q-S-Input}} = \frac{1}{\eta_{\text{Inv}}} \cdot \frac{1}{\eta_{\text{Motor}}} \cdot \frac{1}{\eta_{\text{Gears}}} \cdot \frac{1}{4} \cdot 1.05 \cdot P_N = 1832 \text{ kW}$$

$$2. U_{\text{Smax}} = (1 - 2 \cdot f_Z \cdot T_{\text{min}}) \cdot \frac{U_{\text{dN}}}{\sqrt{2}} = 1782 \text{ V}$$

$$3. U_{\text{T2}} = (1 + \sigma) \cdot U_{\text{T2N}} \quad (\sigma = 0.15)$$

$$u_{\text{xN}} = \frac{I_{\text{FN}} \cdot X_{\text{T}}}{U_{\text{T2N}}}, \quad U_{\text{X}} = u_{\text{x}} \cdot U_{\text{T2N}} = \frac{I_{\text{T2N}} \cdot X_{\text{T}}}{(1 + \sigma) \cdot U_{\text{T2N}}} \cdot U_{\text{T2N}} \quad \rightarrow \quad U_{\text{X}} = u_{\text{xN}} \frac{U_{\text{T2N}}}{(1 + \sigma)}$$

$$u_{\text{rN}} = \frac{I_{\text{FN}} \cdot R_{\text{F}}}{U_{\text{T2N}}}, \quad U_{\text{R}} = u_{\text{r}} \cdot U_{\text{T2N}} = \frac{I_{\text{T2N}} \cdot R_{\text{F}}}{(1 + \sigma) \cdot U_{\text{T2N}}} \cdot U_{\text{T2N}} \quad \rightarrow \quad U_{\text{R}} = u_{\text{rN}} \frac{U_{\text{T2N}}}{(1 + \sigma)}$$

$$U_{\text{S}}^2 = (U_{\text{F}} - U_{\text{R}})^2 + U_{\text{X}}^2$$

$$U_{\text{S}}^2 = \left((1 + \sigma) \cdot U_{\text{FN}} - u_{\text{rN}} \cdot \frac{U_{\text{FN}}}{(1 + \sigma)} \right)^2 + \left(u_{\text{xN}} \cdot \frac{U_{\text{FN}}}{(1 + \sigma)} \right)^2$$

$$U_{\text{T2N}} = \frac{U_{\text{S}}}{(1 + \sigma) \sqrt{\left(1 - \frac{u_{\text{rN}}}{(1 + \sigma)} \right)^2 + \left(\frac{u_{\text{xN}}}{(1 + \sigma)} \right)^2}}$$

=>

$$4. P_{\text{Line}} = U_{\text{T2}} \cdot I_{\text{T2}} \cdot \cos \varphi \quad \text{with } \cos \varphi = 1$$

$$P_{\text{Line}} = P_{\text{4q-S-Input}} \cdot \frac{1}{\eta_{\text{Ttransfo}}} = P_{\text{4q-S-Input}} \cdot \frac{1}{1 - 0.05}$$

$$I_{\text{T2N}} = 1238 \text{ A} \quad \rightarrow$$

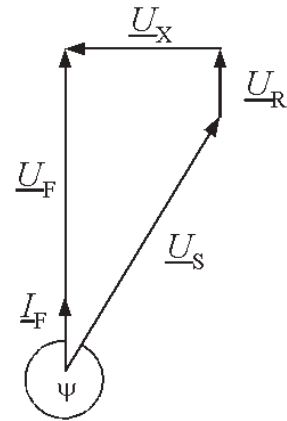


Fig. 17.13 4q-C input quantities at $\cos \varphi = 1$

$$u_{\text{rN}} = \frac{I_{\text{T2}} \cdot R_{\text{T}}}{U_{\text{T2N}}} \quad \rightarrow \quad R_{\text{T}} = u_{\text{rN}} \frac{U_{\text{T2N}}}{I_{\text{T2N}}} = 63 \text{ m}\Omega$$

$$u_{\text{xN}} = \frac{I_{\text{T2N}} \cdot X_{\text{T2}}}{U_{\text{T2N}}} \quad \rightarrow \quad X_{\text{T}} = u_{\text{xN}} \frac{U_{\text{T2N}}}{I_{\text{T2N}}} = 0.42 \Omega \quad \rightarrow \quad L_{\text{F}} = \frac{X_{\text{F}}}{2 \cdot \pi \cdot f} = 4 \text{ mH}$$

$$U_{\text{S}}^2 = U_{\text{T2N}}^2 \cdot \left[(1 - u_{\text{rN}})^2 + u_{\text{xN}}^2 \right] \quad \rightarrow \quad U_{\text{S}} = 1568 \text{ V}$$

$$\varphi_1 = \arcsin \frac{U_{\text{FN}} \cdot u_{\text{xN}}}{U_{\text{S}}} = -19.3^\circ$$

$$5. \quad \bar{i}_d = \frac{P_{4q-S-Input}}{U_d} = 654.3 \text{ A}$$

$$I_{d2} = \frac{1}{2} \cdot \hat{k}_1 \cdot I_{T2} = \frac{1}{2} \cdot \frac{\sqrt{2} \cdot U_S}{U_d} \cdot I_{T2} = 490 \text{ A} \quad \text{with } \hat{k}_1 = \text{control factor of 4q-C}$$

$$\hat{u}_{C2} = \hat{i}_{d2} \cdot \frac{1}{\omega_E \cdot C_2}; \quad \omega_E = 2 \cdot \omega_N \text{ angular frequency of resonant tank circuit} =$$

double line frequency $\rightarrow C_2 = \frac{\hat{i}_{d2}}{\hat{u}_{C2}} \cdot \frac{1}{2 \cdot \omega_N} = \frac{\sqrt{2} \cdot I_{d2}}{\hat{u}_{C2} \cdot 4 \cdot \pi \cdot f} = 4.13 \text{ mF}$

Resonance frequency of resonant circuit $L_2, C_2: \omega_E^2 = \frac{1}{L_2 C_2} \rightarrow L_2 = 5.5 \text{ mH}$

6. Harmonic distortion current

$$\hat{i}_D = \frac{1}{L_T} \cdot \int_0^{1/8f_z} \frac{U_d}{2} dt = \frac{1}{L_T} \cdot \frac{U_d}{2} \cdot \frac{1}{8 \cdot f_z} = 175 \text{ A}$$

$$I_D^2 = \frac{4}{T} \cdot \int_0^{T/4} \left(\frac{1}{2} \cdot \frac{\Delta i_D}{T/4} \cdot t \right)^2 \cdot dt$$

$$\rightarrow I_D = \frac{1}{\sqrt{3}} \cdot \frac{\Delta i_D}{2} = \frac{1}{\sqrt{3}} \cdot \hat{i}_D = 101 \text{ A}$$

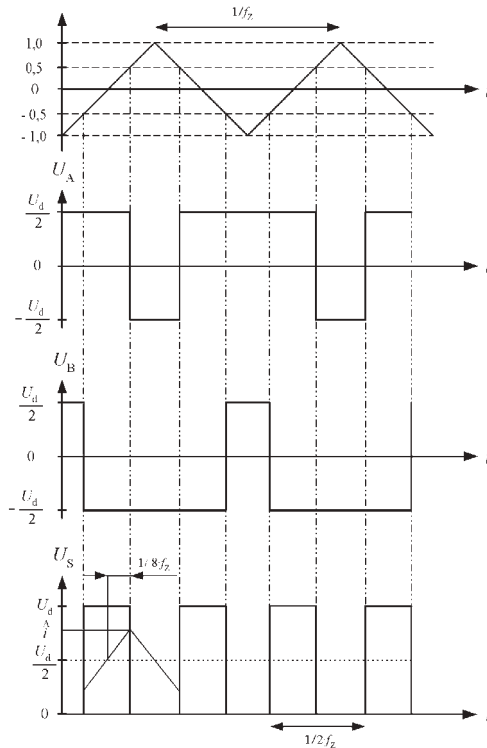


Fig.17.14: 4q-C voltage waveform and input current ripple

7. At regenerative braking power flows from wheels to 4q-C. The power at the input side of the 4q-C is:

$$P_{4q-S} = -1.05 \cdot \frac{P_N}{4} \cdot \eta_{\text{Gears}} \cdot \eta_{\text{Motor}} \cdot \eta_{\text{Inverter}} = -1541 \text{ kW}$$

$$U_{T2N} \cdot I_{T2} \cdot \cos \varphi = P_{4q-S} + I_{T2}^2 \cdot R_T \Rightarrow I_{T2} = 952.5 \text{ A}$$

$$U_S = \sqrt{(U_{T2N} + I_{T2} \cdot R_T)^2 + (I_{T2} \cdot X_T)^2} = 1666 \text{ V}$$

$$\psi_1 = \arcsin \frac{I_{T2} \cdot X_T}{U_S} = 13.9^\circ$$

$$\hat{i}_d = \frac{P_{4q-S}}{U_d} = -550 \text{ A}$$

$$I_{d2} = \frac{1}{2} \cdot \hat{k} \cdot I_{T2} = \frac{1}{2} \cdot \frac{\sqrt{2} \cdot U_S}{U_d} \cdot I_{T2} = 401 \text{ A}$$

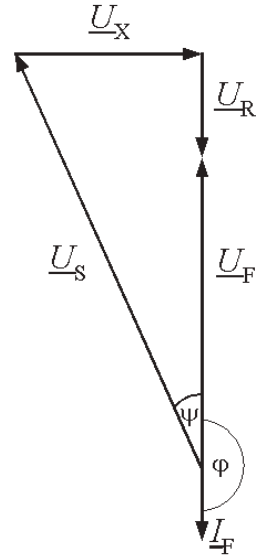


Fig. 17.15: Braking at $\cos \varphi = -1$

8. Braking with inductive line-current component

$$I_{T2} = \frac{U_{T2}}{2 \cdot R_T} \cdot \cos \varphi \pm \sqrt{\left(\frac{U_{T2}}{2 \cdot R_T} \cdot \cos \varphi \right)^2 - \frac{P_{4q-S}}{R_T}}$$

$$= 867.3 \text{ A}$$

$$\psi_1 = \arcsin \frac{-R_T \cdot I_{T2} \cdot \sin \varphi + X_T \cdot I_{T2} \cdot \cos \varphi}{U_S} = 11.8^\circ$$

$$\hat{i}_d = \frac{P_{4q-S}}{U_d} = -550 \text{ A}$$

$$I_{d2} = \frac{1}{2} \cdot \hat{k} \cdot I_{T2} = \frac{1}{2} \cdot \frac{\sqrt{2} \cdot U_S}{U_d} \cdot I_{T2} = 390 \text{ A}$$

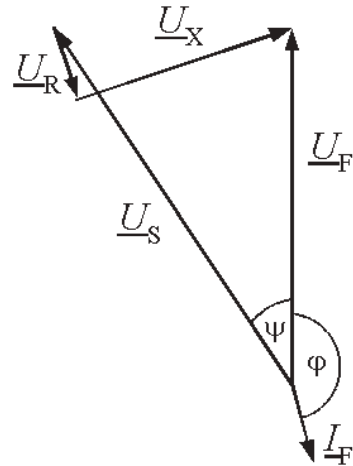


Fig. 17.16: "Inductive" braking, $\varphi = 164^\circ$

$$U_S = \sqrt{(U_{T2} - X_T \cdot I_{T2} \cdot \sin \varphi - I_{T2} \cdot R_T \cdot \cos \varphi)^2 + (I_{T2} \cdot X_T \cdot \cos \varphi - I_{T2} \cdot R_T \cdot \sin \varphi)^2}$$

$$= 1782 \text{ V}$$

17.9 Stopping distance of a Light Rapid Transit Train with and without magnetic rail brake

A fully-occupied Light Rapid Transit eight-axle double train-set (similar to Stuttgart DT 8) with a total mass of $m = 85$ moves on a 70 ‰ slope with an initial speed of $v_0 = 45$ kph. It is to be brought to stand-still by means of the standard wheel brake only or with the Magnetic Rail Brake (MRB), additionally to the wheel brake. The task is to calculate the respective stopping distances.

Additional data:

- Adhesion coefficient of wheels at braking $f_R = 0.15$
- 8 brake magnets, attraction (normal) force of one magnet $F_{NM} = 60$ kN
- Adhesion coefficient of brake magnets $\mu_M = 0.2$

- 1 Calculate the braking effort of the wheels!
- 2 Calculate the total braking effort of the brake magnets.
- 3 Calculate the brace deceleration a_b and the stopping distance s_b
 - a) braking with the wheel brake and the MRB in the slope of 70 ‰
 - b) braking only with the wheel brake in the slope of 70 ‰
 - c) braking with the wheel brake and the MRB in the plain level
 - d) braking only with the wheel brake in the plain level.
- 4 Calculations c) and d) are to be repeated for $v_{0max} = 80$ kph.
1. The braking force of all wheels is:

$$F_{BW} = F_N \cdot f_R = F_G \cdot \cos^2 \cdot f_R = m \cdot g \cdot \cos^2 \cdot f_R = 124.8 \text{ kN} \quad \text{with } \alpha = \arctan(0.070) = 4^\circ$$

2. The braking force of the magnets is:

$$F_{BM} = 8 \cdot F_{NM} \cdot \mu_M = 96 \text{ kN}$$

3. The total braking force (wheels and magnets) is:

$$F_{Btot} = F_{BR} + F_{BW} = 220.8 \text{ kN}$$

The deceleration of the train in the slope is:

$$a_H = \frac{m \cdot g \cdot \sin^2}{m} = 0.69 \frac{\text{m}}{\text{s}^2}$$

$$\text{a) } a_{Bres} = a_{Bges} - a_H = \frac{F_{Btot}}{m} - a_H = 1.91 \frac{\text{m}}{\text{s}^2} \quad s_B = \frac{1}{2} \cdot a_{Bres} \cdot t^2 = \frac{1}{2} \cdot a_{Bres} \cdot \left(\frac{v_0}{a_{Bres}} \right)^2 = 41 \text{ m}$$

$$\text{b) } a_{Bres} = a_{BW} - a_H = \frac{F_{BW}}{m} - a_H = 0.78 \frac{\text{m}}{\text{s}^2} \quad s_B = \frac{1}{2} \cdot a_{Bres} \cdot t^2 = \frac{1}{2} \cdot a_{Bres} \cdot \left(\frac{v_0}{a_{Bres}} \right)^2 = 100 \text{ m}$$

$$\text{Braking in plain level: } a_H = 0 \frac{\text{m}}{\text{s}^2}$$

$$\text{c) } a_{\text{Bres}} = \frac{F_{\text{Btot}}}{m} = 2.6 \frac{\text{m}}{\text{s}^2} \quad s_{\text{B}} = \frac{1}{2} \cdot a_{\text{Bres}} \cdot t^2 = \frac{1}{2} \cdot a_{\text{Bres}} \cdot \left(\frac{v_0}{a_{\text{Bres}}} \right)^2 = 30 \text{ m}$$

$$\text{d) } a_{\text{Bres}} = \frac{F_{\text{BW}}}{m} = 1.47 \frac{\text{m}}{\text{s}^2} \quad s_{\text{B}} = \frac{1}{2} \cdot a_{\text{Bres}} \cdot t^2 = \frac{1}{2} \cdot a_{\text{Bres}} \cdot \left(\frac{v_0}{a_{\text{Bres}}} \right)^2 = 53 \text{ m}$$

$$4. \text{ a) } a_{\text{Bres}} = \frac{F_{\text{Btot}}}{m} = 2.6 \frac{\text{m}}{\text{s}^2} \text{ (cf. 3c)} \quad s_{\text{B}} = \frac{1}{2} \cdot a_{\text{Bres}} \cdot t^2 = \frac{1}{2} \cdot a_{\text{Bres}} \cdot \left(\frac{v_{0,\text{max}}}{a_{\text{Bres}}} \right)^2 = 95 \text{ m}$$

$$\text{b) } a_{\text{Bres}} = \frac{F_{\text{BW}}}{m} = 1.47 \frac{\text{m}}{\text{s}^2} \text{ (cf. 3d)} \quad s_{\text{B}} = \frac{1}{2} \cdot a_{\text{Bres}} \cdot t^2 = \frac{1}{2} \cdot a_{\text{Bres}} \cdot \left(\frac{v_{0,\text{max}}}{a_{\text{Bres}}} \right)^2 = 168 \text{ m}$$

17.10 Supply of electric railway lines from the 50-Hz utility

This exercise shall discuss – in a much simplified manner – reasoning which were decisive for electrification schemes in the 50es/60es of the last century; in recent system studies much more questions have to be investigated!

A two-track electrified section of a length $L = 80 \text{ km}$ is supplied from both ends by identical substations with the transformer data

$$\begin{aligned} S_{\text{N}} &= 20 \text{ MVA} \\ U_0 &= 1.1 U_{\text{N}} \\ u_{\text{xN}} &= 10 \% \text{ (defined at } U_0) \\ u_{\text{r}} &= 0 \end{aligned}$$

The catenaries are transversely coupled and described by the per-unit length parameters

$$\begin{aligned} l' &= 1.2 \text{ mH / km} \\ r' &= 0.118 \Omega / \text{km} \end{aligned}$$

The short-circuit power S_{K} of the feeding utility is assumed first as infinite. Power consumption shall be assumed concentrated in the midth of the section.

1. The section will be supplied with $U_{\text{FN}} = 15 \text{ kV}$, $f_{\text{N}} = 16 \frac{2}{3} \text{ Hz}$; the traction vehicles are dominantly equipped with AC commutator motors, so that the fundamental displacement factor is (simplified) $\cos \varphi_1 = 1$.

What is the maximum value of the active power P , so that the voltage at the pantograph UF does not sink under $90\% \cdot U_{\text{N}}$?

2. Which nominal value U_{FN} of the line voltage is to be selected (at identical transformer and catenary data), so that with a supply frequency of 50 Hz and a fundamental displacement factor $\cos \varphi_2 = 0.91$ ind. the voltage at the pantograph UF does not sink under $90\% \cdot U_{\text{N}}$? ($\cos \varphi = 0.91$ takes into account that most traction units are equipped with thyristor phase-angle control; the cross-section of the line and by that the resist-

ance shall be assumed as above (in spite of the smaller current), not to make calculations too complicated!

- At 50-Hz, 25-kV supply the section acc. to 2. is to be fed from the conductors L1 and L2 of a three-phase utility. Calculate the conductor currents I_{L1} , I_{L2} und I_{L3} and positive-sequence system $\underline{I}' = \frac{1}{3} (\underline{I}_{L1} + \underline{a} \cdot \underline{I}_{L2} + \underline{a}^2 \cdot \underline{I}_{L3})$ and negative-sequence system $\underline{I}'' = \frac{1}{3} (\underline{I}_{L1} + \underline{a}^2 \cdot \underline{I}_{L2} + \underline{a} \cdot \underline{I}_{L3})$, with $\underline{a} = e^{j120^\circ}$ and $\underline{a}^2 = e^{-j120^\circ}$!
- What is the minimal value of the short-circuit power S_K of the three-phase utility, so that the negative-sequence system of the line voltage U_F'' does not exceed 1% of U_{FN} ?
Equivalent Circuit Diagram of line with consumers concentrated in the mid-point of the line

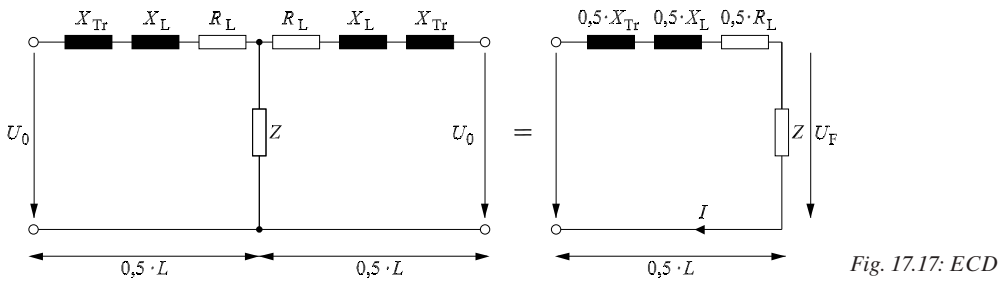


Fig. 17.17: ECD

$$R = r' \cdot 0,5 \cdot L = 4,72 \Omega; \quad X_{Line} = l' \cdot 0,5 \cdot L \cdot 2 \cdot \pi \cdot f = 5,03 \Omega; \quad X_T = u_{xN} \cdot \frac{U_0^2}{S_N} = 1,36 \Omega$$

$$Z_{Line} = \sqrt{(0,5 \cdot R_{Line})^2 + (0,5 \cdot (X_{Line} + X_T))^2} = 3,98 \Omega$$

- Due to $\cos \varphi = 1$ \underline{U}_p and \underline{I} must be in phase.
Thus:

$$U_0^2 = (U_p + 0,5 \cdot R_{Line})^2 + (0,5 \cdot (X_{Line} + X_T) \cdot I)^2$$

$$U_F = 0,9 \cdot U_{FN} \quad \text{and} \quad P = U_F \cdot I$$

$$P_{1/2} = -\frac{0,5 \cdot R_{Line} \cdot U_F^2}{Z_{Line}^2} \pm \frac{U_F}{Z_{Line}} \cdot \sqrt{(U_0^2 + U_F^2) + \frac{(0,5 \cdot R_{Line})^2 \cdot U_F^2}{Z_{Line}^2}}$$

→ $P = 14,95 \text{ MW}$ (only the positive solution is valid)

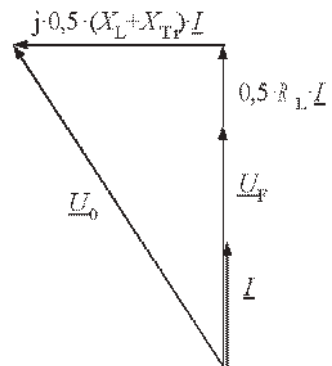


Fig. 17.18: 16 2/3 Hz operation

$$2. X_L = 2 \cdot \pi \cdot f_N \cdot 0,5 \cdot l' = 15,08 \Omega$$

$$X_T = u_x \cdot \frac{U_0^2}{S_N} = u_x \cdot \frac{(1,1 \cdot U_{FN})^2}{S_N} = u_x \cdot \left(\frac{1,1}{0,9}\right)^2 \cdot \frac{U_F^2}{S_N}$$

$$\varphi = \arccos 0,91 = 24,5^\circ \text{ (inductive)}$$

$$R = 0,5 \cdot R_{\text{Line}} = 2,36 \Omega \text{ and } X = 0,5 \cdot (X_{\text{Line}} + X_T)$$

$$U_{\parallel} = R \cdot I \cdot \cos \varphi + X \cdot I \cdot \sin \varphi$$

$$U_{\perp} = X \cdot I \cdot \cos \varphi - R \cdot I \cdot \sin \varphi$$

$$U_0^2 = (U_F + U_{\parallel})^2 + U_{\perp}^2; \text{ with } P = U_F \cdot I \cdot \cos \varphi$$

$$\rightarrow U_F = 22,480 \text{ V}$$

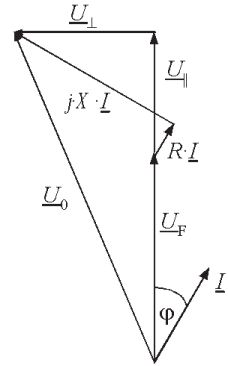


Fig. 17.19: 50-Hz operation

And finally the wanted nominal value of the line voltage: $\rightarrow U_N = \frac{U_P}{0,9} = 24,985 \text{ V}$

$$3. \underline{I}_{L1} = -\underline{I}_{L2}$$

$$|I_{L1}| = |I_{L2}| = \frac{S}{U_F} = \frac{P_1}{U_F \cdot \cos \varphi} = 731 \text{ A}; I_{L3} = 0 \text{ A}$$

$$\underline{U}_{\text{Line}} = \underline{U}_0 - \underline{U}_F$$

$$\rightarrow U_{\text{Line}}^2 = (I \cdot R)^2 + (I \cdot X)^2 \rightarrow U_{\text{Line}} = 7,395 \text{ V}$$

Acc. to the Cosine Theorem:

$$U_{\text{Line}}^2 = U_F^2 + U_0^2 - 2 \cdot U_F \cdot U_0 \cdot \cos \alpha$$

$$\rightarrow \alpha = \arccos \left(\frac{U_F^2 + U_0^2 - U_{\text{Line}}^2}{2 \cdot U_F \cdot U_0} \right) = 11,6^\circ$$

$$\angle(U_0, I_p) = 30^\circ - (\varphi_L + \alpha) = -6,1^\circ$$

$$\underline{I}_{L1} = 731 \text{ A} \cdot e^{-j6,1^\circ} \quad \underline{I}_{L2} = -731 \text{ A} \cdot e^{-j6,1^\circ}$$

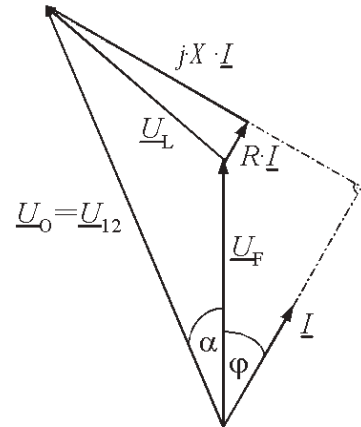


Fig. 17.20: Line voltage drop

Fortescue Components:

$$\underline{I}' = \frac{1}{3} \cdot (\underline{I}_{L1} + \underline{a} \cdot \underline{I}_{L2} + \underline{a}^2 \cdot \underline{I}_{L3}) = \frac{1}{3} \cdot (1 - \underline{a}) \cdot \underline{I}_{L1} = 422 \text{ A} \cdot e^{-j36.1^\circ}$$

$$\underline{I}'' = \frac{1}{3} \cdot (\underline{I}_{L1} + \underline{a}^2 \cdot \underline{I}_{L2} + \underline{a} \cdot \underline{I}_{L3}) = \frac{1}{3} \cdot (1 - \underline{a}^2) \cdot \underline{I}_{L1} = 422 \text{ A} \cdot e^{j23.9^\circ}$$

$$4. \quad U_{\text{Fmax}}'' = 0.01 \cdot \frac{U_0}{\sqrt{3}} = 158.6 \text{ V}$$

Negative-sequence voltage system:

$$U_{\text{F}}'' = X_{\text{K}} \cdot I'' \quad \rightarrow \quad X_{\text{K}} = \frac{U_{\text{F}}''}{I''} = 0.01 \cdot \frac{U_0}{I'' \cdot \sqrt{3}}$$

$$\rightarrow S_{\text{K}}'' = \frac{U_0^2}{X_{\text{K}}} = 100 \cdot U_0 \cdot I'' \cdot \sqrt{3} \approx 2 \text{ GVA}$$

The same result is obtained with equ. (13.1)

$$S_{\text{K}} = \frac{U_0}{U_{\text{F}}''} \cdot S_{\text{N}}$$

and the nominal line power: $S_{\text{N}} = U_0 \cdot I \approx 20 \text{ MVA}$

Index

Symbole

100% low-floor tram 165
100-Hz track circuit 241
110-kV transmission 198
3AC bus bar 213
50-Hz supply mains 206
60-Hz supply mains 206
70 % low-floor tram 165

A

AC-side sequential control 115, 229
AC commutator motor 28, 64, 75, 76, 117, 197
accumulator 171, 195
active current 227
active power 94
adhesion 91, 169, 190
adhesion coefficient 31
admissible tolerances of line voltage 95
air gap 49, 180, 190, 191
all-electric vehicle 178, 216
alternating current system 6
Alweg railway 183
apparent power 94, 227
arcing 64
armature current 49, 52, 143
armature quadrature-axis field 52
armature winding 50, 56
articulated train 160, 164, 184
associations 14
asynchronous motor 75
audio-frequency track circuit 230, 241
authorities 14
automatic field weakening 59, 162
Autosequential Current-Source Inverter 104, 161, 224
autotransformer 65, 209, 224, 240
auxiliary converter 122
auxiliary thyristor 98
average traveling time 35

axle-counter 222
axle-guide 18

B

balanced three-phase current system 70
base frequency 85
base speed 27, 82
BBC Servo-Field Controller 143
bevel gear 47, 128, 141, 166, 168
bidirectional train 161
blocking voltage 99
bogie 18, 19, 28, 38, 45, 75, 91, 123, 126, 151, 165, 166, 168, 182, 190, 231
bogie frame 18
bogie production 12
booster transformer 240
bottom-coil side bar 50, 70
brake
 air-brake control valve 175
 brake chopper 59, 104, 169
 brake contactor 74
 brake deceleration 59
 brake disc 45
 brake pipe 175
 brake resistor 74, 104, 118, 150, 153, 209
 braking effort 59
 braking energy 214
 braking power 59
 braking resistor 59, 66
 compound brake resistor 59
 disk brake 177
 emergency brake valve 175
 linear eddy-current brake 180
 magnet rail brake 169, 179
 regenerative braking 62, 83, 104, 172
 spring-storage brake 178
 triple valve 175
braking 53, 58, 71, 74, 94
break-down angular frequency 79, 92
break-down torque 78, 86, 92, 121, 134, 169
bridge in fully-controllable connection 62
brush 51, 64, 76, 215
brushless excitation 143

C

camshaft-controlled series resistors 54
Cape Gauge 15, 211

cardan hollow shaft 43, 74
cardan shaft 21, 38, 128, 141, 166
cascade connection 81
catenary 75, 80, 129, 152, 207, 209, 214, 226, 236
central mains 197, 198
centrifugal acceleration 23
characteristic wave impedance 236
chording 70
circular current 65
CITADIS 153, 166, 219
clamp diodes 103
classification of traction vehicle types 37
collector 50
collector head 214
Combino 168
commutation 6, 52, 64, 65, 222
 blocking-voltage-free commutation 99
 commutation-pole resistive shunts 64
 commutation capability 100, 148
 commutation capacitor 98, 105, 107
 commutation control 100
 commutation failure 62
 commutation period 99
 commutation pole 52, 54, 57, 64
 commutation reactor 98, 115, 229
 commutation thyristor 89, 98, 107
 phase commutation 100, 144
commutator 50, 69
commutator motor 28
commutator segments 50, 64
commuter 3, 155, 191
compatibility 239
compensation 64, 199
compensation winding 52, 65
concentric lap winding 70
conductor rail 218
conduit 219
conical running profile 17
conicity 17
contact line 211, 214, 236
contact rail 221
contact strip 214, 216
contact wire 240
control 49, 65
control angle margin 62
control trailer 37
converter 195, 221, 236
converter equivalent voltage 232

converter motor 71
cooling 105, 191
 air cooling 105, 111
 evaporation cooling 106, 119, 148, 149, 188
 Freon R113 106
 immersed cooling 105
 liquid cooling 105
 mineral-oil cooling 106
 oil can cooling 106, 107
 radiator 106, 140
 raw-water cooling 106
 silicon oils or esters 106
 water cooling 106, 166, 169
 water intermediate circuit 106
corridor arrangement 151
cost of transshipping 16
Coulomb friction 31
coupling 222, 239
coupling rod 18, 19, 43
current-divider reactor 65, 66
current-source inverter (CSI) 104
current collector 214
current harmonics 148, 223
currents harmonics 93
Curtius/Kniffler 32
curvature-dependant body-tilting equipment 128
curve 17, 23, 26, 32, 91, 160, 166
curved-tooth coupling 45
cycloconverter 141, 202

D

damper 20, 202
damper winding 71
DB II-Wear Profile 17
DC-chopper 131, 161
DC-link 83
DC-link capacitor 94, 102, 107, 135, 237
DC-link current 71, 85, 224
DC-link current harmonics 226
DC-link reactor 74
DC-link voltage 71, 85, 134, 145, 147, 148, 195, 234
DC-link voltage ripple 235, 242
DC chopper 73, 153, 161, 164, 172, 184, 195
DC commutator motor 49, 139, 141, 147
DC railway 221

decentralized supply 198
 deep-draft rods 30
 degrees of liberty 18
 deregulation 4, 124, 134
 diesel-electric locomotive 7, 75, 91, 92, 139, 140, 142, 144, 146, 148, 150, 152
 diesel-electric power transmission 139
 diesel engine 139
 diesel locomotive 7
 diesel traction 11
 difference speed 31
 diode bridge rectifier 60, 74, 152, 212
 direct-current railway system 8
 direct current 8
 Direct Self Control (DSC) 148
 Direct Self Control (DSC) 90
 displacement factor \cos 62, 192
 distortion current 227, 234
 DMU 126
 double-deck motive power 159
 Double-Layer Capacitors 213
 double-star motor 74, 135
 doubly-articulated train 160, 163
 drawbar 28
 drive 39
 AEG-Kleinow helical spring-coil drive 42
 ALSTHOM dancing ring 43
 Alsthom Hollow Shaft drive 43
 axle-hung drive 40, 124, 155, 159
 axle-riding drive 45
 bipolar motor drive 39
 bogie-mounted drive motor 42
 cardan hollow-shaft drive with rubber joints 43, 126, 165
 DÜWAG twin-axle longitudinal drive 47
 electric drive chain 139, 141, 143
 gear-centre distance 40
 gearless drive 39, 74, 165
 high-performance drive with brake shaft 45
 hydraulic drive chain 139, 141, 143
 inclined oblige driving rods 40
 intermediate gear wheel 45
 INTRA drive 74
 Monomoteur drive 74, 113, 132
 parallel-crank drive 18, 39
 pin-and-nose drive 40
 single wheelset drive 40

 SSW rubber circular-spring drive 41, 65
 SYNTEGRA drive 74
 two-axle longitudinal drive 160, 161, 164
 Westinghouse drive 42, 65
 Winterthur drive 40
 DSP 90
 dual-frequency locomotive 124
 dual-layer winding 75
 dual-mode traction vehicle 152
 dual-system 74
 dual-system Light Rapid Transit vehicle 162
 dual-system locomotive 131
 duty cycle 56, 85, 93
 Dynamic Field Weakening 90

E

economical continuous speed 80
 eddy current 86
 eddy currents 191
 efficiency 11, 54, 74, 83, 92, 105
 electric railway 8
 electric traction 11
 electrification 8, 198, 211, 218
 electro-pneumatic wheelset balance 30, 117
 emission 236
 EMU 126, 156
 energy consumption 11
 energy recovery 11
 European railway industry 12, 13
 European Standard Gauge 15
 excitation winding 49, 73
 exciter current 49
 exterior starting resistors 80

F

feeder line 209
 feeding section 207
 fiber-optic 112
 field-oriented control 89, 148, 192
 field-weakening shunt 54
 field weakening 27, 53, 74, 89, 172
 filling set value 143
 flange 3, 150
 flash-over 54
 Flexicoil 18, 19, 40, 45, 165
 Flexity Classic 168
 flicker 207

flux threshold 90
flywheel 173
forced-commutation circuit 56, 59, 74, 98
four-quadrant converter 93, 124, 134, 136, 163, 204, 230, 235, 242
four-system locomotive 112, 133
free-wheeling diode 57
friction 4, 33
fundamental factor 228
fundamental frequency 83
fundamental reactive power 63

G

gate unit 108, 111, 112
gauge 5
generator 69, 152, 173, 188, 238
 auxiliary generator 143, 147, 148
 DC generator 141
 generator dimensioning 147
 heating generator 141
 permanent-magnet synchronous generator 152
 synchronous generator 141, 202, 226
 tacho generator 143
gradient 26, 127, 193
gradient resistance 26
great cogwheel 40
group supply of motors connected in parallel 74, 91, 123
GTO thyristor 56, 59, 73, 75, 100, 105, 109, 122, 134, 148, 195, 204
guidance 3, 181, 190, 195

H

Hard-Drive technology 204
harmonic currents 121, 198, 227
haul truck 188
Head-End Power 153
high-performance drive with brake shaft 124
high-performance locomotive 19
high-power locomotive 75
high-speed line 127, 198, 205, 207
high-speed train 3, 37, 75, 119, 126
high-voltage switch gear 65
hold-off time 99
Höllental trial line 6, 221
hollow shaft 21, 41

HV connection cable 129
hydrodynamic (Föttinger) converter 7, 139
hydroelectric plant 198
hydroelectric power 11
hysteresis 90

I

ICE 1 108, 126, 129, 177
ICE 2 37, 108, 129
ICE 3 45, 128, 129, 135, 178, 180, 193, 196
idler wheelset 19
IGBT 56, 75, 83, 89, 102, 105, 111, 136, 169
IGCT 204
Ignitron 60, 131
impulse encoder 71
incremental impulse encode 87
Indirect Stator-quantities Control (ISC) 90
induction 49
induction machine (motor) 74, 75, 76, 78, 80, 82, 84, 86, 88, 90, 92, 94, 96, 98, 100, 102, 104, 106, 108, 110, 112, 202
input filter 57, 137, 222
insulating joint 241
insulation gap 80
Integrated Complete Drive 21, 45, 122
Intelligent Power Module (IPM) 112
interaction of vehicles with four-quadrant converters 238
Intercity train 37
interharmonics 204
interleaving 224, 231
interurban 156
inverter 69, 80, 83, 192
 circuit and construction technology 98
 GTO inverter 134, 153, 157, 165
 IGBT inverter 74, 102, 166, 169, 186, 195
 Neutral-Point-Clamped (NPC) 103
 three-level inverter 103
 thyristor inverter 75, 145, 148
 two-level inverter 83
iron losses 52

J

Jacobs' bogie 126, 158, 160

K

Kando system 80
 Klingel's oscillations 17, 190
 Kloss Formula 79

L

leakage inductivity 77, 81, 86, 137
 leasing of rolling stock 12
 lemniscatic guidance 18
 length of exposed section 239
 lengths of system network 10
 LEW AC controller 66
 Light Rail System 4, 156, 159
 Light Rapid Transit 4, 155, 159, 161
 linear motor 190

- linear generator 195
- linear synchronous long-stator motor 192
- short-stator induction motor 192

 line filter 73, 122
 line frequency 6, 65
 line interference 115, 209, 221, 222, 226, 228, 230, 232, 234, 236, 238, 240, 242
 LIREX 152
 load-commutated inverter 71
 load transfer 28, 91, 117, 234
 locomotive 5, 113, 219
 London Underground 39
 long-distance railway 5, 64
 longitudinal coupling 209
 low-floor technology 159
 low-floor tramway 153, 169
 low-floor vehicle 164
 low-frequent signaling interference 235
 low-frequent subharmonics 85
 low-voltage control 65
 low force attack point 30
 lyra bow collector 160, 216

M

M-n plain 71
 machine model 90
 magnetic field 190, 212
 magnetic flux 49
 magnetic pole 49
 magnetizing inductivity 77
 mainline locomotive 19
 manufacturer 13, 14
 mass transit 4, 156

mercury-vapor rectifier 6
 mercury-vapour rectifier 212
 metre gauge 15, 161
 Metro 156
 mid-point 83
 mid-point potential 103
 minimum fuel consumption 139, 147
 mining railway 16
 minor railway 15
 mixed excitation 30
 modularization 107
 moment of inertia 18, 20, 216
 motor coach 75, 126, 152, 172, 219
 motor headcar 73
 motor series reactor 121
 motor star voltage 83
 motor car 37
 motor coach 37
 motor headcar 37
 multi-system locomotive 103, 151, 218, 242
 multi-system traction vehicle 74, 128, 131, 132, 134, 136, 138
 multiple control 126
 multiple unit (MU) 37, 128, 155

N

narrow gauge 5, 15
 national railways 3
 negative-sequence system 207
 neutral zone 49, 52, 64
 nominal power 27, 54
 nonactive current 227
 nonpositive link 31
 normalized short-circuit voltage 231
 number of parallel branches 51
 number of pole pairs 49, 80
 number of thermal cycles 102

O

ohmic commutation-pole shunt 6
 opposed-forced guidance of wheelsets 22
 oscillation 20
 overhead line 236
 oversize factor 147
 overvoltage protection chopper module 109

P

- pantograph 62, 80, 129, 160, 214, 216, 237
passenger-flow system 160
passengers' comfort 23
Pendolino 23, 128
people mover 4, 10, 182
permanent-magnet synchronous motor (PMSM) 74, 173
phase-angle control 61, 63, 93, 113, 226, 237
phase-angle delay 66
phase-control rectifier 60
phase-shifting capacitor 228
phase building block 107, 108, 112
phase separation 207
phasor 76, 93
PI controller 89
pinion 40
pivot 19, 30, 165
plastic-moulded module 102
platform 12, 124, 128, 151
platform (station) 158, 164, 182
point of common coupling 207, 221
point of constant power 147
point of constant power 82
pole 70
pole pitch 49, 192
pole shoe 49, 52
positive-fit 31
positive-sequence system 207
power-electronic control 157, 198, 223, 226, 239
power-frequency control 198
power at maximal speed 137
power at maximum speed 83, 134
power factor 93, 228
power headcar 37, 119, 126, 134
power supply 209, 226
power transmission 19, 39
pressure-contact device 102
pressurized rubber-tire wheel 181
PRIMA 124, 151
psophometric weighting 222
psophometric interference current 239
psophometric weighting 231
public-service railway 4
pulse number 231
Pulse Width Modulation (PWM) 56, 84, 89, 144, 242
pump storage plant 199
push-pull train 37
- Q
quenchable half-controllable bridge (LUB) 63
quenching-angle control 63
- R
rack railway 26, 31
radar slip control 33
radially-steerable single-wheel running gears (KERF) 152, 157
radially-steered single-wheel trailing running gear (EEF) 165
rail 3
rail-guidance 15, 17, 19, 21, 23
rail-wheel system 3, 181, 190
railway 3
railway electrical supply network 8, 9
railway product market 13
rail car 37
reactive current 94, 199, 227
reactive power 73, 204
recovery time 99
rectifier 212, 221, 222
rectifier overlap 222
recuperation 12, 59, 66, 173, 186, 199, 208, 209, 227
reinforcement line 209
resilient wheel 47
resonance 237
resonance frequency 17, 99, 215, 240
resonant commutation circuit 99
resonant impedance 99
resonantly-earthed system 198
resonant quality 100
resonant tank circuit 108, 111, 121, 204, 229, 237
return current 212, 221, 240
rod collector 155, 159, 215
rolling resistance 25
rotary converter 80, 198, 199, 201, 212, 239
rotary field 207
rotating energy-storage 219
rotating energy storage 173, 213
rotating field 69, 70, 75
rotating reference system 90
rotor 49, 54, 69, 74, 75, 143
 drum-type rotor pattern 49
 dual-layer winding 50
 loop winding 50
 rotor bar 50, 83, 86, 92

- rotor lamination 50
- rotor winding resistance 77
- squirrel-cage rotor 173
- rotor-flux-oriented or Vector Control 90
- running resistance 20
- S
- sags of the traction effort 66
- saturation 52
- screw spring 18
- secondary suspension 19, 40
- section-change methods 194
- self-steering wheelsets 22, 150
- separate excitation (Sepex) 53, 113
- sequential control 60, 131
- sequential phase control 228
- series-parallel regrouping 54, 131
- series-resonant circuit 94
- series-wound commutator motor 6, 52
- series compensation 199
- series resistor control 54
- shaft power 77
- shell diagram 141
- Shin Kansen 7, 126
- short-circuit ring 76
- short-circuit time constant 84, 89
- shunting 53
- shunt locomotive 83, 86, 92, 144
- side-band frequencies 225
- Simplon Tunnel 75, 106
- simulated series motor 53, 115
- single-arm pantograph 216
- single-axle drive 19, 38, 150
- single-phase alternating current 8
- single-phase alternating current railway system 9
- single-phase load 207
- single-wheel running gear 164, 165, 167, 168
- single-wire system 212
- sinusoidal oscillation 18
- slip 17, 26, 52, 77, 207
- Slip-frequency-stator-current characteristics control 87, 144, 145
- slip-ring rotor 76
- slip rings 69, 76, 80
- slot 50, 70, 192, 195
- smoothing reactor 57, 62, 71, 93, 104, 135, 204, 223, 229
- snubber 101, 106, 110
- Marquardt-Undeland snubber circuit 101, 108, 110
- McMurray snubber circuit 102, 109
- RCD-LRD snubber circuit 101
- Space-Vector Modulation 85
- spectra 231
- speed 27, 35, 64
- speed-torque characteristic 52
- speed observer 90
- spring suspension 18, 39, 40
- square-wave (block) modulation 83, 89, 195, 204, 226
- squeezing of diesel-engine speed 143
- squirrel-cage induction motor 6, 75
- squirrel-cage winding 76
- Stadtbahn 161
- standard gauge 15, 156, 161, 214
- star-delta re-grouping 137
- static converter 204, 239
- stator 49, 54, 69, 75
- stator-winding-fixed reference system 90
- stator frequency 77, 195
- stator winding 192
- steam locomotive 4
- step-down chopper 56, 223
- step-up chopper 58
- stranded conductors 122
- stray current 212, 219
- striking angle 20, 22, 26
- substation 198, 199, 207, 209, 212, 222
- substation rectifier 59
- subterranean power feed 219
- suburban railway 4
- superconductive coil 191
- supersynchronous braking operation 80
- supply frequency 69, 197
- support 190, 195
- surface roughness 32
- suspension railway 183
- switching frequency 56, 83, 85, 90, 93, 103, 228
- switching loss 103
- Symmetrized Sinusoidal Modulation 85
- Synchrone Bicourant (SYBIC) 74, 132
- synchronous displacement angle 71
- synchronously induced voltage 70, 147
- synchronous motor 119
- synchronous reactance 71
- synchronous switching patterns 85

T

Talent 152
Talgo 129
Taurus 45, 109, 124
technical standard 5
telephone harmonic form factor 222
tertiary winding 122, 234
TGV-A 73, 119
Thalys 73, 119
thermal power station 198, 199
thermal time constant 28
third rail 152, 156
three-level inverter 123, 136, 195, 196, 205
three-phase current 6, 8
three-phase drive 93, 144
three-phase drive technology 7, 20, 124, 134, 152, 163, 164, 188, 209, 228
three-phase motor 28
Three-Phase Reference Source 89
three-phase winding 69, 70, 74, 75
three-system locomotive 131
three-wire system 212
threshold voltage 61, 99
throttle position 143, 145
thyristor 55, 65, 98, 229
tilting 23, 152, 183, 193
 active tilting technology 24
 cant deficiency 23
 passive tilting technology 24
 rotating pole 24
time-variant voltage ratio 93
tire wear 17, 164
top-coil side bar 50, 70
torque 51, 65, 71, 85, 87, 145
 torque control 33, 166
 torque equation 81
 torque oscillation 207
 torque pulsation 65, 74
touch voltage 212
track 3, 181
track circuit 222, 241
traction motor 49
tractive-effort vs. speed diagram 28
tractive effort 27, 145
trailer 37, 156, 160, 171
train line 10, 121, 141, 149
train resistance 25, 126, 190, 191
train safety system 134
Tram Train 163

tramway 4, 8, 47, 155, 159, 214, 219, 222
transformer 28, 45, 93, 117, 122, 195, 205, 231
transformer e.m.f. 64
transformer tap-changer 60, 65, 156, 172
TRANSRAPID 190
transversal slip 32
traveling time loss 35
TRAXX 124, 151
trolley bus 111, 186
tunnel 152, 156, 214, 215, 218
turn loop 161, 186
two-phase motor block relay 241
two-pulse bridge in half-controllable connection of pairs of arms with sequential control 228
two-pulse bridge in half-controllable connection of pairs of arms with sequential phase control 60, 73, 93, 113
two-quadrant converter 134
U
U/fr - characteristic control with impulse encoder 87
UM-AN 126
underground railway 4, 8, 155, 222
undulating-current motor 133, 157, 229
unidirectional train 161
unipolar switching 96, 231
universal locomotive 7, 28, 83, 113
unsprung mass 39, 40
V
VAL 182
Variotram 165, 168
voltage-source inverter (VSI) 83, 98, 144, 225
voltage control 82
voltage drop 5, 214, 228
voltage harmonics 222, 226, 230
voltage quality 221
W
wear 17
weight-to-power ratio 5
wheel 3
wheel-creep control 33
wheel arrangement 38
wheelbase 20, 160, 182
wheel contact point 28
wheel diameter difference 91, 92, 150
wheel profile 17
wheelset 16, 18, 28, 38, 91, 141, 156
wheelset load 16, 126, 128

wheelsettrack system 17

wheel tire 91

winding insulation 103

wing-train concept 127

Y

yoke 49

Z

zero-sequence portion 83

zig-zag 214, 215, 218